

## Appendix A

# Driven-Thin Experimental Procedure and Data

Included here is the checklist and all data recorded during the driven-thin detonation experiments. All experiments were performed with Kliulai Chow-Yee.

### A.1 Driven-Thin Checklist

Checklist for experiments performed in the driven-thin detonation tube in 26 Guggenheim, Caltech.

**Operators:** Jason Damazo and Kliulai Chow-Yee

1. Turn on data acquisition system.
2. Turn on vacuum pump and heat exchanger.
3. Open hand valves for gases.
4. Turn on gas key, evacuate line, turn off gas key.
5. Open bottle farm valves.
6. Open all electronic valves to evacuate specimen tube. Wait until  $p_{\text{vacuum}} < 40 \text{ mTorr}$ . Zero fill pressure gauge.
7. Check position of rotary valve.

8. Turn on strain gauge signal conditioning amplifiers; zero strain gauges. In tube 9, the amplifiers used a signal gain of 50 with a strain gauge excitation voltage of 10 V. For tubes 10 and 11, the amplifiers used a signal gain of 10 with an excitation voltage of 10 V.
9. Close door to experiment room and seal room.
10. Turn on warning light.
11. Don ear protection.
12. Evacuate the gas fill line.
13. Pressurize the gas fill line with oxygen.
14. Open valves and fill the detonation tube with oxygen to the target oxygen fill pressure.
15. Evacuate the fill line.
16. Pressurize the gas fill line with ethylene.
17. Open valves and fill the detonation tube with ethylene to the target fill pressure.
18. Evacuate the fill line.
19. Run circulation pump for at least 5 minutes.
20. Record the pre-shot temperature and pressure.
21. Close all valves to seal the detonation tube.
22. Verify interlocks are green.
23. Arm data acquisition.
24. Arm glow-plug.
25. Turn on glow plug and wait for ignition. Fire!

26. Switch off glow-plug immediately after data acquisition triggers or 30 seconds have elapsed.
27. Open valve to pressure gauge after the temperature is below 30°C.
28. Record post shot pressure and temperature.
29. Evacuate vessel.
30. If it is the last shot of the day, reset the facility.
31. Record data to ASCII files.
32. Back-up data.

## A.2 Tube 9 Data

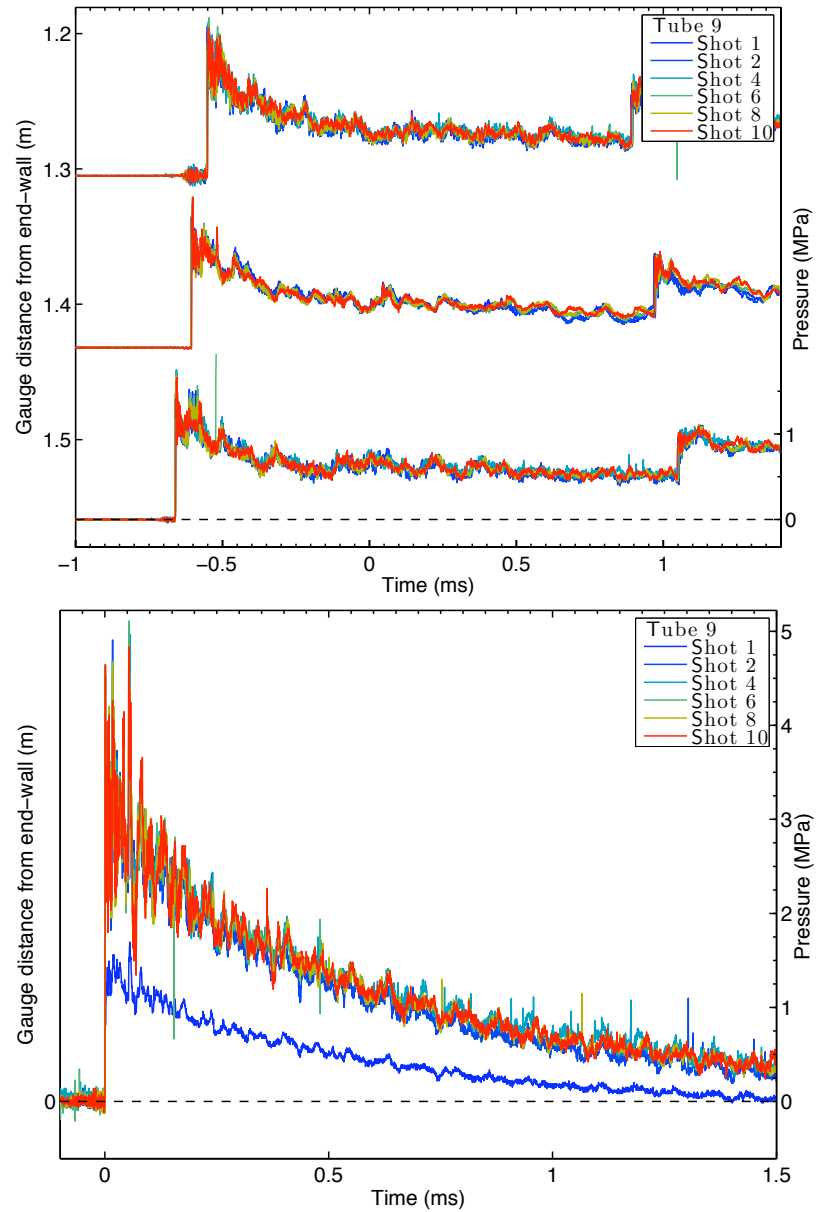


Figure A.1: Time-resolved pressure measurements from elastic shots in tube 9.

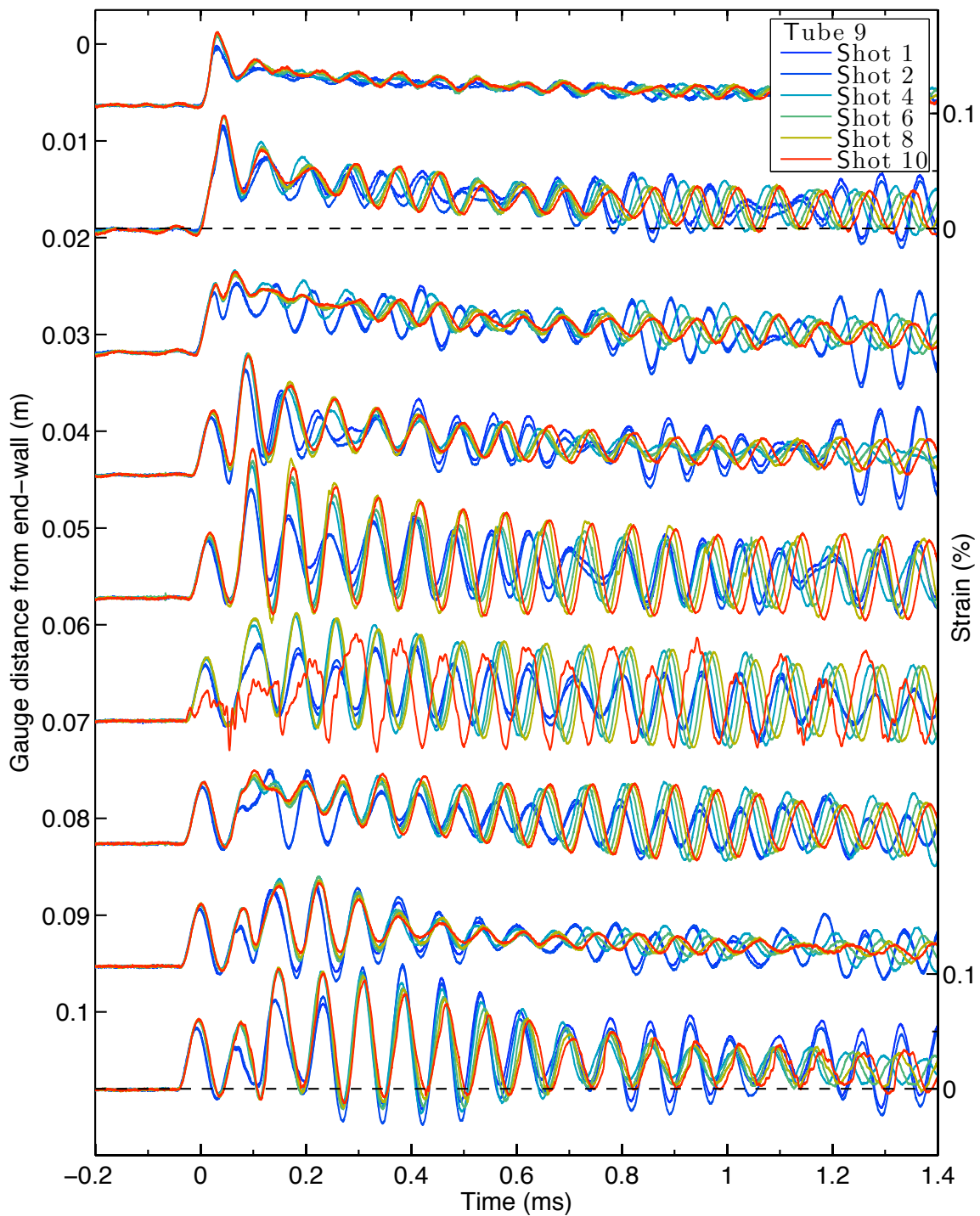


Figure A.2: Time-resolved elastic hoop strain measurements in tube 9, part 1.

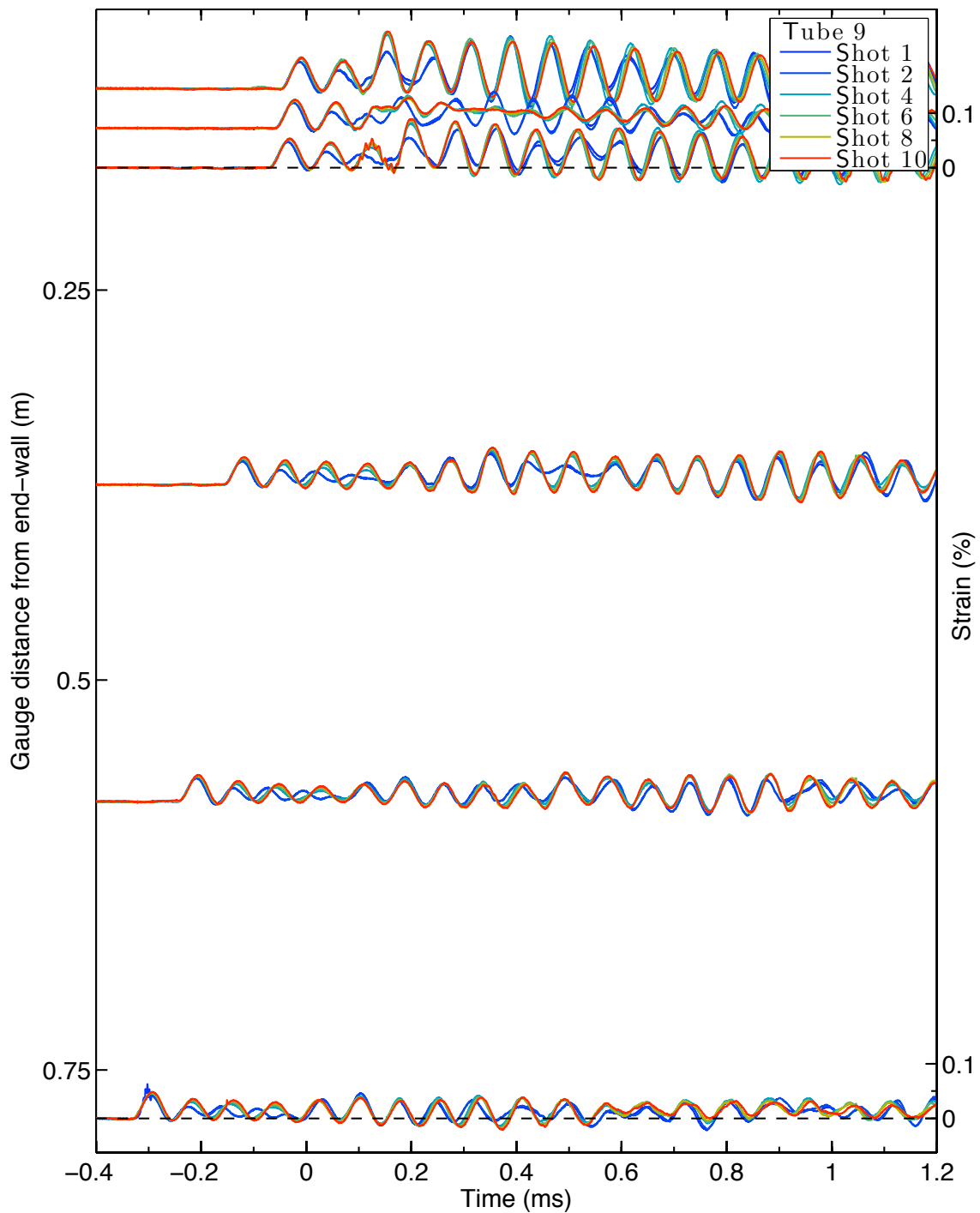


Figure A.3: Time-resolved elastic hoop strain measurements in tube 9, part 2.

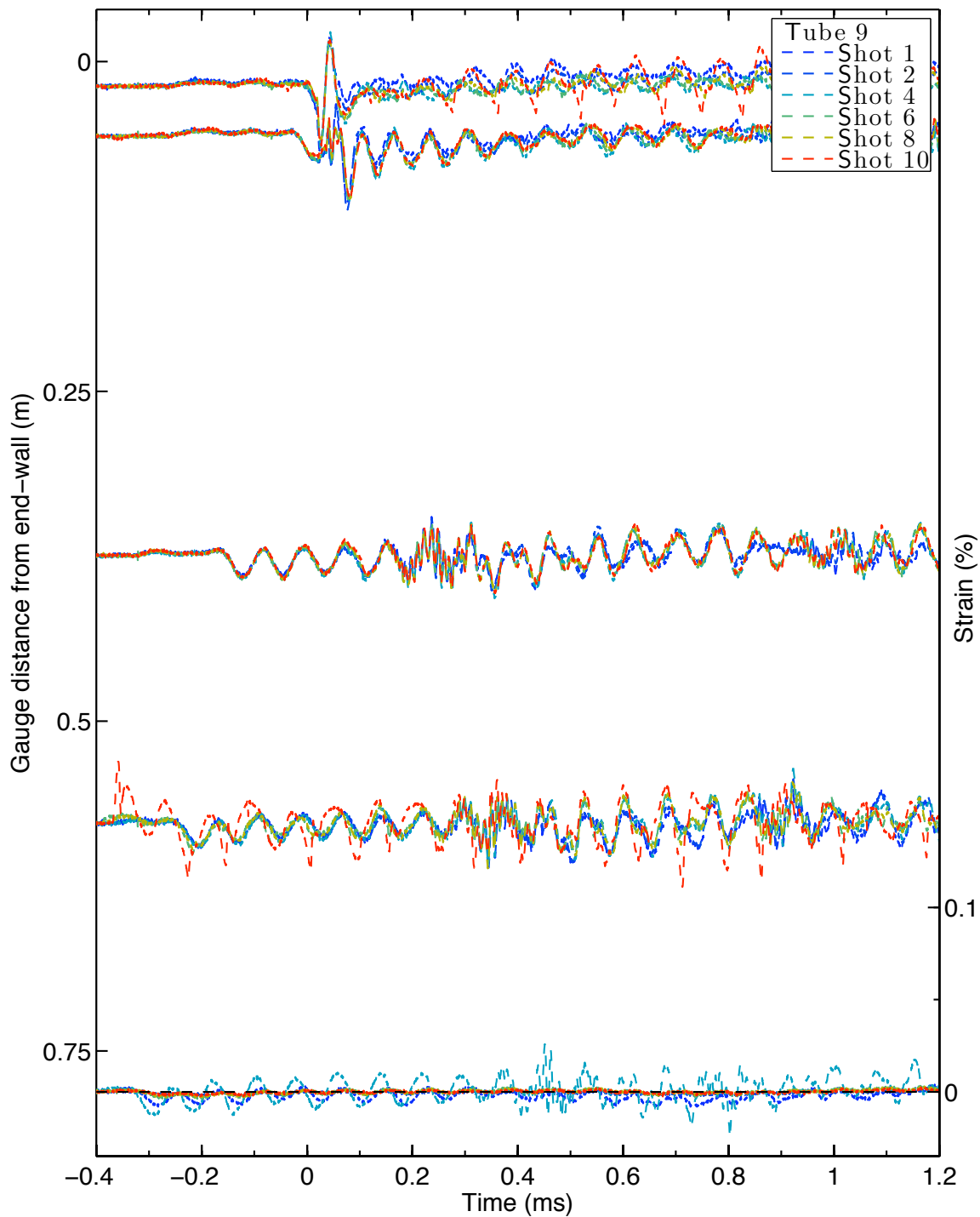


Figure A.4: Time-resolved elastic longitudinal strain measurements in tube 9.

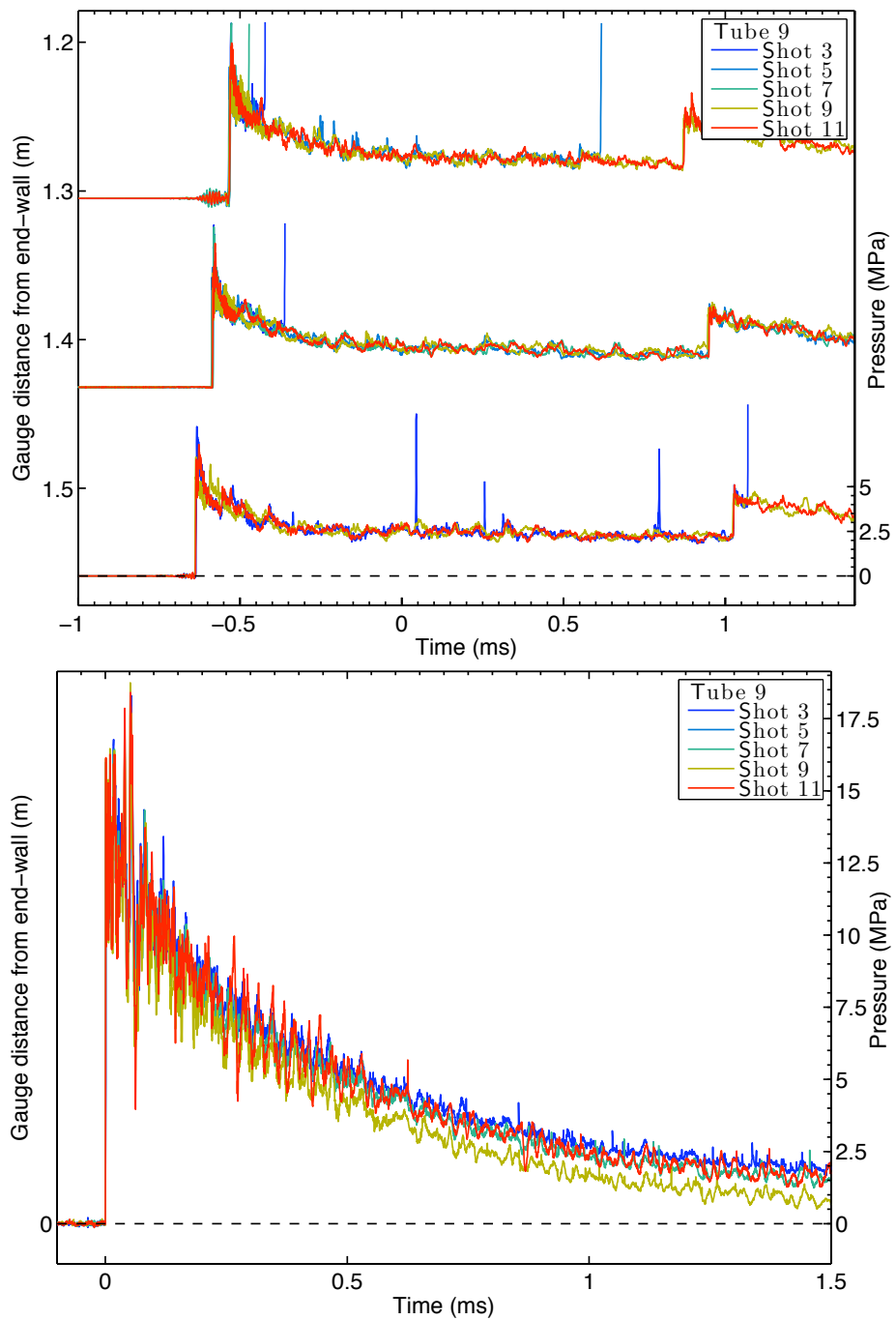


Figure A.5: Time-resolved pressure measurements from plastic shots in tube 9.

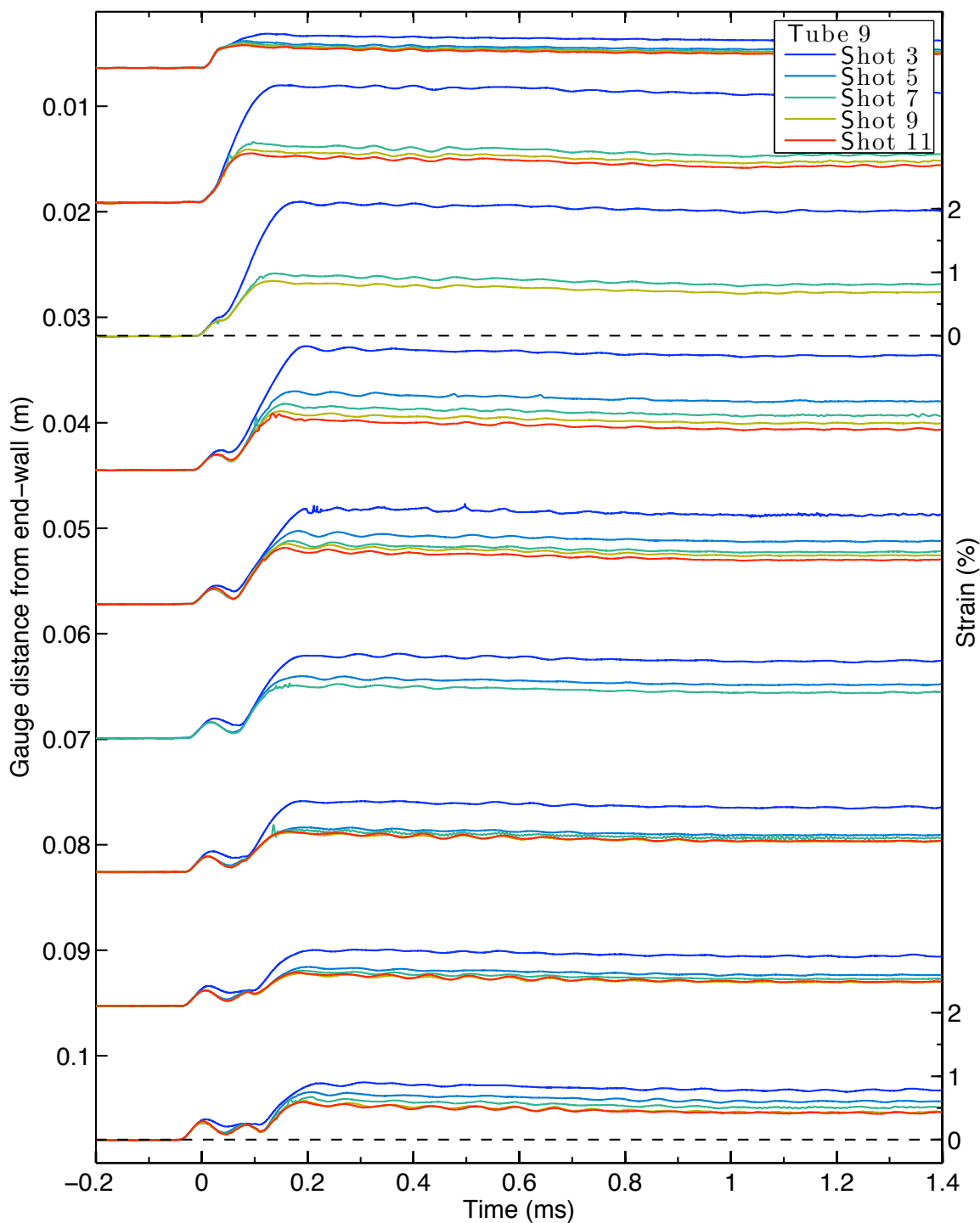


Figure A.6: Time-resolved plastic hoop strain measurements in tube 9, part 1.

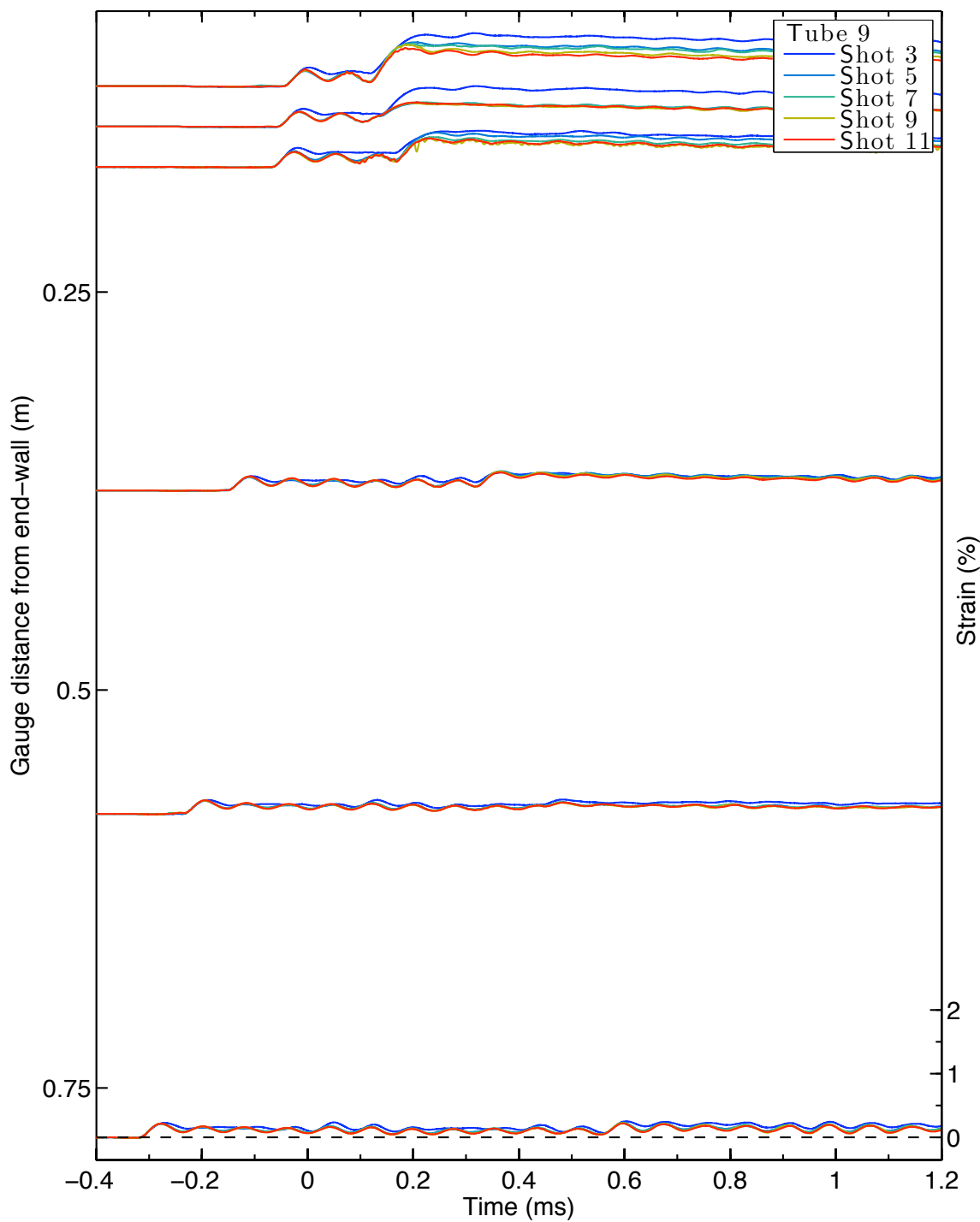


Figure A.7: Time-resolved plastic hoop strain measurements in tube 9, part 2.

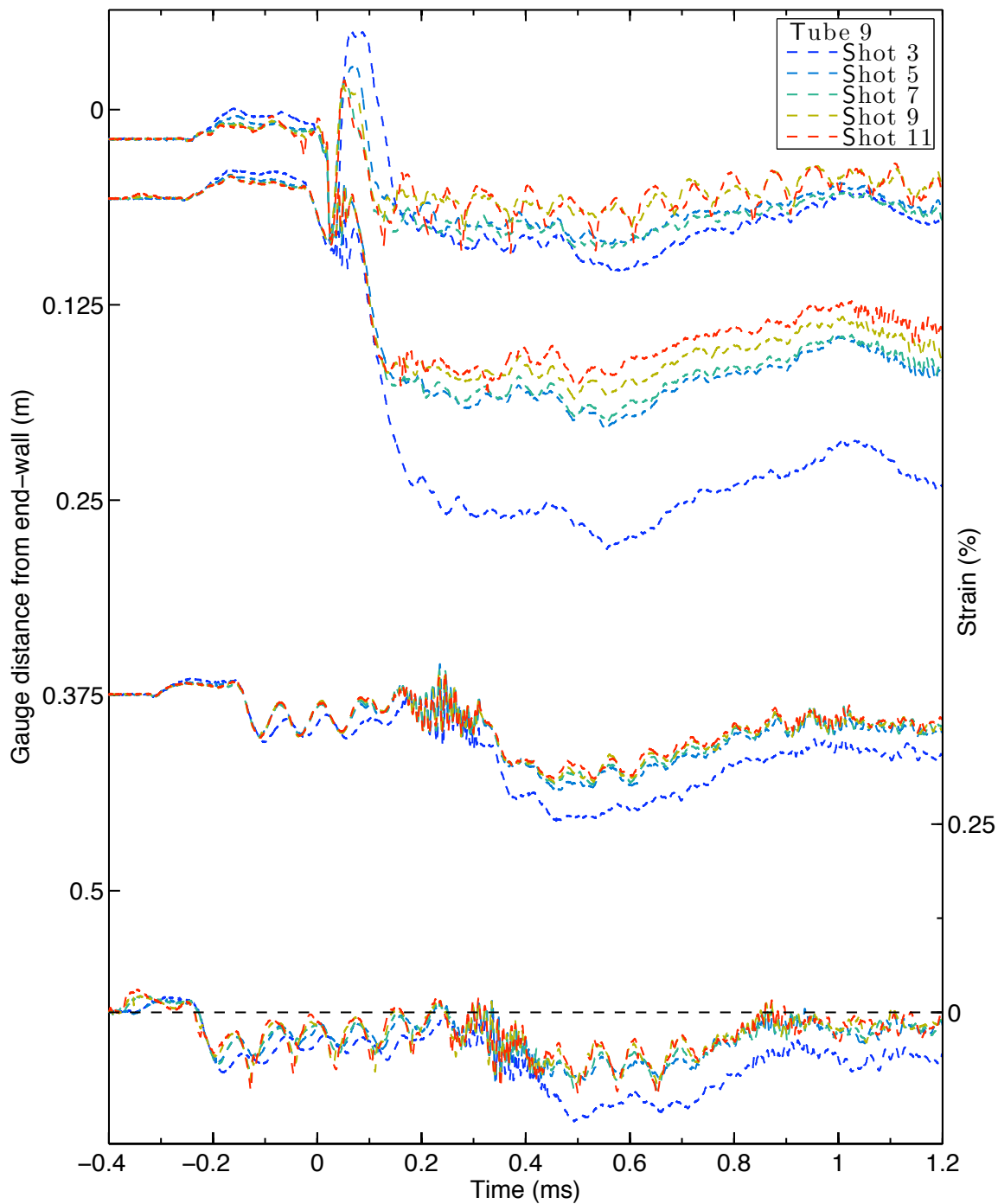


Figure A.8: Time-resolved plastic longitudinal strain measurements in tube 9.

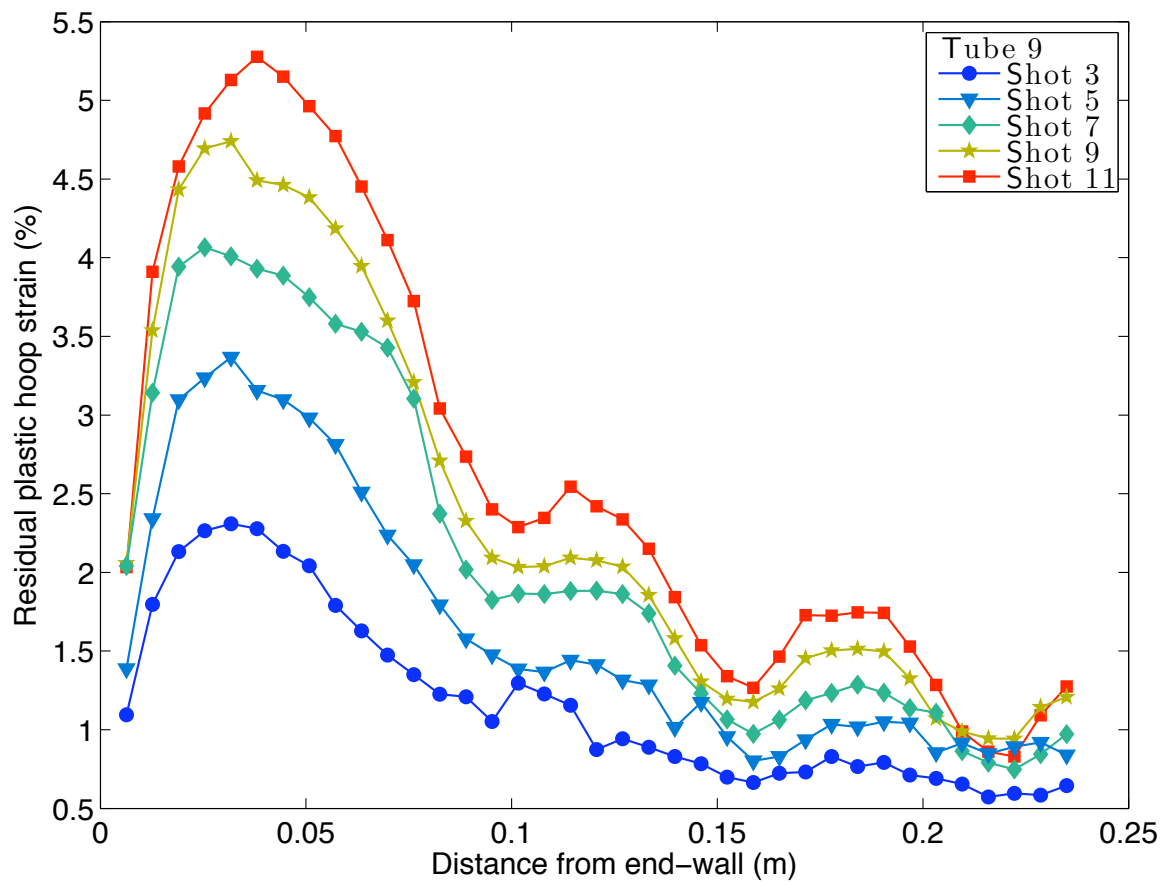


Figure A.9: Residual plastic hoop strain measurements in tube 9.

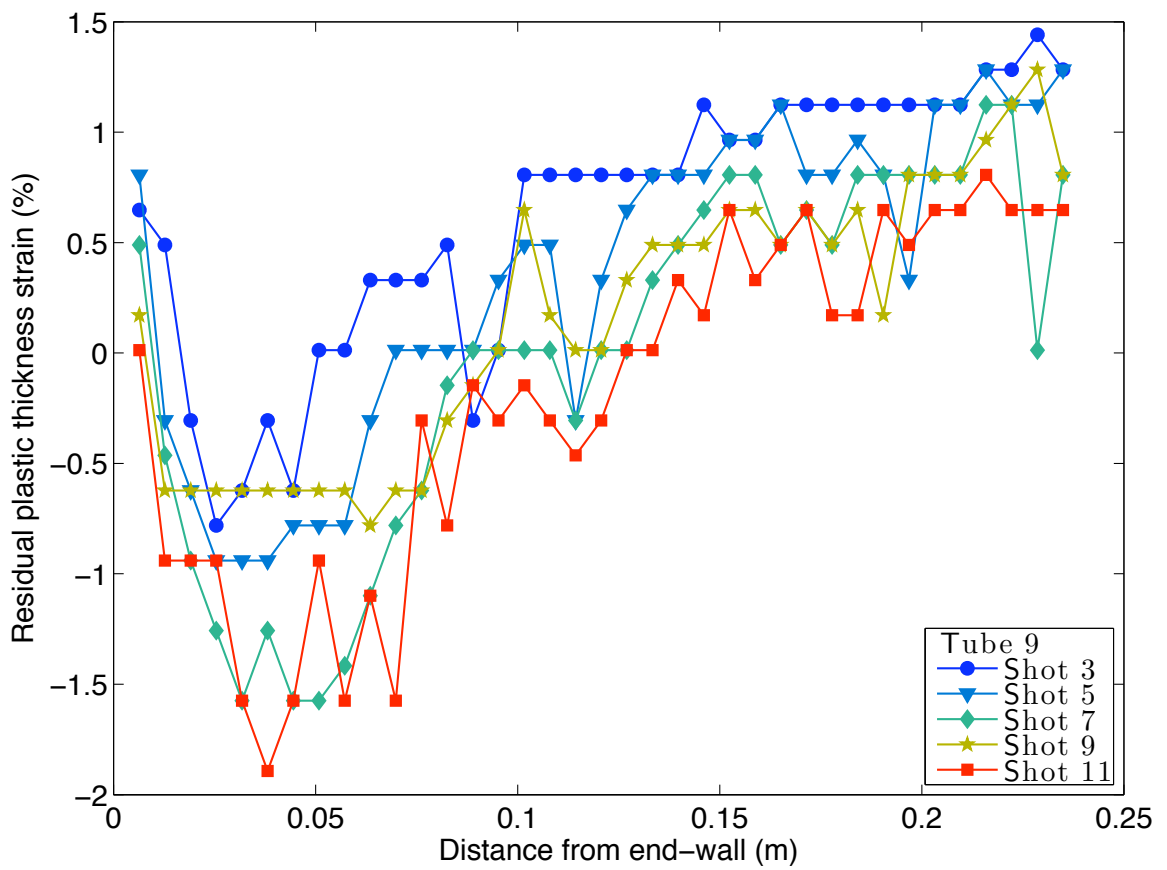


Figure A.10: Residual plastic thickness strain measurements in tube 9.

### A.3 Tube 10 Data

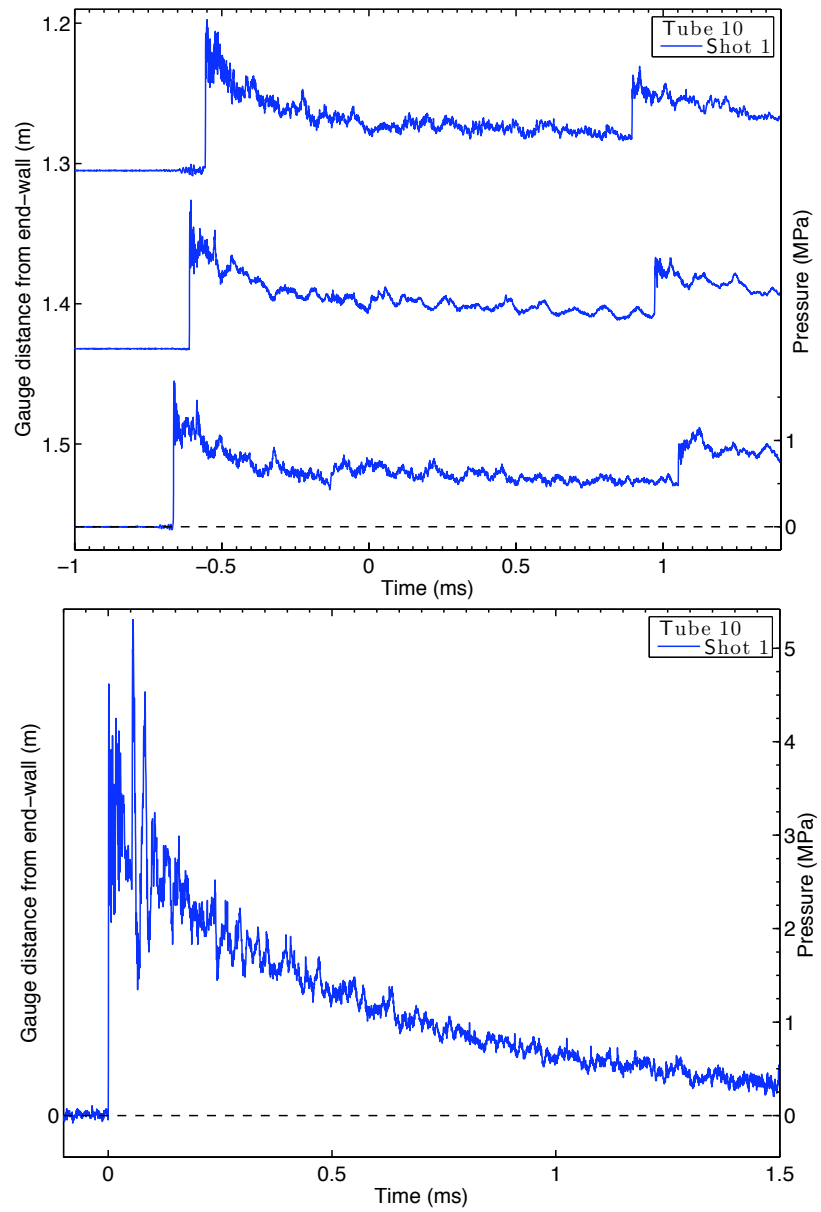


Figure A.11: Time-resolved pressure measurements from elastic shots in tube 10.

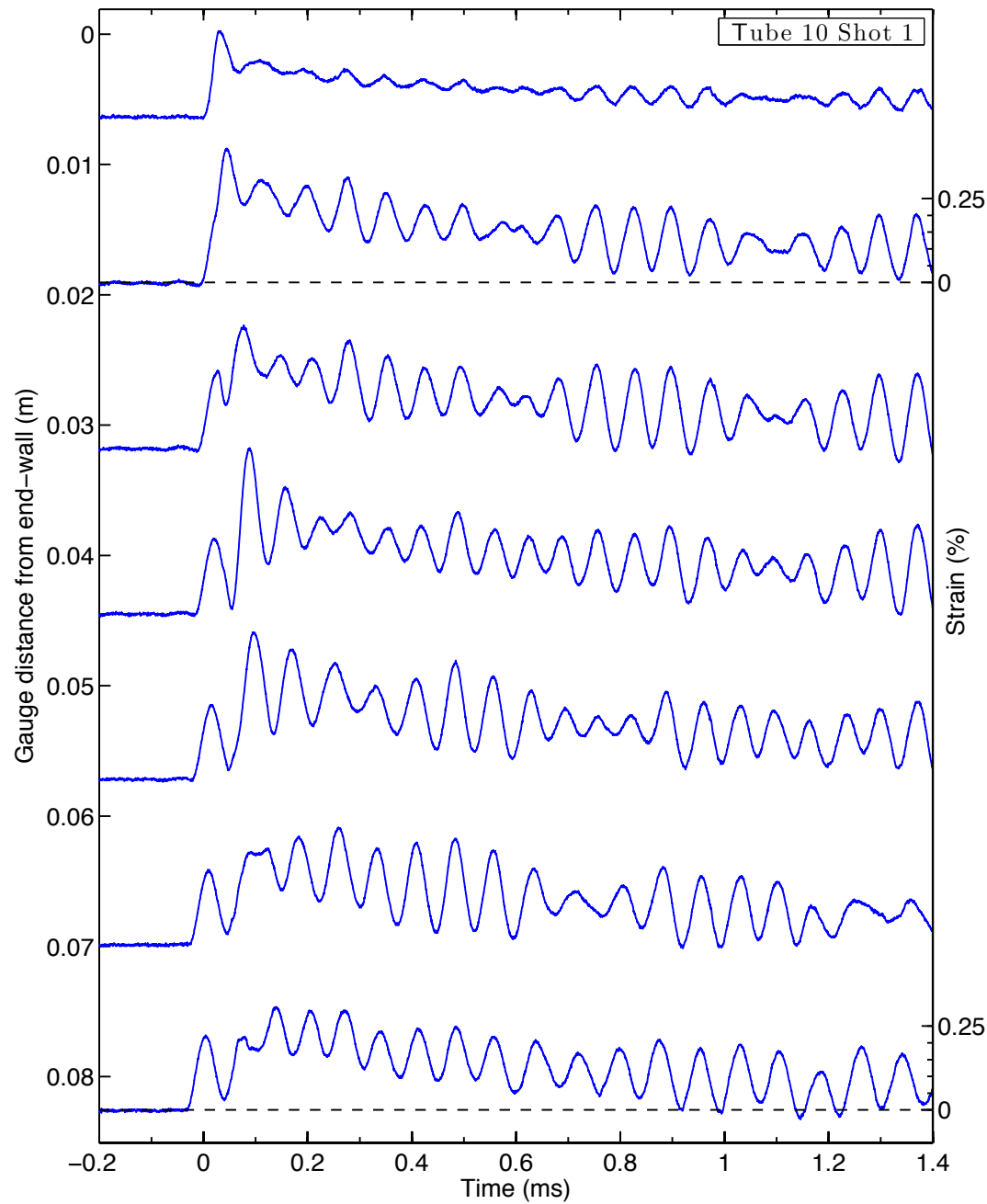


Figure A.12: Time-resolved elastic hoop strain measurements in tube 10, part 1.

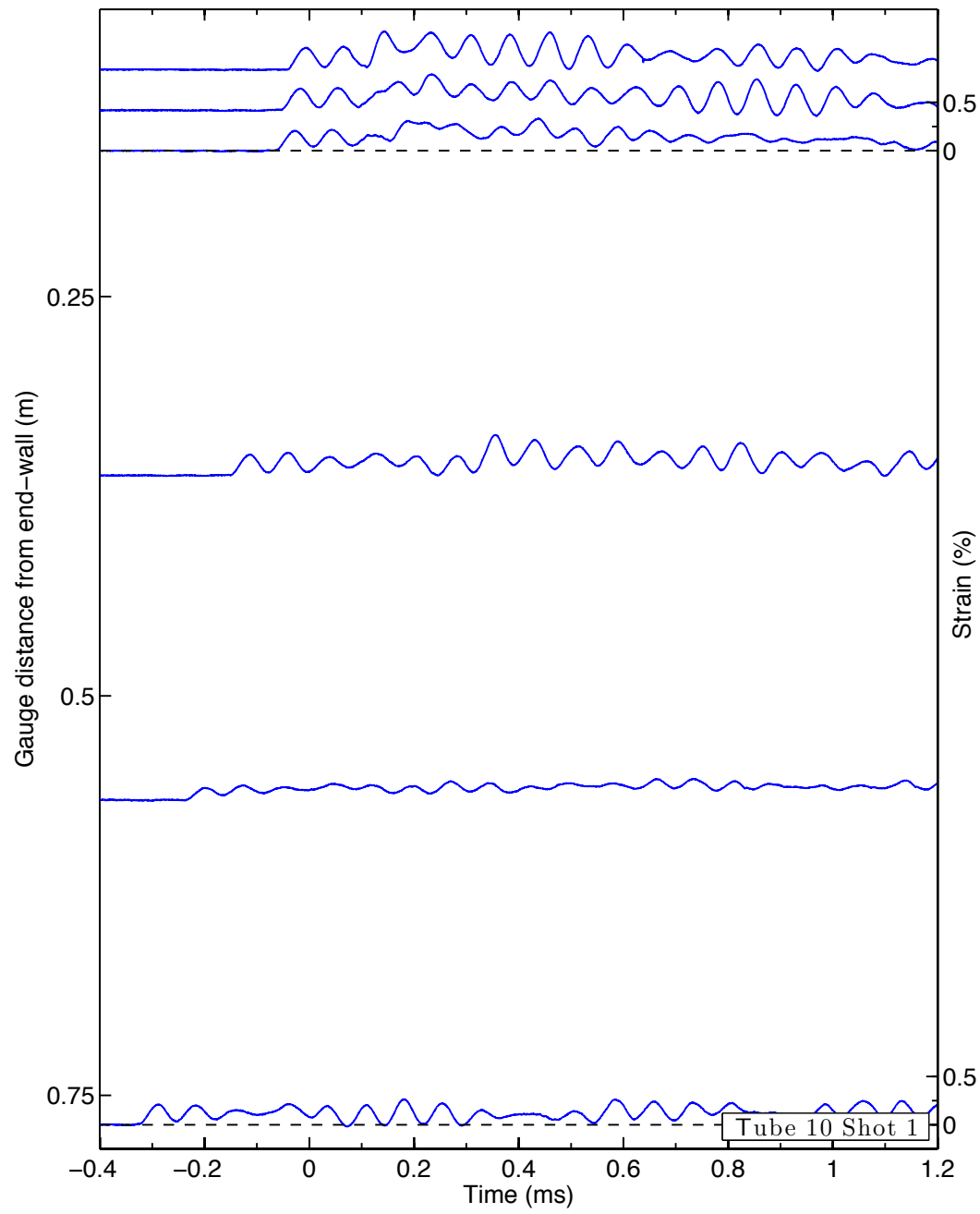


Figure A.13: Time-resolved elastic hoop strain measurements in tube 10, part 2.

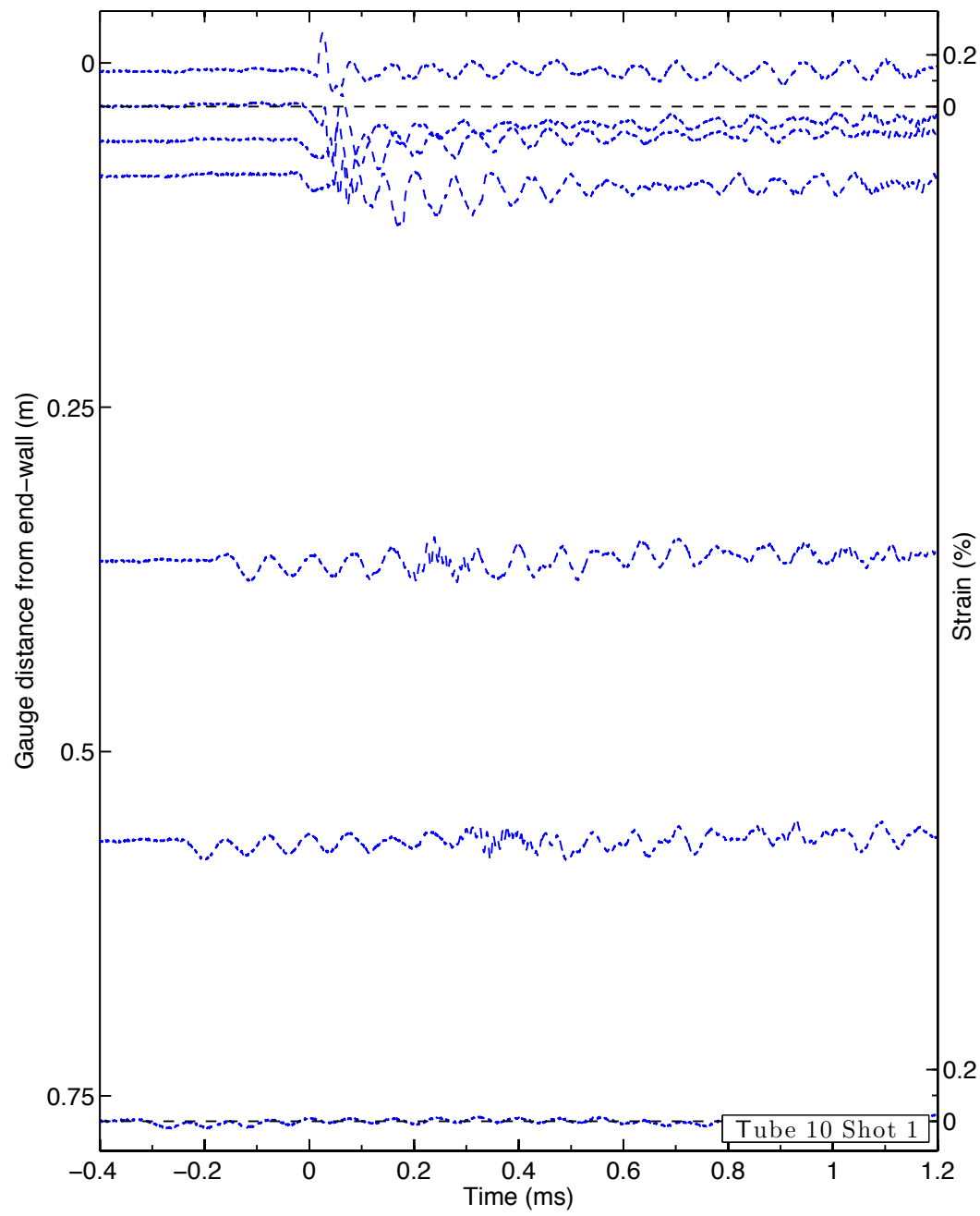


Figure A.14: Time-resolved elastic longitudinal strain measurements in tube 10.

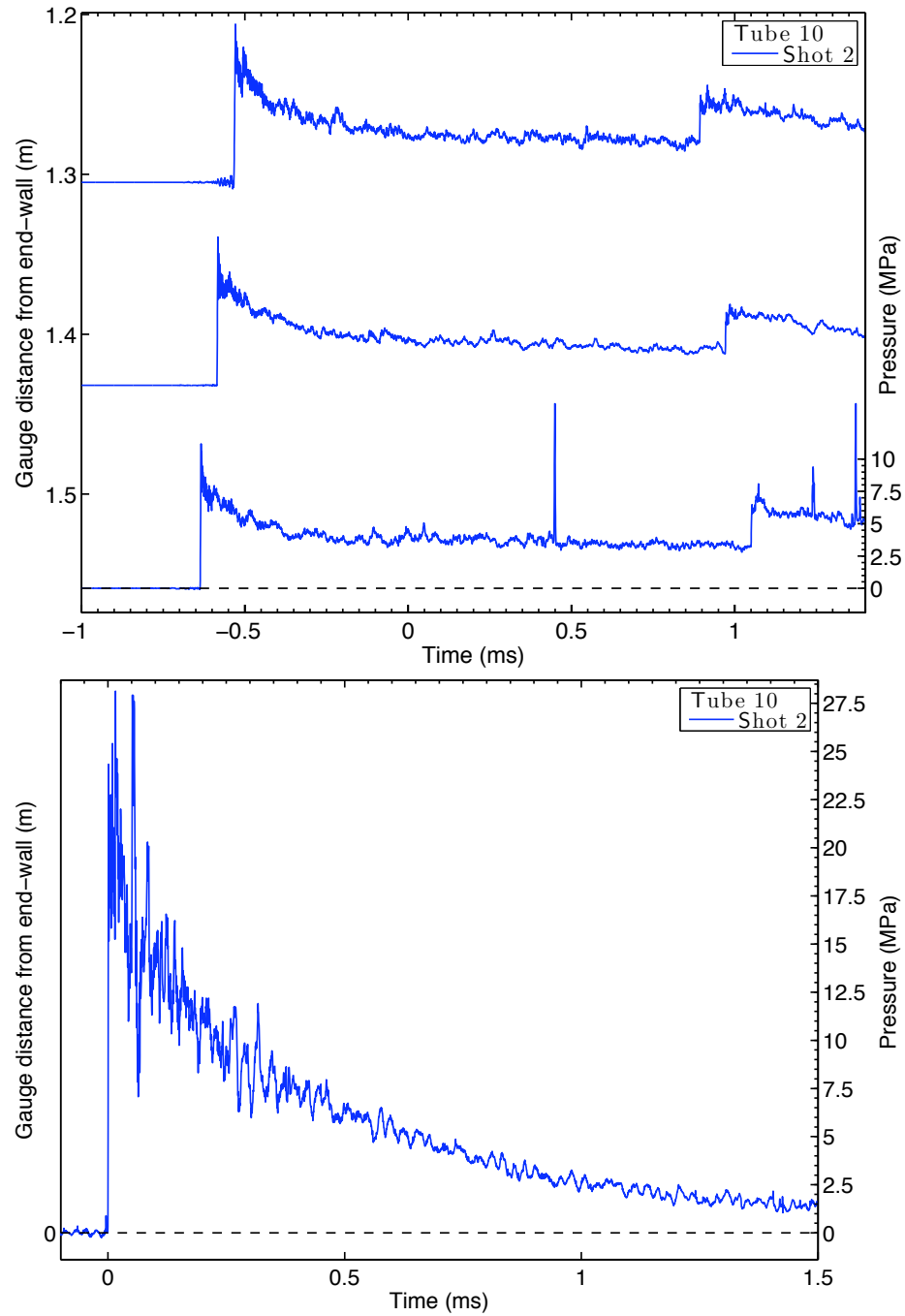


Figure A.15: Time-resolved pressure measurements from plastic shots in tube 10.

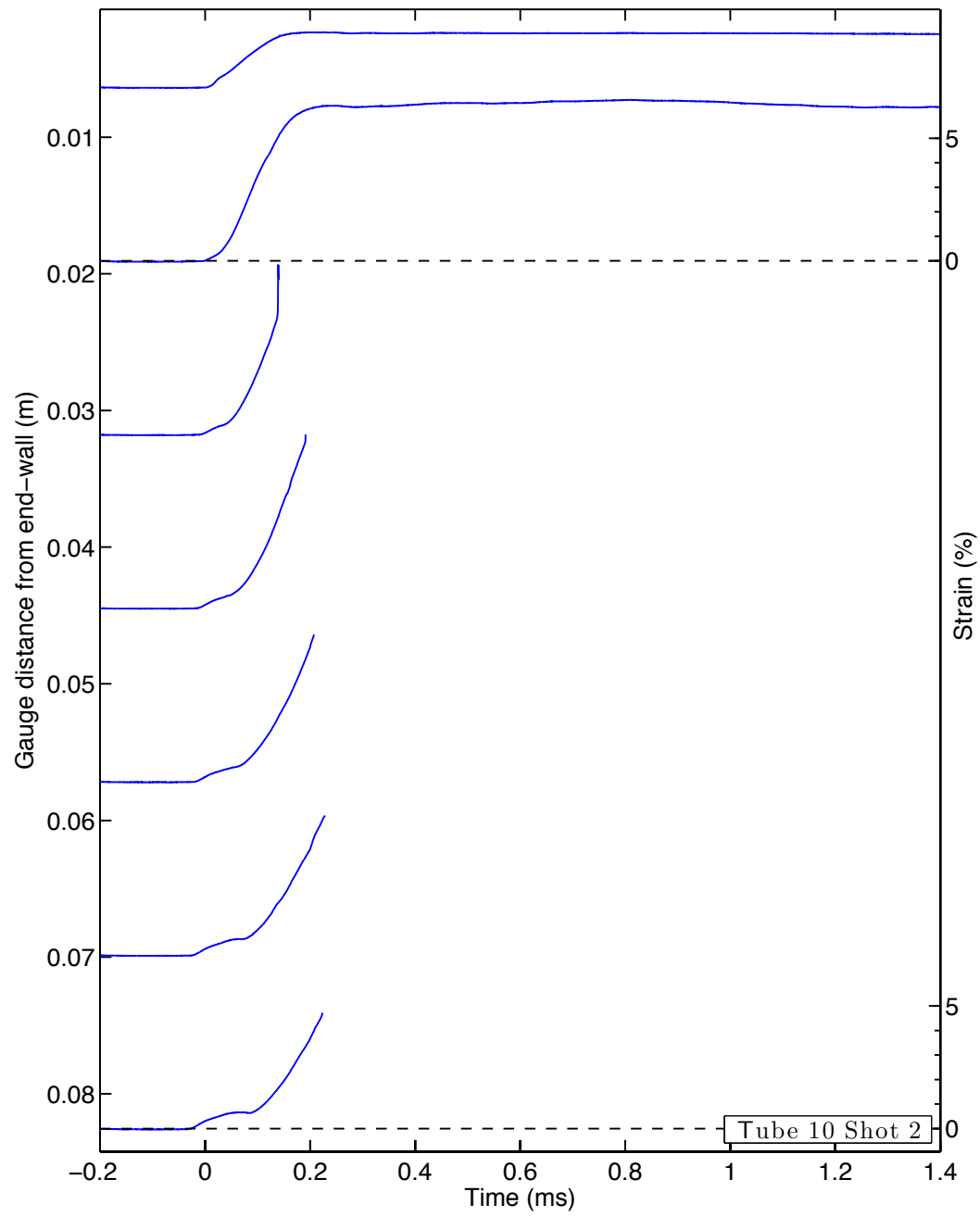


Figure A.16: Time-resolved plastic hoop strain measurements in tube 10, part 1.

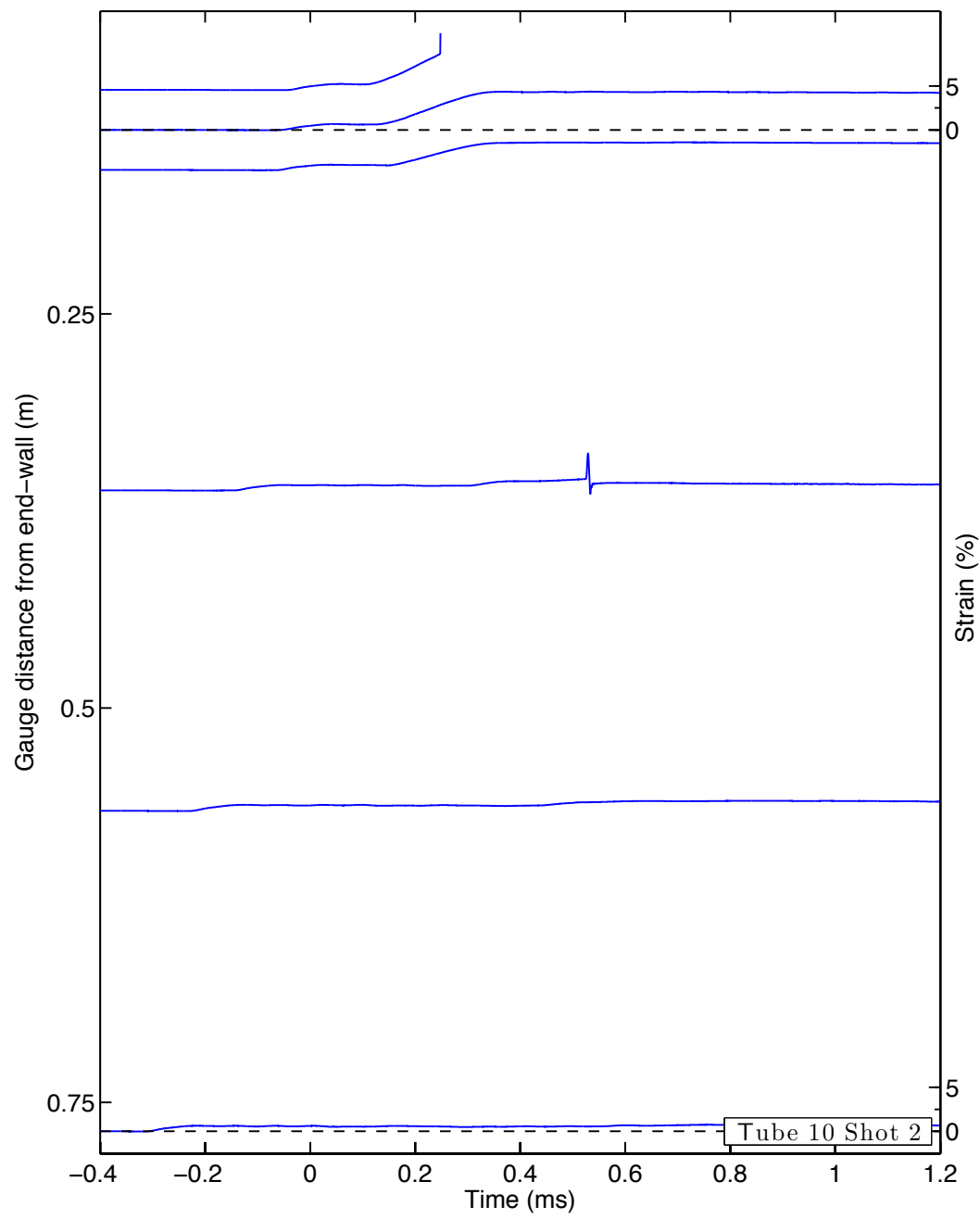


Figure A.17: Time-resolved plastic hoop strain measurements in tube 10, part 2.

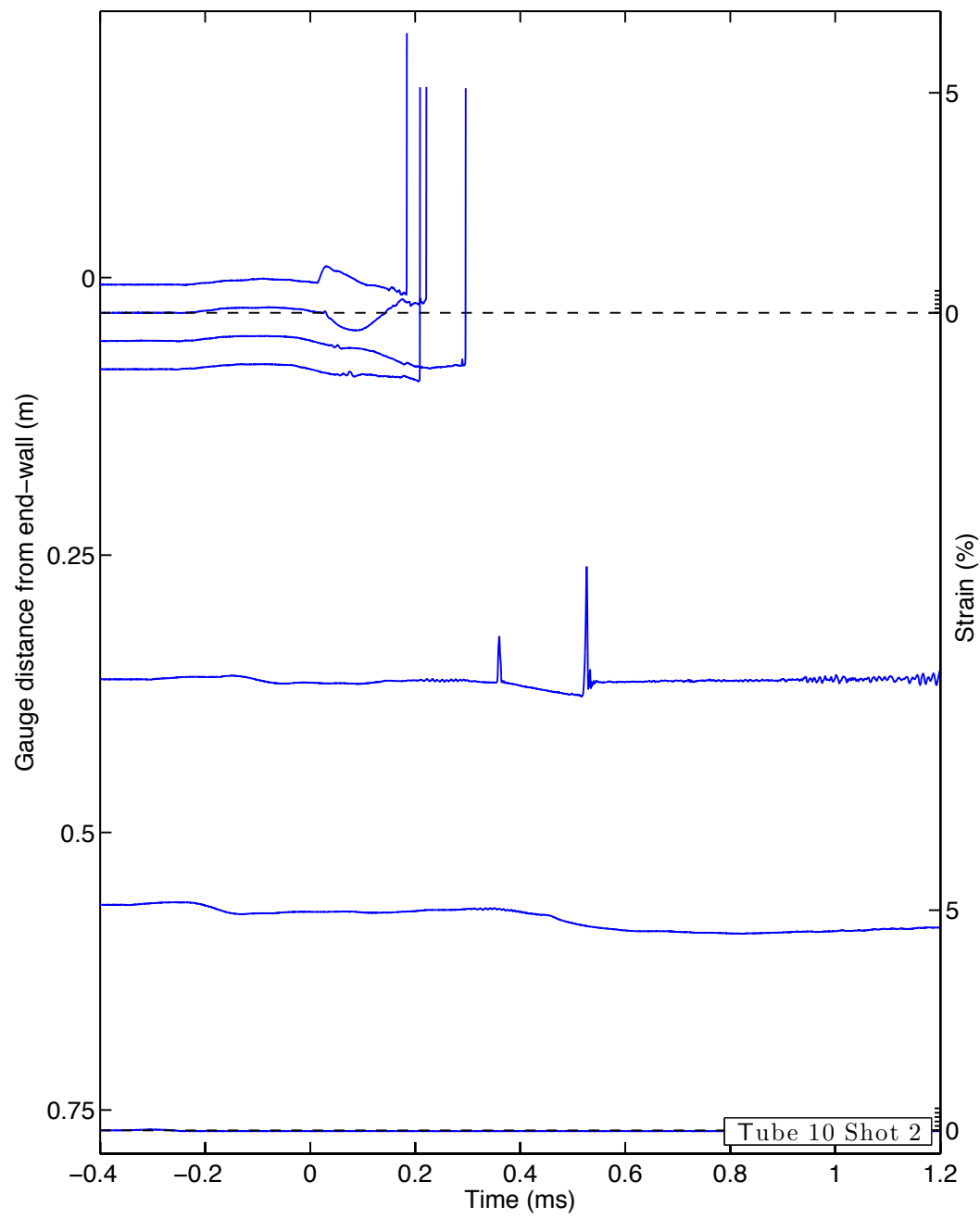


Figure A.18: Time-resolved plastic longitudinal strain measurements in tube 10.

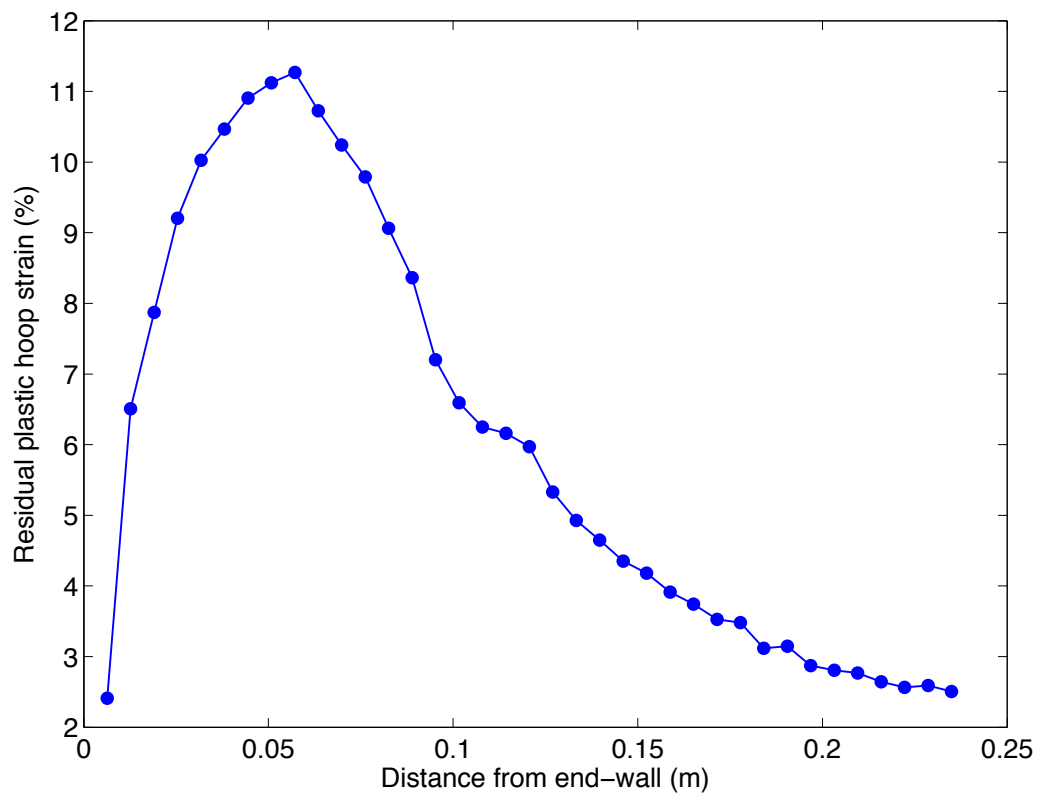


Figure A.19: Residual plastic hoop strain measurements in tube 10.

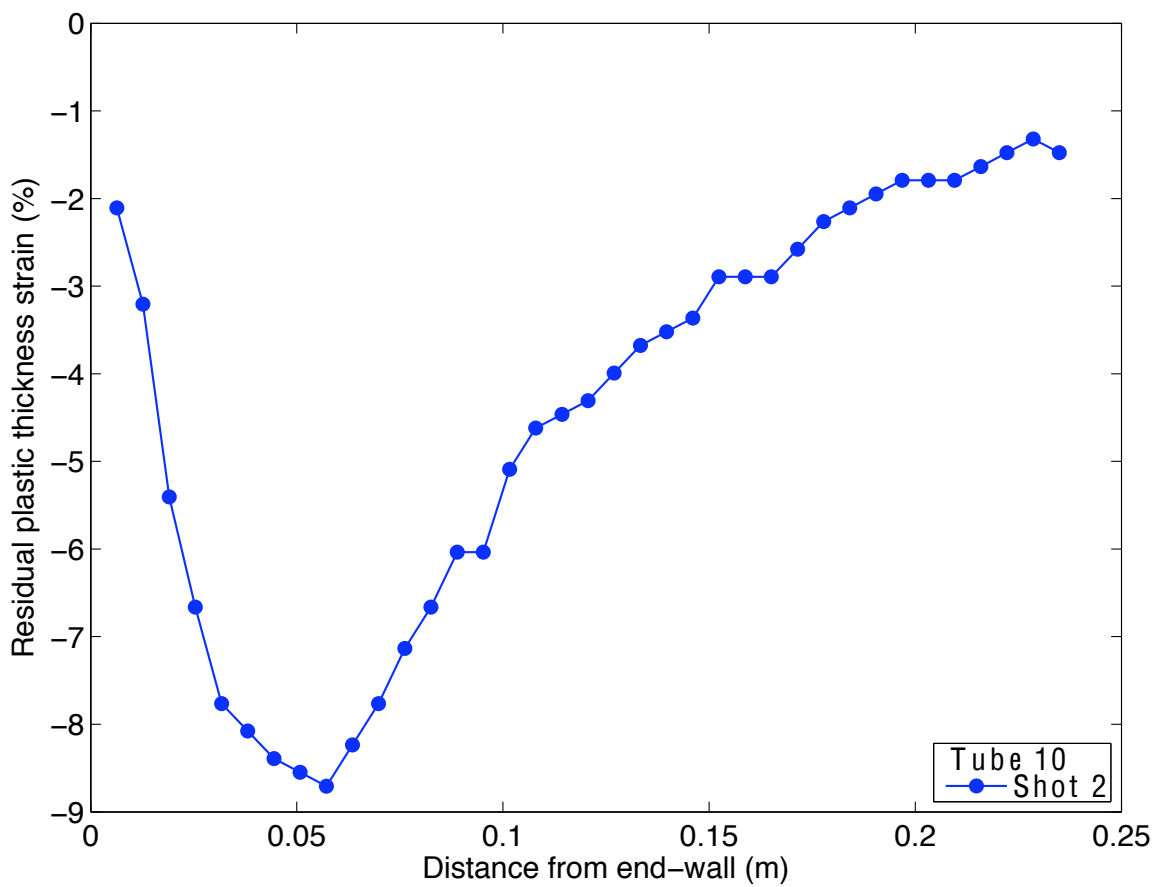


Figure A.20: Residual plastic thickness strain measurements in tube 10.

## A.4 Tube 11 Data

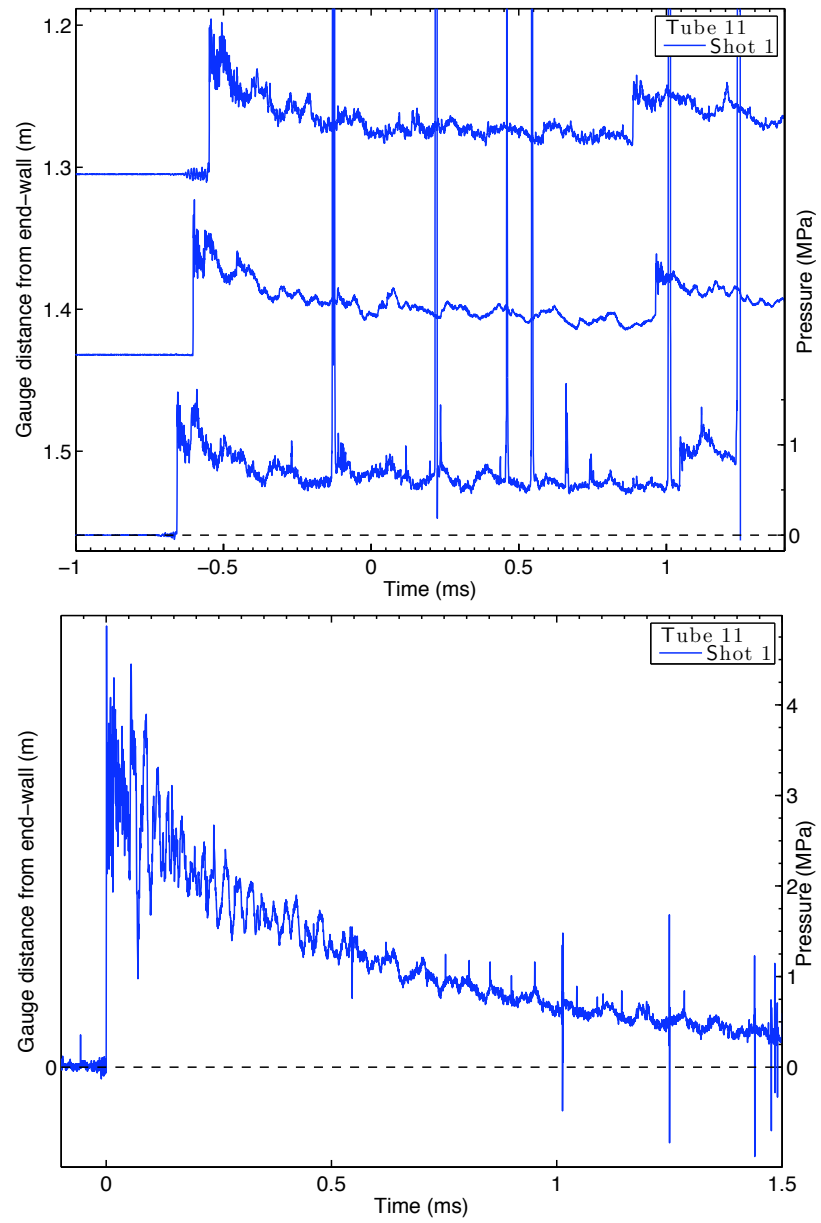


Figure A.21: Time-resolved pressure measurements from elastic shots in tube 11.

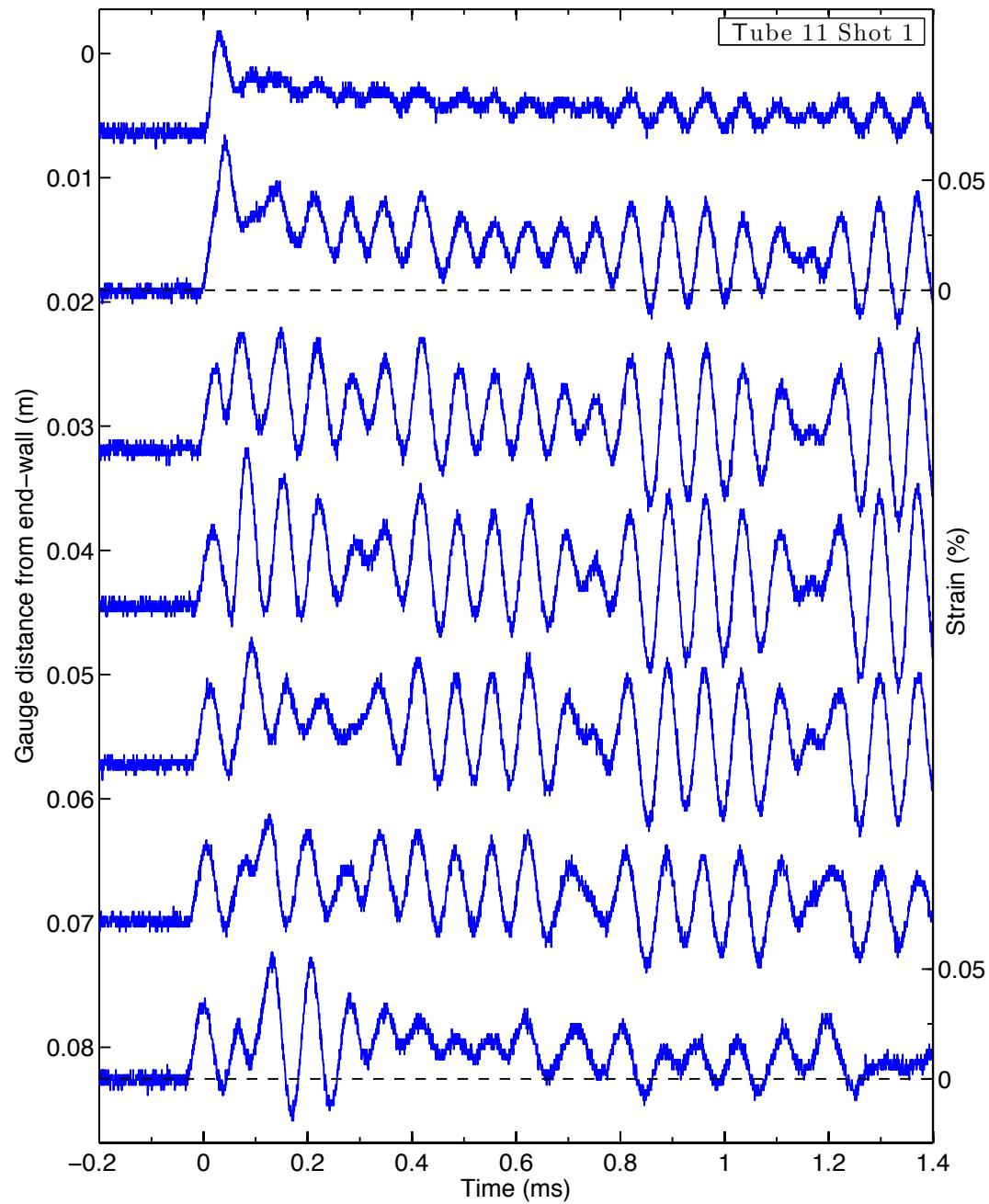


Figure A.22: Time-resolved elastic hoop strain measurements in tube 11, part 1.

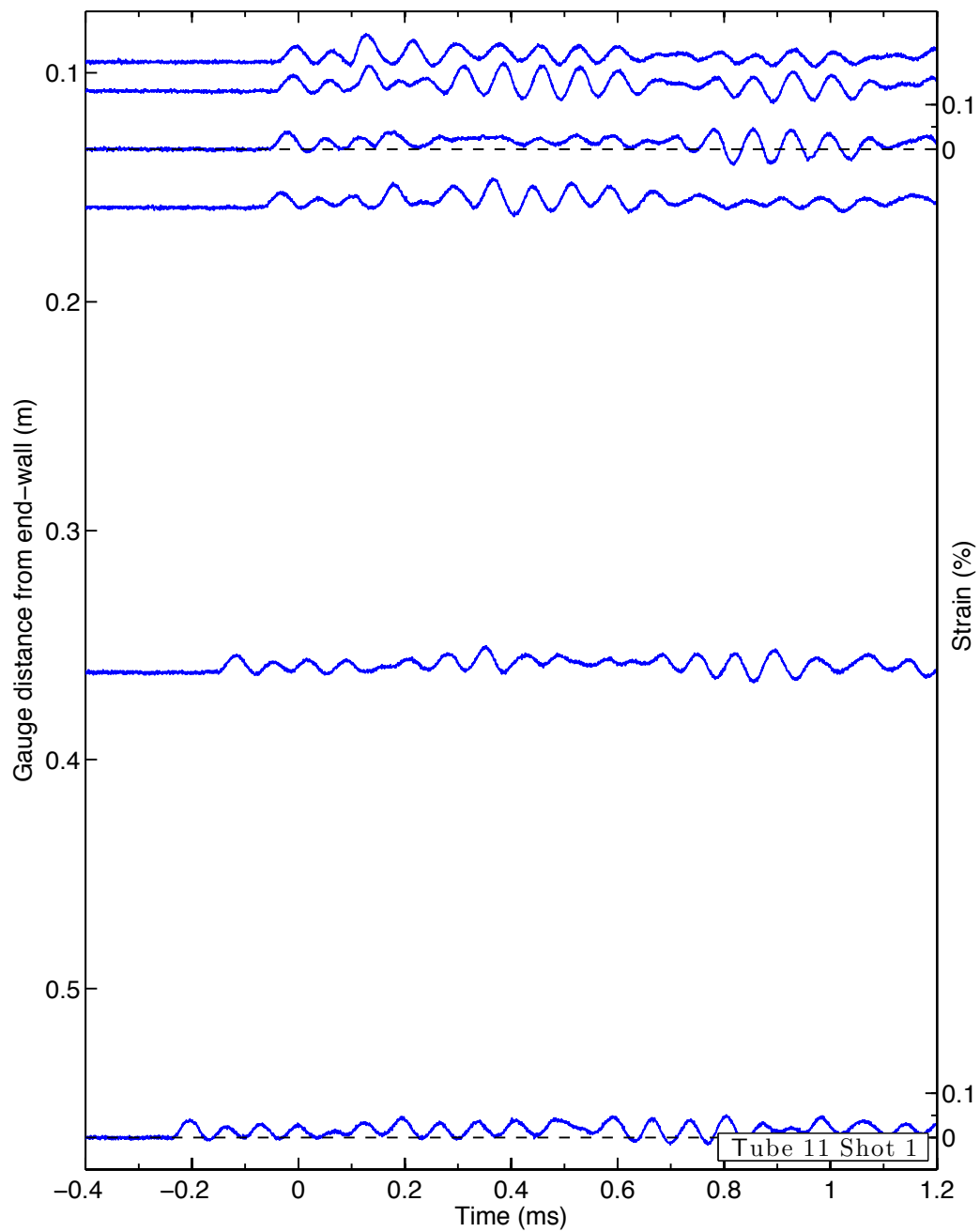


Figure A.23: Time-resolved elastic hoop strain measurements in tube 11, part 2.

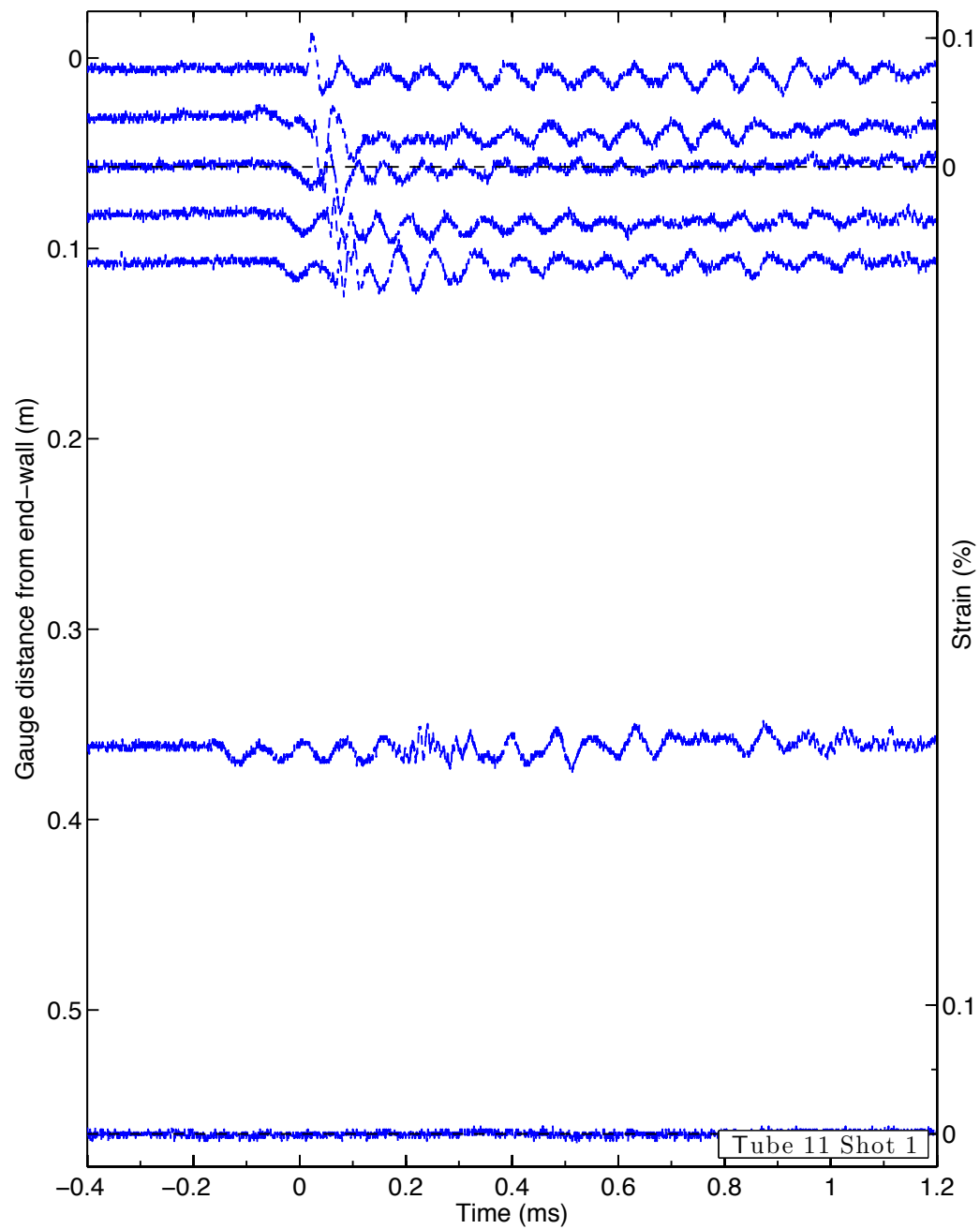


Figure A.24: Time-resolved elastic longitudinal strain measurements in tube 11.

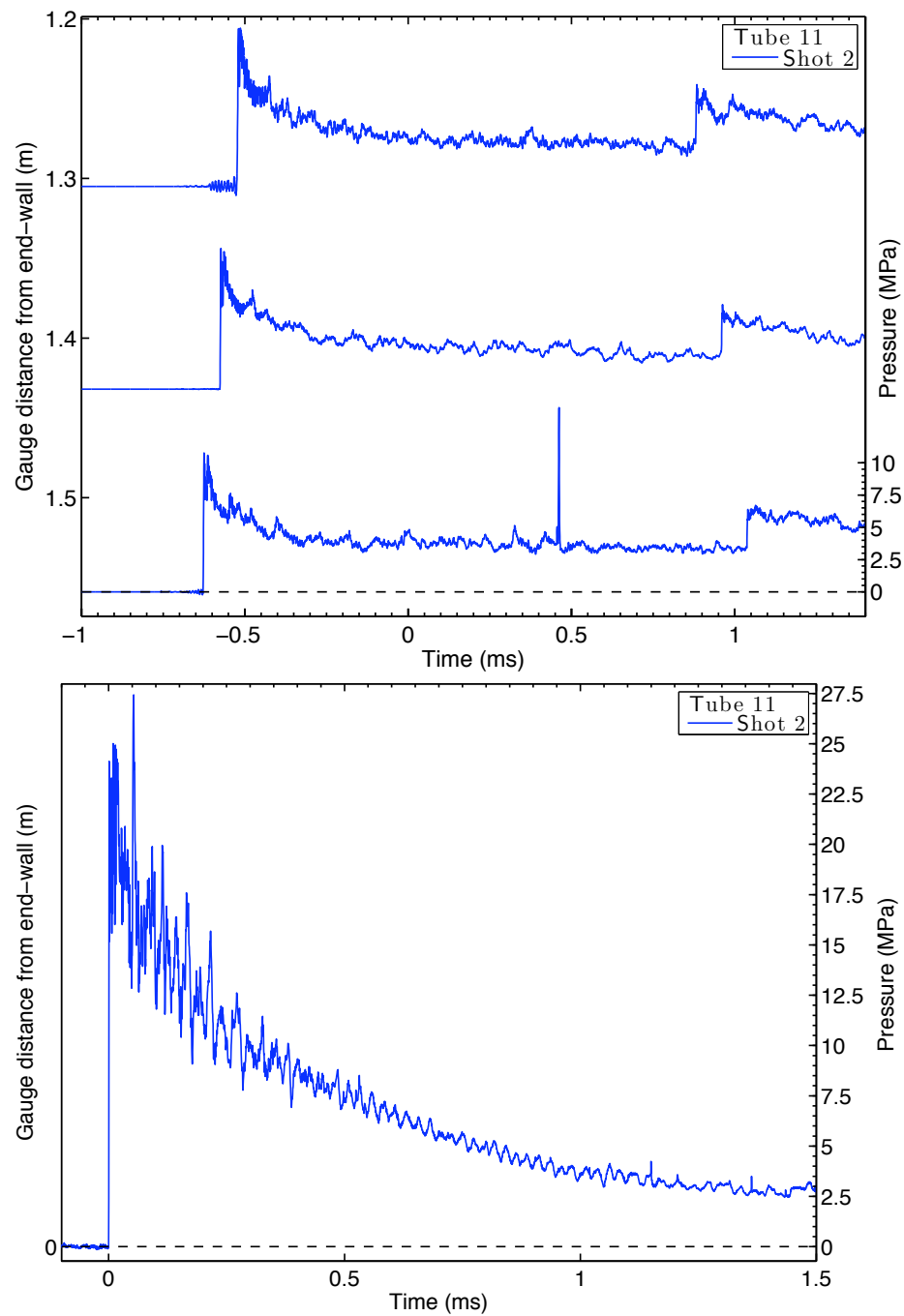


Figure A.25: Time-resolved pressure measurements from plastic shots in tube 11.

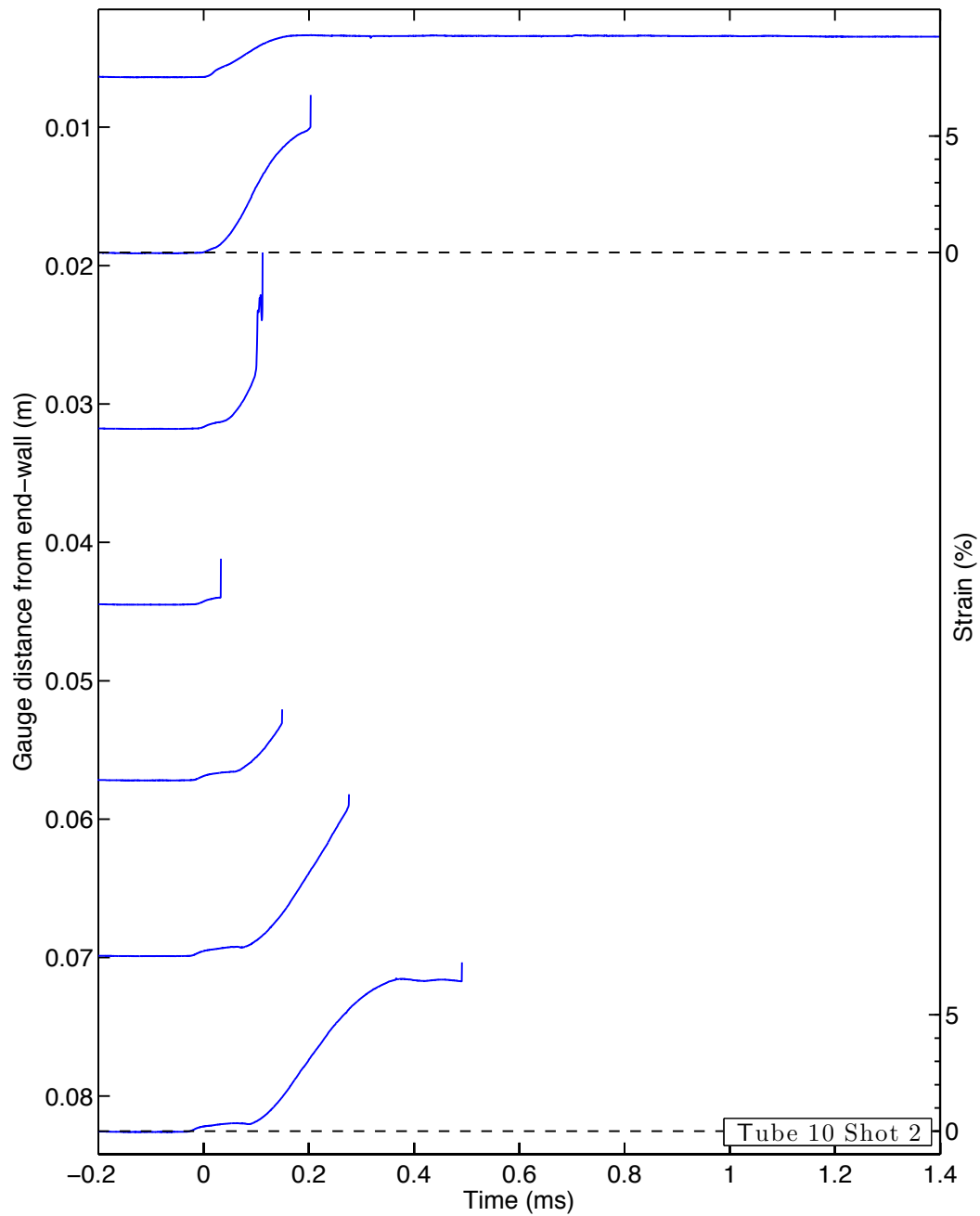


Figure A.26: Time-resolved plastic hoop strain measurements in tube 11, part 1.

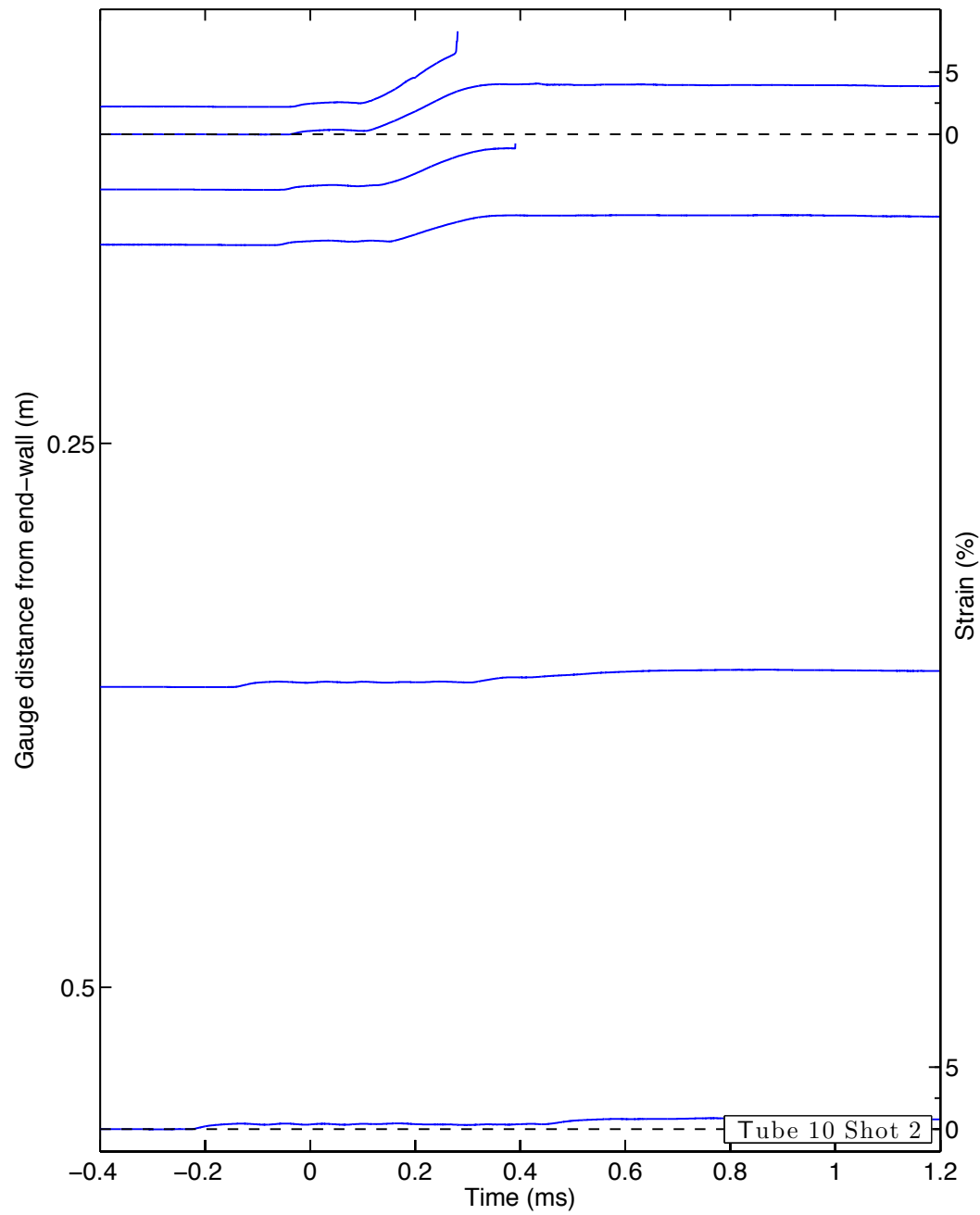


Figure A.27: Time-resolved plastic hoop strain measurements in tube 11, part 2.

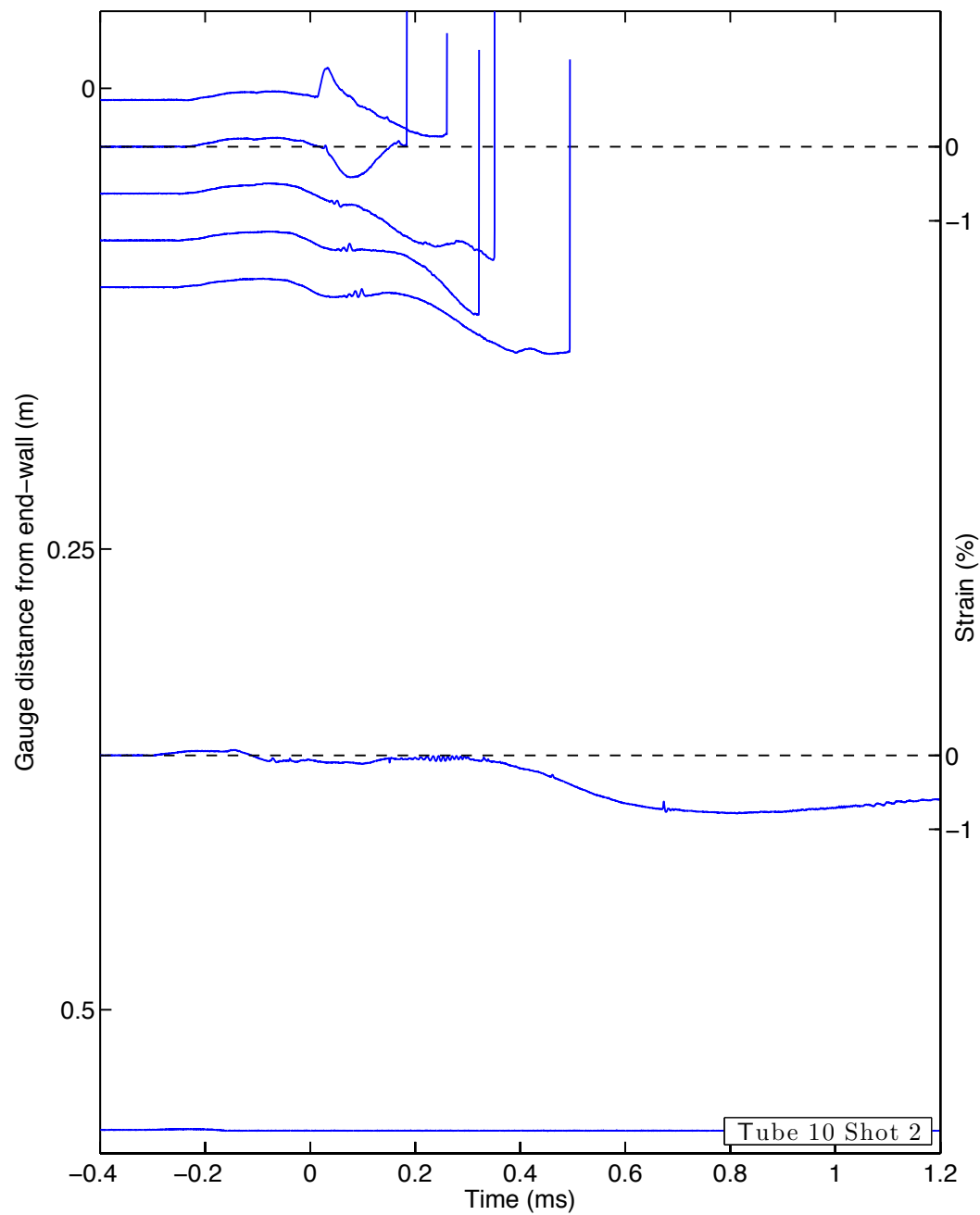


Figure A.28: Time-resolved plastic longitudinal strain measurements in tube 11.

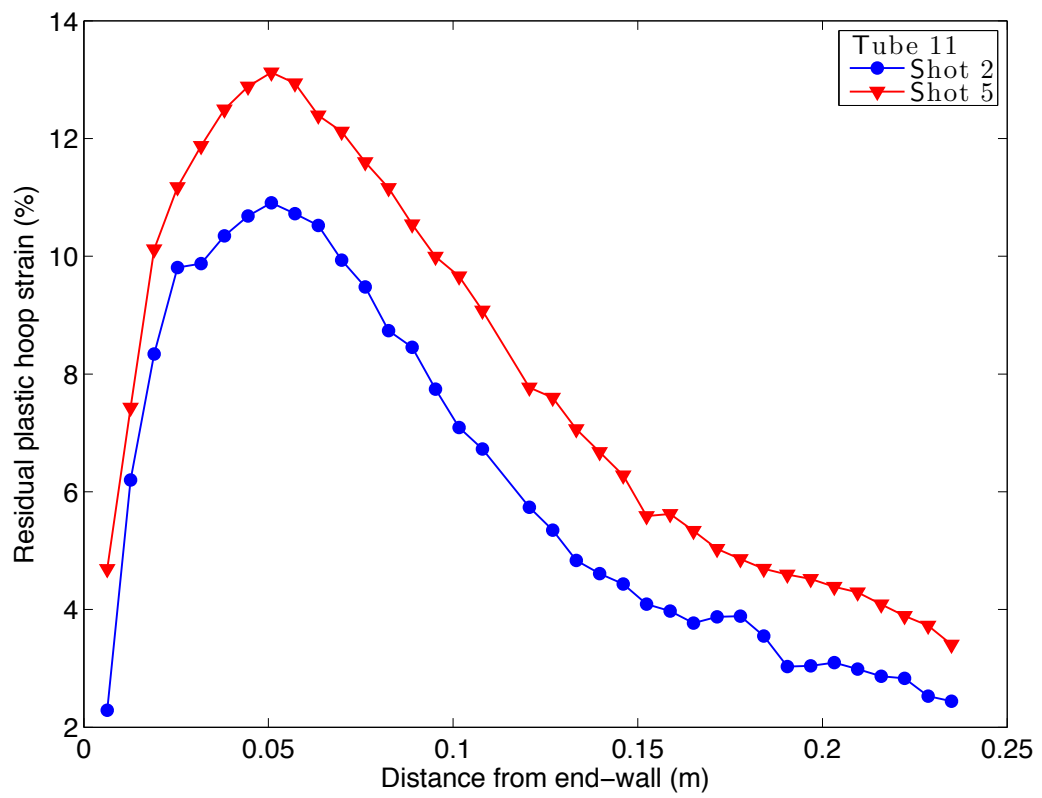


Figure A.29: Residual plastic hoop strain measurements in tube 11.

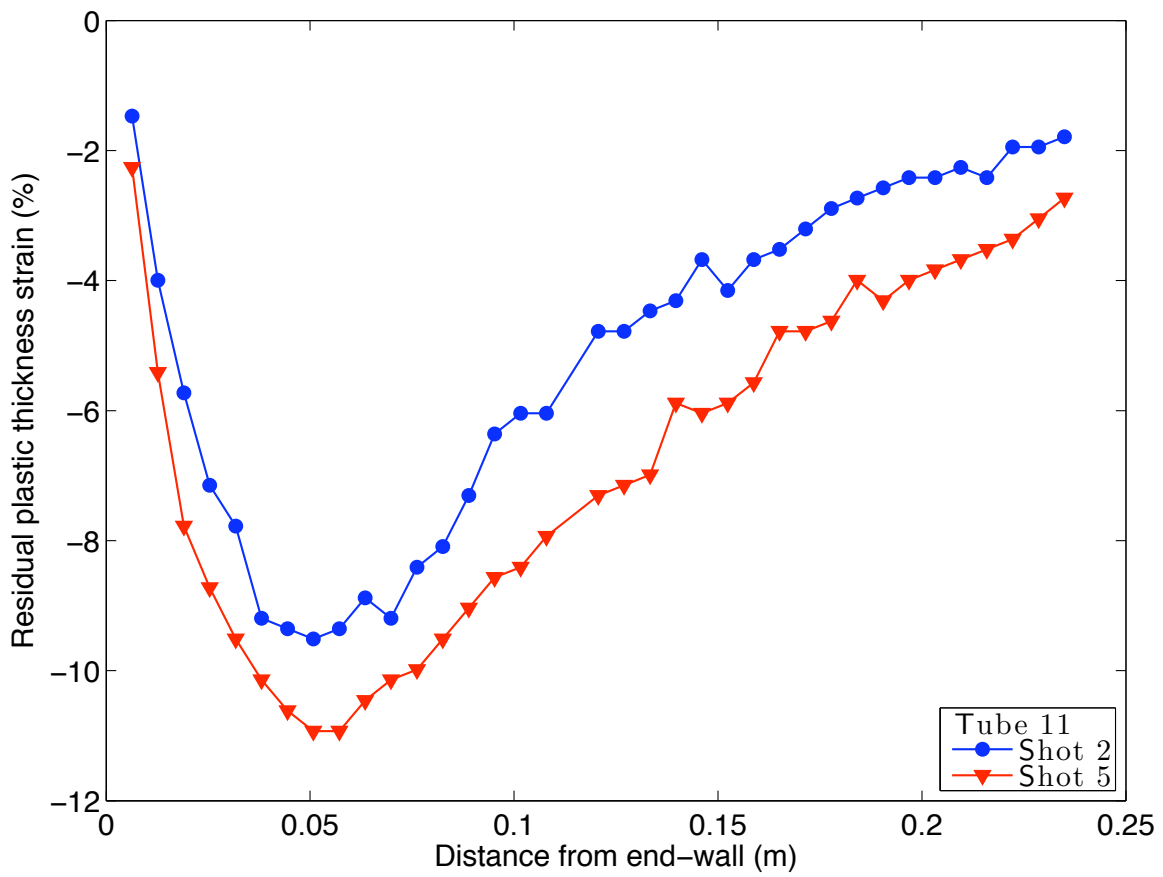


Figure A.30: Residual plastic thickness strain measurements in tube 11.

# Appendix B

## Single Degree of Freedom Model

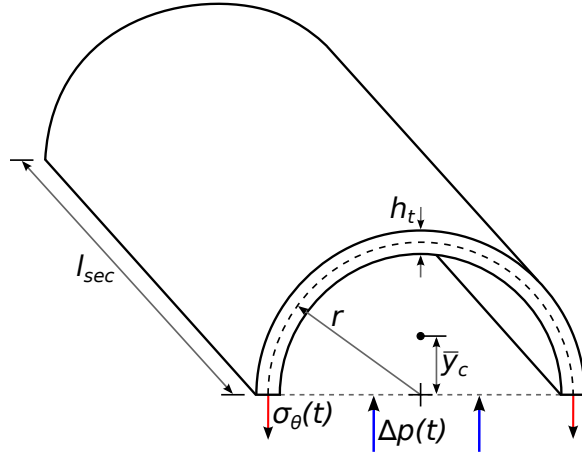


Figure B.1: Sketch of the forces applied to a thin-walled tube of infinite length.

The equations of motion for the single degree of freedom oscillator are derived here. Applying Newton's second law to the shell shown in figure B.1, we see

$$m_{sec} \frac{d^2 \bar{y}_c}{dt^2} = 2rl_{sec}\Delta p(t) - 2h_t l_{sec}\sigma_\theta(t) \quad (\text{B.1})$$

where  $m_{sec}$  is the mass of the tube section,  $\bar{y}_c$  is the location of the centroid of the tube,  $r$  is the tube radius,  $l_{sec}$  is the length of the tube section,  $\Delta p(t)$  is the time-dependent difference in pressure across the tube wall,  $h_t$  is the thickness of the tube, and  $\sigma_\theta(t)$  is the time-dependent hoop stress in the shell wall. Using the density of the tube,  $\rho_t$ , we see

$$\pi r h_t l_{sec} \rho_t \frac{d^2 \bar{y}_c}{dt^2} = 2rl_{sec} \Delta p(t) - 2h_t l_{sec} \sigma_\theta(t) \quad (\text{B.2})$$

$$\frac{\pi}{2} \frac{d^2 \bar{y}_c}{dt^2} = \frac{\Delta p(t)}{\rho_t h_t} - \frac{\sigma_\theta(t)}{\rho_t r}. \quad (\text{B.3})$$

The location of the centroid for a half-circle is given by

$$\bar{y}_c = \frac{2r}{\pi} \quad (\text{B.4})$$

implying

$$\frac{d^2 \bar{y}_c}{dt^2} = \frac{2}{\pi} \frac{d^2 r}{dt^2} = \frac{2}{\pi} \frac{d^2 r'}{dt^2} \quad (\text{B.5})$$

with  $r' = r - r_0$ , since  $d^2 r_0 / dt^2 = 0$ . Thus we have

$$\frac{d^2 r'}{dt^2} = \frac{\Delta p(t)}{\rho_t h_t} - \frac{\sigma_\theta(t)}{\rho_t r}. \quad (\text{B.6})$$

The hoop stress can be determined from

$$\sigma_\theta = \begin{cases} E_1 \epsilon_\theta & \sigma \leq \sigma_y \\ \sigma_y + E_2 (\epsilon - \epsilon_y) & \sigma > \sigma_y \end{cases} \quad (\text{B.7})$$

where  $\sigma_y$  is the yield stress tracked by the additional equation

$$\frac{d\sigma_y}{dt} = \frac{d\sigma_y}{d\sigma_\theta} \frac{d\sigma_\theta}{dt} \quad (\text{B.8})$$

with

$$\frac{d\sigma_y}{d\sigma_\theta} = \begin{cases} 1 & \sigma \geq \sigma_y \\ 0 & \sigma < \sigma_y \end{cases}. \quad (\text{B.9})$$

The equation for  $\sigma_\theta$  assumes a state of unidirectional stress. This is justified since the tube thickness,  $h_t$ , is much smaller than the other dimensions,  $r$  and  $L$ . The large radius implies that stresses normal to the tube surface are much smaller than the hoop stress term, and, if we consider the dynamic loading of a location far from a restricting boundary condition as is the case for most of the tube if  $L$  is large, axial stress will only come from the inertia of the tube wall; this is also much less than the hoop stress term because the small thickness implies the mass of the tube per unit length is negligible relative to the pressure and hoop stress terms.

## Appendix C

# GDT Experimental Procedure and Drawings

Contained herein are the checklist, shot list, and drawing files pertaining to experiments performed in the GALCIT detonation tube. A description of the visualization systems employed is included in appendix D and all data gathered are included in appendix E.

### C.1 GDT Checklist

Checklist for experiments performed in the GALCIT detonation tube.

**Operator:** Jason Damazo

**Beginning of shot series**

1. Turn on vacuum pump and heat exchanger.
2. Turn on desired bottles in bottle farm.
3. Turn on driver gases, record regulator settings.
4. Tighten endplate bolts.

**Preparation and pump down**

5. Load firing plug with wire.
6. Check that clamp bolts are snug and clamp movement is clear.

7. Pressurize hydraulics to 3500 psi, make sure all clamps engage backing plate surface.
8. Enable Main Control Panel power.
9. Turn on Main Control Panel 12 V relay.
10. Open valves: E1, T1, T2, T3, V1, V2, V3, MKS, G1, and N1.
11. Close valve: L1.
12. Wait for pressure to drop below 100 mTorr.
13. Zero fill pressure gauge.
14. Close valves: V1, V2, and V3.
15. Record final vacuum pressure.

### **Gas fill**

16. Turn on warning lights and check that doors are closed (Laboratory access is restricted).
17. Don ear protection.
18. Fill GDT until internal pressure meets desired fill pressure, record achieved pressures.
19. Close valves: G1 and N1.
20. Turn on mixing pump, mix for 5 minutes.
21. Close valves: E1, T1, T2, T3, and MKS.

### **Firing procedure**

22. Switch off 12 V relay.
23. Check that ‘Fire Ready’ light is on.

24. Turn on wire exploder.
25. Turn on Charge switch.
26. Charge for 2 minutes.
27. Arm data acquisition.
28. Arm wire exploder key switch.
29. Fire: Press run on delay generator (wait for detonation to occur).
30. Turn off Charge switch.
31. Disarm wire exploder key switch.
32. Turn off wire exploder.
33. If no combustion, dilute mixture.
34. Turn off warning lights (Laboratory access is unrestricted).
35. Record shot time.

### Cleanup

36. Switch on 12 V relay on Main Control Panel.
37. Open valve: MKS, record post-detonation pressure.
38. Open valves: V1, V2, V3, T1, T2, T3, and E1, wait for vacuum.
39. Turn off driver gases.
40. Turn off vacuum pump.
41. Open valve: L1.
42. Turn off bottles in bottle farm.
43. Back-up and convert data.

## C.2 GDT Shotlist

Below is the shotlist for all detonations in the GDT during my tenure at Caltech (November 19, 2010–May 31, 2013). Initial tests (shots 1930–1962) were preliminary experiments performed before a splitter plate was designed; their primary purpose was to gain knowledge with the operation of the GDT and to take preliminary detonation and reflection pictures. Shot numbers 1963–2021 used an early implementation of the splitter plate that did not have pressure and heat-flux gauges. The remaining tests (2022–2199) were performed with the splitter plate that was equipped with pressure and heat-flux measurement gauges, however it was only beginning with shot 2071 that the new data acquisition system described in chapter 3 was obtained and all pressure and heat-flux data were recorded. The pressure gauge located 25.4 mm from the reflecting end-wall was incorrectly calibrated for shots 2022–2112.

Table C.1: Shot list for experiments performed in the GDT. The data column indicates what was recorded for a particular test: ‘p’ indicates that time-resolved pressure data were saved, ‘q’ represents time-resolve heat-flux data, and ‘i’ is an image or video.

Shot number	$p_1$ (kPa)	Mixture	Data	Visualization
1930	7	C2H2:1 O2:1		phoenix <sup>1</sup>
1931	10	C2H2:1 O2:1		phoenix
1932	~5	C2H2:1 O2:1	i	phoenix
1933	13	C2H2:1 O2:1	i	phoenix
1934	9	C2H2:1 O2:1	i	phoenix
1935	12	C2H2:1 O2:1	i	greenarrow <sup>2</sup>

Continued on next page

<sup>1</sup>The “Phoenix” visualization system used the Phantom v7.10 equipped with a camera lens pointed at the GDT window to record a simple movie of the detonation.

<sup>2</sup>The “Green arrow” visualization system used the Phantom v7.10 with a 200 mW, 532 nm interferometer laser in a Z-type schlieren set-up.

**Table C.1 – continued from previous page**

Shot number	$p_1$ (kPa)	Mixture	Data	Visualization
1936	12	C2H2:1 O2:1	i	greenarrow
1937	12	C2H2:1 O2:1		storm
1938	12	C2H2:1 O2:1		storm
1939	12	C2H2:1 O2:1		storm
1940	12	C2H2:1 O2:1		storm
1941	12	C2H2:1 O2:1		storm
1942	12	C2H2:1 O2:1		storm
1943	12	C2H2:1 O2:1		storm
1944	20	H2:2 O2:1 AR:12	i	storm
1945	20	H2:2 O2:1 AR:12	i	storm
1946	20	H2:2 O2:1 AR:12		storm
1947	20	H2:2 O2:1 AR:12		storm
1948	15	H2:2 O2:1 AR:12	i	storm
1949	15	H2:2 O2:1 AR:12		storm
1950	15	H2:2 O2:1 AR:12	i	storm
1951	15	H2:2 O2:1 AR:12	i	storm
1952	15	H2:2 O2:1 AR:12	i	storm
1953	15	H2:2 O2:1 HE:12	i	storm
1954	15	H2:2 O2:1 HE:12	i	storm
1955	15	H2:2 O2:1 HE:12	i	storm
1956	15	H2:2 O2:1 HE:12	i	storm
1957	5	H2:2 O2:1		storm
1958	5	H2:2 O2:1	i	storm
1959	5	H2:2 O2:1	i	storm
1960	5	H2:2 O2:1	i	storm
1961	5	H2:2 O2:1		storm

Continued on next page

**Table C.1 – continued from previous page**

Shot number	$p_1$ (kPa)	Mixture	Data	Visualization
1962	5	H2:2 O2:1		storm
1963	15	H2:2 O2:1 AR:12	i	storm
1964	15	H2:2 O2:1 AR:12	i	storm
1965	15	H2:2 O2:1 AR:12	i	storm
1966	15	H2:2 O2:1 AR:12	i	storm
1967	15	H2:2 O2:1 AR:12	i	storm
1968	10	H2:2 O2:1	i	storm
1969	10	H2:2 O2:1	i	storm
1970	10	H2:2 O2:1		storm
1971	10	H2:2 O2:1	i	storm
1972	15	H2:2 O2:1 N2:12	i	storm
1973	15	H2:2 O2:1 N2:12	i	storm
1974	15	H2:2 O2:1 N2:12	i	storm
1975	15	H2:2 O2:1 N2:12	i	storm
1976	15	H2:2 O2:1	i	storm
1977	15	H2:2 O2:1	i	storm
1978	15	H2:2 O2:1	i	storm
1979	15	H2:2 O2:1	i	storm
1980	15	H2:14 O2:1	i	storm
1981	15	H2:14 O2:1	i	storm
1982	15	H2:14 O2:1	i	storm
1983	15	H2:14 O2:1	i	storm
1984	15	H2:14 O2:1	i	storm
1985	15	H2:13 O2:2	i	storm
1986	15	H2:13 O2:2		storm
1987	15	H2:13 O2:2	i	storm

Continued on next page

**Table C.1 – continued from previous page**

Shot number	$p_1$ (kPa)	Mixture	Data	Visualization
1988	15	H2:13 O2:2	i	storm
1989	15	H2:13 O2:2	i	storm
1990	15	H2:13 O2:2	i	storm
1991	15	H2:13 O2:2	i	storm
1992	25	air		storm
1993	25	air	i	storm
1994	25	air	i	storm
1995	25	air	i	storm
1996	25	air	i	storm
1997	25	air	i	storm
1998	25	air	i	storm
1999	25	air	i	storm
2000	25	air	i	storm
2001	15	N2O:1		storm
2002	15	N2O:1	i	storm
2003	15	N2O:1	i	storm
2004	15	H2:6 N2O:94	i	storm
2005	15	H2:6 N2O:94	i	storm
2006	16	H2:6 N2O:94	i	storm
2007	15	H2:6 N2O:94	i	storm
2008	15	H2:1 N2O:9	i	storm
2009	15	H2:1 N2O:9		storm
2010	15	H2:1 N2O:9		storm
2011	15	H2:1 N2O:9	i	storm
2012	10	H2:2 O2:1		storm
2013	15	H2:2 O2:1		greenlantern

Continued on next page

**Table C.1 – continued from previous page**

Shot number	$p_1$ (kPa)	Mixture	Data	Visualization
2014	15	H2:2 O2:1		greenlantern
2015	15	H2:2 O2:1		greenlantern
2016	15	H2:2 O2:1	i	greenlantern
2017	15	H2:2 O2:1	i	greenlantern
2018	15	H2:2 O2:1	i	greenlantern
2019	15	H2:1 N2O:9	i	greenlantern
2020	15	H2:1 N2O:9	i	greenlantern
2021	15	H2:1 N2O:9	i	greenlantern
2022	15	H2:1 N2O:9		greenlantern
2023	15	N2O:1	i	greenlantern
2024	15	N2O:1	i	greenlantern
2025	15	N2O:1	i	greenlantern
2026	15	N2O:1	i	greenlantern
2027	15	N2O:1	i	greenlantern
2028	15	H2:1 N2O:9	i	greenlantern
2029	15	H2:1 N2O:9	i	greenlantern
2030	15	H2:1 N2O:9	i	greenlantern
2031	15	N2O:1	i	greenlantern
2032	15	N2O:1	i	greenlantern
2033	15	N2O:1	i	greenlantern
2034	15	N2O:1	i	greenlantern
2035	16	air	i	greenlantern
2036	15	N2O:1	i	greenlantern
2037	14	air	i	greenlantern
2038	14	air	i	greenlantern
2039	15	air	i	greenlantern

Continued on next page

**Table C.1 – continued from previous page**

Shot number	$p_1$ (kPa)	Mixture	Data	Visualization
2040	~100	air	i	greenlantern
2041	15	N2O:1	p,i	greenlantern
2042	15	N2O:1	p,i	greenlantern
2043	15	N2O:1	p,i	greenlantern
2044	15	N2O:1	p,i	greenlantern
2045	15	N2O:1	p,i	greenlantern
2046	15	N2O:1	p,i	greenlantern
2047	15	N2O:1	p,i	greenlantern
2048	15	H2:1 N2O:9	p	greenlantern
2049	15	H2:15 N2O:85	p	greenlantern
2050	15	H2:2 N2O:8	p	greenlantern
2051	15	H2:25 N2O:75	p	greenlantern
2052	15	H2:3 N2O:7	p	greenlantern
2053	15	H2:35 N2O:65	p	greenlantern
2054	15	N2O:1	p,i	greenlantern
2055	15	N2O:1	p,i	greenlantern
2056	15	N2O:1	p	greenlantern
2057	15	N2O:1	p,i	greenlantern
2058	15	HE:1	p,i	greenlantern
2059	15	HE:1	p,i	greenlantern
2060	15	HE:1	p,i	greenlantern
2061	15	H2:2 O2:1	p	greenlantern
2062	15	H2:2 O2:1	p	ghostintheshell
2063	15	H2:2 O2:1	p,i	ghostintheshell
2064	15	H2:2 O2:1	p,i	ghostintheshell
2065	15	H2:2 O2:1	p,i	ghostintheshell

Continued on next page

**Table C.1 – continued from previous page**

Shot number	$p_1$ (kPa)	Mixture	Data	Visualization
2066	15	H2:2 O2:1	p,i	ghostintheshell
2067	15	H2:2 O2:1	p,i	ghostintheshell
2068	15	H2:2 O2:1	p	ghostintheshell
2069	15	H2:2 O2:1	p,i	ghostintheshell
2070	15	H2:2 O2:1	p,i	ghostintheshell
2071	15	H2:2 O2:1	p,q	watchmen
2072	15	H2:2 O2:1	p,q	watchmen
2073	30	H2:2 O2:1	p,q	watchmen
2074	5	H2:2 O2:1	p,q	watchmen
2075	99	air		watchmen
2076	25	N2O:1	p,q	watchmen
2077	25	N2O:1	p,q,i	watchmen
2078	25	N2O:1	p,q,i	watchmen
2079	25	H2:2 O2:1	p,q,i	watchmen
2080	25	H2:2 O2:1	p,q,i	watchmen
2081	25	H2:2 O2:1	p,q	watchmen
2082	25	H2:2 O2:1	p,q	watchmen
2083	25	H2:2 O2:1	p,q	watchmen
2084	25	H2:2 O2:1	p,q,i	watchmen
2085	25	H2:2 O2:1	p,q,i	watchmen
2086	25	H2:2 O2:1	p,q,i	watchmen
2087	10	H2:2 O2:1	p,q	watchmen
2088	10	H2:2 O2:1	i	watchmen
2089	10	H2:2 O2:1	p,q,i	watchmen
2090	25	H2:2 O2:1	p,q,i	watchmen
2091	40	H2:2 O2:1	p,q,i	watchmen

Continued on next page

**Table C.1 – continued from previous page**

Shot number	$p_1$ (kPa)	Mixture	Data	Visualization
2092	40	H2:2 O2:1	p,q,i	watchmen
2093	40	H2:2 O2:1 AR:3	p,q,i	watchmen
2094	40	H2:2 O2:1 AR:3	p,q,i	watchmen
2095	40	H2:2 O2:1 AR:3	p,q,i	watchmen
2096	40	H2:2 O2:1 AR:6	p,q,i	watchmen
2097	40	H2:2 O2:1 AR:6	p,q,i	watchmen
2098	40	H2:2 O2:1 AR:6	p,q,i	watchmen
2099	40	H2:2 O2:1 AR:15	p,q,i	watchmen
2100	40	H2:2 O2:1 AR:15	p,q,i	watchmen
2101	40	H2:2 O2:1 AR:15	p,q,i	watchmen
2102	25	H2:2 O2:1 AR:15	p,q,i	watchmen
2103	25	H2:2 O2:1 AR:6	p,q,i	watchmen
2104	25	H2:2 O2:1 AR:3	p,q,i	watchmen
2105	10	H2:2 O2:1 AR:3	p,q,i	watchmen
2106	10	H2:2 O2:1 AR:3	p,q,i	watchmen
2107	10	H2:2 O2:1 AR:6	p,q,i	watchmen
2108	10	H2:2 O2:1 AR:15	p,q,i	watchmen
2109	10	H2:2 O2:1 AR:15	p,q,i	watchmen
2110	25	AR:1	p,q,i	watchmen
2111	25	AR:1	p,q,i	watchmen
2112	25	AR:1	p,q,i	watchmen
2113	25	AR:1	p,q,i	watchmen
2114	25	H2:2 O2:1 AR:15	p,q	watchmen
2115	25	H2:2 O2:1 AR:15	p,q,i	watchmen
2116	25	H2:2 O2:1	p,q	watchmen
2117	25	H2:2 O2:1	p,q,i	watchmen

Continued on next page

**Table C.1 – continued from previous page**

Shot number	$p_1$ (kPa)	Mixture	Data	Visualization
2118	25	H2:2 O2:1	p,q,i	watchmen
2119	25	H2:2 O2:1	p,q,i	watchmen
2120	25	H2:2 O2:1	p,q,i	watchmen
2121	10	AR:1	p,q	watchmen
2122	25	C2H4:1 O2:3	p,q	watchmen
2123	25	C2H4:1 O2:3	p,q,i	watchmen
2124	25	C2H4:1 O2:3	p,q,i	watchmen
2125	25	C2H4:1 O2:3	p,q,i	watchmen
2126	25	H2:2 O2:1	p,q	watchmen
2127	25	C2H4:1 O2:3	p,q	watchmen
2128	25	C2H4:1 O2:3	p,q,i	watchmen
2129	25	C2H4:1 O2:3	p,q,i	watchmen
2130	25	C2H4:1 O2:3	p,q,i	watchmen
2131	25	C2H4:1 O2:3	p,q,i	watchmen
2132	25	C2H4:1 O2:3	p,q,i	watchmen
2133	25	C2H4:1 O2:3	p,q,i	watchmen
2134	25	C2H4:1 O2:3	p,q,i	watchmen
2135	25	C2H4:1 O2:3	p,q,i	watchmen
2136	25	C2H4:1 O2:3	p,q,i	watchmen
2137	25	C2H4:1 O2:3	p,q,i	watchmen
2138	25	C2H4:1 O2:3	p,q,i	watchmen
2139	25	C2H4:1 O2:3	p,q,i	watchmen
2140	25	C2H4:1 O2:3	p,q,i	watchmen
2141	25	C2H4:1 O2:3	p,q,i	watchmen
2142	25	C2H4:1 O2:3	p,q	watchmen
2143	25	H2:2 O2:1	p,q	watchmen

Continued on next page

**Table C.1 – continued from previous page**

Shot number	$p_1$ (kPa)	Mixture	Data	Visualization
2144	25	H2:2 O2:1 CO2:3	p,q	watchmen
2145	25	H2:4 O2:2 CO2:3	p,q	watchmen
2146	25	H2:2 O2:1	p,q	sandman
2147	25	H2:2 O2:1	p,q	sandman
2148	25	H2:2 O2:1	p,q	sandman
2149	25	H2:2 O2:1	p,q	sandman
2150	25	H2:2 O2:1	p,q	sandman
2151	25	H2:2 O2:1	p,q,i	sandman
2152	25	H2:2 O2:1	p,q,i	sandman
2153	25	H2:2 O2:1 CO2:3	p,q	sandman
2154	25	H2:4 O2:2 CO2:3		sandman
2155	25	H2:2 O2:1 CO2:1	p,q	sandman
2156	25	H2:2 O2:1 CO2:1	p,q,i	sandman
2157	25	H2:2 O2:1 CO2:1	i	sandman
2158	25	H2:4 O2:2 CO2:3	p,q,i	sandman
2159	25	H2:2 O2:1 N2:3	p,q	sandman
2160	25	H2:2 O2:1 N2:3	p,q,i	sandman
2161	25	H2:2 O2:1 AR:3	p,q,i	sandman
2162	25	H2:2 O2:1 AR:12	p,q,i	sandman
2163	10	H2:2 O2:1	p,q,i	sandman
2164	10	H2:2 O2:1 AR:3	p,q,i	sandman
2165	10	H2:2 O2:1 AR:12	p,q	sandman
2166	10	H2:2 O2:1 AR:12	p,q,i	sandman
2167	10	H2:2 O2:1 N2:3	p,q,i	sandman
2168	10	H2:4 O2:2 CO2:3	p,q,i	sandman
2169	50	H2:2 O2:1 AR:12	p,q,i	sandman

Continued on next page

**Table C.1 – continued from previous page**

Shot number	$p_1$ (kPa)	Mixture	Data	Visualization
2170	50	H2:2 O2:1 AR:3	p,q,i	sandman
2171	50	H2:2 O2:1 N2:3	p,q,i	sandman
2172	50	H2:4 O2:2 CO2:3	p,q	sandman
2173	50	H2:4 O2:2 CO2:3	p,q	sandman
2174	50	H2:4 O2:2 CO2:3	p,q	sandman
2175	25	AR:1	p,q	sandman
2176	25	AR:1	p,q	sandman
2177	25	AR:1	p,q,i	sandman
2178	25	AR:1	p,q	sandman
2179	25	H2:2 O2:1	p,q,i	sandman
2180	50	H2:2 O2:1	p,q,i	sandman
2181	50	H2:4 O2:2 CO2:3	p,q,i	sandman
2182	25	AR:1	p,q	sandman
2183	25	AR:1	p,q	sandman
2184	25	AR:1	p,q,i	sandman
2185	25	CO2:1	p,q	sandman
2186	50	H2:2 O2:1	p,q,i	sandman
2187	50	H2:2 O2:1 AR:12	p,q,i	sandman
2188	50	C2H4:1 O2:3	p,q,i	sandman
2189	50	C2H4:1 O2:3 CO2:4	p,q,i	sandman
2190	25	H2:2 O2:1 AR:12	p,q	cyclops
2191	50	H2:2 O2:1 AR:27	p,q	cyclops
2192	25	H2:2 O2:1 AR:12	p,q	cyclops
2193	25	H2:2 O2:1 AR:12	p,q,i	cyclops
2194	25	H2:2 O2:1 AR:12	p,q	cyclops
2195	25	H2:2 O2:1 AR:12	p,q,i	cyclops

Continued on next page

**Table C.1 – continued from previous page**

Shot number	$p_1$ (kPa)	Mixture	Data	Visualization
2196	25	H2:2 O2:1	p,q,i	watchmen
2197	25	H2:2 O2:1	p,q,i	watchmen
2198	25	H2:2 O2:1	p,q,i	watchmen

### C.3 Drawings

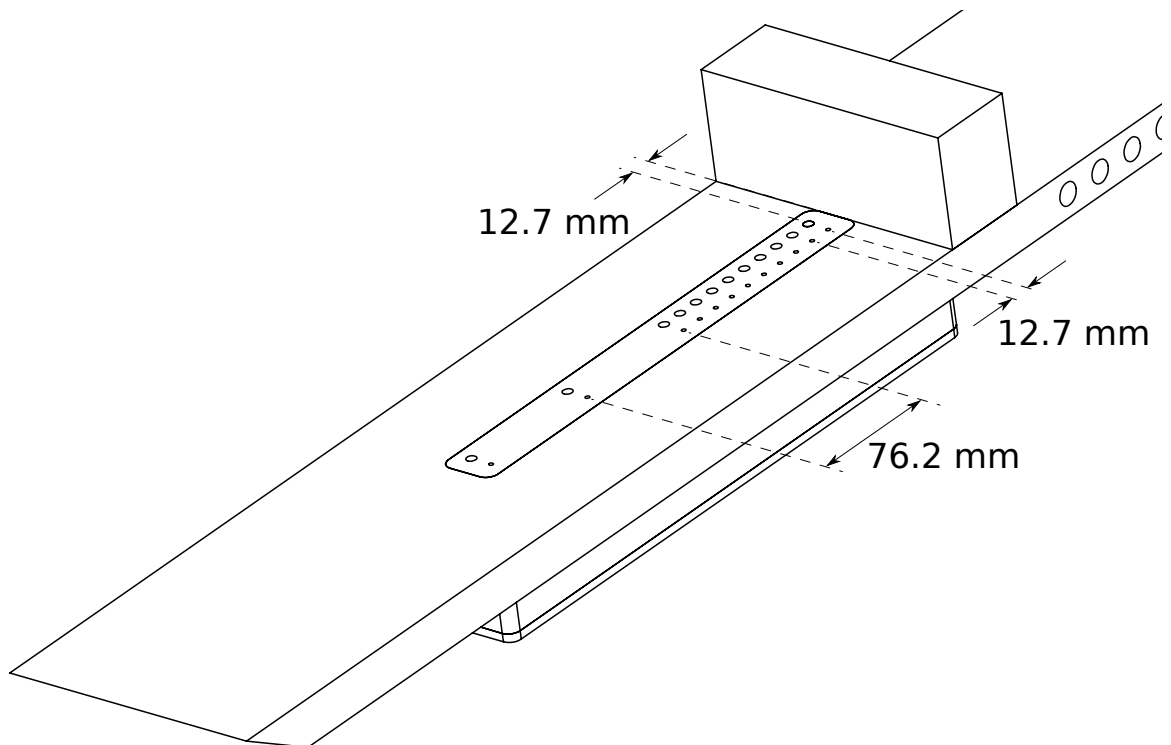


Figure C.1: Drawings of the GDT splitter plate, part 1.

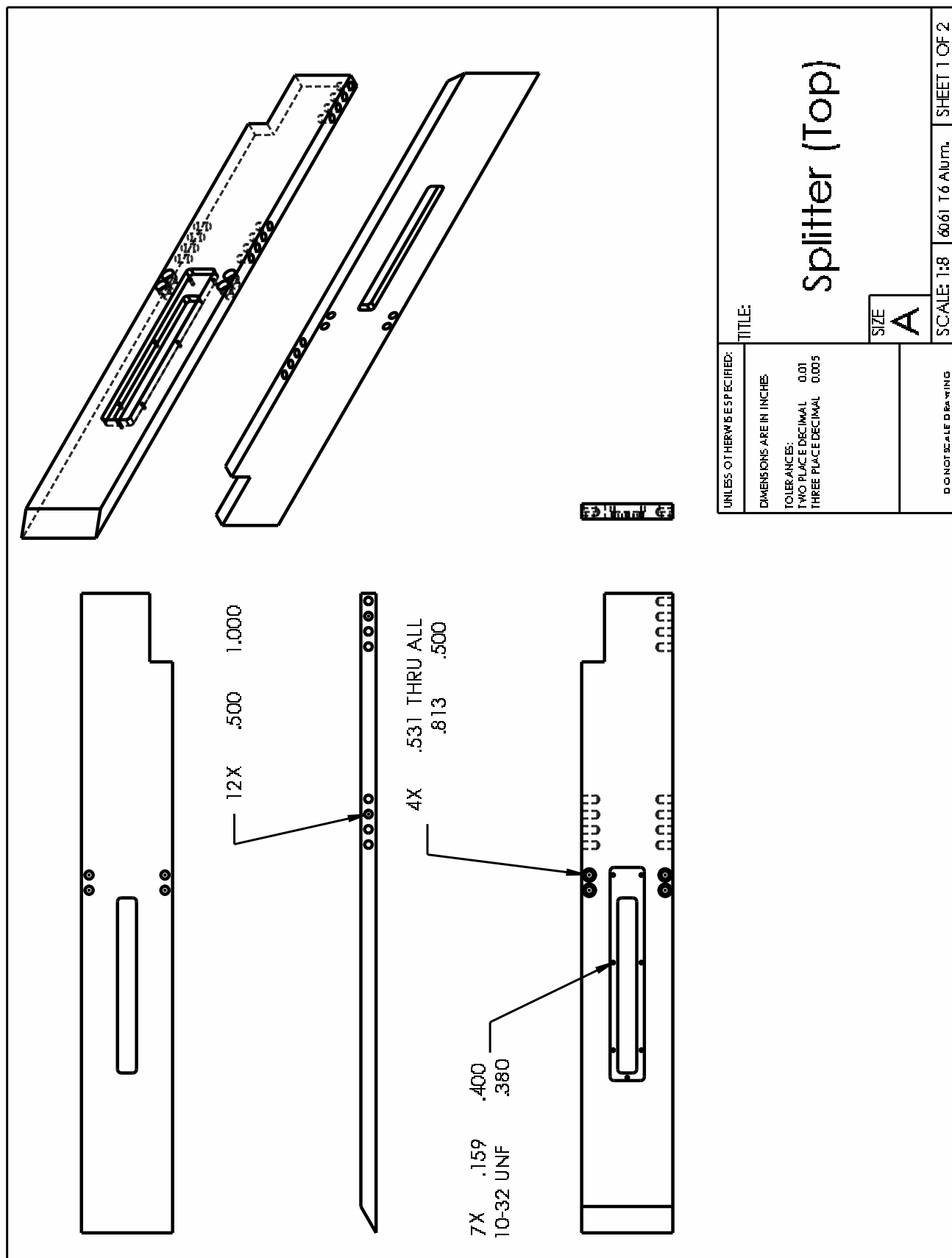


Figure C.2: Drawings of the GDT splitter plate, part 2.

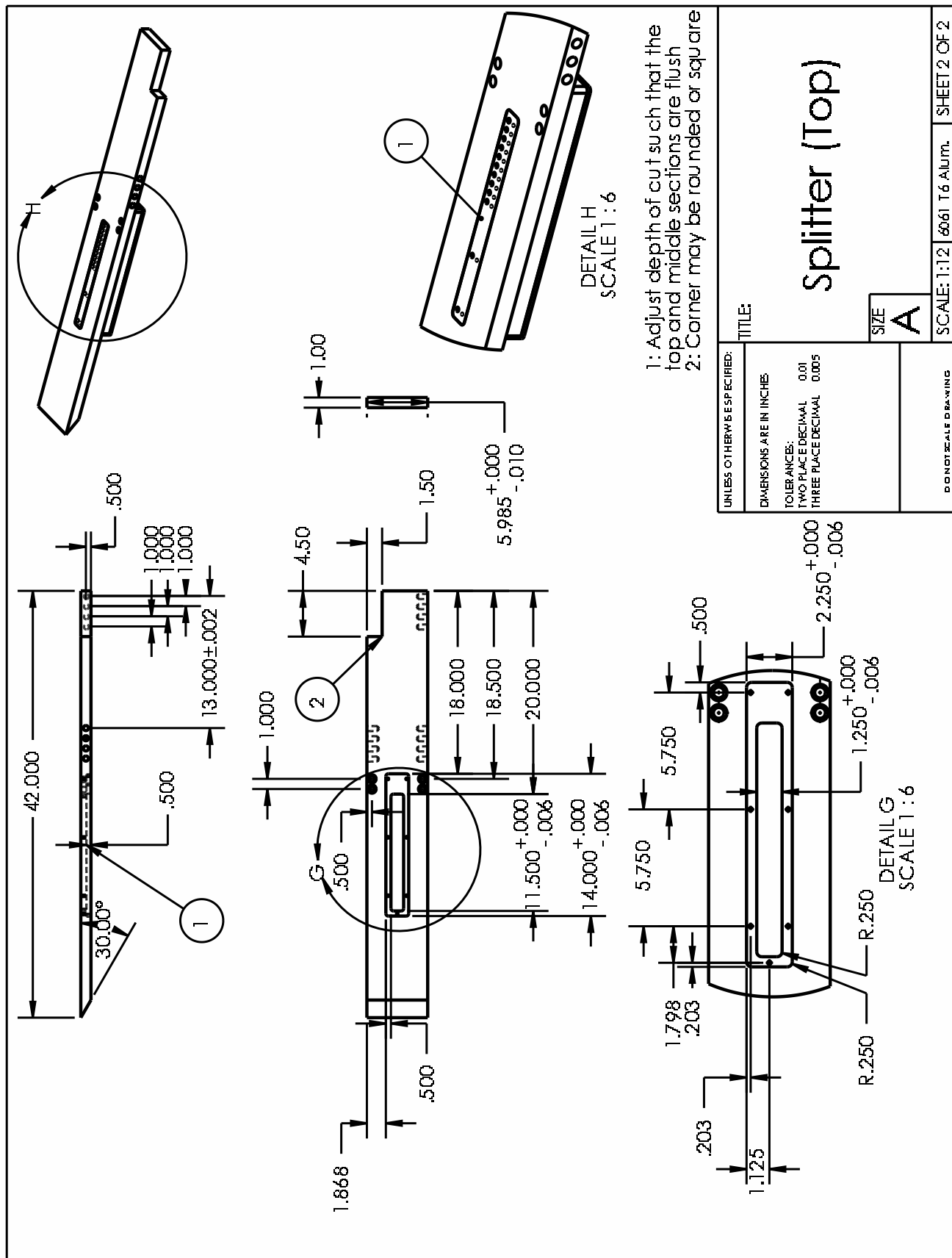


Figure C.3: Drawings of the GDT splitter plate, part 3.

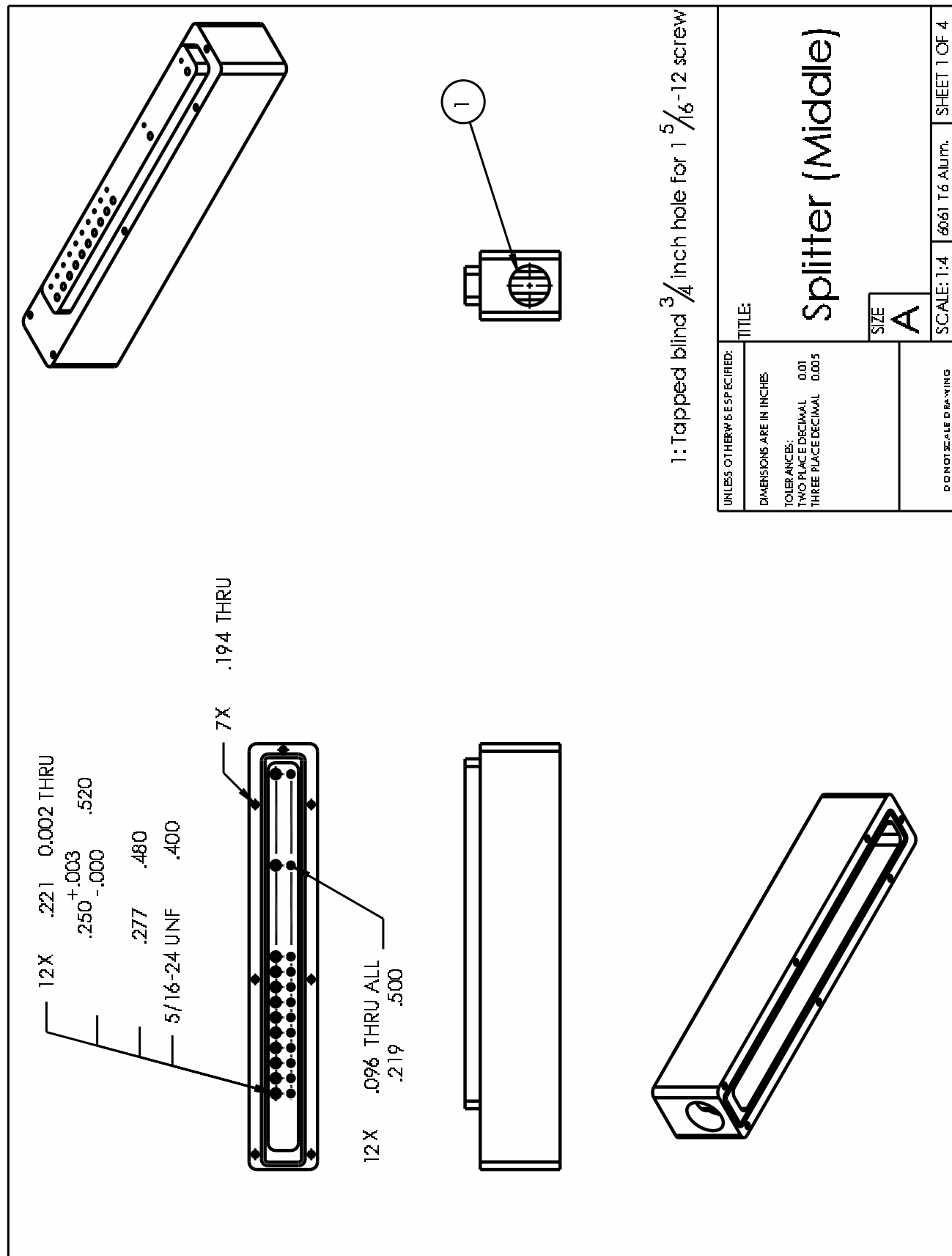


Figure C.4: Drawings of the GDT splitter plate, part 4.

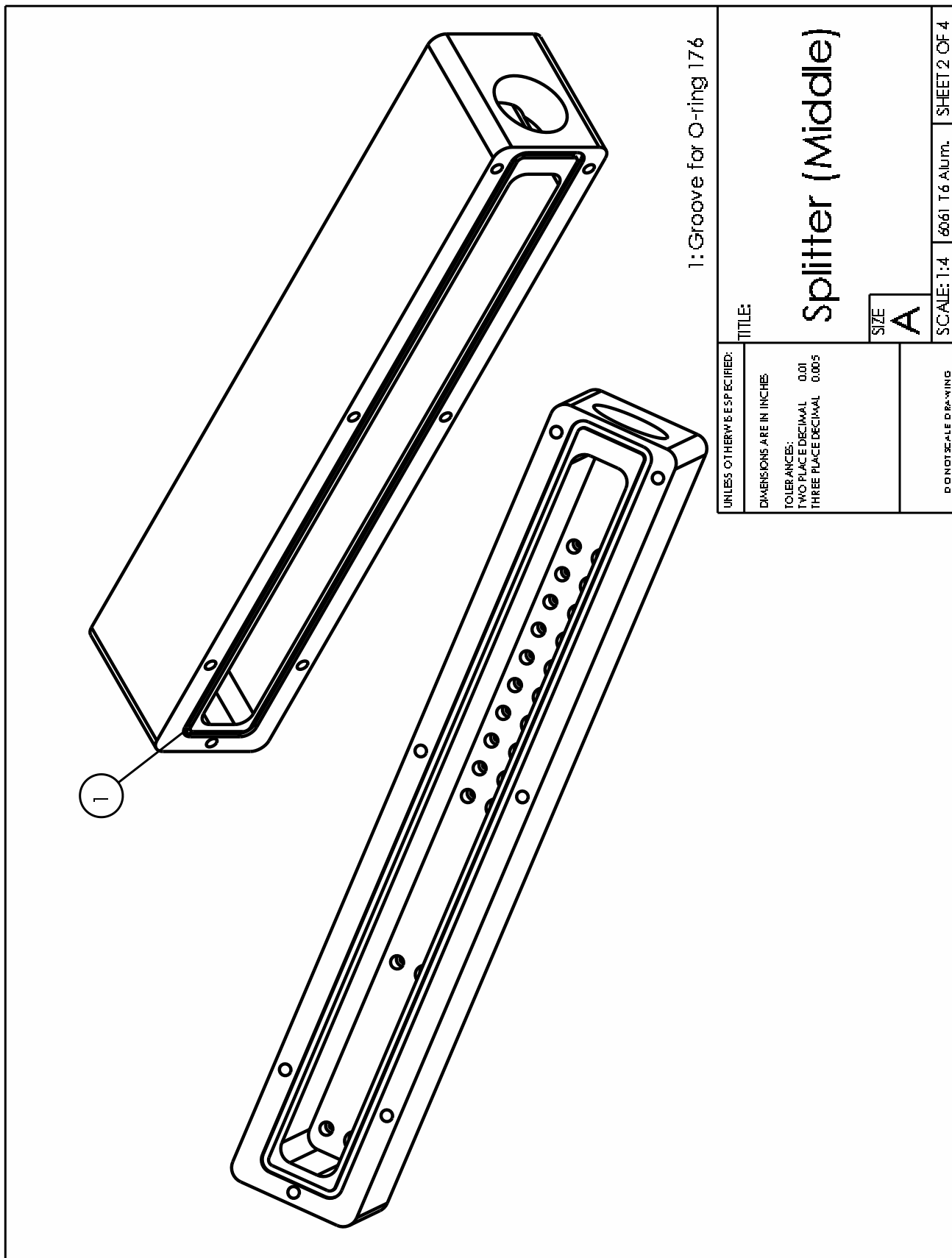


Figure C.5: Drawings of the GDT splitter plate, part 5.

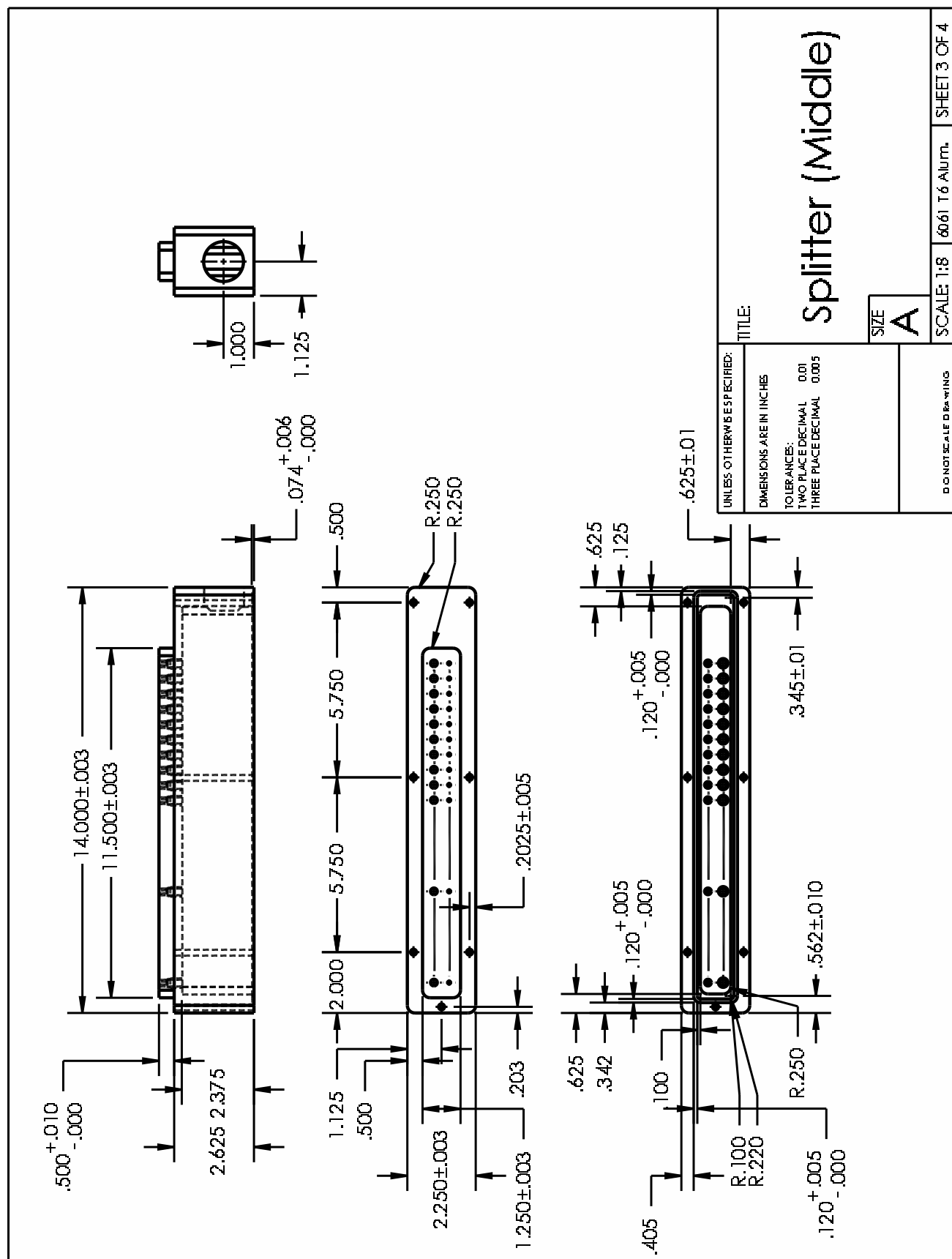


Figure C.6: Drawings of the GDT splitter plate, part 6.

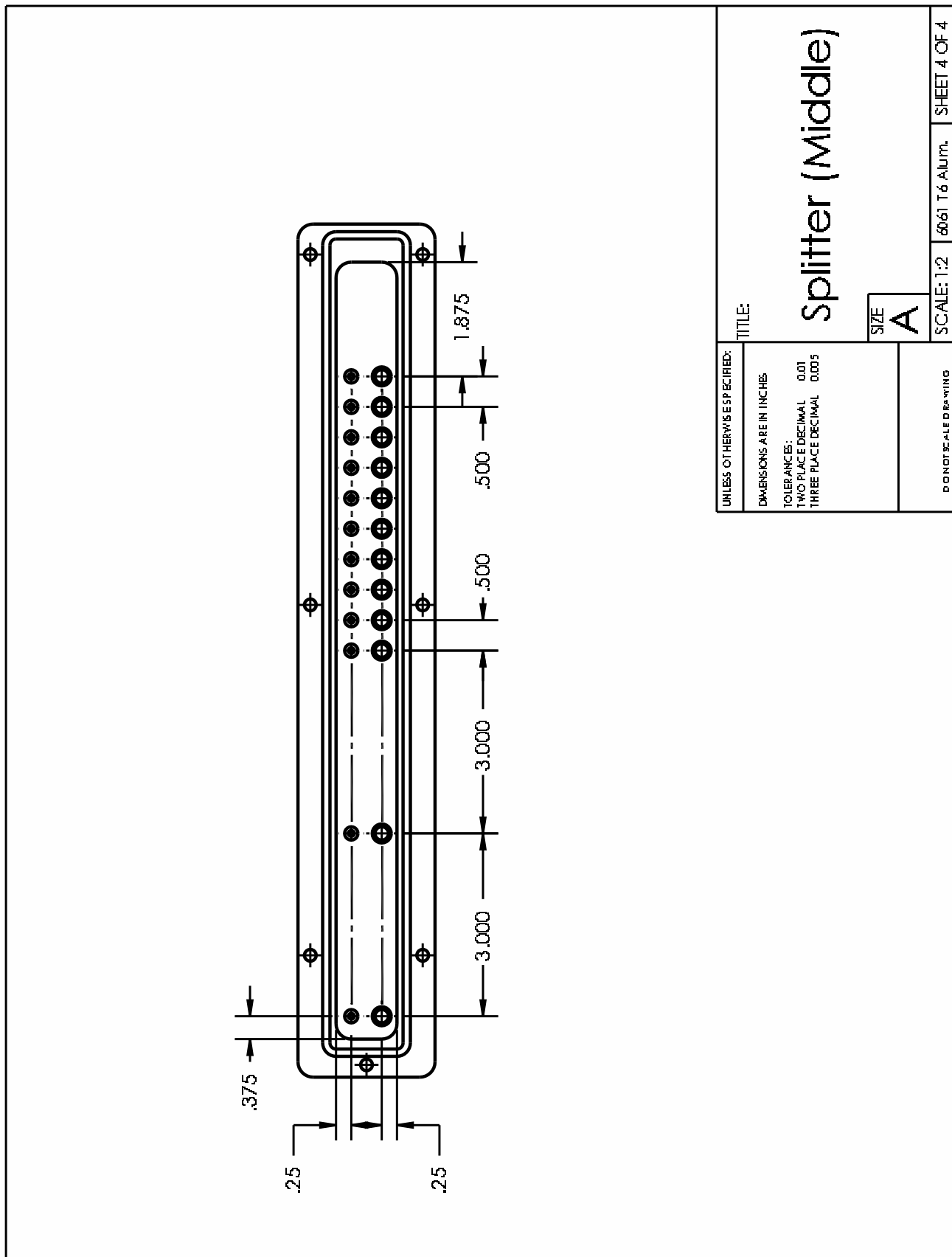


Figure C.7: Drawings of the GDT splitter plate, part 7.

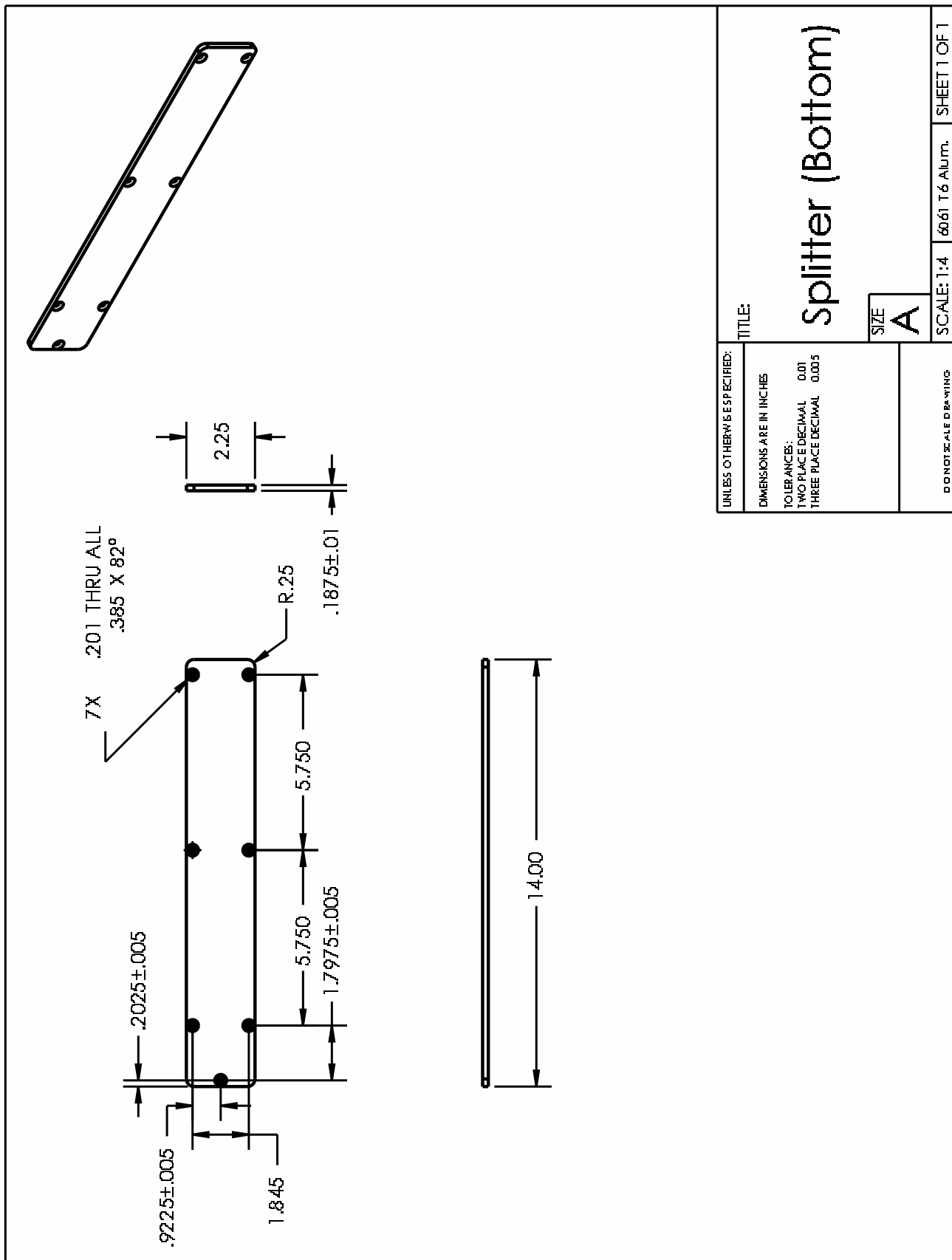


Figure C.8: Drawings of the GDT splitter plate, part 8.

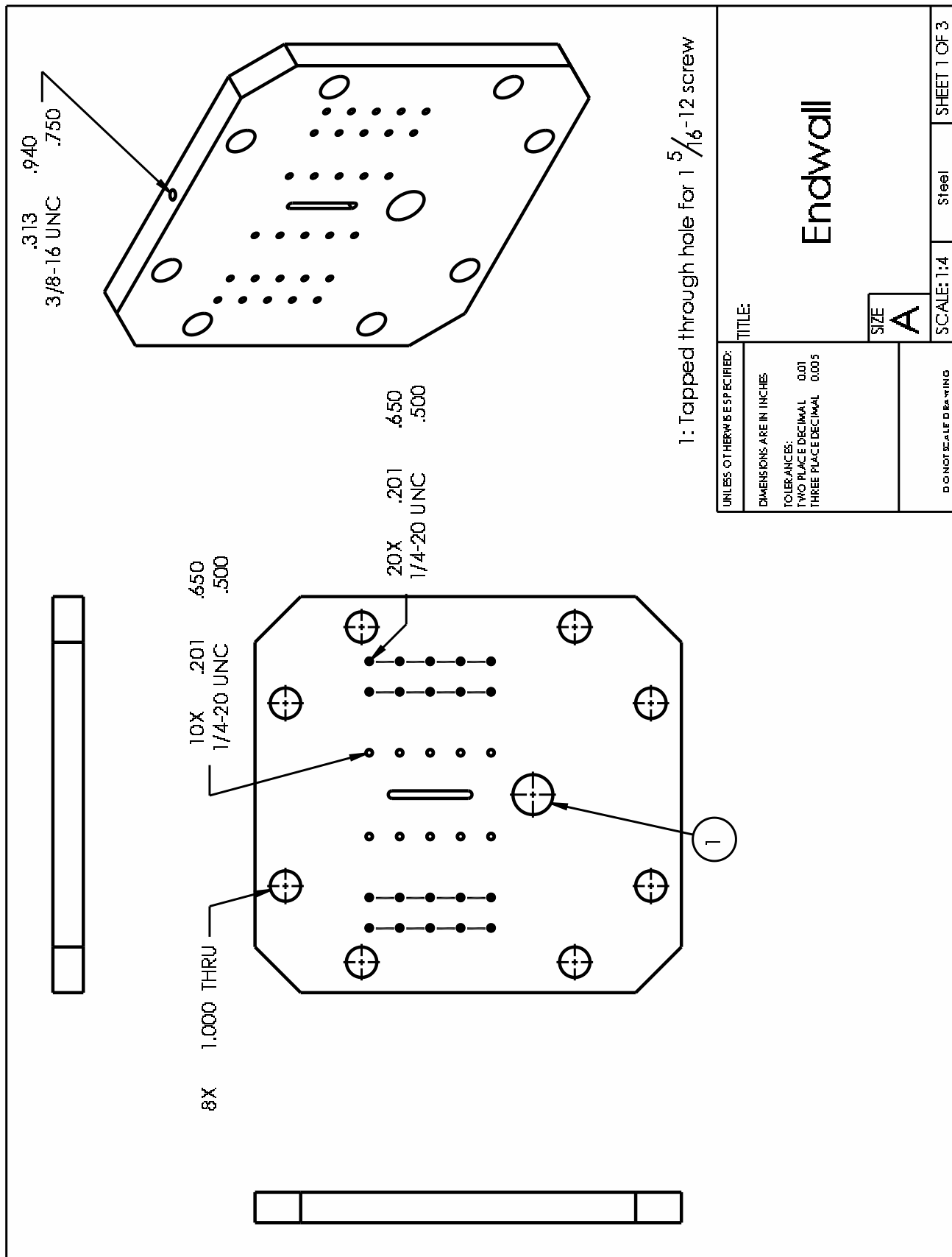


Figure C.9: Drawings of the GDT splitter plate, part 9.

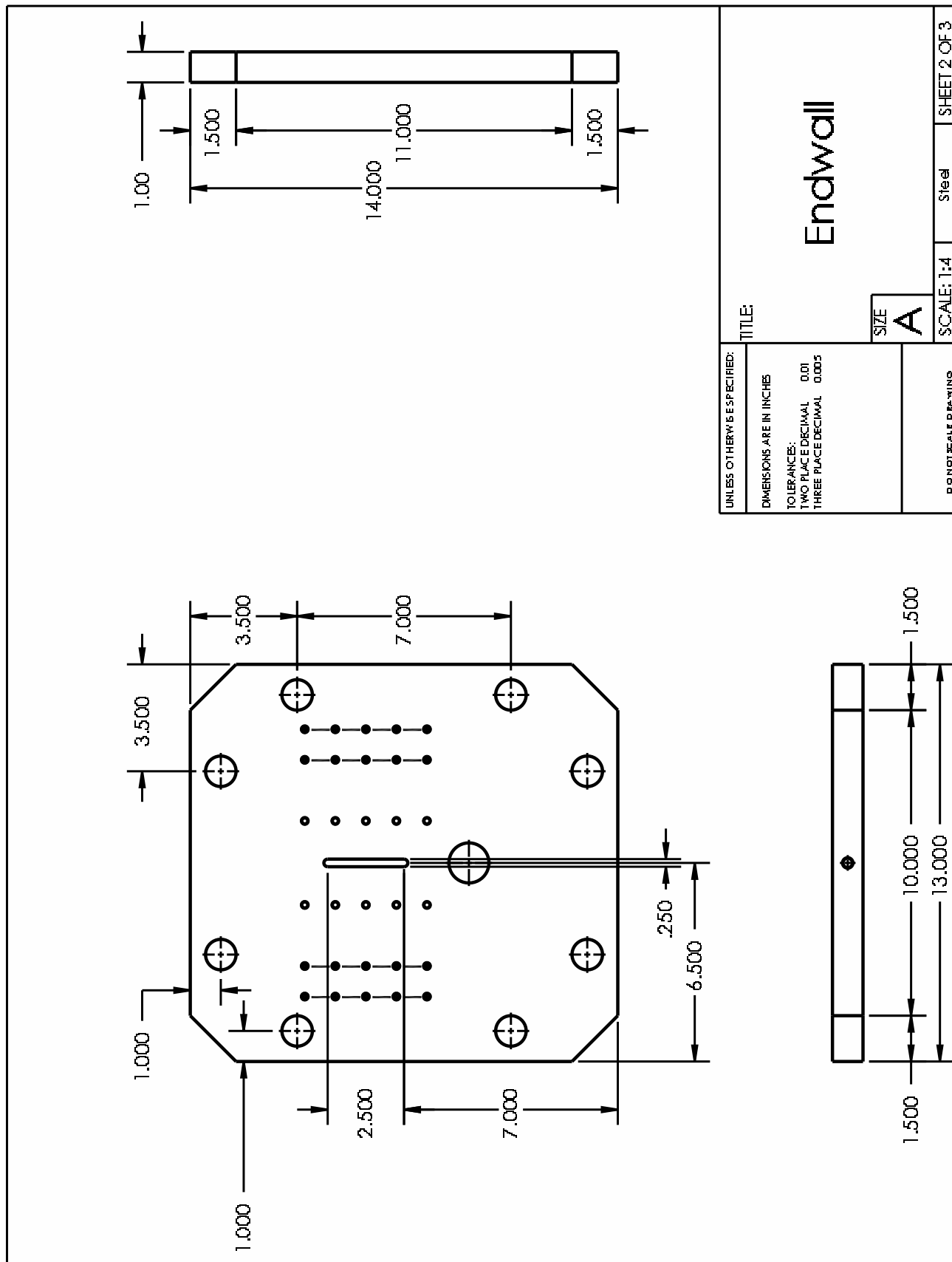


Figure C.10: Drawings of the GDT splitter plate, part 10.

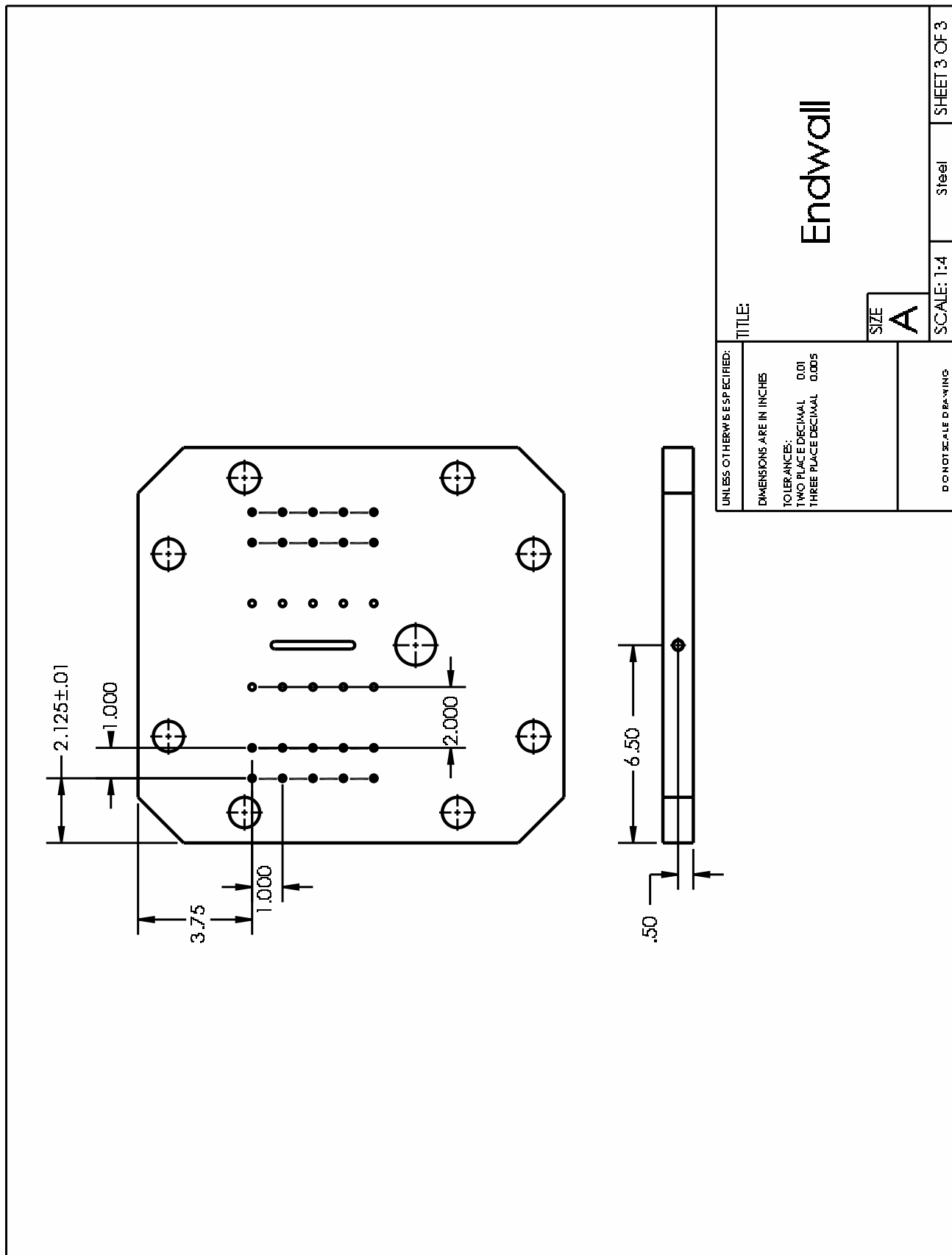


Figure C.11: Drawings of the GDT splitter plate, part 11.

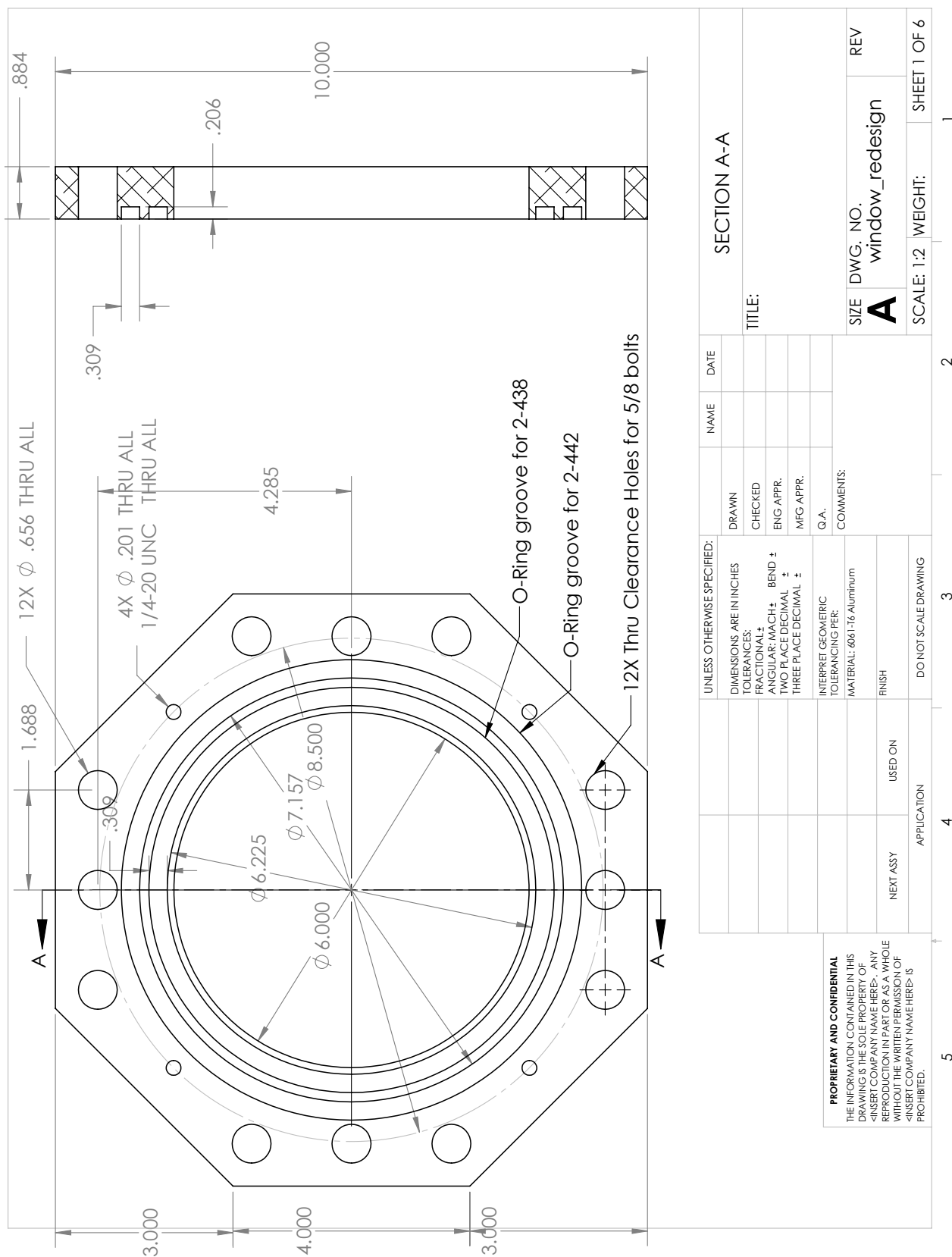


Figure C.12: Drawings of the redesigned GDT test section window, part 1.

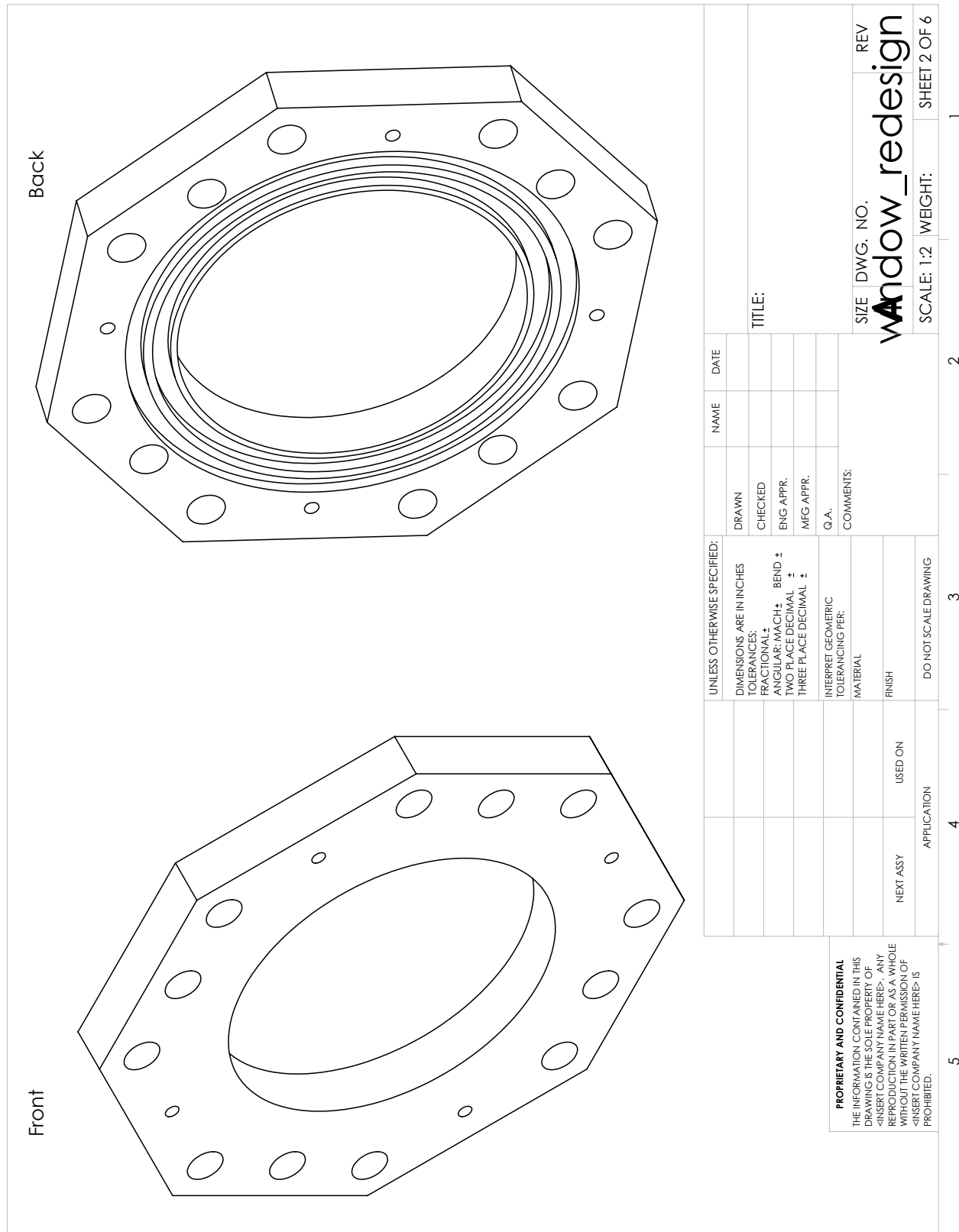


Figure C.13: Drawings of the redesigned GDT test section window, part 2.

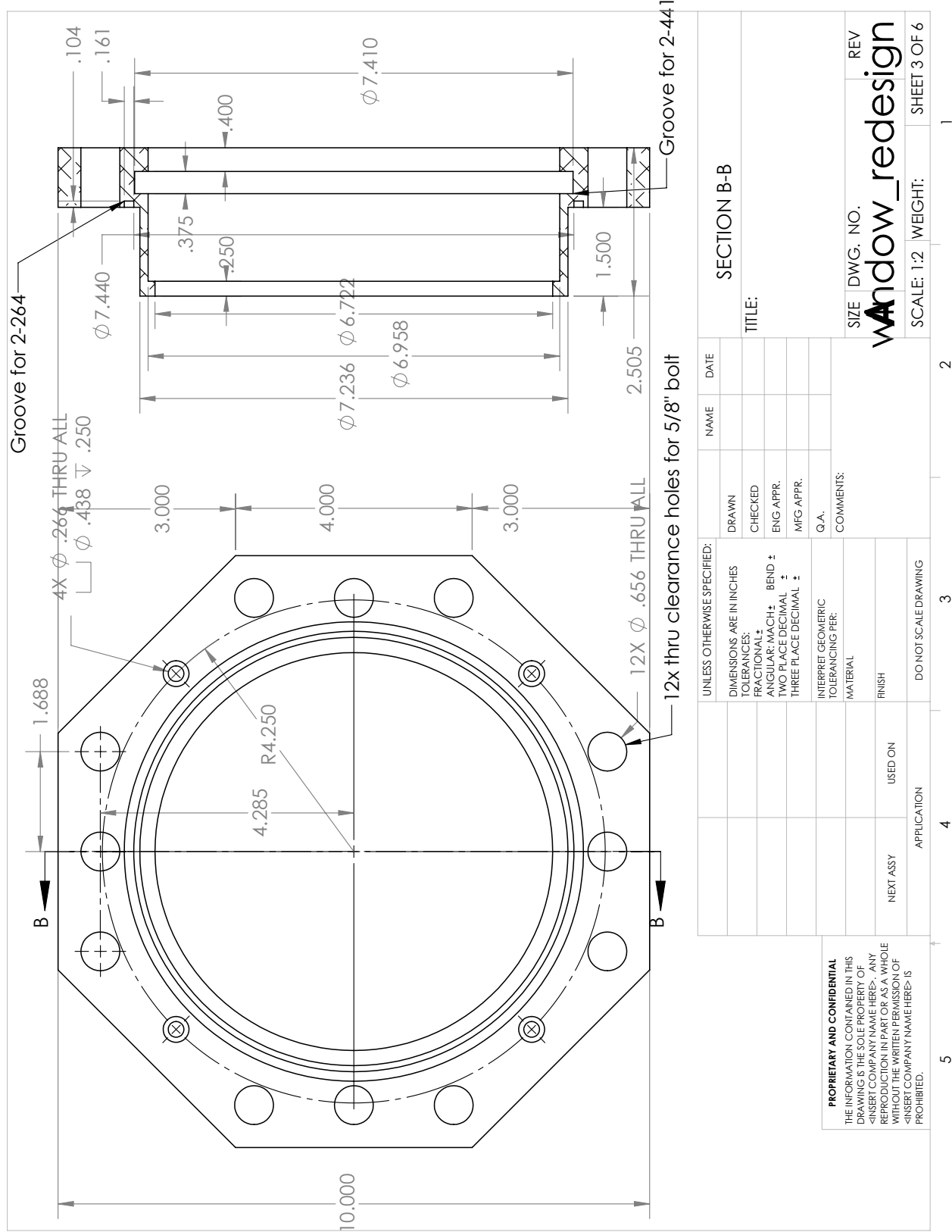


Figure C.14: Drawings of the redesigned GDT test section window, part 3.

		UNLESS OTHERWISE SPECIFIED: DIMENSIONS ARE IN INCHES TOLERANCES: FRACTIONAL: ANGULAR: MACH. ± TWO PLACE DECIMAL ± THREE PLACE DECIMAL ± MFG APPR. INTERPRET GEOMETRIC TOLERANCING PER: MATERIAL		DRAWN CHECKED ENG APPR. MFG APPR. Q.A. COMMENTS:	NAME DATE
<b>PROPRIETARY AND CONFIDENTIAL</b> THE INFORMATION CONTAINED IN THIS DRAWING IS THE SOLE PROPERTY OF <INSERT COMPANY NAME HERE>. ANY REPRODUCTION IN PART OR AS A WHOLE WITHOUT THE WRITTEN PERMISSION OF <INSERT COMPANY NAME HERE> IS PROHIBITED.		NEXT ASSY  APPLICATION	USED ON  DO NOT SCALE DRAWING		DWG. NO. <b>Window_redesign</b> REV
					SCALE: 1:2 WEIGHT: SHEET 4 OF 6
					1 2 3 4 5

Figure C.15: Drawings of the redesigned GDT test section window, part 4.

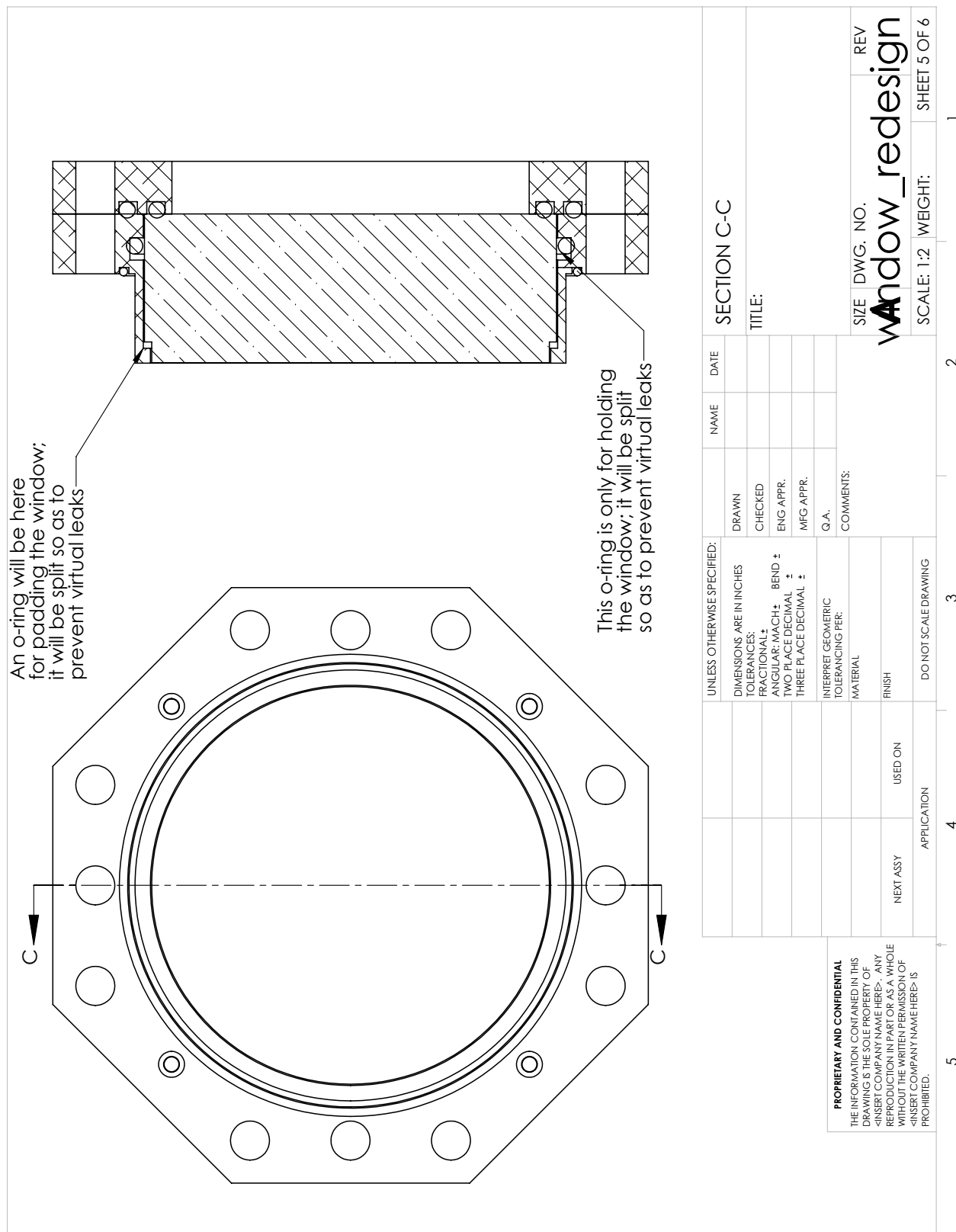


Figure C.16: Drawings of the redesigned GDT test section window, part 5.

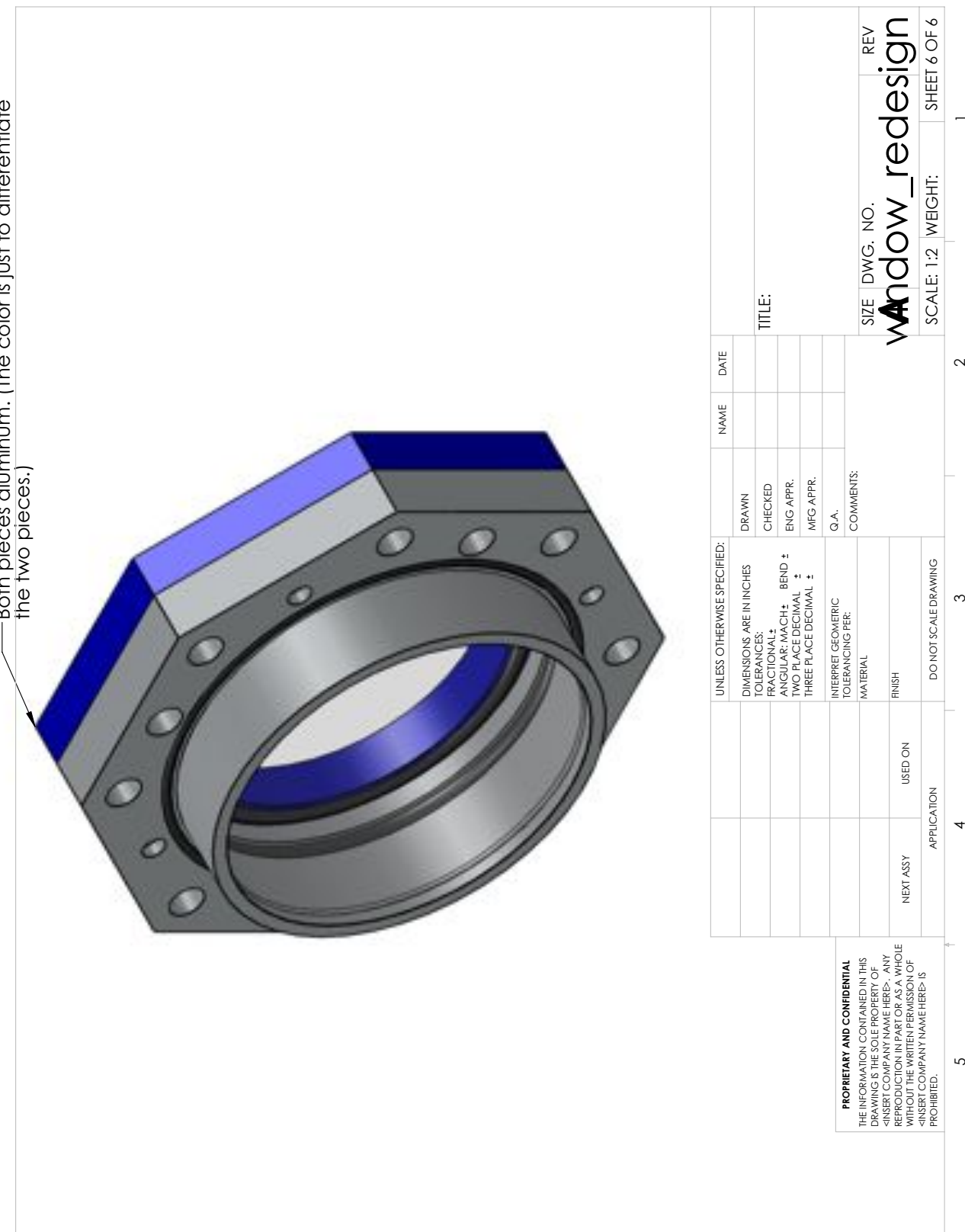


Figure C.17: Drawings of the redesigned GDT test section window, part 6.

# Appendix D

## Visualization Systems

Details for each visualization system employed are given below organized by type of system (focused or unfocused) and the light source used. A more complete set of images is included with the pressure and heat-flux data in appendix E.

### D.1 Unfocused Schlieren Systems

A list of focal lengths and magnifications are shown in table D.1. A list of run conditions for each system is given in appendix C.

Table D.1: Details of unfocused schlieren configurations.

#	Light source	Camera	$f_1$ (mm)	$f_2$ (mm)	$M$	$t_{exp}$ (ns)
1	Sparker	Nikon D200	1500	1600	0.5	300
2	SLD1332V	Phantom v7.10	1500	1600	2	50
3	SMART Cavidux	Phantom v7.10	1500	1000	0.5	10
4	PL1000DRC	SI SIMD16	1500	1000	1	20

#### D.1.1 Sparker

A sparker light source built by Shepherd (1981), nicknamed “Storm” in the data files, was used as a schlieren source to obtain pictures such as those shown below. The exposure time of 300 ns was a half-width, half-maximum value as recorded by a photodiode and should only be considered as an approximate exposure time. The

camera used was a 3872 x 2592 pixel Nikon D200. It was triggered off the exploding wire and the shutter remained open on the order of 50 ms. The sparker was then triggered off a pressure gauge with appropriate delay to produce the pictures.

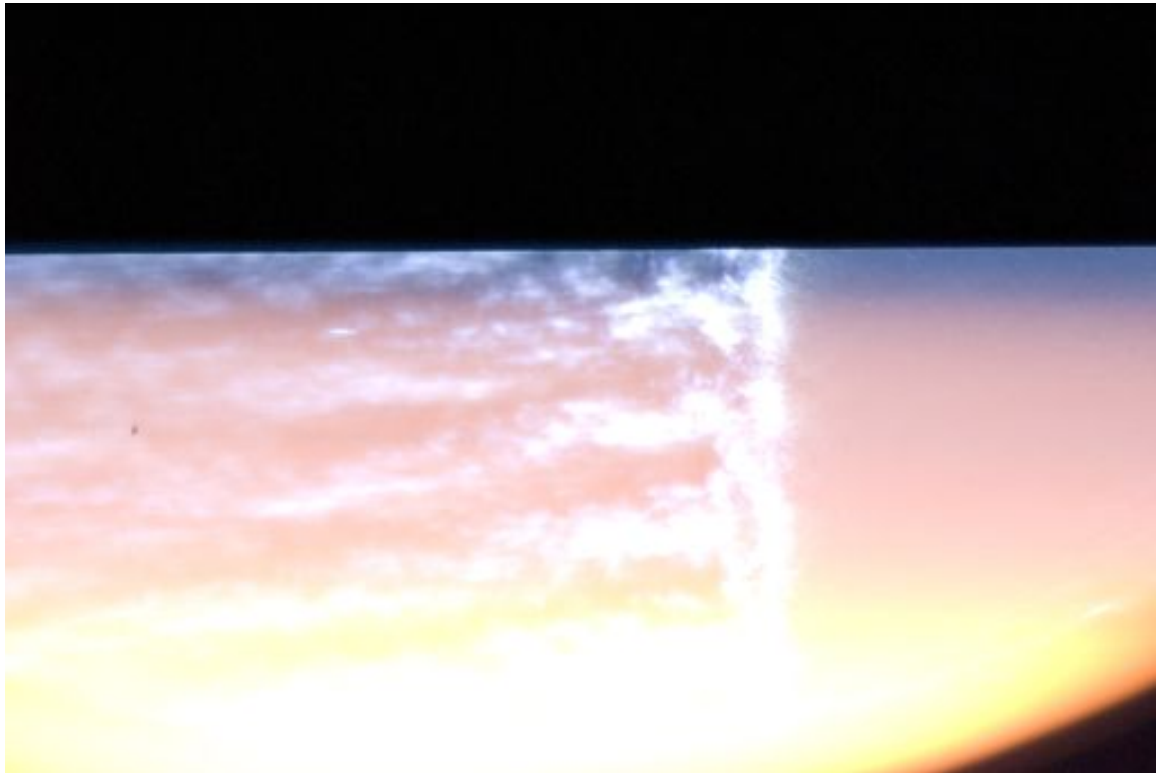


Figure D.1: Unfocused schlieren image of shot 1944. The field of view is approximately 45 mm wide.

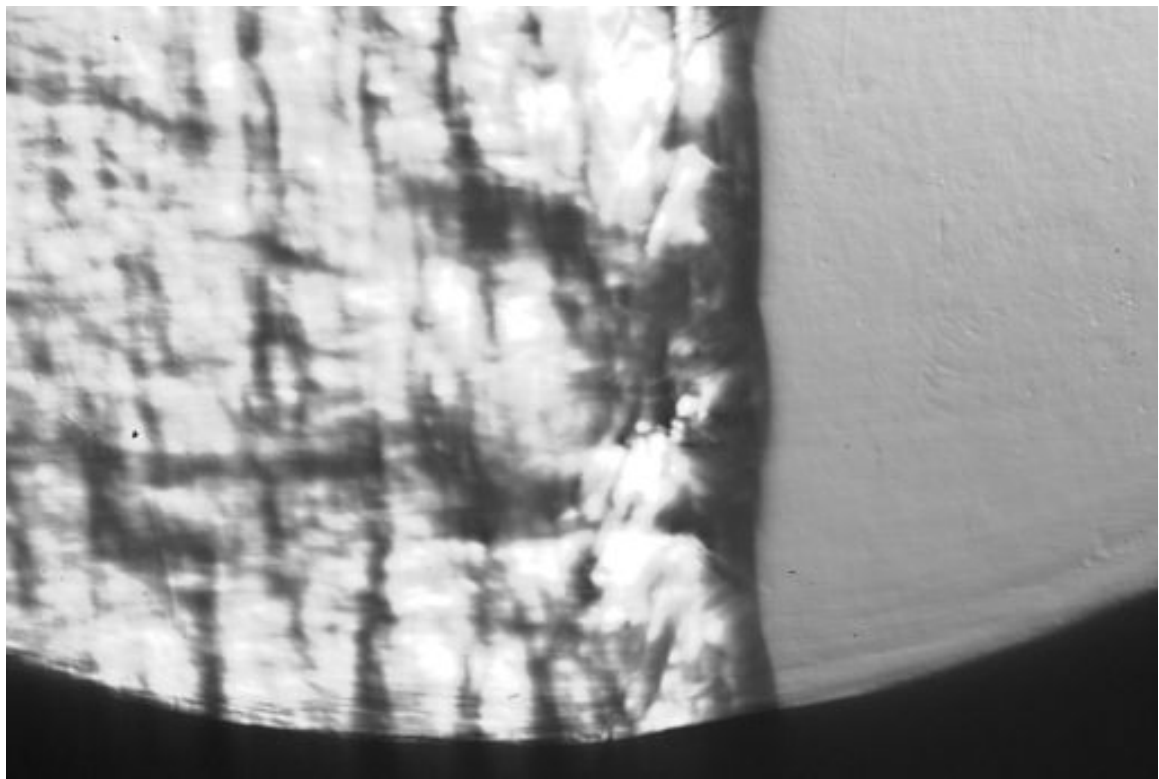


Figure D.2: Unfocused schlieren image of shot 1945. The field of view is approximately 45 mm wide.

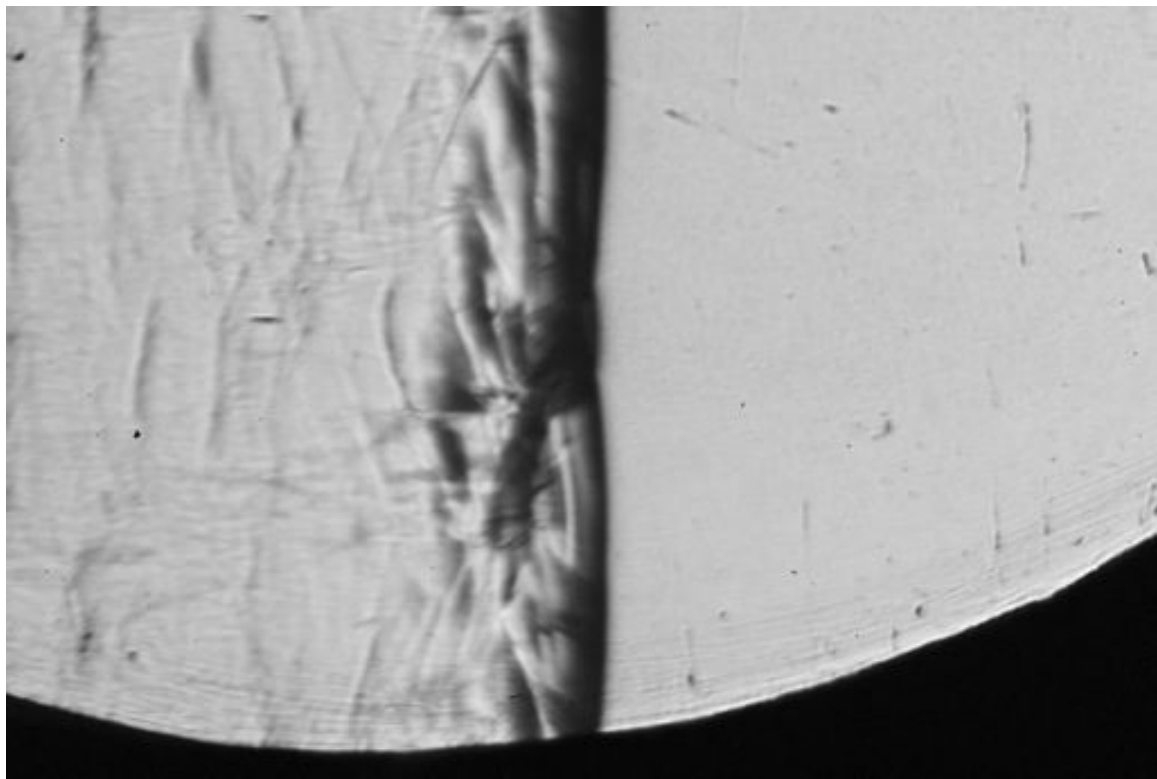


Figure D.3: Unfocused schlieren image of shot 1948. The field of view is approximately 45 mm wide.

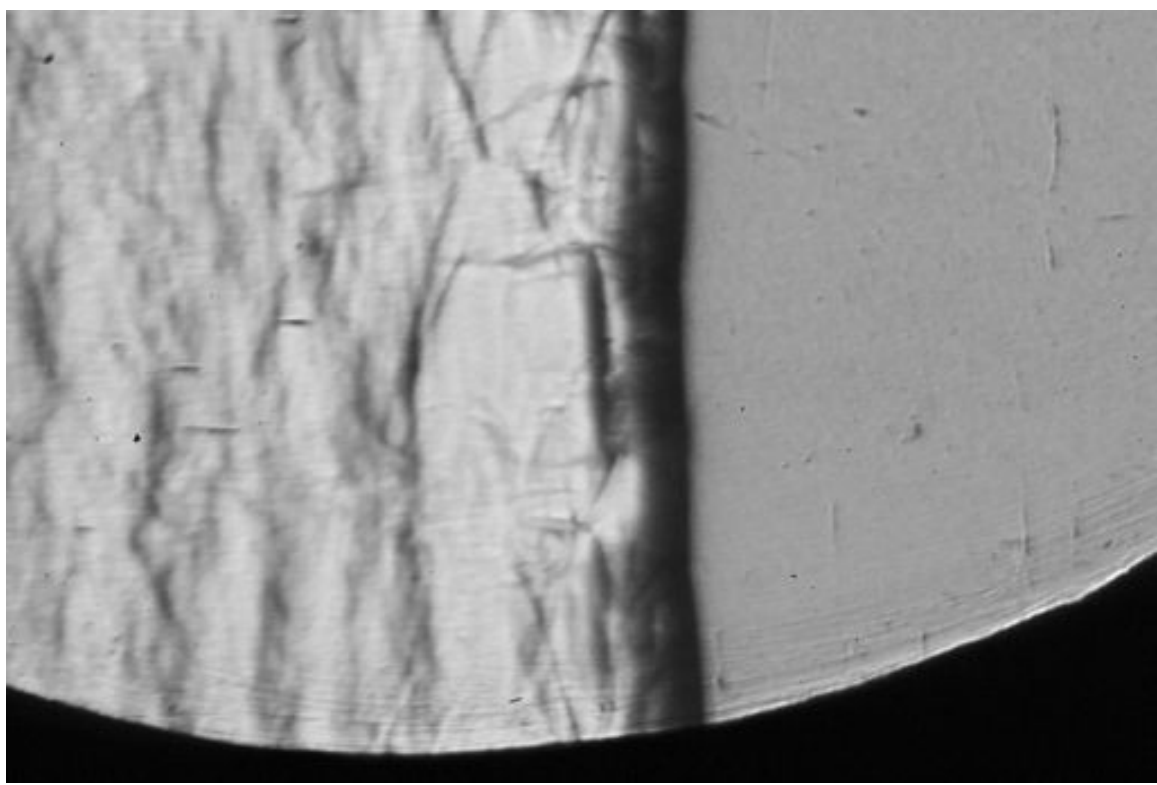


Figure D.4: Unfocused schlieren image of shot 1950. The field of view is approximately 45 mm wide.

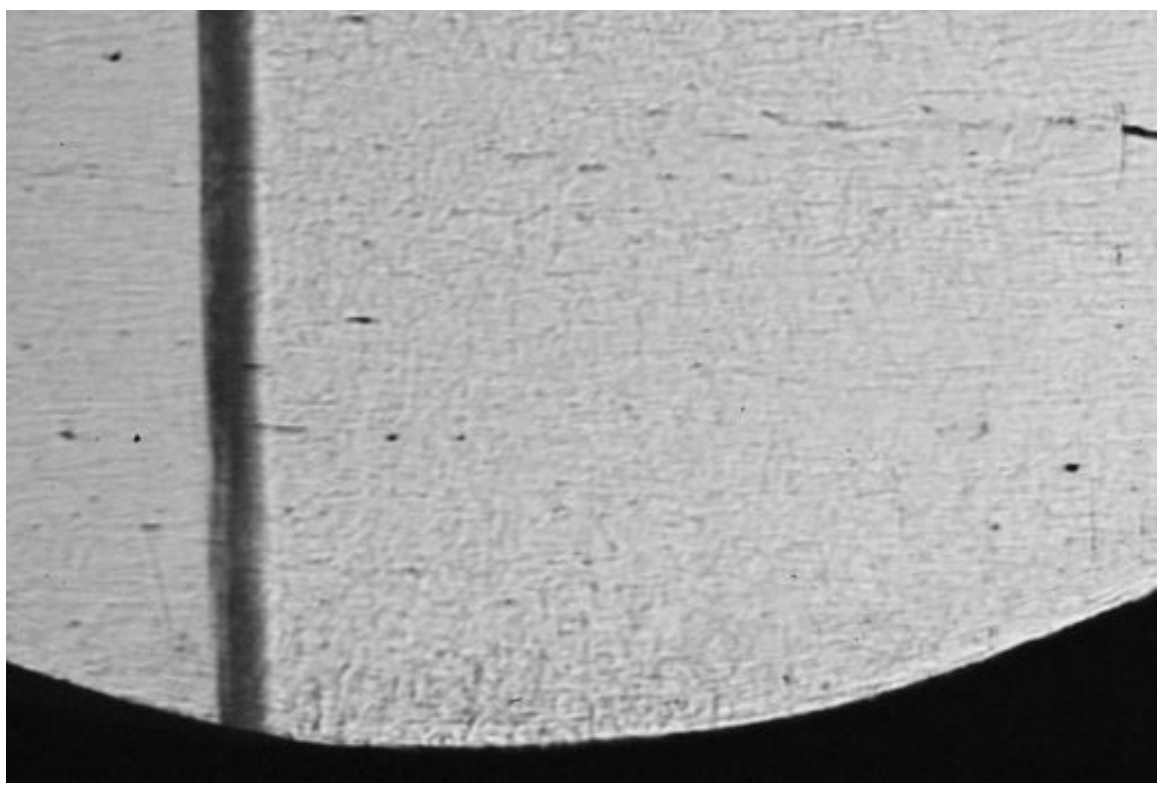


Figure D.5: Unfocused schlieren image of shot 1951. The field of view is approximately 45 mm wide.

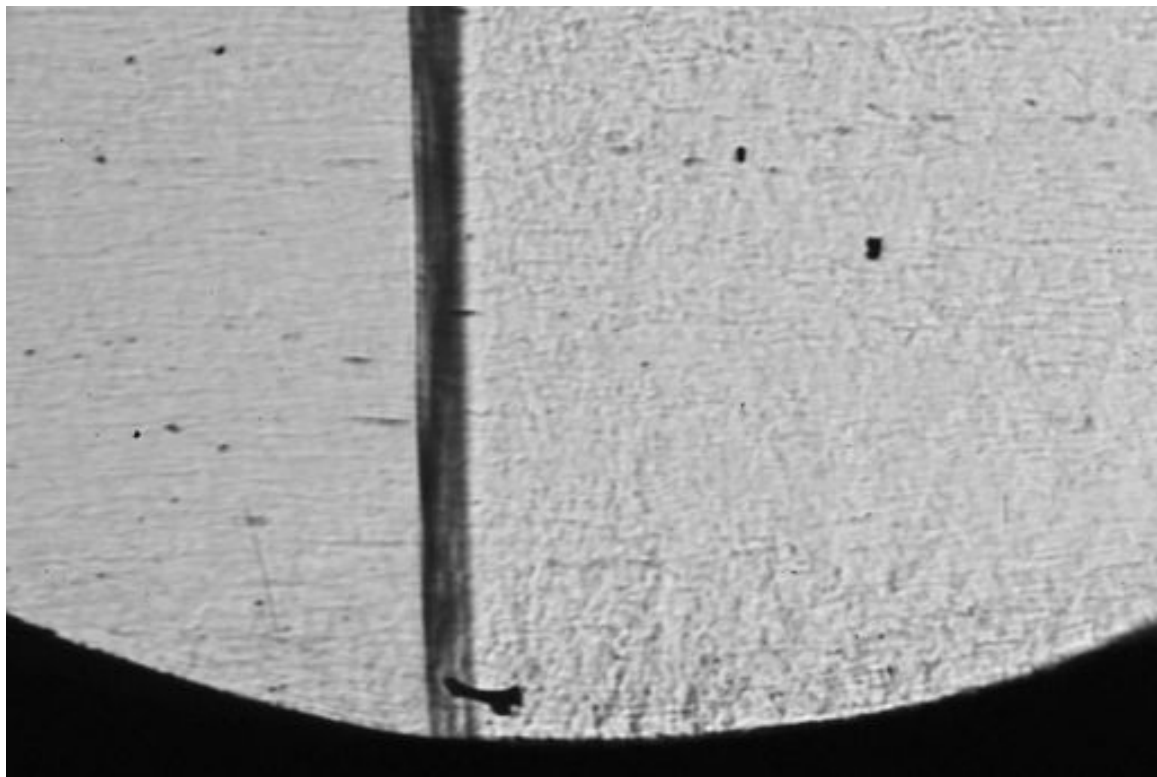


Figure D.6: Unfocused schlieren image of shot 1952. The field of view is approximately 45 mm wide.

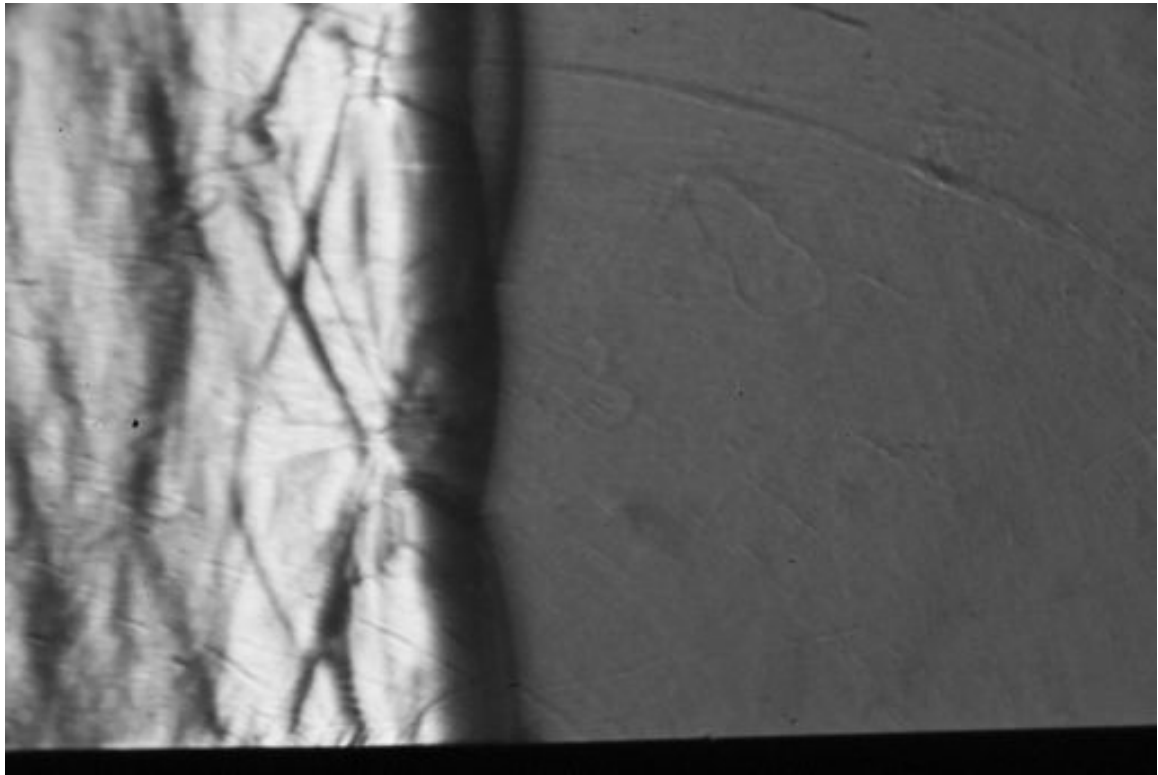


Figure D.7: Unfocused schlieren image of shot 1963. The field of view is approximately 45 mm wide.

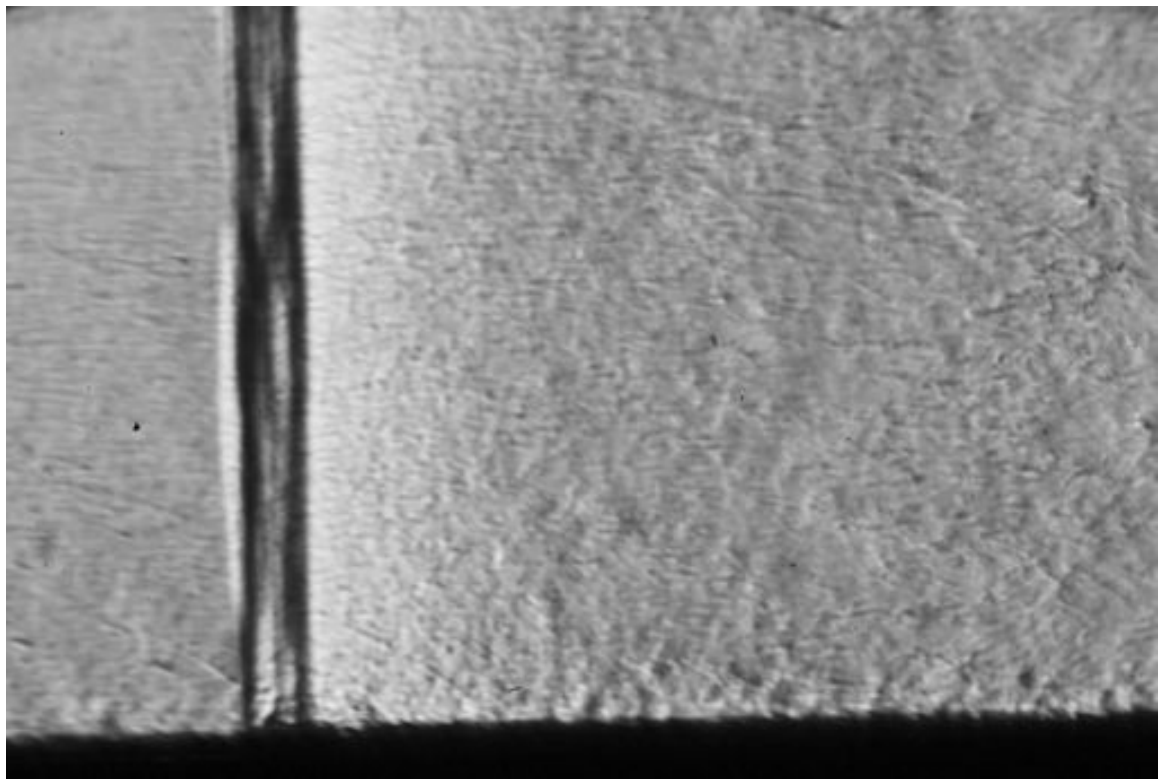


Figure D.8: Unfocused schlieren image of shot 1964. The field of view is approximately 45 mm wide.

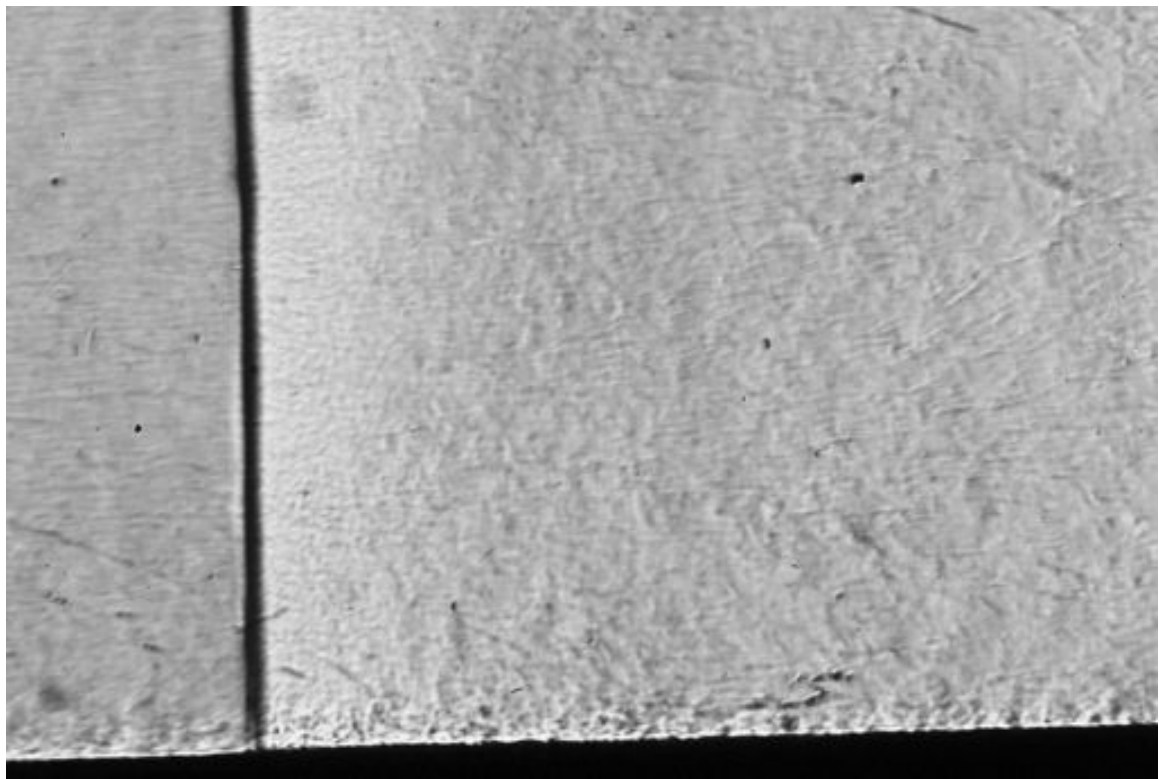


Figure D.9: Unfocused schlieren image of shot 1965. The field of view is approximately 45 mm wide.

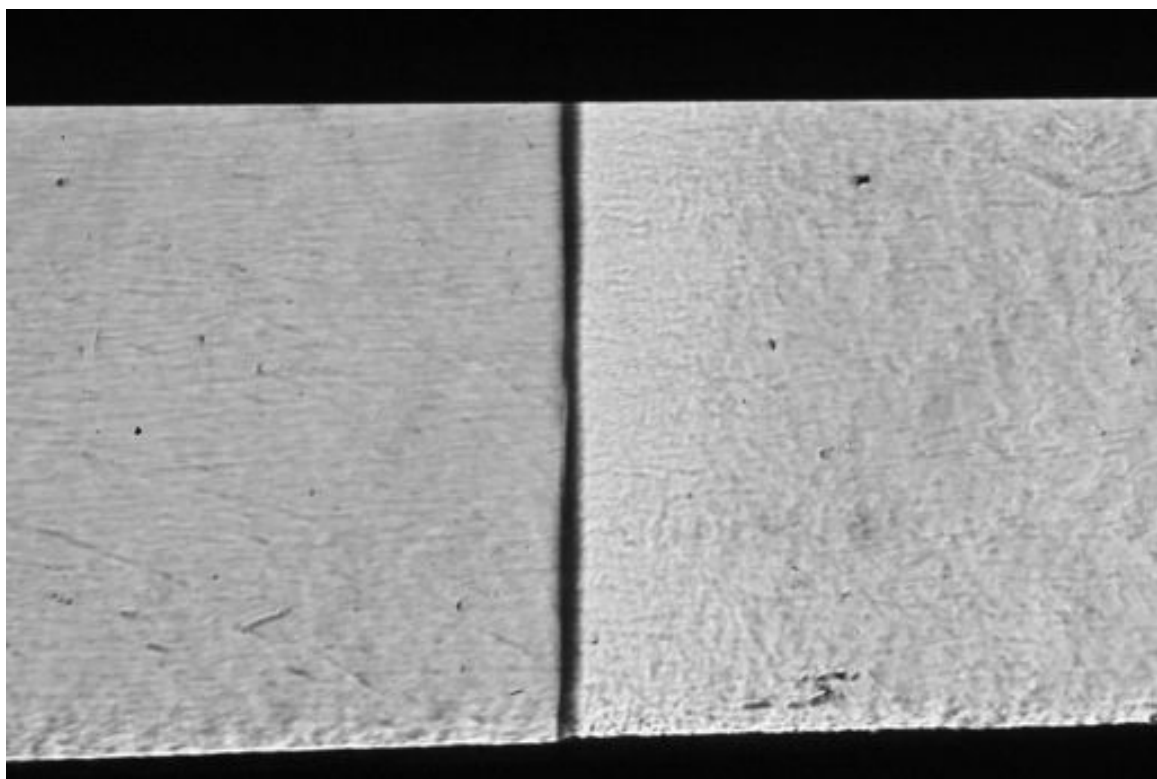


Figure D.10: Unfocused schlieren image of shot 1966. The field of view is approximately 45 mm wide.

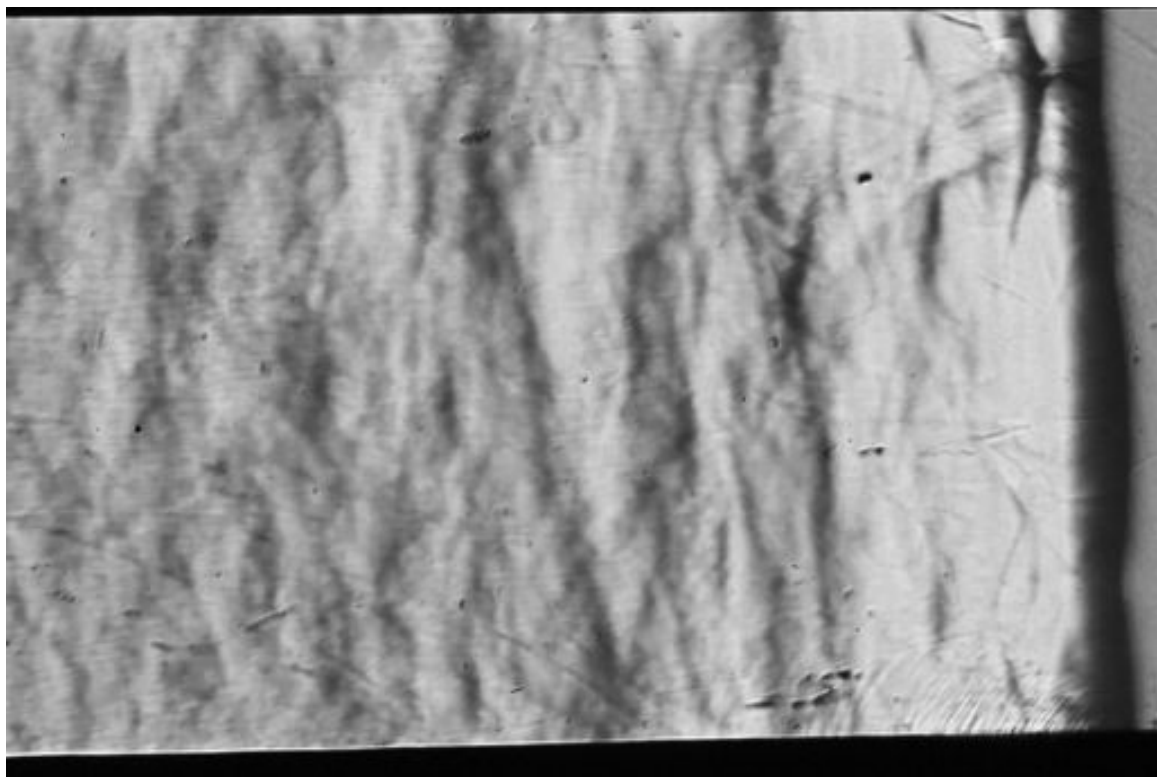


Figure D.11: Unfocused schlieren image of shot 1967. The field of view is approximately 45 mm wide.

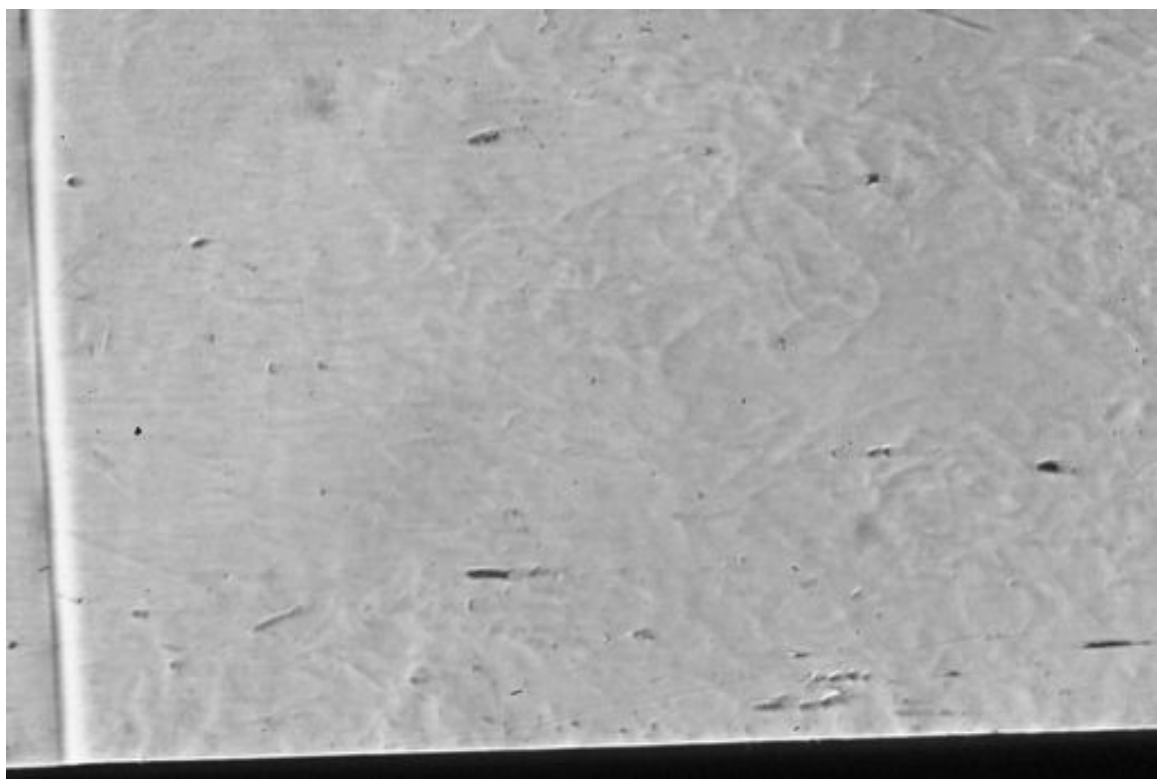


Figure D.12: Unfocused schlieren image of shot 1971. The field of view is approximately 45 mm wide.

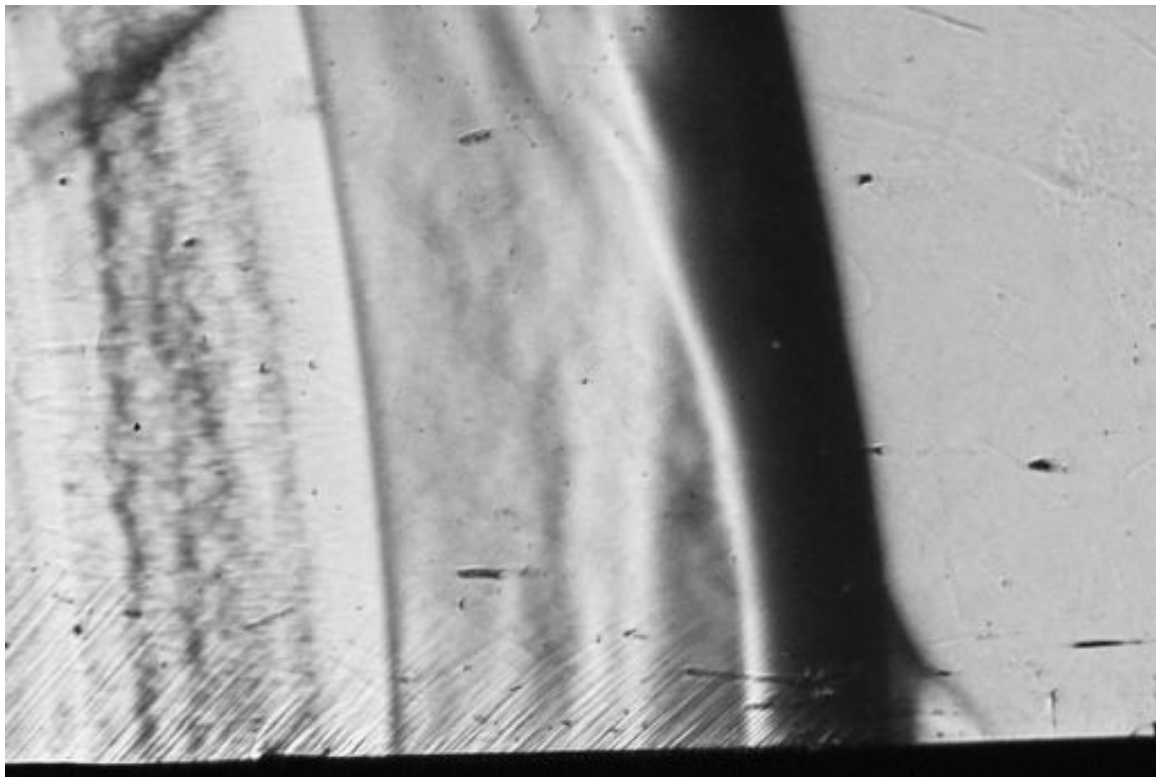


Figure D.13: Unfocused schlieren image of shot 1972. The field of view is approximately 45 mm wide.

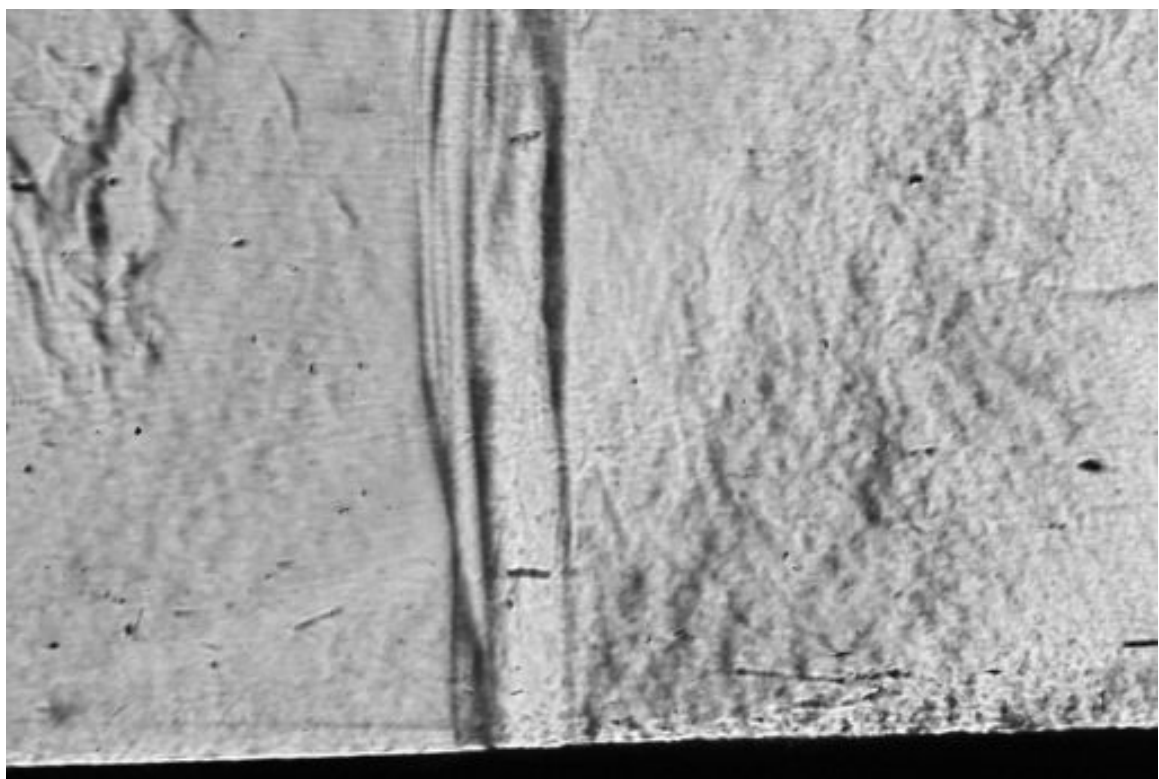


Figure D.14: Unfocused schlieren image of shot 1975. The field of view is approximately 45 mm wide.

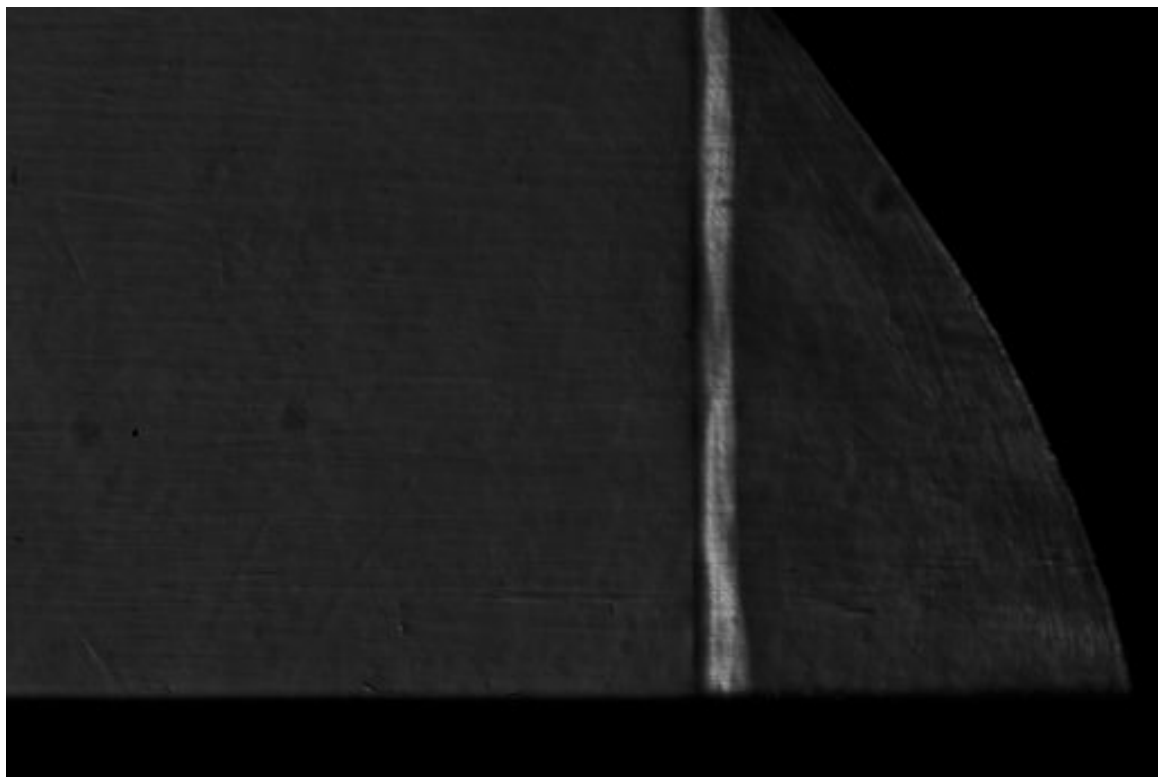


Figure D.15: Unfocused schlieren image of shot 1978. The field of view is approximately 45 mm wide.

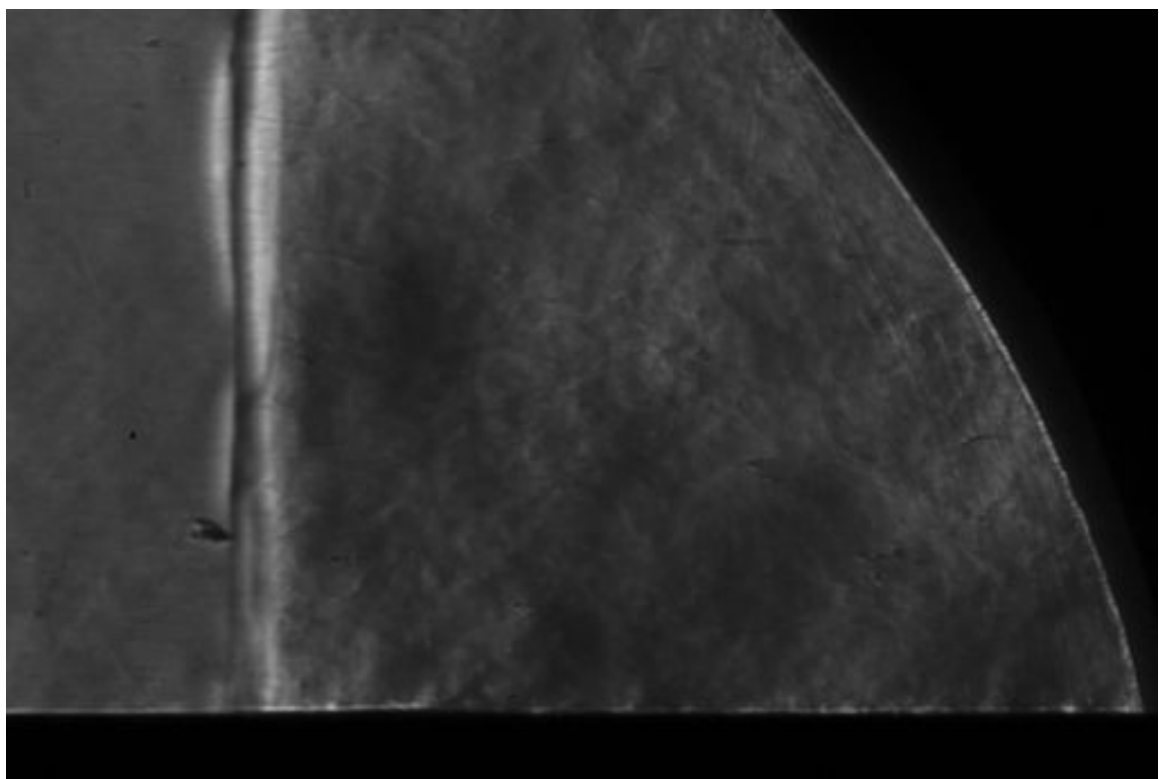


Figure D.16: Unfocused schlieren image of shot 1991. The field of view is approximately 45 mm wide.

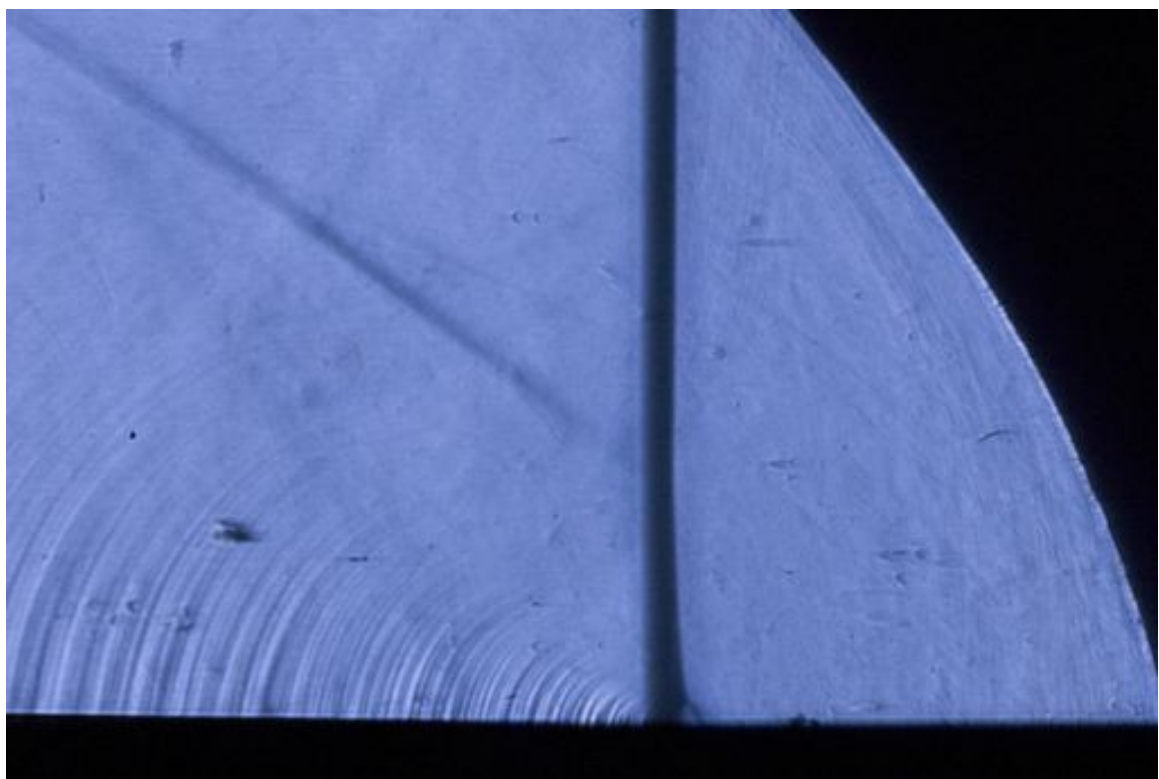


Figure D.17: Unfocused schlieren image of shot 1997. The field of view is approximately 45 mm wide.

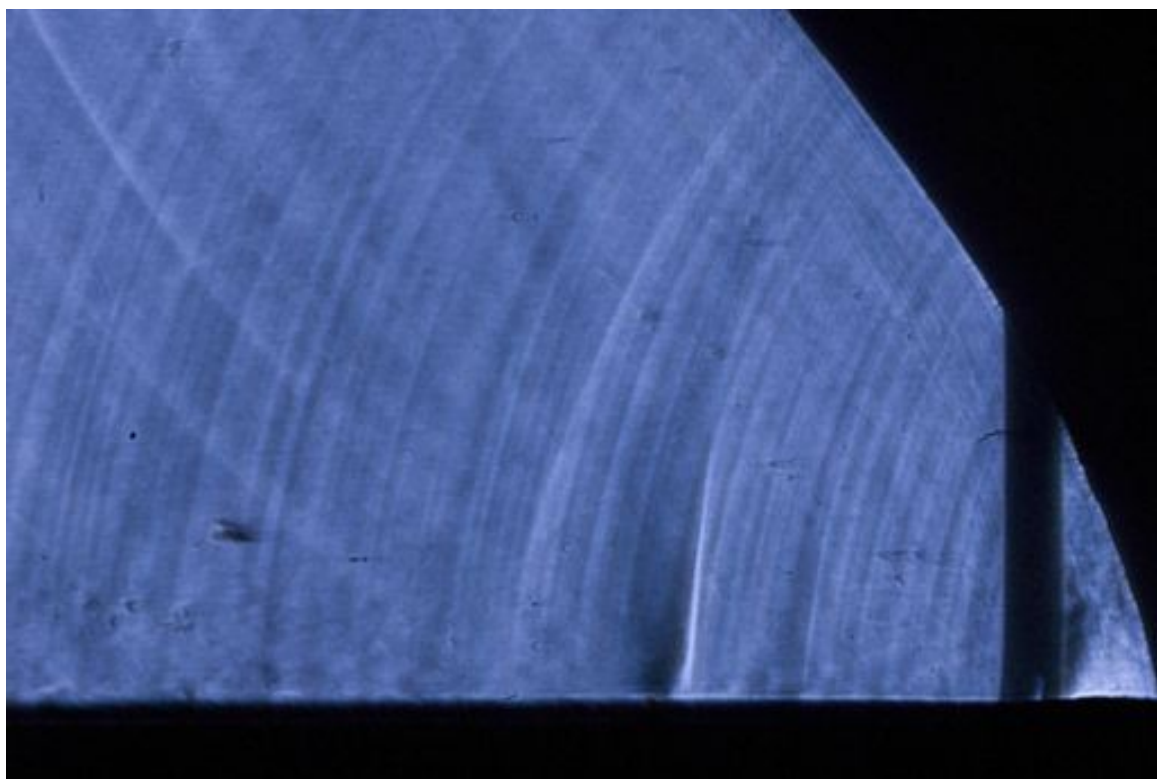


Figure D.18: Unfocused schlieren image of shot 1999. The field of view is approximately 45 mm wide.

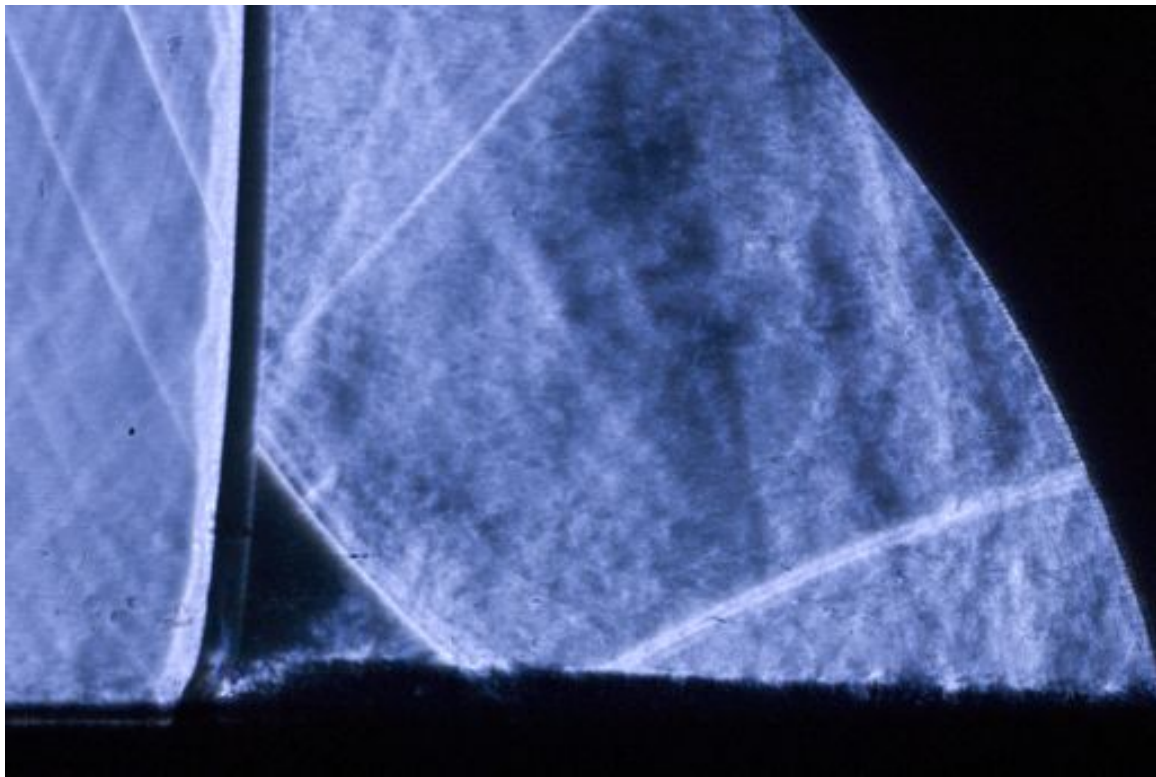


Figure D.19: Unfocused schlieren image of shot 2000. The field of view is approximately 45 mm wide.

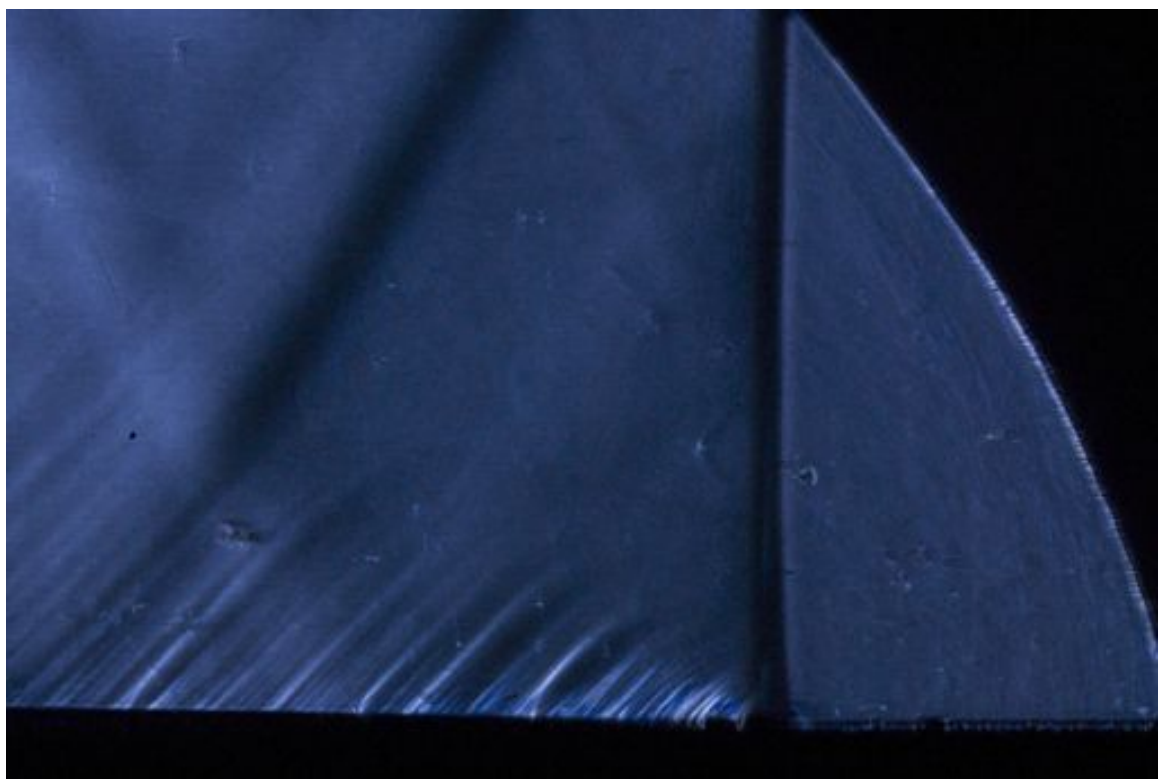


Figure D.20: Unfocused schlieren image of shot 2002. The field of view is approximately 45 mm wide.

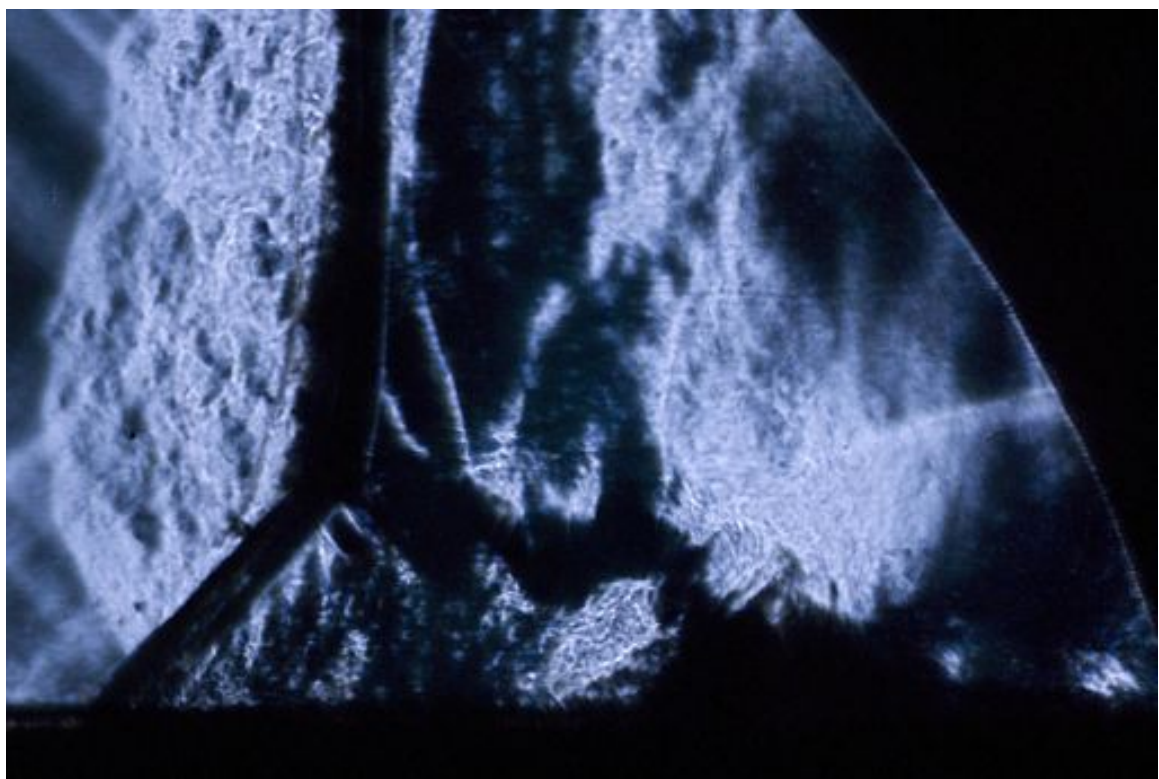


Figure D.21: Unfocused schlieren image of shot 2003. The field of view is approximately 45 mm wide.

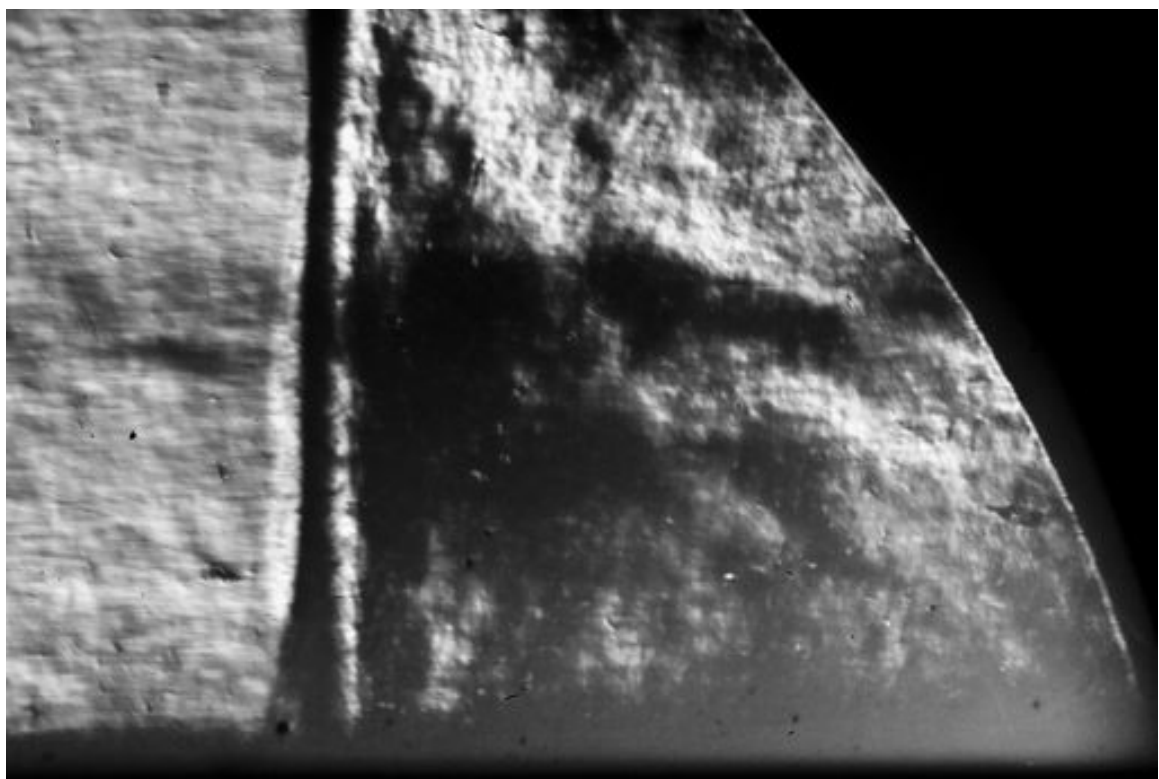


Figure D.22: Unfocused schlieren image of shot 2011. The field of view is approximately 45 mm wide.

### D.1.2 SLD1332V

A Sony SLD1332V laser diode, nicknamed “Ghost in the Shell” in the data files, was used in conjunction with an LDP-V 03-100 UF3 current driver and a Phantom v7.10 high-speed camera to obtain images with a much shorter exposure time than was possible with the spark light source. A laser line filter was positioned in front of the camera; this made imaging detonation waves much easier. Both laser and camera were driven by a BNC delay generator that was triggered from a pressure signal. This visualization system was developed with Dr. Nick Parziale, who used it to great effect in the T5 hypervelocity wind tunnel.

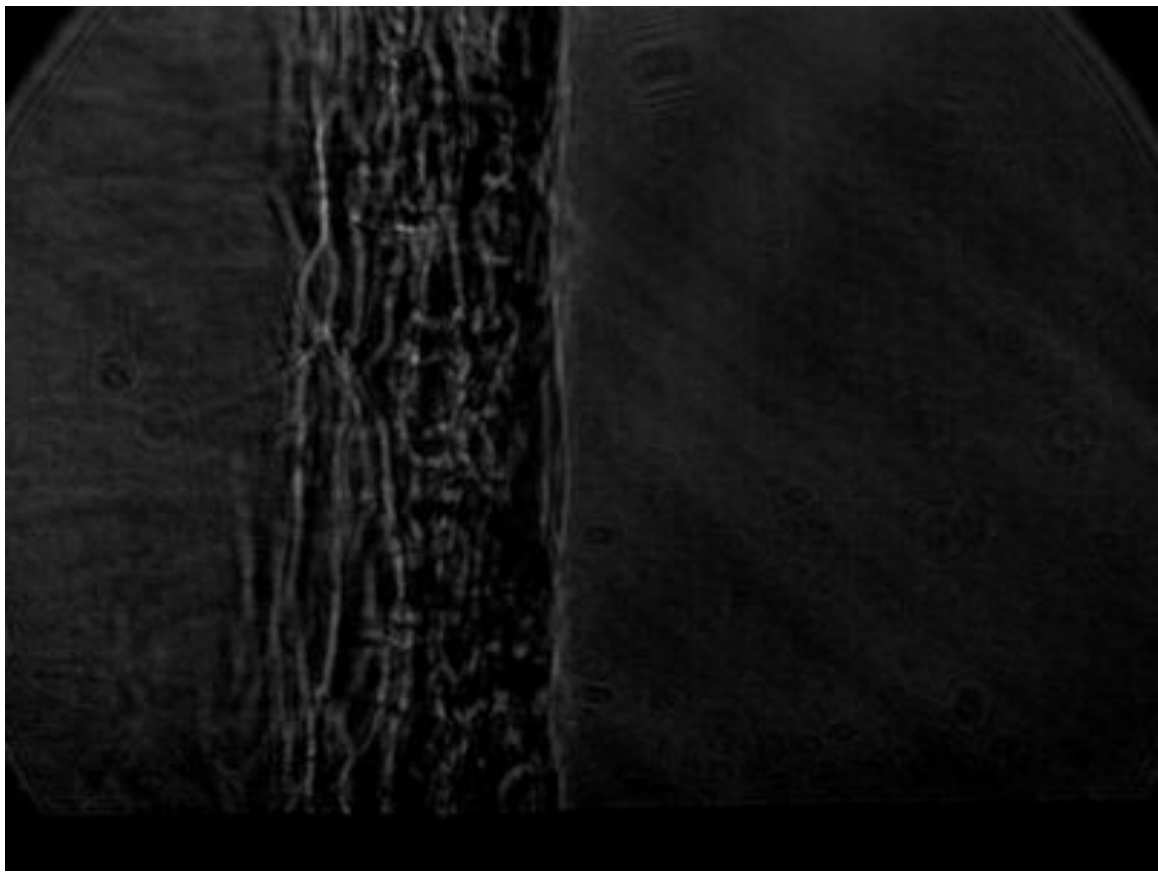


Figure D.23: Unfocused schlieren image of shot 2067. The field of view is approximately 10 mm wide.

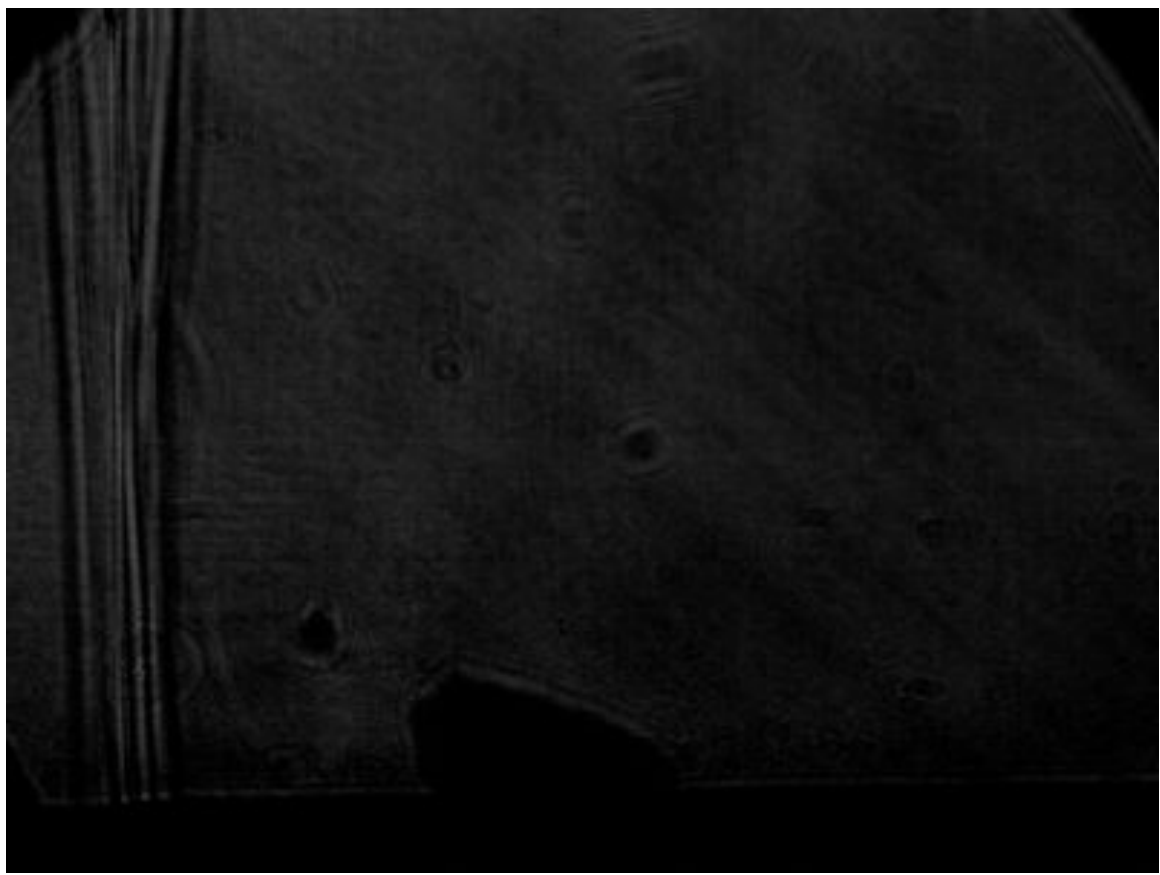


Figure D.24: Unfocused schlieren image of shot 2069. The field of view is approximately 10 mm wide.

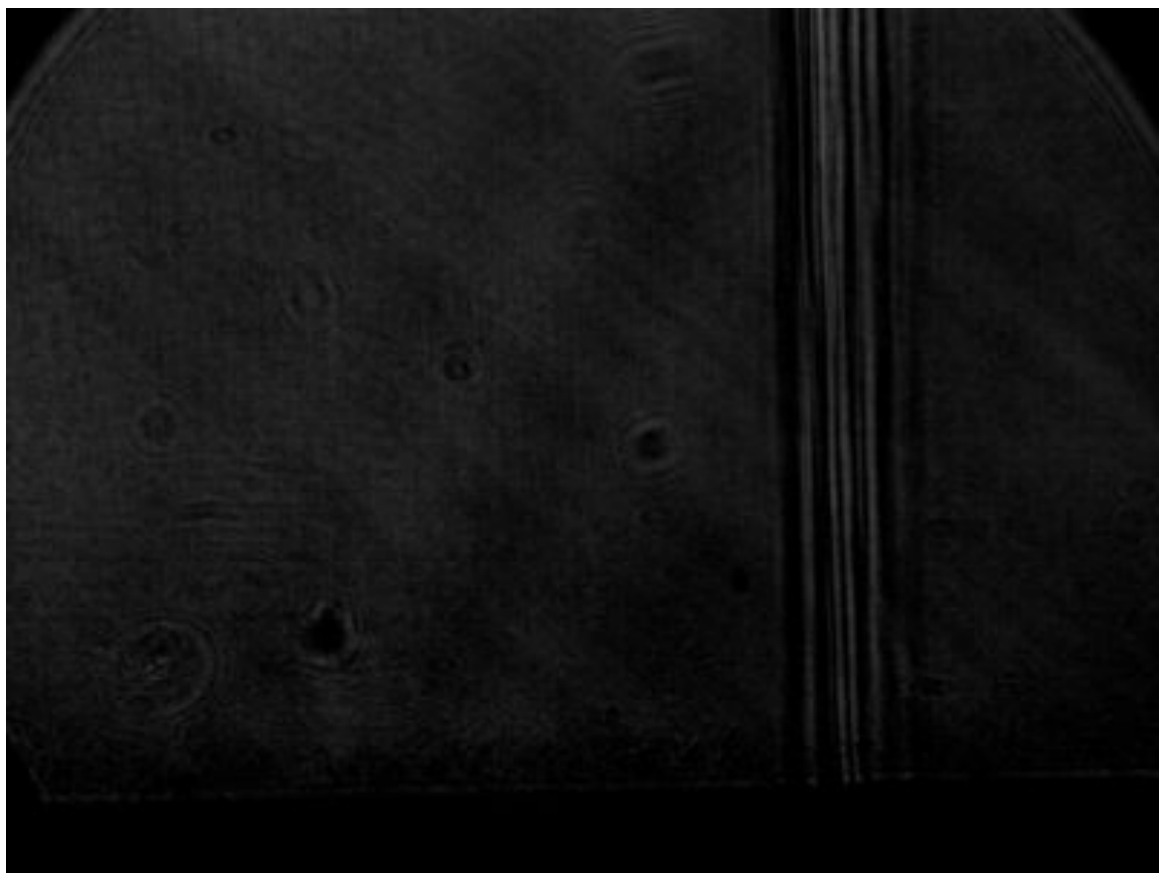


Figure D.25: Unfocused schlieren image of shot 2070. The field of view is approximately 10 mm wide.

### D.1.3 SMART Cavilux

The SMART Cavilux laser, named “Cyclops” in the data files, was demoed for an afternoon to explore if it would be useful for detonation imaging. The laser was similar in capability to the SLD1332V system, but was slightly more user friendly in operation. The laser was run such that it would produce two sets of five 10 ns pulses in conjunction with the Phantom v7.10 camera. For an unknown reason, only four pulses were produced. In practice, it proved less useful than the SLD1332V laser.

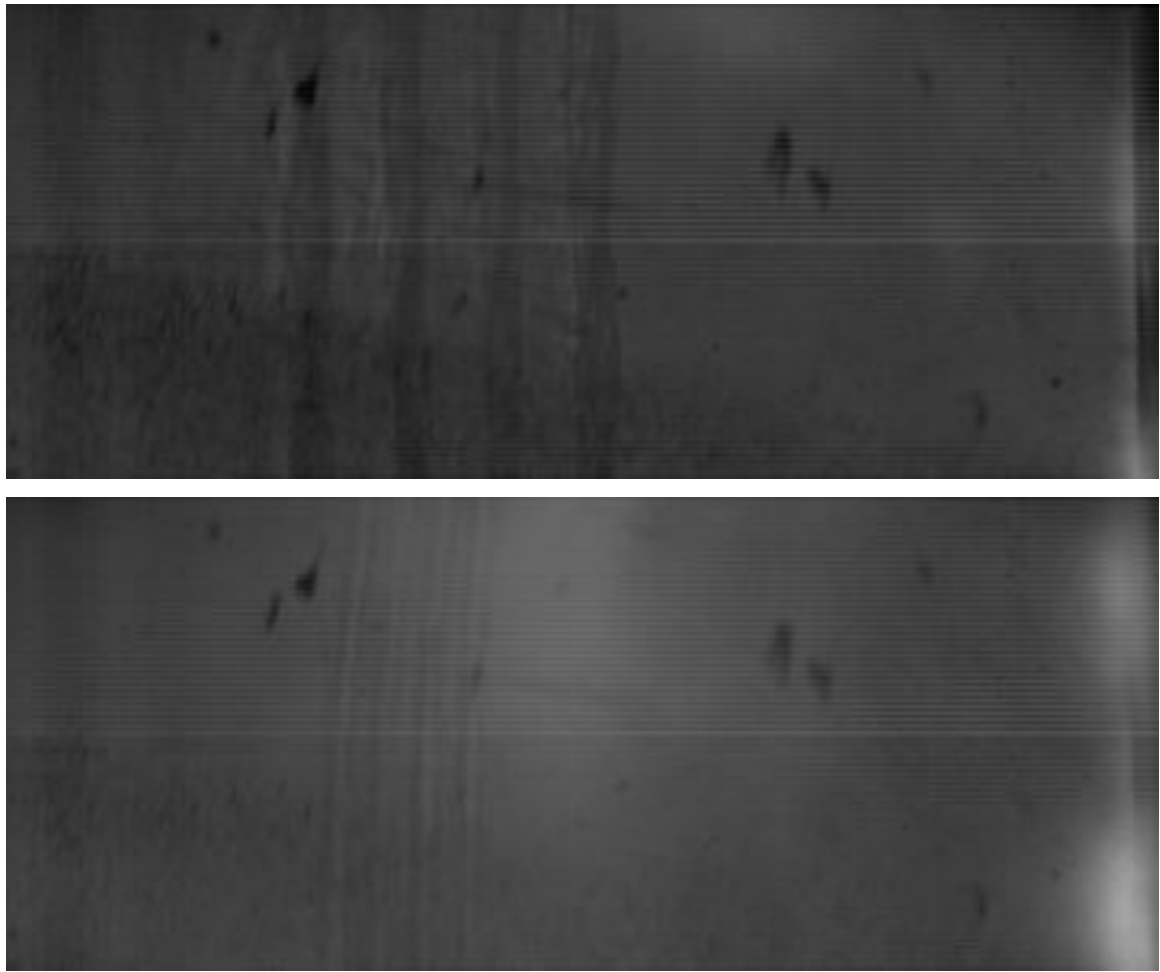


Figure D.26: Unfocused schlieren images of shot 2195. The field of view is approximately 66 mm wide.

#### D.1.4 PL1000DRC

The best images obtained were recorded using a PL1000DRC flash lamp with a SIMD16 Ultra Fast Framing Camera, nicknamed “Sandman.” This allowed for 16 images at essentially arbitrary frame rate and exposure time. The light source was triggered off an upstream pressure gauge (so that it would have ample time to warm up and produce light). The camera, which had a trigger-to-picture delay time of 65 ns, was triggered off of a separate pressure gauge in the field of view. The low trigger-to-picture time meant that most every detonation performed resulted in a picture. The camera produced a 5 V output whenever the camera was recording an image; this signal was fed into the data acquisition system to relate the pressure signals and images. A USAF 1951 target was used to quantify the resolving power of this system to be 223  $\mu\text{m}$  horizontally and 125  $\mu\text{m}$  vertically as measured with the target at the center of the test section.

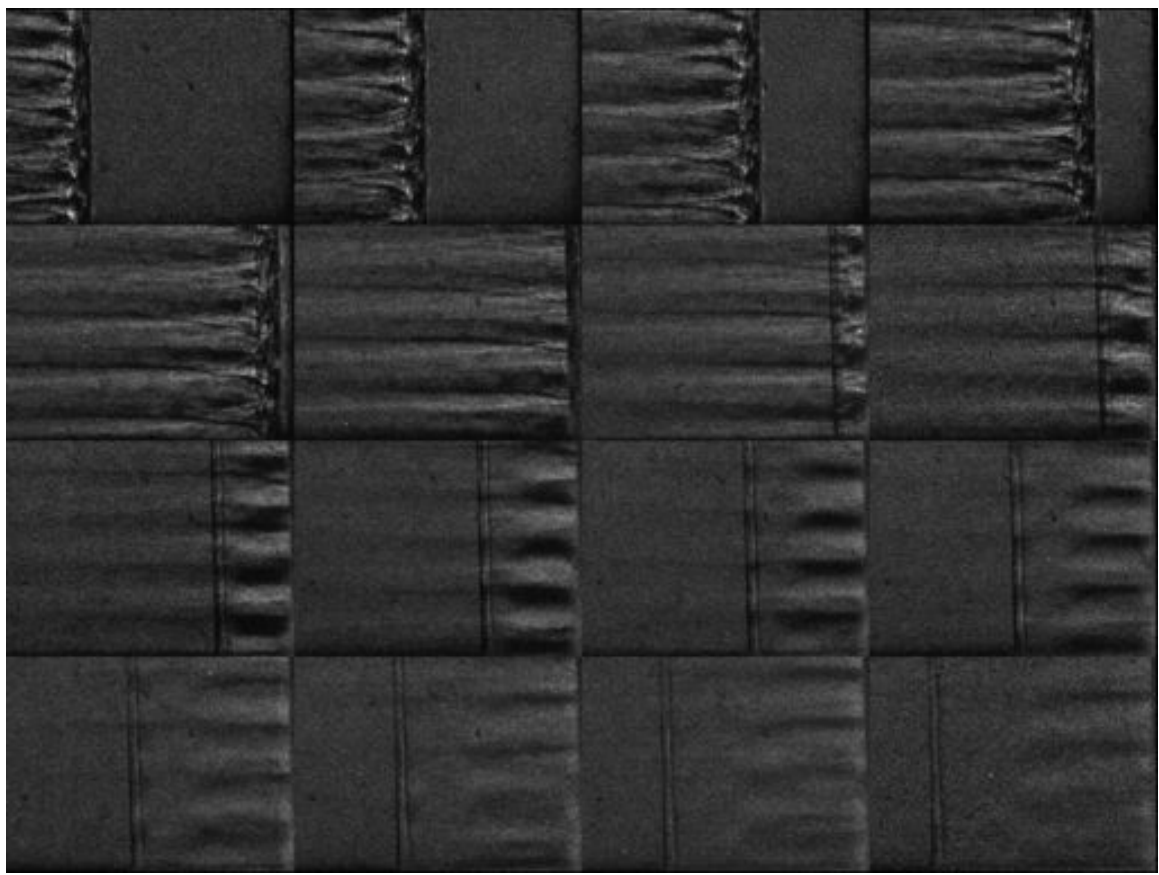


Figure D.27: Unfocused schlieren image of shot 2161. The field of view is approximately 30 mm wide.

## D.2 Focused Schlieren Systems

Design considerations for a focused schlieren system as well as specifics for each focused visualization system employed are given below organized by the light source used. A list of focal lengths and magnifications are included in table D.2, although these sometimes changed between images and thus the scale for each individual picture should be checked. Run conditions are given in appendix C.

Table D.2: Details of focused schlieren configurations.

#	Light source	Camera	$b$ (mm)	$f_1$ (mm)	$f_2$ (mm)	$M$	$t_{exp}$ (ns)
5	HardSoft IL-106G	Nikon D200	50	500	750	1	250
6	EverGreen70	PCO.2000	25	500	1000	1	10

### D.2.1 Focused Schlieren Design Considerations

Building a focused schlieren system requires more care than a similar unfocused system. Reducing the depth of focus (and thereby increasing the focusing effect) is achieved by increasing the camera aperture angle,  $\alpha$ . This was accomplished by increasing the height of the schlieren source,  $b$ , as illustrated in figure D.28. The aperture angle of the source,  $\alpha_s$ , (which may be larger than the camera aperture angle for reasons discussed later) may be calculated as follows:

$$\tan \frac{\alpha_s}{2} = \frac{b}{2f_1} \quad (\text{D.1})$$

$$\Rightarrow \alpha_s \approx \frac{b}{f_1} \quad (\text{D.2})$$

where  $f_1$  is the focal length of the collimating optical element and the small angle approximation has been applied. However, this source aperture angle may be reduced if the schlieren object is too far from the focusing mirror. We observe that, in order for a given source aperture angle to have the optimal focusing effect, the maximum distance between the collimating optical element and the schlieren object,  $d_{1s,max}$ , is a function of  $f_1$ ,  $\phi_1$ , and  $b$ , where  $\phi_1$  is the diameter of the collimating element.

$$\tan \frac{\alpha_s}{2} = \frac{\phi_1}{2d_{1s,max}} \quad (\text{D.3})$$

$$\Rightarrow d_{1s,max} = \frac{f_1\phi_1}{b} \quad (\text{D.4})$$

If  $d_{1s} > d_{1s,max}$ , an effective aperture angle for the collimating optical element is determined by

$$\alpha_1 = \frac{\phi_1}{d_{1s}}. \quad (\text{D.5})$$

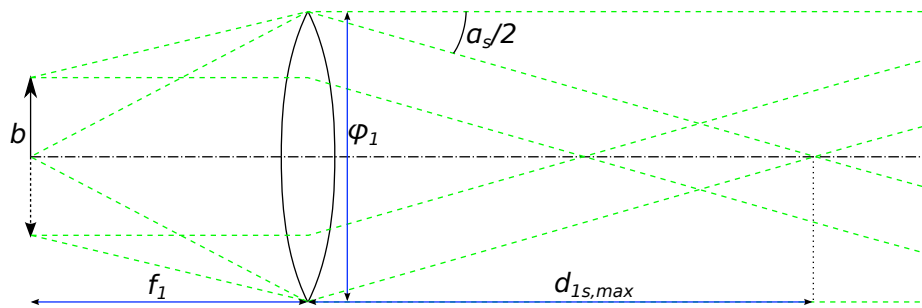


Figure D.28: The light source side of an extended schlieren system.

Figure D.29 depicts the camera side of the focused schlieren system. Similarly to the case of the schlieren object being too far from the collimating optical element, if the distance between the schlieren object and the focusing element,  $d_{s2}$ , is too large the light may not impinge upon the focusing optical element. In this case there is the

limiting distance,  $d_{s2,max}$ , determined by

$$d_{s2,max} = \frac{\phi_2}{\alpha} \quad (\text{D.6})$$

$$= \frac{f_1 \phi_2}{b} \quad (\text{D.7})$$

in the case that this distance is exceeded, there is an effective aperture angle,  $\alpha_2$ , determined by

$$\alpha_2 = \frac{\phi_2}{d_{s2}} \quad (\text{D.8})$$

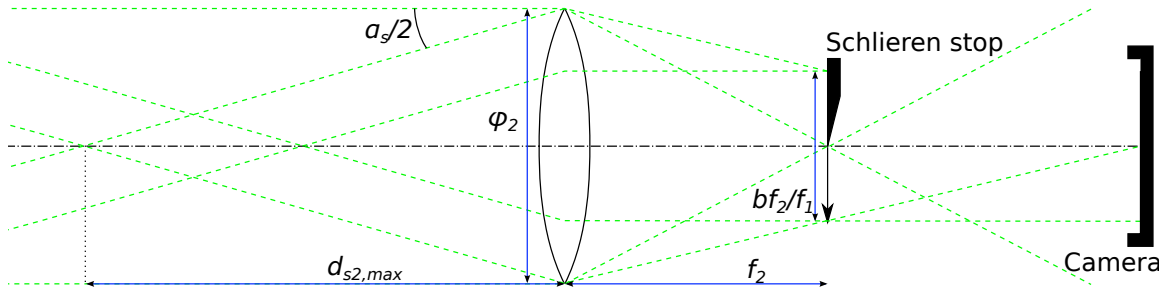


Figure D.29: The camera side of an extended schlieren system.

The true aperture angle,  $\alpha$ , used to determine the depth of focus is the minimum of  $\alpha_s$ ,  $\alpha_1$ , and  $\alpha_2$  given in equations (D.2), (D.5), and (D.8). The sensitivity of the schlieren system increases for increased  $d_{s2}$  and thus an optimal sensitivity for a given aperture angle may be determined:

$$d_{s2} = d_{s2,max} = \frac{\phi_1}{\alpha} = \frac{f_1 \phi_2}{b} \quad (\text{D.9})$$

as illustrated in figure D.30; this choice also limits light loss. In practice, this distance was often exceeded to allow for greater schlieren sensitivity and to limit the effect of the test section floor discussed next.

As illustrated in figure D.31, increasing the aperture angle also results in a reduced illumination near the test section walls. For a given aperture angle and distance from

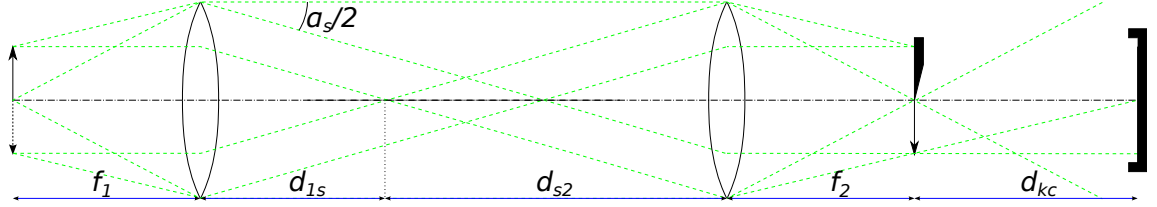


Figure D.30: An extended source schlieren system designed to obtain maximum sensitivity and depth of focus.

the side-wall,  $y$ , we can determine the fraction of light,  $\xi$ , transmitted through the test section of width  $w$  without impinging upon the wall from the equation

$$\xi = \frac{A'}{A} \quad (\text{D.10})$$

$$A = \pi r_s^2 \quad (\text{D.11})$$

$$r_s = \frac{\alpha w}{2} \quad (\text{D.12})$$

$$A' = \begin{cases} A & \text{if } y \geq r_s \\ A - 2r_s^2 \cos^{-1} \left( \frac{y}{r_s} \right) + 2y\sqrt{r_s^2 - y^2} & \text{if } y < r_s \end{cases} \quad (\text{D.13})$$

or defining  $y'$  as

$$y' = \frac{y}{r_s} \quad (\text{D.14})$$

we have

$$\xi = \begin{cases} 1 & \text{if } y' \geq 1 \\ 1 - \frac{2}{\pi} \cos^{-1} y' + \frac{2y'}{\pi} \sqrt{1 - y'^2} & \text{if } y' < 1. \end{cases} \quad (\text{D.15})$$

The above analysis assumed only one focusing element was employed (such as was the case in the current investigation). Adding further elements requires repeated consideration of each element to determine the limiting camera aperture angle.

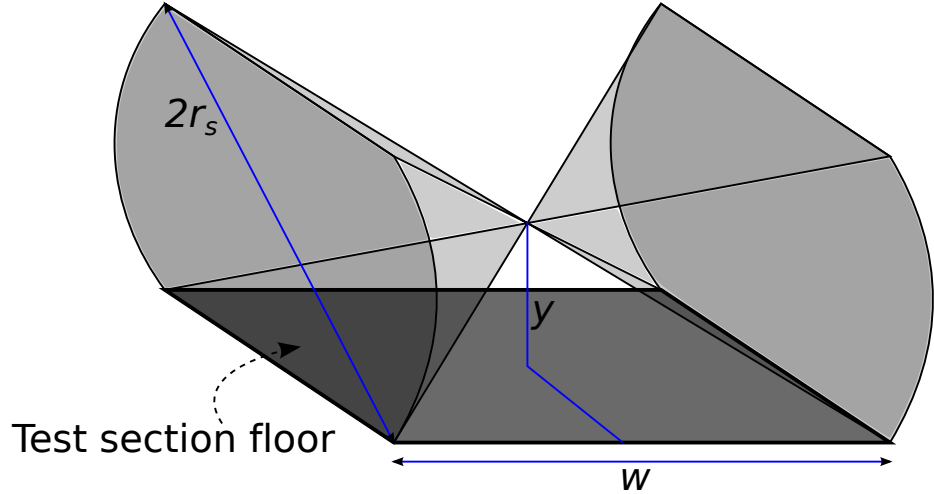


Figure D.31: The effect of the test section floor on the light paths.

### D.2.2 HardSoft IL

This was a green LED light source, named the “Green Lantern” in data files, that was capable of producing light pulses down to 250 ns in duration. It was paired with the Nikon D200 camera discussed in section D.1.1. This source was ideal for use as a focused light source because of the shape of the LED array (which was 50 mm tall), and its ability to be pulsed. However, the light produced was not of short enough duration to adequately freeze the detonation, and the wavelength of the light was  $\pm \sim 50$  nm making it impossible to adequately filter the light. For these reasons, this source was only used to visualize shock waves. The camera was triggered off of the exploding wire and the LED source triggered off of an appropriate pressure gauge. This visualization system was assembled and tested with the help of Jeff Odell.



Figure D.32: Focused schlieren image of shot 2042. The field of view is approximately 20 mm wide.



Figure D.33: Focused schlieren image of shot 2044. The field of view is approximately 20 mm wide.

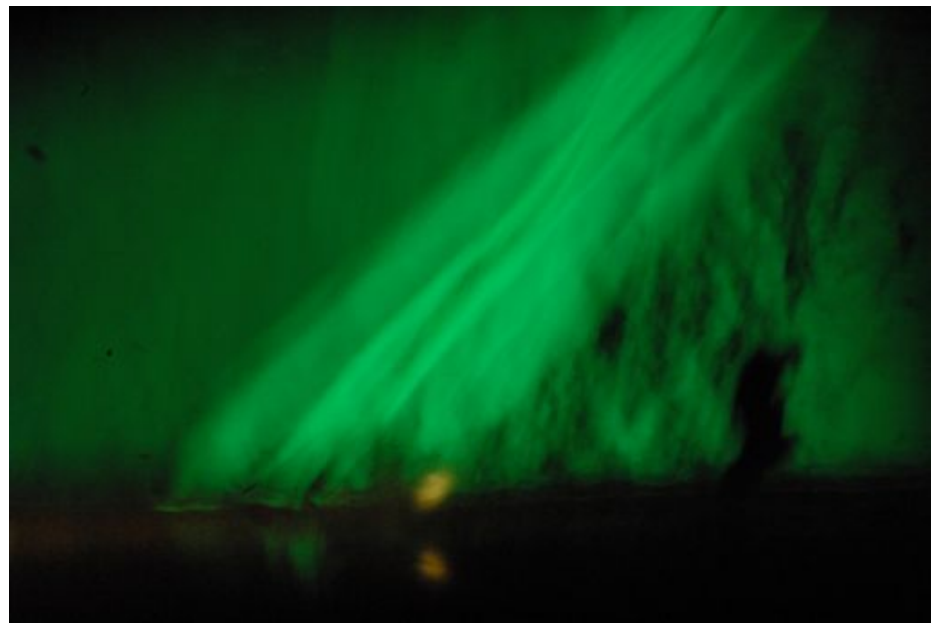


Figure D.34: Focused schlieren image of shot 2045. The field of view is approximately 20 mm wide.



Figure D.35: Focused schlieren image of shot 2055. The field of view is approximately 20 mm wide.

### D.2.3 EverGreen70

The EverGreen70 Q-switched pulsed PIV laser combined with the 4 megapixel 14 bit PCO.2000 camera produced some exceptional images. The laser emitted two 10 ns duration laser pulses at 530 nm wavelength with 70 mJ pulse energy. An extended source was created by expanding the beam with a cylindrical lens into a sheet that impinged on either a white screen or an engineered optical diffuser. The diffuser had a diameter of 25.4 mm and a diffusion angle of 20° to create a line of light that functioned as the schlieren source. The EverGreen70 required a delay of 135  $\mu$ s between trigger and light emission. This made it difficult to time the images and frequently repeated tests were required to get a successful image. A USAF 1951 target was used to determine that this system had a horizontal resolution of 63  $\mu$ m and a vertical resolution of 44  $\mu$ m in the center of the test section and less than 250  $\mu$ m at the windows.

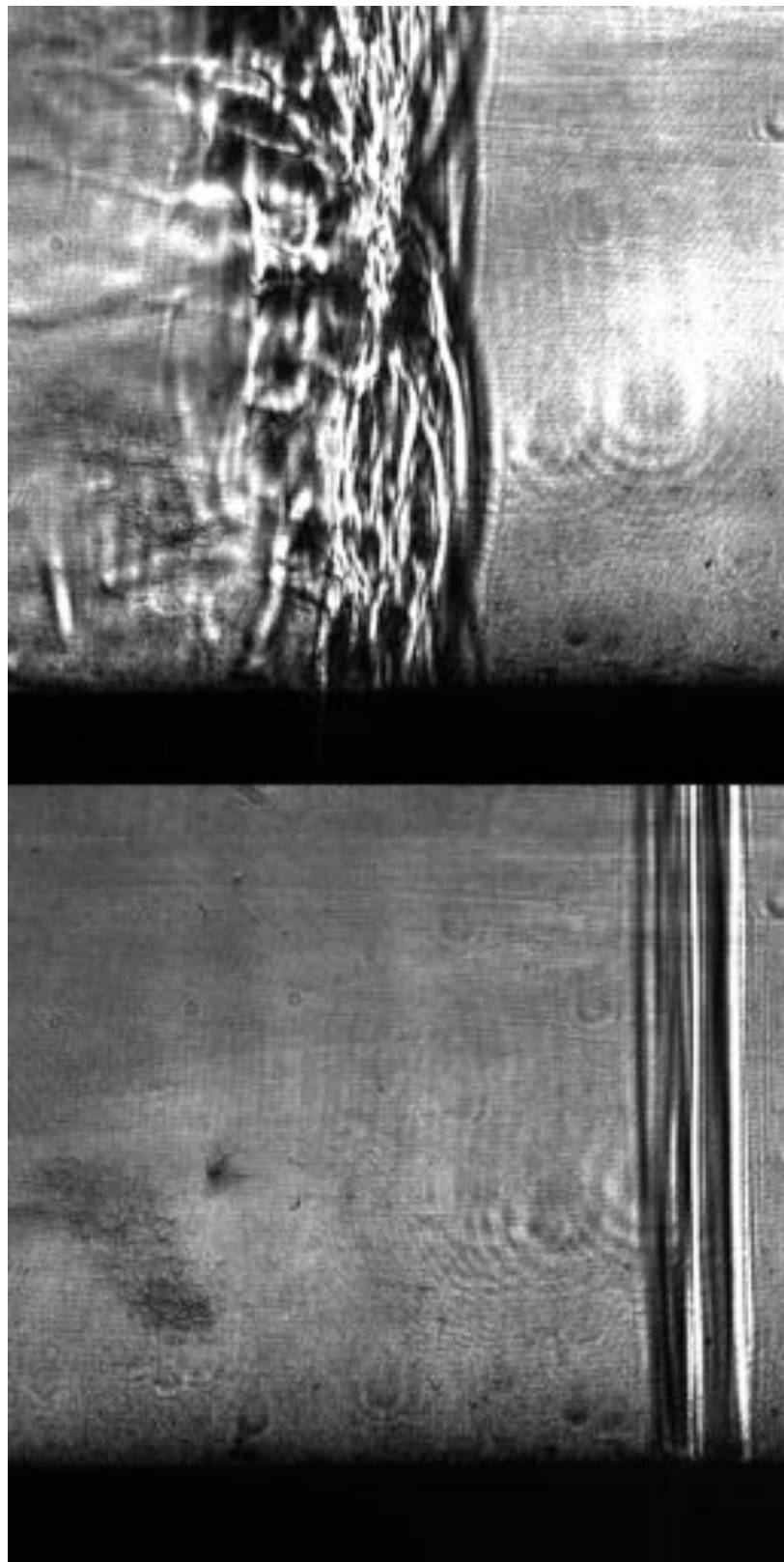


Figure D.36: Focused schlieren image of shot 2088. The field of view is approximately 14 mm wide.

# Appendix E

## GDT Pressure and Heat-Flux Data

A nearly complete set of data for the GDT experiments is included here. The data are organized by mixture and fill pressure. Pressure, heat-flux, and image data are included where appropriate. Signals that were dominated by noise and images that were indecipherable are not included.

### E.1 Hydrogen-Oxygen

Figures [E.1–E.51](#).

### E.2 Hydrogen-Oxygen-Argon

Figures [E.56–E.121](#).

### E.3 Hydrogen-Oxygen-Nitrogen

Figures [E.124–E.132](#).

### E.4 Hydrogen-Oxygen-Carbon Dioxide

Figures [E.136–E.147](#).

## E.5 Hydrogen-Nitrous Oxide

Figure E.151.

## E.6 Ethylene-Oxygen

Figures E.154–E.179.

## E.7 Shock Waves

Figures E.183–E.189.

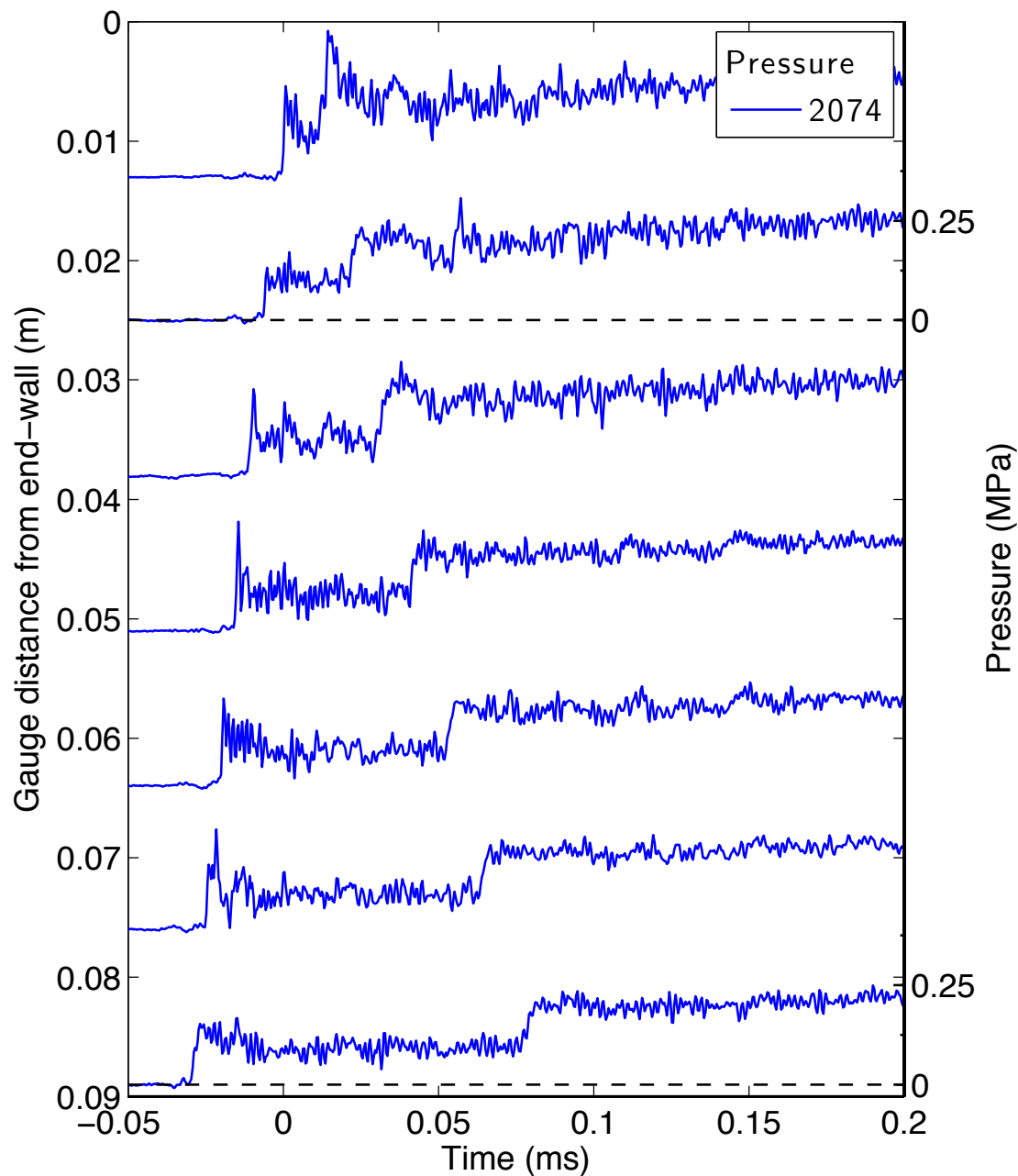


Figure E.1: Pressure traces for a detonation in stoichiometric hydrogen-oxygen at fill pressure 5 kPa, part 1.

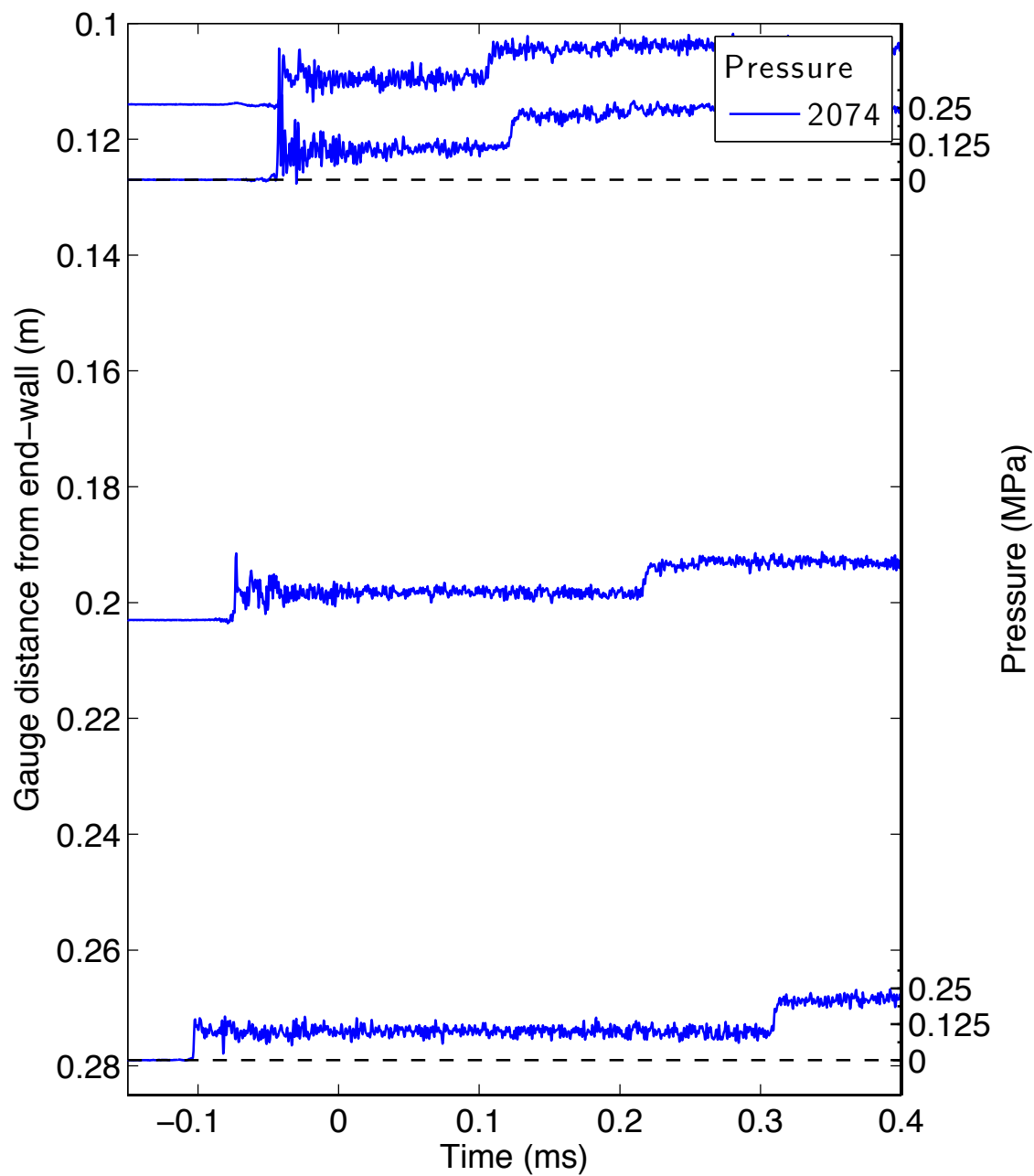


Figure E.2: Pressure traces for a detonation in stoichiometric hydrogen-oxygen at fill pressure 5 kPa, part 2.

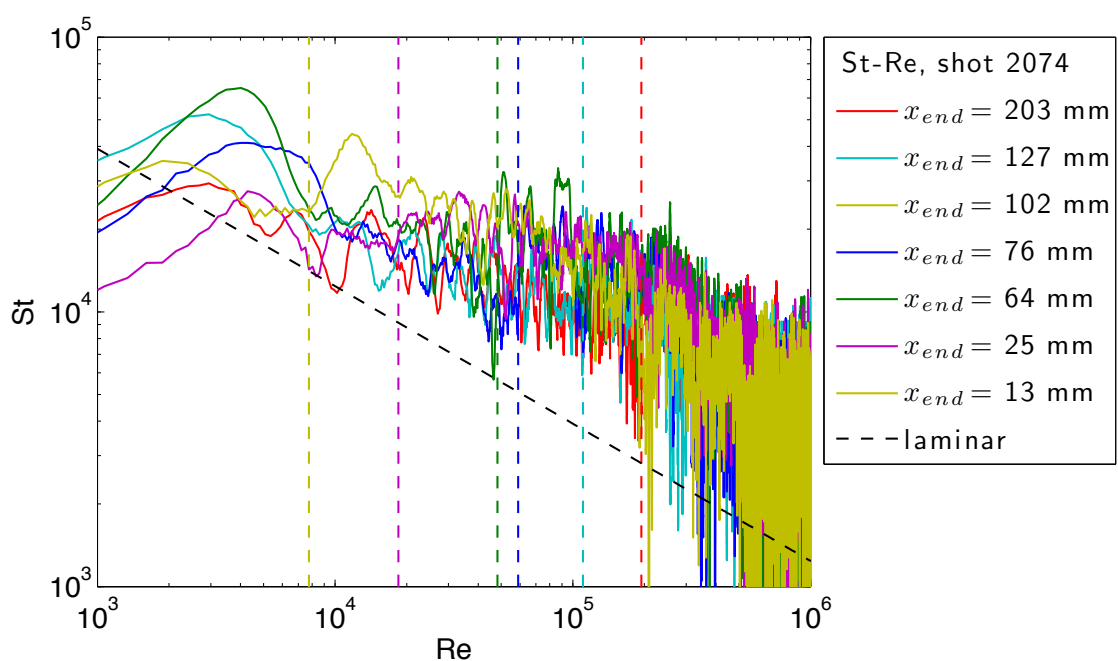


Figure E.3: Stanton-Reynolds number traces from shot 2074, a detonation in stoichiometric hydrogen-oxygen at fill pressure 5 kPa. The dashed vertical lines represent the arrival of the reflected shock wave.

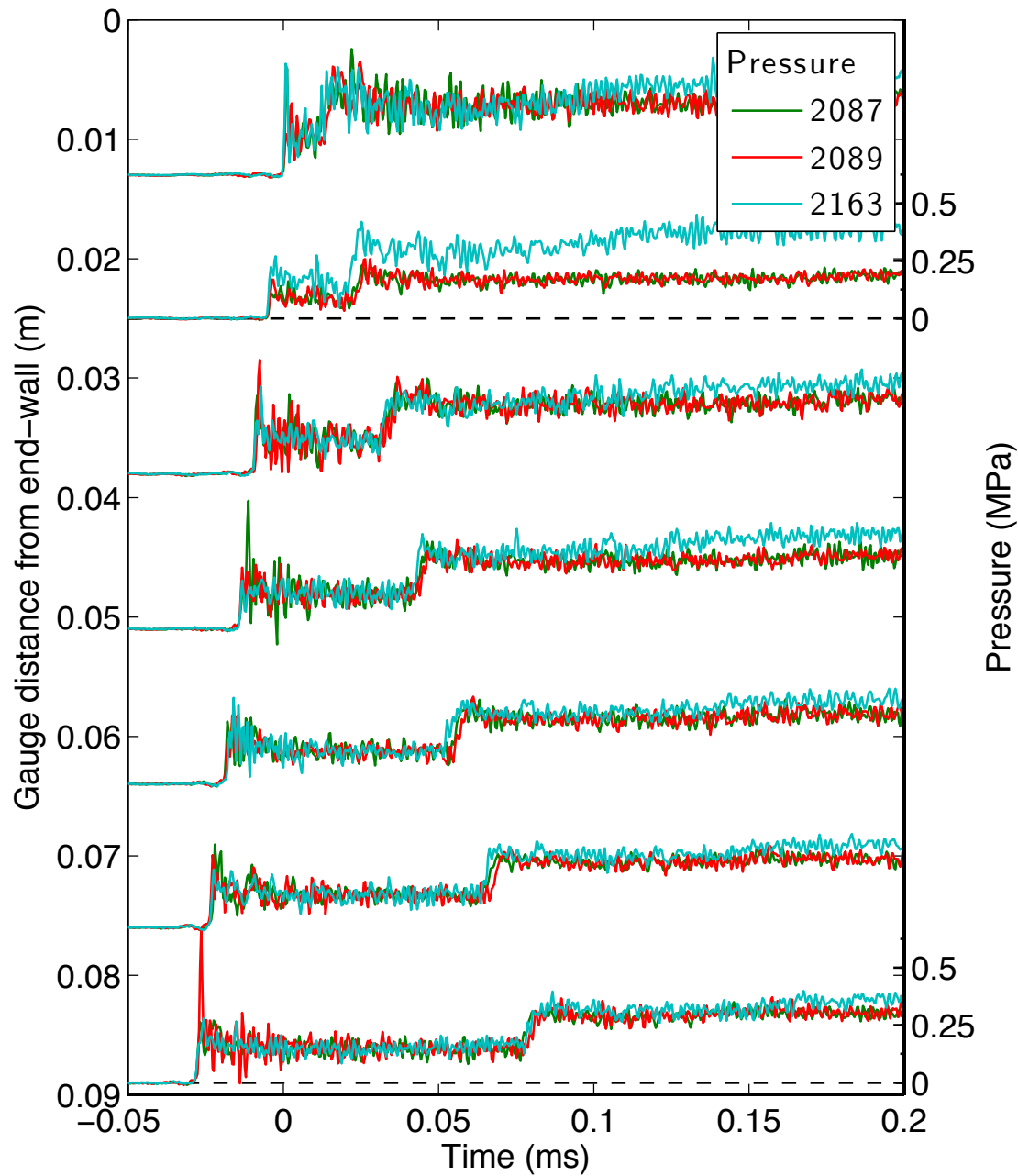


Figure E.4: Pressure traces for a detonation in stoichiometric hydrogen-oxygen at fill pressure 10 kPa, part 1.

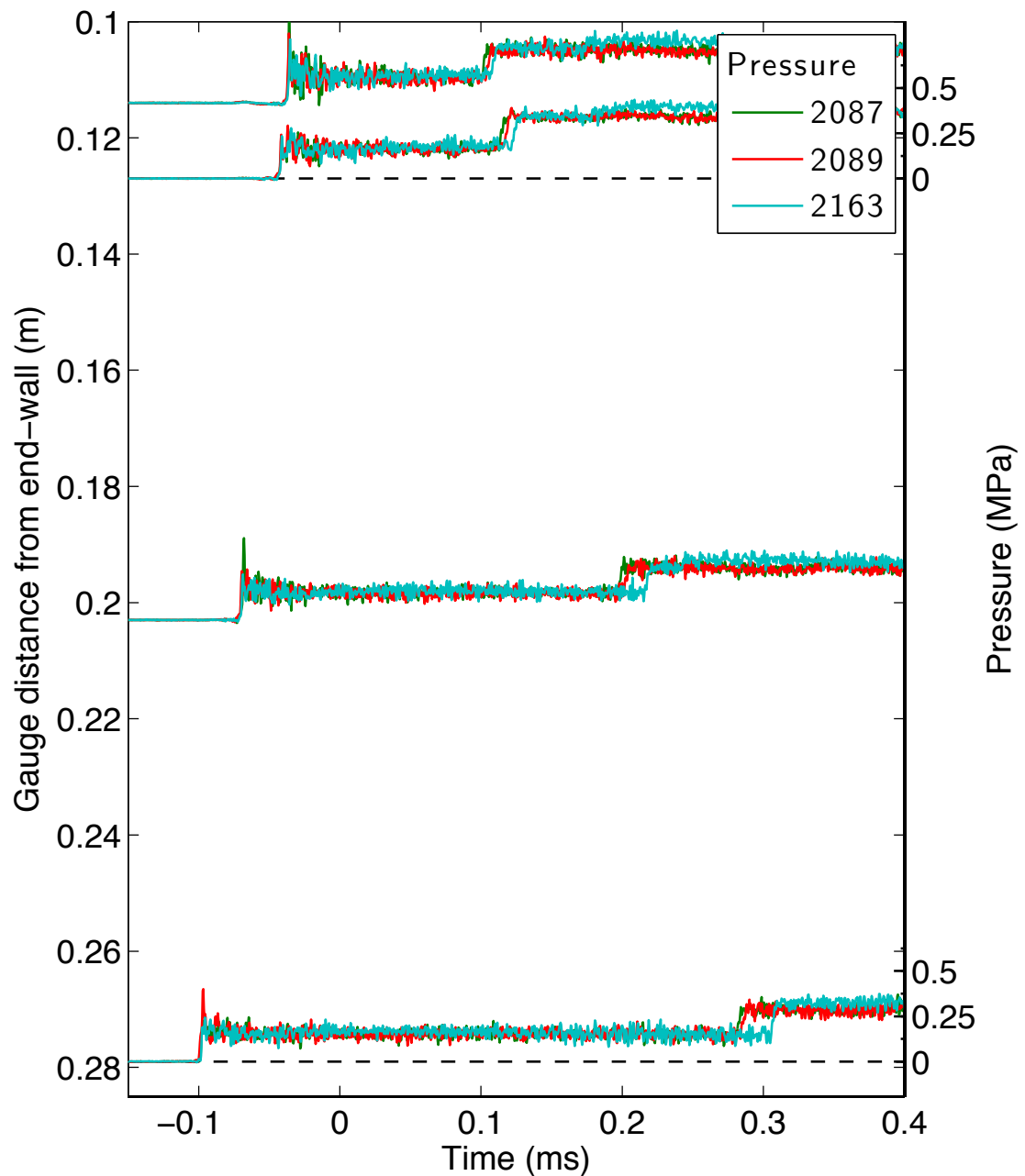


Figure E.5: Pressure traces for a detonation in stoichiometric hydrogen-oxygen at fill pressure 10 kPa, part 2.

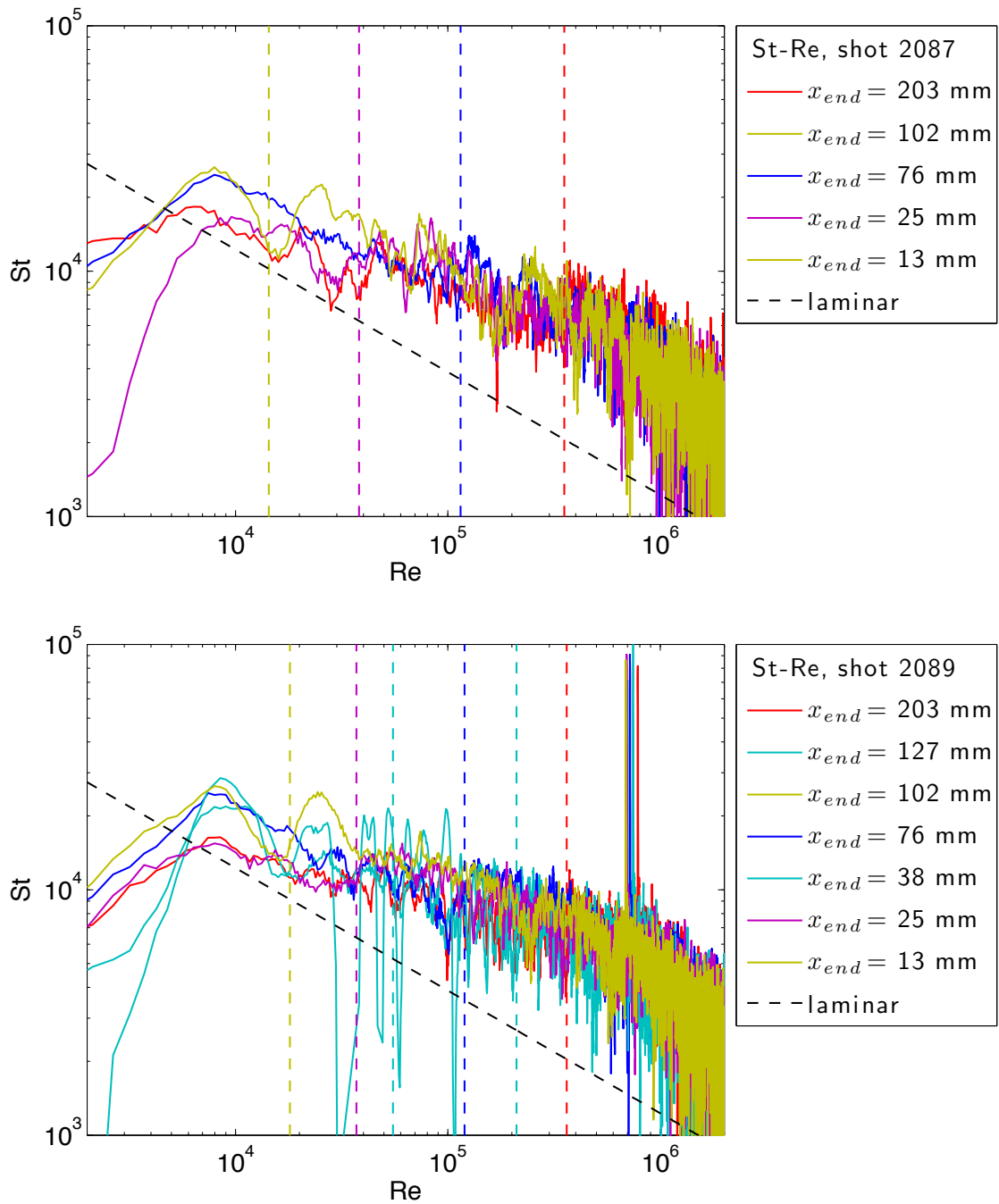


Figure E.6: Stanton-Reynolds number traces from shot 2089, a detonation in stoichiometric hydrogen-oxygen at fill pressure 10 kPa. The dashed vertical lines represent the arrival of the reflected shock wave.

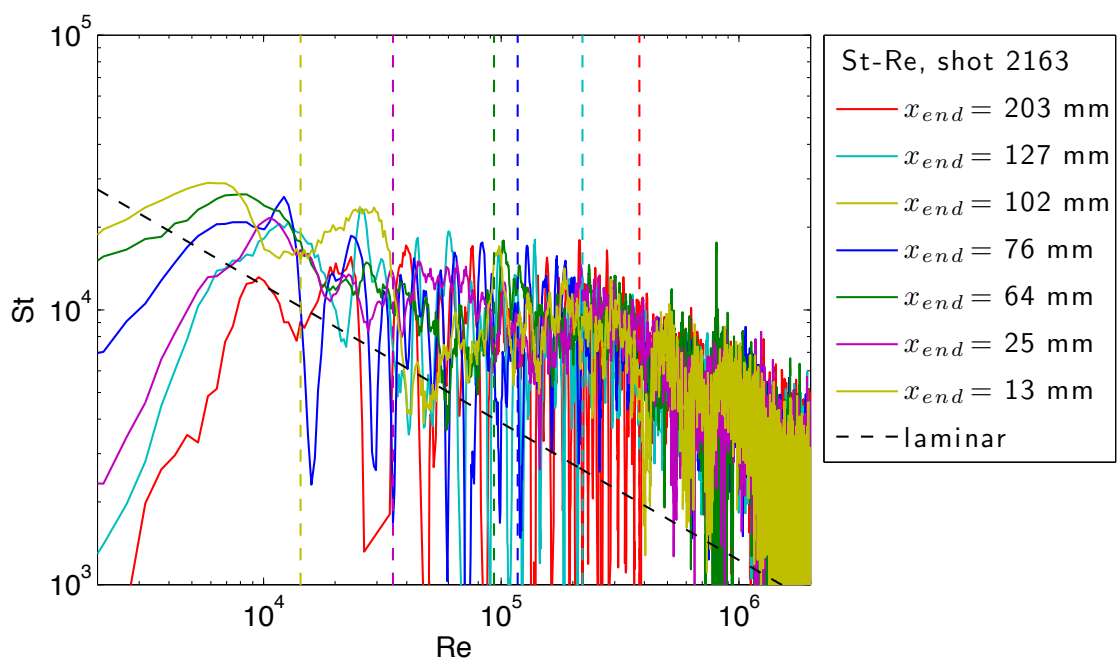


Figure E.7: Stanton-Reynolds number traces from shot 2163, a detonation in stoichiometric hydrogen-oxygen at fill pressure 10 kPa. The dashed vertical lines represent the arrival of the reflected shock wave.

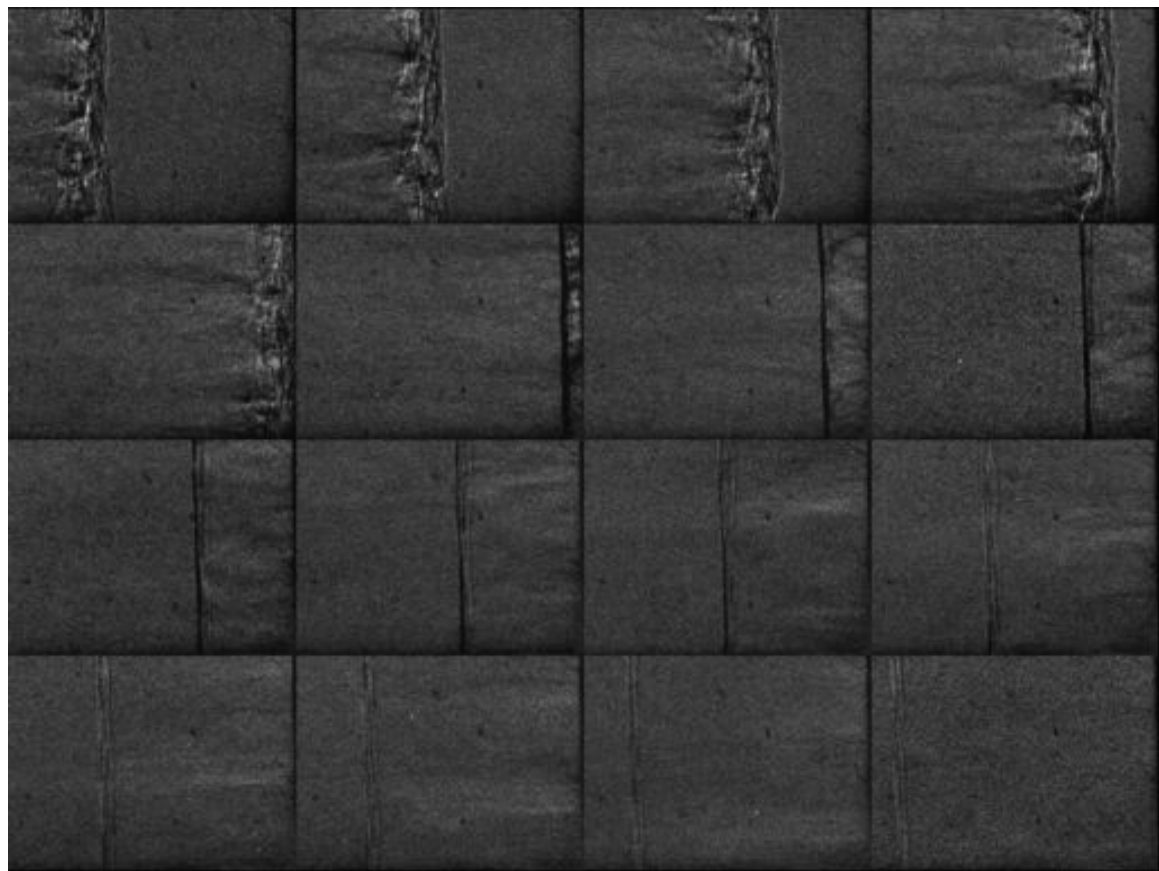


Figure E.8: Unfocused schlieren image of shot 2163. The field of view is approximately 30 mm wide.

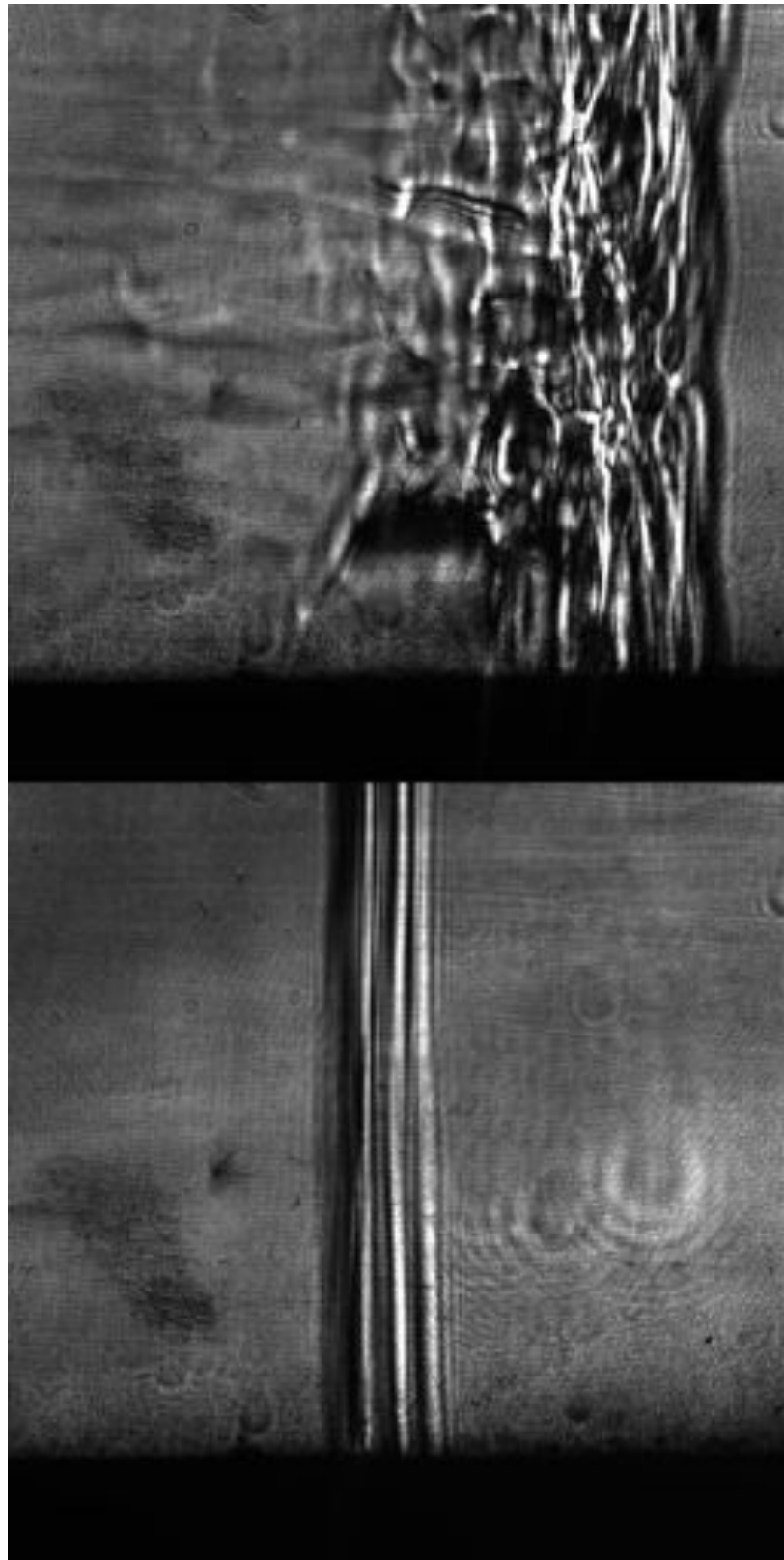


Figure E.9: Focused schlieren image of shot 2089. The field of view is approximately 14 mm wide.

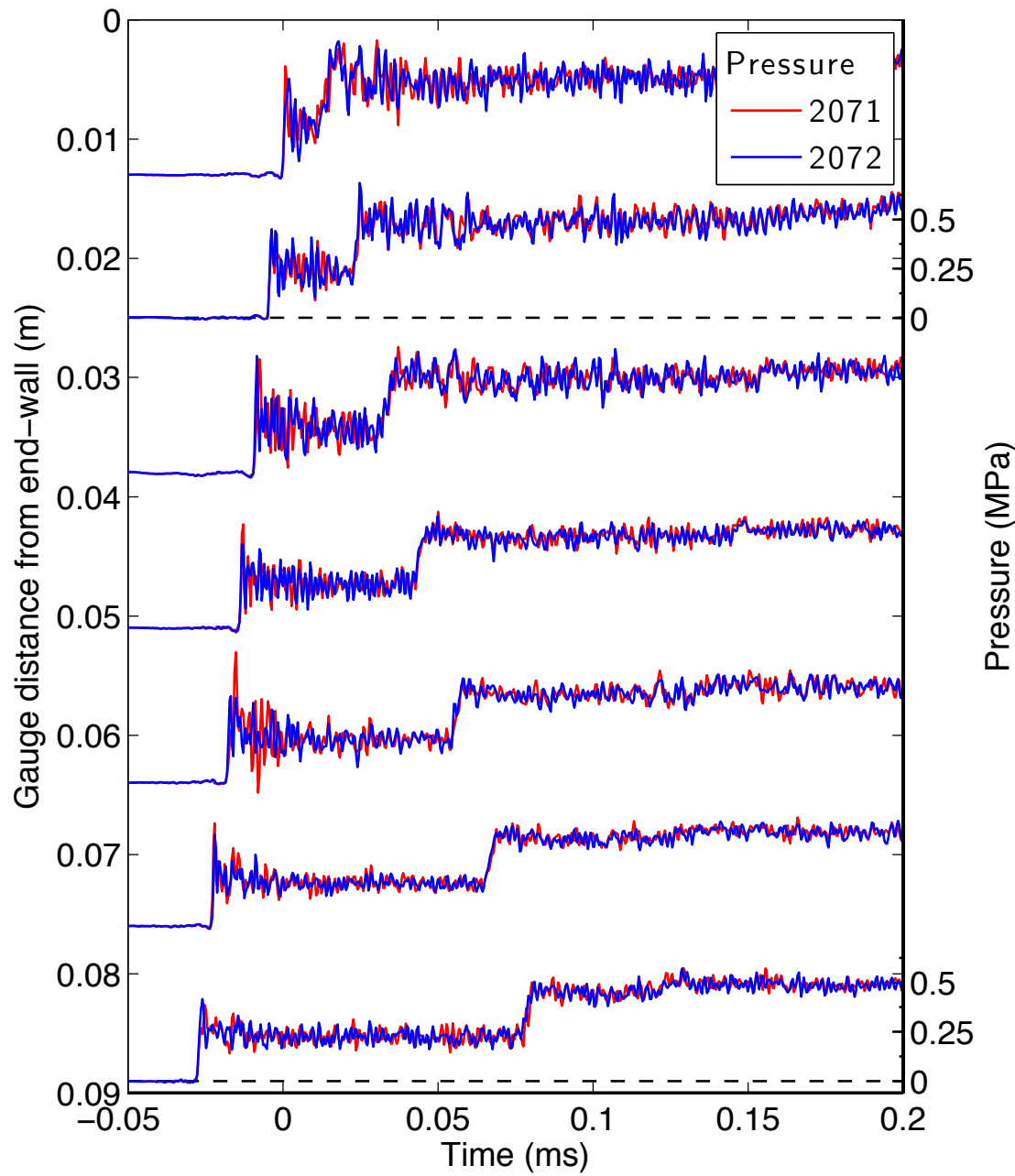


Figure E.10: Pressure traces for a detonation in stoichiometric hydrogen-oxygen at fill pressure 15 kPa, part 1.

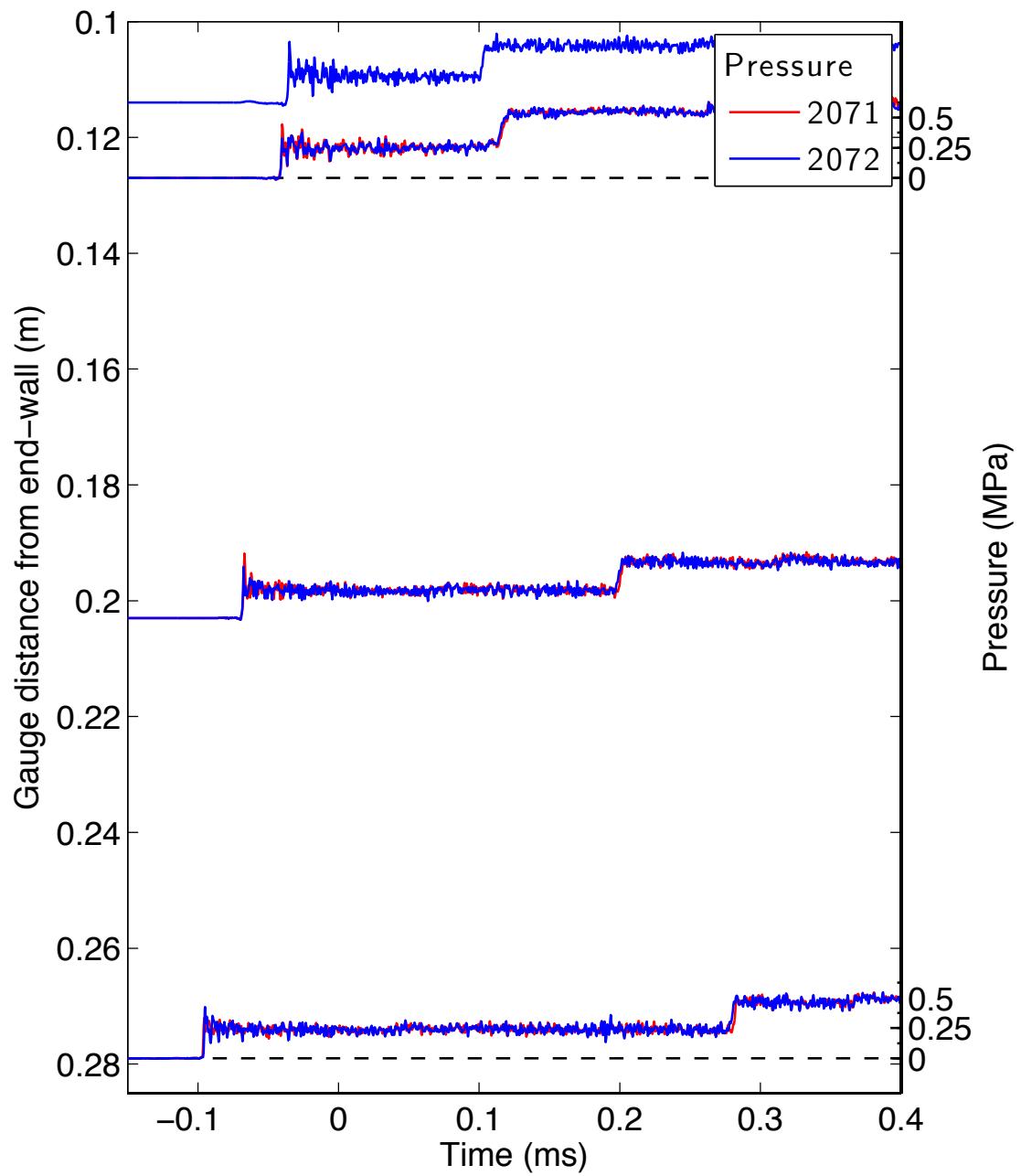


Figure E.11: Pressure traces for a detonation in stoichiometric hydrogen-oxygen at fill pressure 15 kPa, part 2.

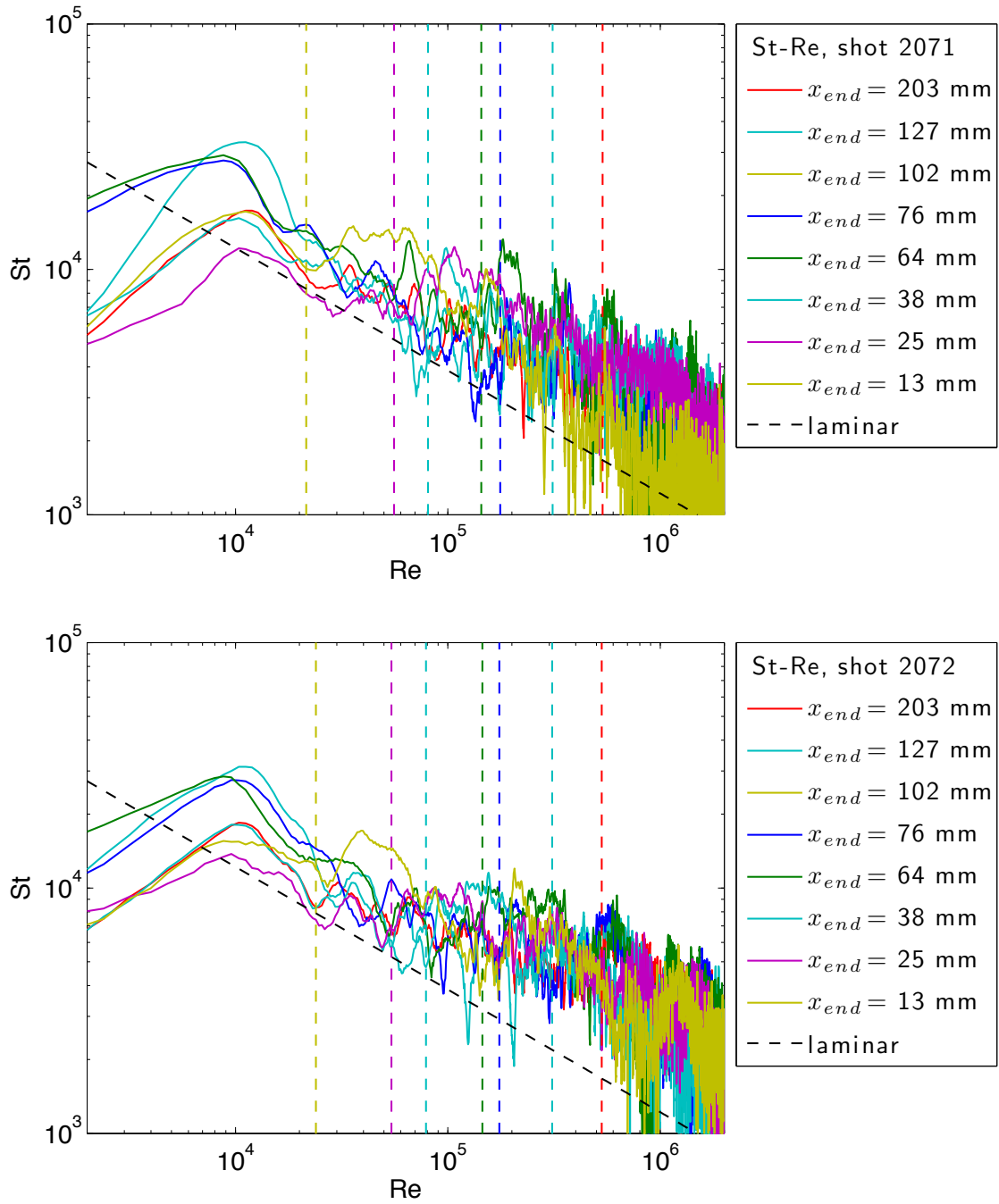


Figure E.12: Stanton-Reynolds number traces from shot 2072, a detonation in stoichiometric hydrogen-oxygen at fill pressure 15 kPa. The dashed vertical lines represent the arrival of the reflected shock wave.

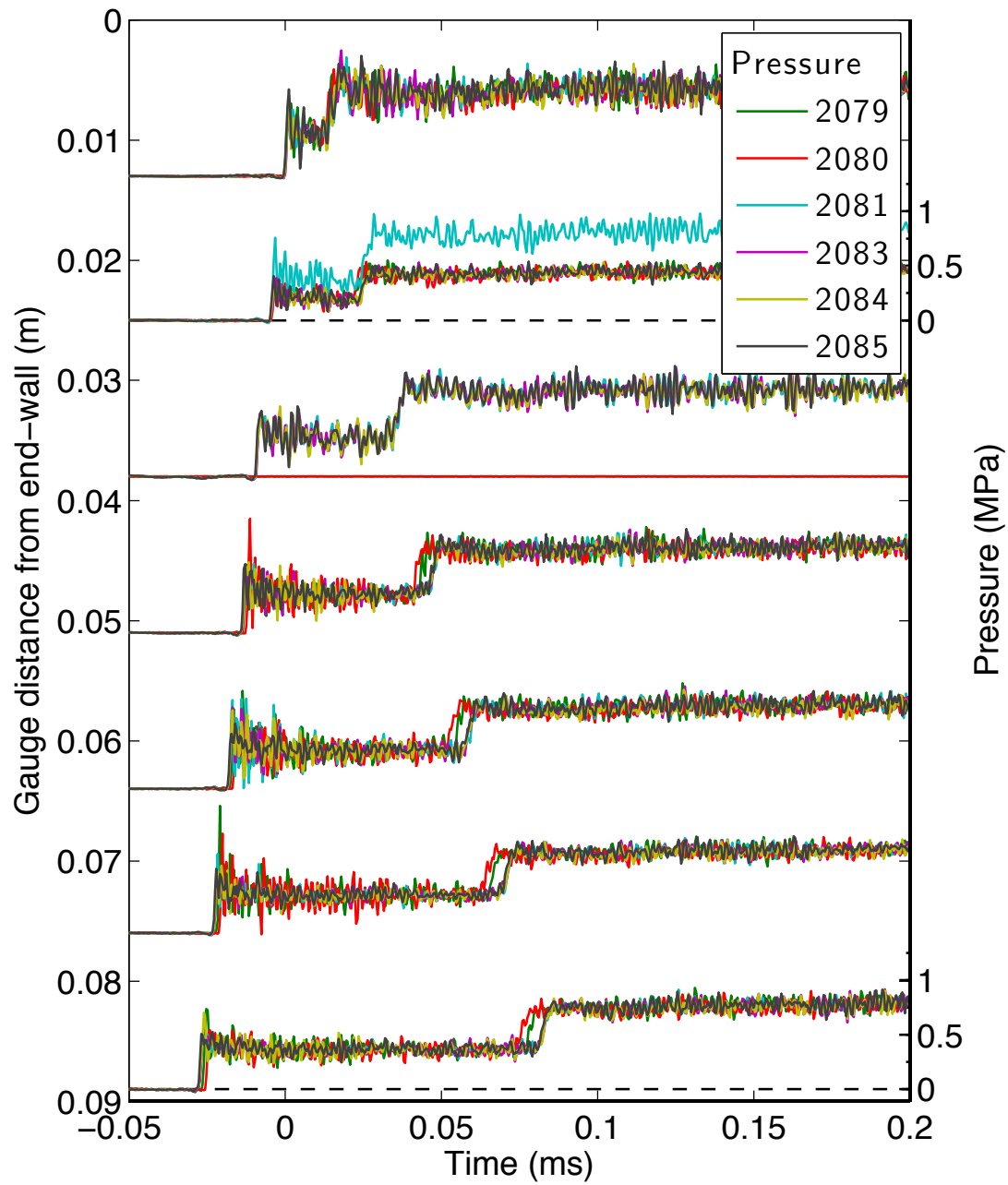


Figure E.13: Pressure traces for a detonation in stoichiometric hydrogen-oxygen at fill pressure 25 kPa, part 1.

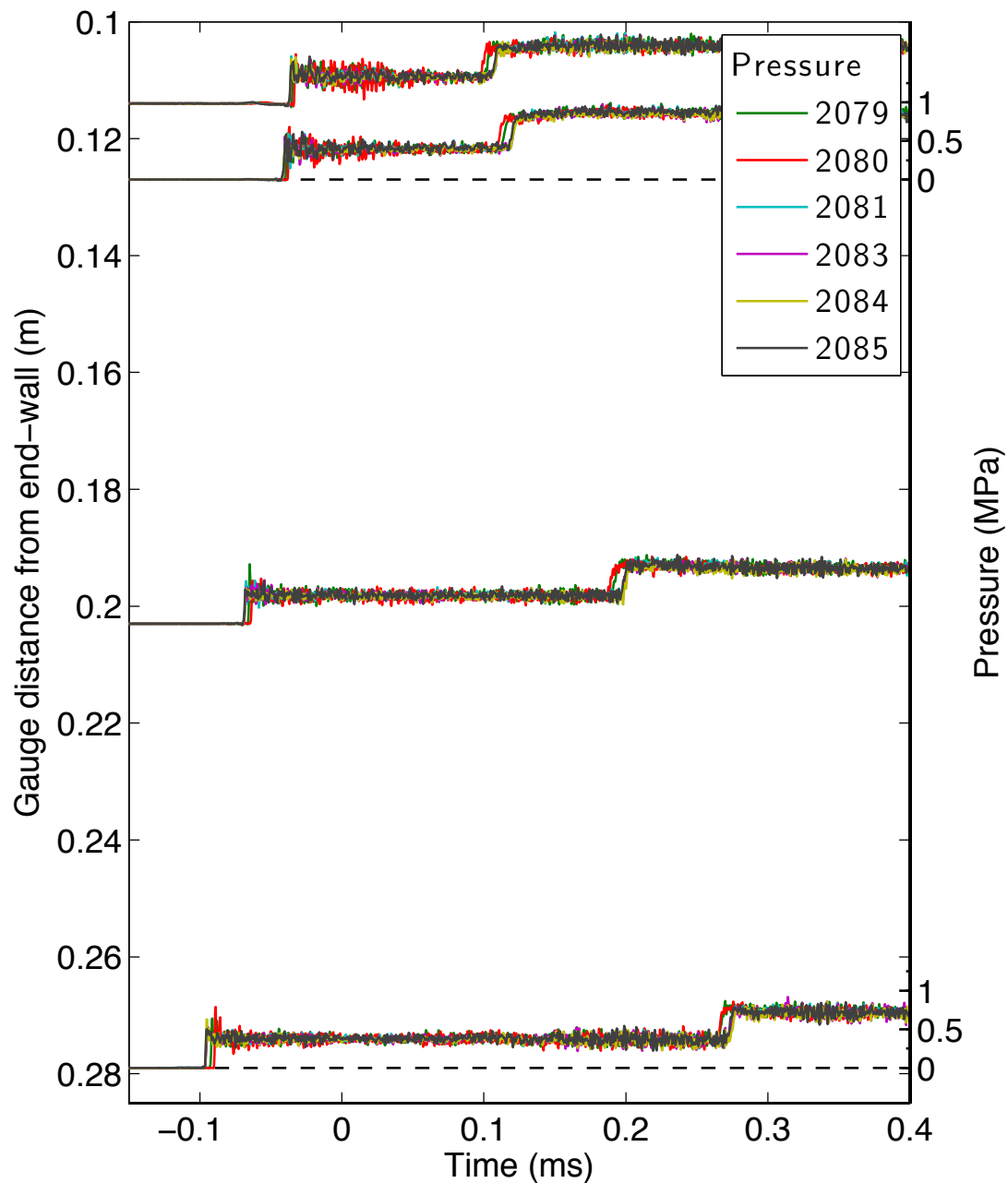


Figure E.14: Pressure traces for a detonation in stoichiometric hydrogen-oxygen at fill pressure 25 kPa, part 2.

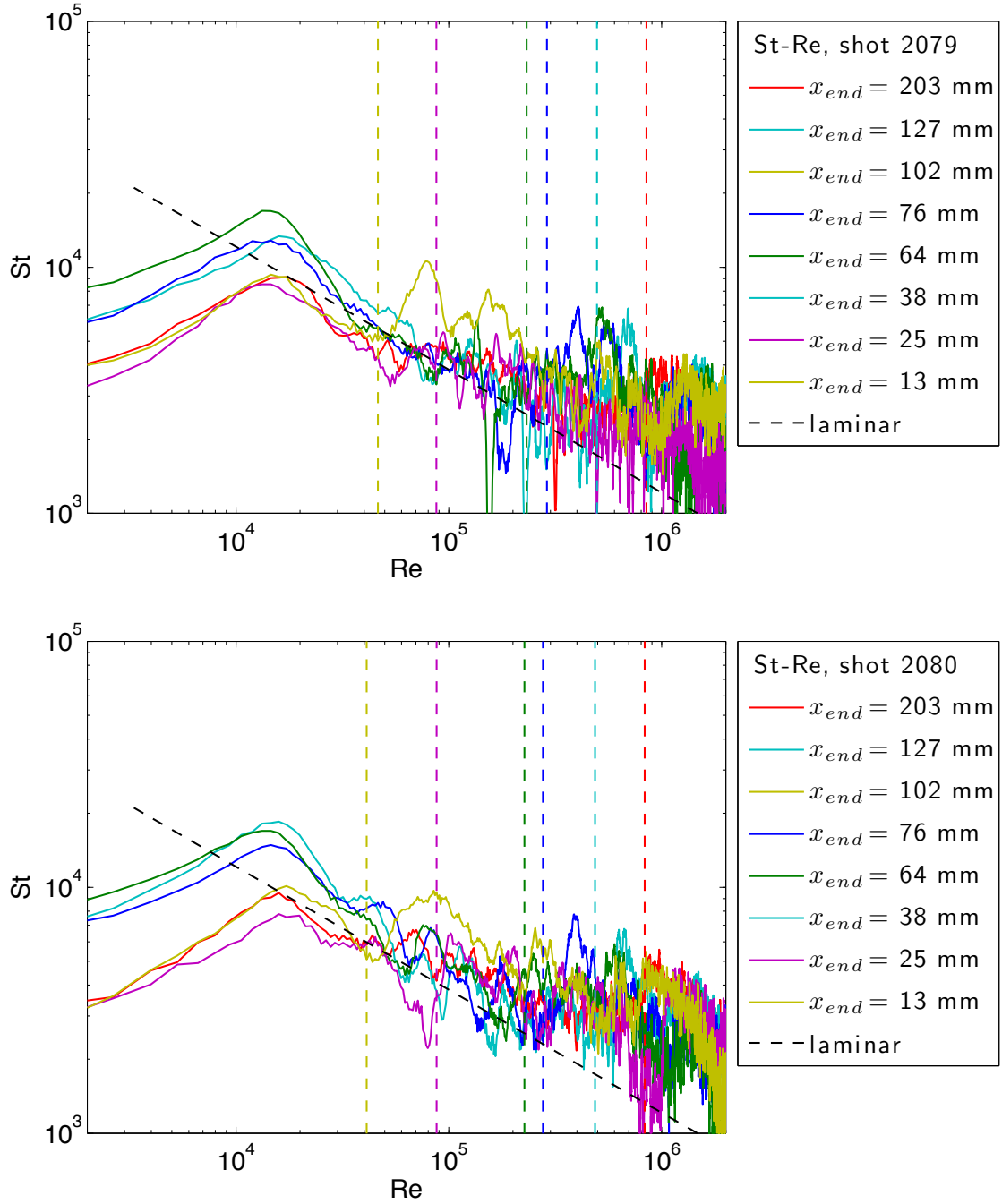


Figure E.15: Stanton-Reynolds number traces from shot 2080, a detonation in stoichiometric hydrogen-oxygen at fill pressure 25 kPa. The dashed vertical lines represent the arrival of the reflected shock wave.

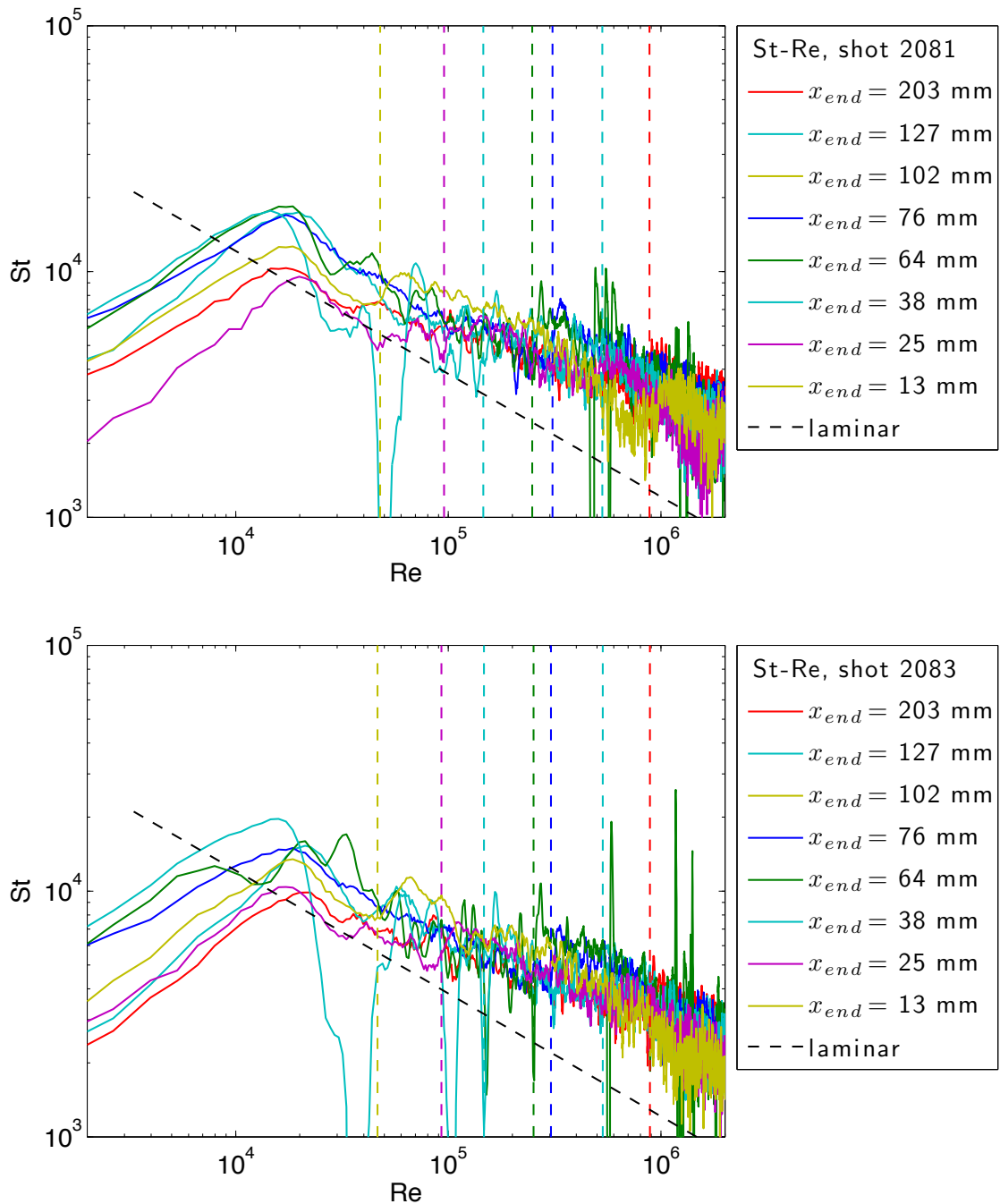


Figure E.16: Stanton-Reynolds number traces from shot 2083, a detonation in stoichiometric hydrogen-oxygen at fill pressure 25 kPa. The dashed vertical lines represent the arrival of the reflected shock wave.

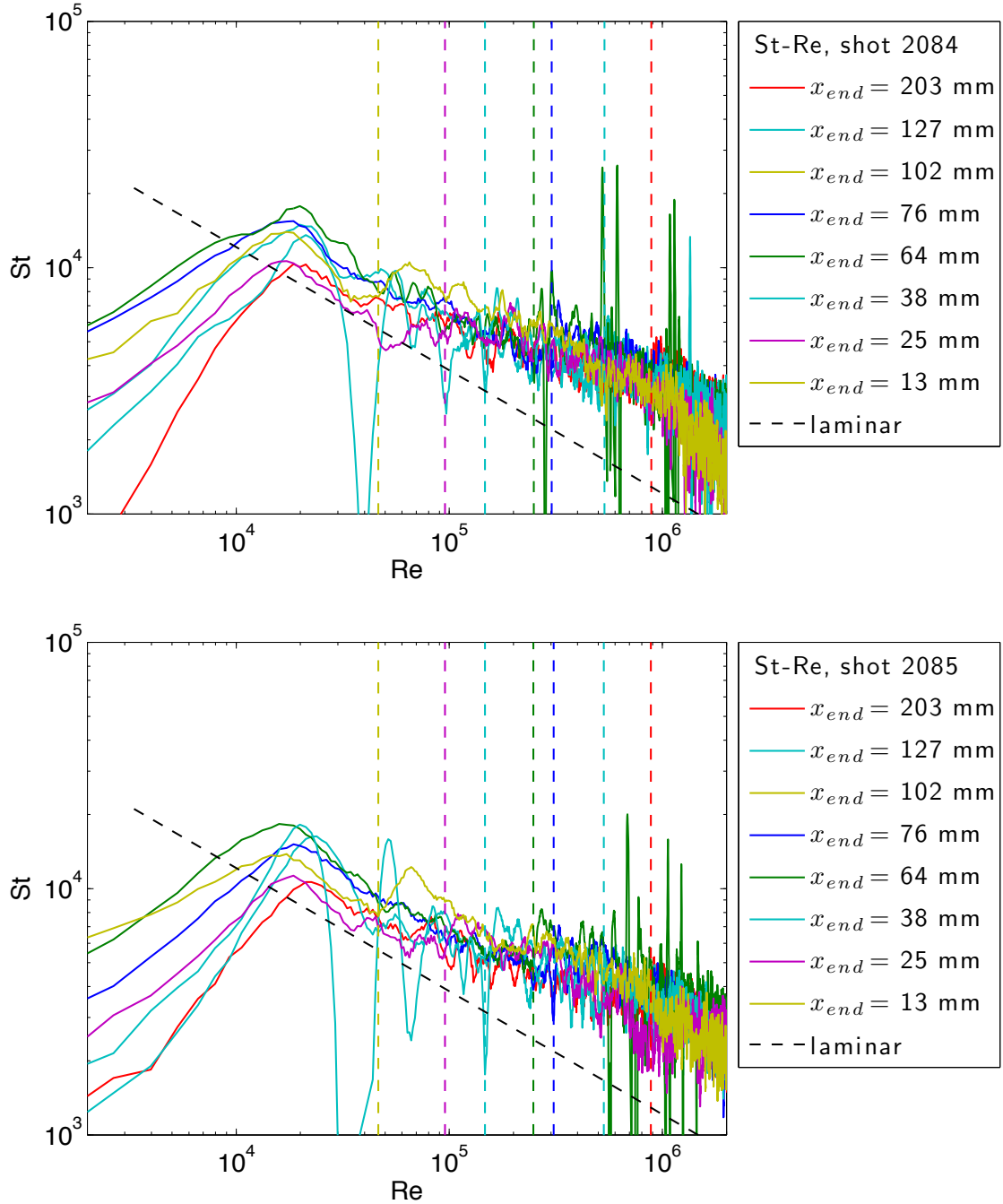


Figure E.17: Stanton-Reynolds number traces from shot 2085, a detonation in stoichiometric hydrogen-oxygen at fill pressure 25 kPa. The dashed vertical lines represent the arrival of the reflected shock wave.

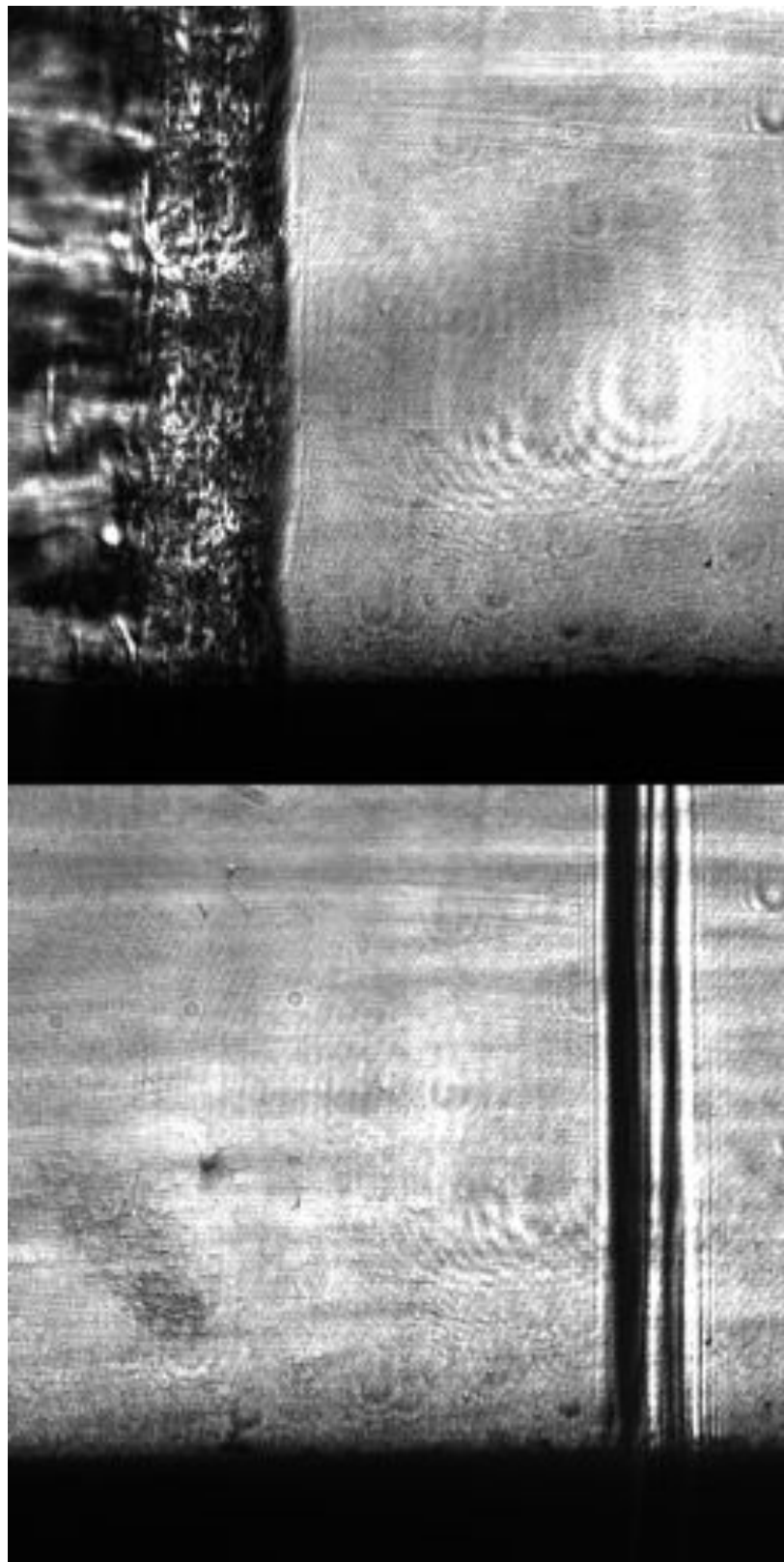


Figure E.18: Focused schlieren image of shot 2084. The field of view is approximately 14 mm wide.

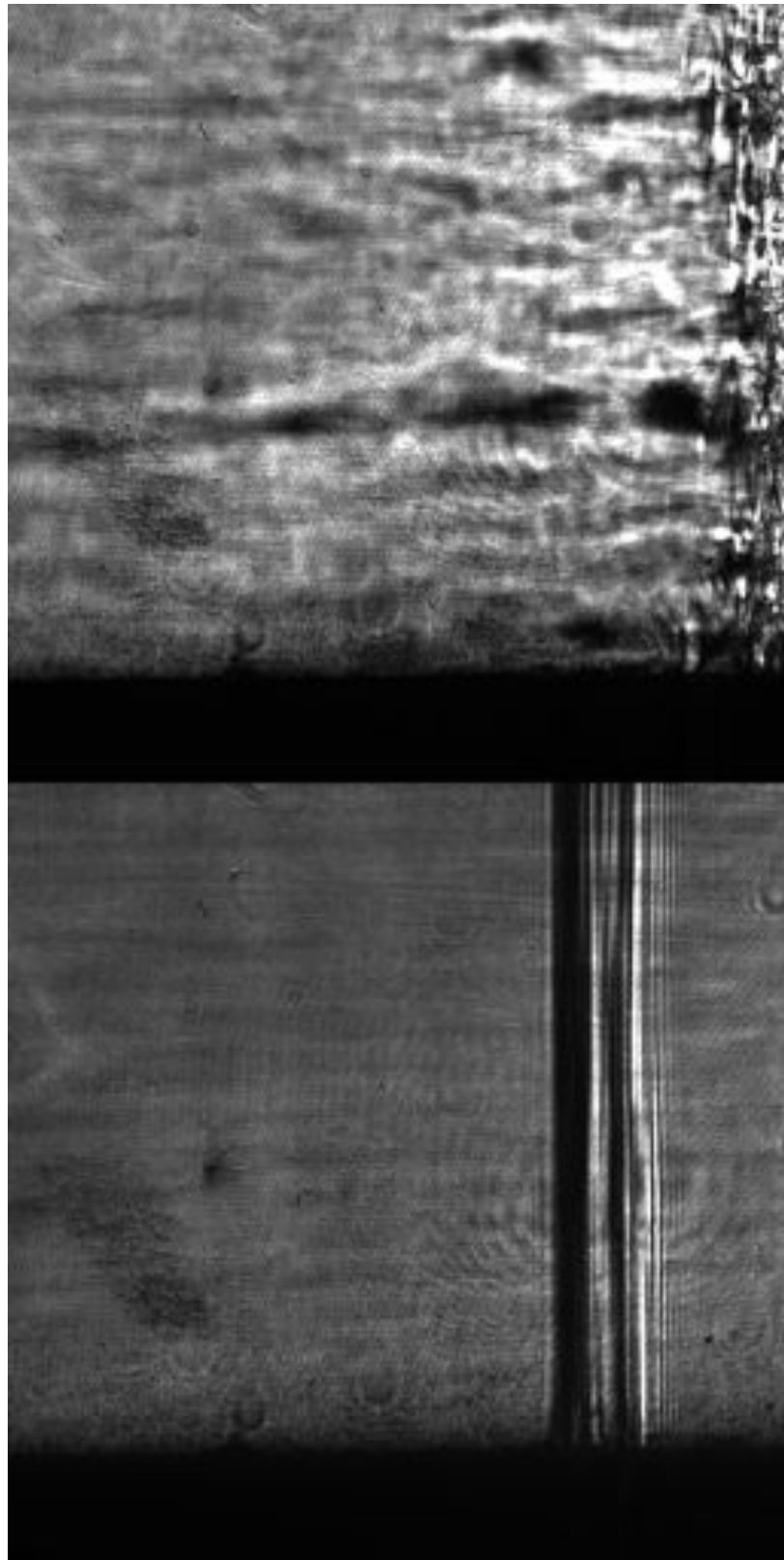


Figure E.19: Focused schlieren image of shot 2085. The field of view is approximately 14 mm wide.

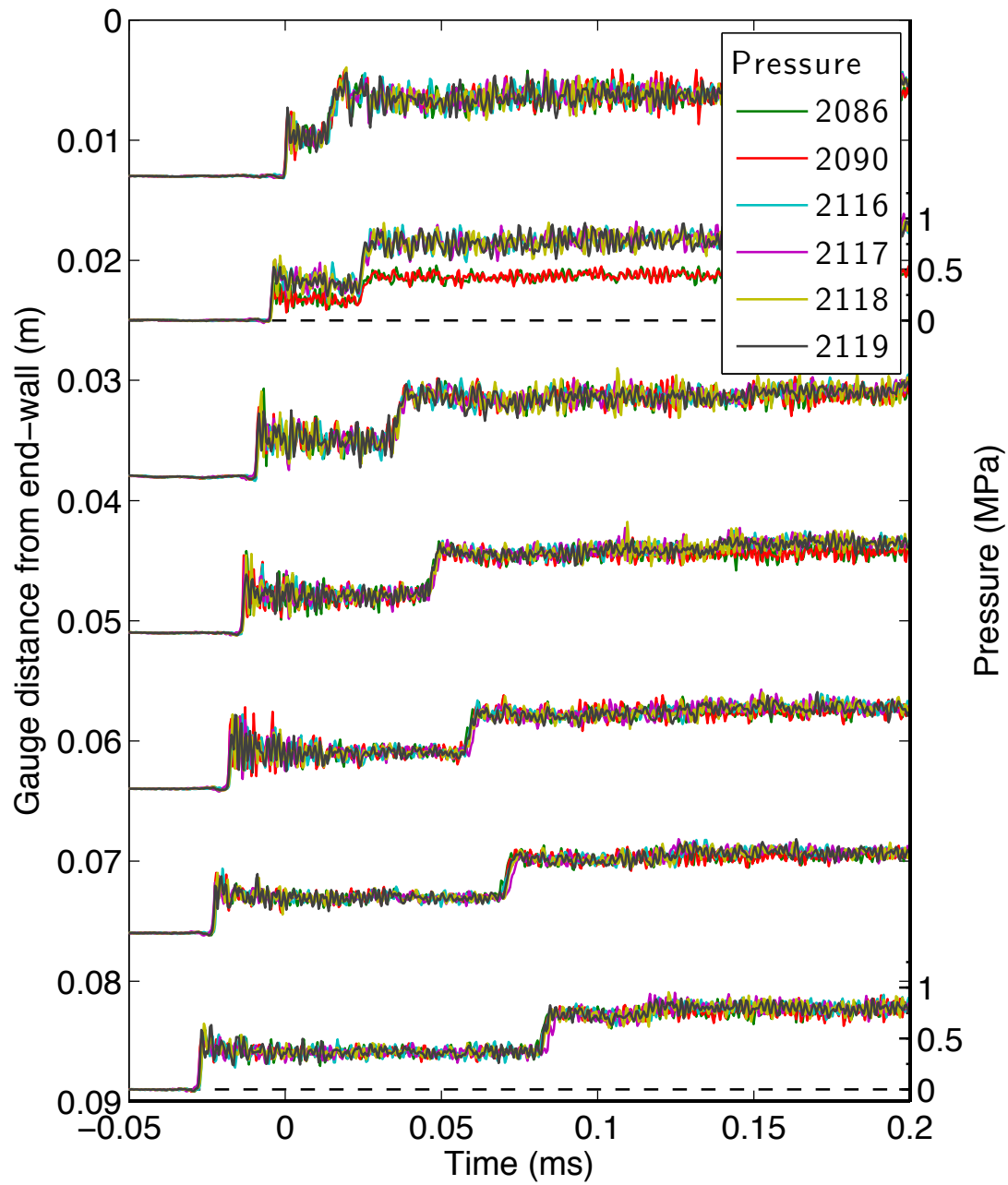


Figure E.20: Pressure traces for a detonation in stoichiometric hydrogen-oxygen at fill pressure 25 kPa, part 3.

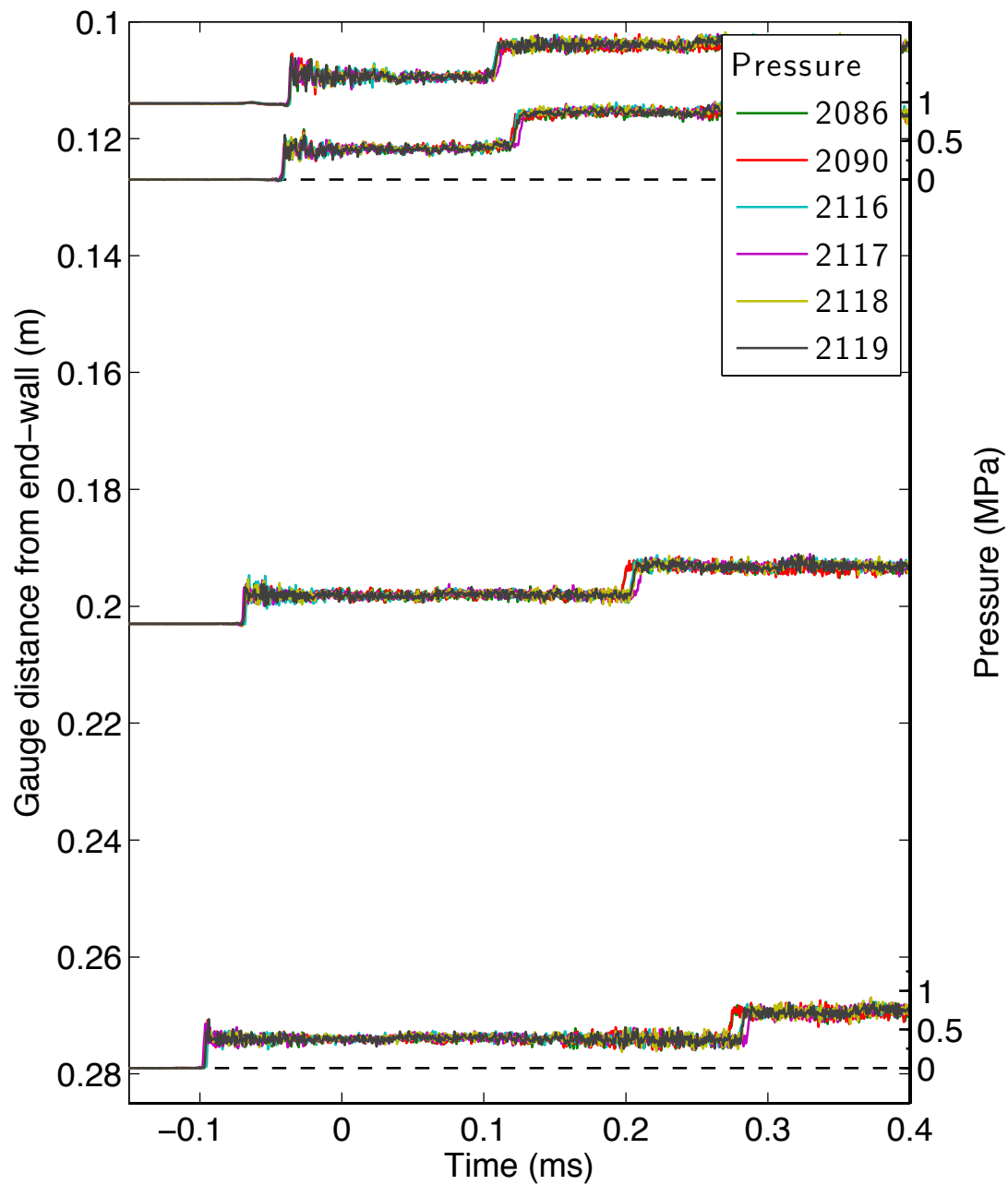


Figure E.21: Pressure traces for a detonation in stoichiometric hydrogen-oxygen at fill pressure 25 kPa, part 4.

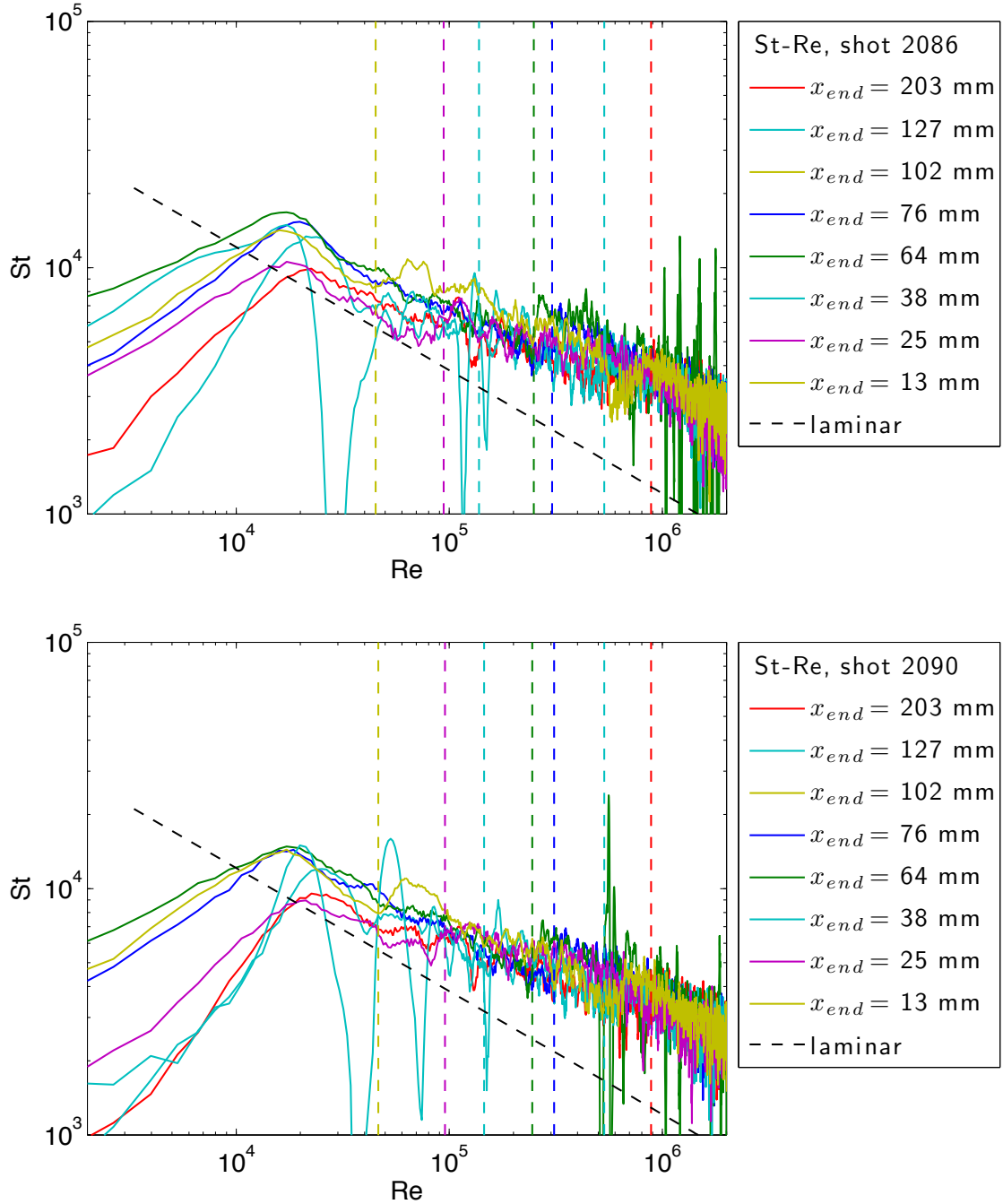


Figure E.22: Stanton-Reynolds number traces from shot 2090, a detonation in stoichiometric hydrogen-oxygen at fill pressure 25 kPa. The dashed vertical lines represent the arrival of the reflected shock wave.

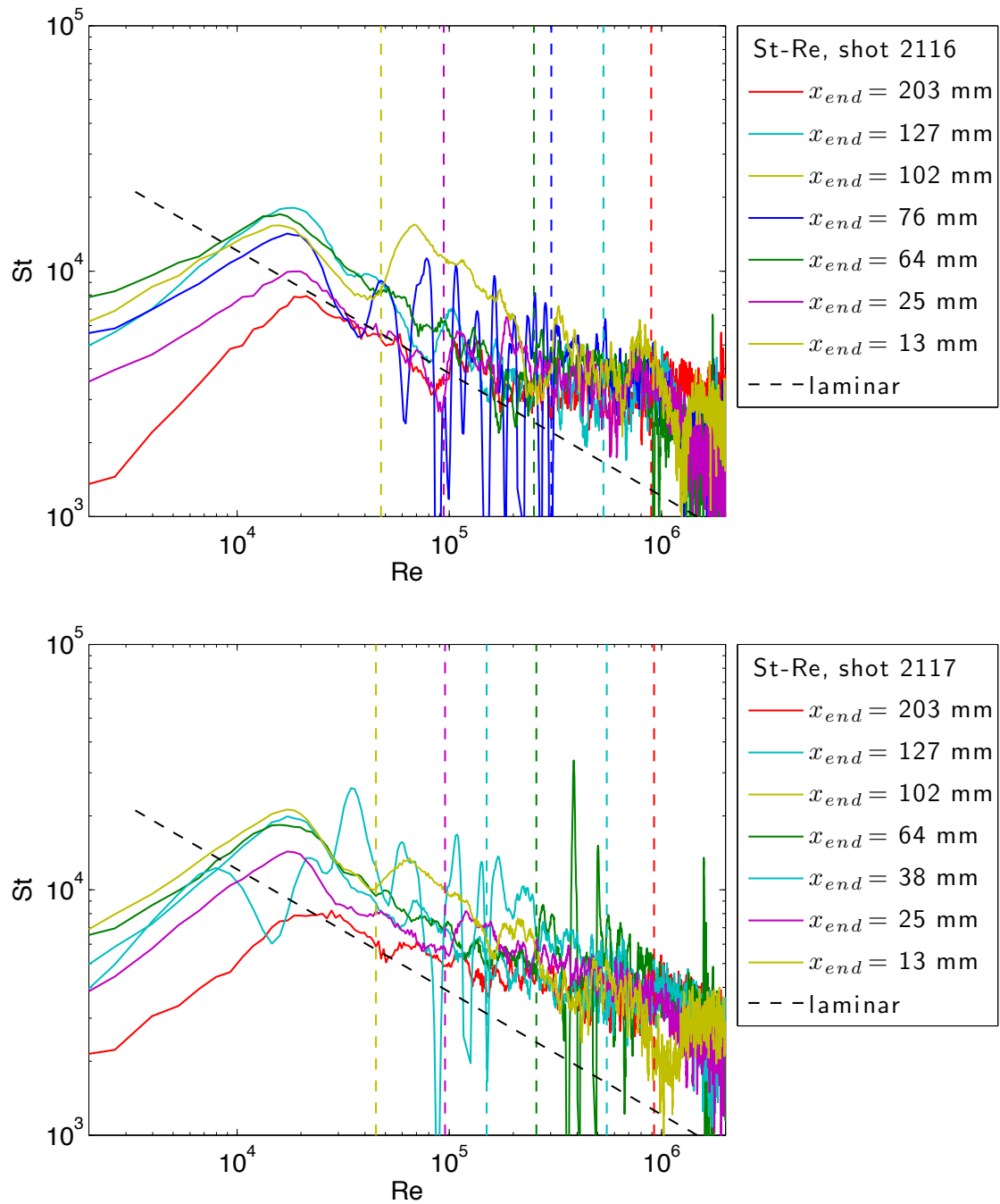


Figure E.23: Stanton-Reynolds number traces from shot 2117, a detonation in stoichiometric hydrogen-oxygen at fill pressure 25 kPa. The dashed vertical lines represent the arrival of the reflected shock wave.

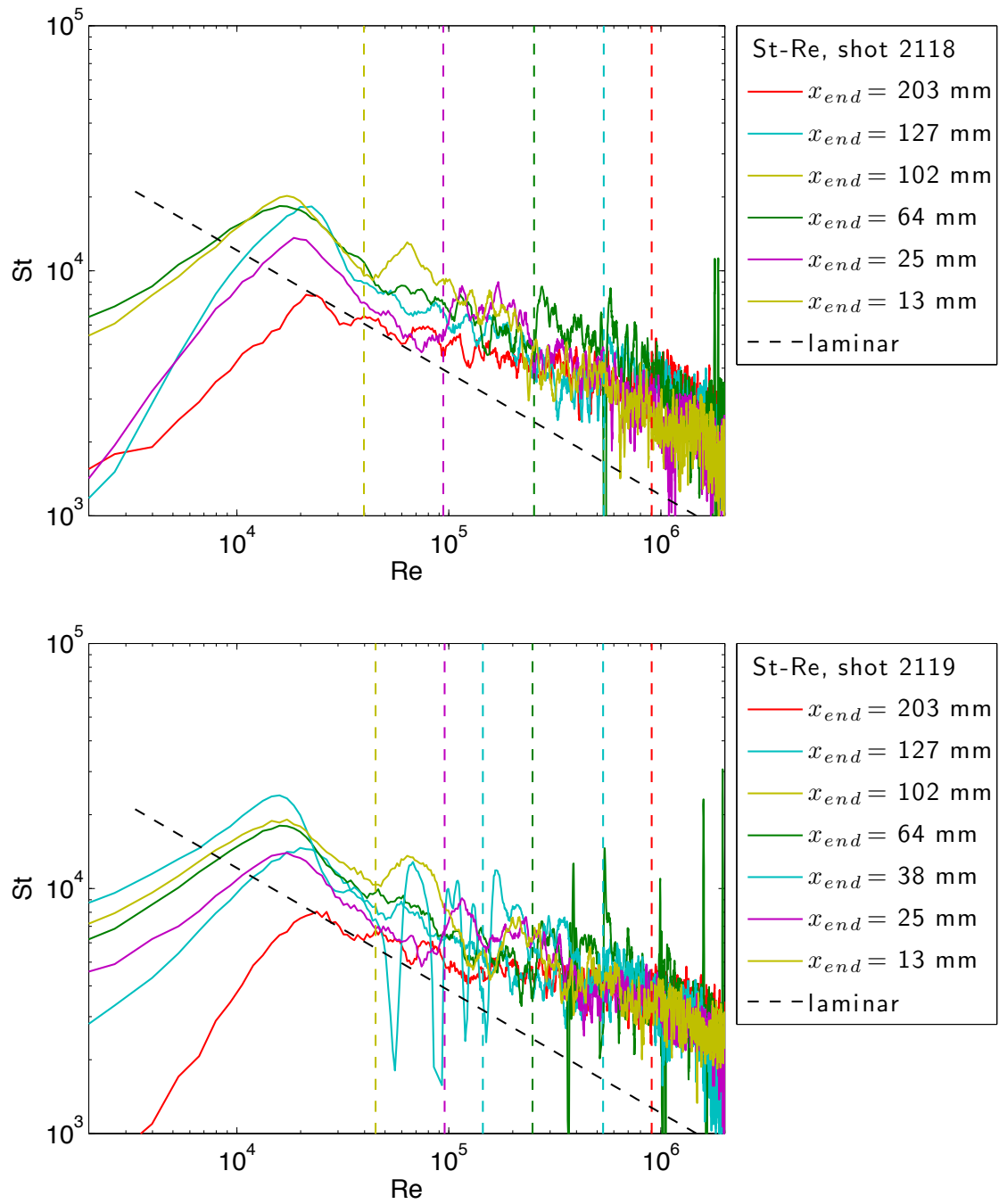


Figure E.24: Stanton-Reynolds number traces from shot 2119, a detonation in stoichiometric hydrogen-oxygen at fill pressure 25 kPa. The dashed vertical lines represent the arrival of the reflected shock wave.

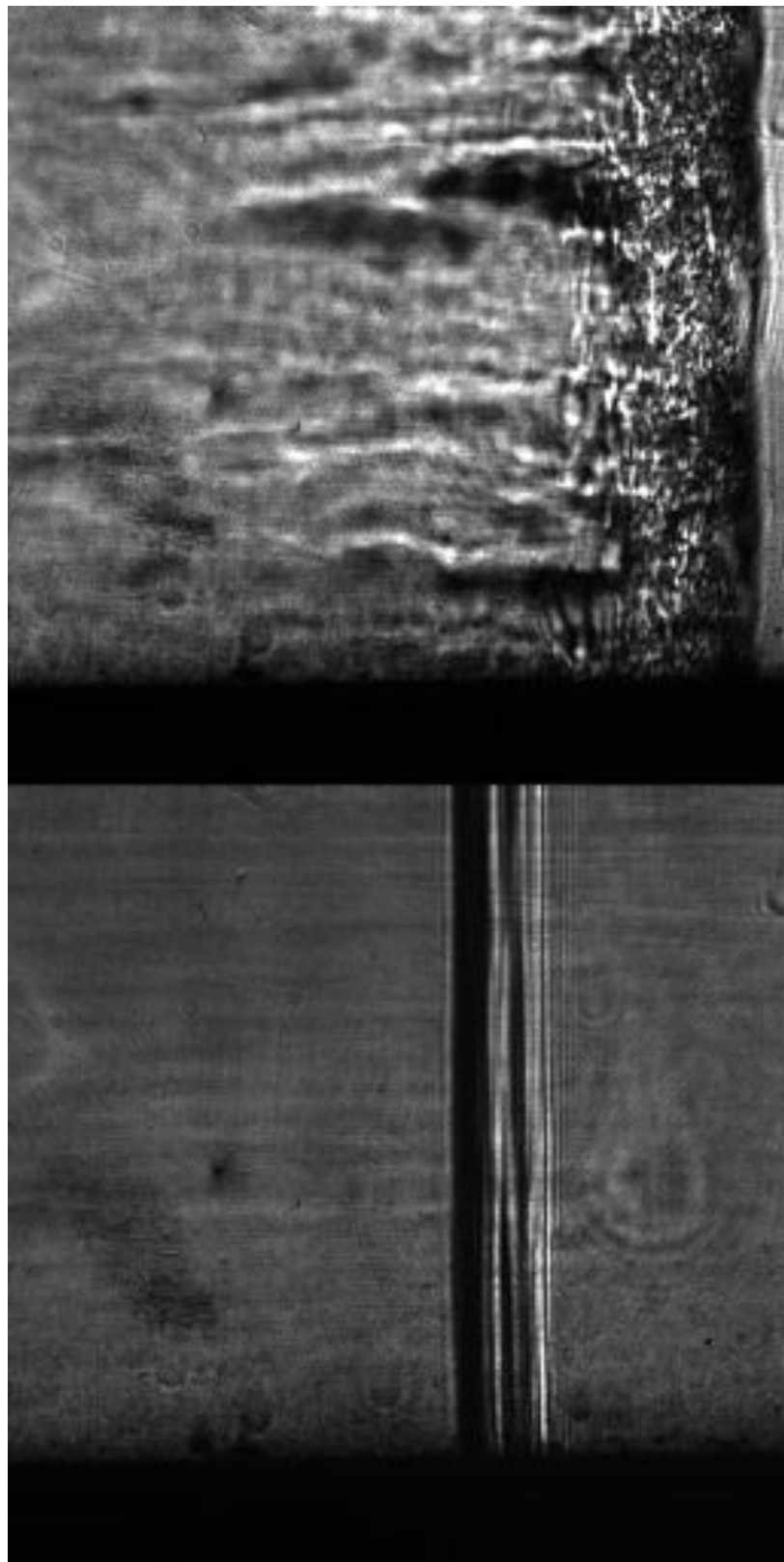


Figure E.25: Focused schlieren image of shot 2090. The field of view is approximately 14 mm wide.

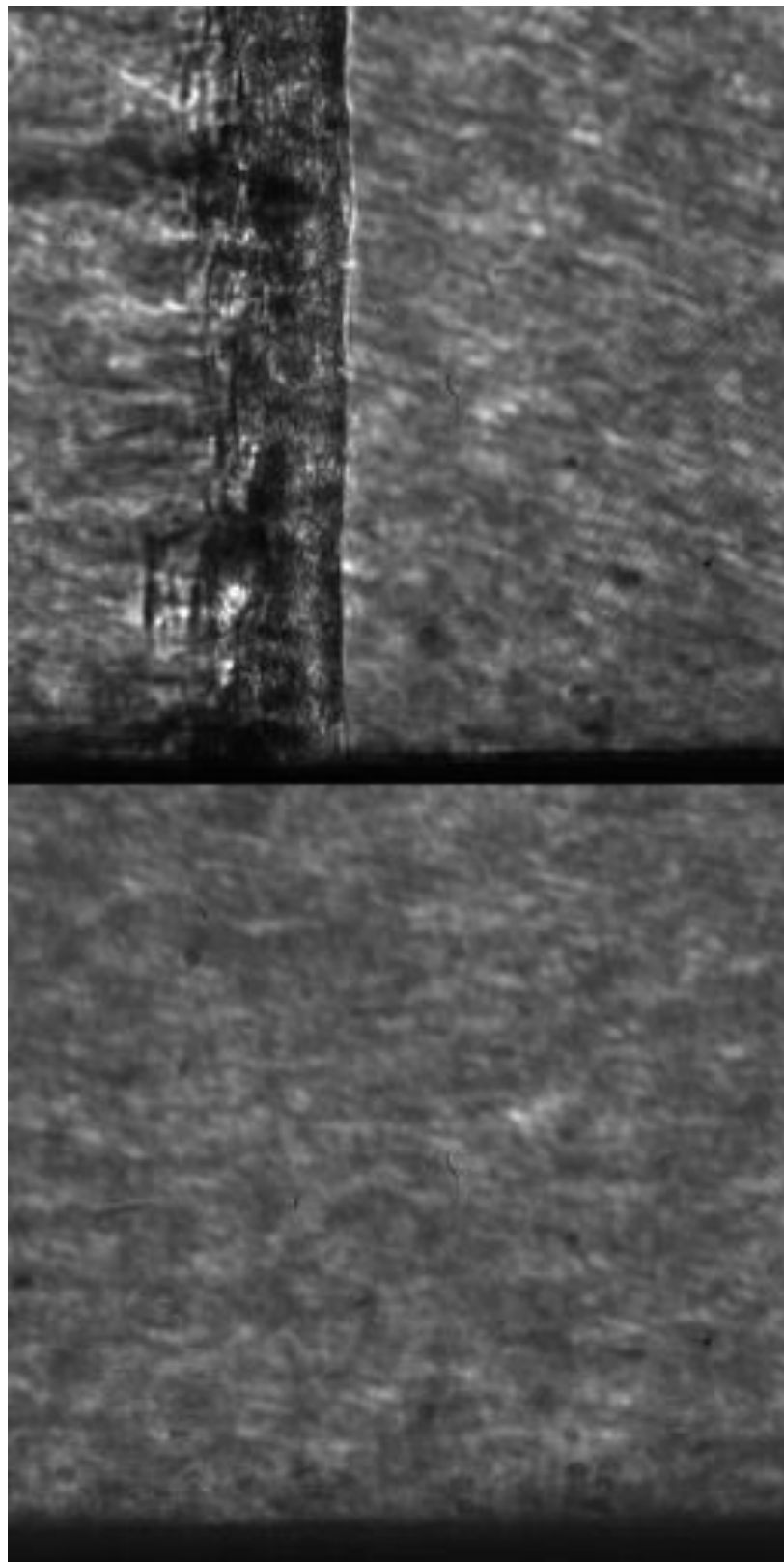


Figure E.26: Focused schlieren image of shot 2117. The field of view is approximately 14 mm wide.

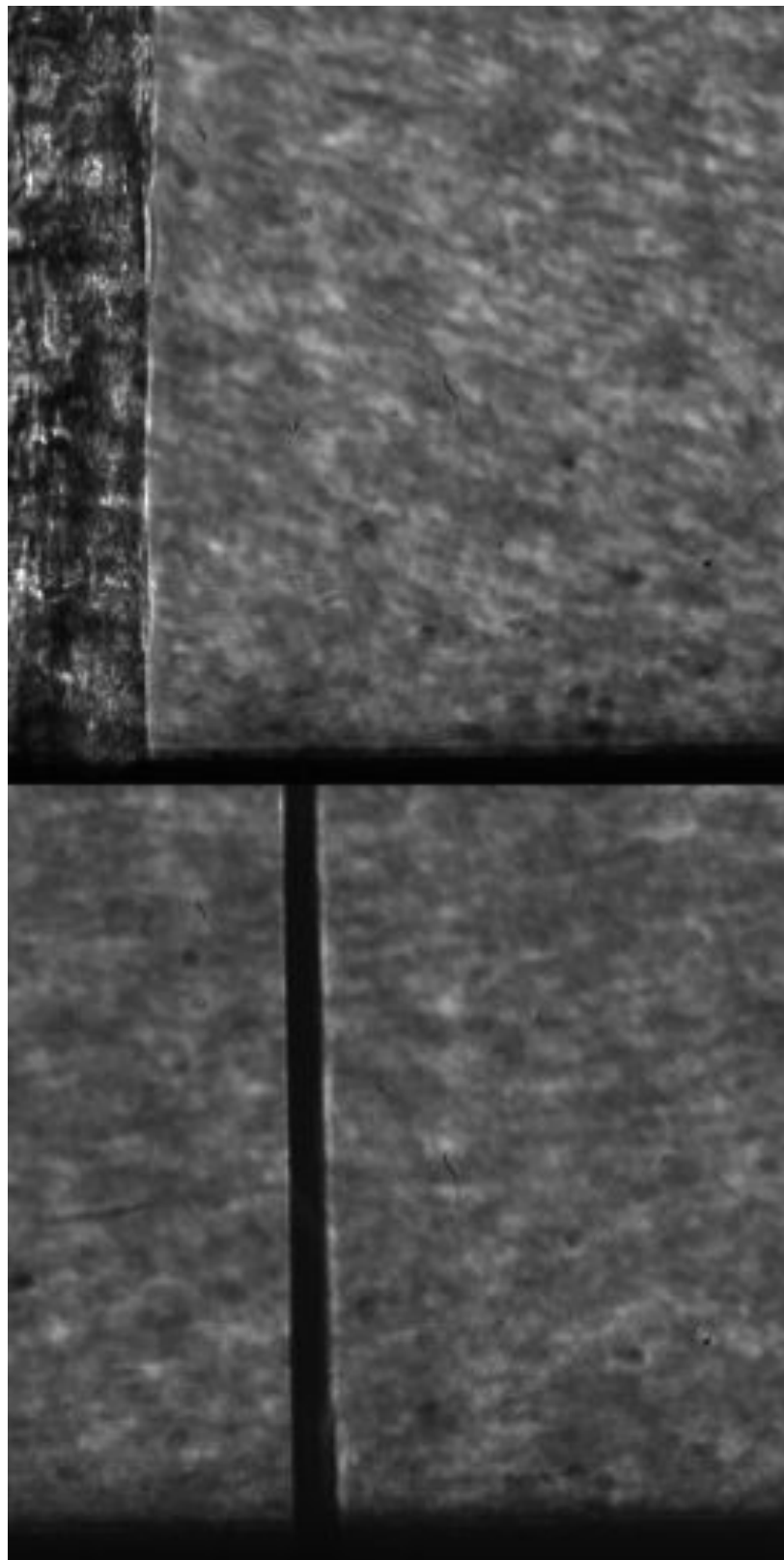


Figure E.27: Focused schlieren image of shot 2119. The field of view is approximately 14 mm wide.

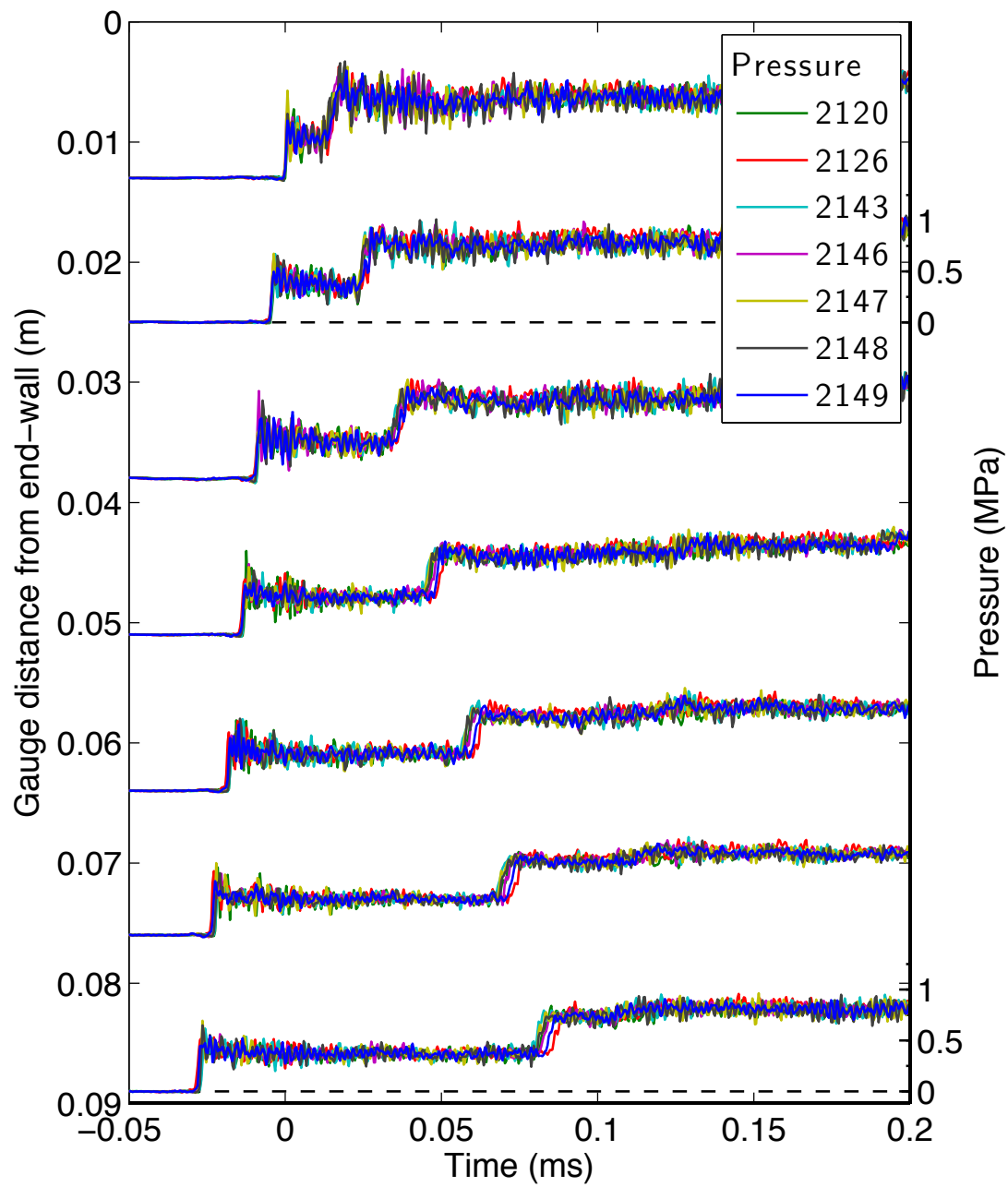


Figure E.28: Pressure traces for a detonation in stoichiometric hydrogen-oxygen at fill pressure 25 kPa, part 5.

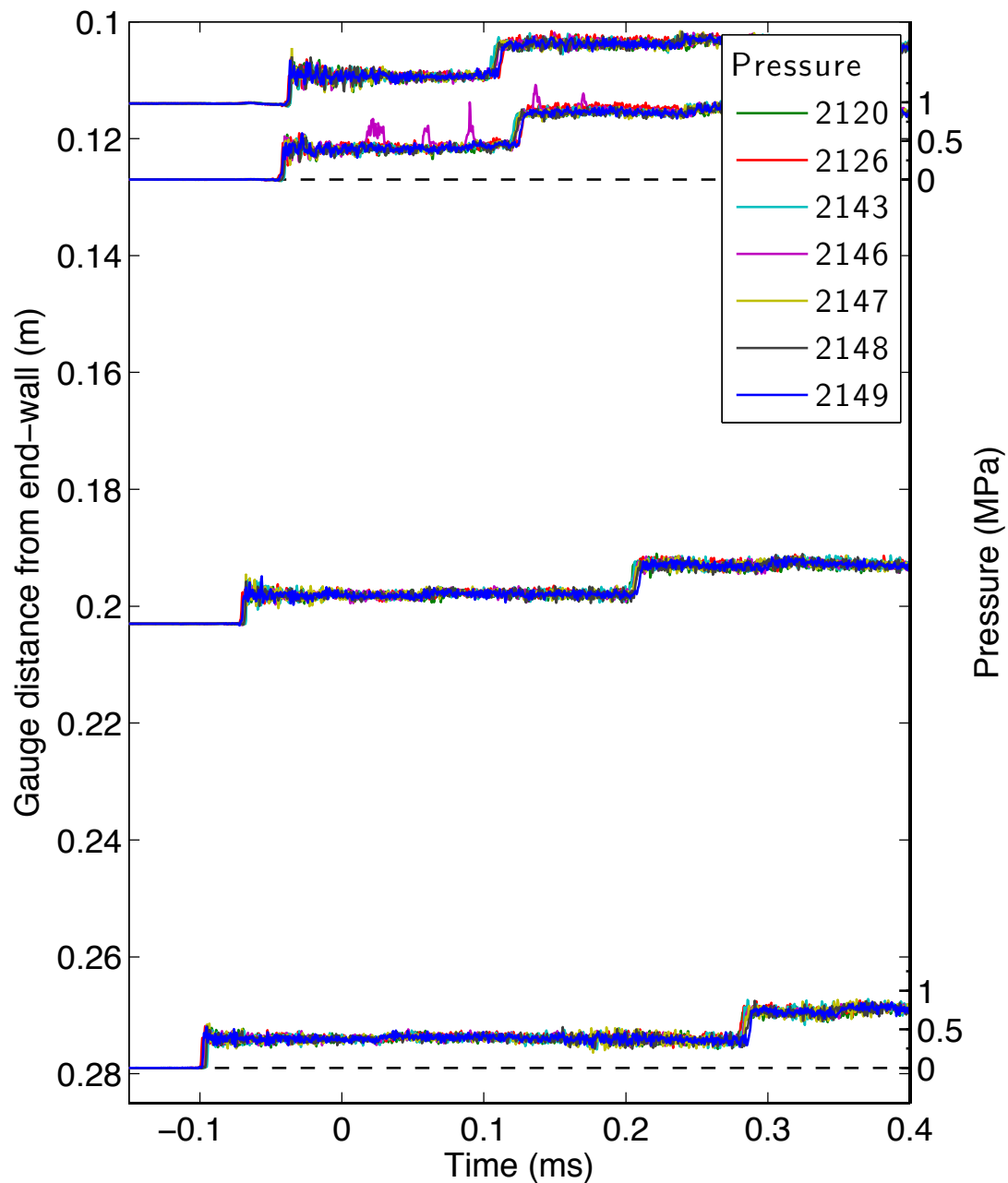


Figure E.29: Pressure traces for a detonation in stoichiometric hydrogen-oxygen at fill pressure 25 kPa, part 6.

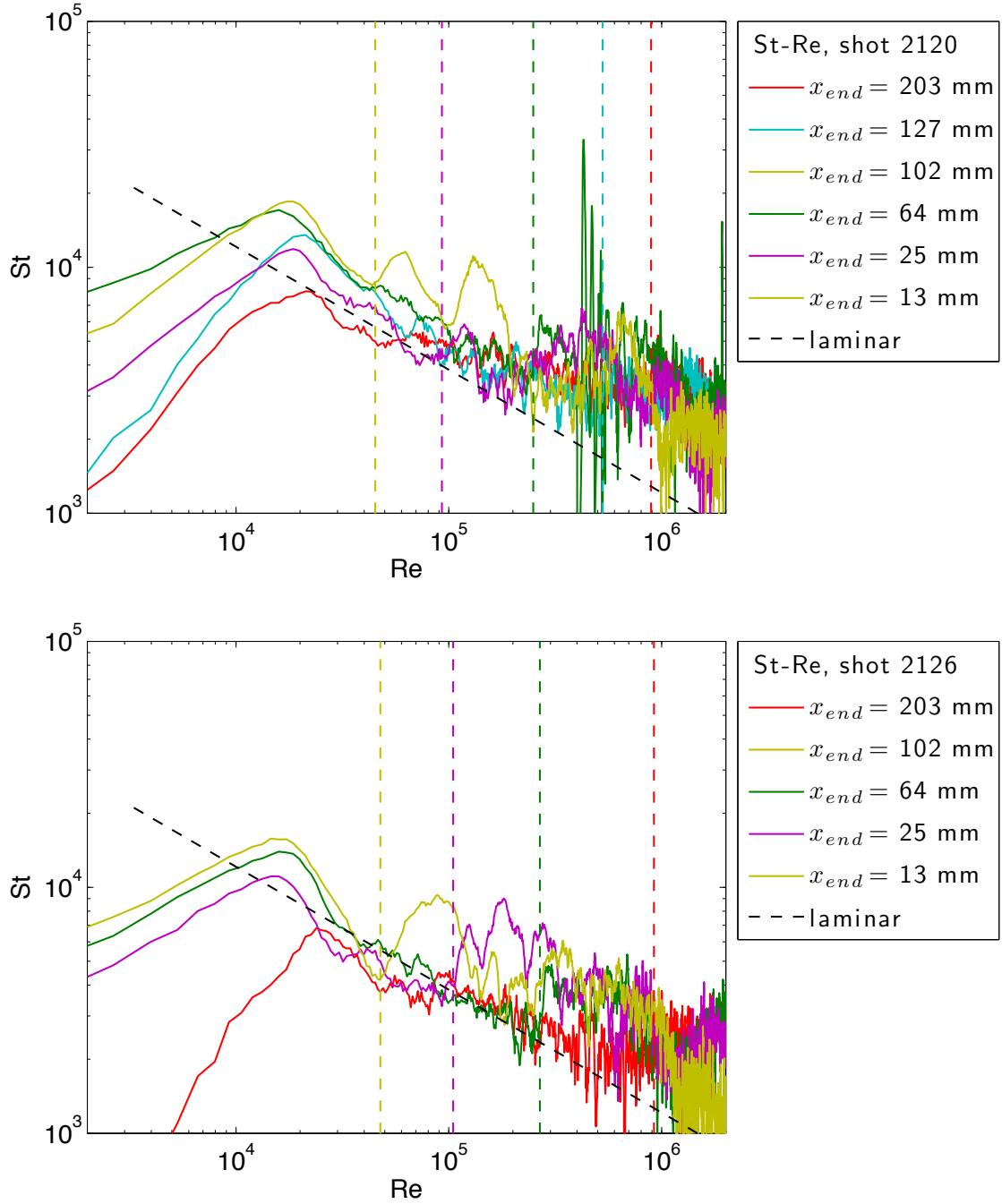


Figure E.30: Stanton-Reynolds number traces from shot 2126, a detonation in stoichiometric hydrogen-oxygen at fill pressure 25 kPa. The dashed vertical lines represent the arrival of the reflected shock wave.

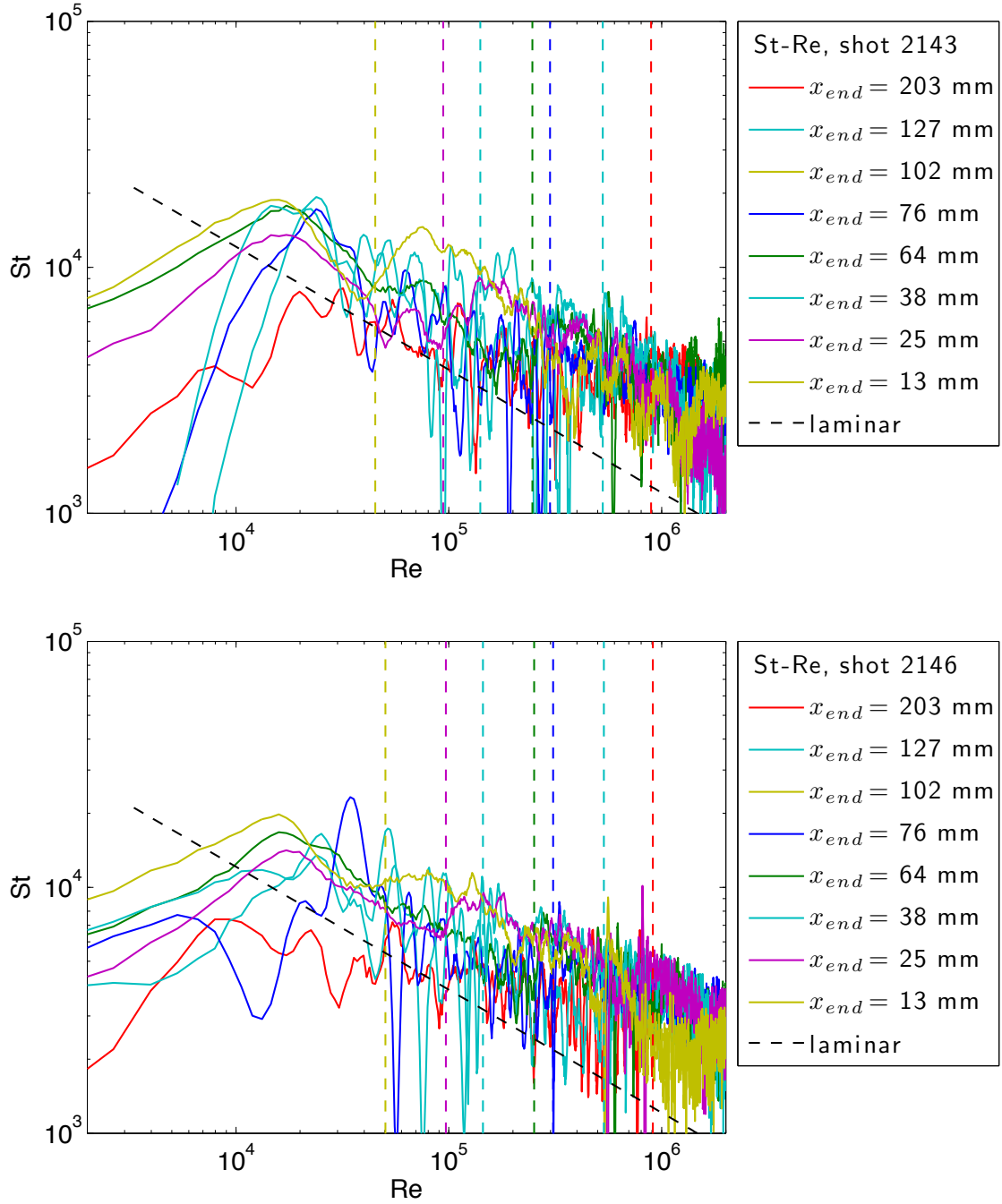


Figure E.31: Stanton-Reynolds number traces from shot 2146, a detonation in stoichiometric hydrogen-oxygen at fill pressure 25 kPa. The dashed vertical lines represent the arrival of the reflected shock wave.

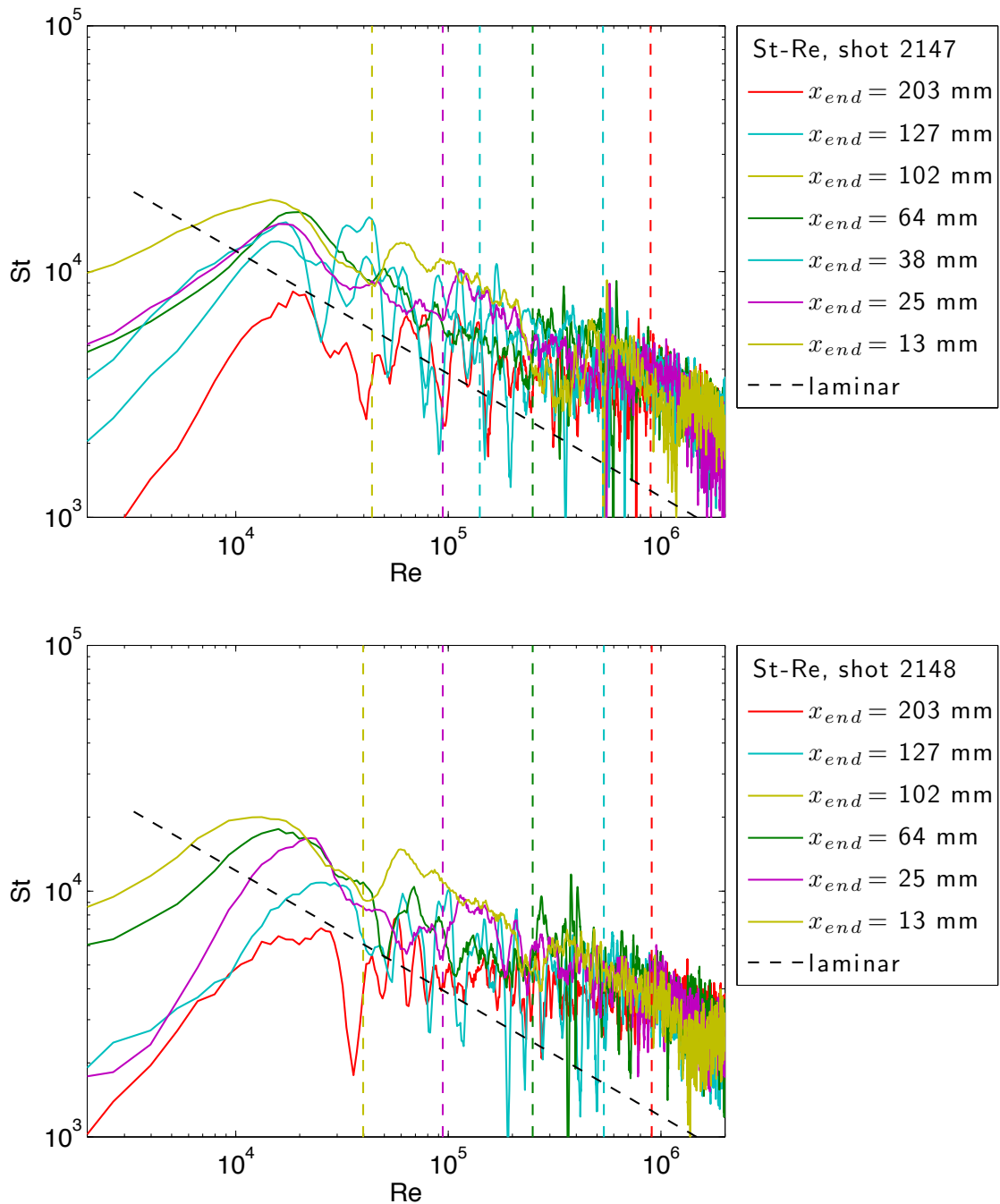


Figure E.32: Stanton-Reynolds number traces from shot 2148, a detonation in stoichiometric hydrogen-oxygen at fill pressure 25 kPa. The dashed vertical lines represent the arrival of the reflected shock wave.

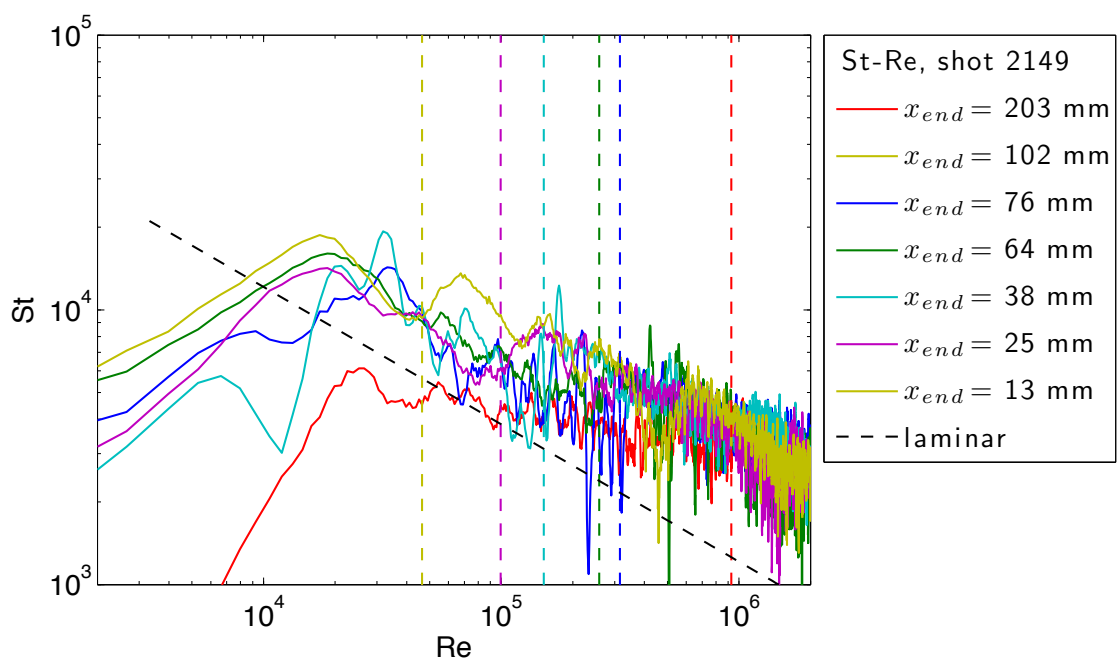


Figure E.33: Stanton-Reynolds number traces from shot 2149, a detonation in stoichiometric hydrogen-oxygen at fill pressure 25 kPa. The dashed vertical lines represent the arrival of the reflected shock wave.

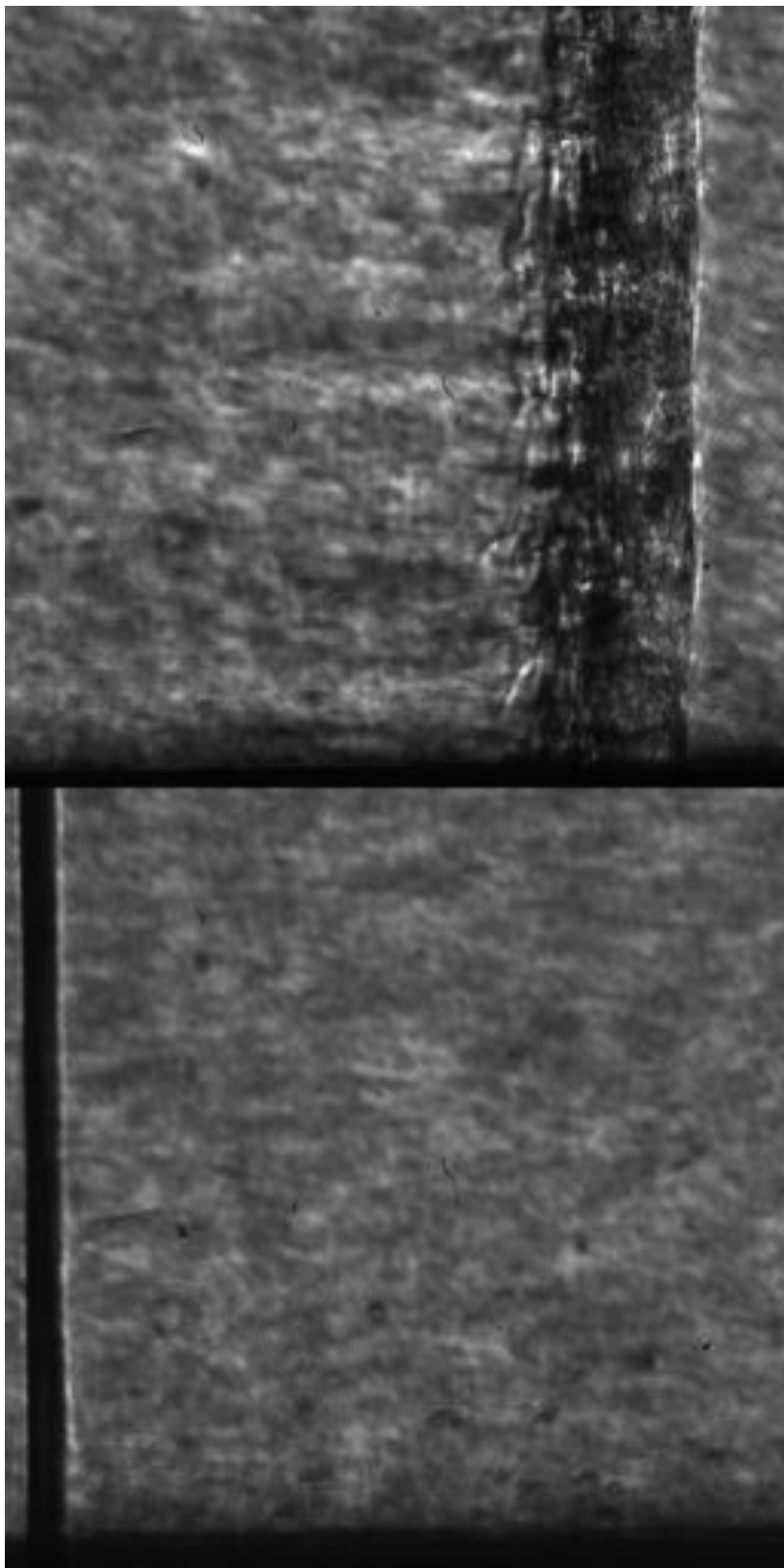


Figure E.34: Focused schlieren image of shot 2120. The field of view is approximately 14 mm wide.

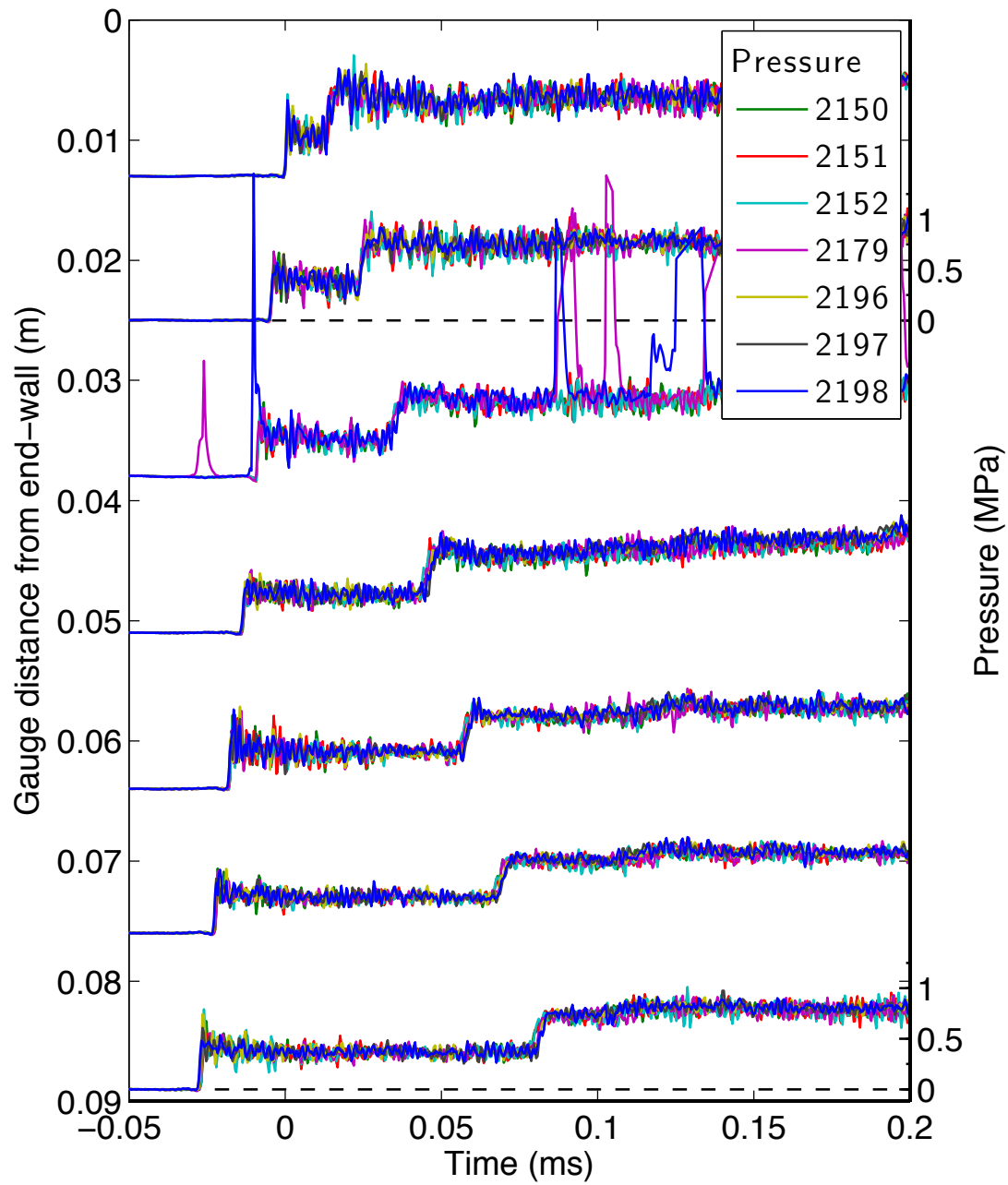


Figure E.35: Pressure traces for a detonation in stoichiometric hydrogen-oxygen at fill pressure 25 kPa, part 7.

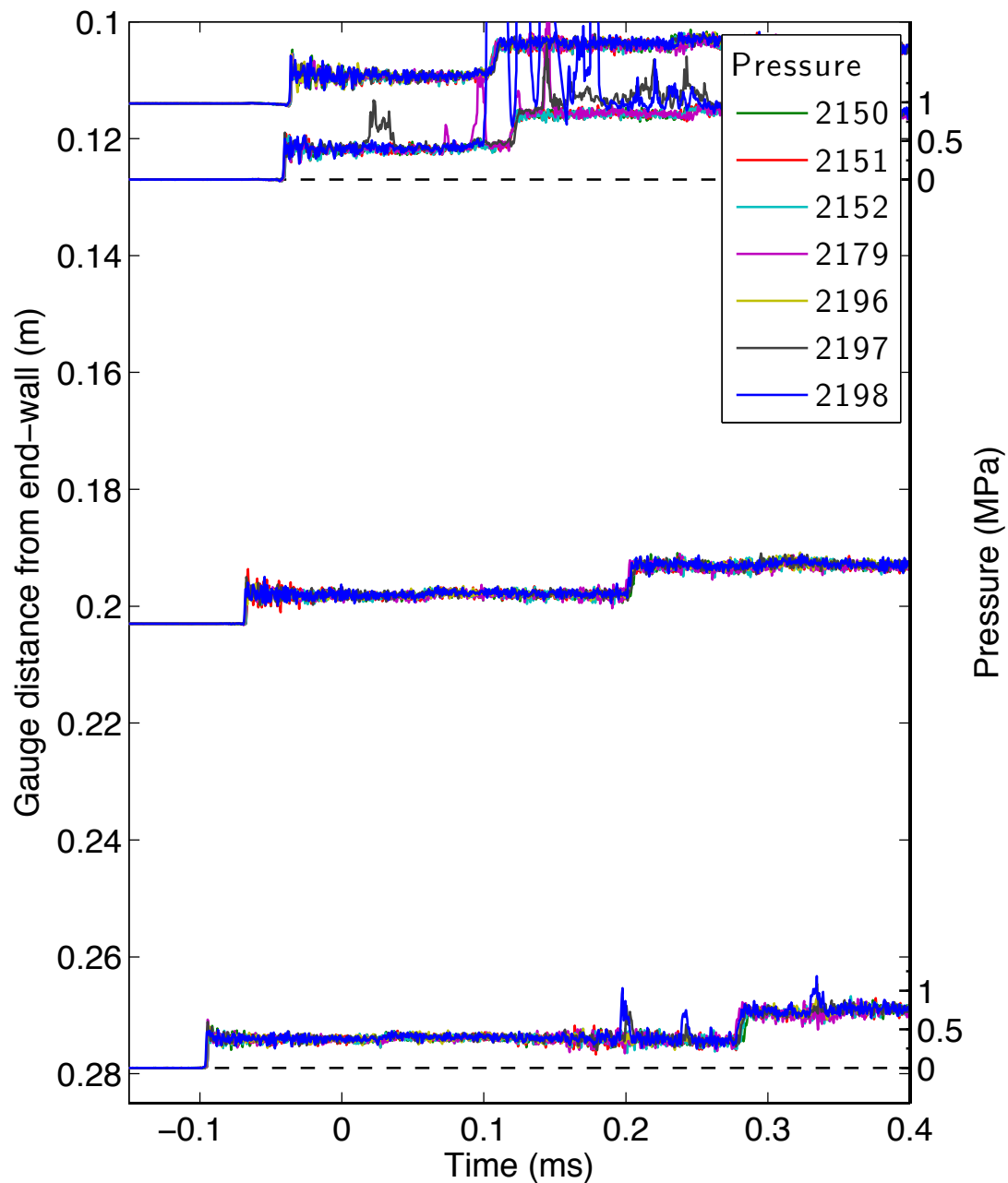


Figure E.36: Pressure traces for a detonation in stoichiometric hydrogen-oxygen at fill pressure 25 kPa, part 8.

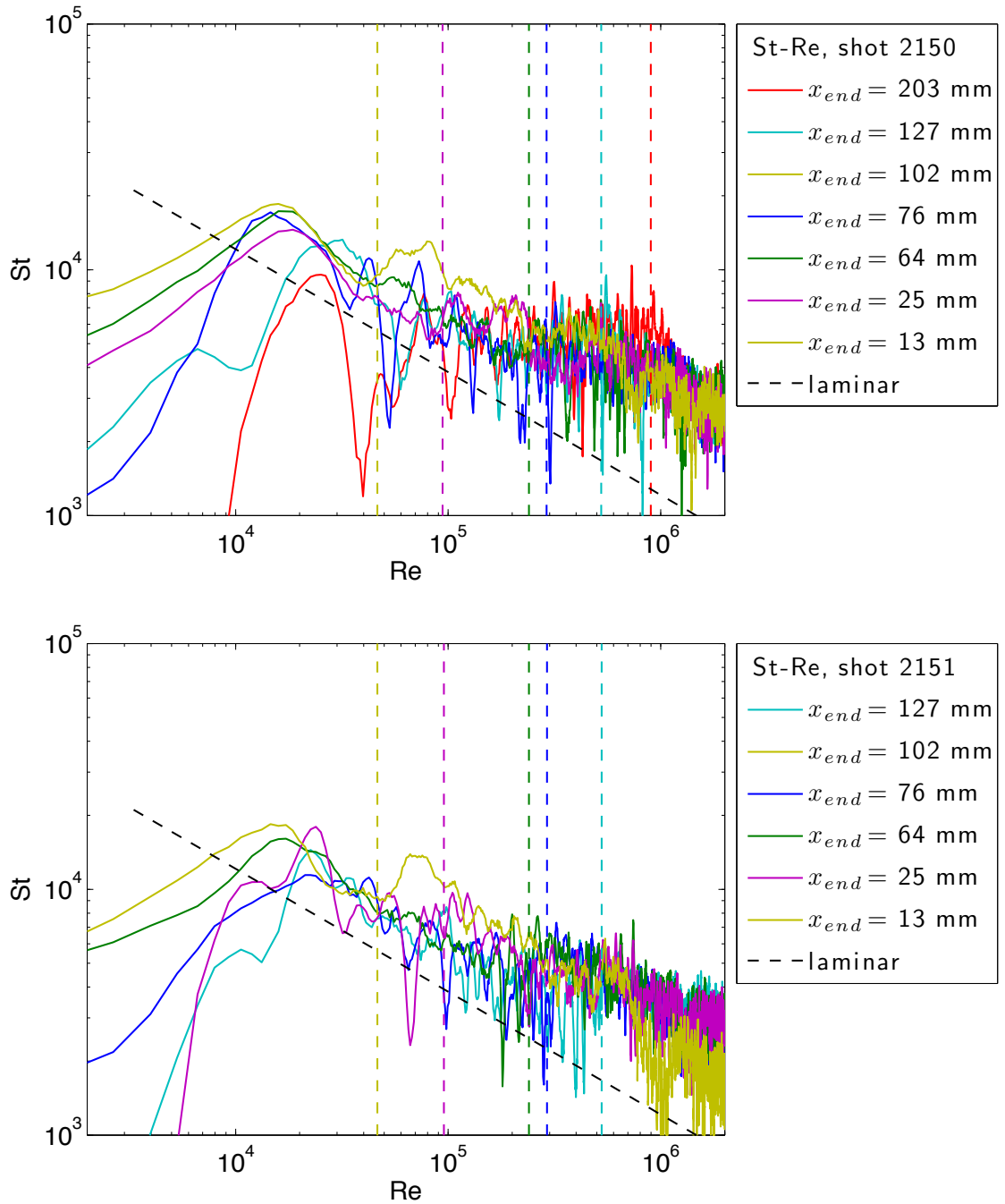


Figure E.37: Stanton-Reynolds number traces from shot 2151, a detonation in stoichiometric hydrogen-oxygen at fill pressure 25 kPa. The dashed vertical lines represent the arrival of the reflected shock wave.

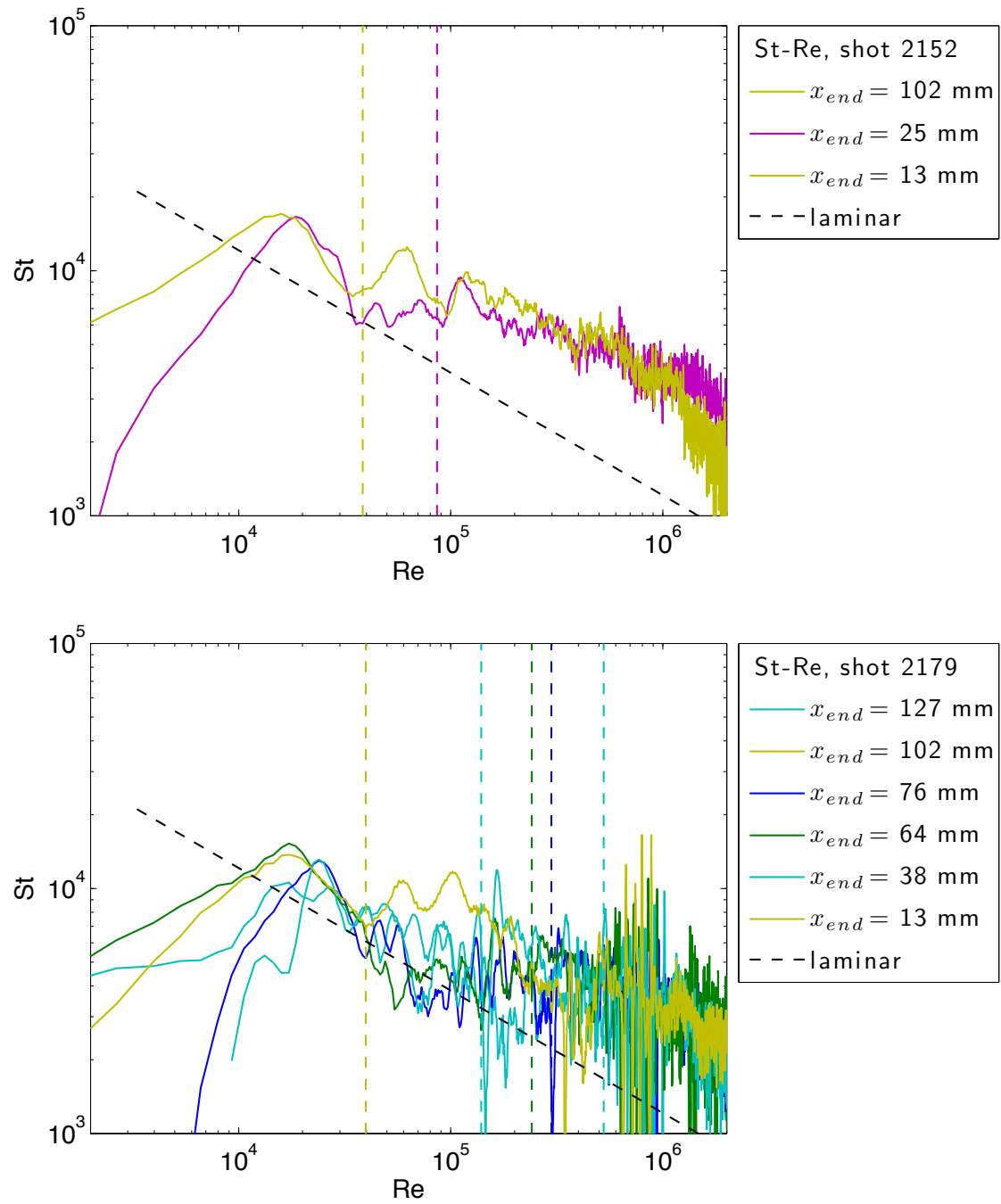


Figure E.38: Stanton-Reynolds number traces from shot 2179, a detonation in stoichiometric hydrogen-oxygen at fill pressure 25 kPa. The dashed vertical lines represent the arrival of the reflected shock wave.

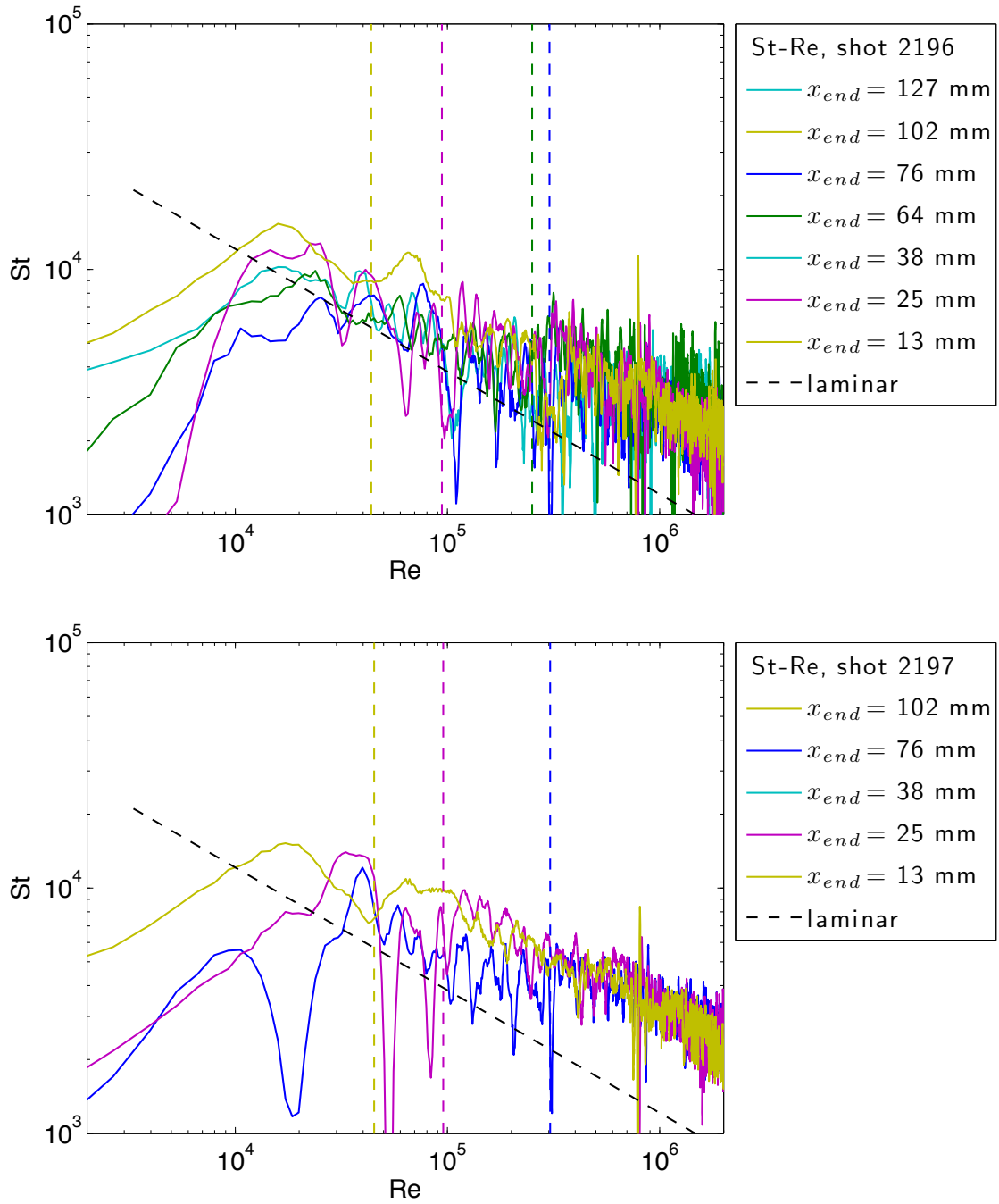


Figure E.39: Stanton-Reynolds number traces from shot 2197, a detonation in stoichiometric hydrogen-oxygen at fill pressure 25 kPa. The dashed vertical lines represent the arrival of the reflected shock wave.

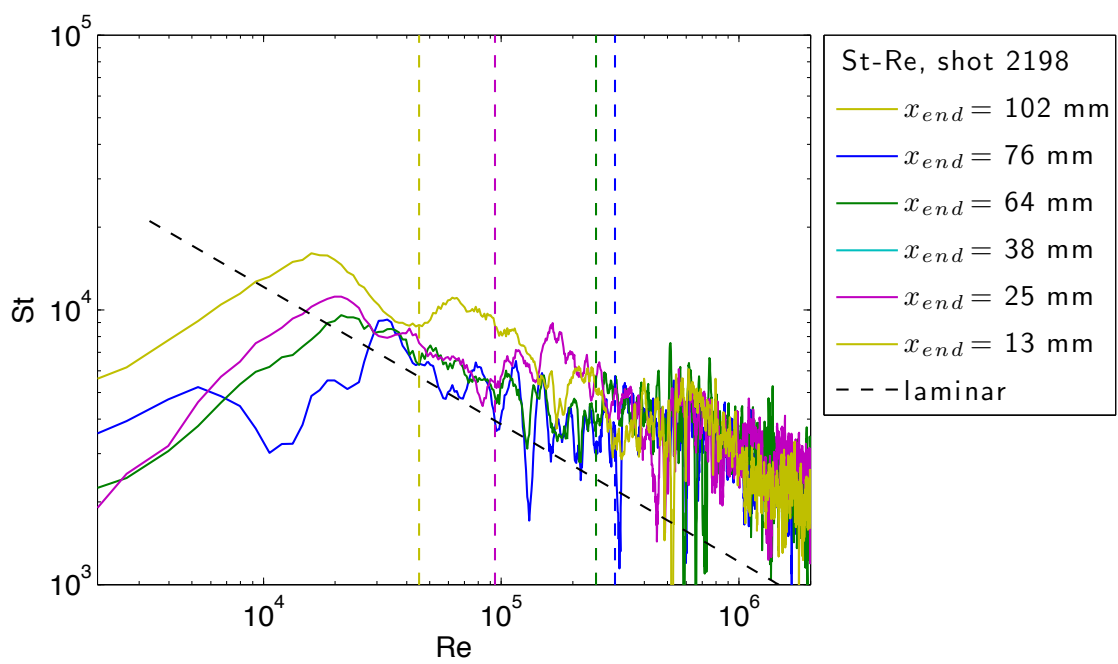


Figure E.40: Stanton-Reynolds number traces from shot 2198, a detonation in stoichiometric hydrogen-oxygen at fill pressure 25 kPa. The dashed vertical lines represent the arrival of the reflected shock wave.

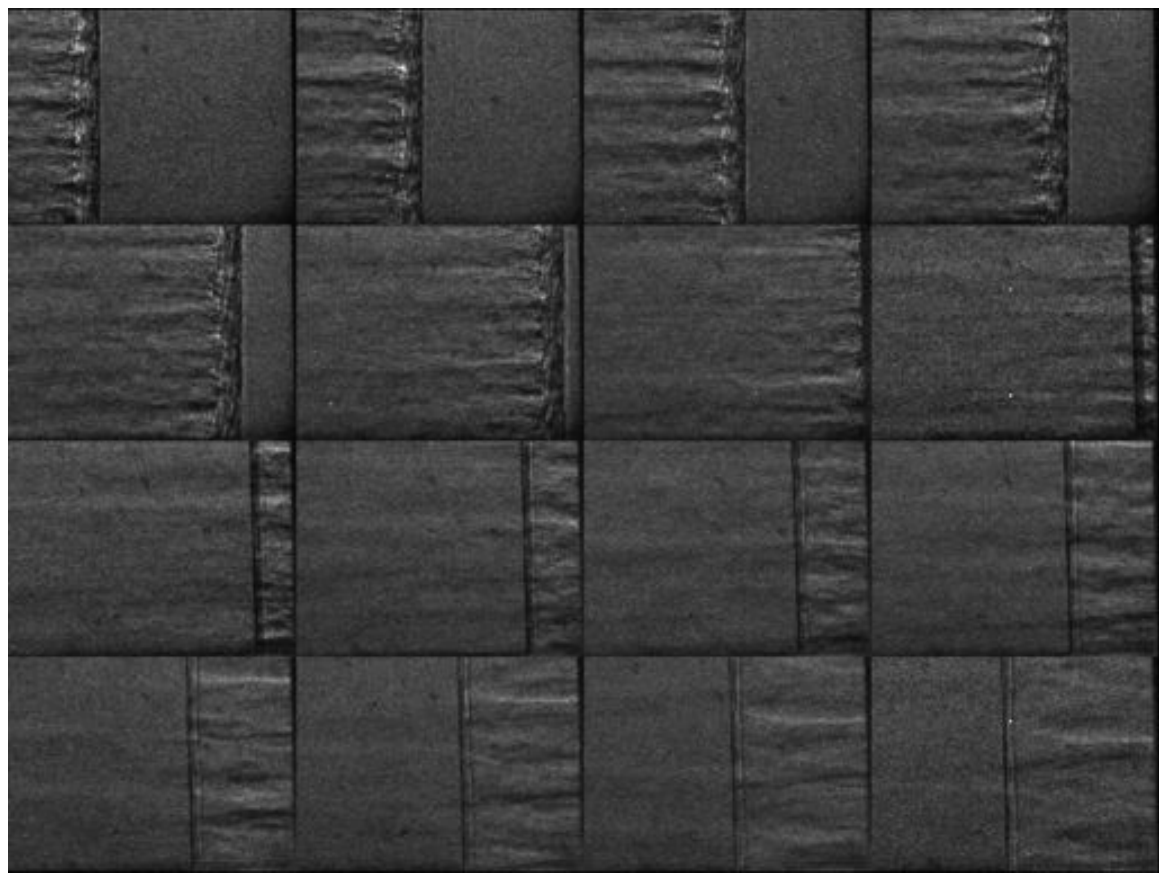


Figure E.41: Unfocused schlieren image of shot 2152. The field of view is approximately 30 mm wide.

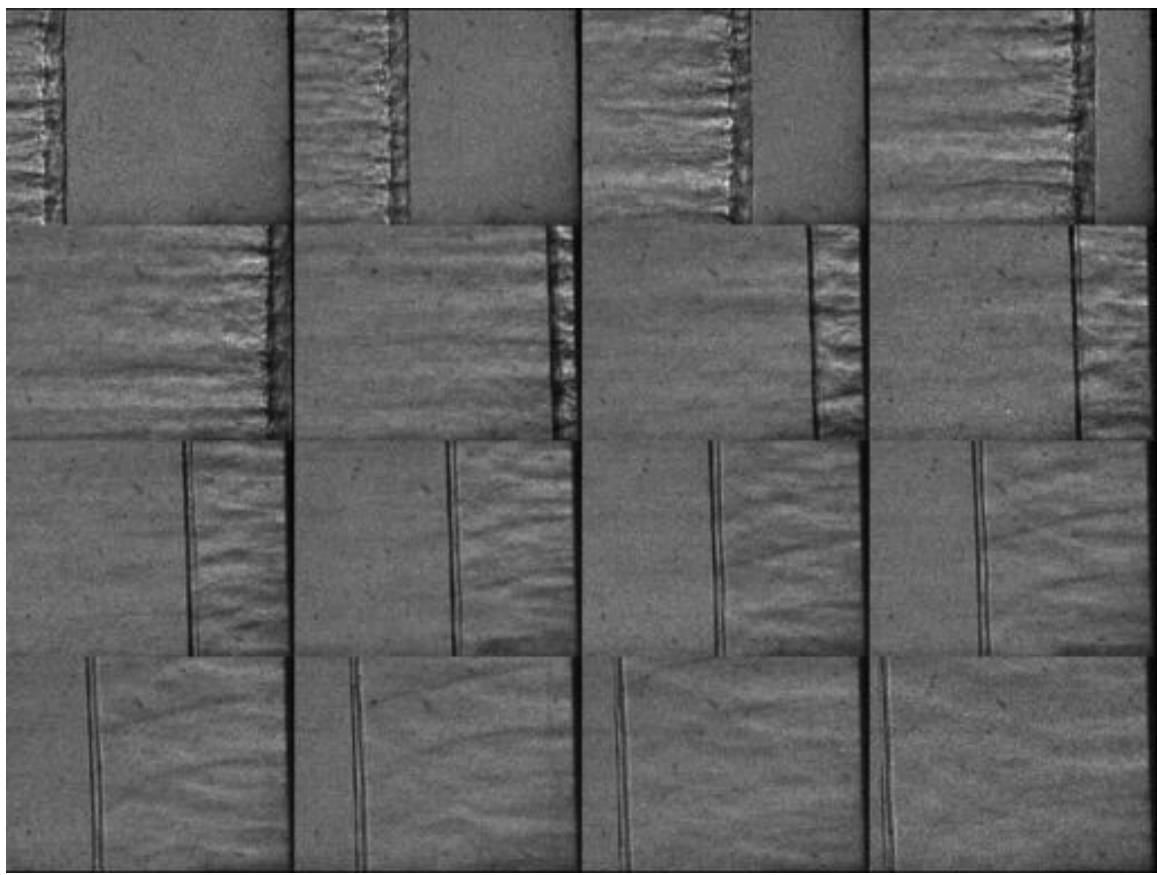


Figure E.42: Unfocused schlieren image of shot 2179. The field of view is approximately 30 mm wide.

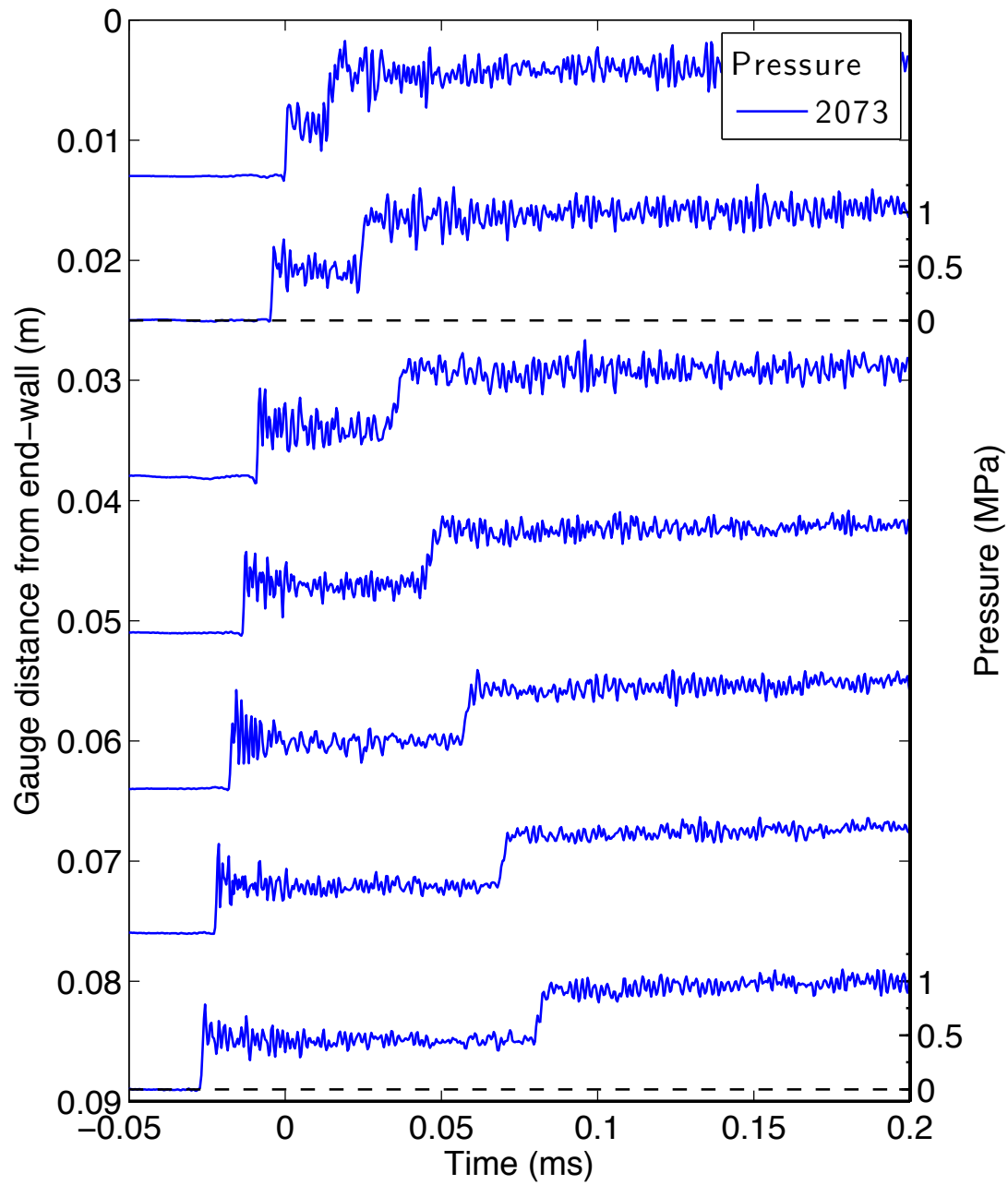


Figure E.43: Pressure traces for a detonation in stoichiometric hydrogen-oxygen at fill pressure 30 kPa, part 1.

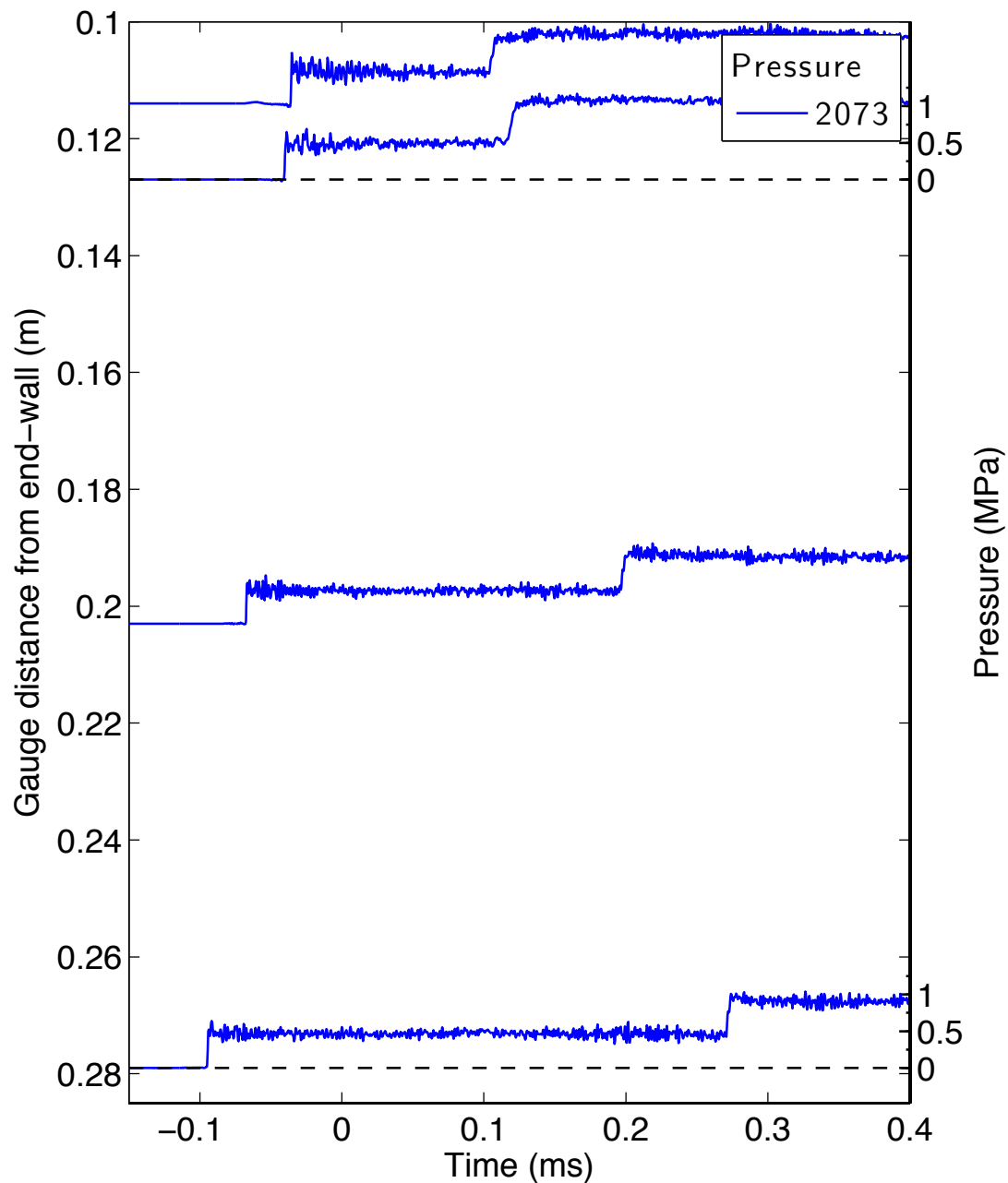


Figure E.44: Pressure traces for a detonation in stoichiometric hydrogen-oxygen at fill pressure 30 kPa, part 2.

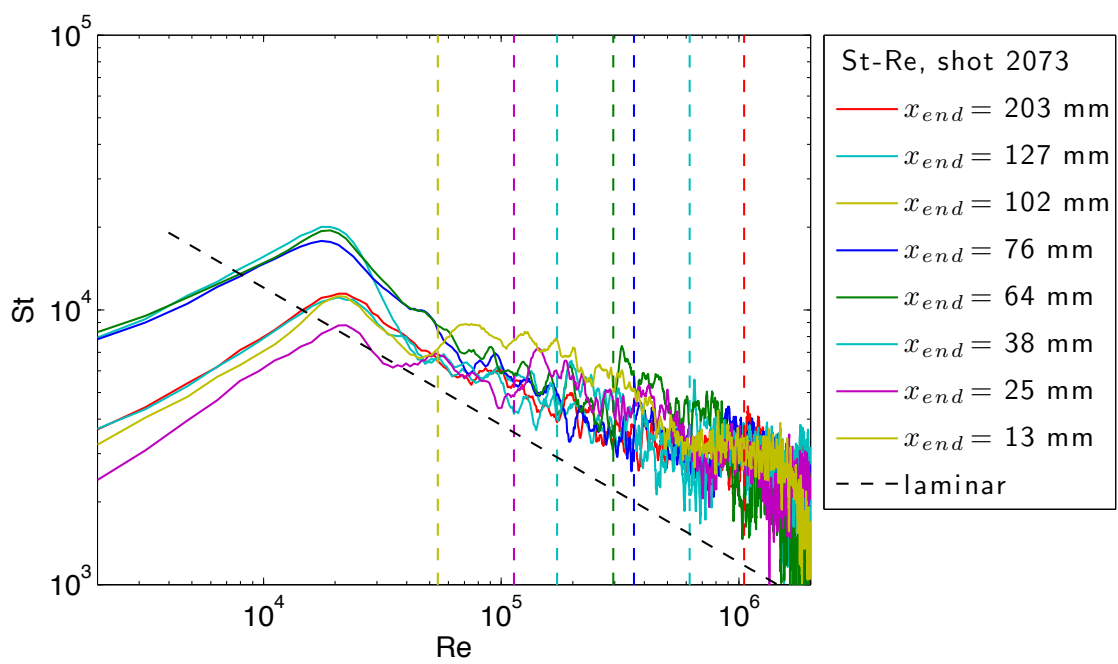


Figure E.45: Stanton-Reynolds number traces from shot 2073, a detonation in stoichiometric hydrogen-oxygen at fill pressure 30 kPa. The dashed vertical lines represent the arrival of the reflected shock wave.

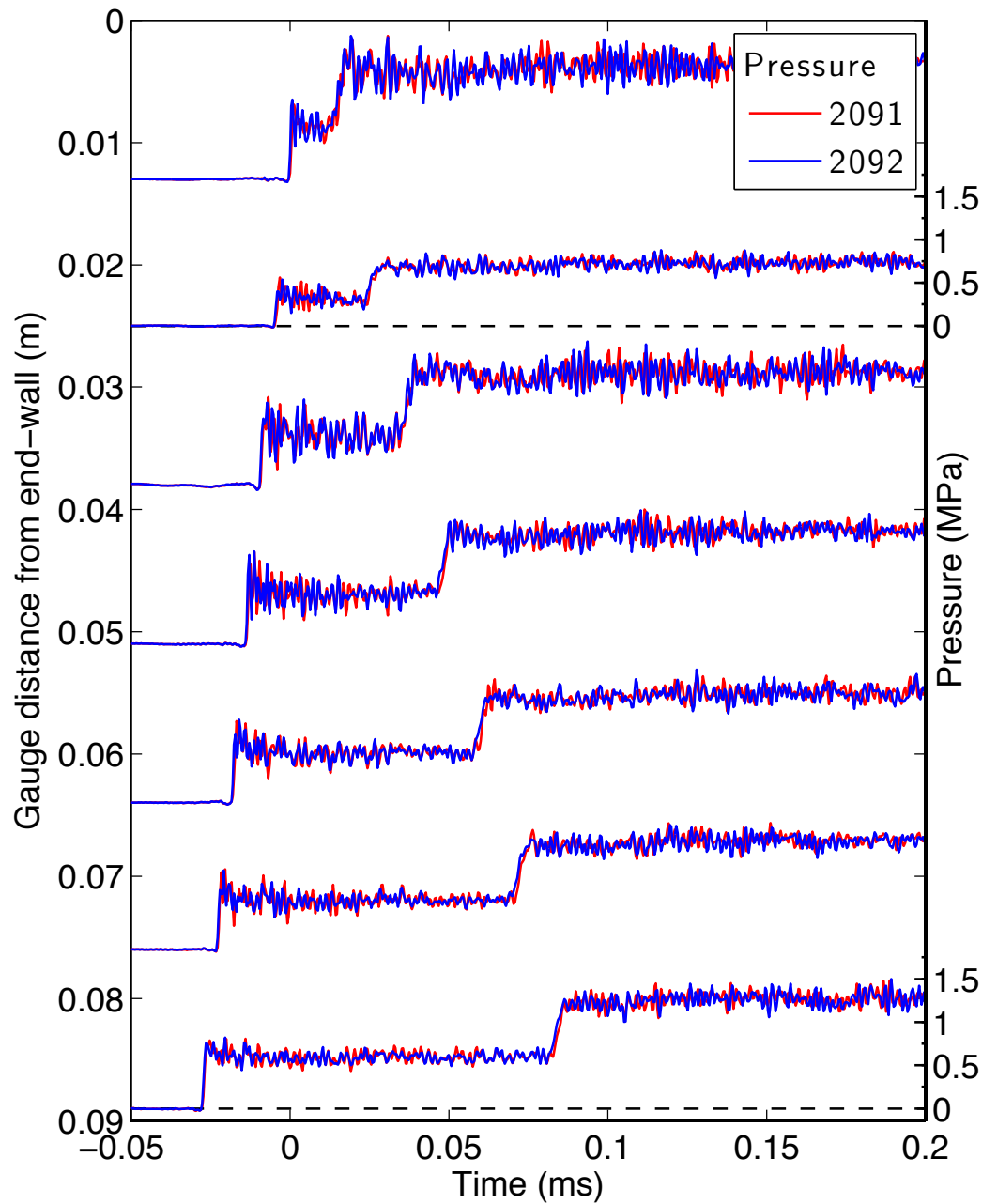


Figure E.46: Pressure traces for a detonation in stoichiometric hydrogen-oxygen at fill pressure 40 kPa, part 1.

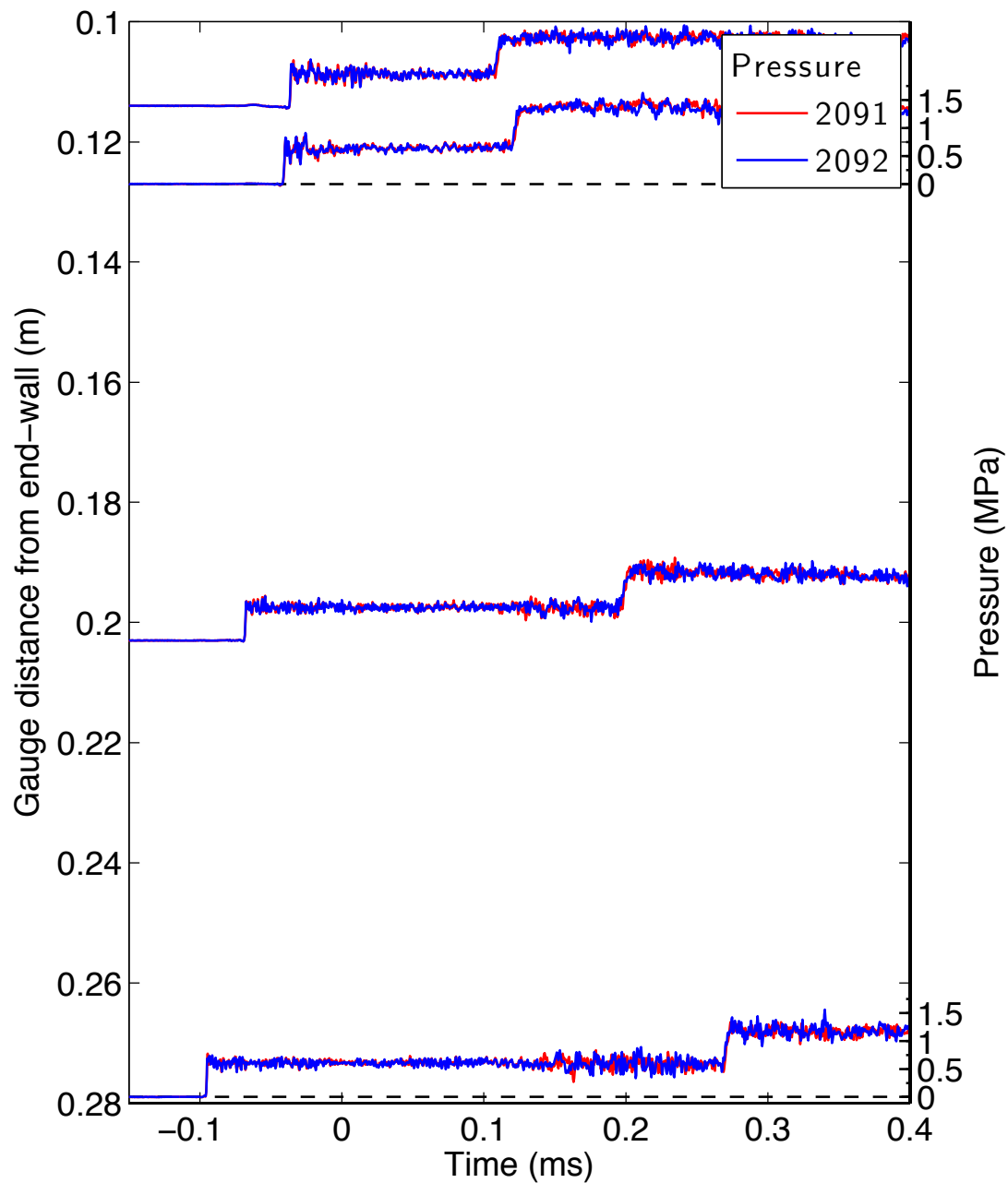


Figure E.47: Pressure traces for a detonation in stoichiometric hydrogen-oxygen at fill pressure 40 kPa, part 2.

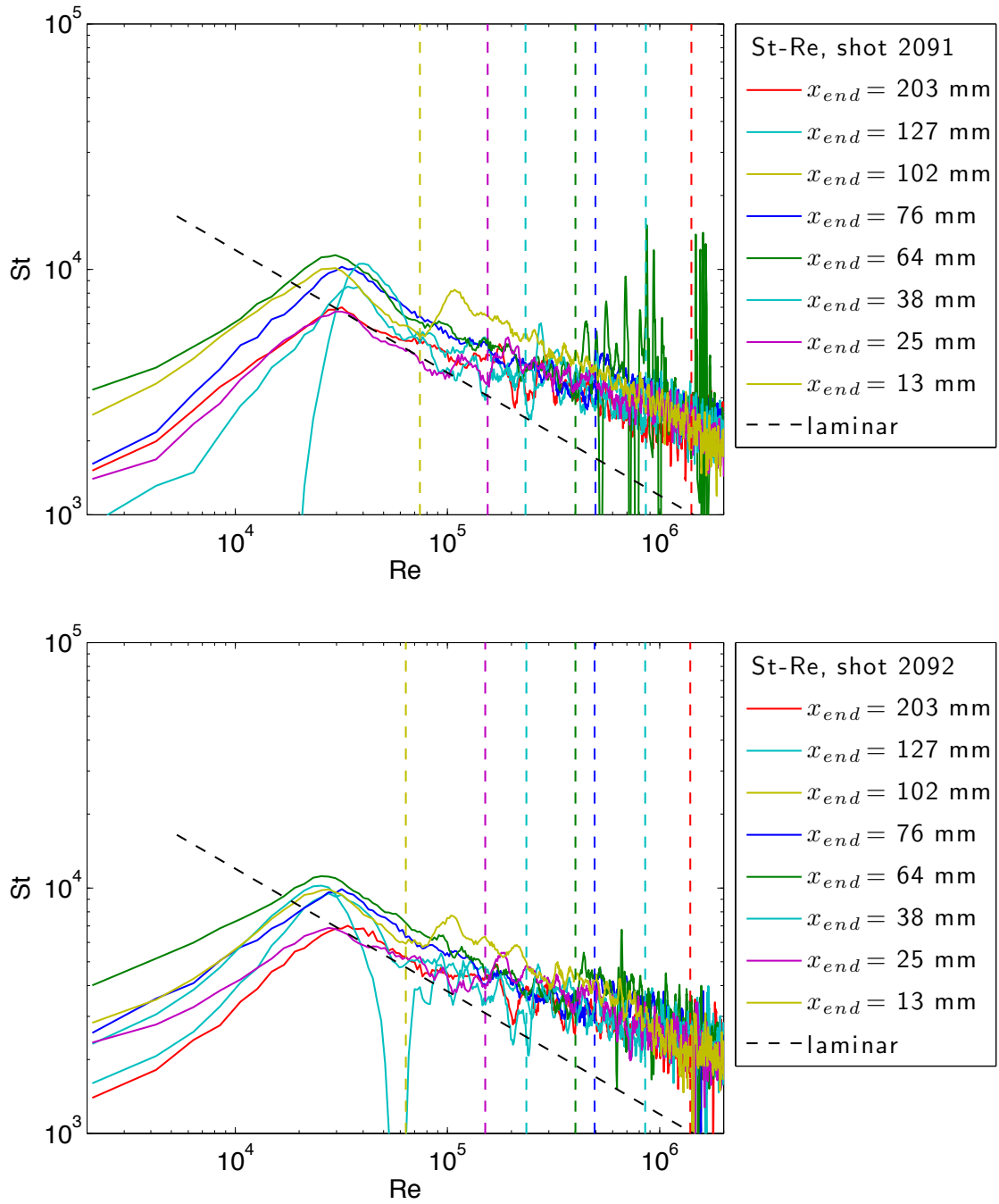


Figure E.48: Stanton-Reynolds number traces from shot 2092, a detonation in stoichiometric hydrogen-oxygen at fill pressure 40 kPa. The dashed vertical lines represent the arrival of the reflected shock wave.

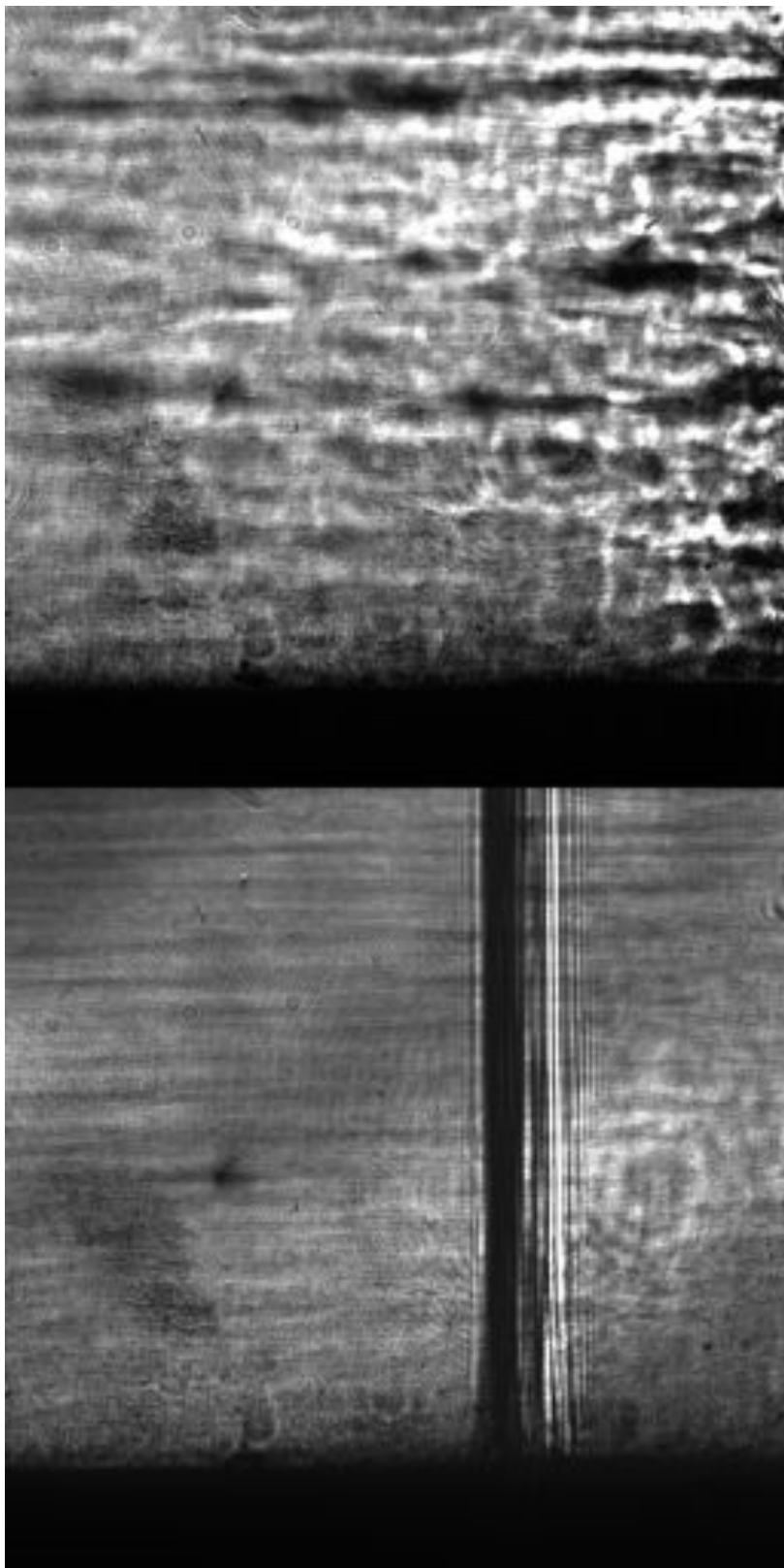


Figure E.49: Focused schlieren image of shot 2091. The field of view is approximately 14 mm wide.

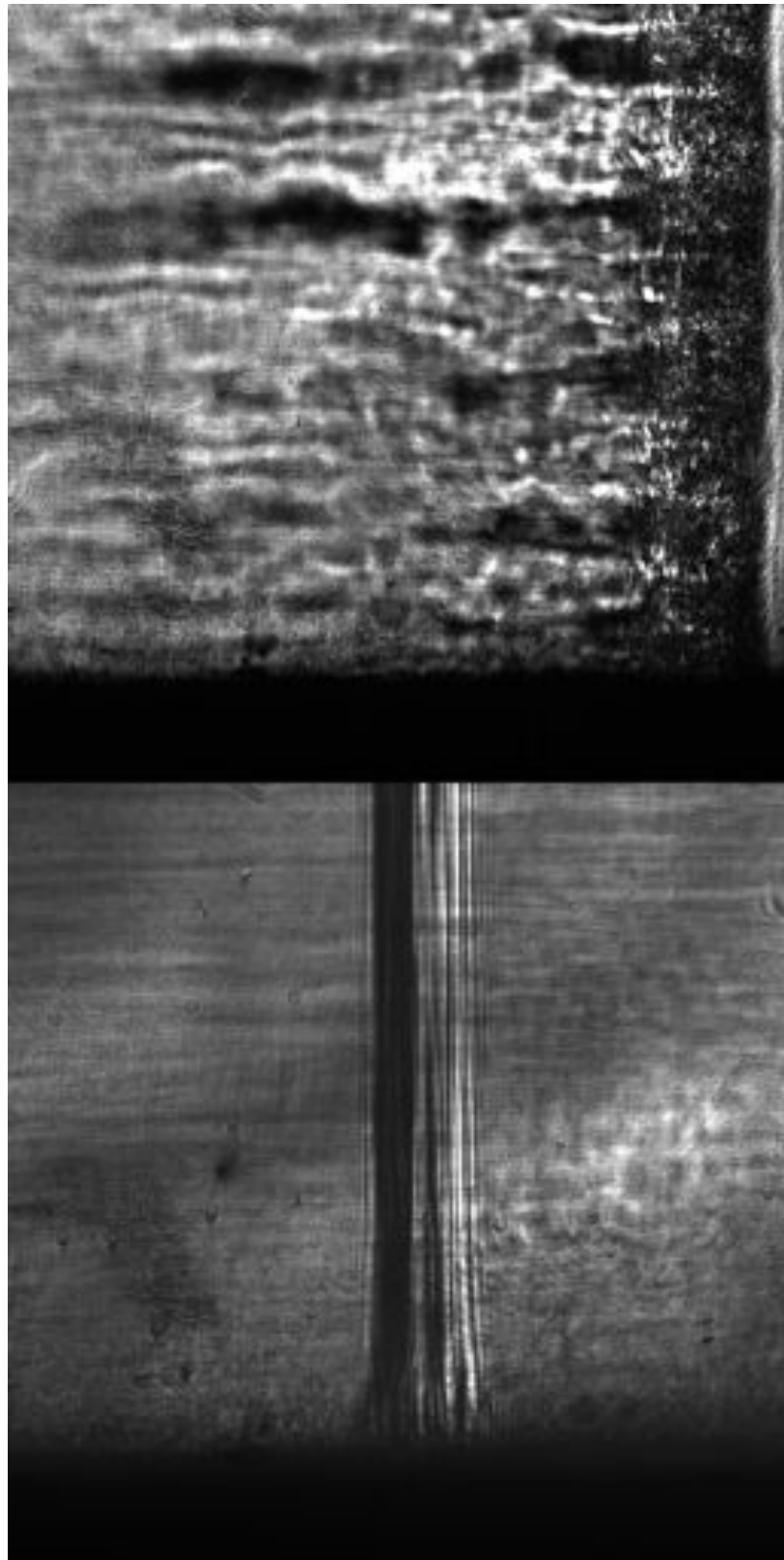


Figure E.50: Focused schlieren image of shot 2092. The field of view is approximately 14 mm wide.

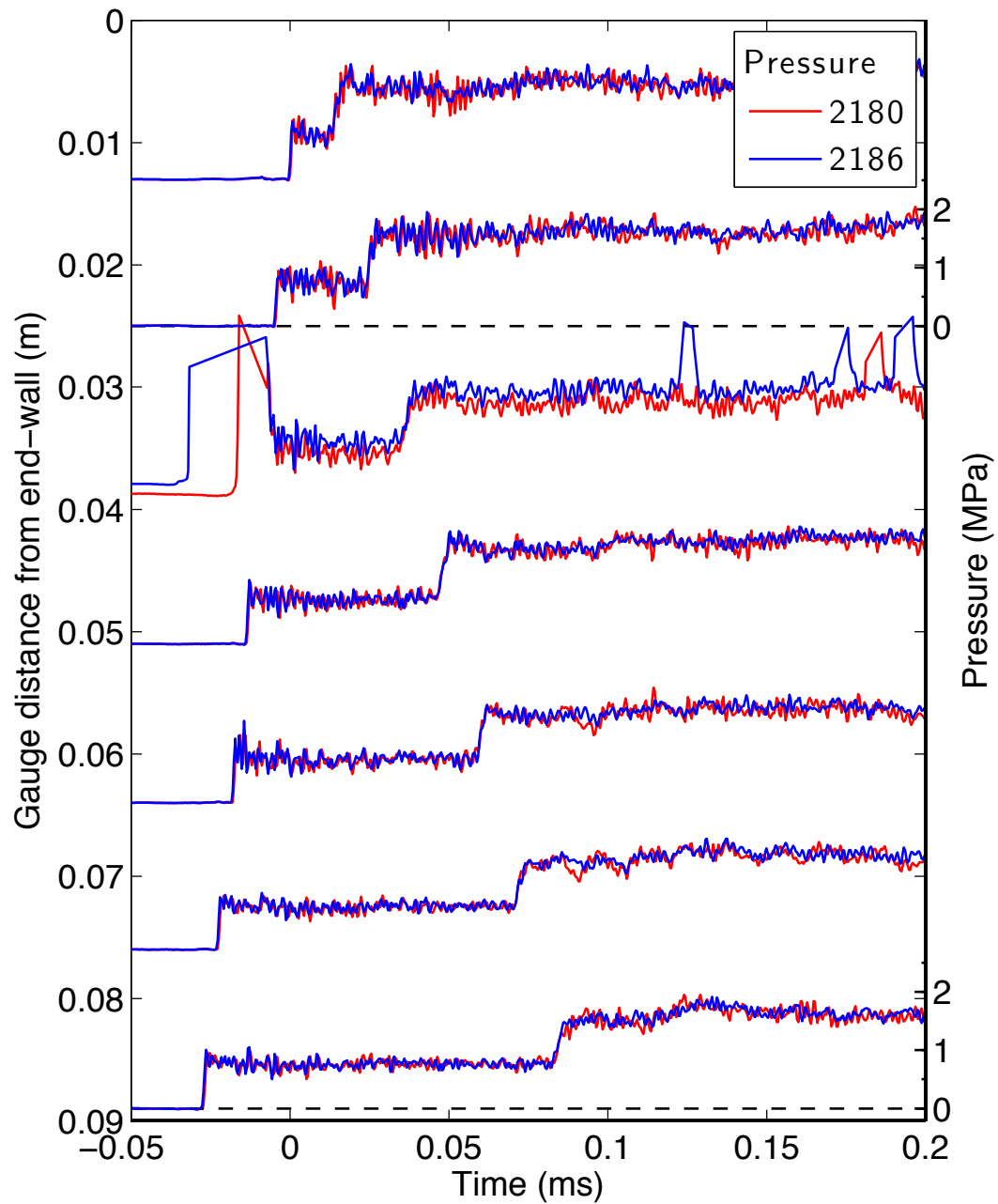


Figure E.51: Pressure traces for a detonation in stoichiometric hydrogen-oxygen at fill pressure 50 kPa, part 1.

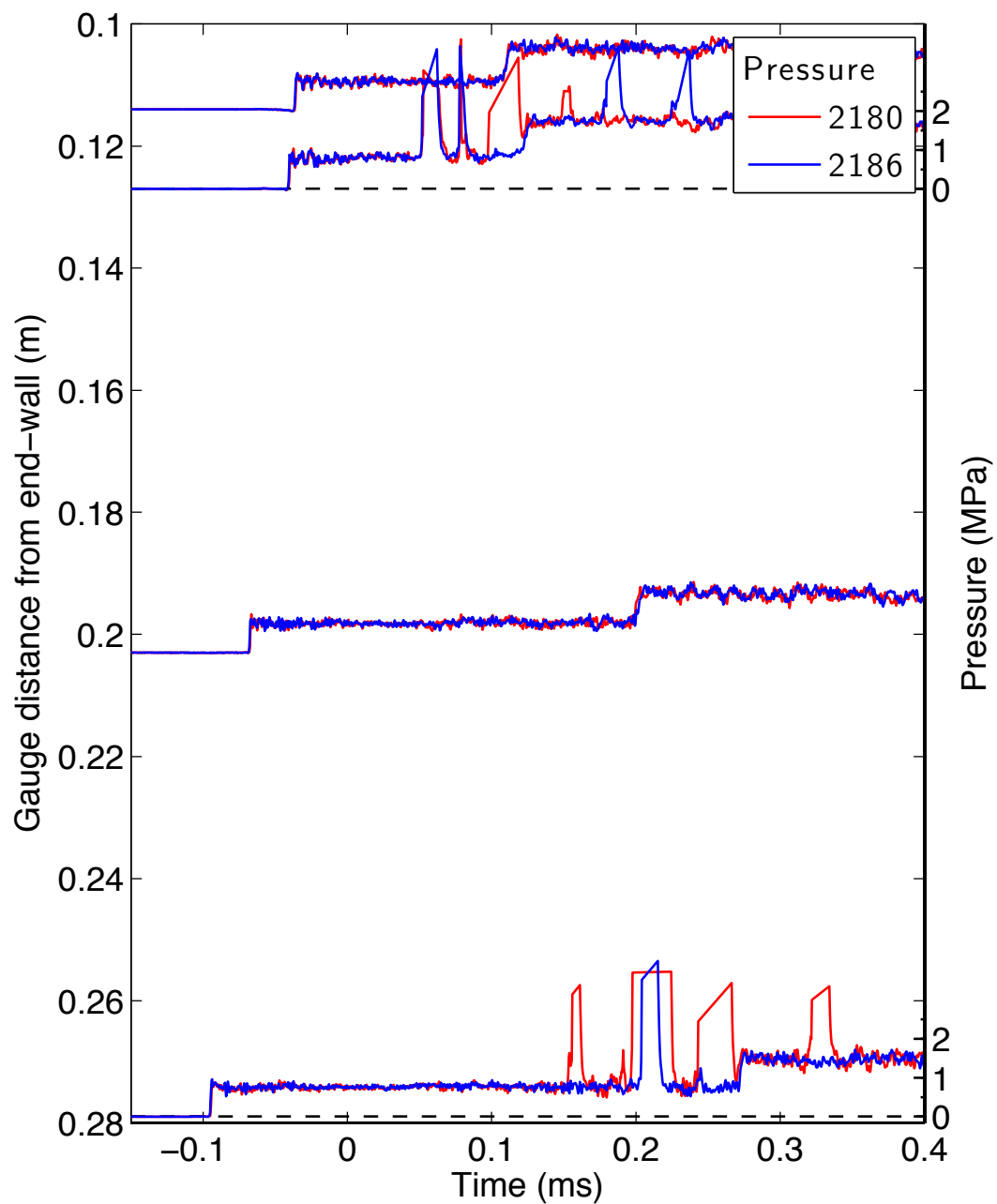


Figure E.52: Pressure traces for a detonation in stoichiometric hydrogen-oxygen at fill pressure 50 kPa, part 2.

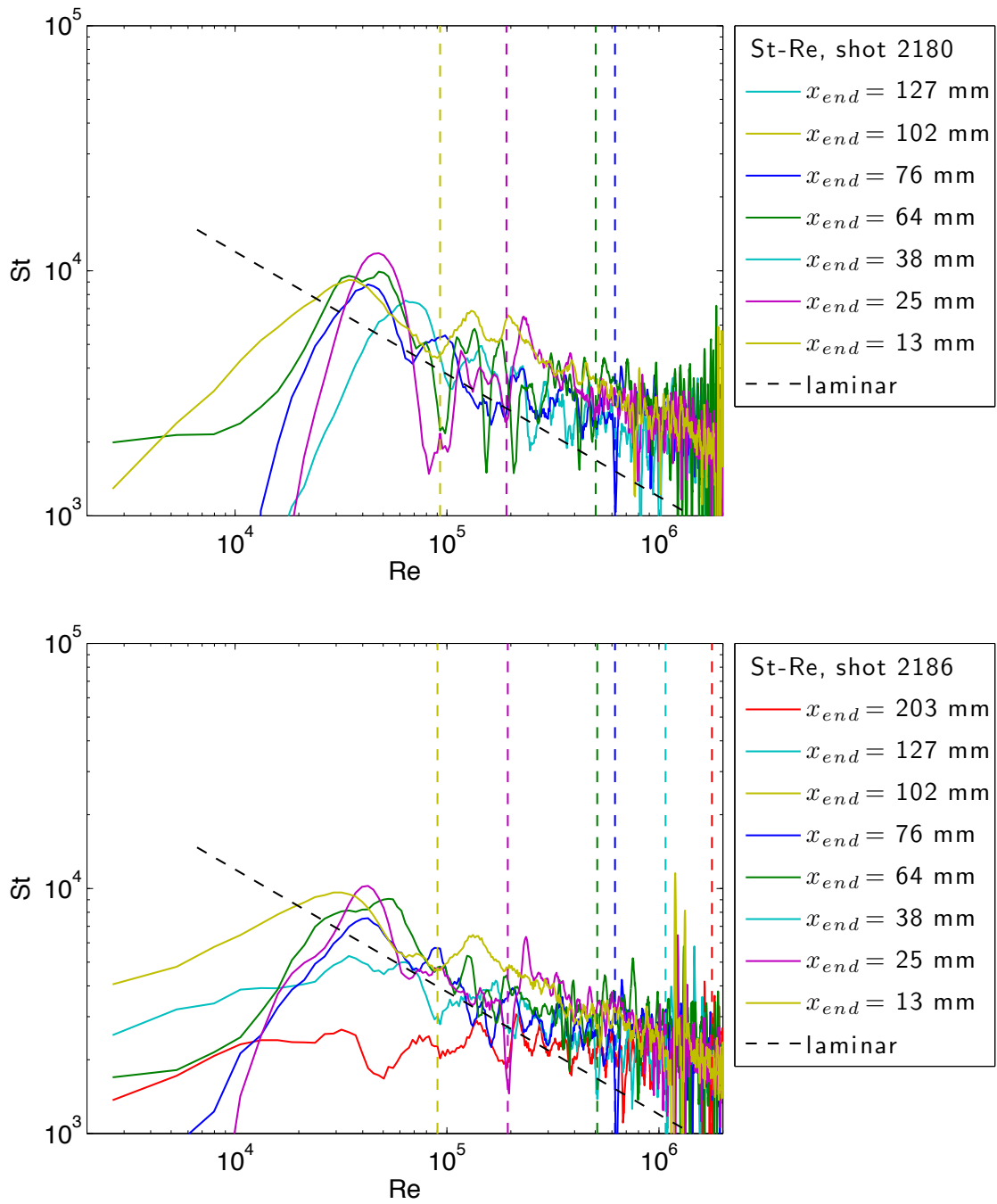


Figure E.53: Stanton-Reynolds number traces from shot 2186, a detonation in stoichiometric hydrogen-oxygen at fill pressure 50 kPa. The dashed vertical lines represent the arrival of the reflected shock wave.

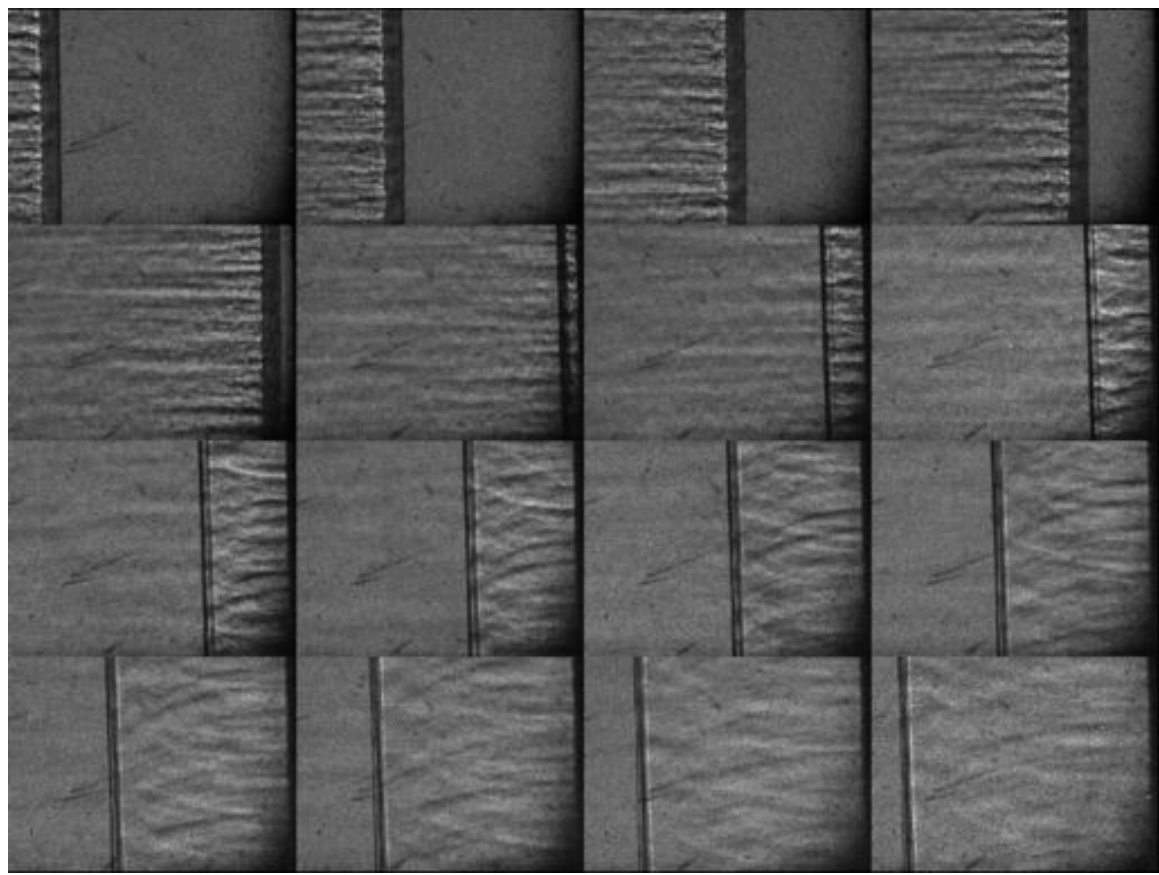


Figure E.54: Unfocused schlieren image of shot 2180. The field of view is approximately 30 mm wide.

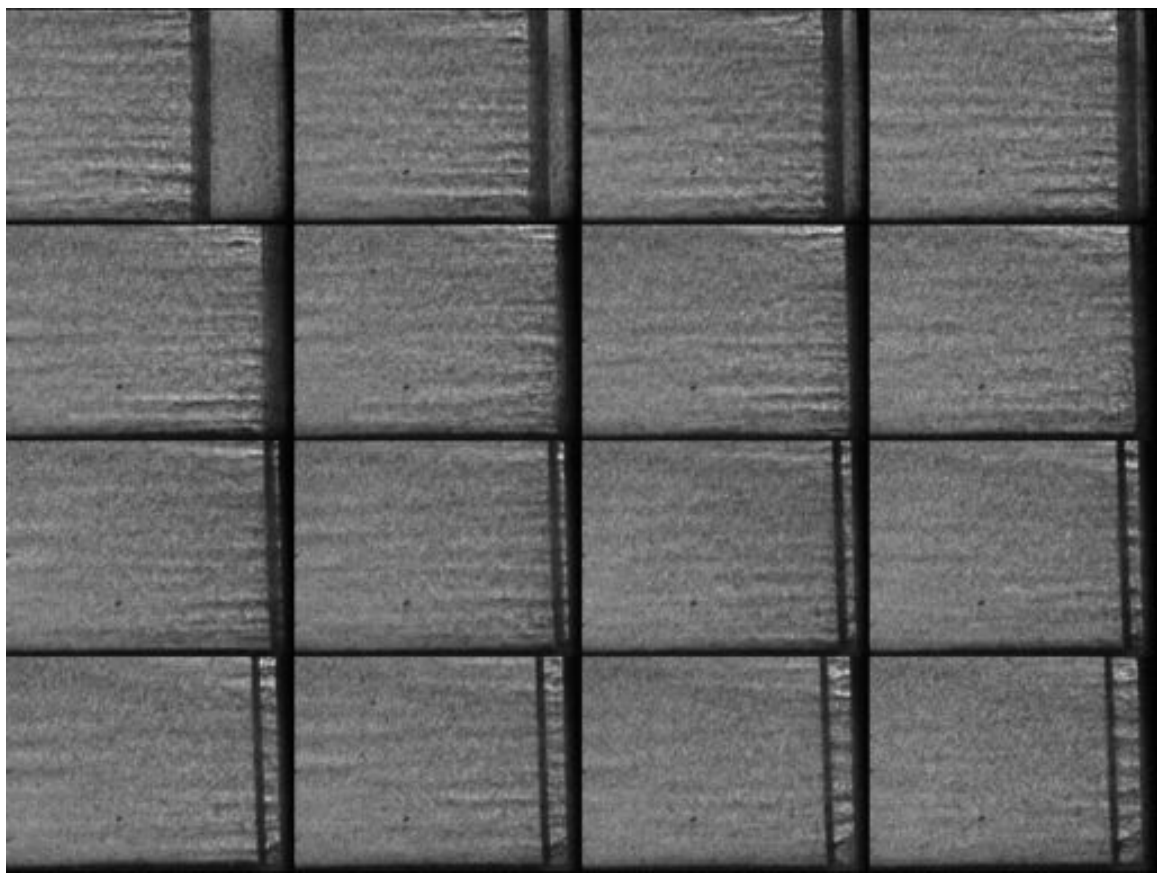


Figure E.55: Unfocused schlieren image of shot 2186. The field of view is approximately 30 mm wide.

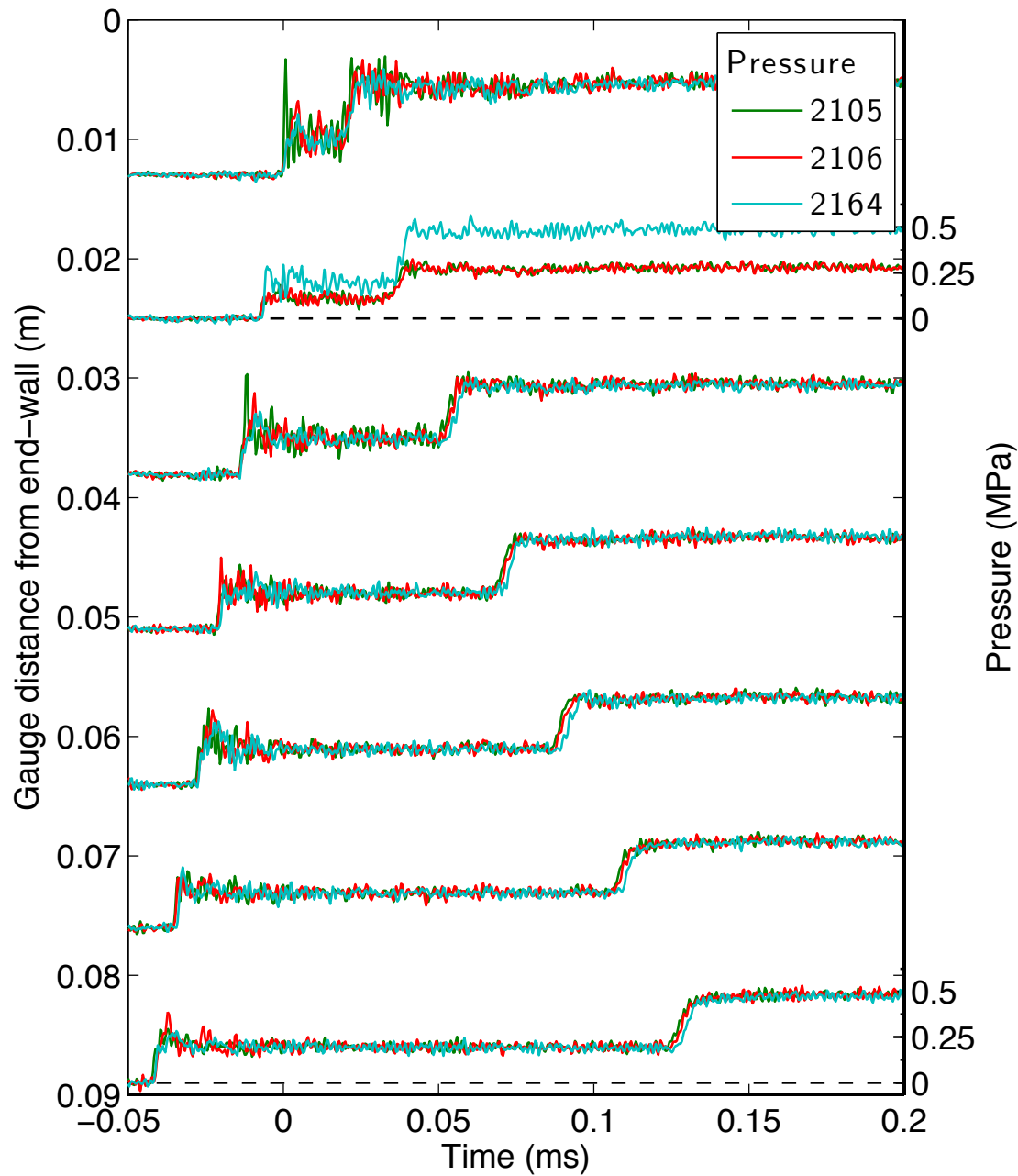


Figure E.56: Pressure traces for a detonation in stoichiometric hydrogen-oxygen with 50% argon dilution at fill pressure 10 kPa, part 1.

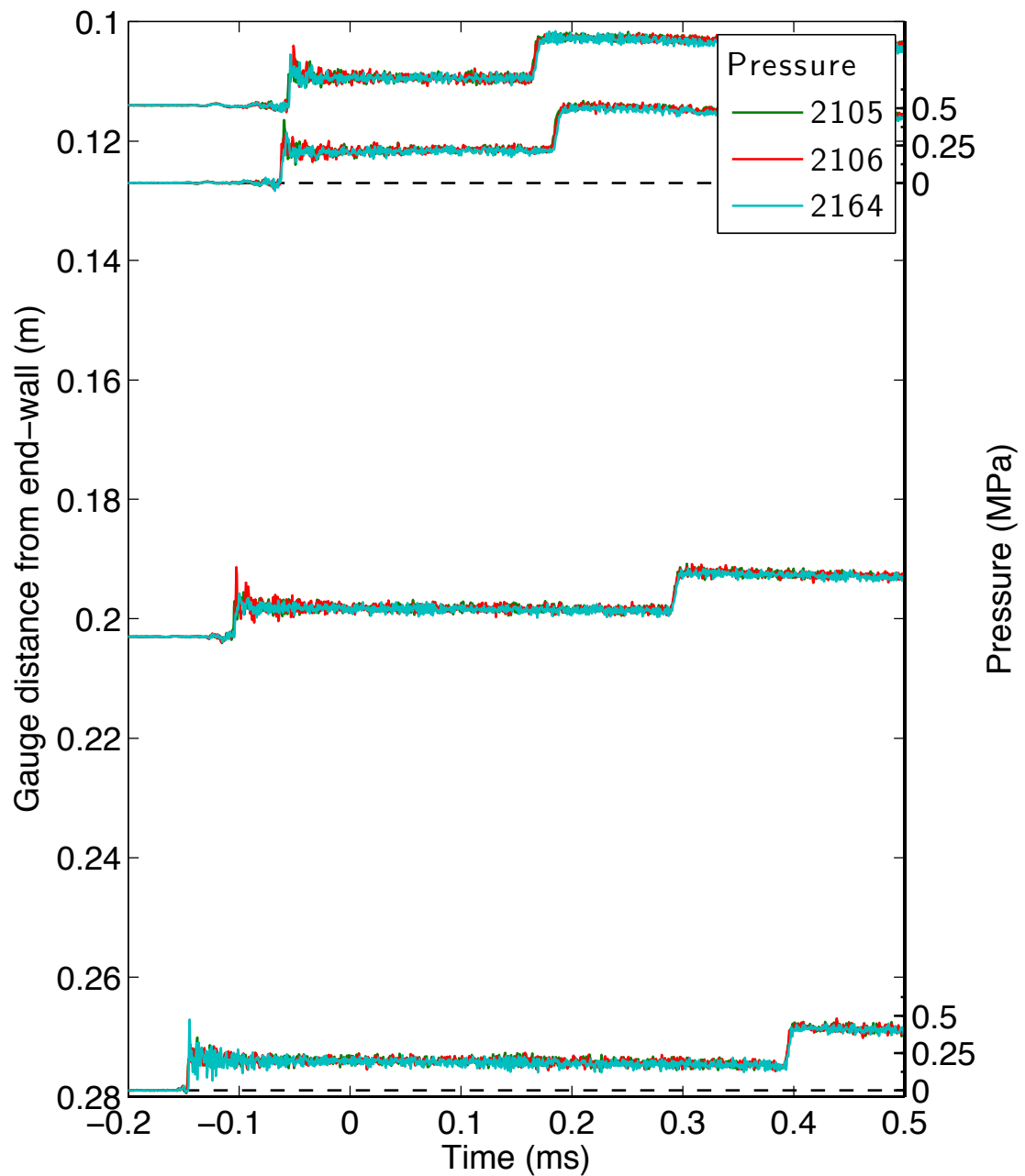


Figure E.57: Pressure traces for a detonation in stoichiometric hydrogen-oxygen with 50% argon dilution at fill pressure 10 kPa, part 2.

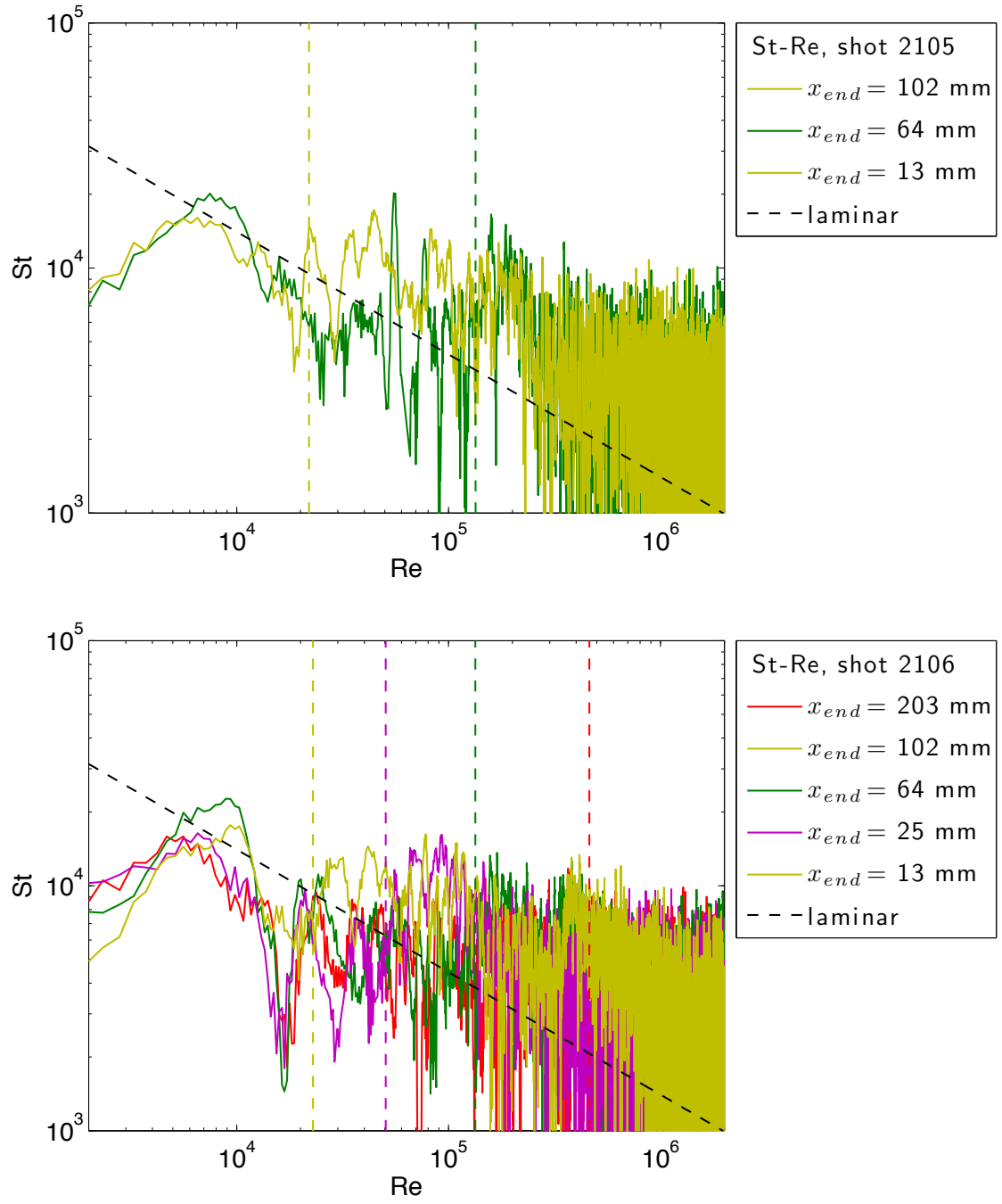


Figure E.58: Stanton-Reynolds number traces from shot 2106, a detonation in stoichiometric hydrogen-oxygen with 50% argon dilution at fill pressure 10 kPa. The dashed vertical lines represent the arrival of the reflected shock wave.

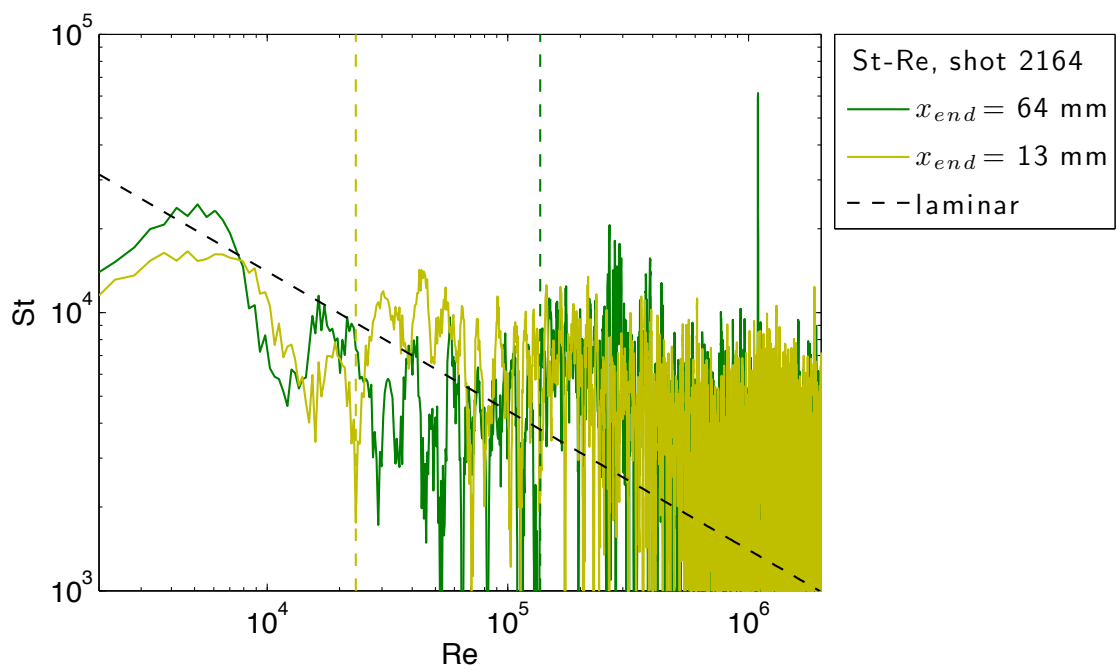


Figure E.59: Stanton-Reynolds number traces from shot 2164, a detonation in stoichiometric hydrogen-oxygen with 50% argon dilution at fill pressure 10 kPa. The dashed vertical lines represent the arrival of the reflected shock wave.

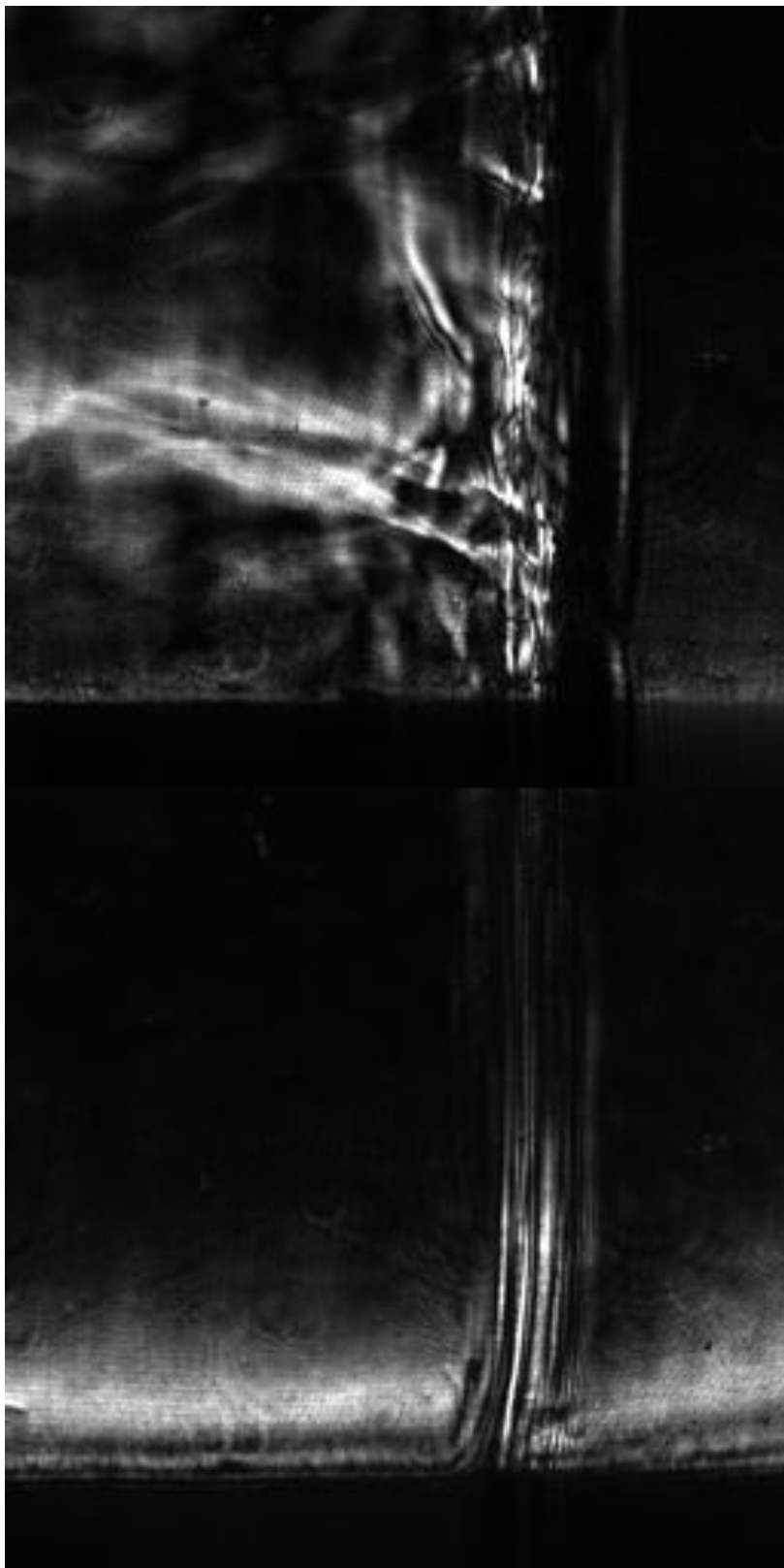


Figure E.60: Focused schlieren image of shot 2106. The field of view is approximately 14 mm wide.

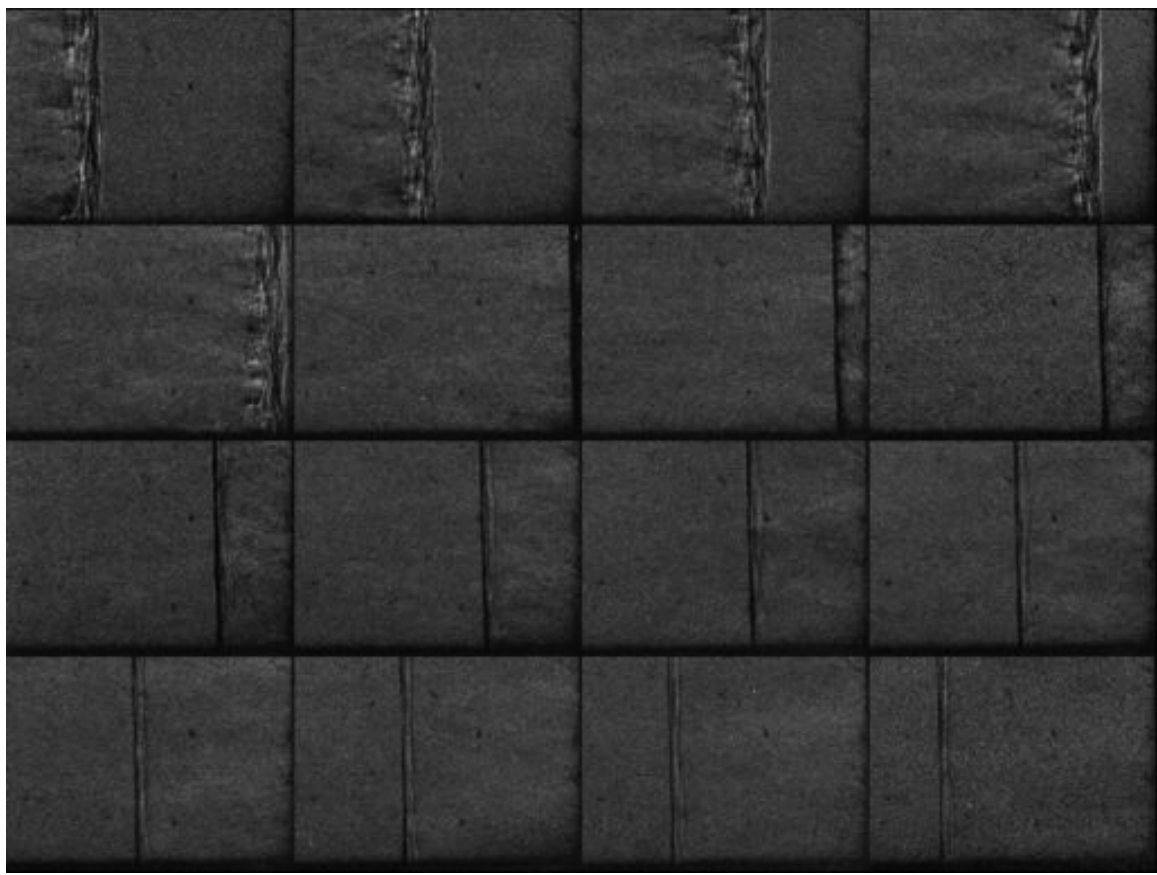


Figure E.61: Unfocused schlieren image of shot 2164. The field of view is approximately 30 mm wide.

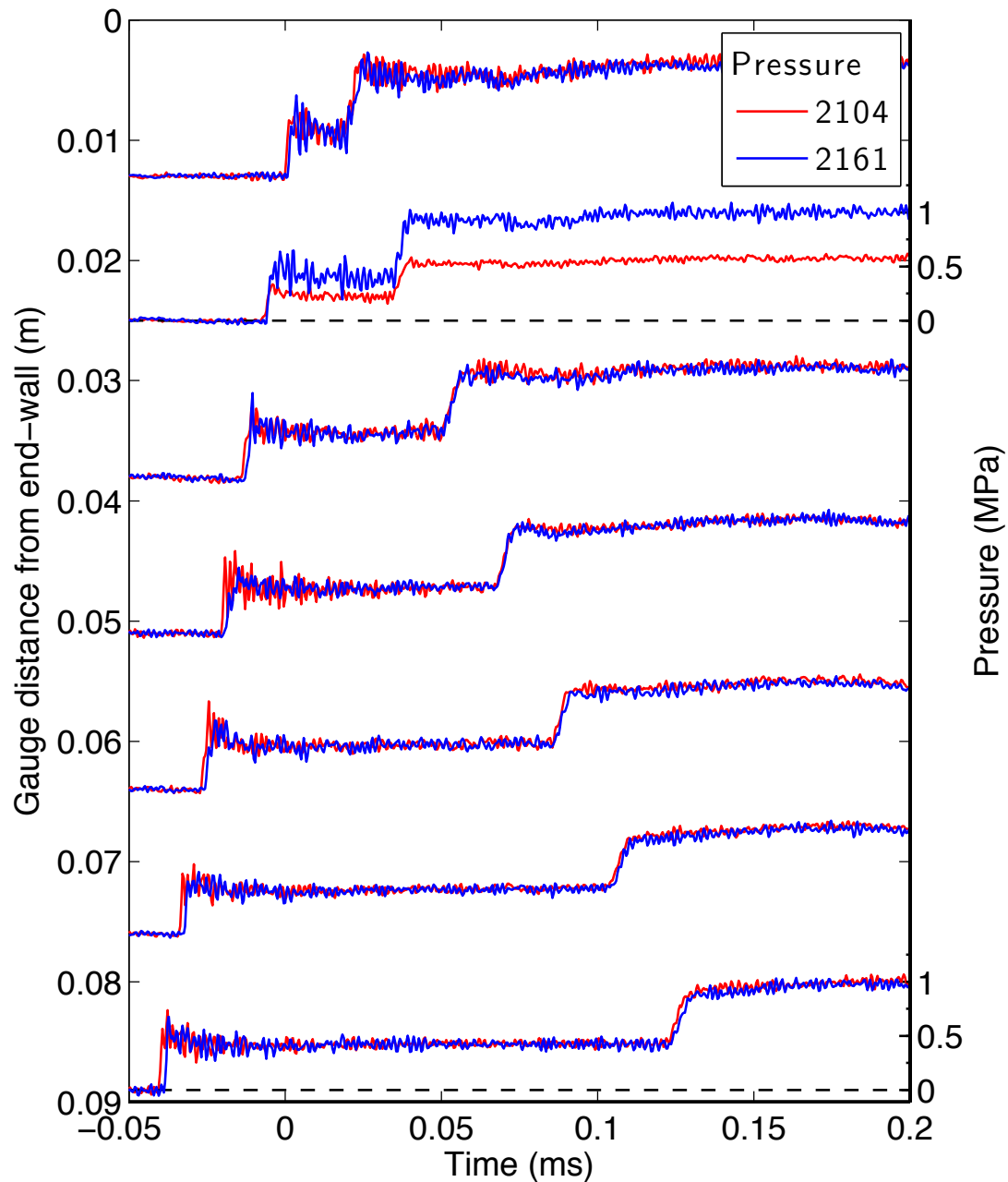


Figure E.62: Pressure traces for a detonation in stoichiometric hydrogen-oxygen with 50% argon dilution at fill pressure 25 kPa, part 1.

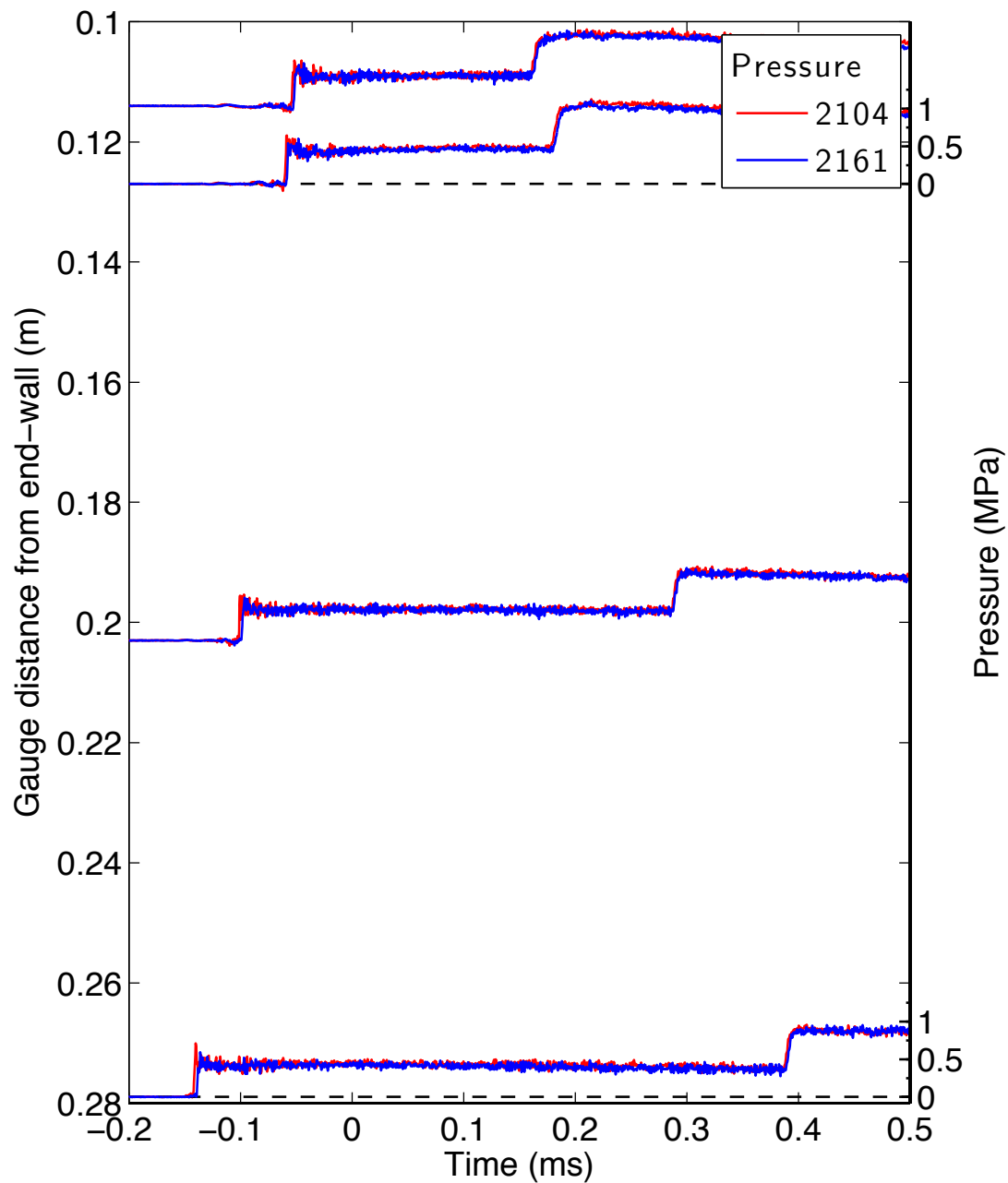


Figure E.63: Pressure traces for a detonation in stoichiometric hydrogen-oxygen with 50% argon dilution at fill pressure 25 kPa, part 2.

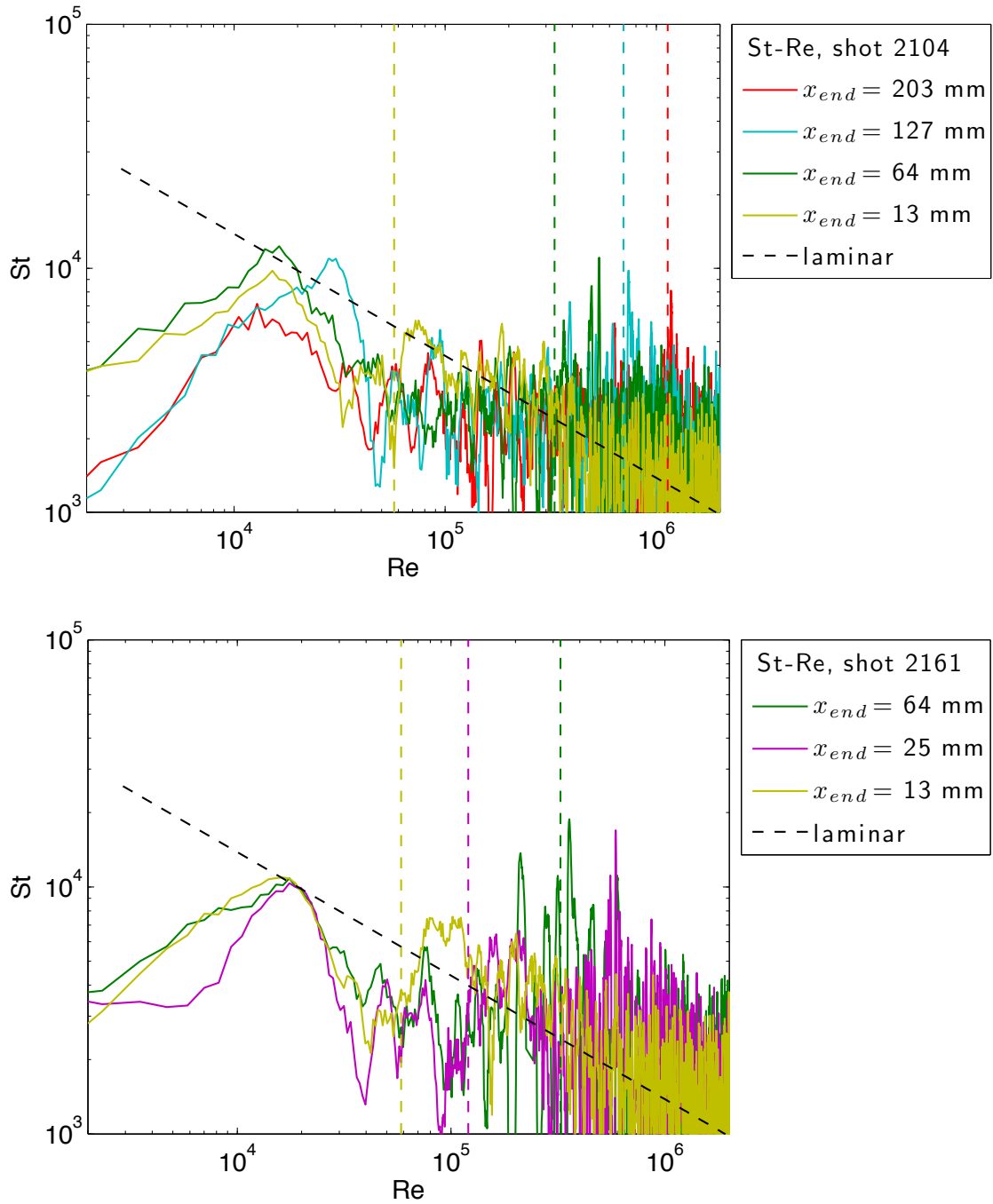


Figure E.64: Stanton-Reynolds number traces from shot 2161, a detonation in stoichiometric hydrogen-oxygen with 50% argon dilution at fill pressure 25 kPa. The dashed vertical lines represent the arrival of the reflected shock wave.

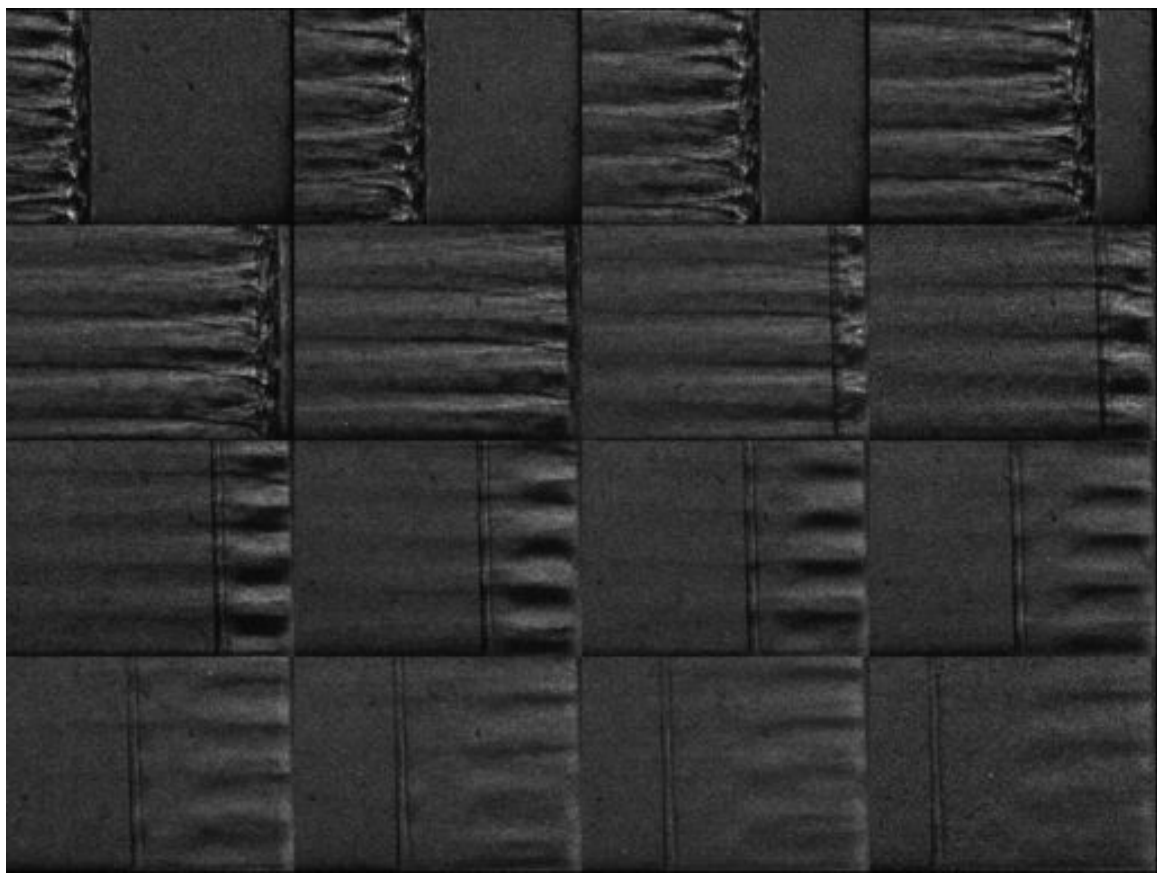


Figure E.65: Unfocused schlieren image of shot 2161. The field of view is approximately 30 mm wide.

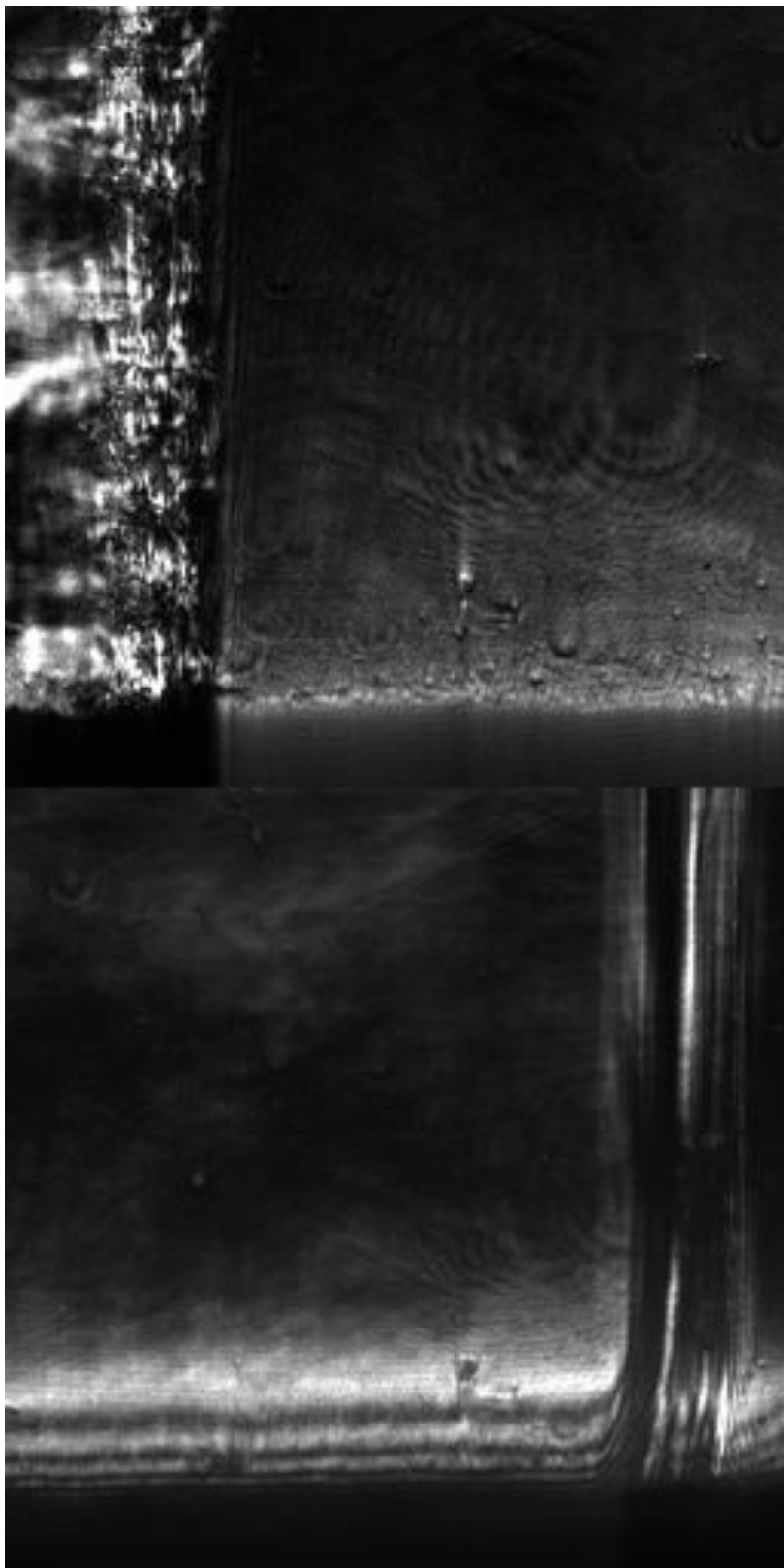


Figure E.66: Focused schlieren image of shot 2104. The field of view is approximately 14 mm wide.

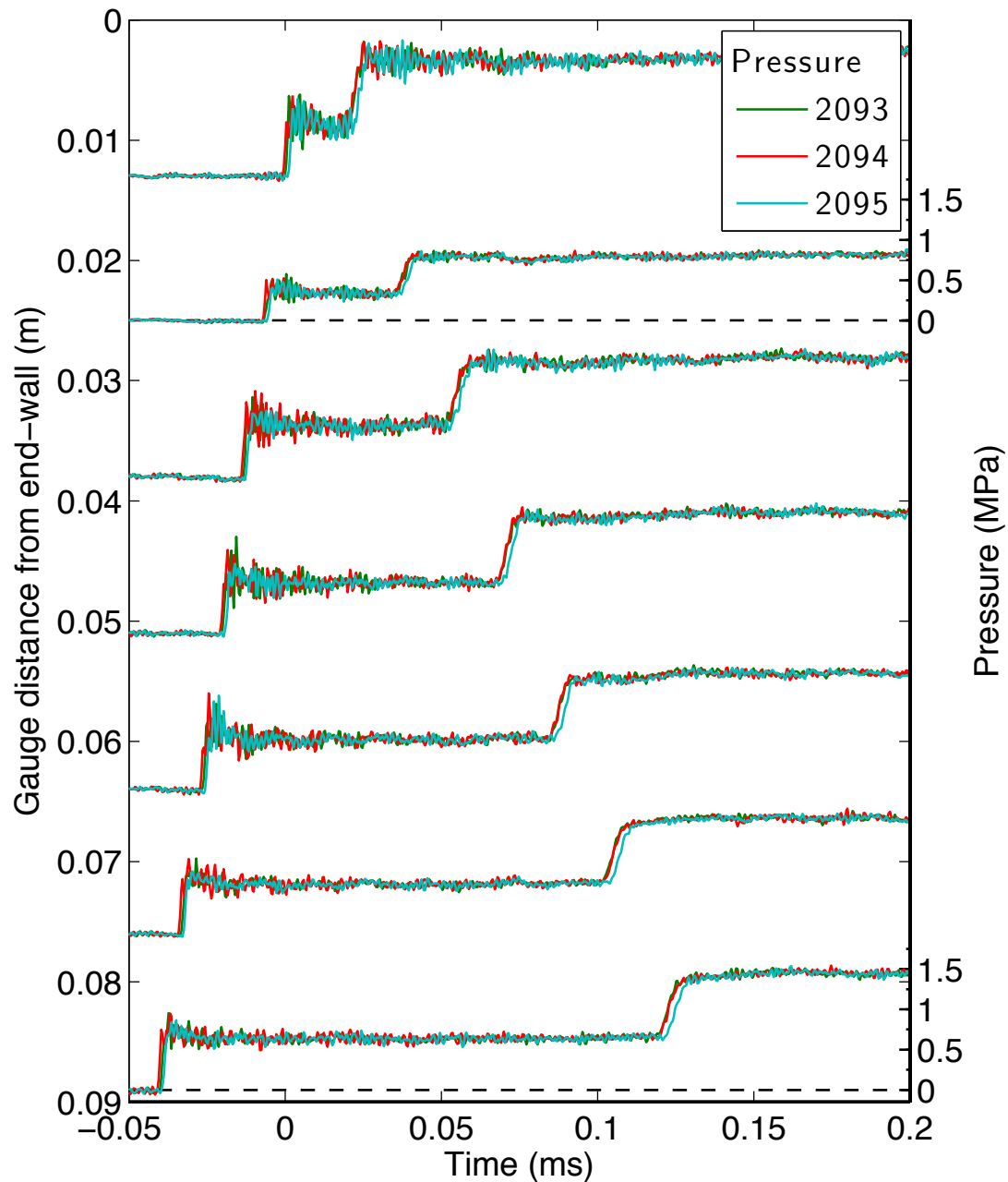


Figure E.67: Pressure traces for a detonation in stoichiometric hydrogen-oxygen with 50% argon dilution at fill pressure 40 kPa, part 1.

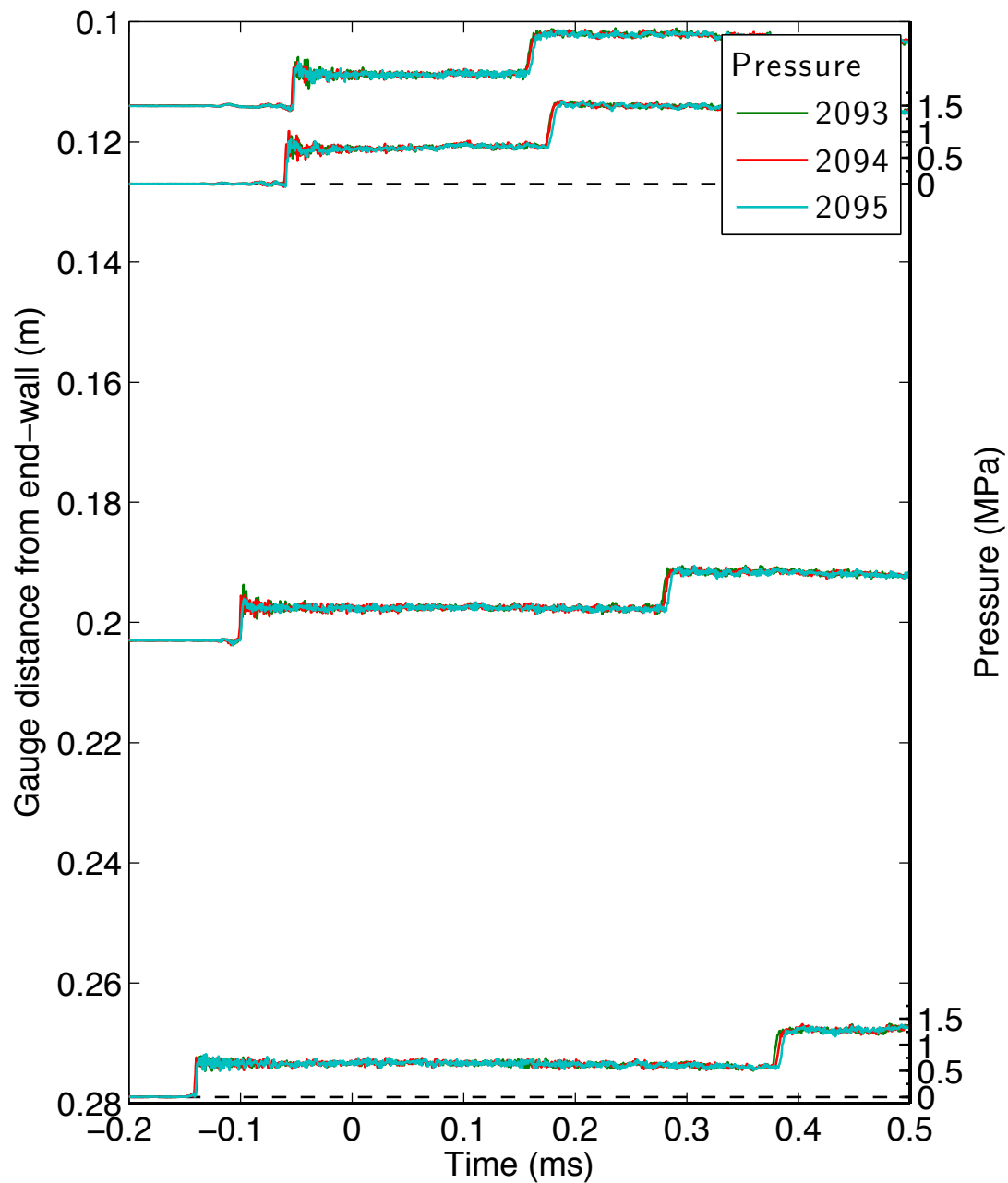


Figure E.68: Pressure traces for a detonation in stoichiometric hydrogen-oxygen with 50% argon dilution at fill pressure 40 kPa, part 2.

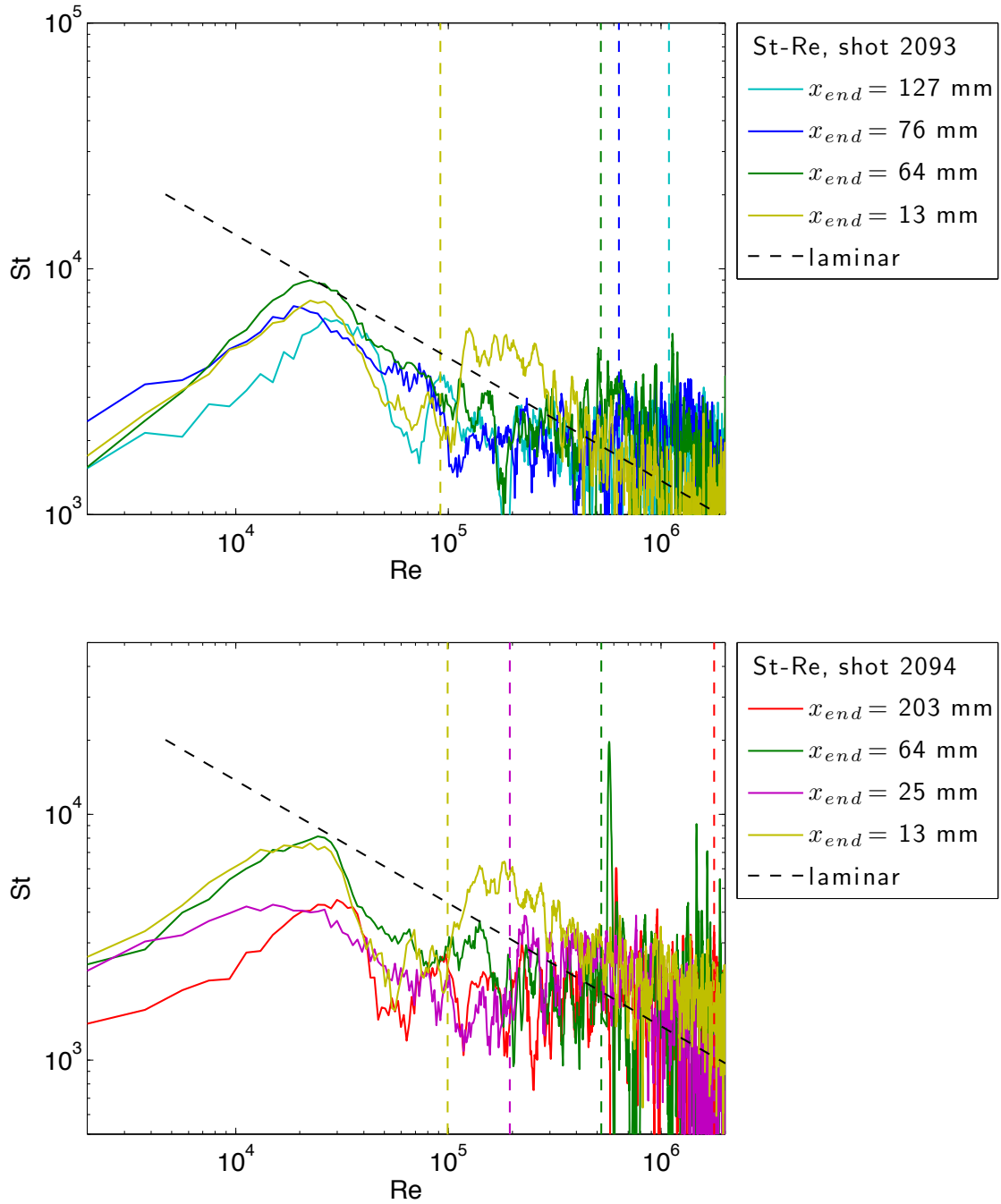


Figure E.69: Stanton-Reynolds number traces from shot 2094, a detonation in stoichiometric hydrogen-oxygen with 50% argon dilution at fill pressure 40 kPa. The dashed vertical lines represent the arrival of the reflected shock wave.

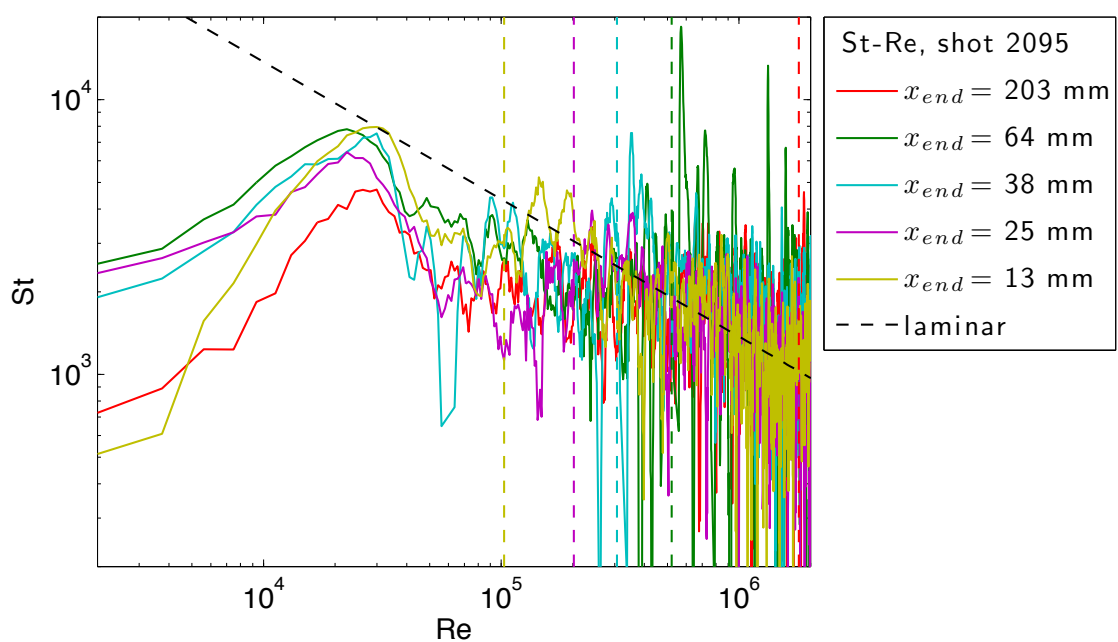


Figure E.70: Stanton-Reynolds number traces from shot 2095, a detonation in stoichiometric hydrogen-oxygen with 50% argon dilution at fill pressure 40 kPa. The dashed vertical lines represent the arrival of the reflected shock wave.

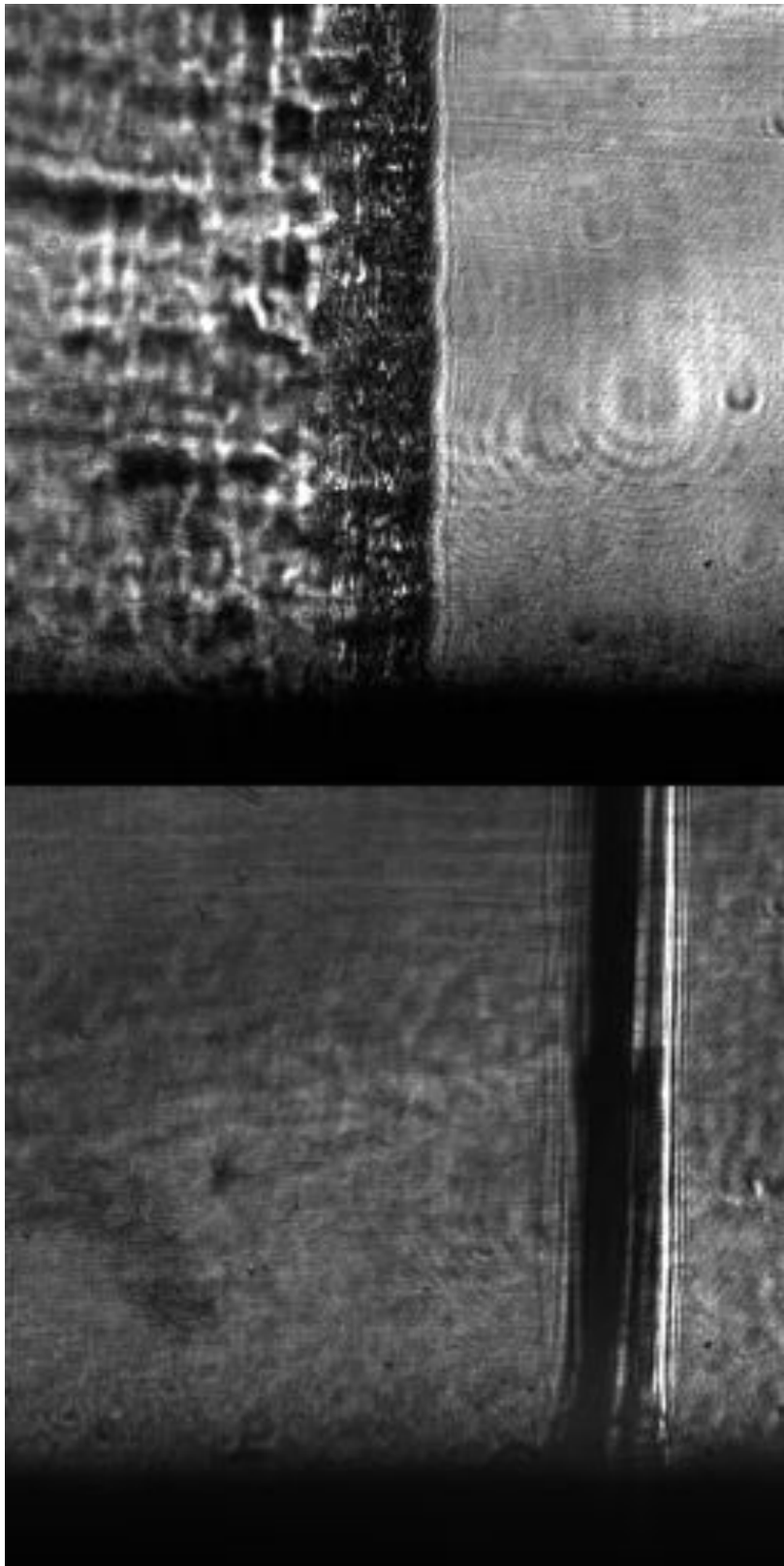


Figure E.71: Focused schlieren image of shot 2095. The field of view is approximately 14 mm wide.

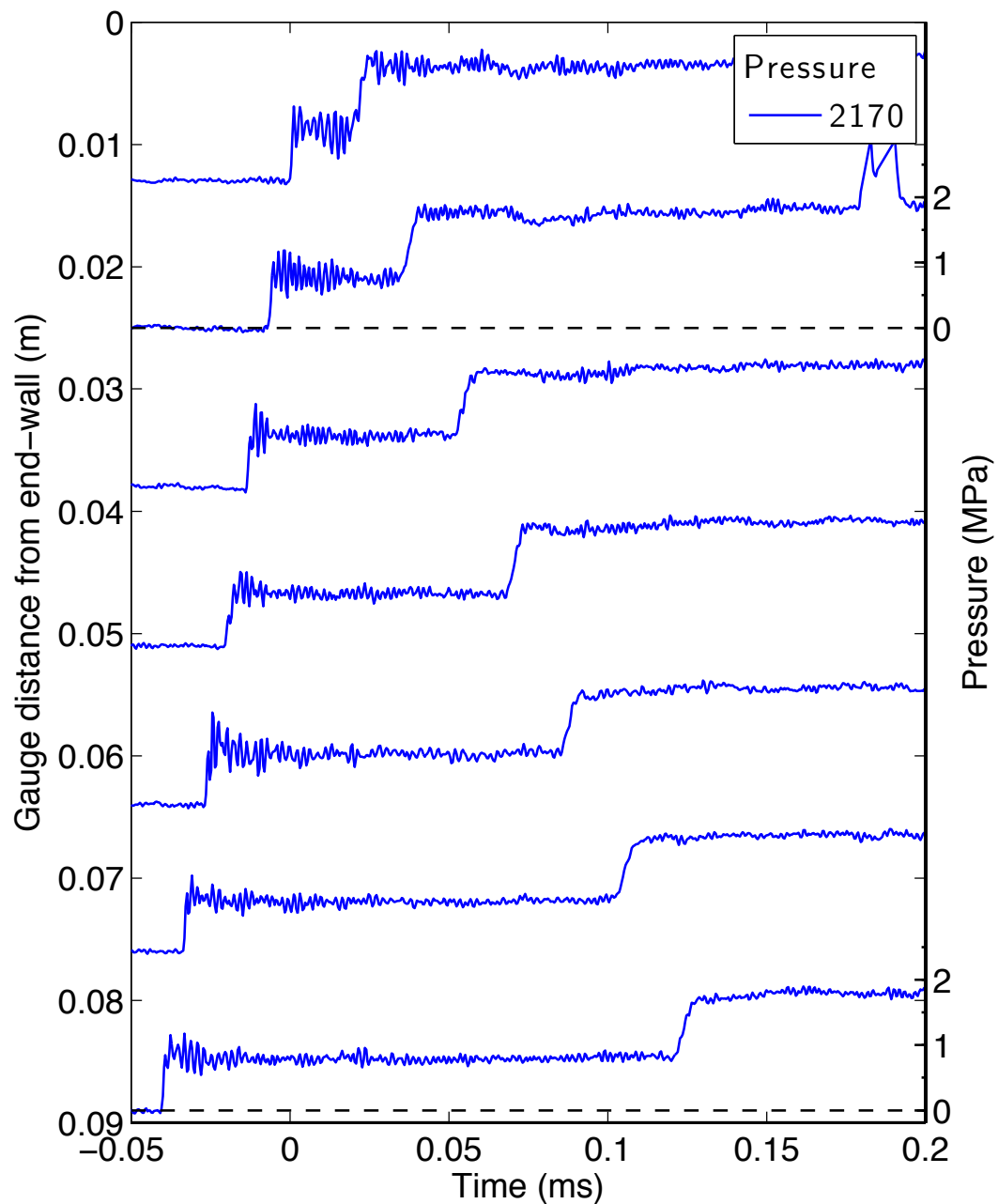


Figure E.72: Pressure traces for a detonation in stoichiometric hydrogen-oxygen with 50% argon dilution at fill pressure 50 kPa, part 1.

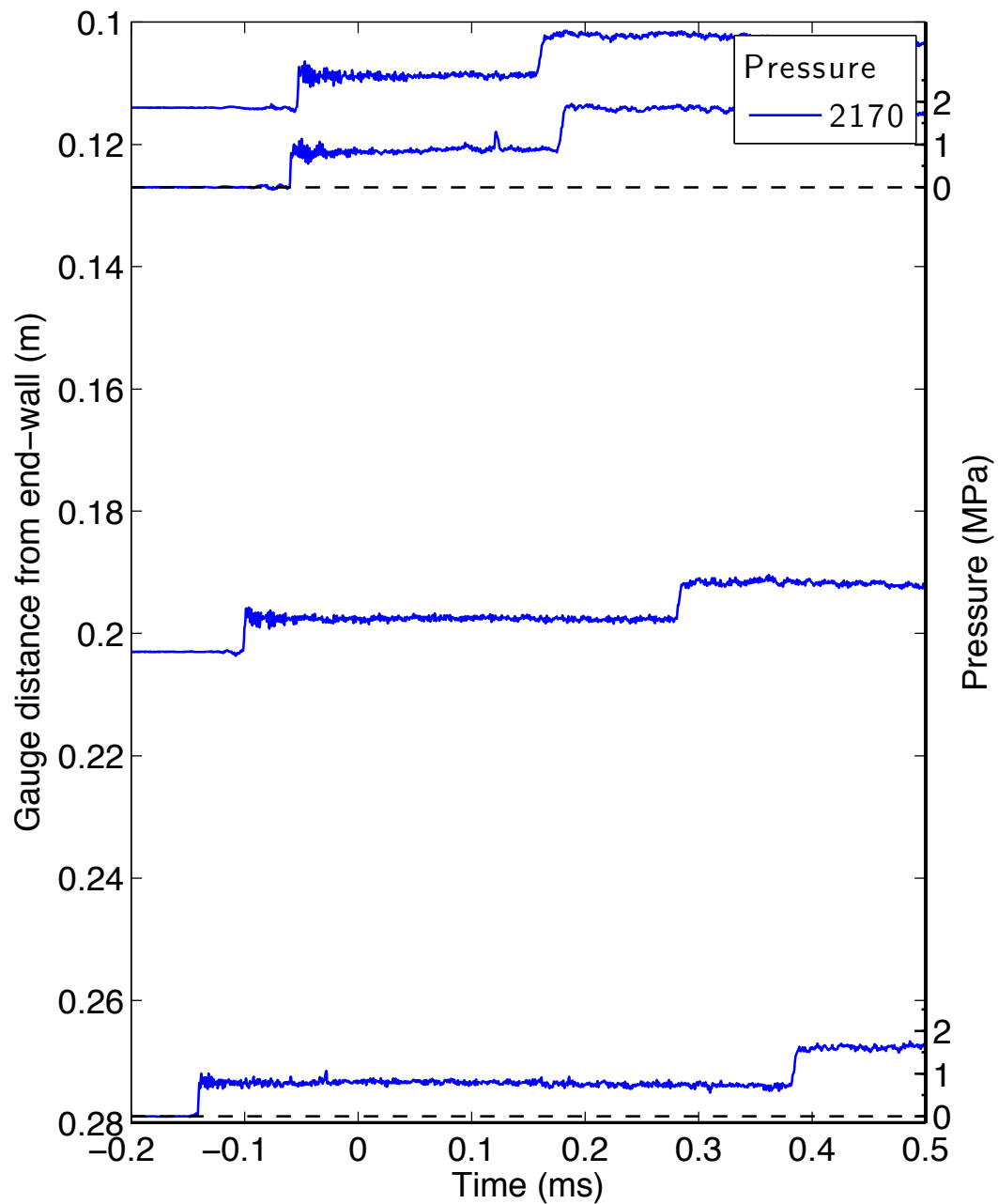


Figure E.73: Pressure traces for a detonation in stoichiometric hydrogen-oxygen with 50% argon dilution at fill pressure 50 kPa, part 2.

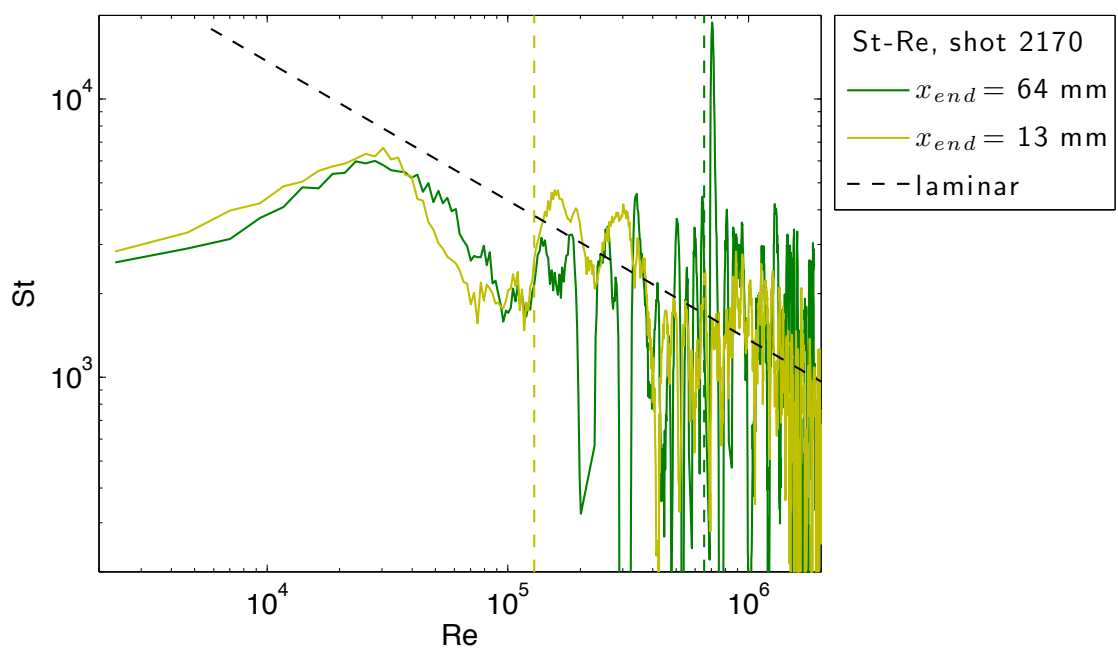


Figure E.74: Stanton-Reynolds number traces from shot 2170, a detonation in stoichiometric hydrogen-oxygen with 50% argon dilution at fill pressure 50 kPa. The dashed vertical lines represent the arrival of the reflected shock wave.

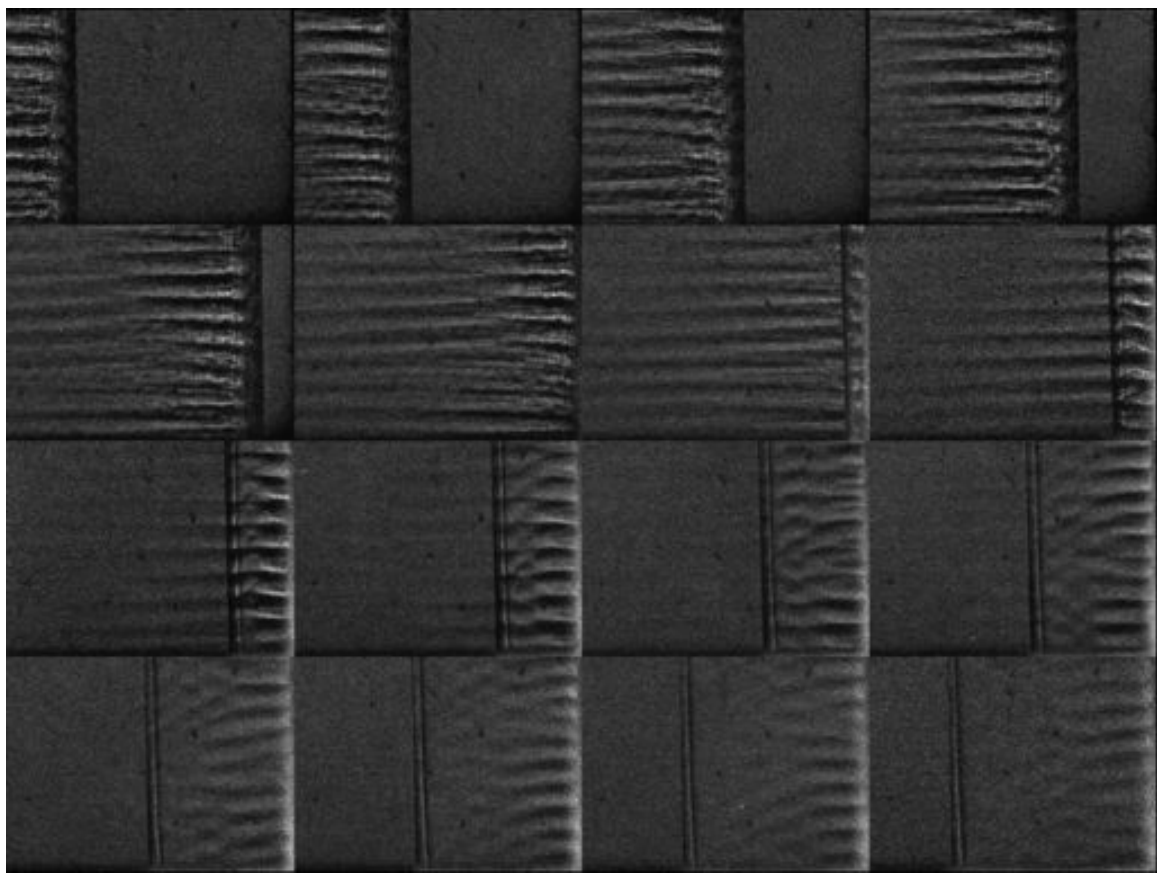


Figure E.75: Unfocused schlieren image of shot 2170. The field of view is approximately 30 mm wide.

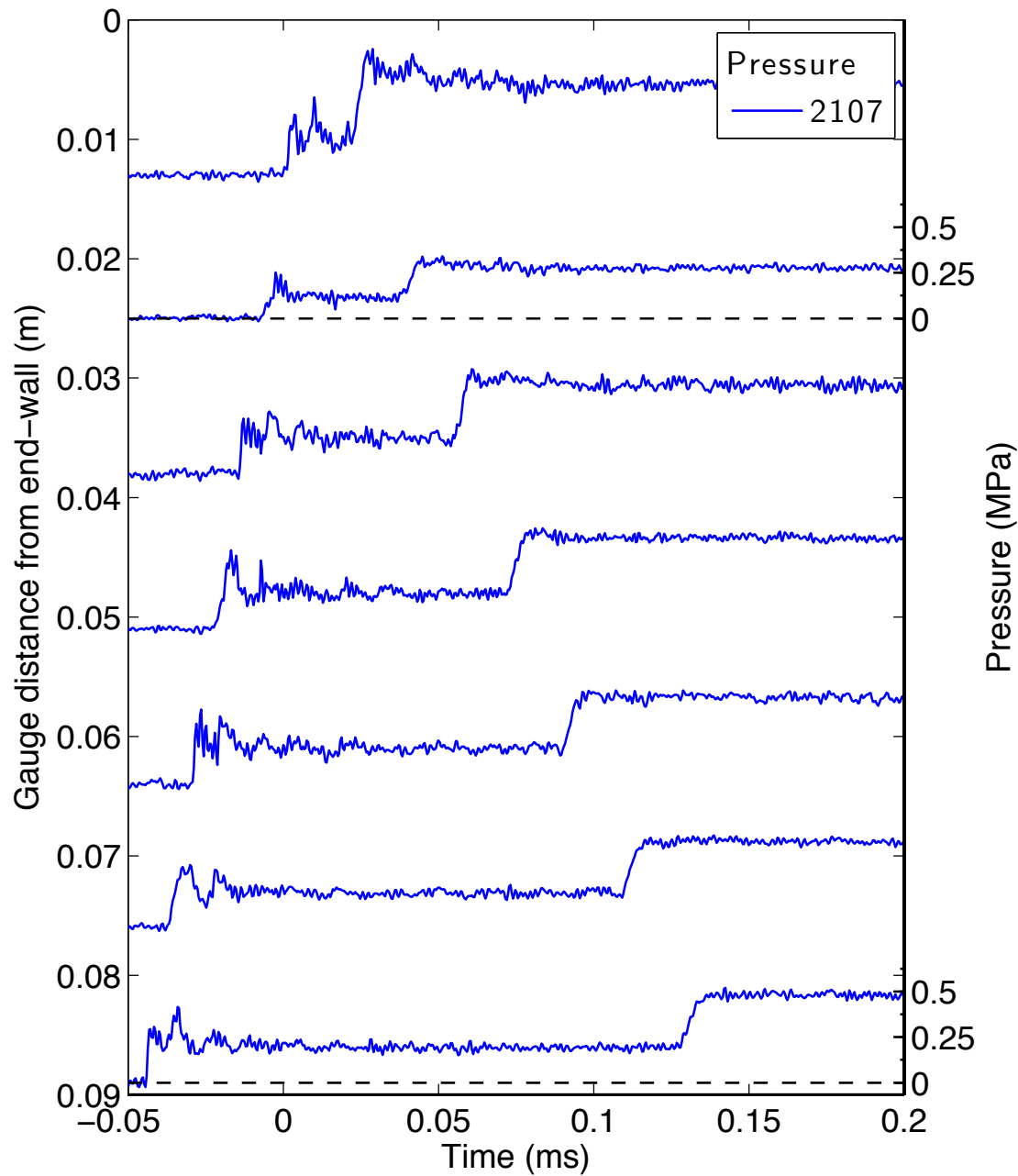


Figure E.76: Pressure traces for a detonation in stoichiometric hydrogen-oxygen with 67% argon dilution at fill pressure 10 kPa, part 1.

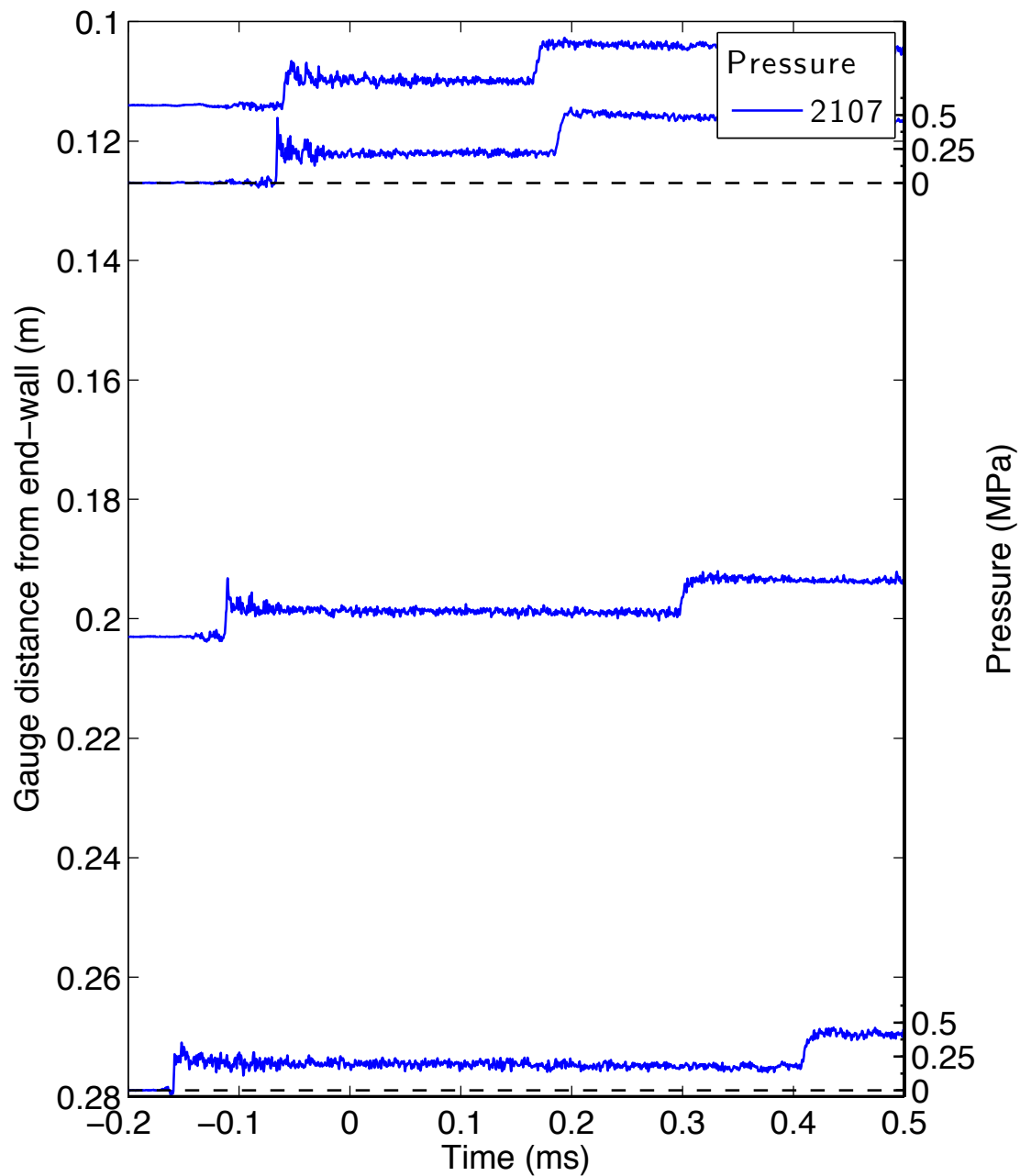


Figure E.77: Pressure traces for a detonation in stoichiometric hydrogen-oxygen with 67% argon dilution at fill pressure 10 kPa, part 2.

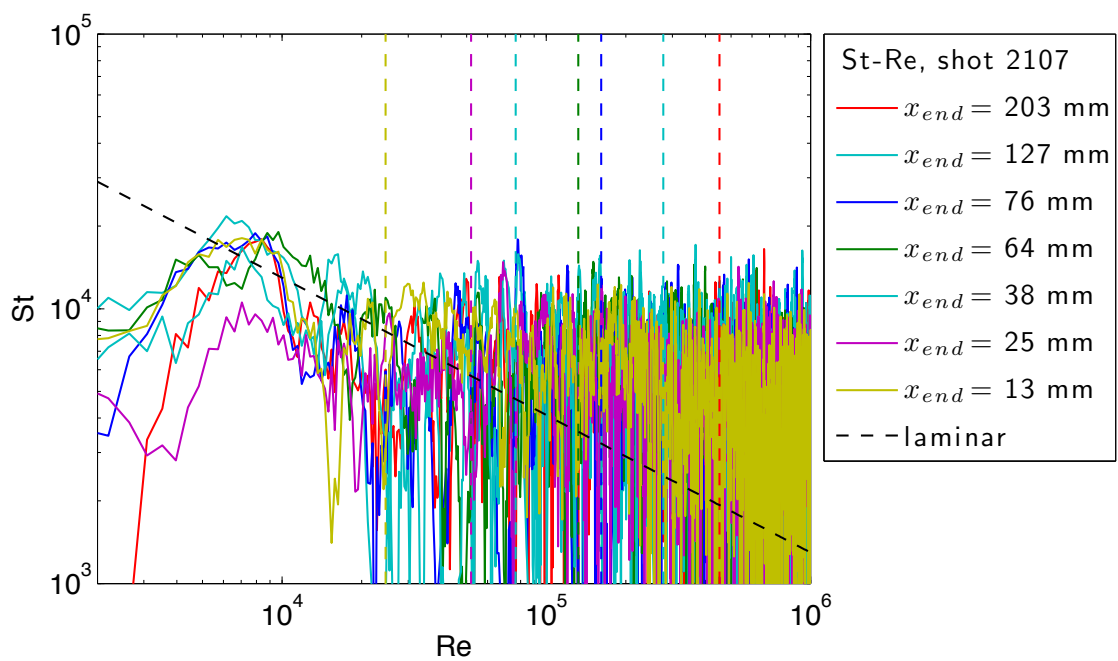


Figure E.78: Stanton-Reynolds number traces from shot 2107, a detonation in stoichiometric hydrogen-oxygen with 67% argon dilution at fill pressure 10 kPa. The dashed vertical lines represent the arrival of the reflected shock wave.

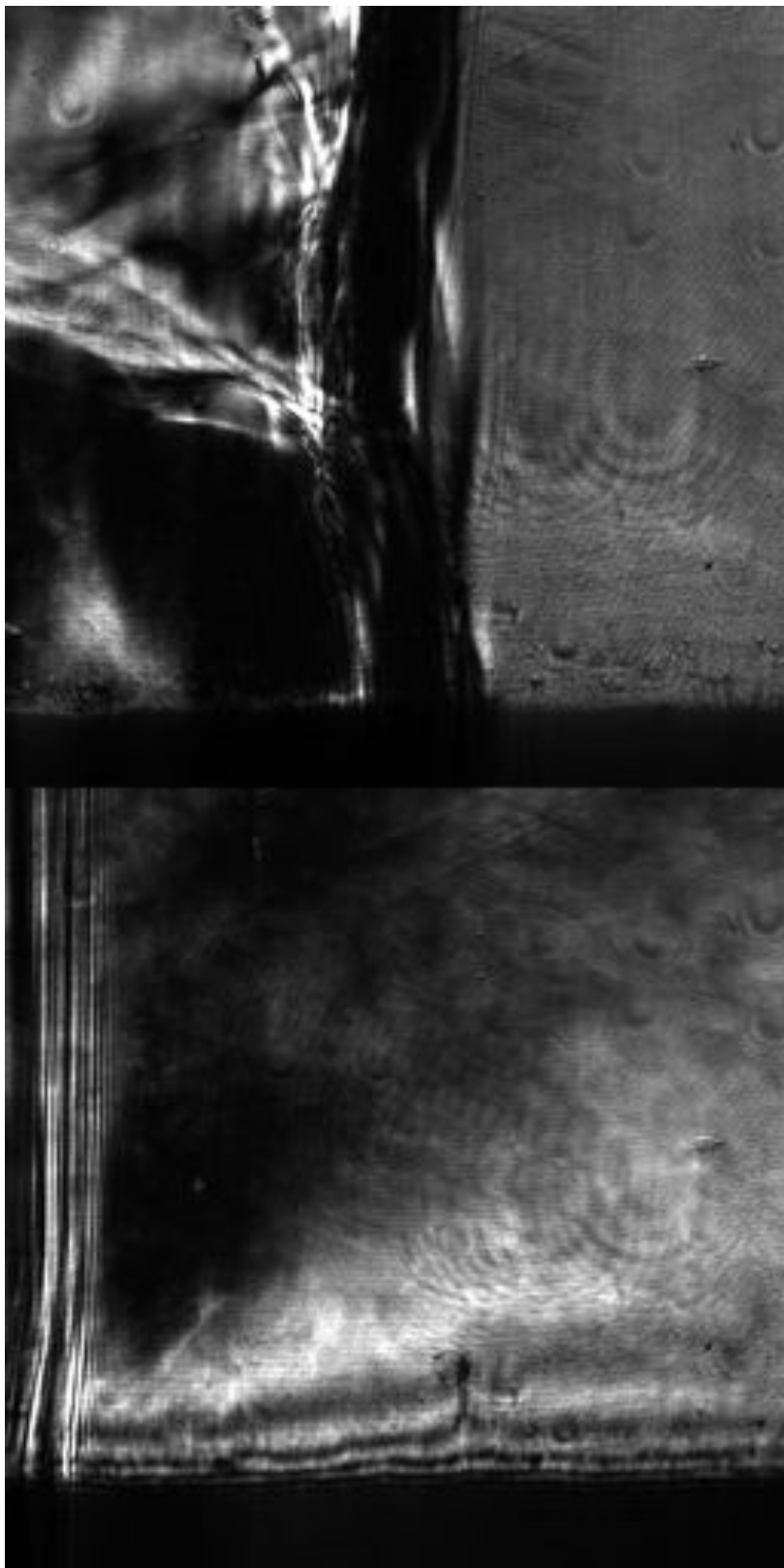


Figure E.79: Focused schlieren image of shot 2107. The field of view is approximately 14 mm wide.

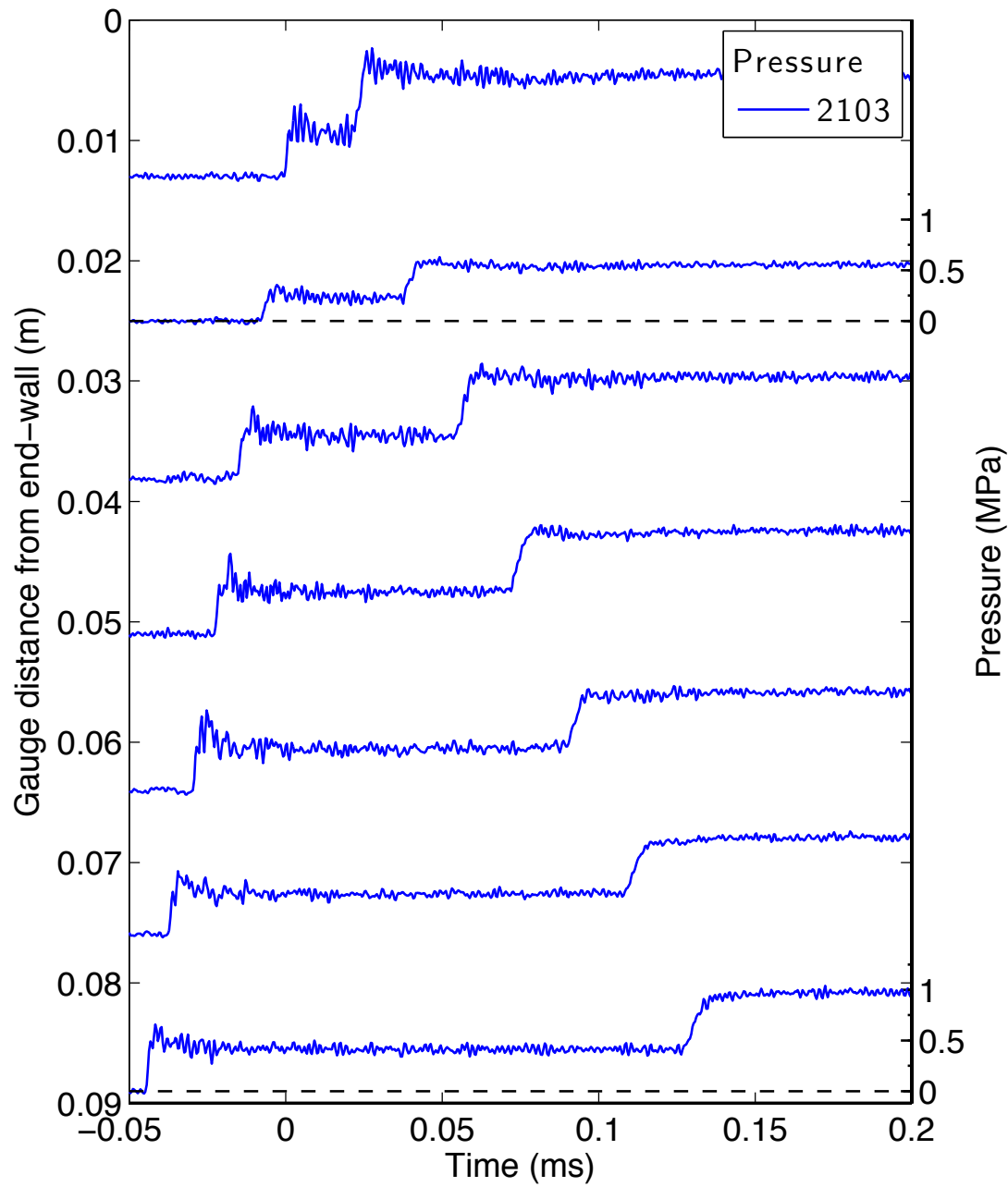


Figure E.80: Pressure traces for a detonation in stoichiometric hydrogen-oxygen with 67% argon dilution at fill pressure 25 kPa, part 1.

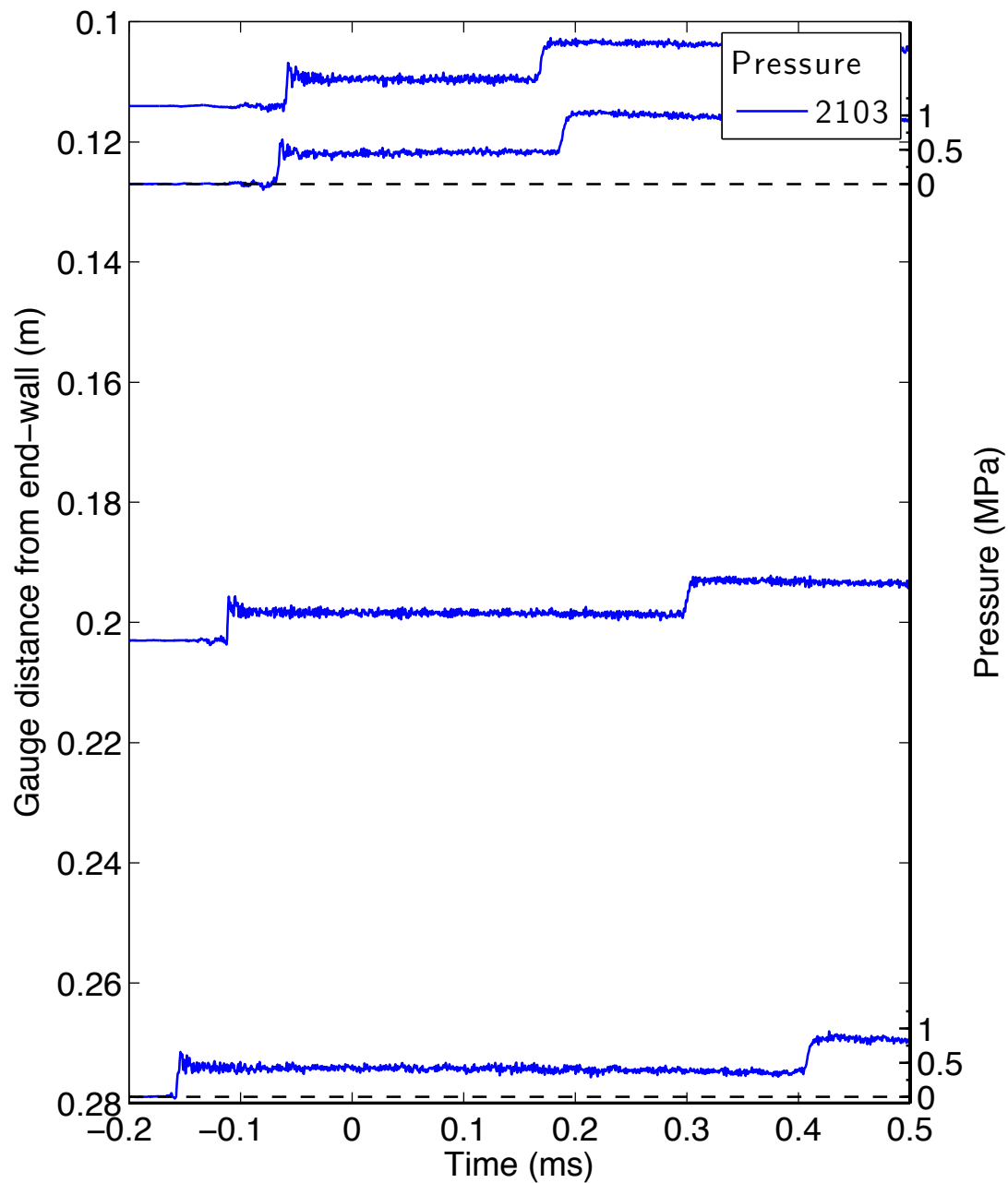


Figure E.81: Pressure traces for a detonation in stoichiometric hydrogen-oxygen with 67% argon dilution at fill pressure 25 kPa, part 2.

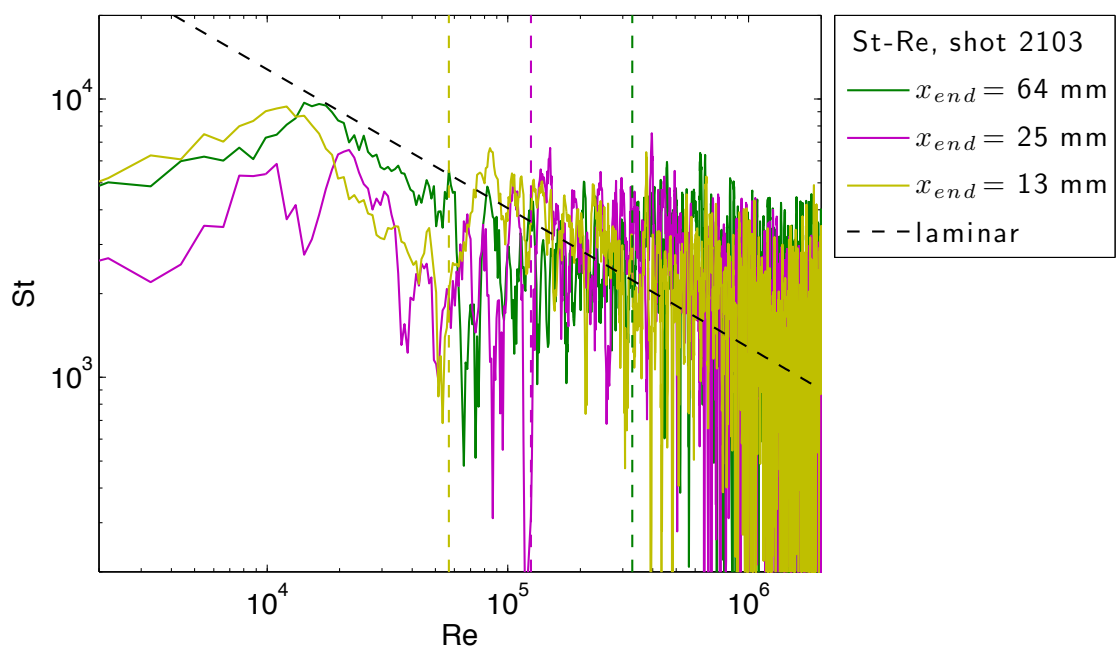


Figure E.82: Stanton-Reynolds number traces from shot 2103, a detonation in stoichiometric hydrogen-oxygen with 67% argon dilution at fill pressure 25 kPa. The dashed vertical lines represent the arrival of the reflected shock wave.

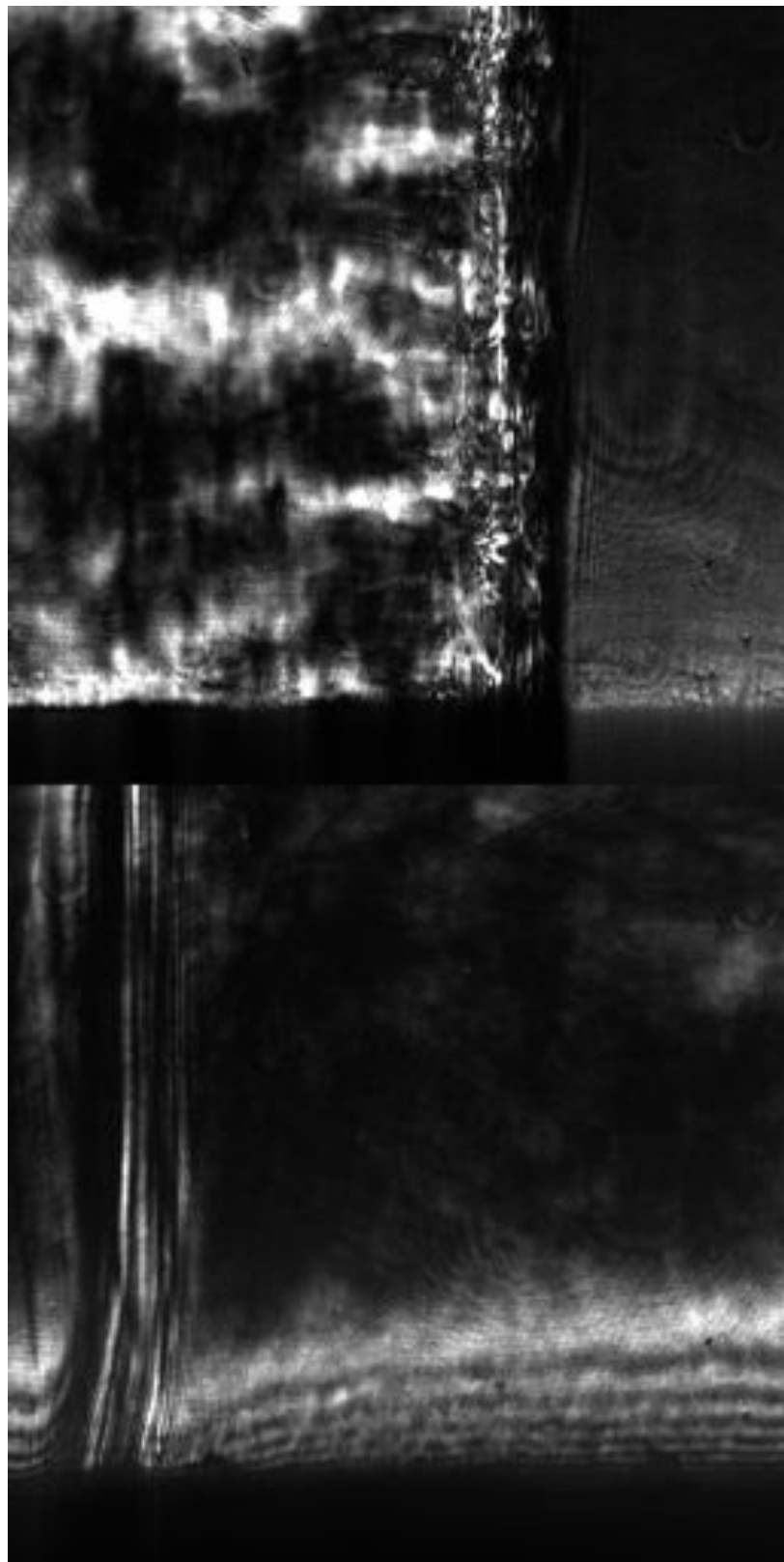


Figure E.83: Focused schlieren image of shot 2103. The field of view is approximately 14 mm wide.

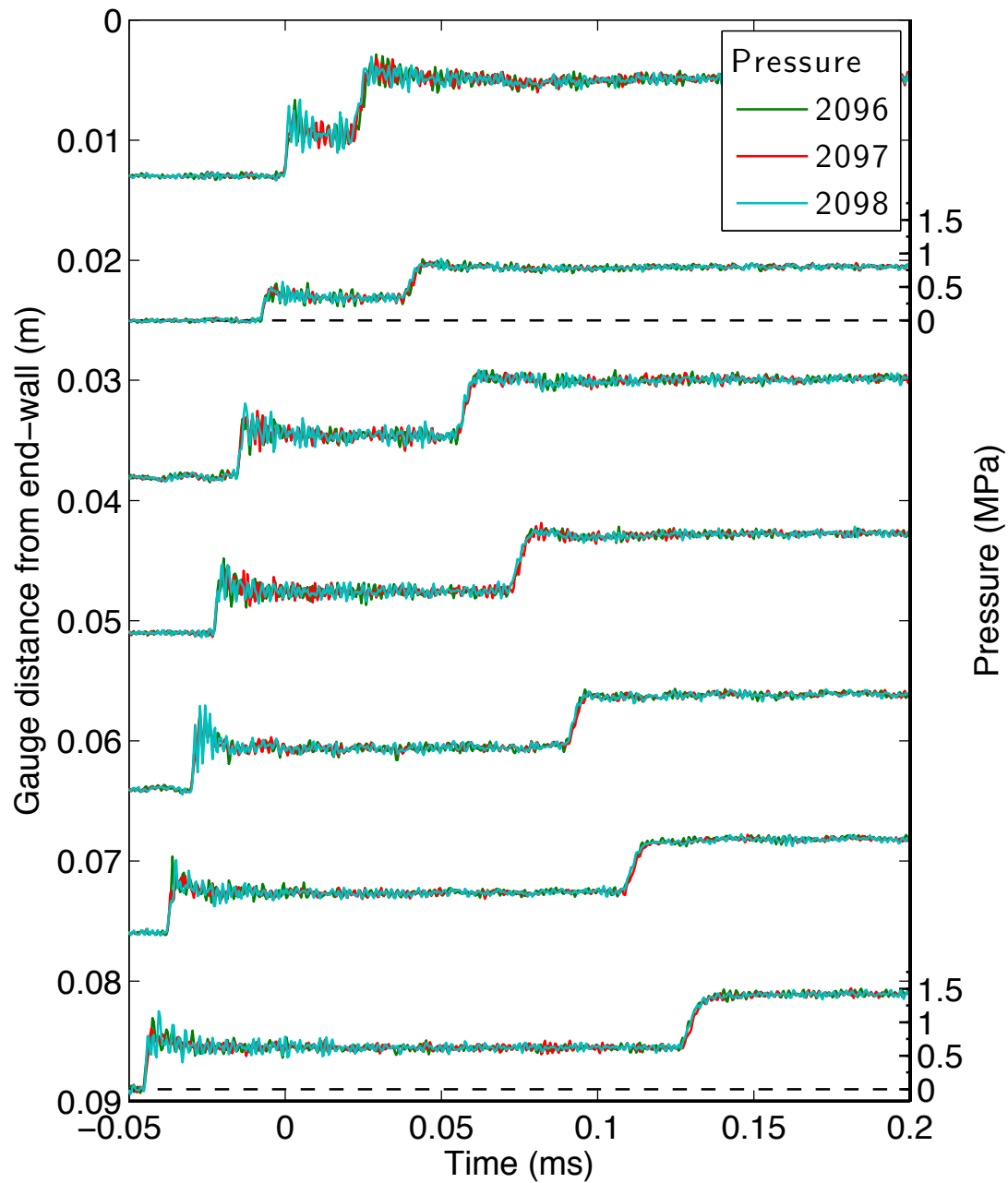


Figure E.84: Pressure traces for a detonation in stoichiometric hydrogen-oxygen with 67% argon dilution at fill pressure 40 kPa, part 1.

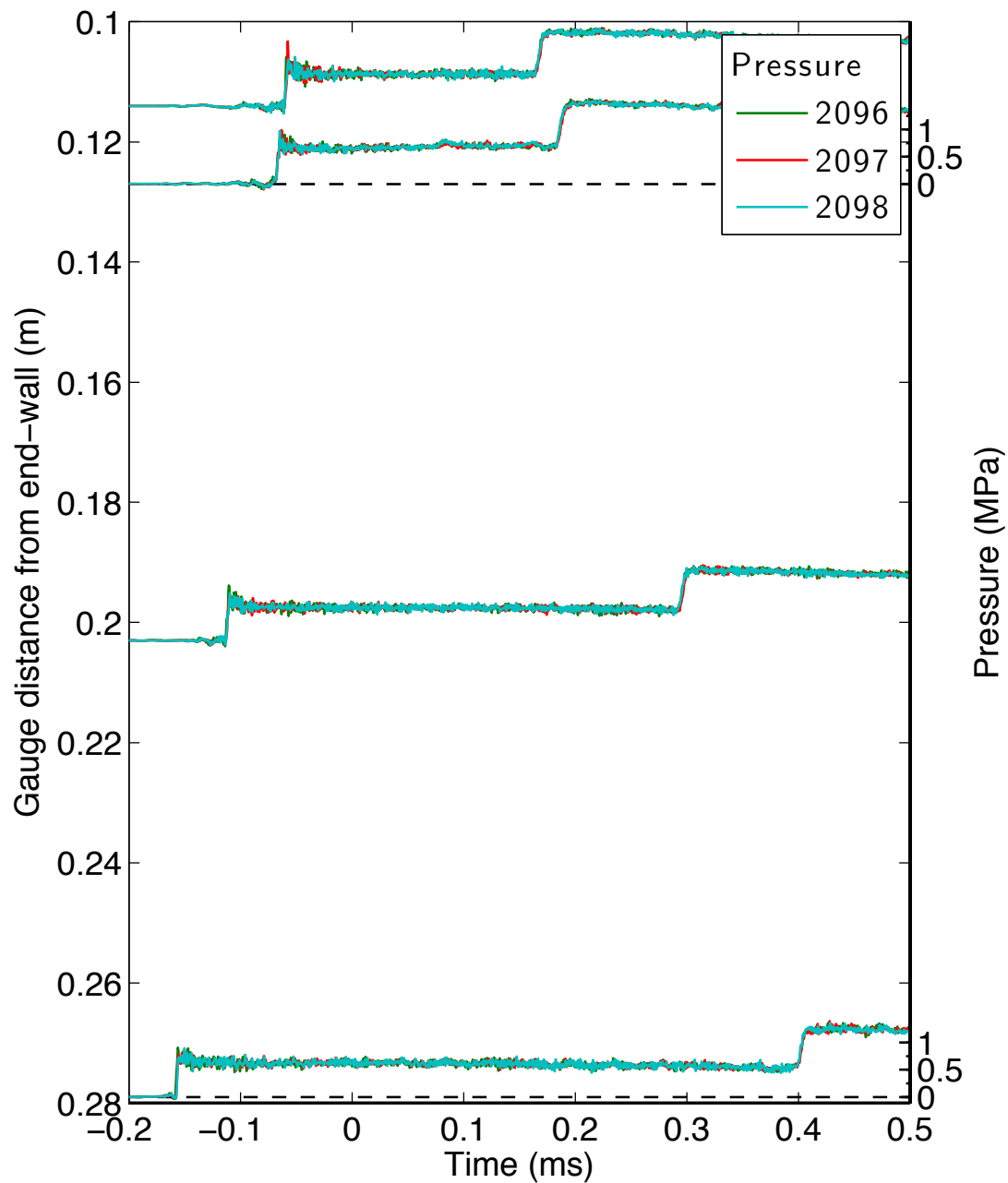


Figure E.85: Pressure traces for a detonation in stoichiometric hydrogen-oxygen with 67% argon dilution at fill pressure 40 kPa, part 2.

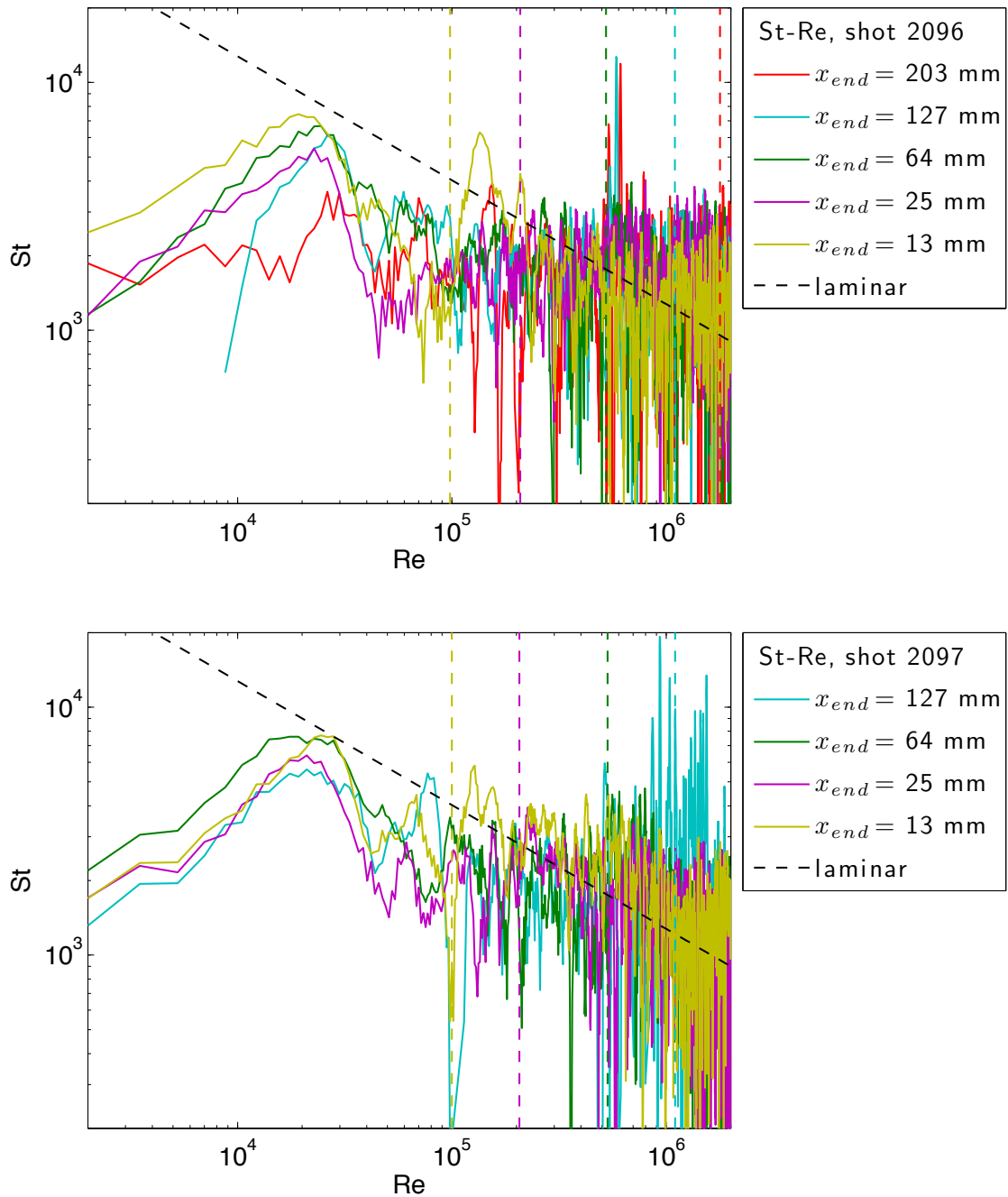


Figure E.86: Stanton-Reynolds number traces from shot 2097, a detonation in stoichiometric hydrogen-oxygen with 67% argon dilution at fill pressure 40 kPa. The dashed vertical lines represent the arrival of the reflected shock wave.

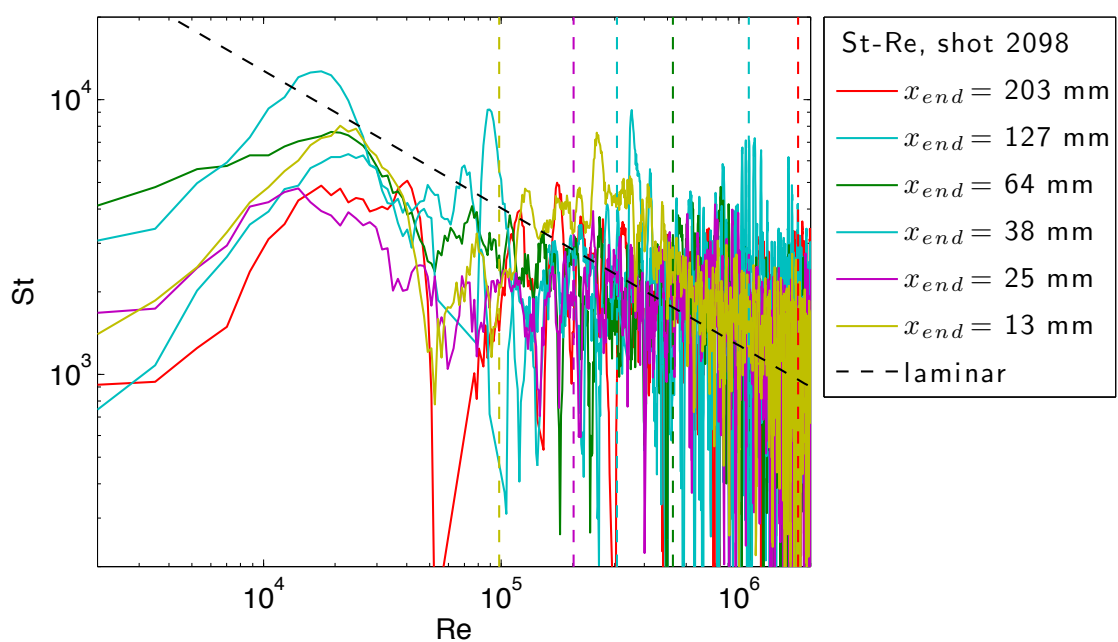


Figure E.87: Stanton-Reynolds number traces from shot 2098, a detonation in stoichiometric hydrogen-oxygen with 67% argon dilution at fill pressure 40 kPa. The dashed vertical lines represent the arrival of the reflected shock wave.

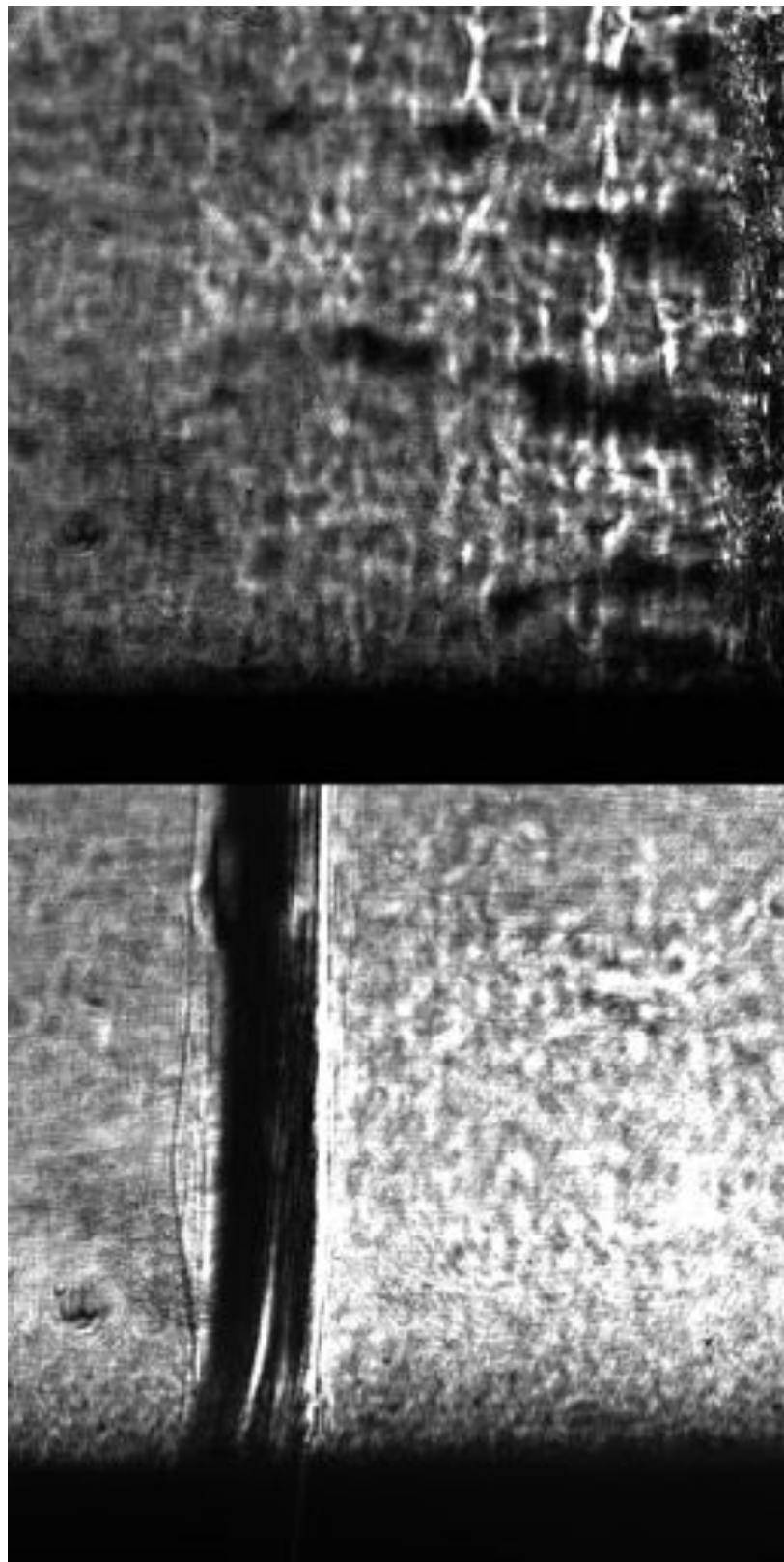


Figure E.88: Focused schlieren image of shot 2097. The field of view is approximately 14 mm wide.

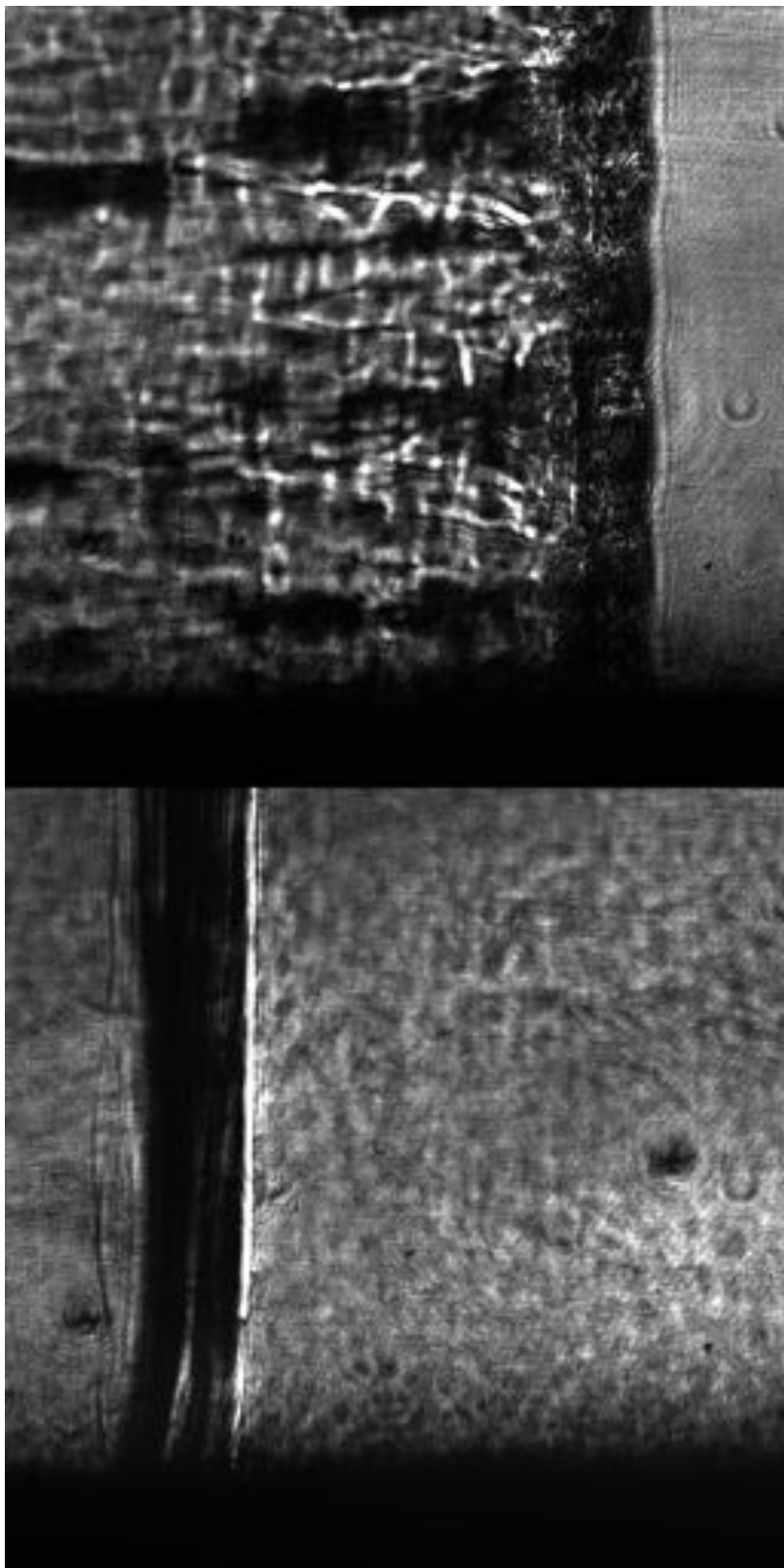


Figure E.89: Focused schlieren image of shot 2098. The field of view is approximately 14 mm wide.

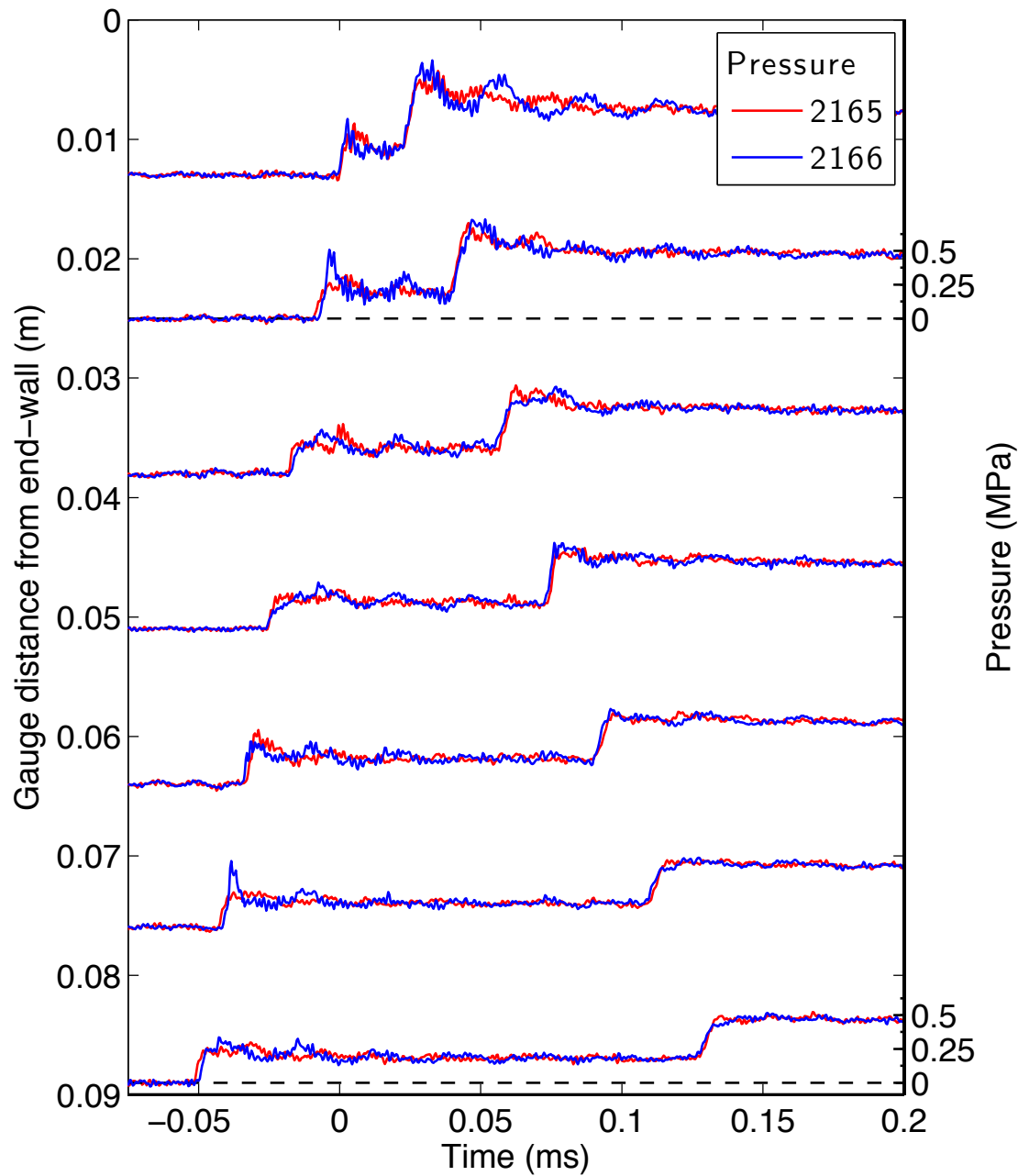


Figure E.90: Pressure traces for a detonation in stoichiometric hydrogen-oxygen with 80% argon dilution at fill pressure 10 kPa, part 1.

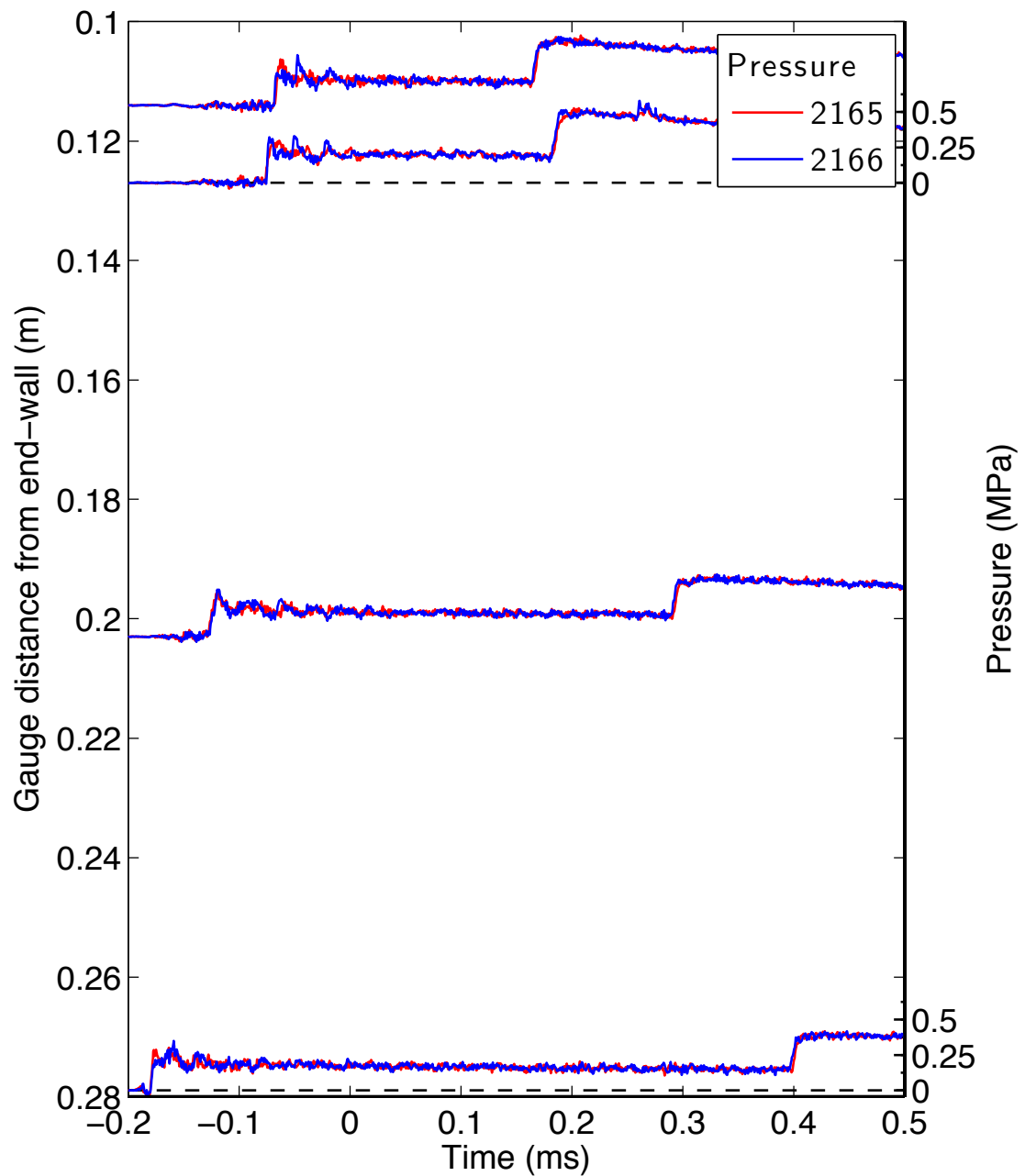


Figure E.91: Pressure traces for a detonation in stoichiometric hydrogen-oxygen with 80% argon dilution at fill pressure 10 kPa, part 2.

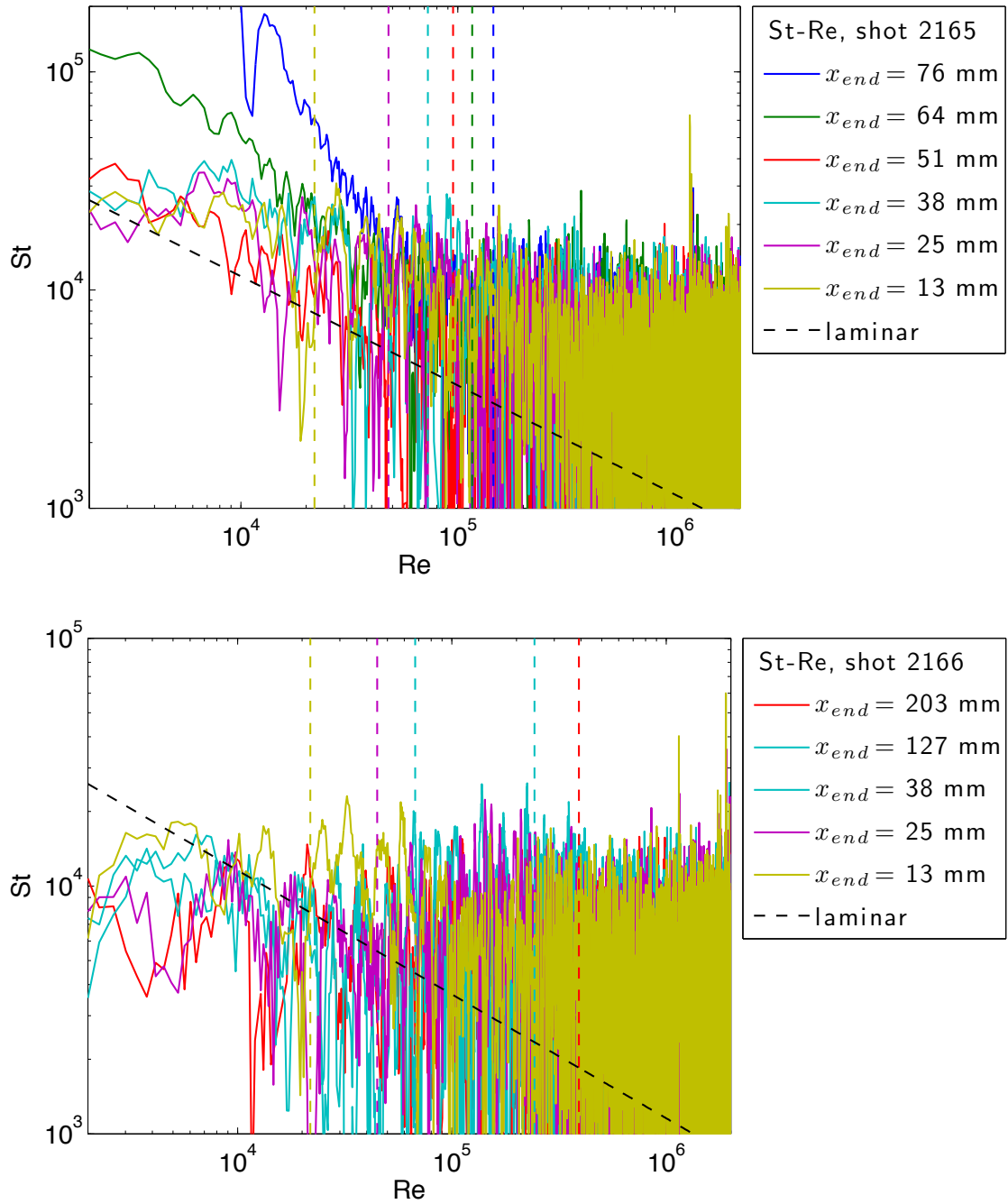


Figure E.92: Stanton-Reynolds number traces from shot 2166, a detonation in stoichiometric hydrogen-oxygen with 80% argon dilution at fill pressure 10 kPa. The dashed vertical lines represent the arrival of the reflected shock wave.

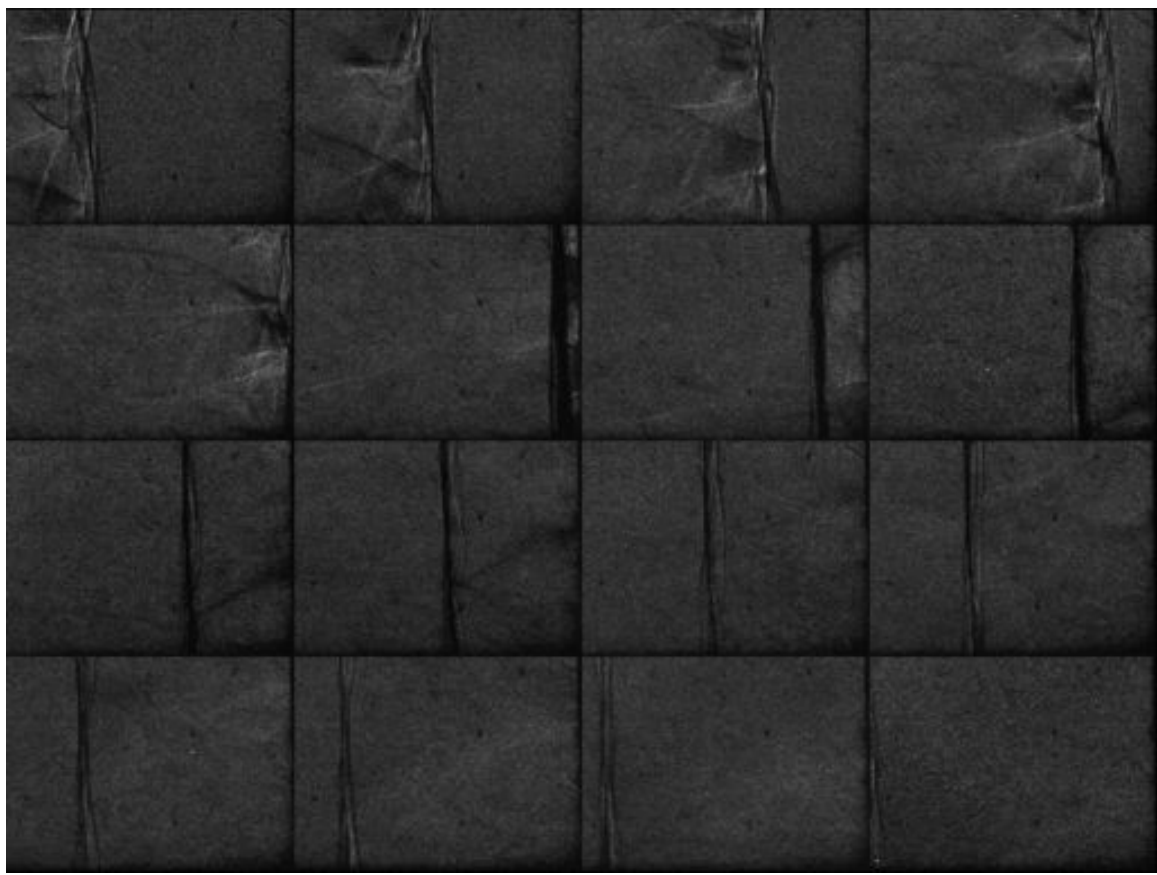


Figure E.93: Unfocused schlieren image of shot 2166. The field of view is approximately 30 mm wide.

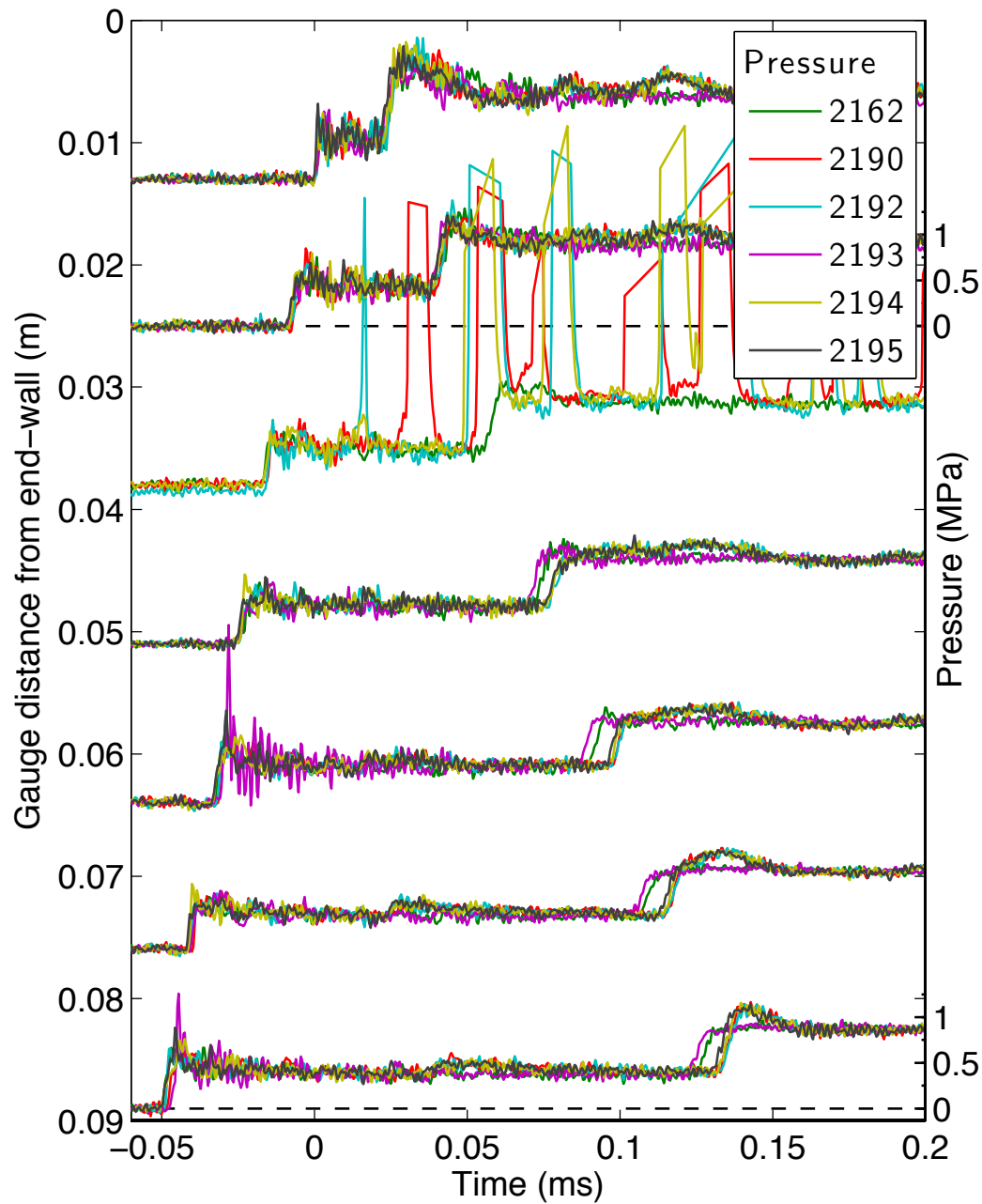


Figure E.94: Pressure traces for a detonation in stoichiometric hydrogen-oxygen with 80% argon dilution at fill pressure 25 kPa, part 1.

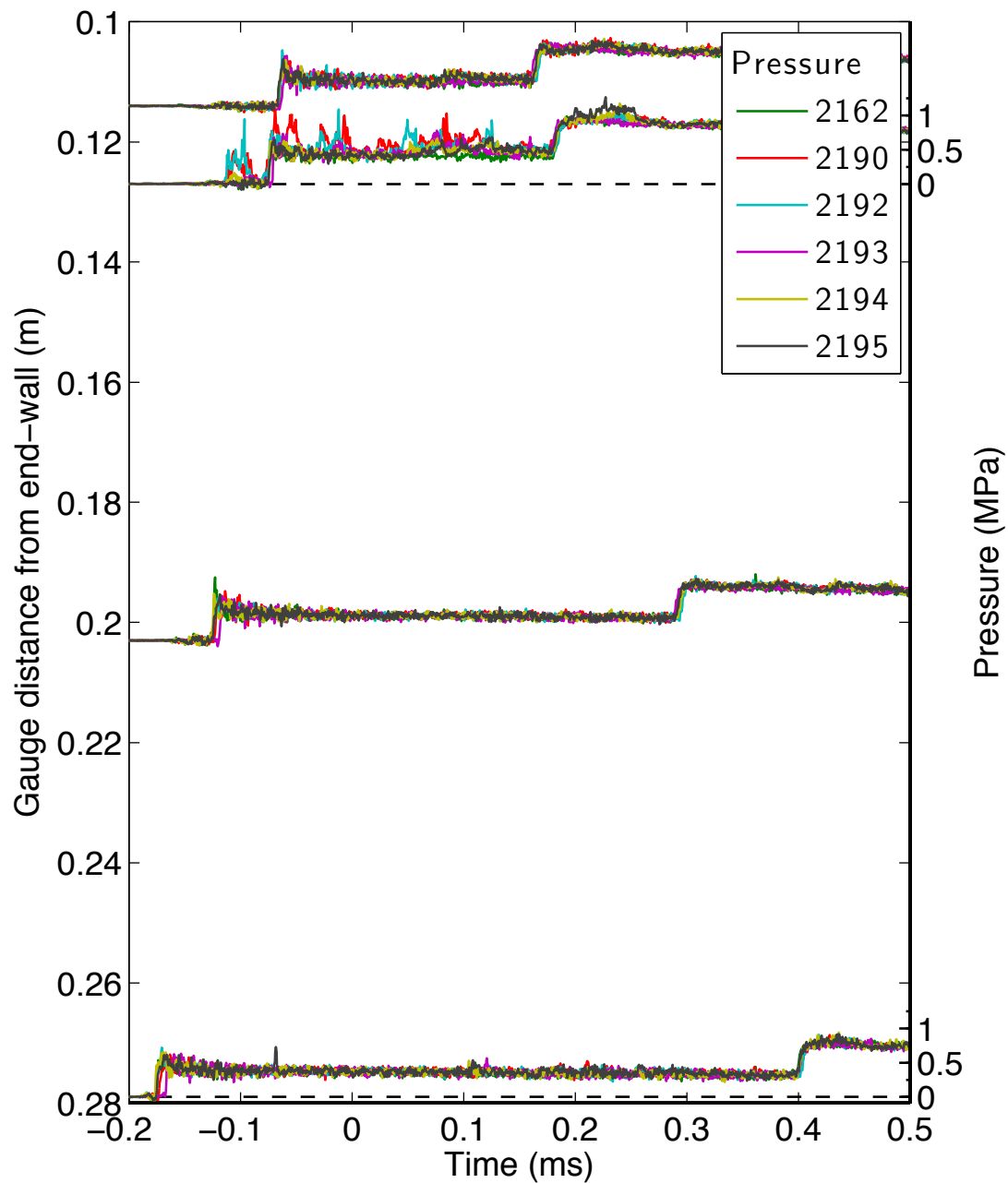


Figure E.95: Pressure traces for a detonation in stoichiometric hydrogen-oxygen with 80% argon dilution at fill pressure 25 kPa, part 2.

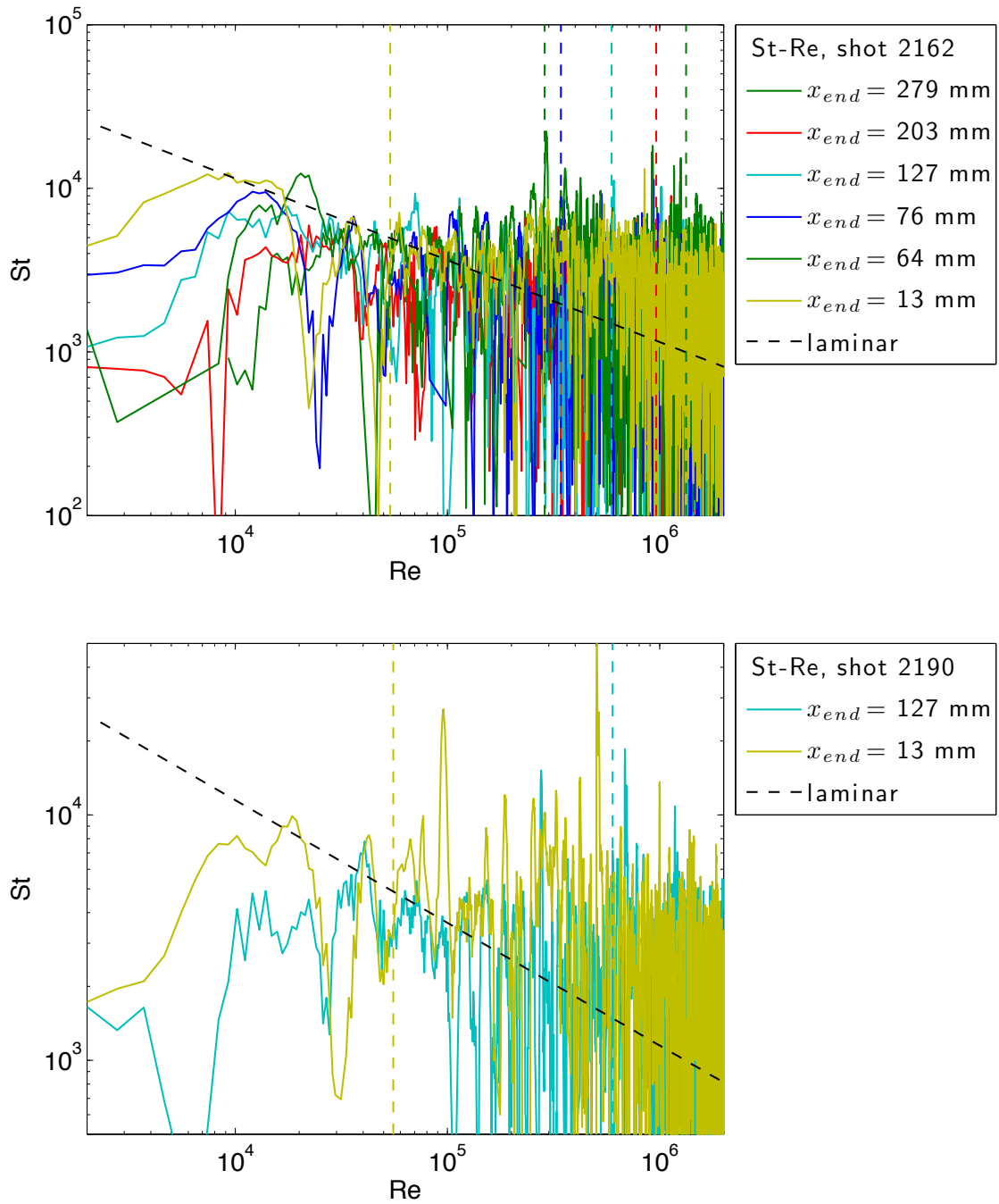


Figure E.96: Stanton-Reynolds number traces from shot 2190, a detonation in stoichiometric hydrogen-oxygen with 80% argon dilution at fill pressure 25 kPa. The dashed vertical lines represent the arrival of the reflected shock wave.

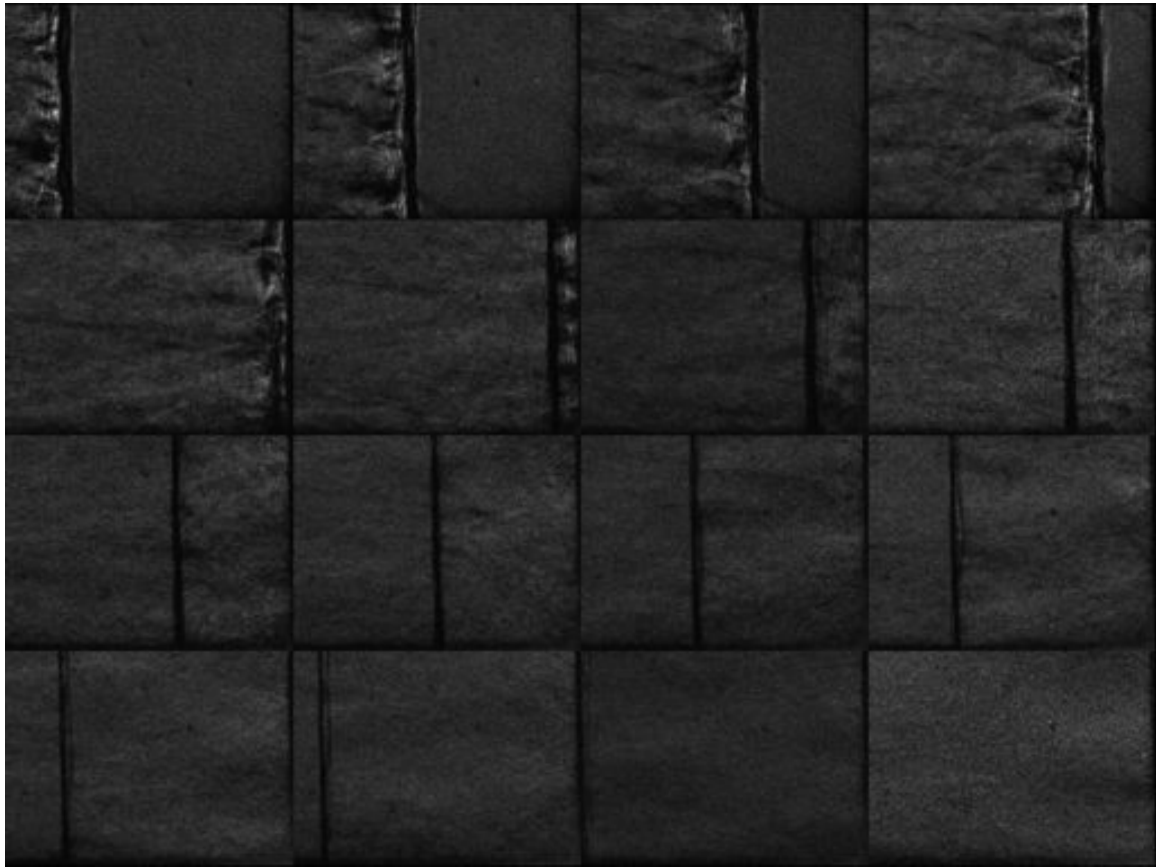


Figure E.97: Unfocused schlieren image of shot 2162. The field of view is approximately 30 mm wide.

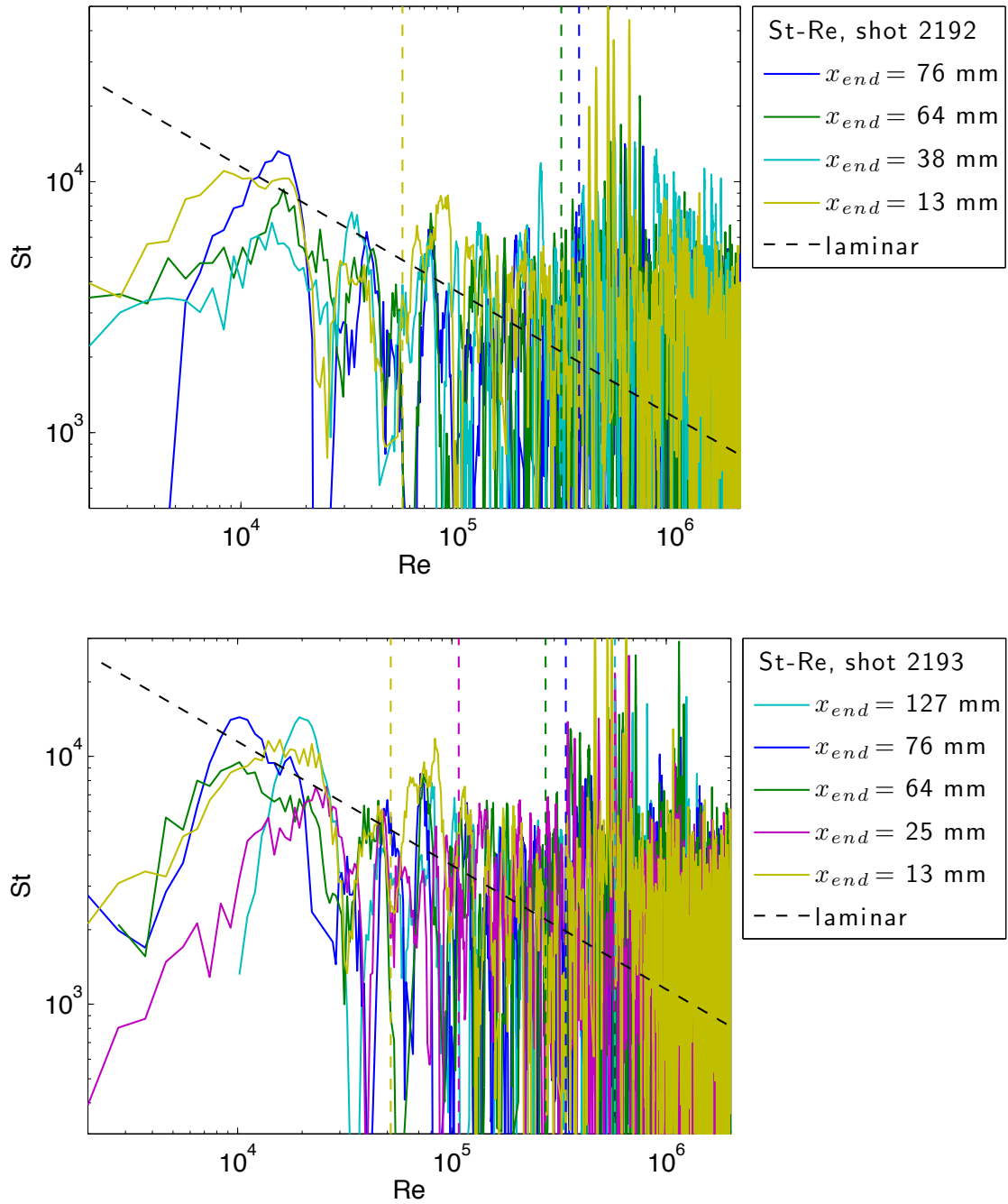


Figure E.98: Stanton-Reynolds number traces from shot 2193, a detonation in stoichiometric hydrogen-oxygen with 80% argon dilution at fill pressure 25 kPa. The dashed vertical lines represent the arrival of the reflected shock wave.

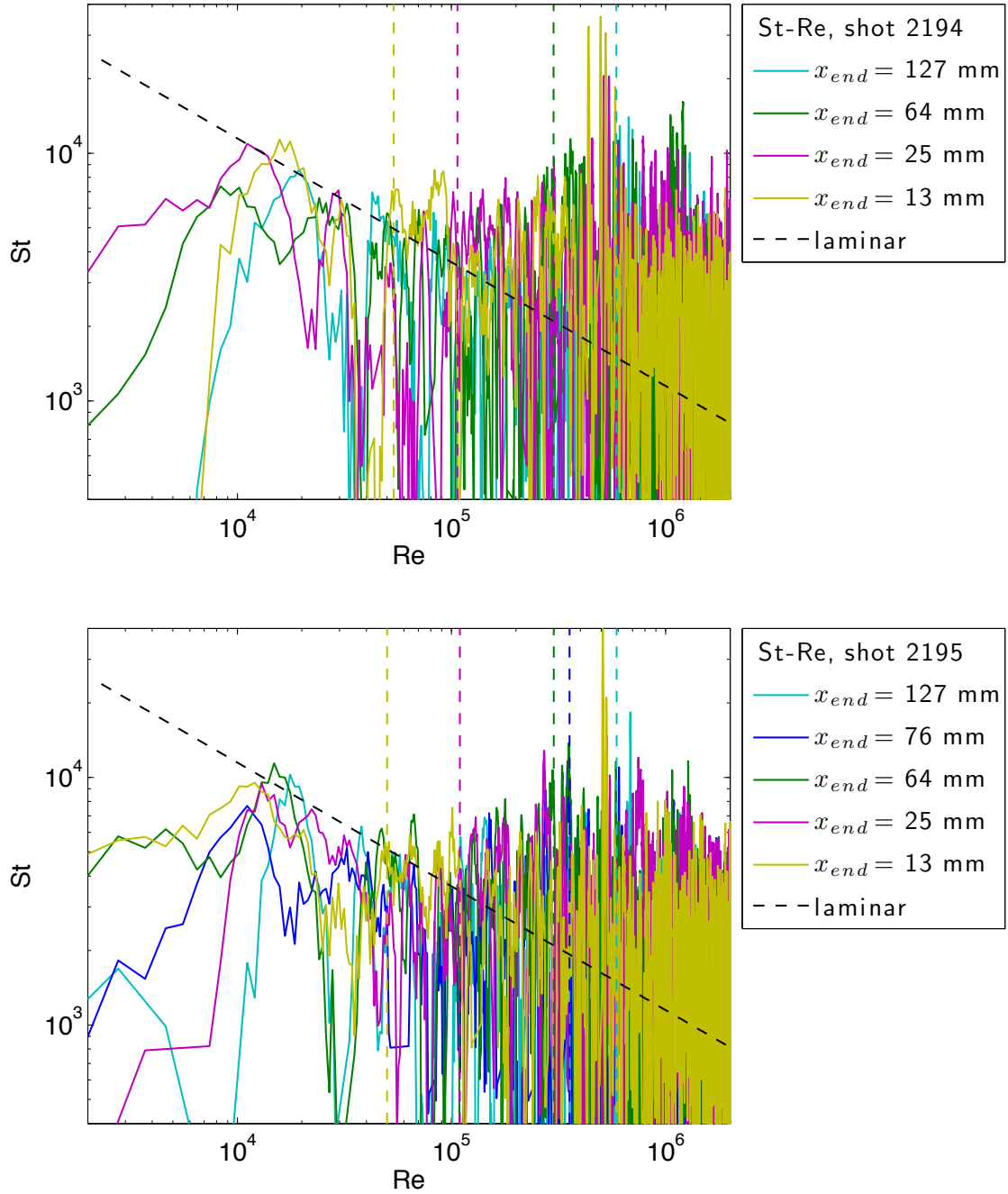


Figure E.99: Stanton-Reynolds number traces from shot 2195, a detonation in stoichiometric hydrogen-oxygen with 80% argon dilution at fill pressure 25 kPa. The dashed vertical lines represent the arrival of the reflected shock wave.

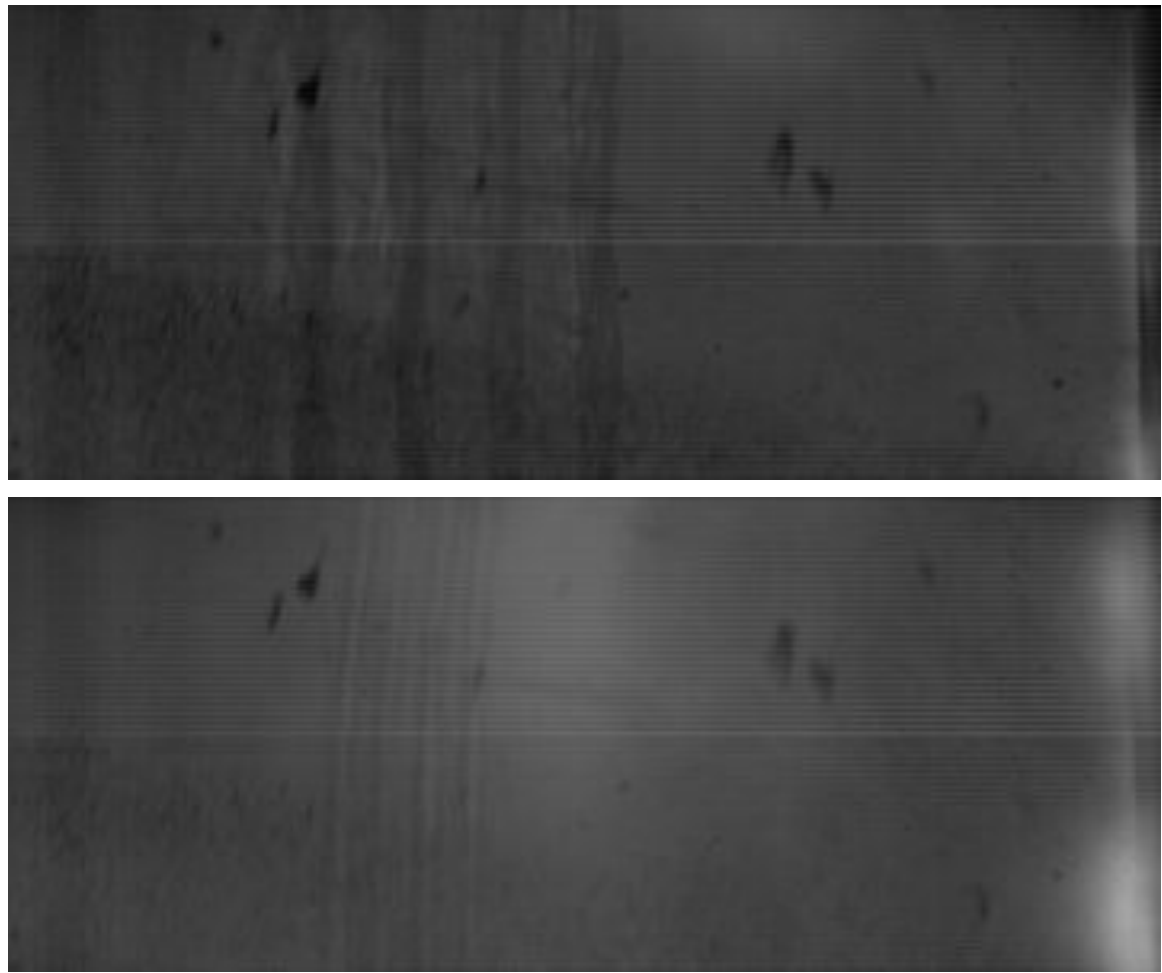


Figure E.100: Unfocused schlieren images of shot 2195. The field of view is approximately 66 mm wide.

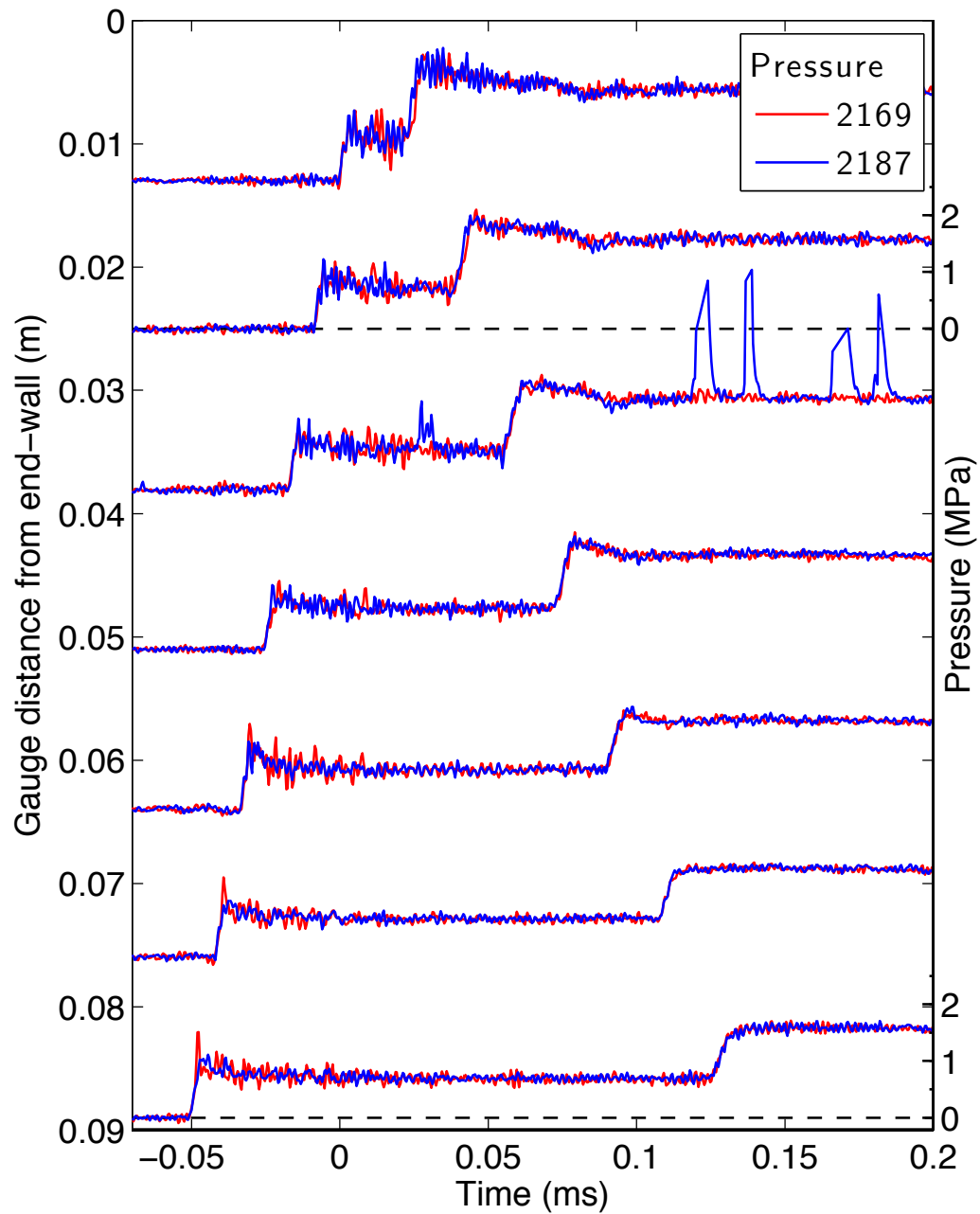


Figure E.101: Pressure traces for a detonation in stoichiometric hydrogen-oxygen with 80% argon dilution at fill pressure 50 kPa, part 1.

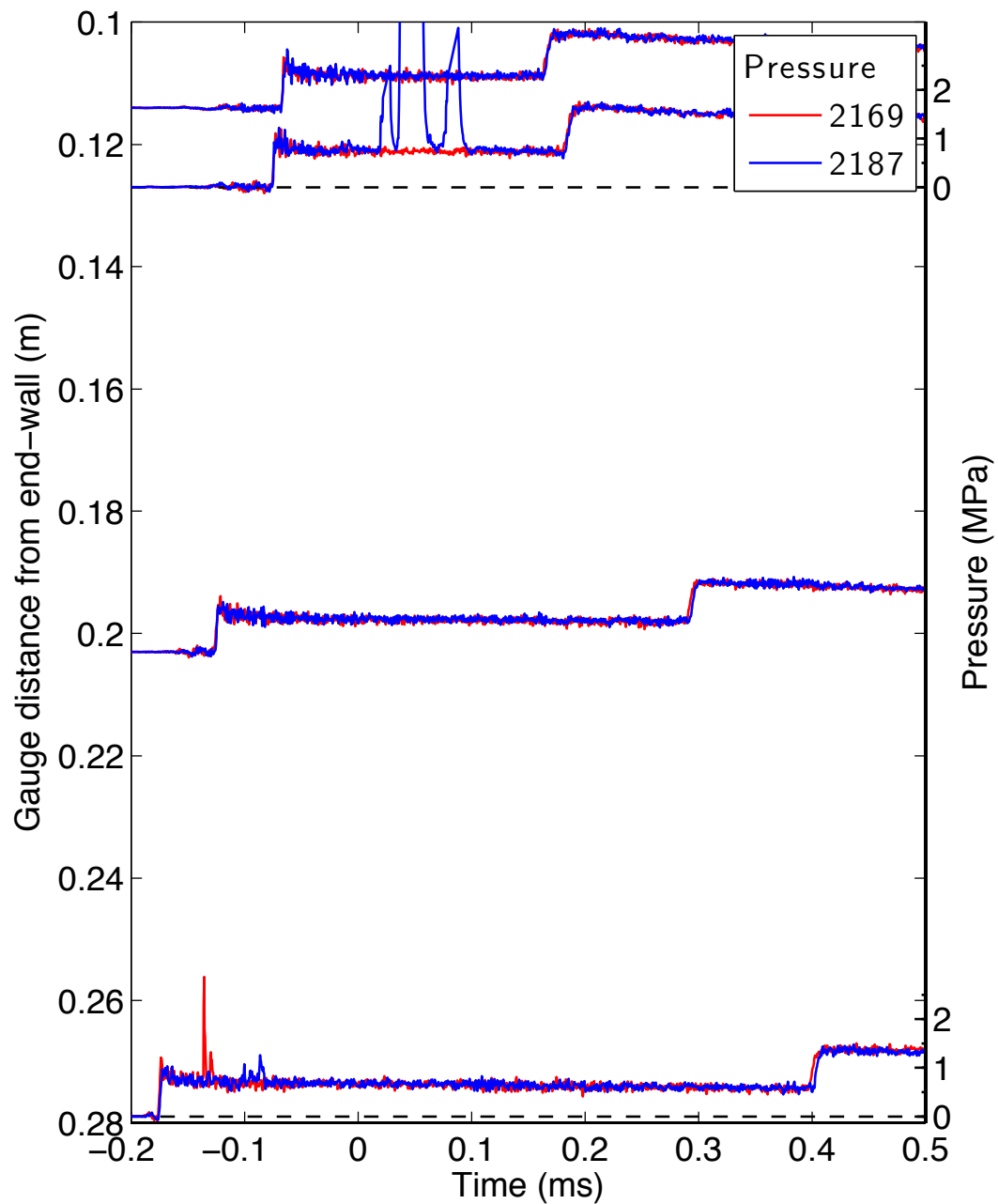


Figure E.102: Pressure traces for a detonation in stoichiometric hydrogen-oxygen with 80% argon dilution at fill pressure 50 kPa, part 2.

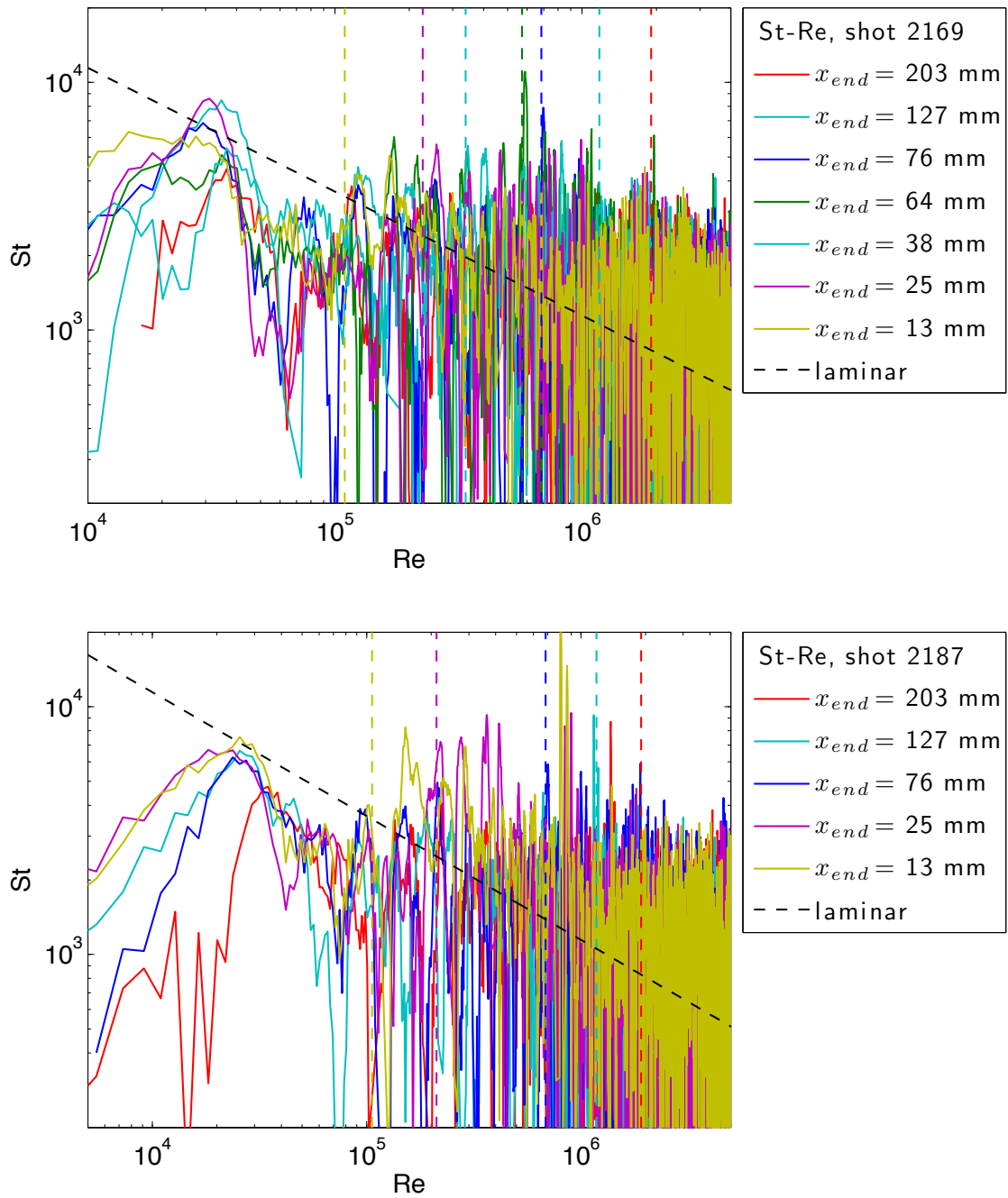


Figure E.103: Stanton-Reynolds number traces from shot 2187, a detonation in stoichiometric hydrogen-oxygen with 80% argon dilution at fill pressure 50 kPa. The dashed vertical lines represent the arrival of the reflected shock wave.

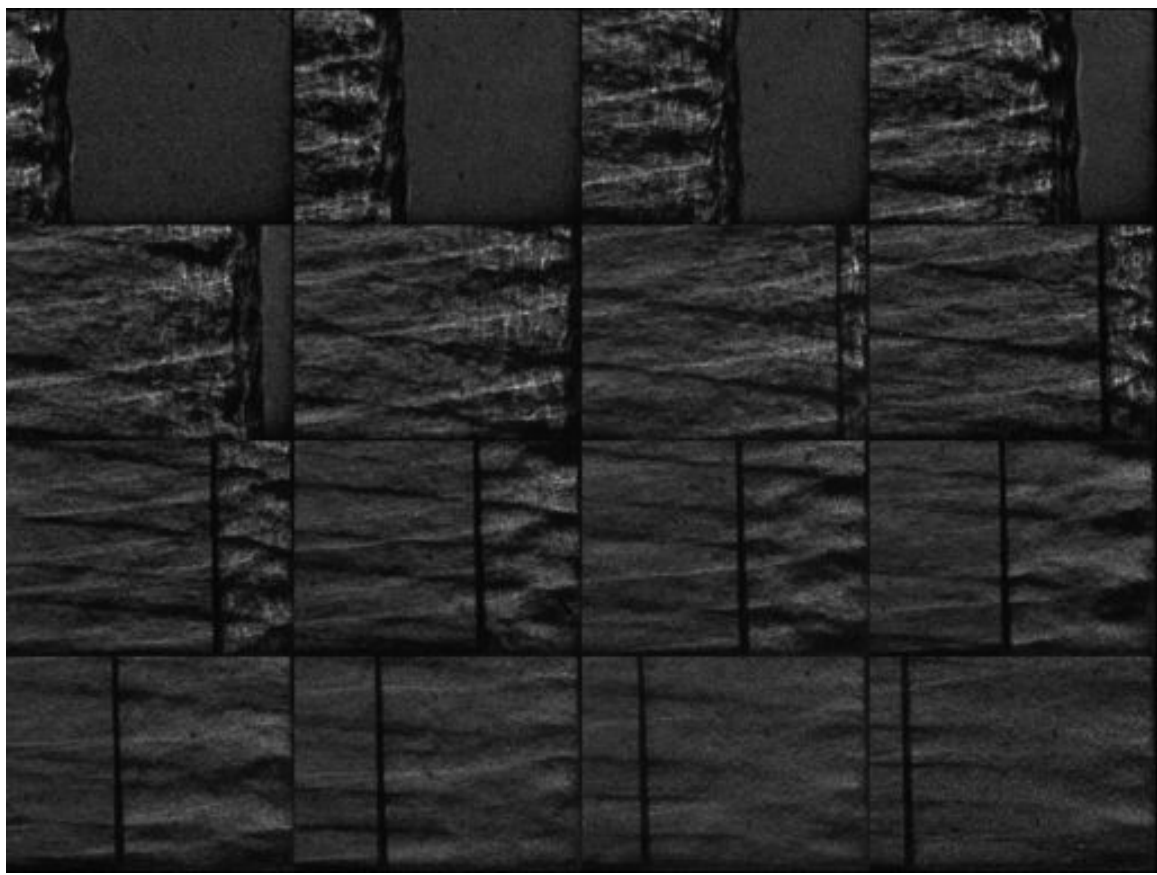


Figure E.104: Unfocused schlieren image of shot 2169. The field of view is approximately 30 mm wide.

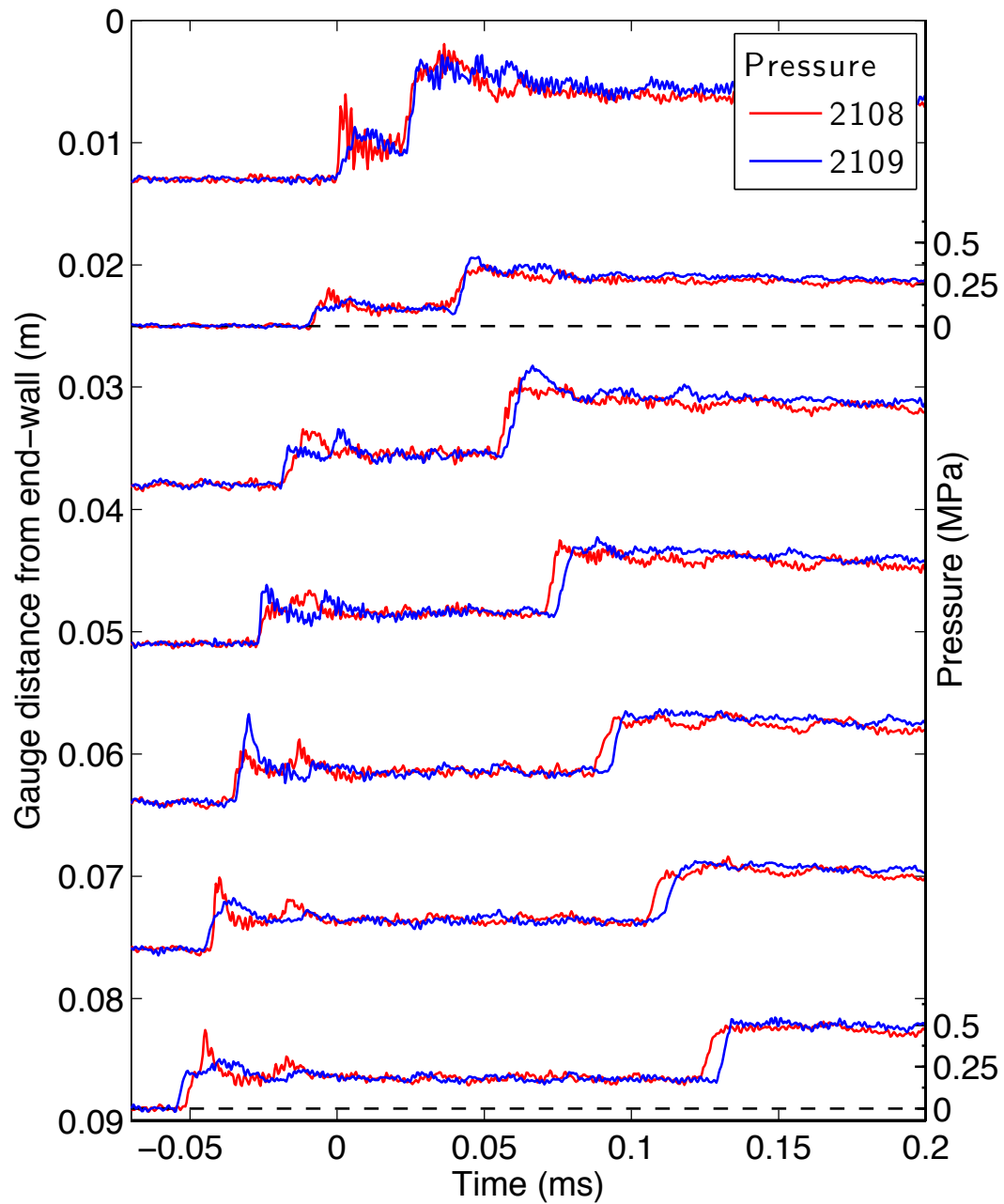


Figure E.105: Pressure traces for a detonation in stoichiometric hydrogen-oxygen with 83% argon dilution at fill pressure 10 kPa, part 1.

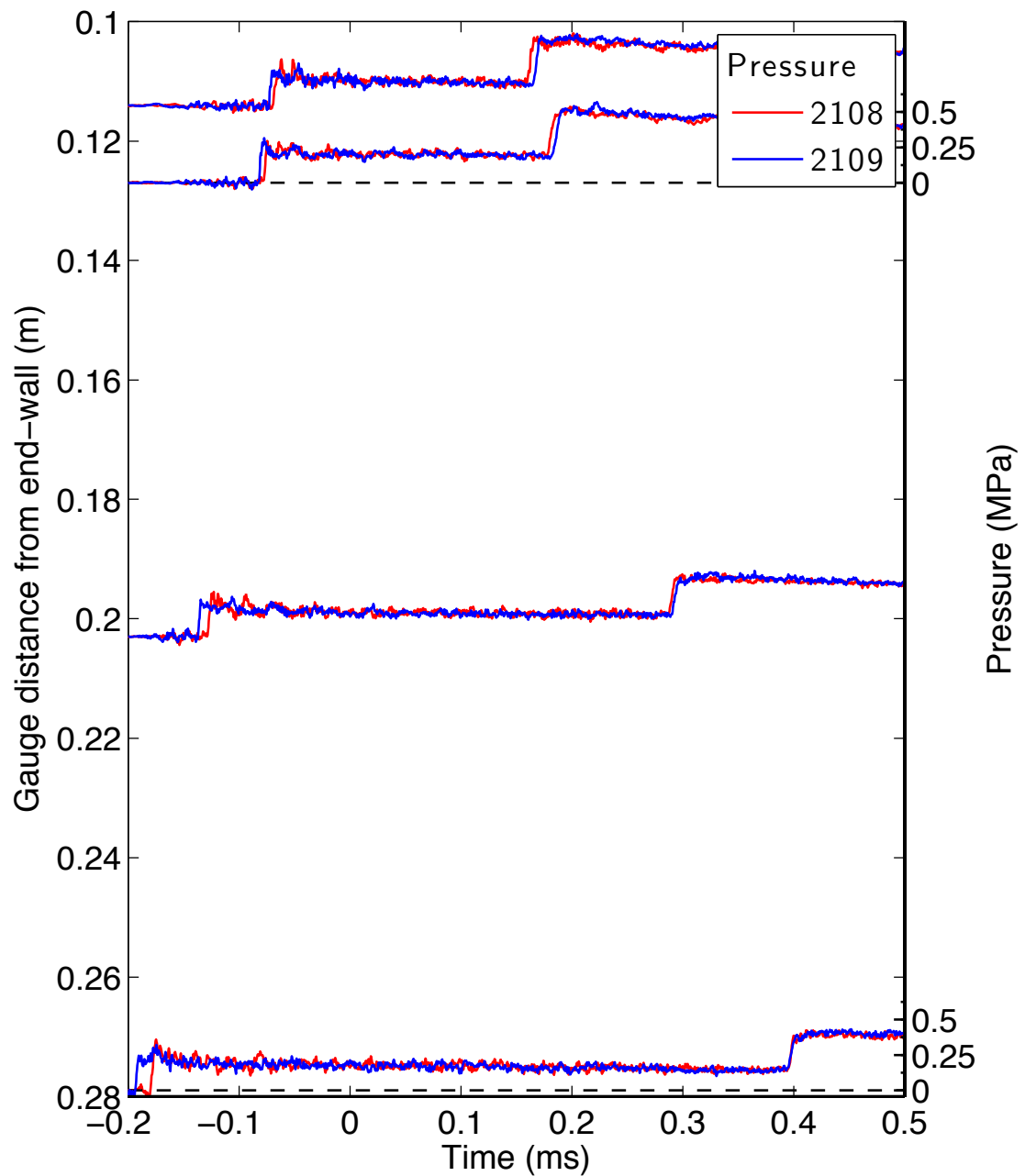


Figure E.106: Pressure traces for a detonation in stoichiometric hydrogen-oxygen with 83% argon dilution at fill pressure 10 kPa, part 2.

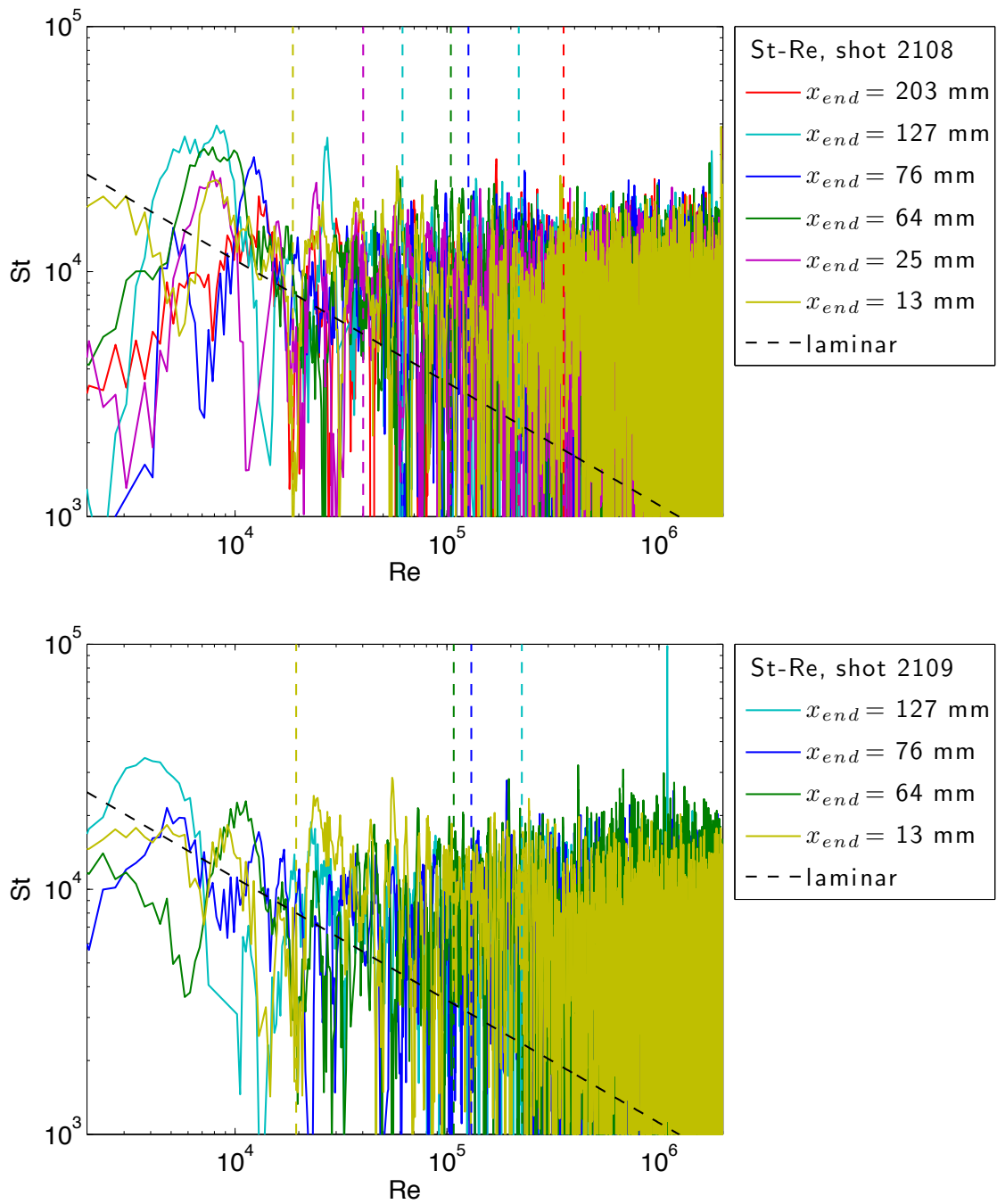


Figure E.107: Stanton-Reynolds number traces from shot 2109, a detonation in stoichiometric hydrogen-oxygen with 83% argon dilution at fill pressure 10 kPa. The dashed vertical lines represent the arrival of the reflected shock wave.

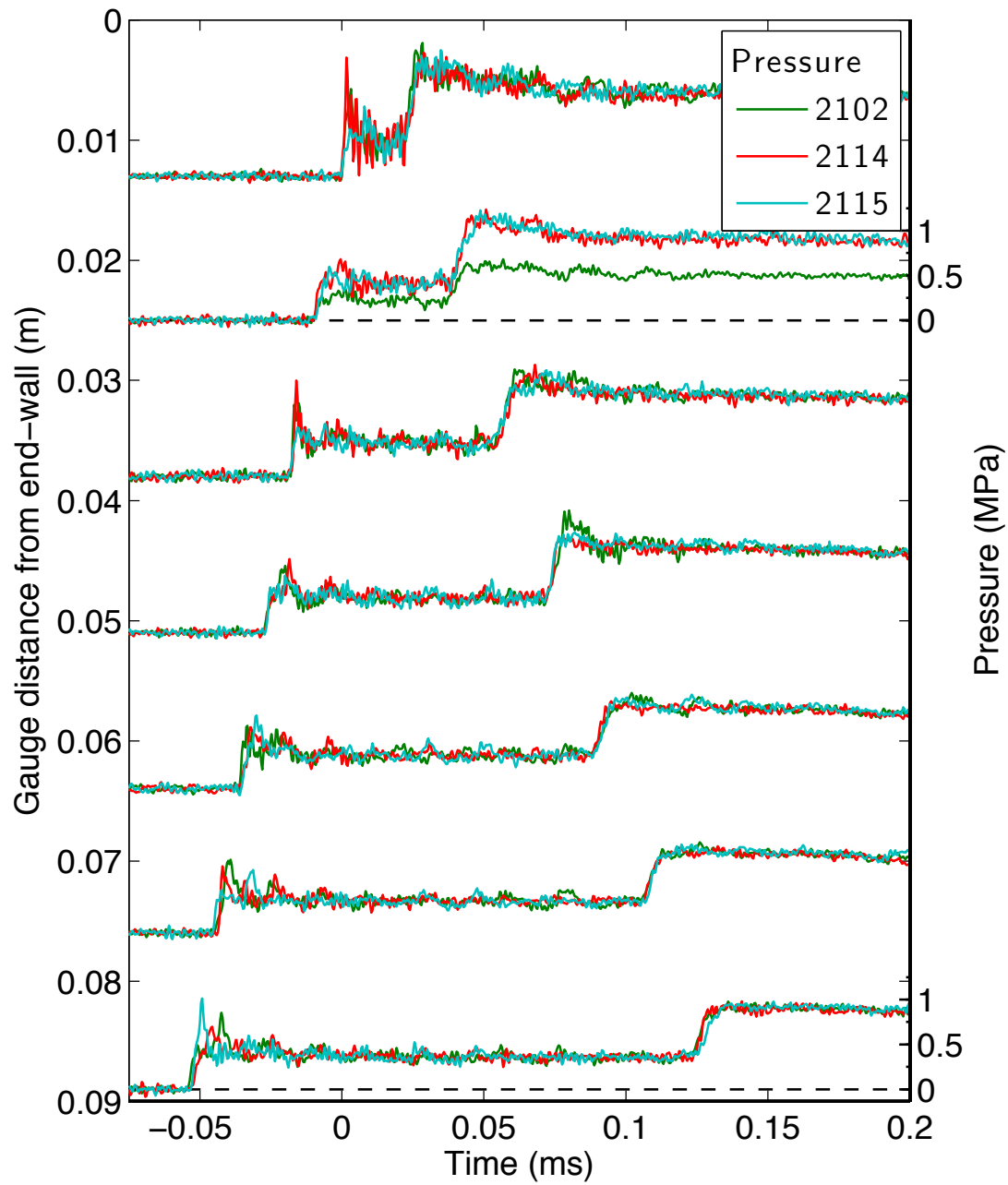


Figure E.108: Pressure traces for a detonation in stoichiometric hydrogen-oxygen with 83% argon dilution at fill pressure 25 kPa, part 1.

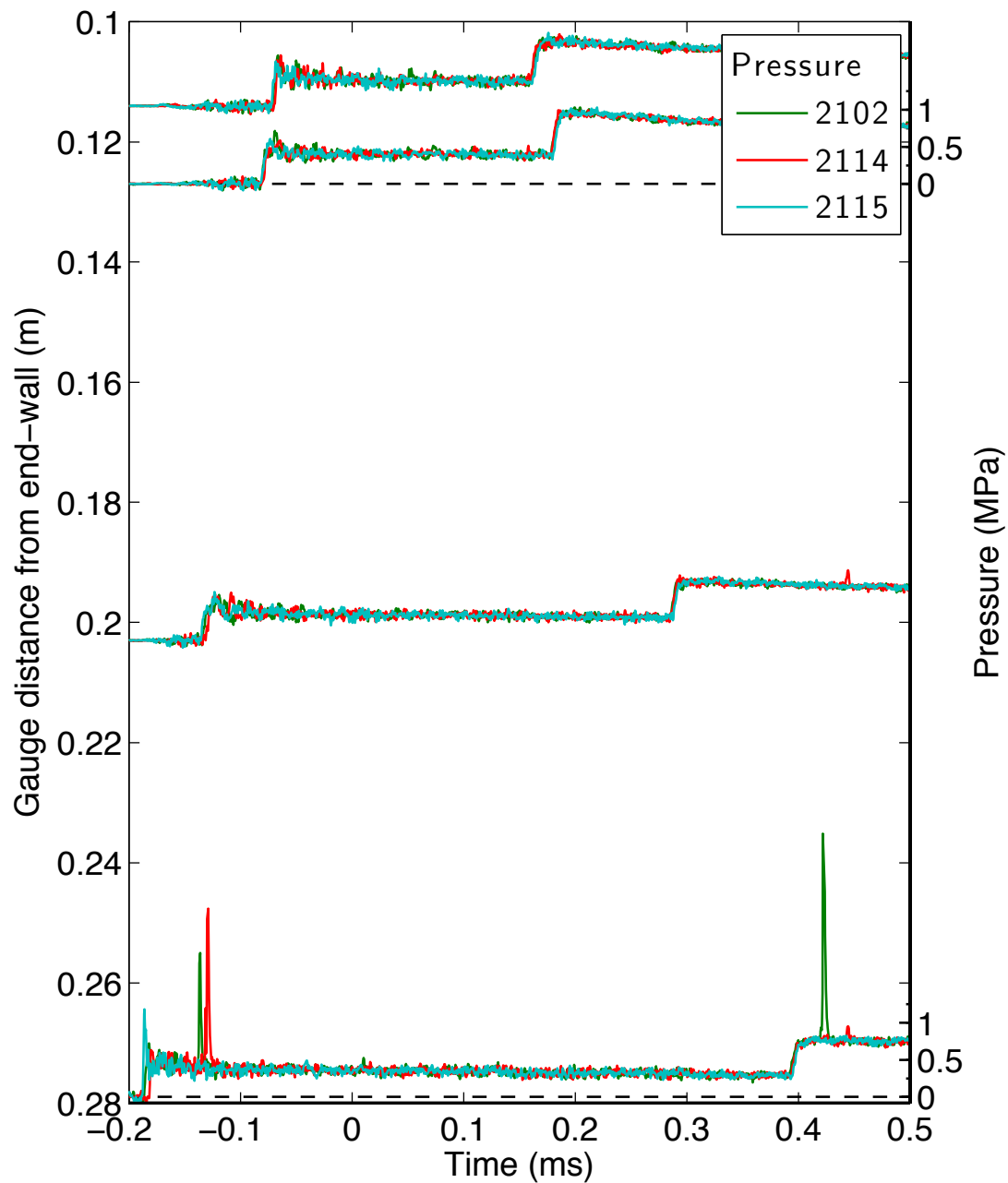


Figure E.109: Pressure traces for a detonation in stoichiometric hydrogen-oxygen with 83% argon dilution at fill pressure 25 kPa, part 2.

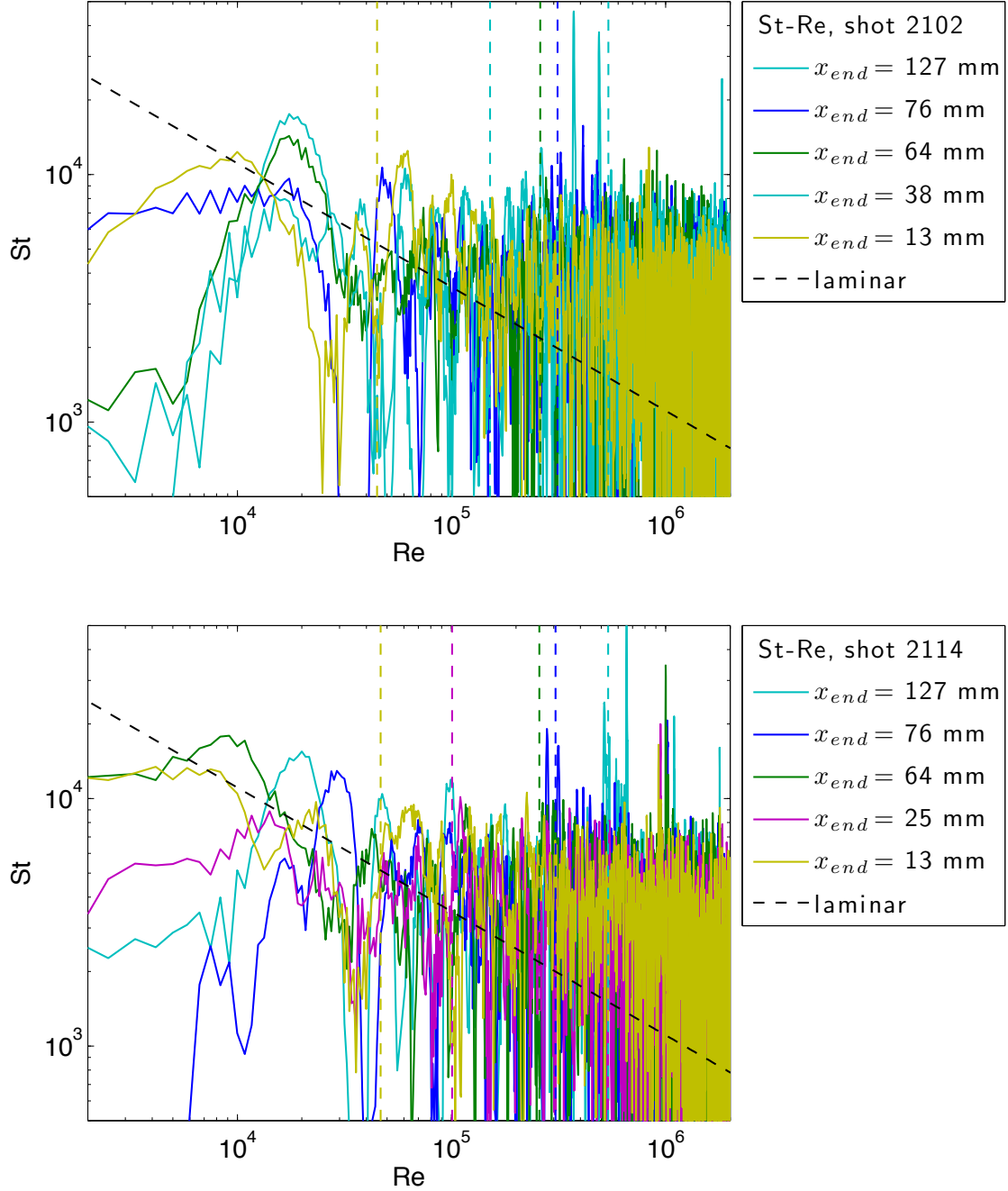


Figure E.110: Stanton-Reynolds number traces from shot 2114, a detonation in stoichiometric hydrogen-oxygen with 83% argon dilution at fill pressure 25 kPa. The dashed vertical lines represent the arrival of the reflected shock wave.

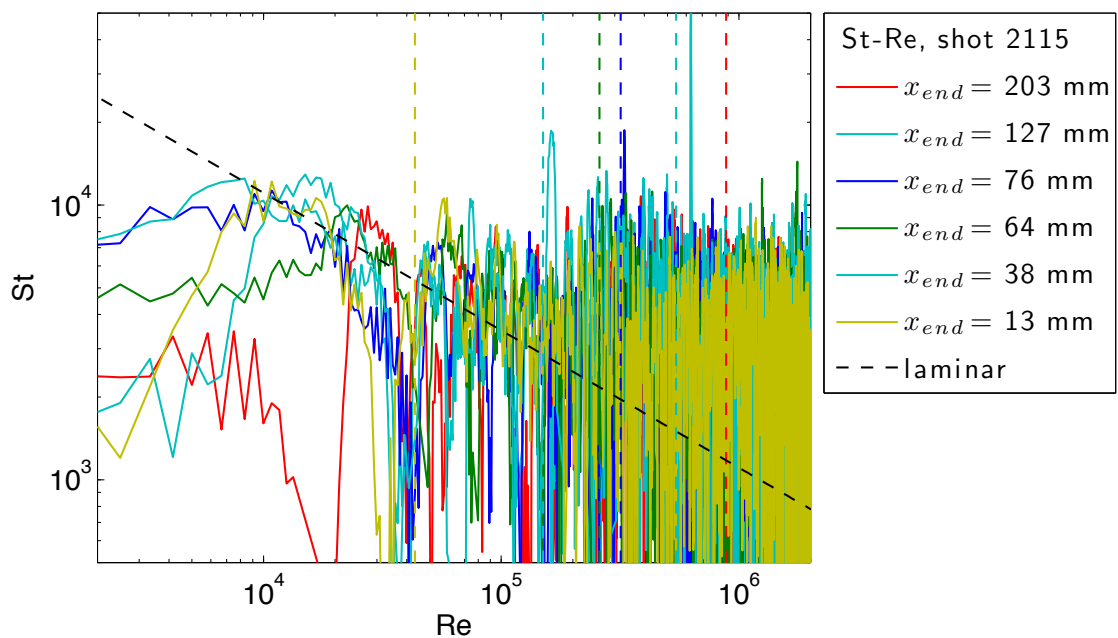


Figure E.111: Stanton-Reynolds number traces from shot 2115, a detonation in stoichiometric hydrogen-oxygen with 83% argon dilution at fill pressure 25 kPa. The dashed vertical lines represent the arrival of the reflected shock wave.

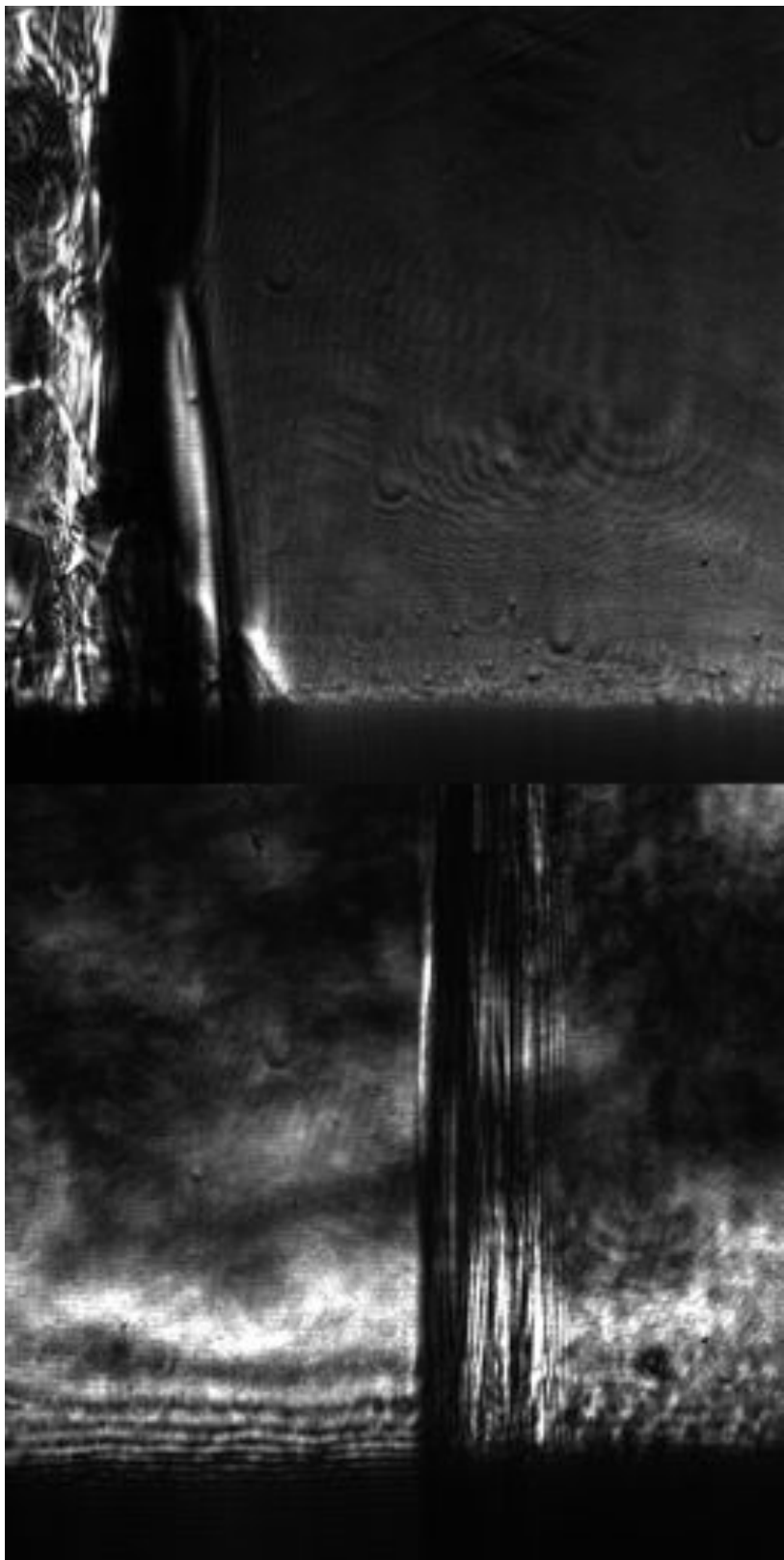


Figure E.112: Focused schlieren image of shot 2102. The field of view is approximately 14 mm wide.

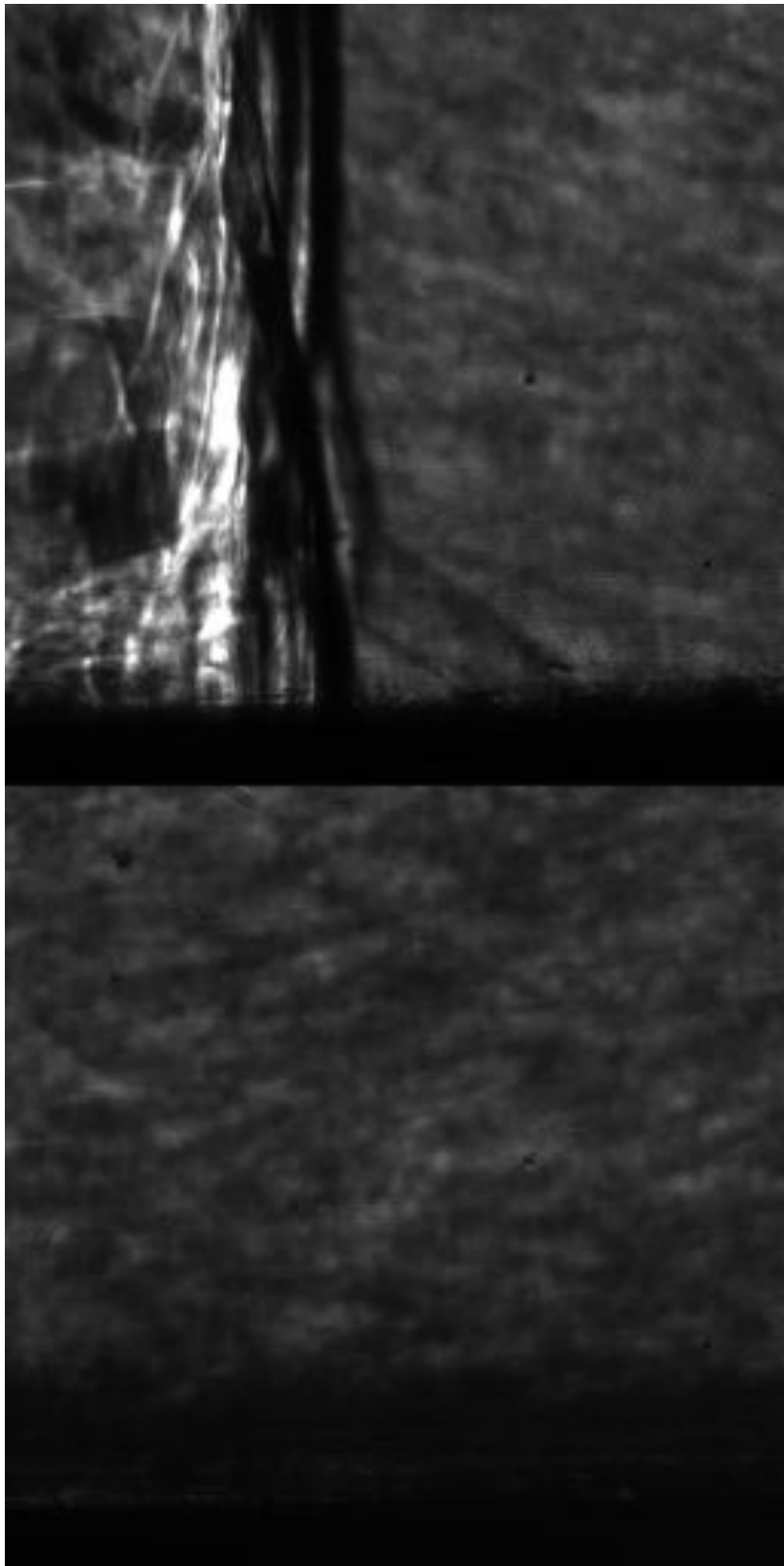


Figure E.113: Focused schlieren image of shot 2115. The field of view is approximately 14 mm wide.

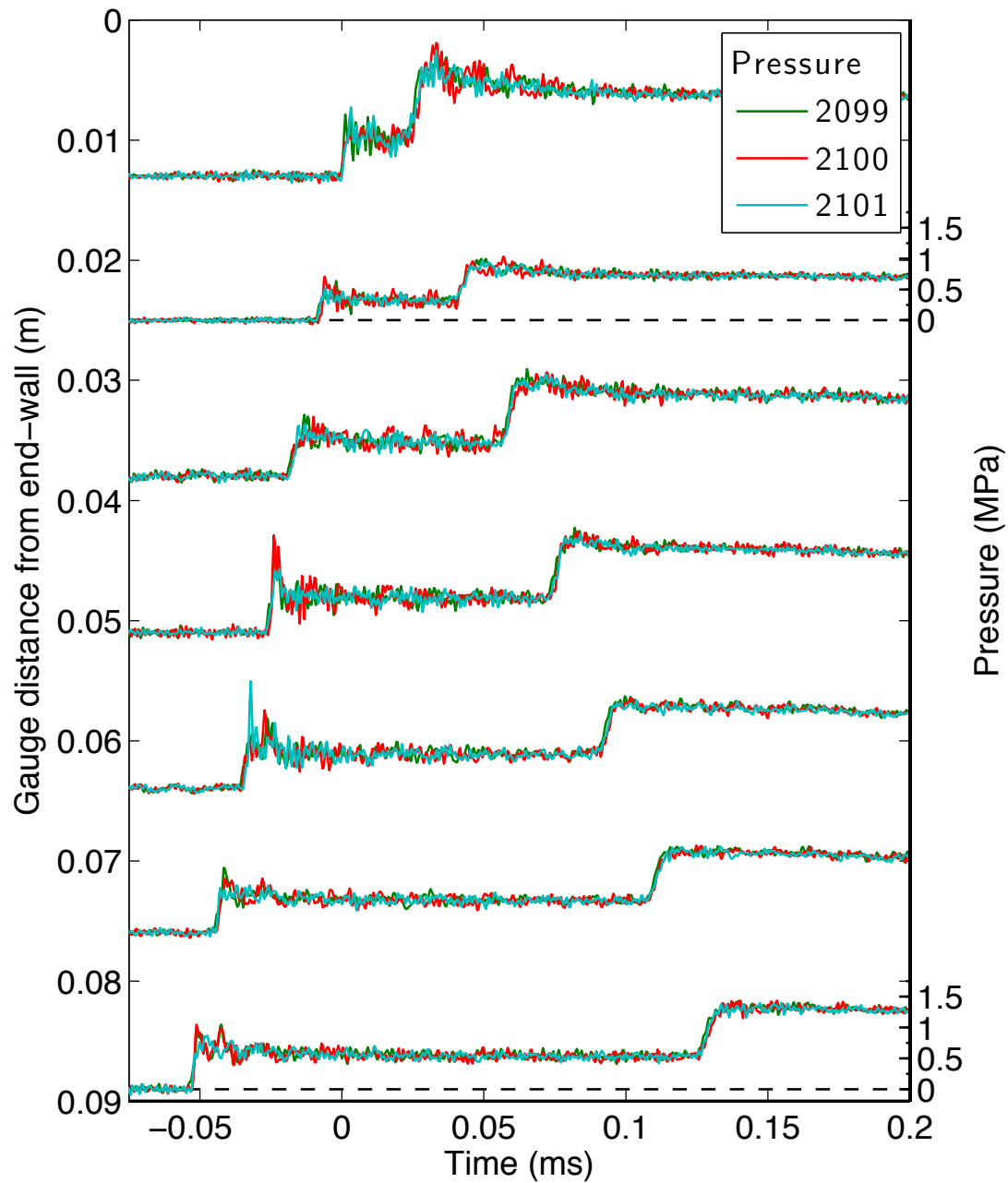


Figure E.114: Pressure traces for a detonation in stoichiometric hydrogen-oxygen with 83% argon dilution at fill pressure 40 kPa, part 1.

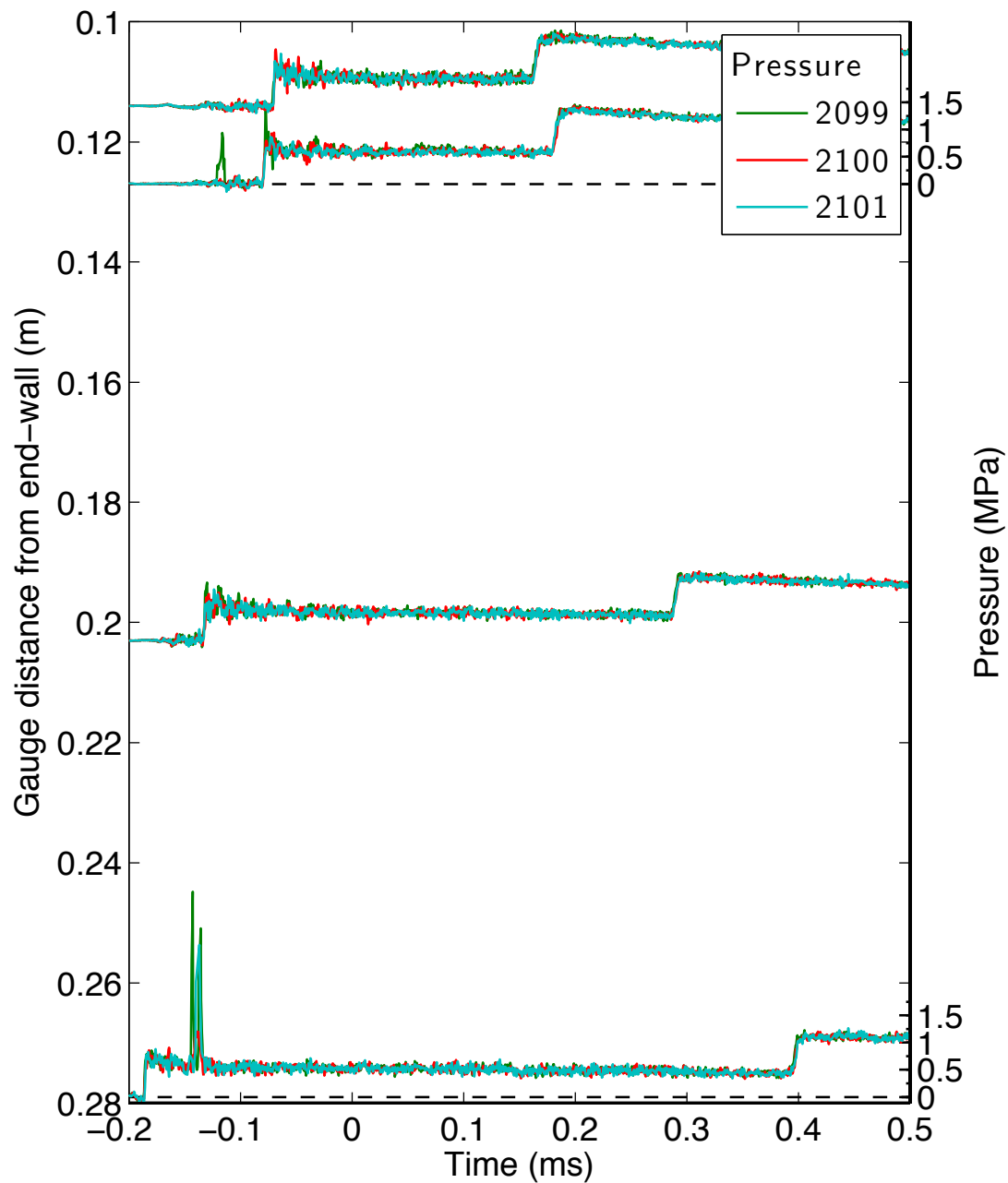


Figure E.115: Pressure traces for a detonation in stoichiometric hydrogen-oxygen with 83% argon dilution at fill pressure 40 kPa, part 2.

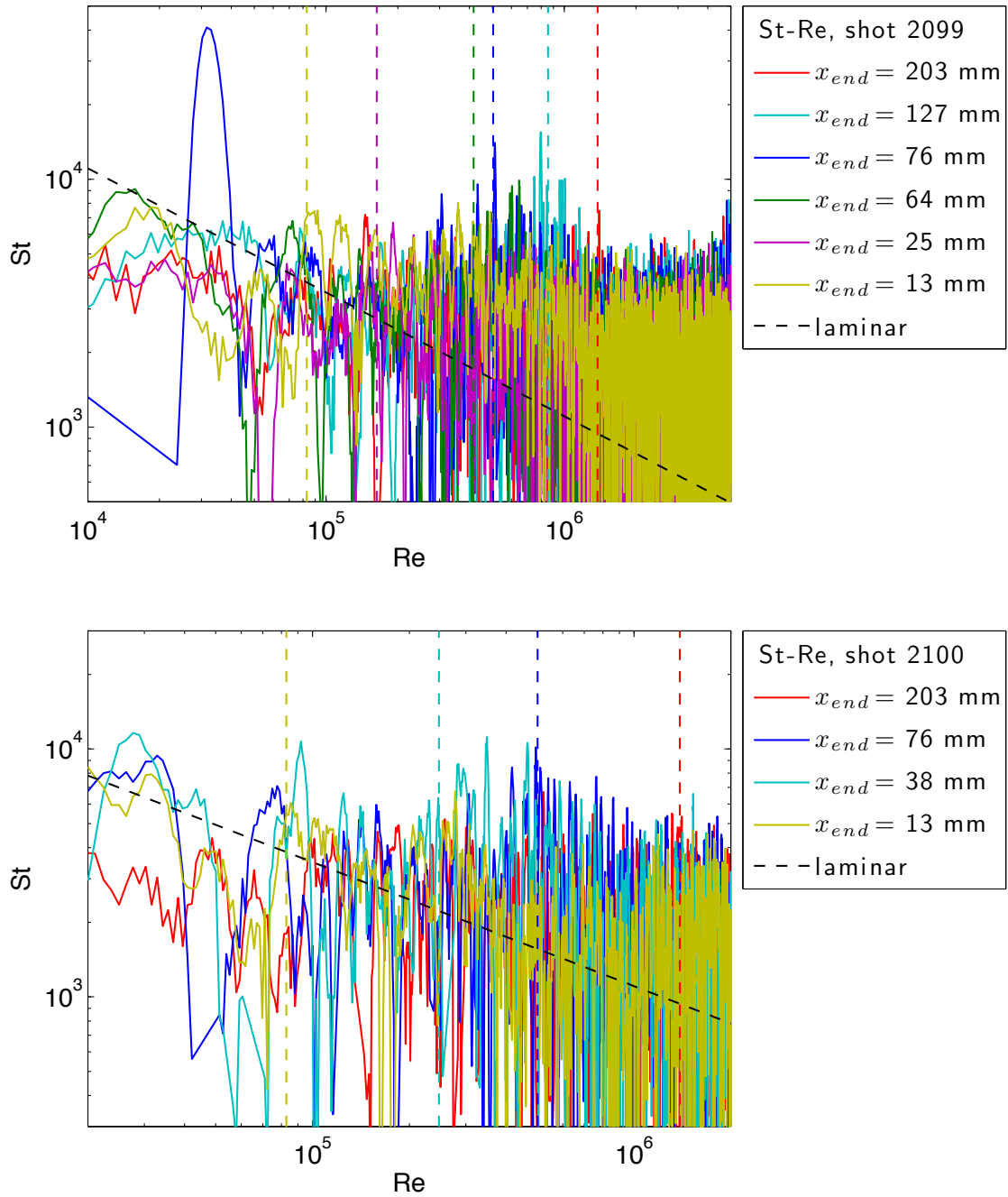


Figure E.116: Stanton-Reynolds number traces from shot 2100, a detonation in stoichiometric hydrogen-oxygen with 83% argon dilution at fill pressure 40 kPa. The dashed vertical lines represent the arrival of the reflected shock wave.

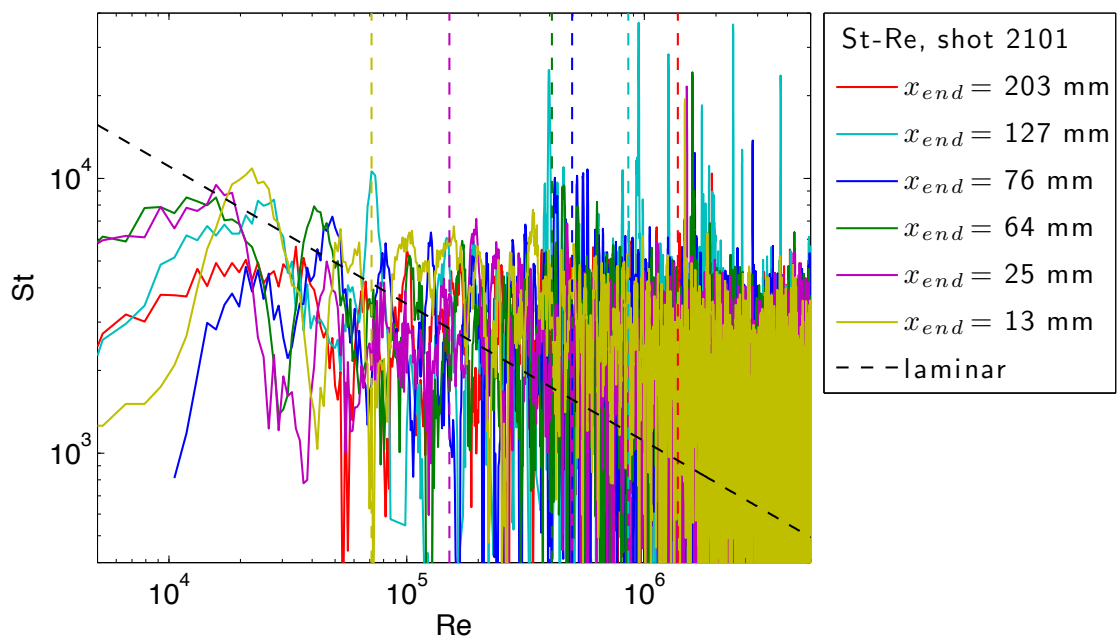


Figure E.117: Stanton-Reynolds number traces from shot 2101, a detonation in stoichiometric hydrogen-oxygen with 83% argon dilution at fill pressure 40 kPa. The dashed vertical lines represent the arrival of the reflected shock wave.

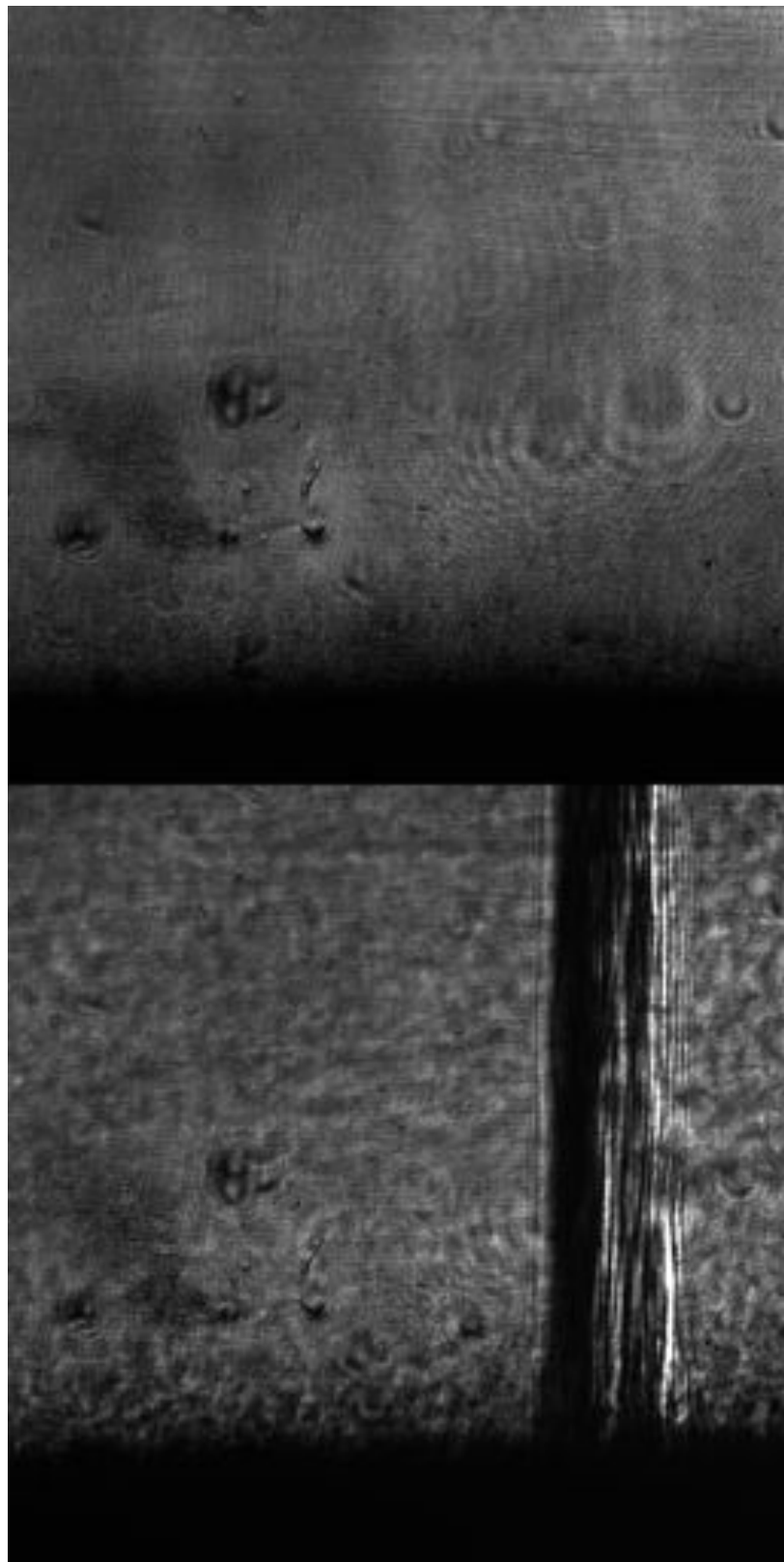


Figure E.118: Focused schlieren image of shot 2099. The field of view is approximately 14 mm wide.

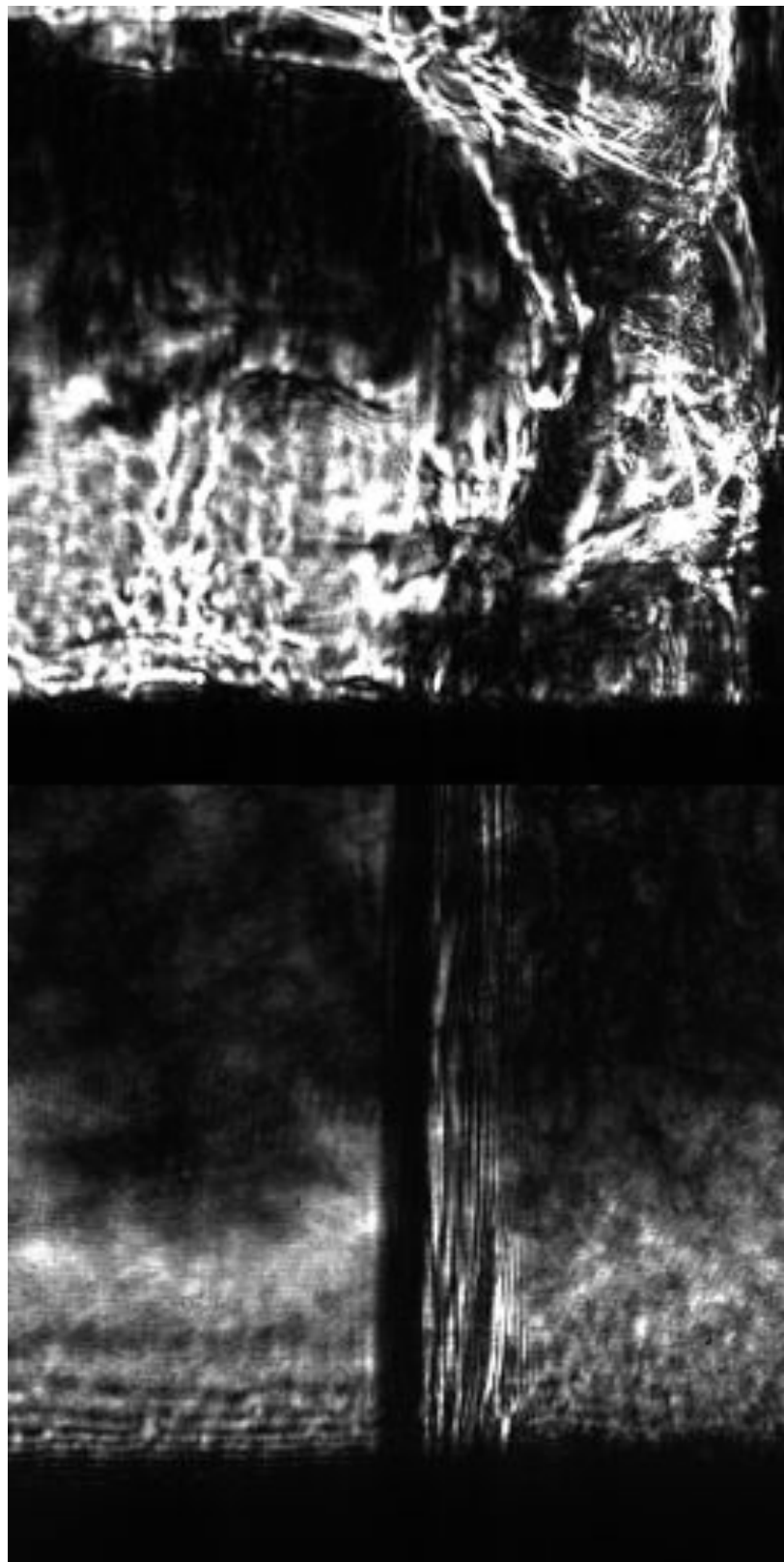


Figure E.119: Focused schlieren image of shot 2100. The field of view is approximately 14 mm wide.

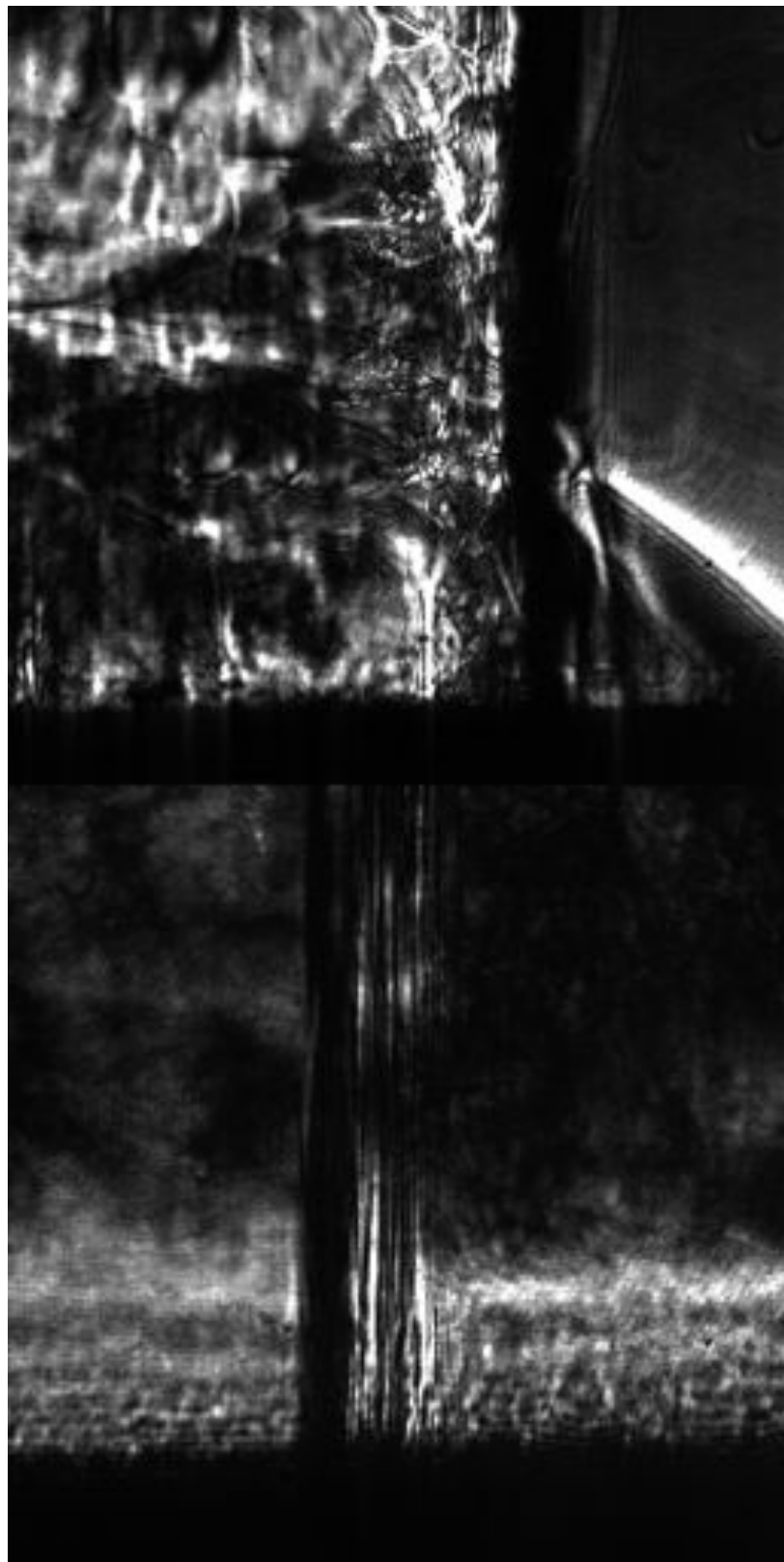


Figure E.120: Focused schlieren image of shot 2101. The field of view is approximately 14 mm wide.

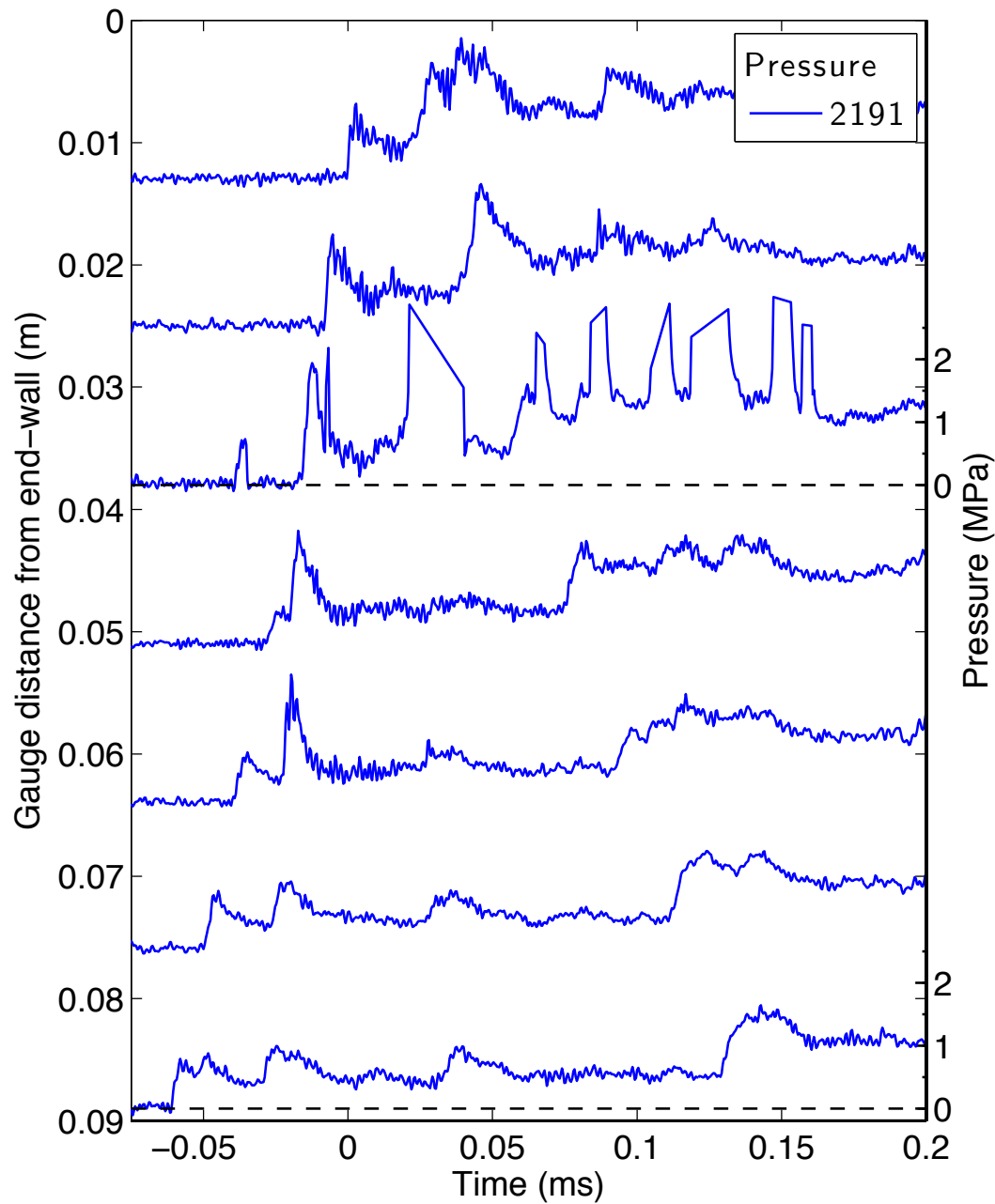


Figure E.121: Pressure traces for a detonation in stoichiometric hydrogen-oxygen with 90% argon dilution at fill pressure 50 kPa, part 1.

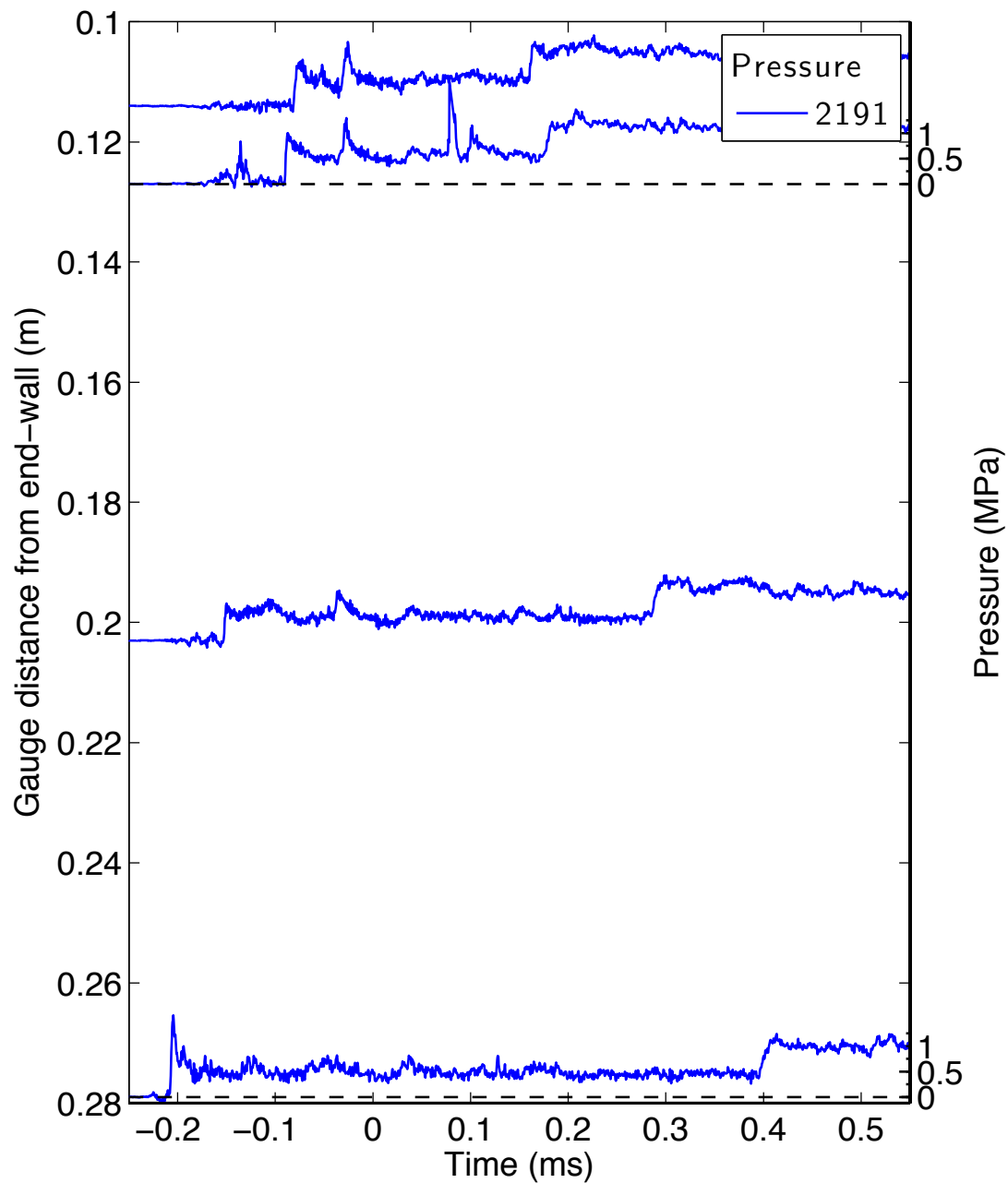


Figure E.122: Pressure traces for a detonation in stoichiometric hydrogen-oxygen with 90% argon dilution at fill pressure 50 kPa, part 2.

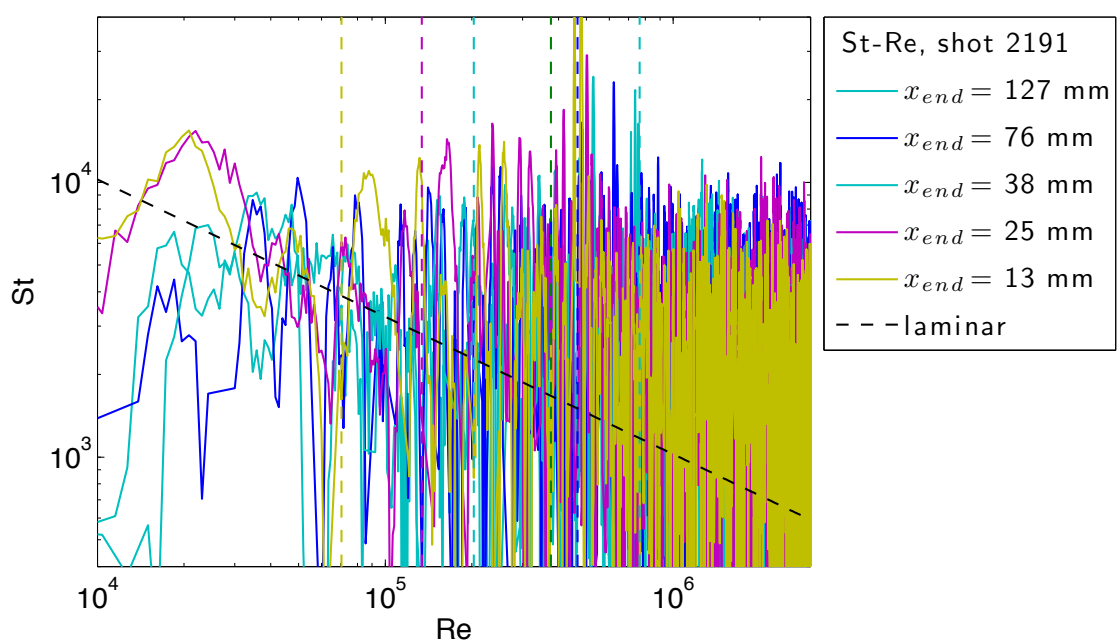


Figure E.123: Stanton-Reynolds number traces from shot 2191, a detonation in stoichiometric hydrogen-oxygen with 90% argon dilution at fill pressure 50 kPa. The dashed vertical lines represent the arrival of the reflected shock wave.

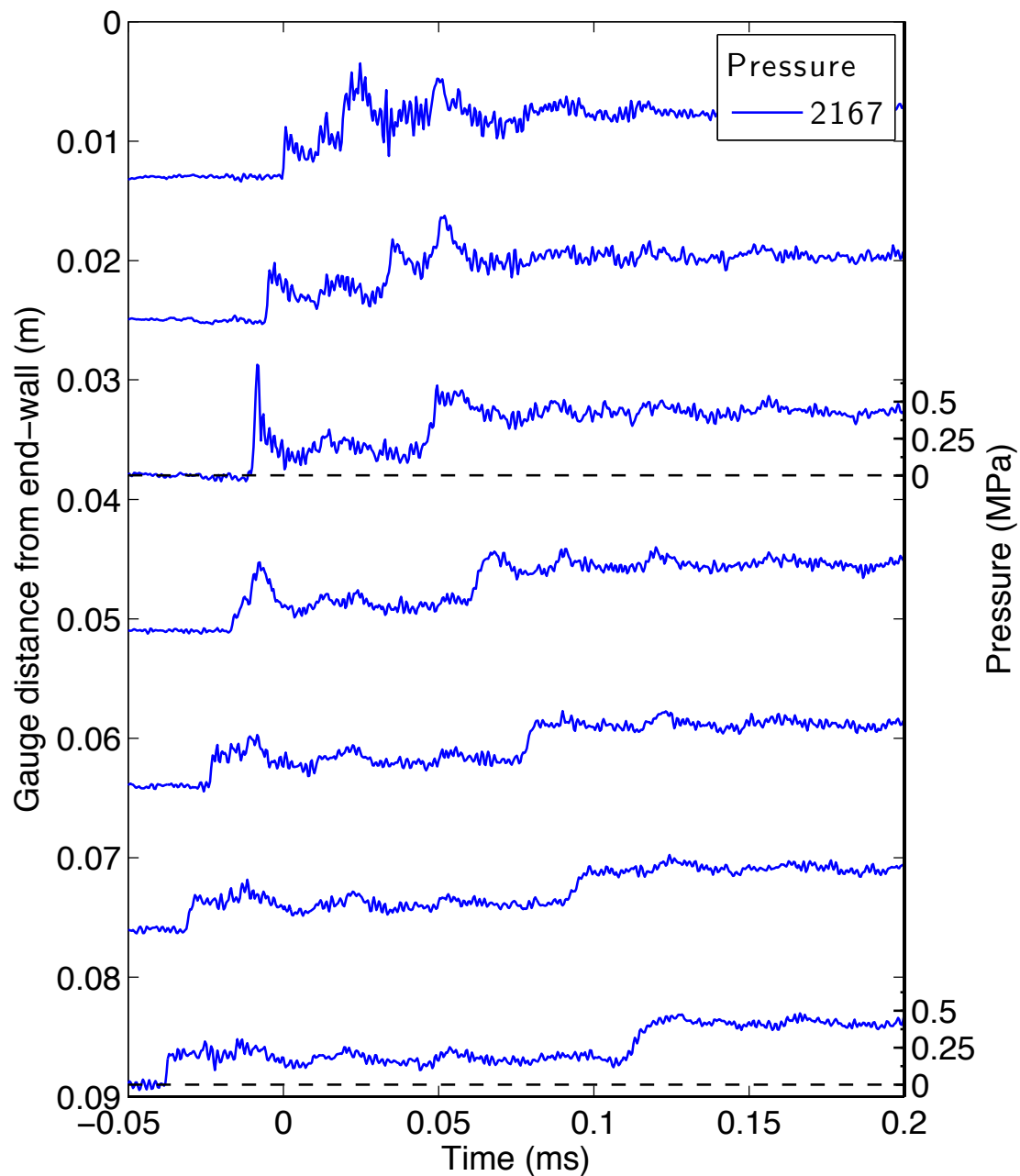


Figure E.124: Pressure traces for a detonation in stoichiometric hydrogen-oxygen with 50% nitrogen dilution at fill pressure 10 kPa, part 1.

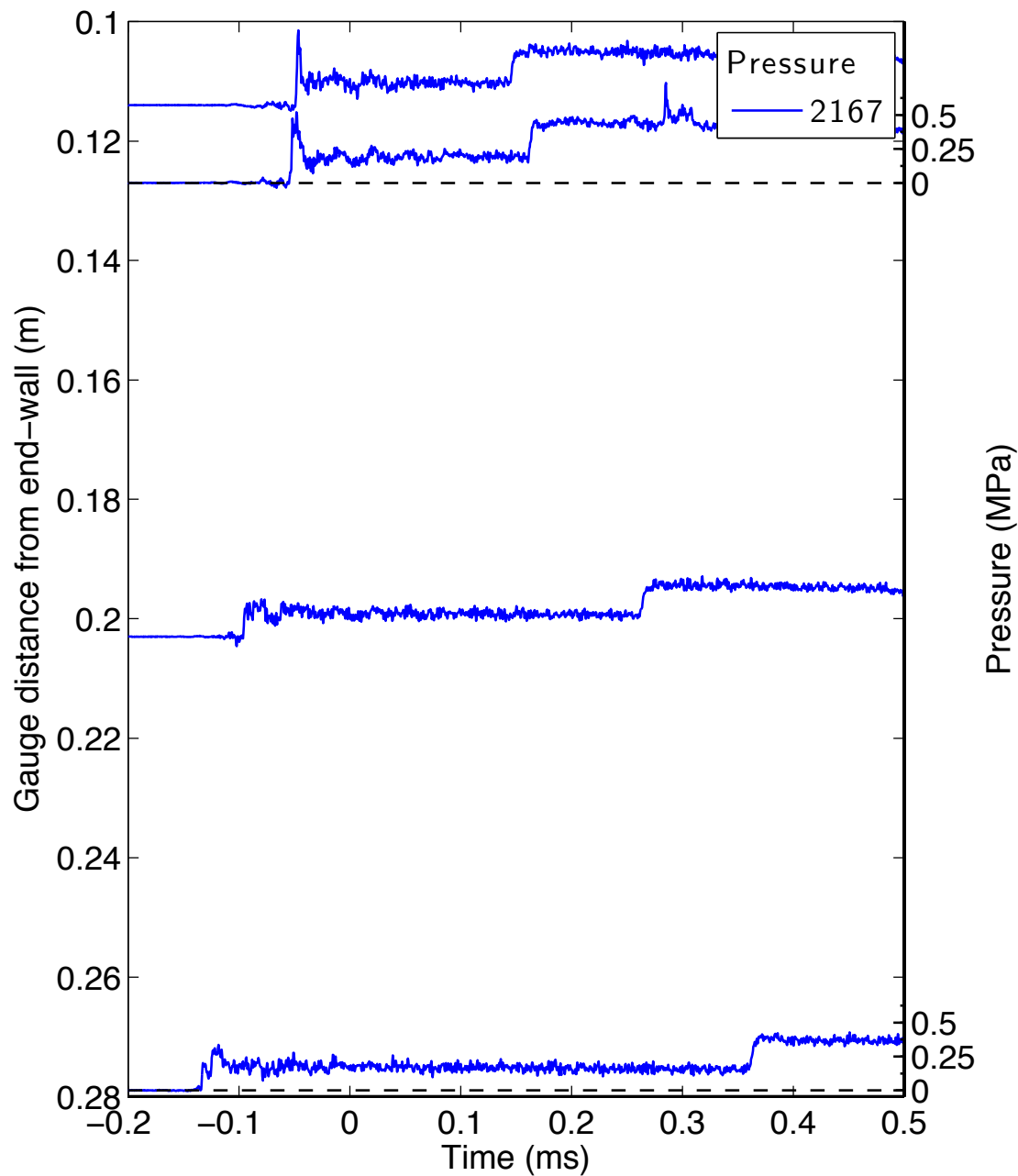


Figure E.125: Pressure traces for a detonation in stoichiometric hydrogen-oxygen with 50% nitrogen dilution at fill pressure 10 kPa, part 2.

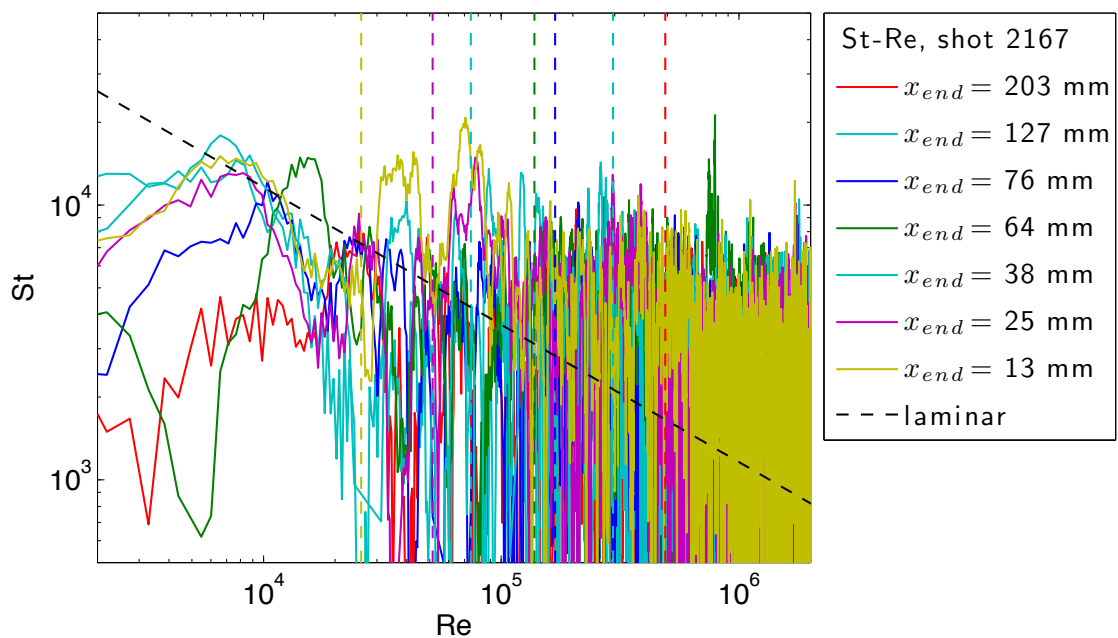


Figure E.126: Stanton-Reynolds number traces from shot 2167, a detonation in stoichiometric hydrogen-oxygen with 50% nitrogen dilution at fill pressure 10 kPa. The dashed vertical lines represent the arrival of the reflected shock wave.

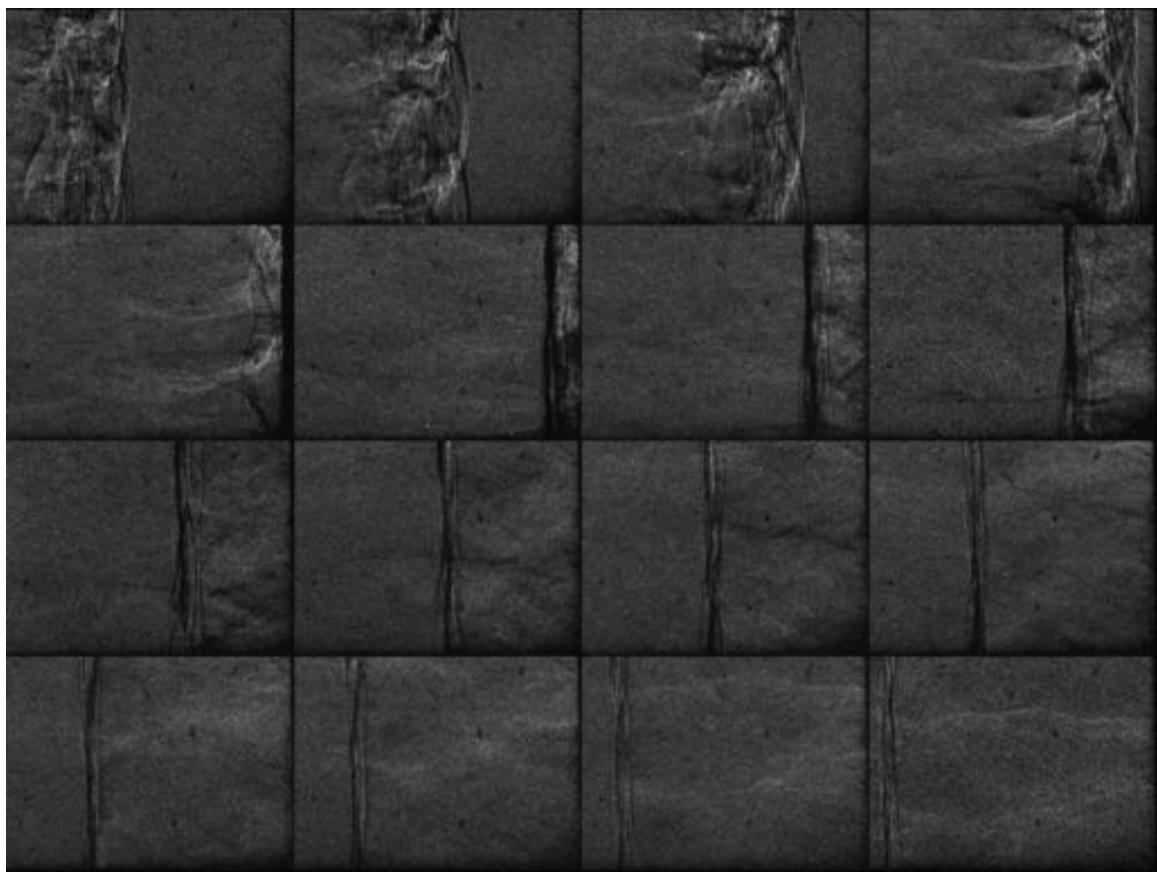


Figure E.127: Unfocused schlieren image of shot 2167. The field of view is approximately 30 mm wide.

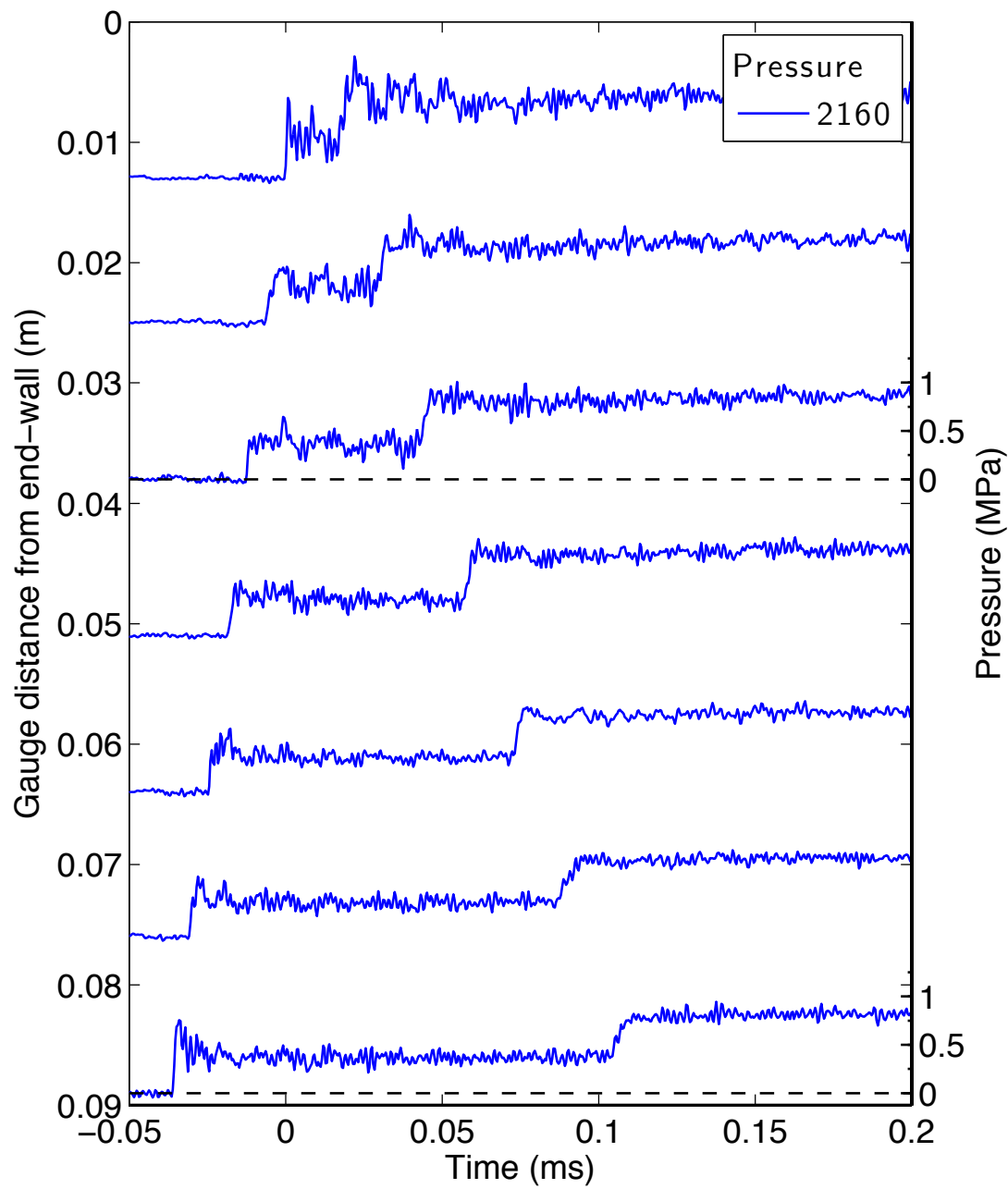


Figure E.128: Pressure traces for a detonation in stoichiometric hydrogen-oxygen with 50% nitrogen dilution at fill pressure 25 kPa, part 1.

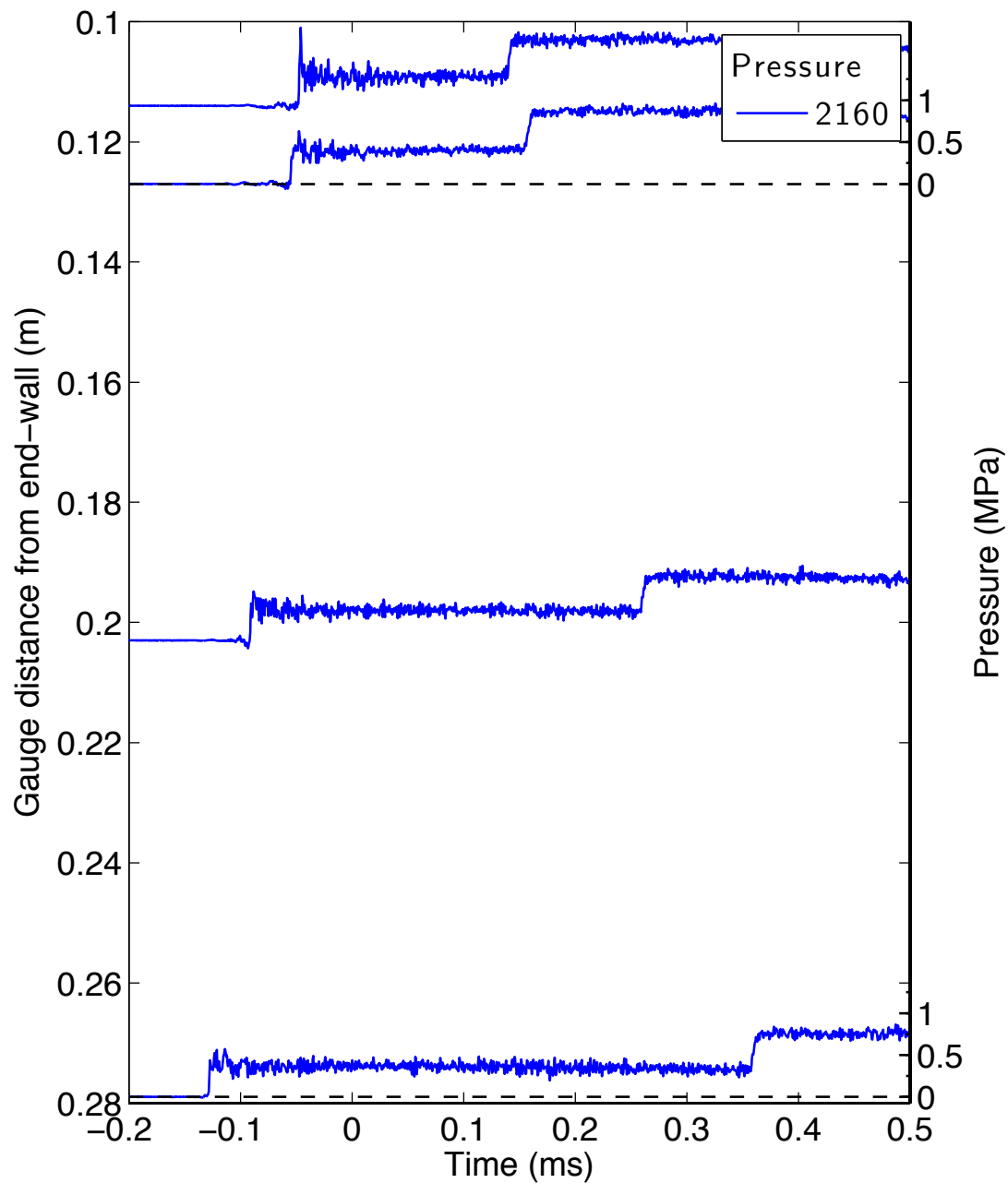


Figure E.129: Pressure traces for a detonation in stoichiometric hydrogen-oxygen with 50% nitrogen dilution at fill pressure 25 kPa, part 2.

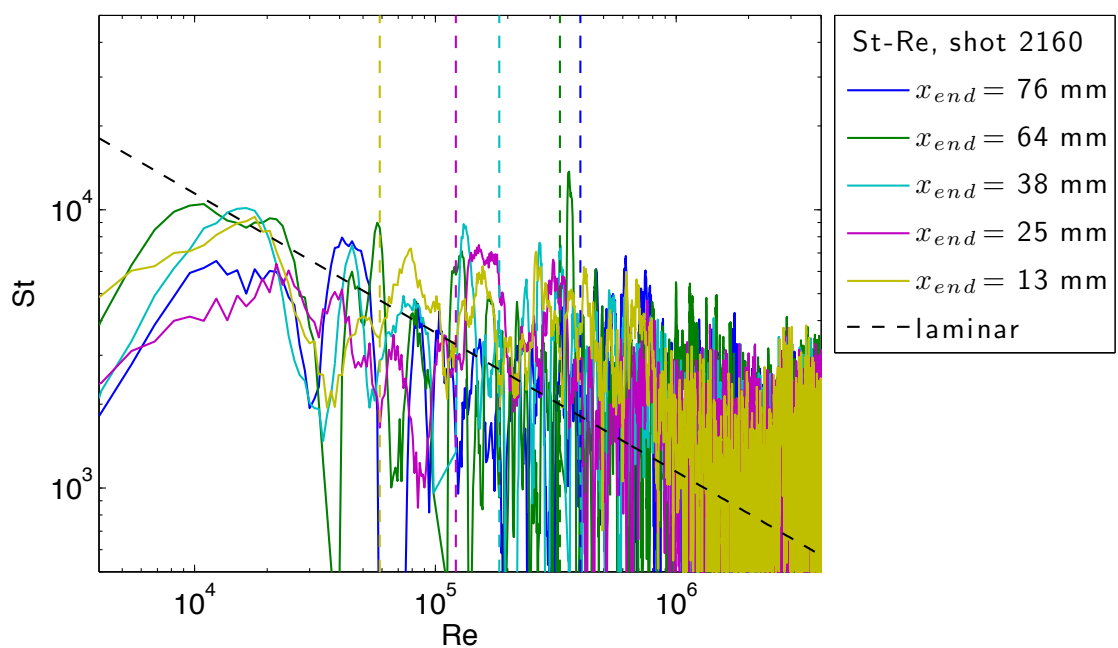


Figure E.130: Stanton-Reynolds number traces from shot 2160, a detonation in stoichiometric hydrogen-oxygen with 50% nitrogen dilution at fill pressure 25 kPa. The dashed vertical lines represent the arrival of the reflected shock wave.

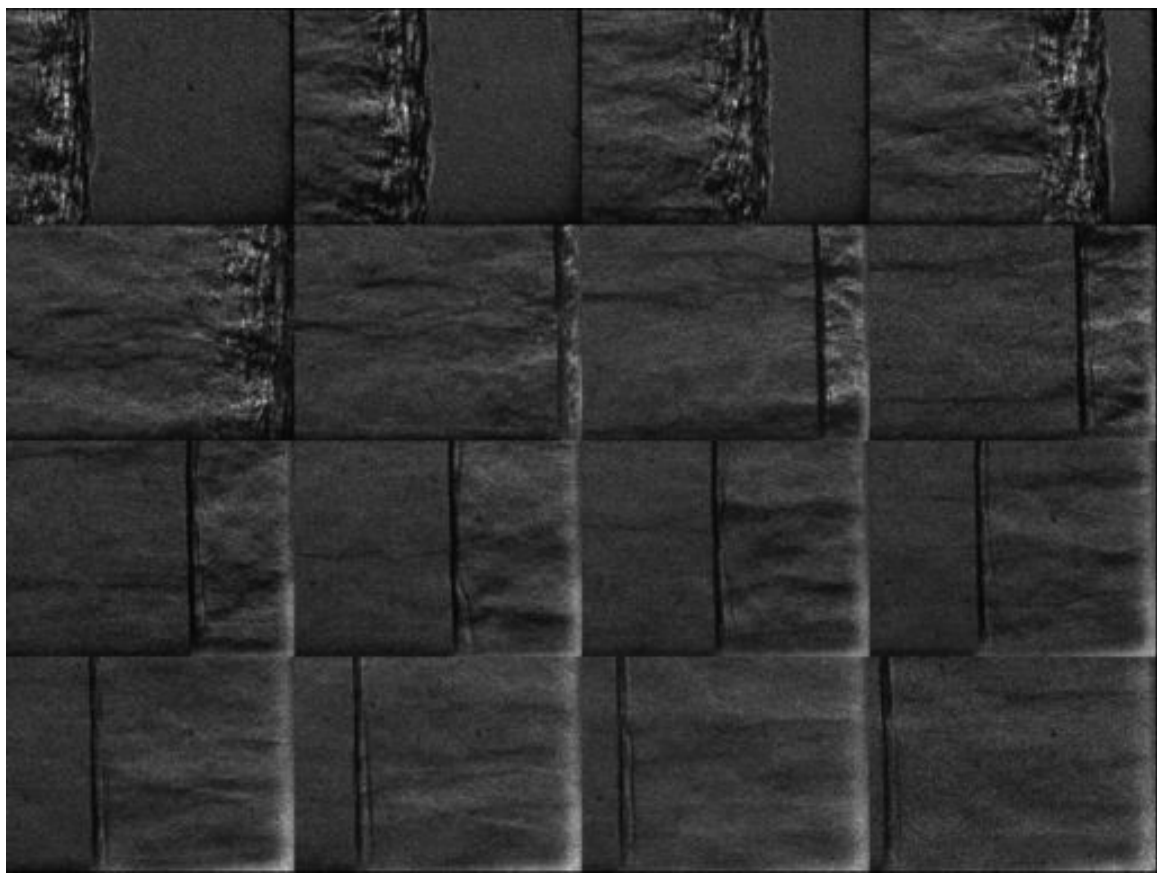


Figure E.131: Unfocused schlieren image of shot 2160. The field of view is approximately 30 mm wide.

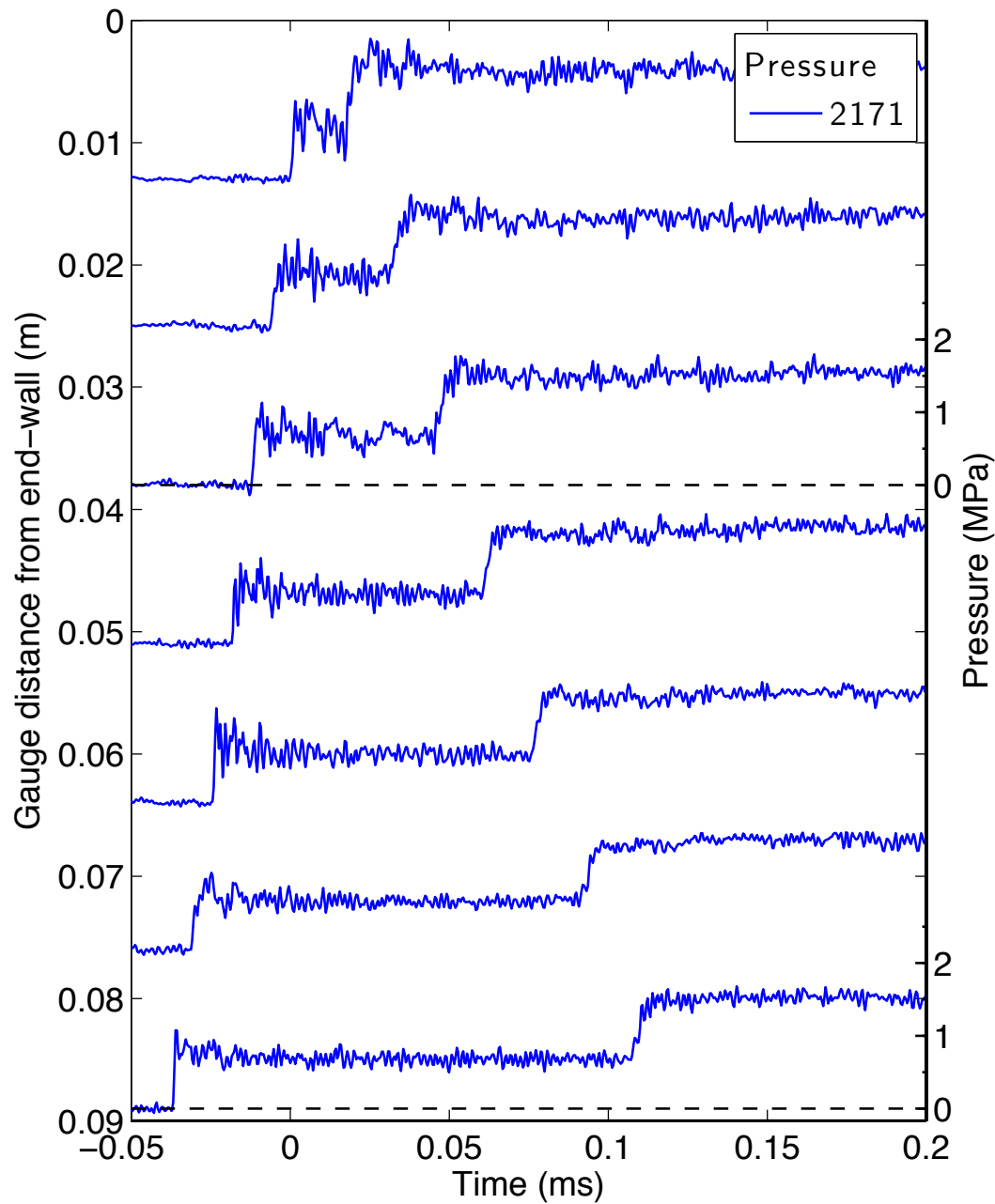


Figure E.132: Pressure traces for a detonation in stoichiometric hydrogen-oxygen with 50% nitrogen dilution at fill pressure 50 kPa, part 1.

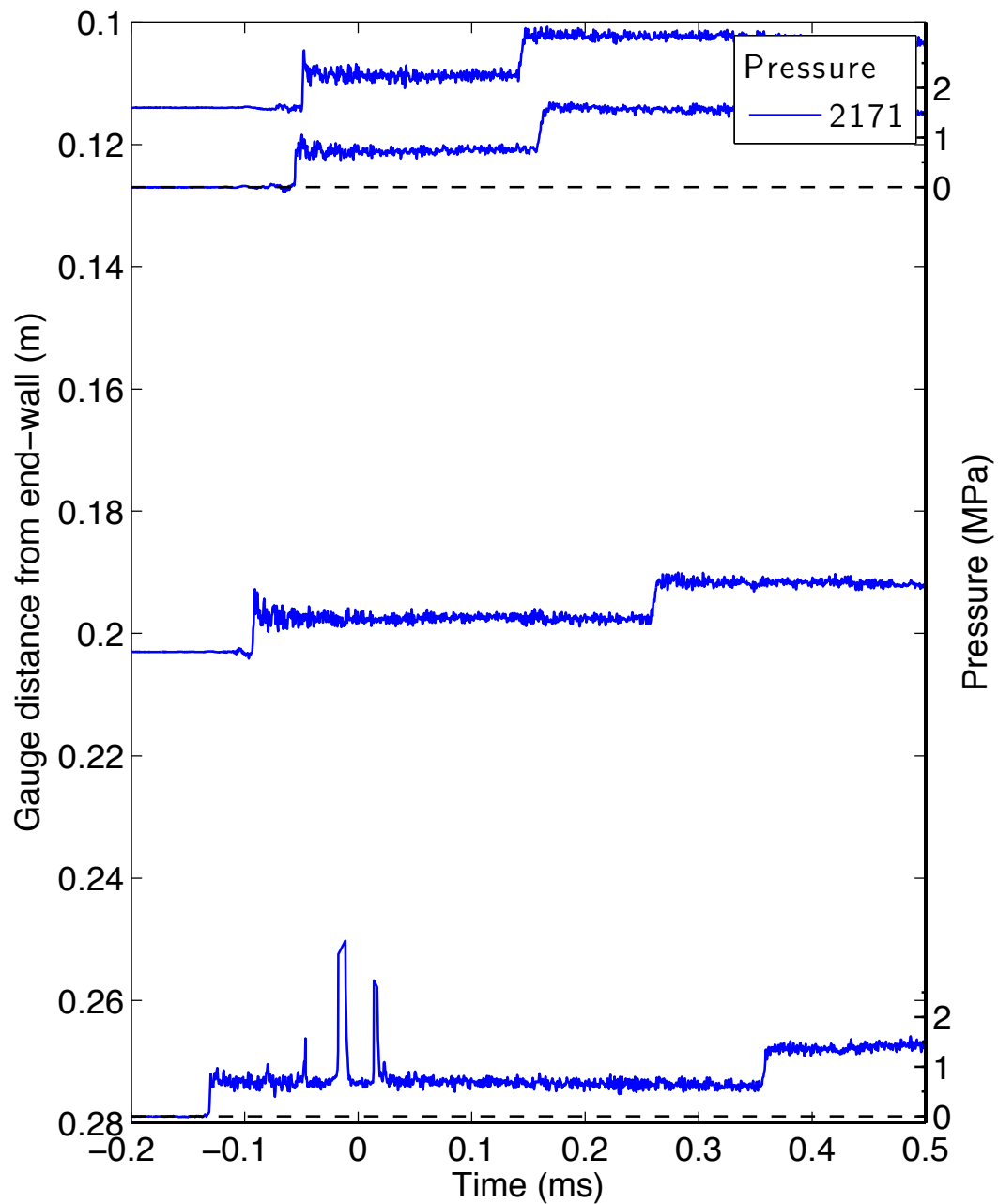


Figure E.133: Pressure traces for a detonation in stoichiometric hydrogen-oxygen with 50% nitrogen dilution at fill pressure 50 kPa, part 2.

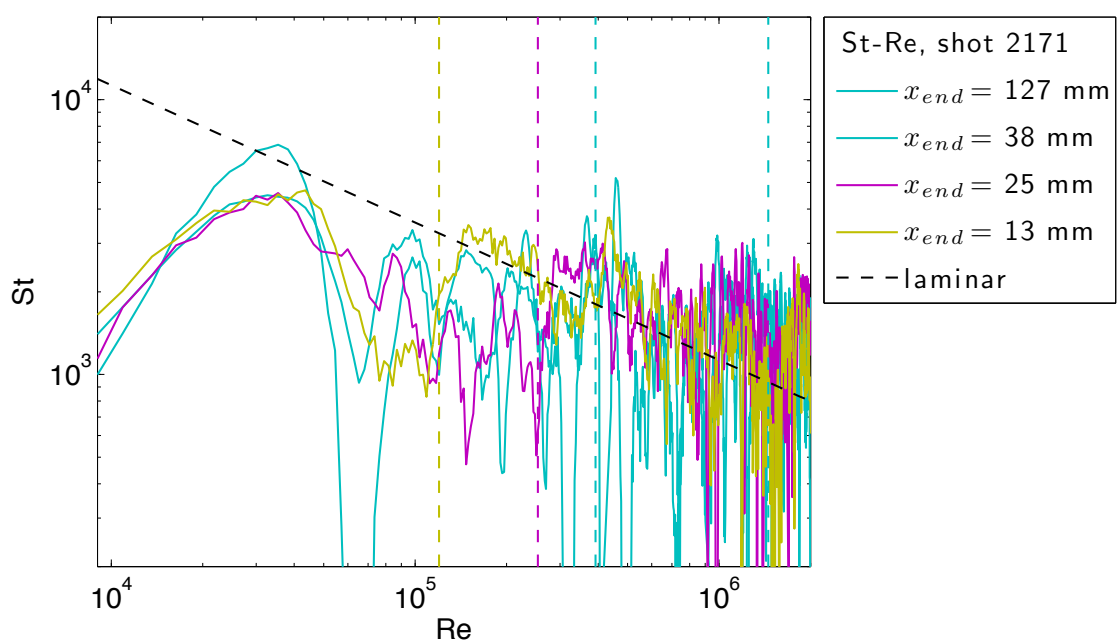


Figure E.134: Stanton-Reynolds number traces from shot 2171, a detonation in stoichiometric hydrogen-oxygen with 50% nitrogen dilution at fill pressure 50 kPa. The dashed vertical lines represent the arrival of the reflected shock wave.

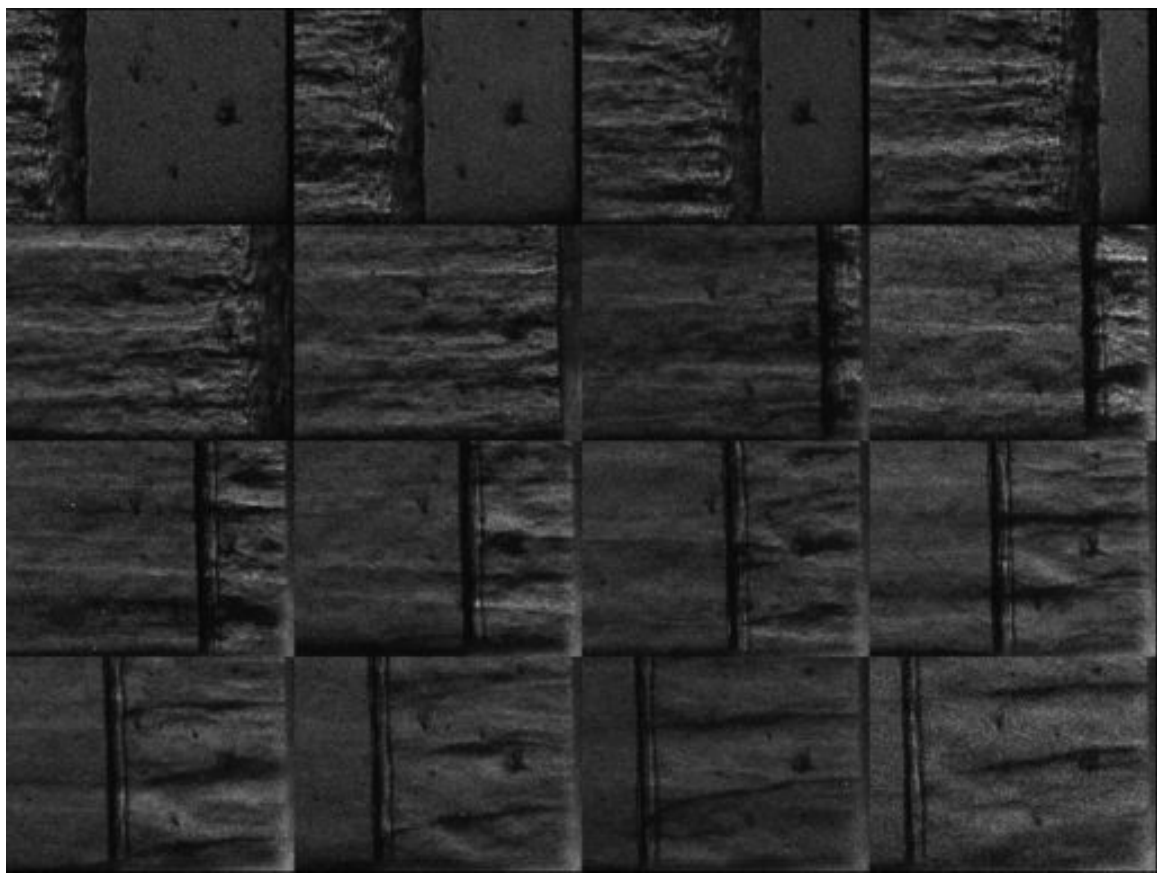


Figure E.135: Unfocused schlieren image of shot 2171. The field of view is approximately 30 mm wide.

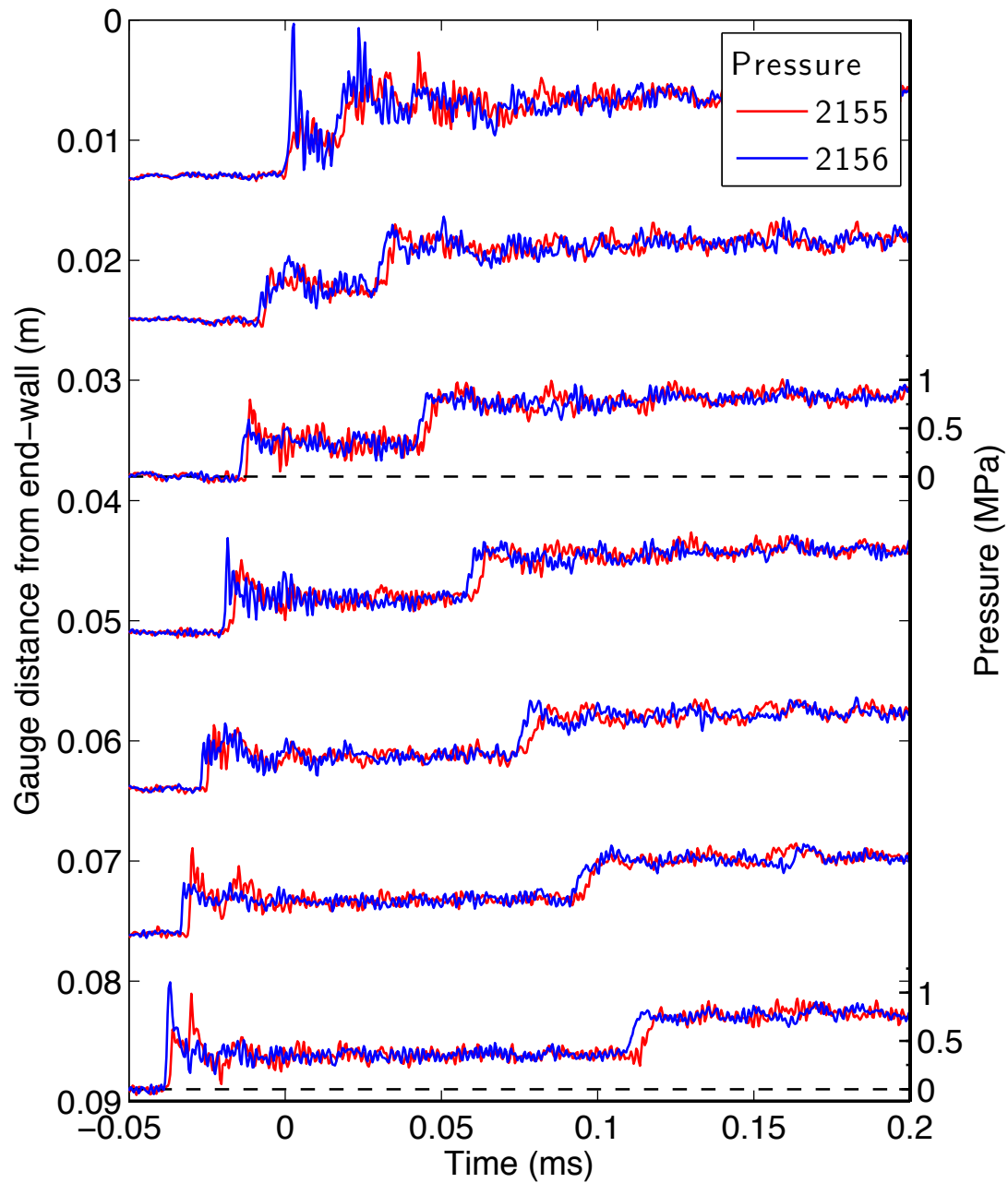


Figure E.136: Pressure traces for a detonation in stoichiometric hydrogen-oxygen with 25% carbon dioxide dilution at fill pressure 25 kPa, part 1.

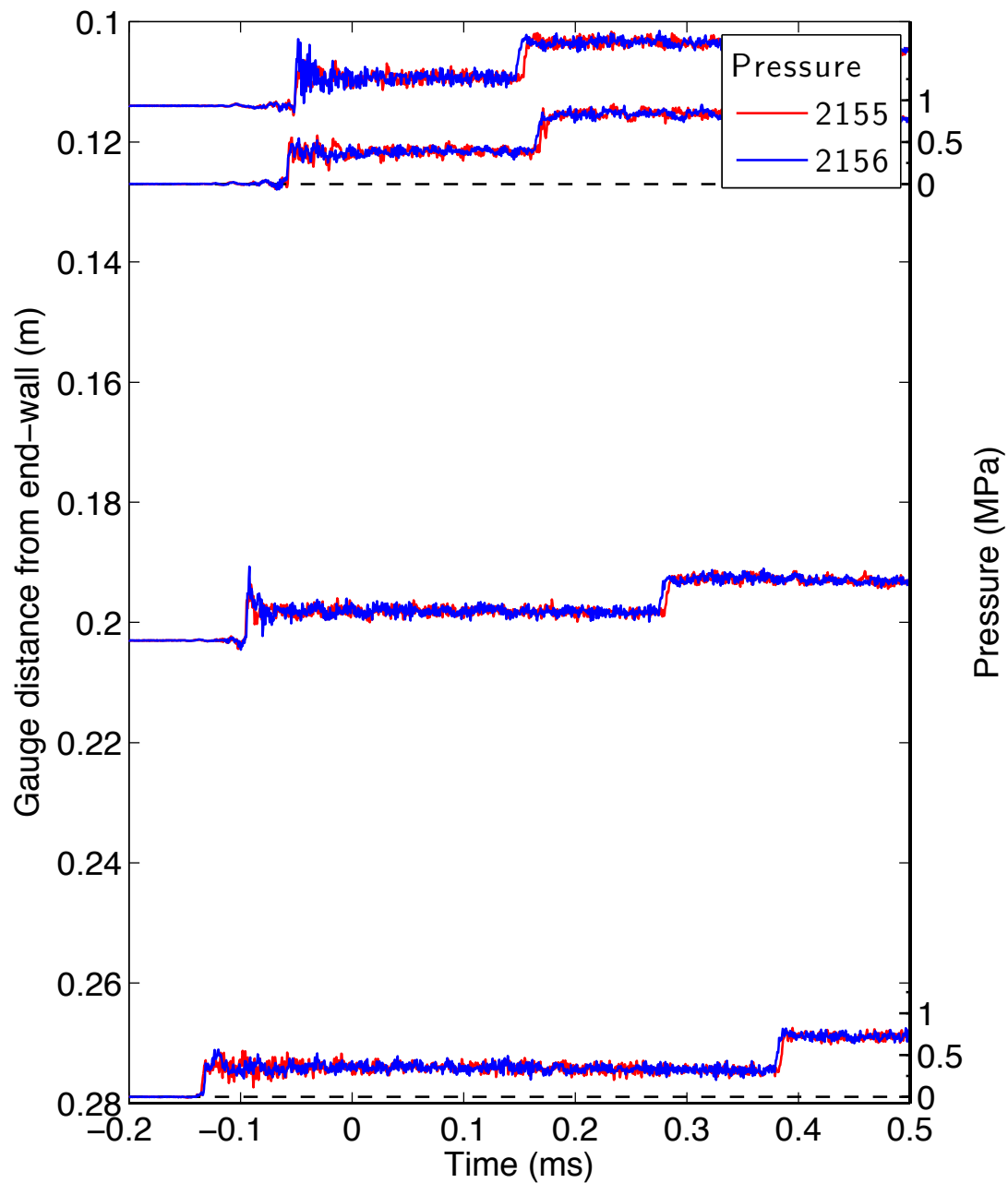


Figure E.137: Pressure traces for a detonation in stoichiometric hydrogen-oxygen with 25% carbon dioxide dilution at fill pressure 25 kPa, part 2.

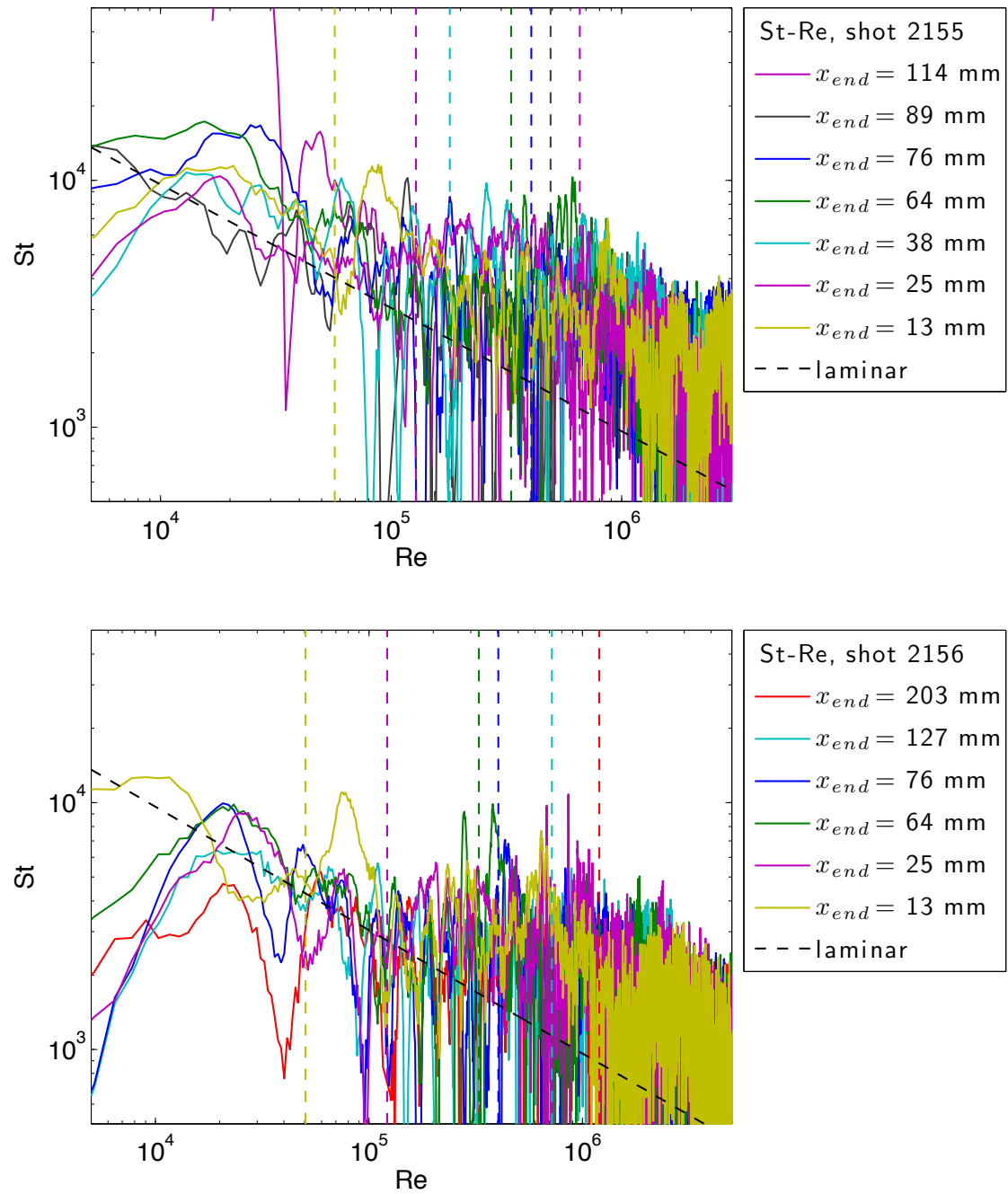


Figure E.138: Stanton-Reynolds number traces from shot 2156, a detonation in stoichiometric hydrogen-oxygen with 25% carbon dioxide dilution at fill pressure 25 kPa. The dashed vertical lines represent the arrival of the reflected shock wave.

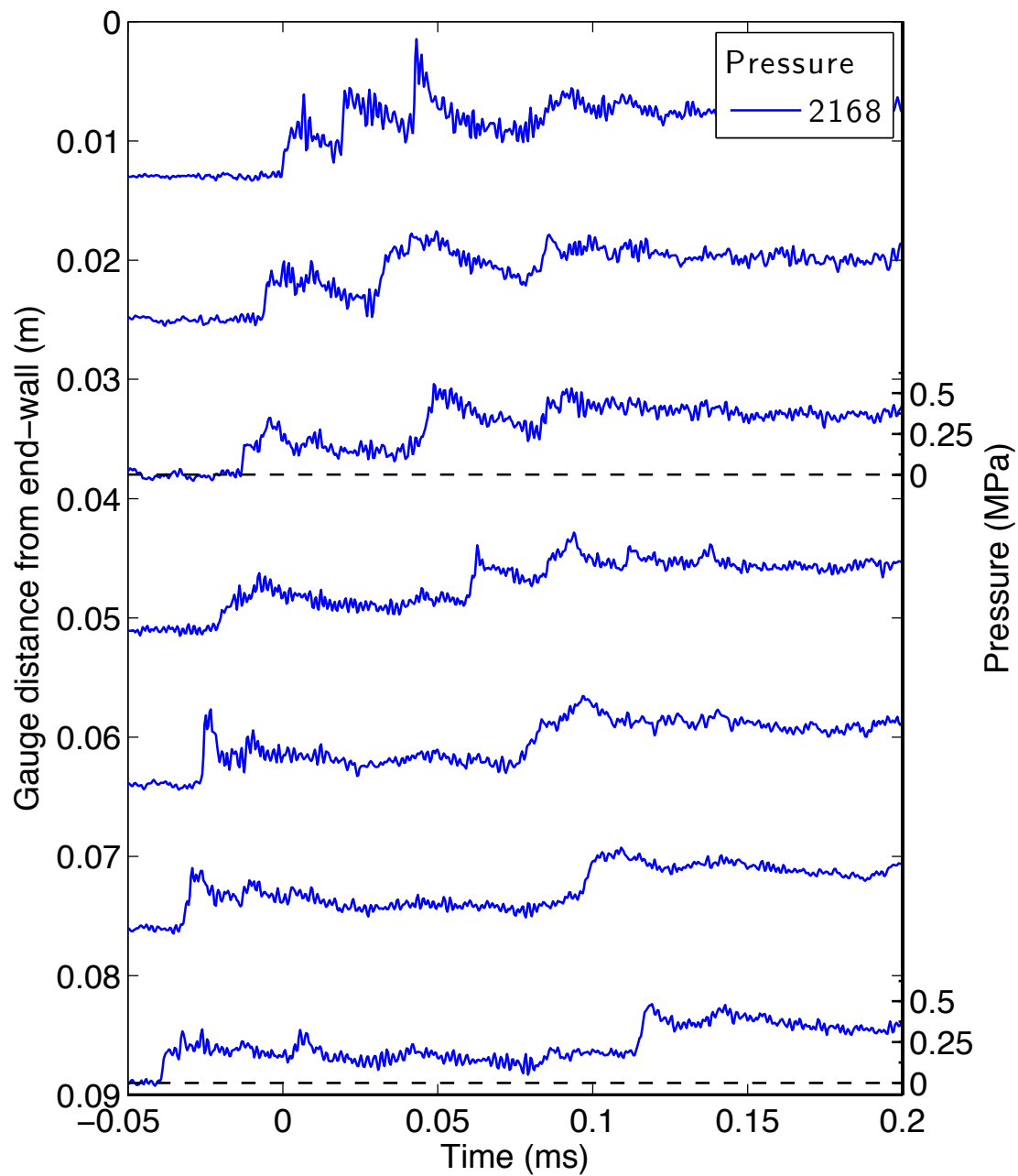


Figure E.139: Pressure traces for a detonation in stoichiometric hydrogen-oxygen with 33% carbon dioxide dilution at fill pressure 10 kPa, part 1.

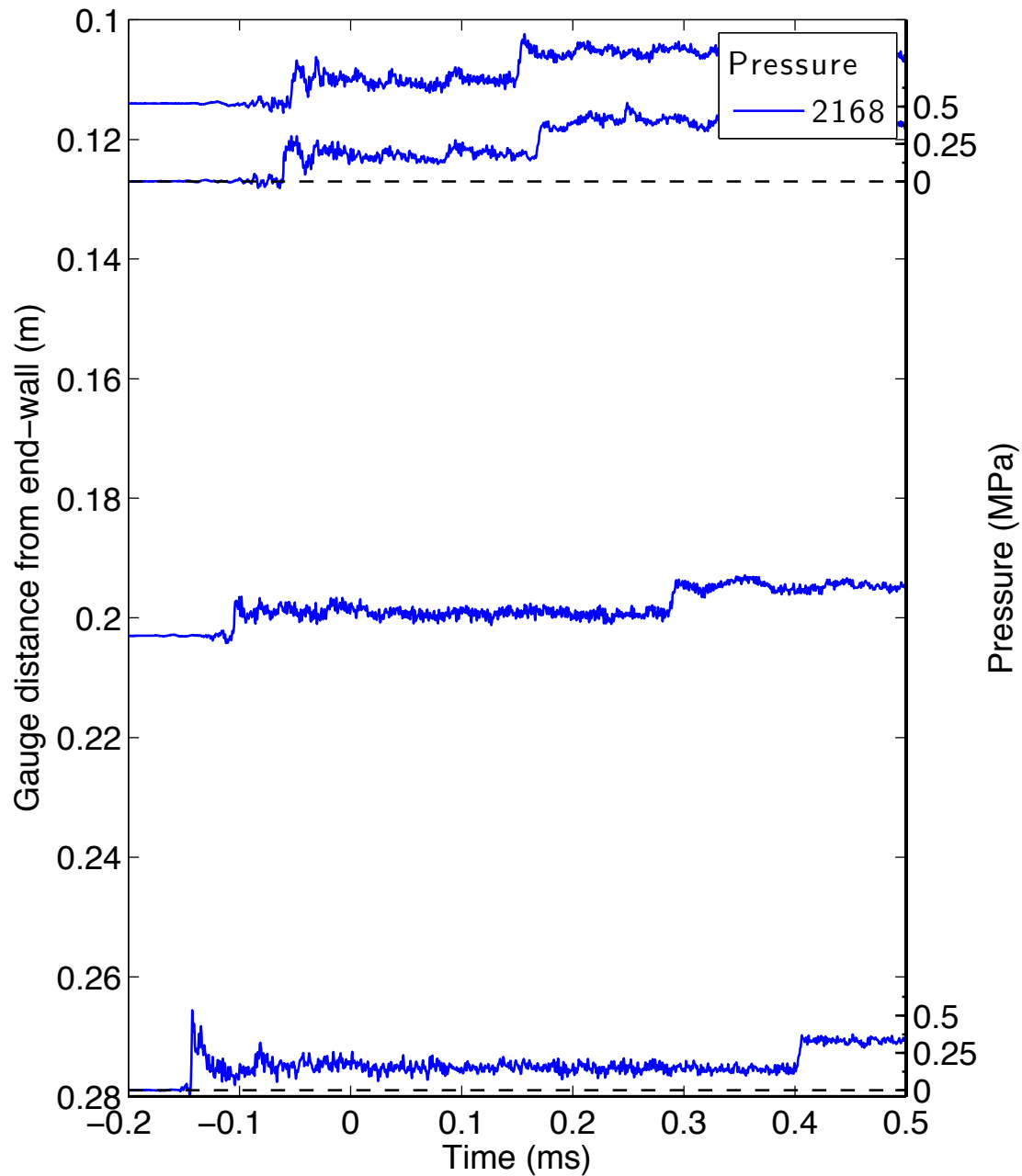


Figure E.140: Pressure traces for a detonation in stoichiometric hydrogen-oxygen with 33% carbon dioxide dilution at fill pressure 10 kPa, part 2.

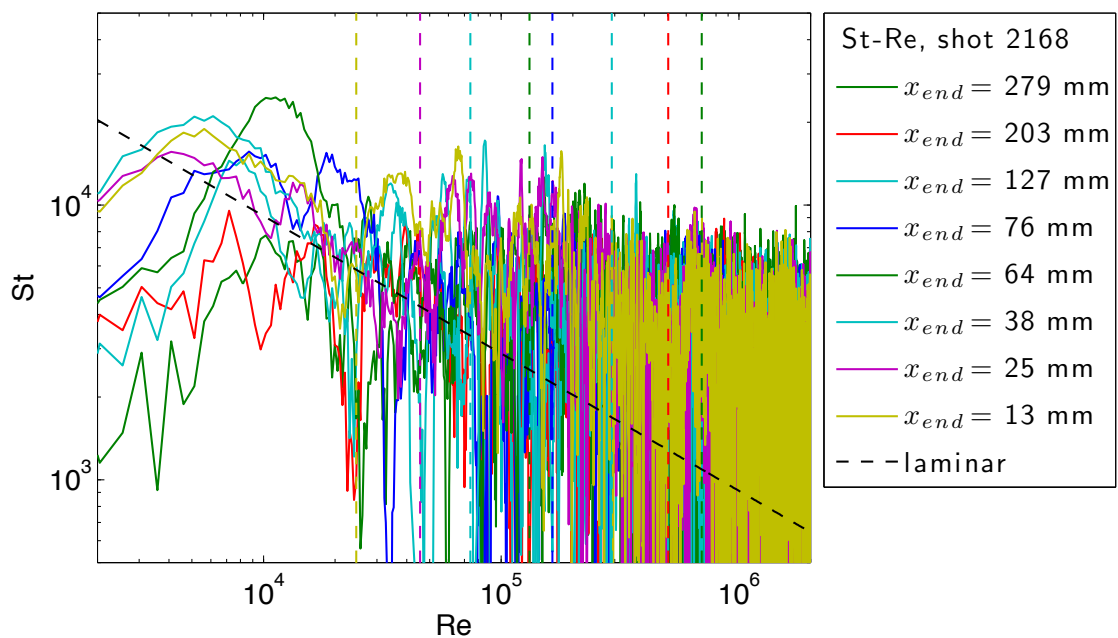


Figure E.141: Stanton-Reynolds number traces from shot 2168, a detonation in stoichiometric hydrogen-oxygen with 33% carbon dioxide dilution at fill pressure 10 kPa. The dashed vertical lines represent the arrival of the reflected shock wave.

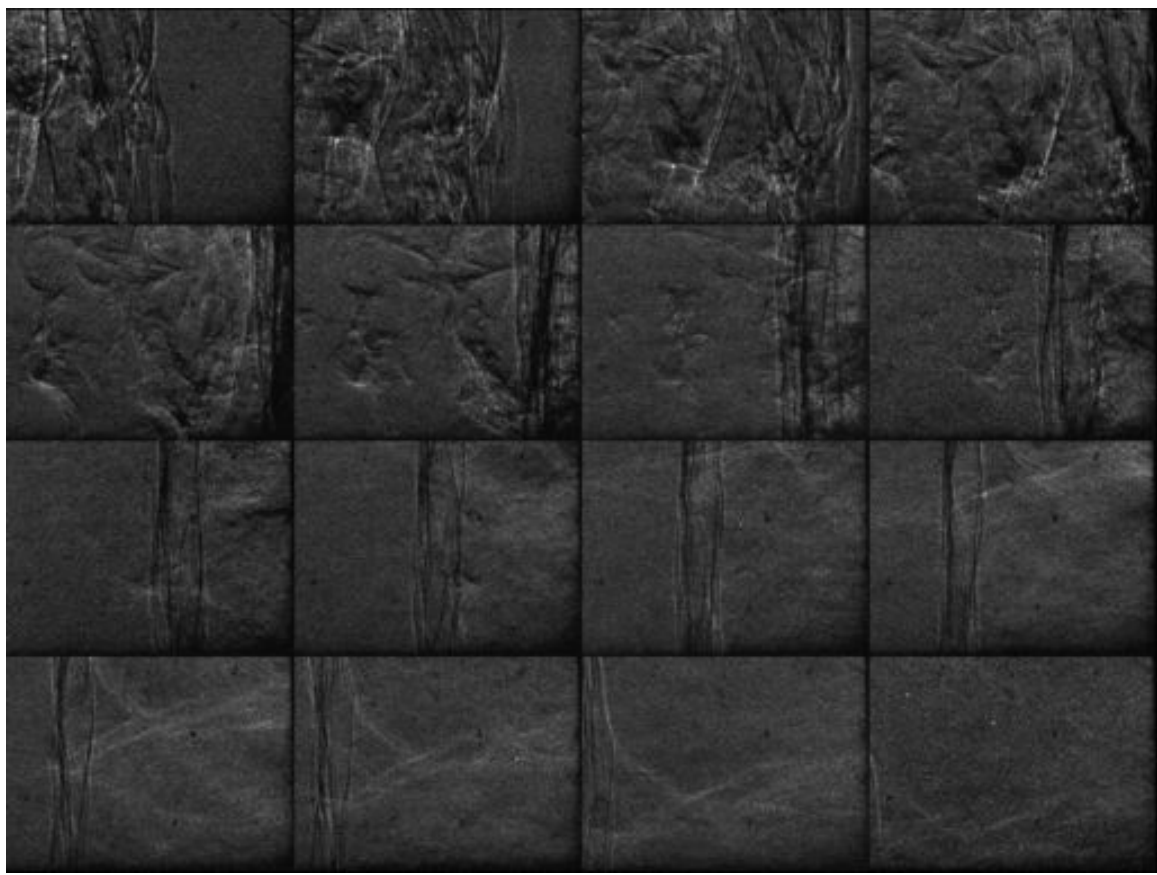


Figure E.142: Unfocused schlieren image of shot 2168. The field of view is approximately 30 mm wide.

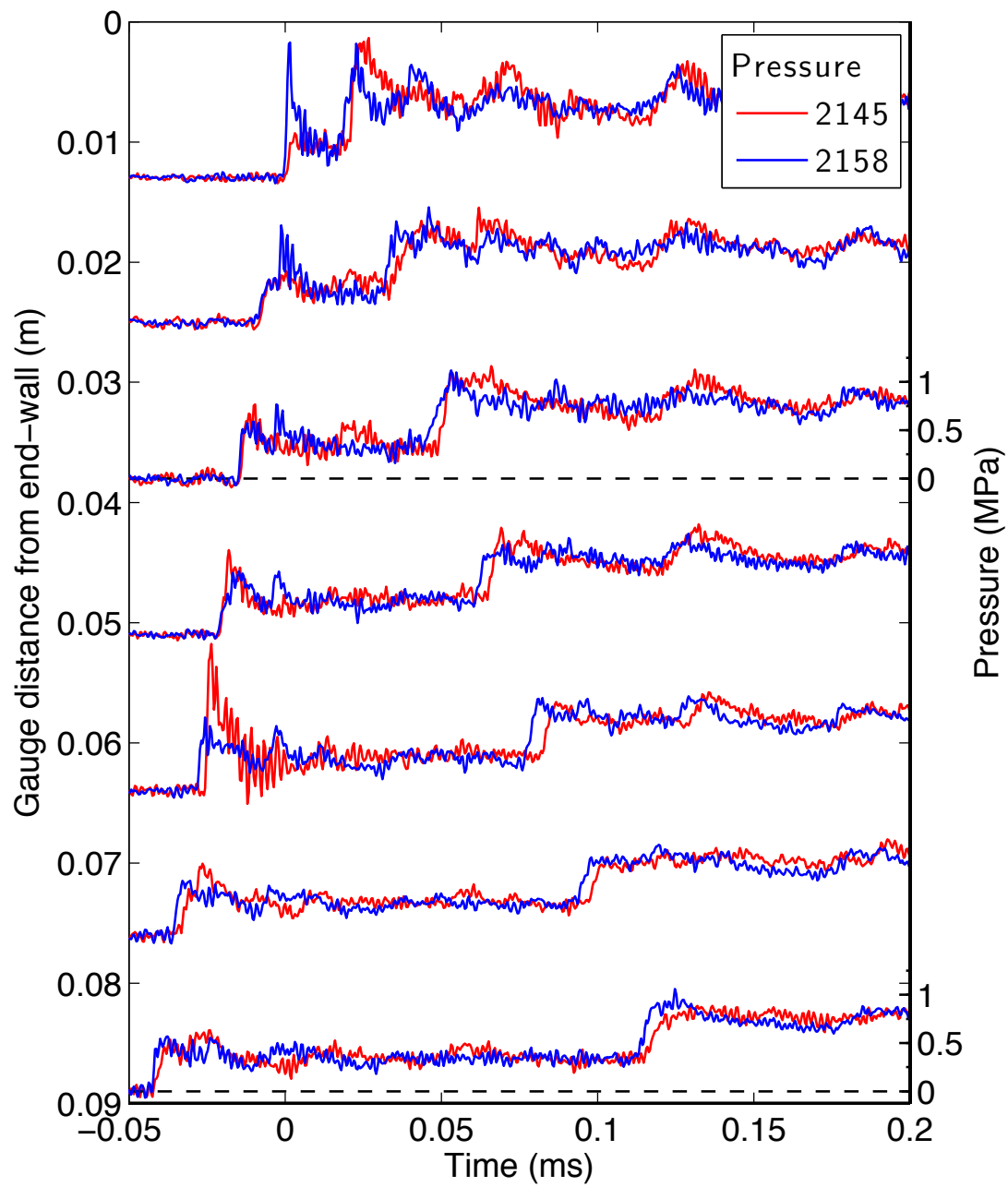


Figure E.143: Pressure traces for a detonation in stoichiometric hydrogen-oxygen with 33% carbon dioxide dilution at fill pressure 25 kPa, part 1.

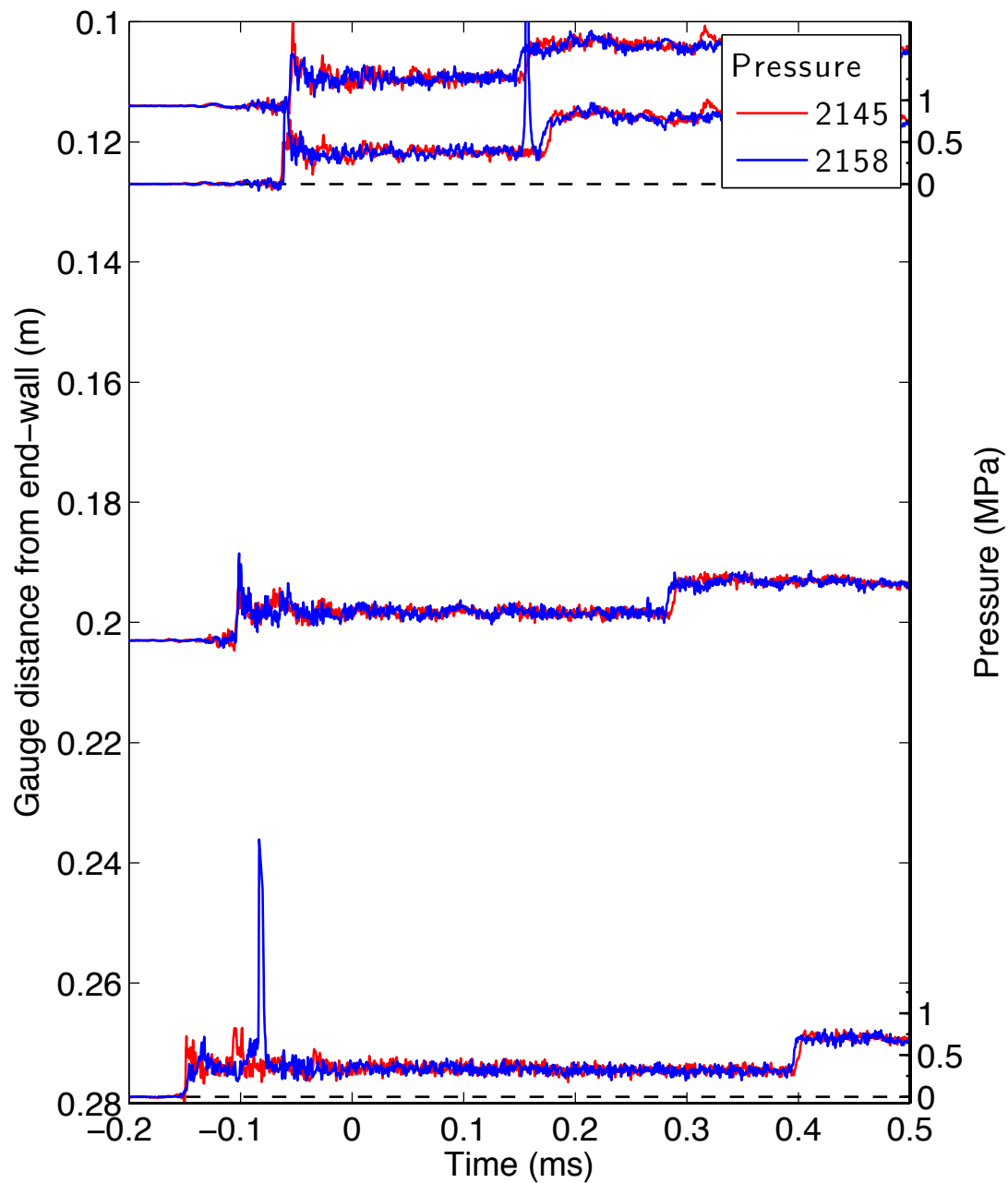


Figure E.144: Pressure traces for a detonation in stoichiometric hydrogen-oxygen with 33% carbon dioxide dilution at fill pressure 25 kPa, part 2.

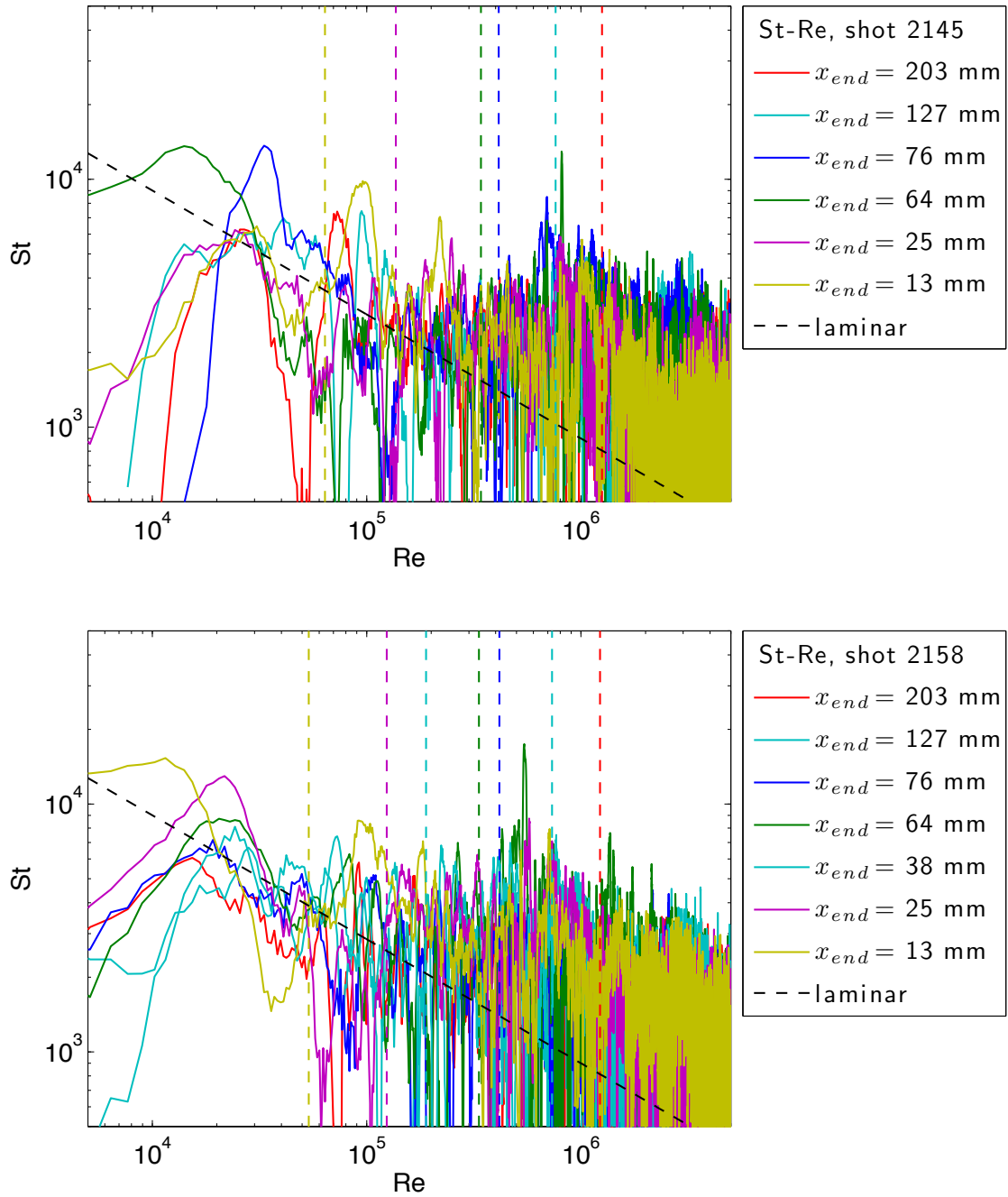


Figure E.145: Stanton-Reynolds number traces from shot 2158, a detonation in stoichiometric hydrogen-oxygen with 33% carbon dioxide dilution at fill pressure 25 kPa. The dashed vertical lines represent the arrival of the reflected shock wave.

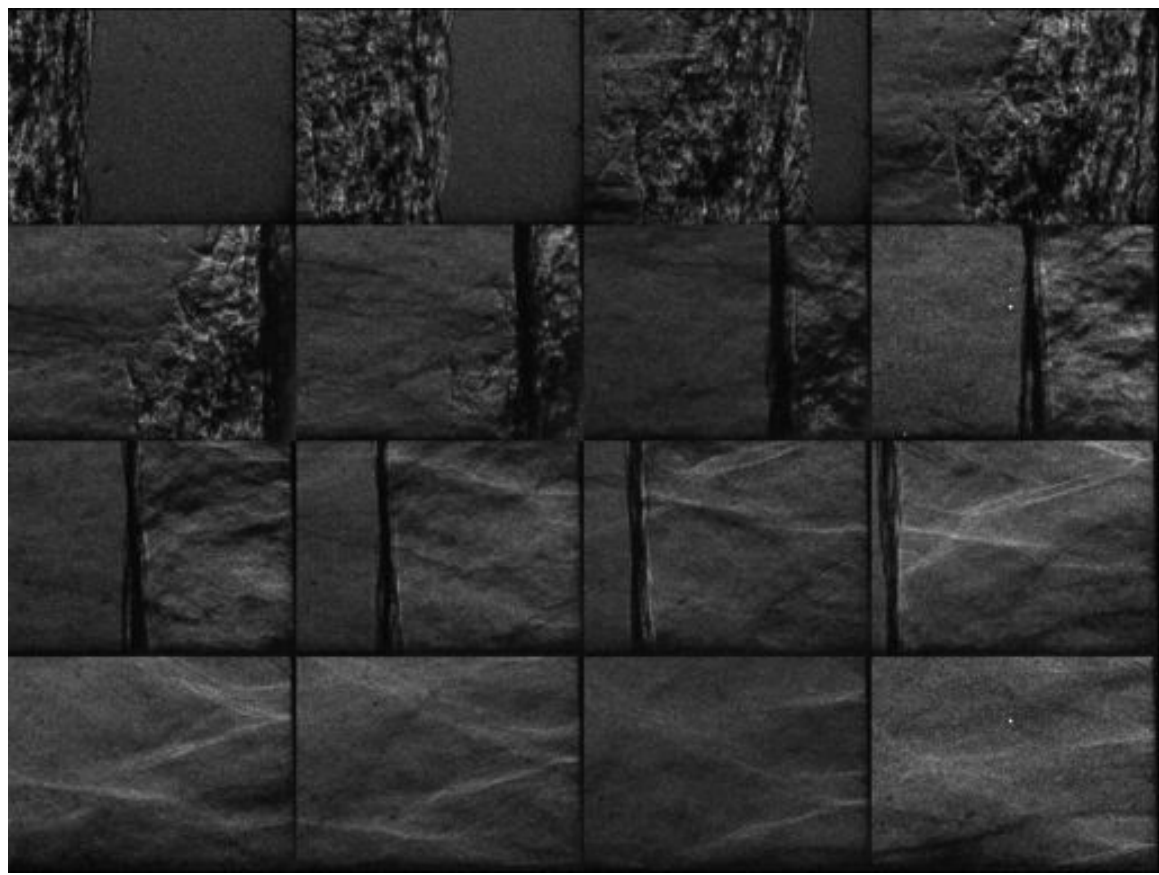


Figure E.146: Unfocused schlieren image of shot 2158. The field of view is approximately 30 mm wide.

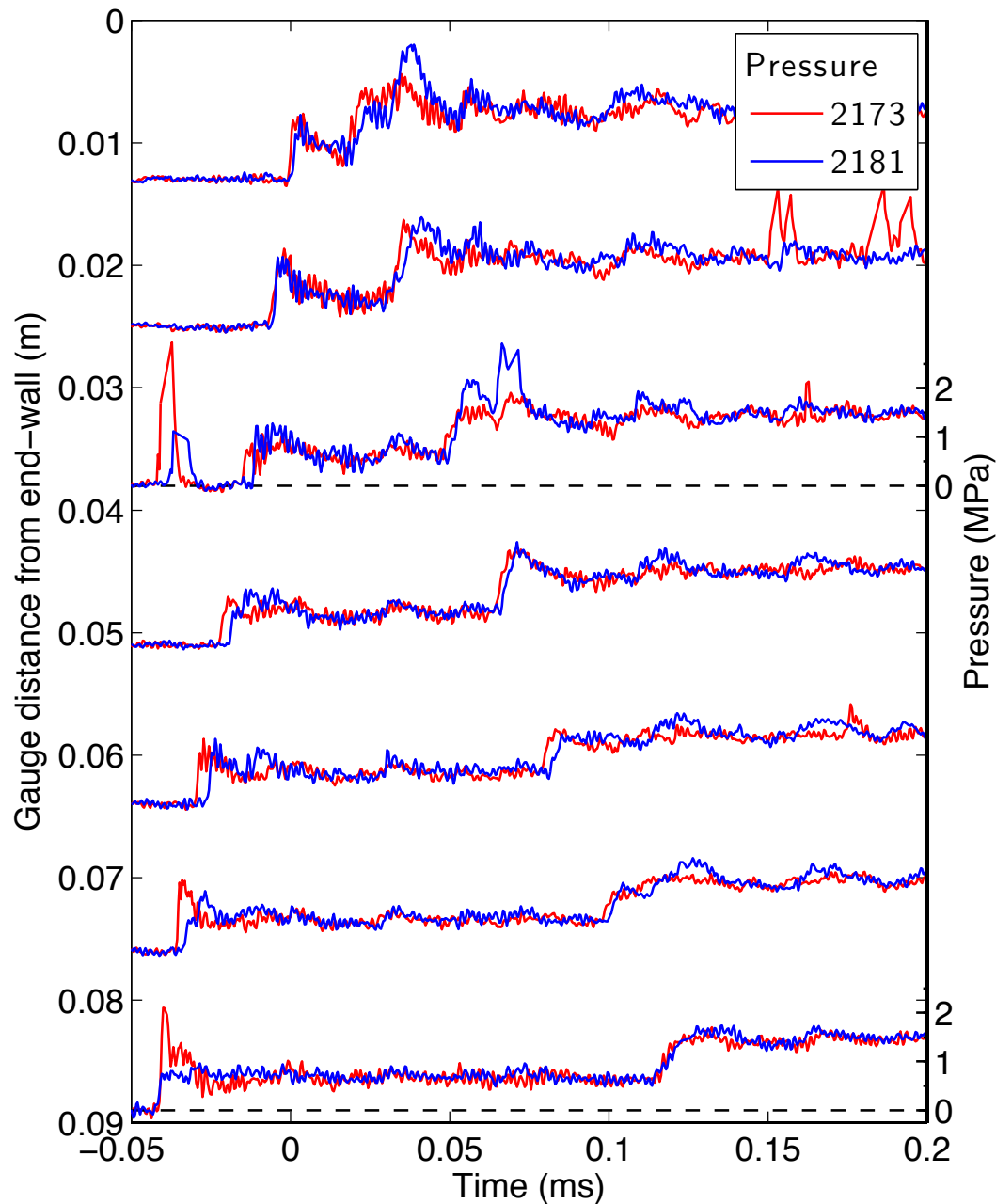


Figure E.147: Pressure traces for a detonation in stoichiometric hydrogen-oxygen with 33% carbon dioxide dilution at fill pressure 50 kPa, part 1.

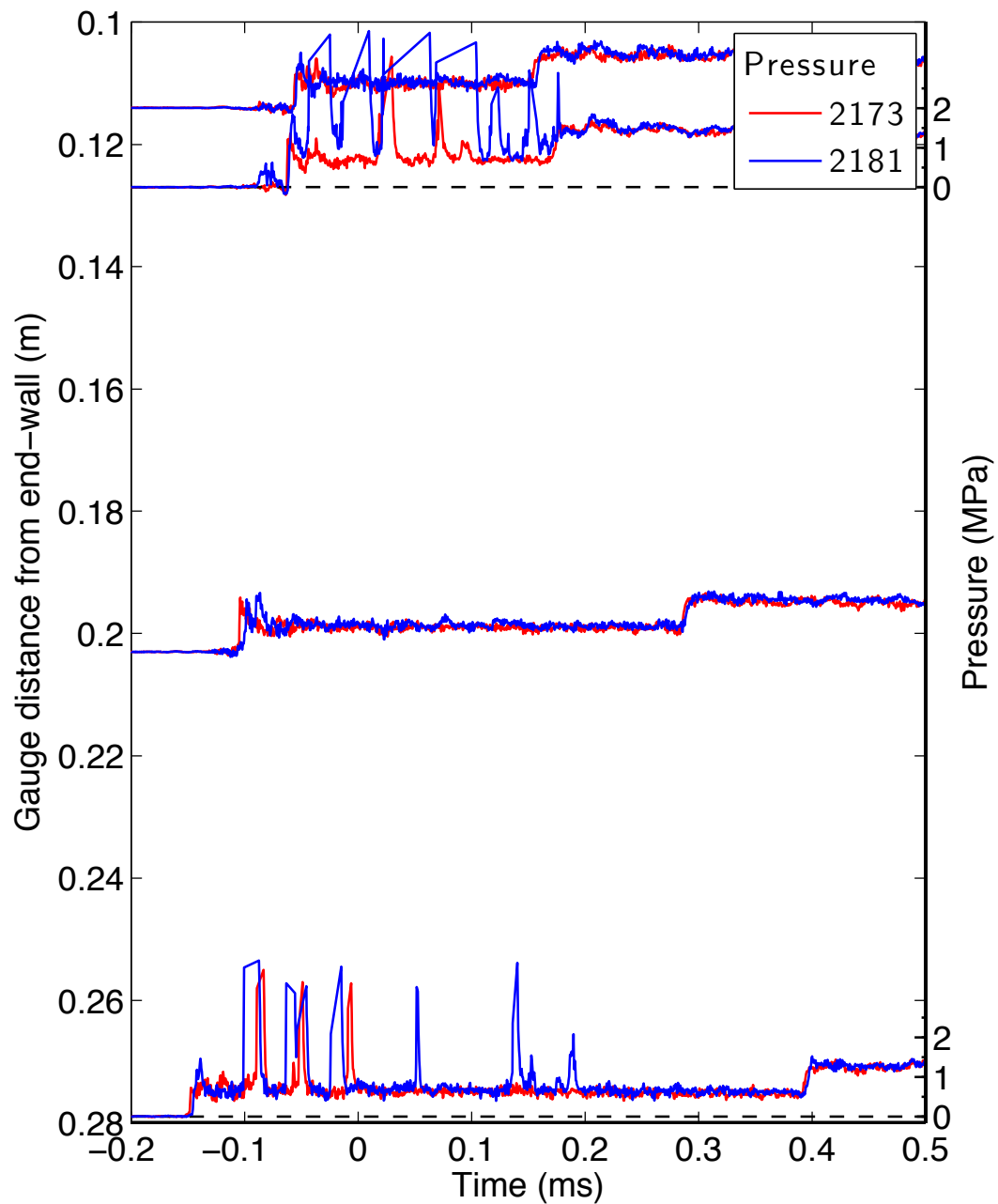


Figure E.148: Pressure traces for a detonation in stoichiometric hydrogen-oxygen with 33% carbon dioxide dilution at fill pressure 50 kPa, part 2.

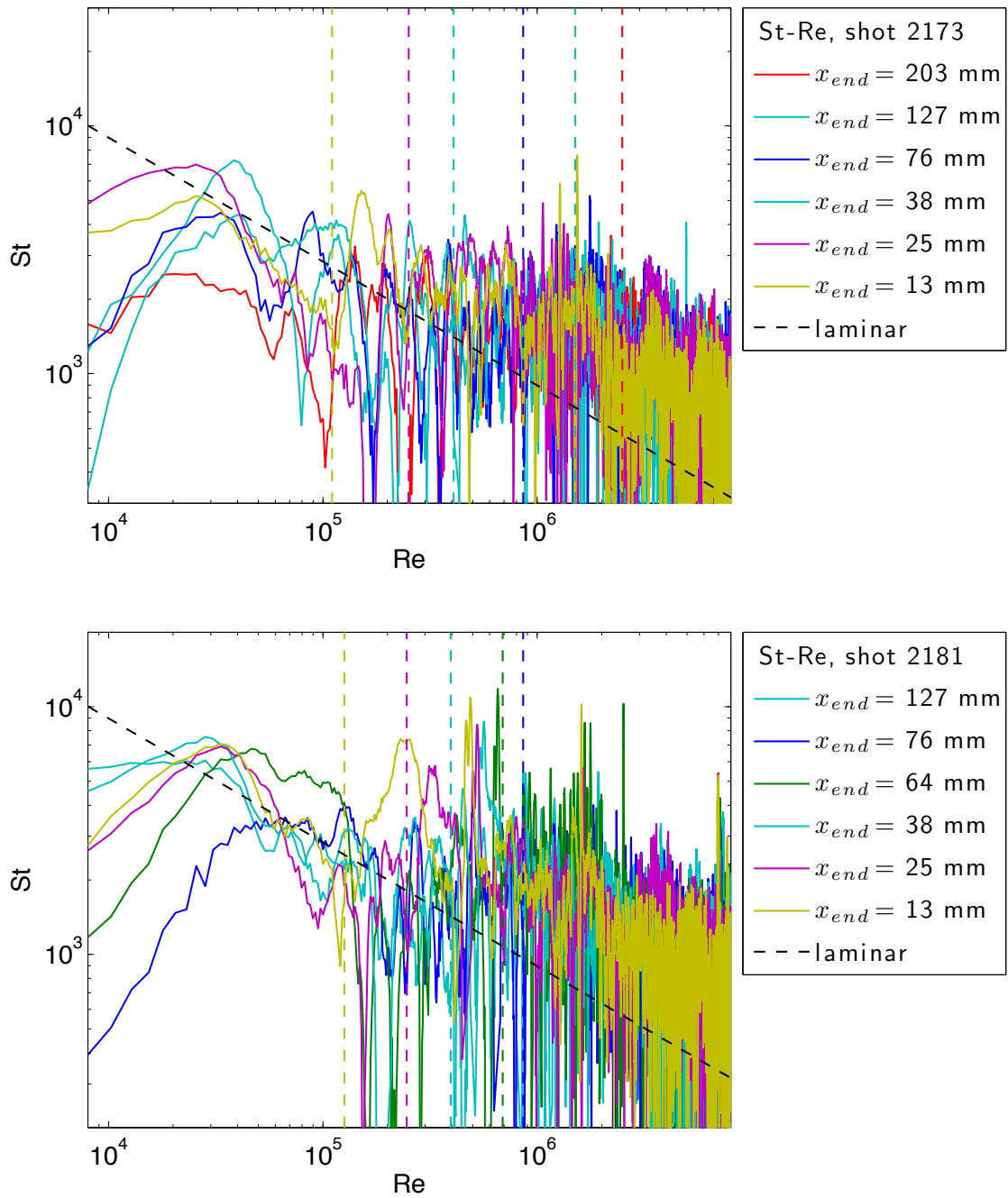


Figure E.149: Stanton-Reynolds number traces from shot 2181, a detonation in stoichiometric hydrogen-oxygen with 33% carbon dioxide dilution at fill pressure 50 kPa. The dashed vertical lines represent the arrival of the reflected shock wave.

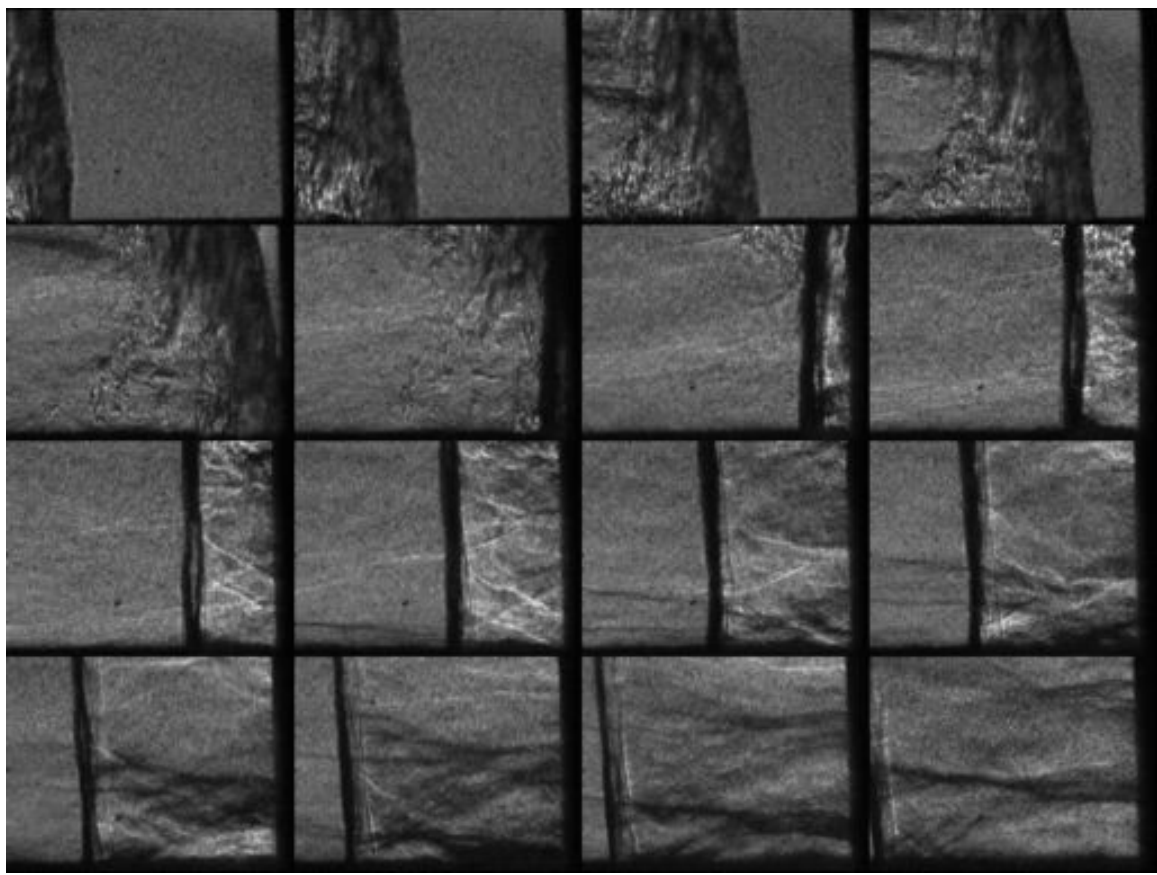


Figure E.150: Unfocused schlieren image of shot 2181. The field of view is approximately 30 mm wide.

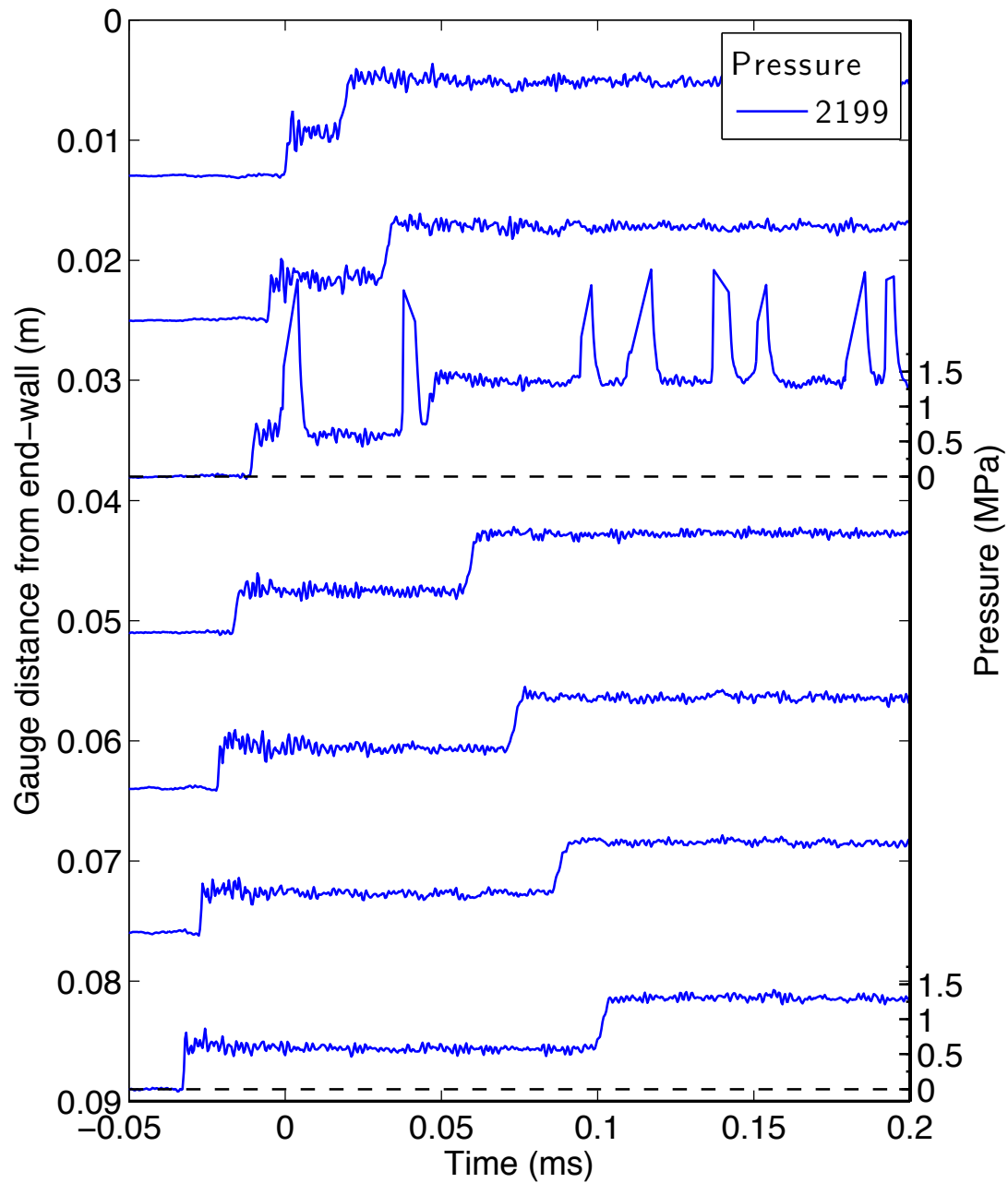


Figure E.151: Pressure traces for a detonation in stoichiometric hydrogen-nitrous oxide at fill pressure 25 kPa, part 1.

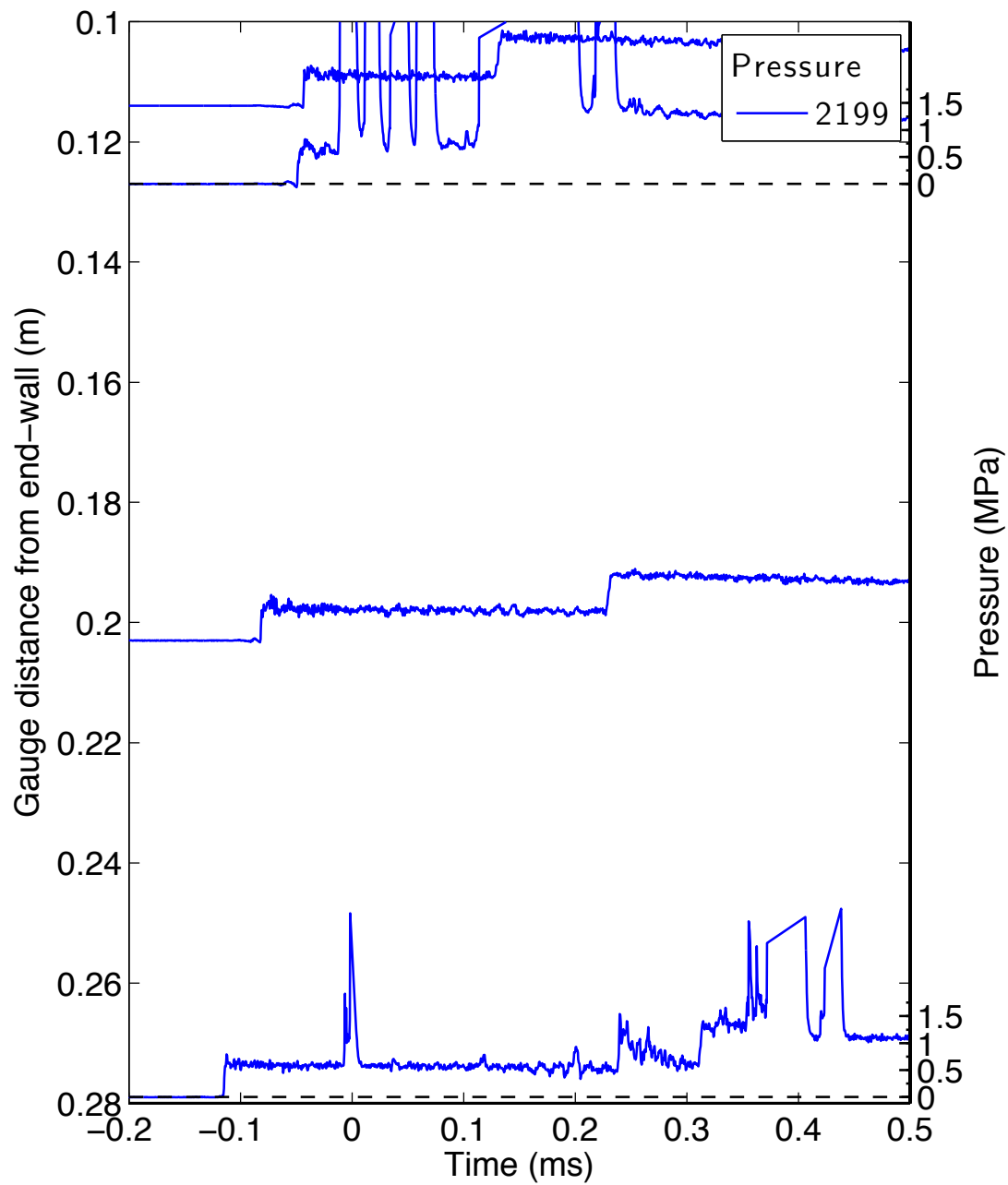


Figure E.152: Pressure traces for a detonation in stoichiometric hydrogen-nitrous oxide at fill pressure 25 kPa, part 2.

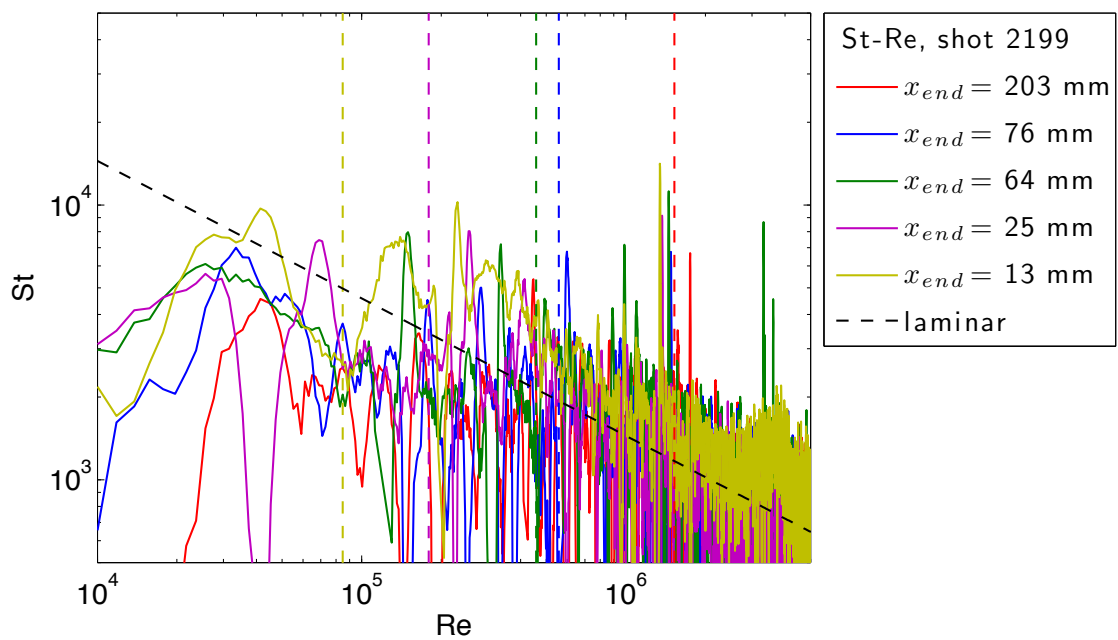


Figure E.153: Stanton-Reynolds number traces from shot 2199, a detonation in stoichiometric hydrogen-nitrous oxide at fill pressure 25 kPa. The dashed vertical lines represent the arrival of the reflected shock wave.

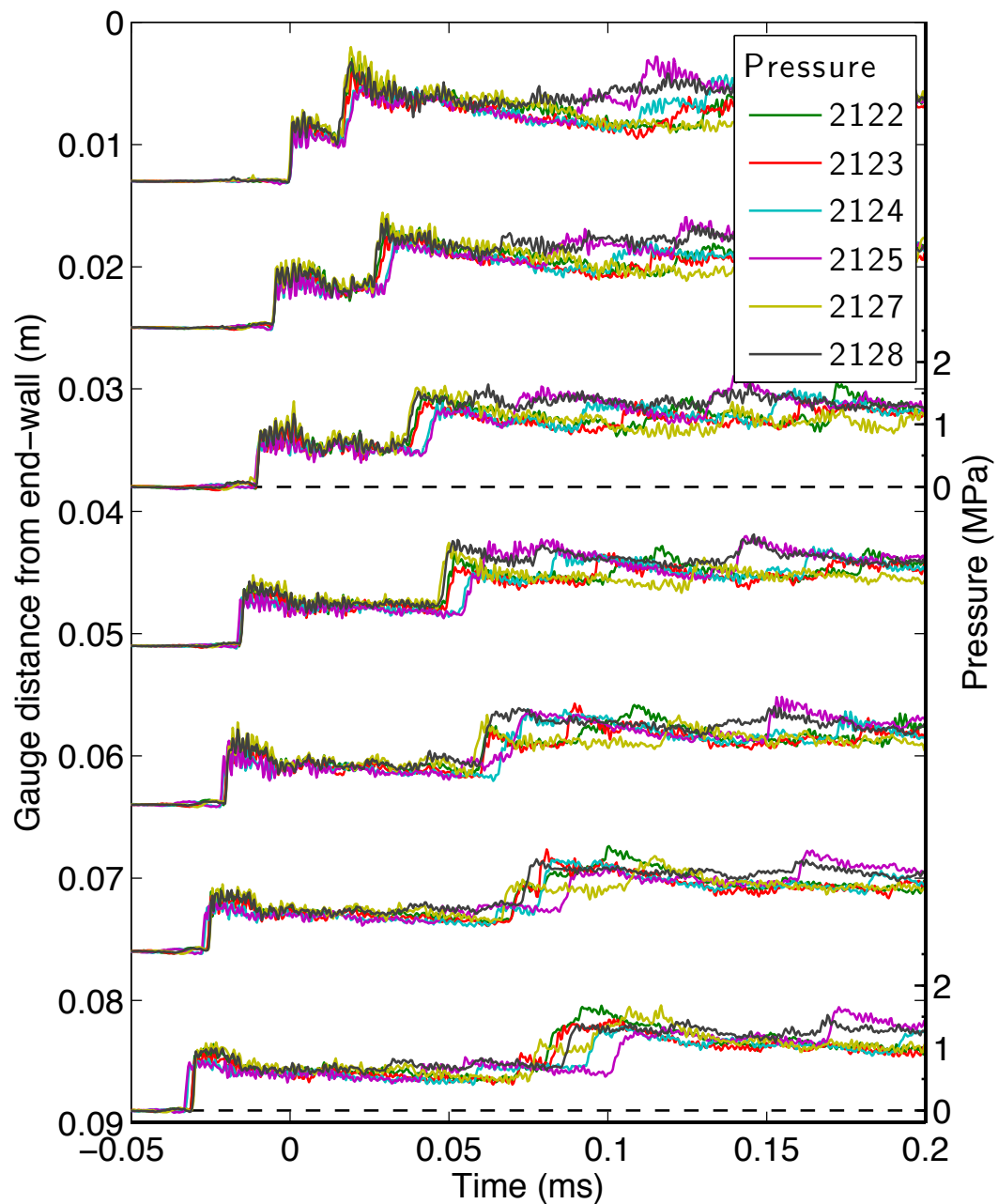


Figure E.154: Pressure traces for a detonation in stoichiometric ethylene-oxygen at fill pressure 25 kPa, part 1.

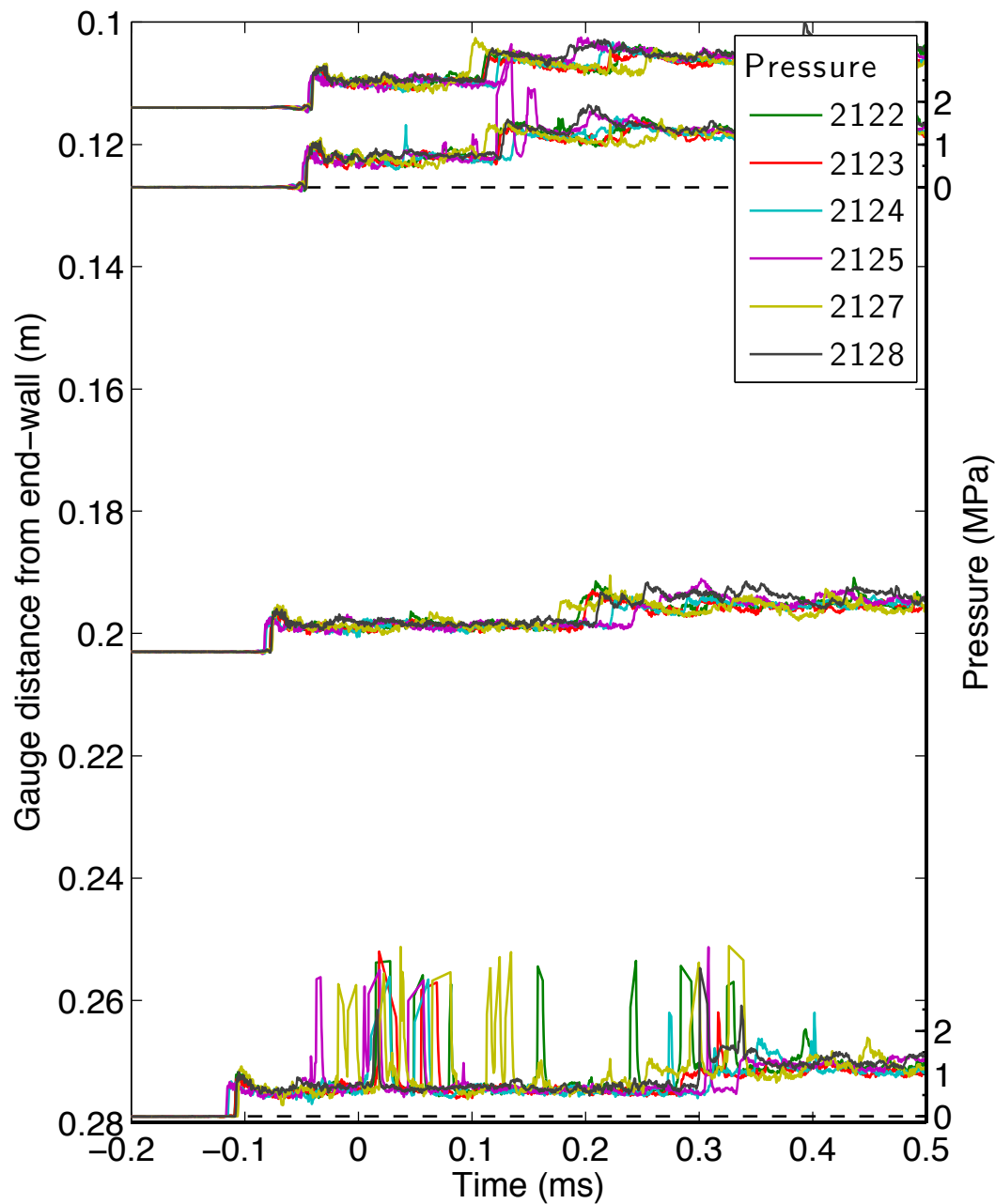


Figure E.155: Pressure traces for a detonation in stoichiometric ethylene-oxygen at fill pressure 25 kPa, part 2.

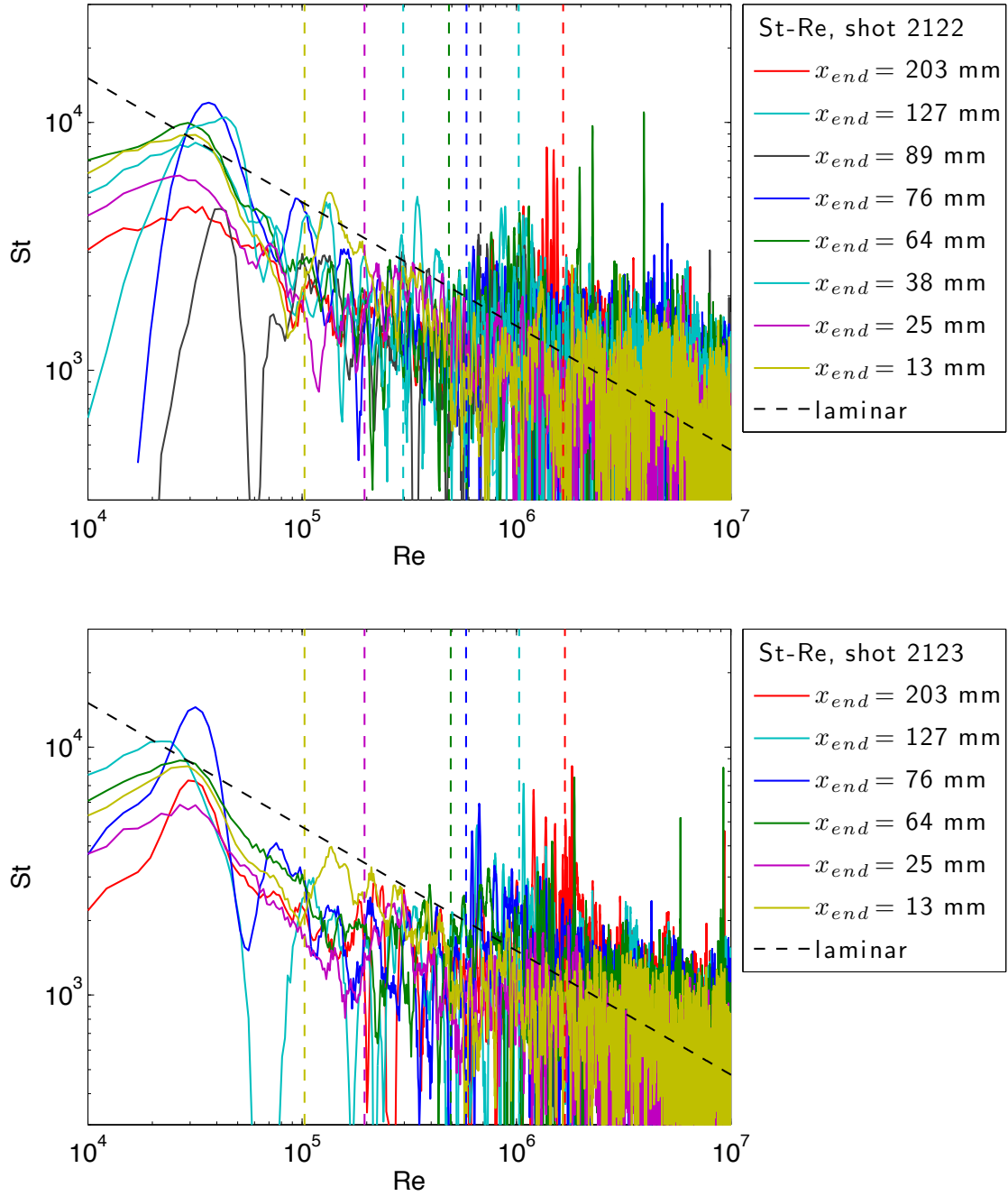


Figure E.156: Stanton-Reynolds number traces from shot 2123, a detonation in stoichiometric ethylene-oxygen at fill pressure 25 kPa. The dashed vertical lines represent the arrival of the reflected shock wave.

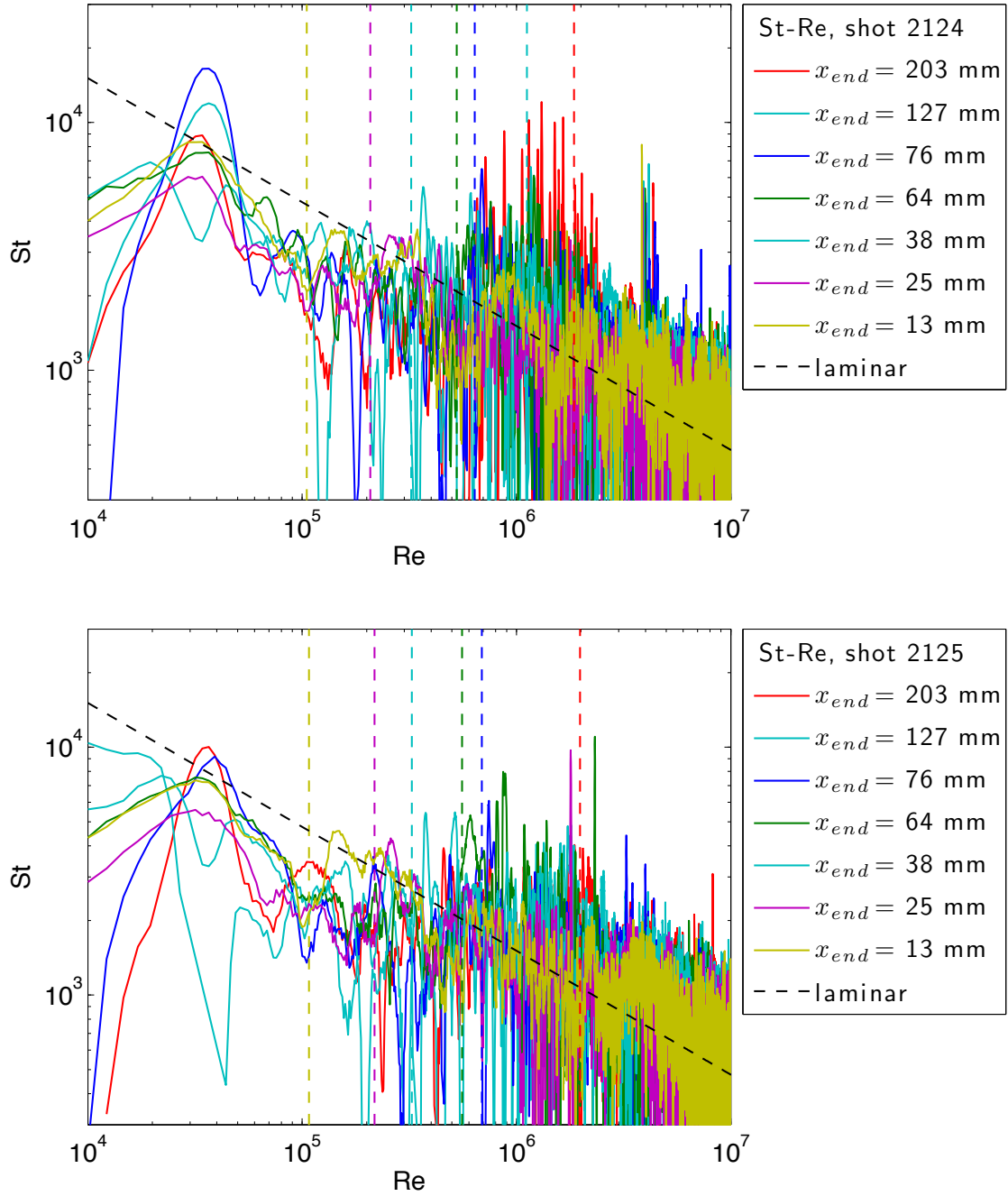


Figure E.157: Stanton-Reynolds number traces from shot 2125, a detonation in stoichiometric ethylene-oxygen at fill pressure 25 kPa. The dashed vertical lines represent the arrival of the reflected shock wave.

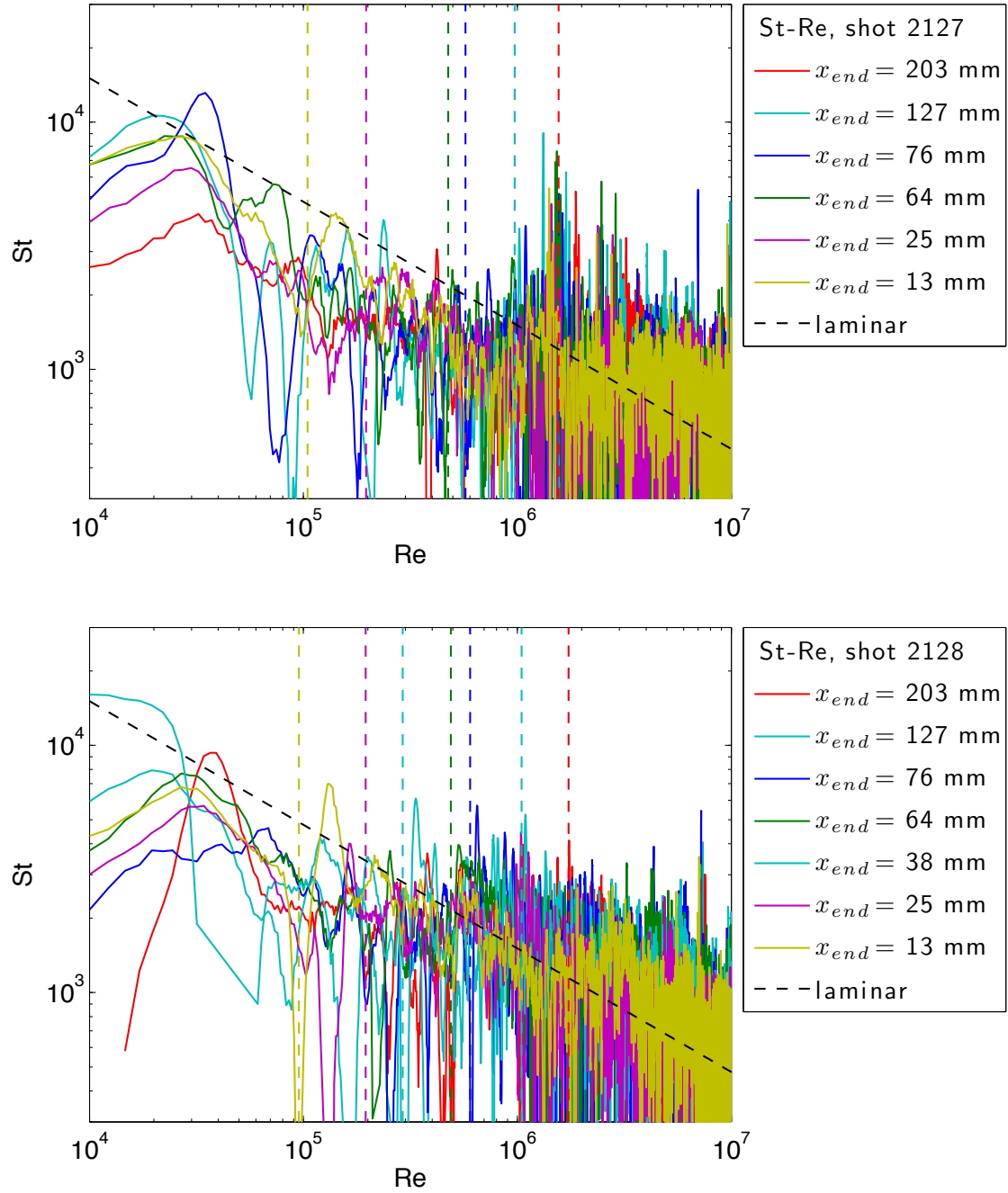


Figure E.158: Stanton-Reynolds number traces from shot 2128, a detonation in stoichiometric ethylene-oxygen at fill pressure 25 kPa. The dashed vertical lines represent the arrival of the reflected shock wave.

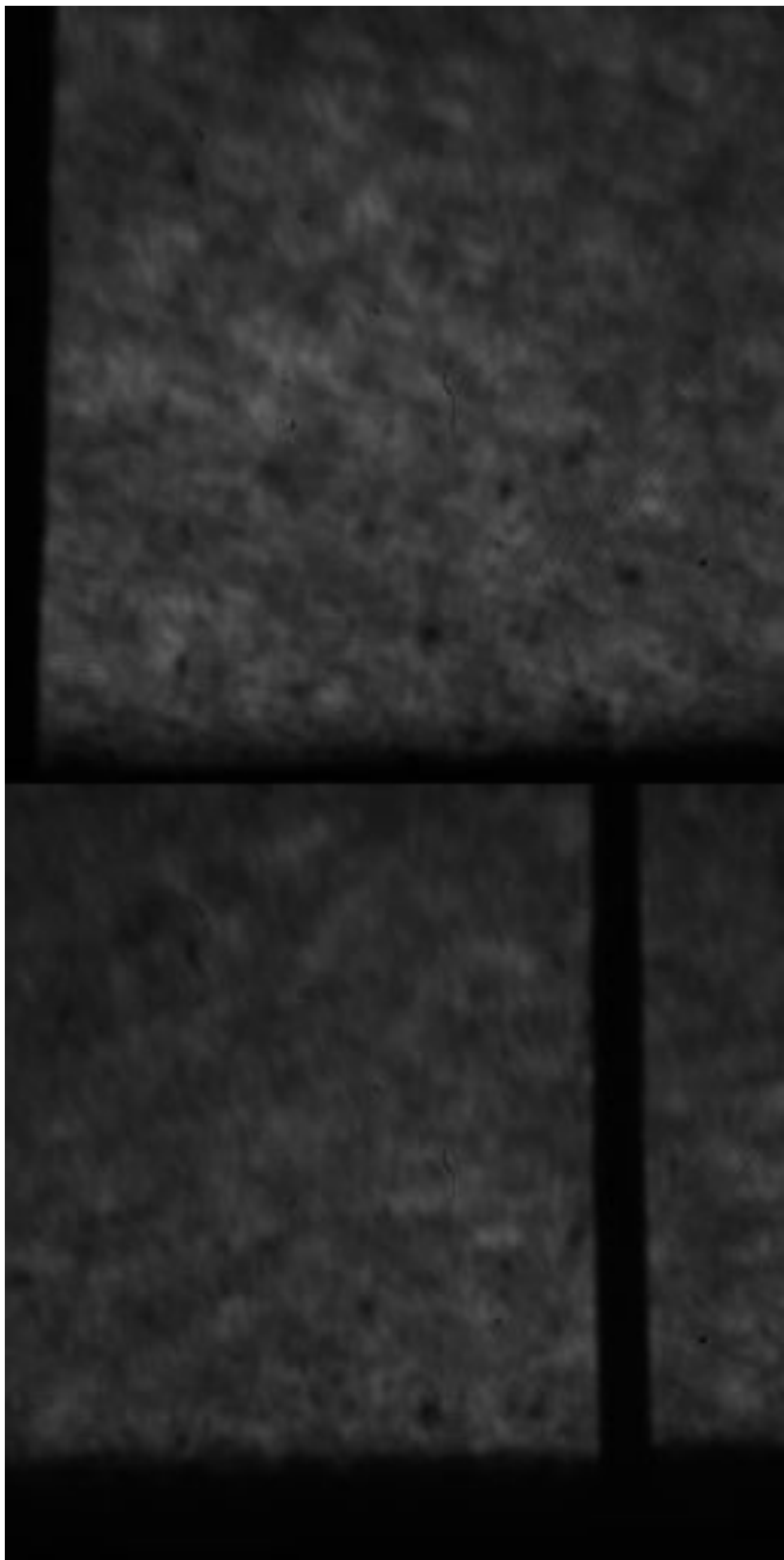


Figure E.159: Focused schlieren image of shot 2125. The field of view is approximately 14 mm wide.

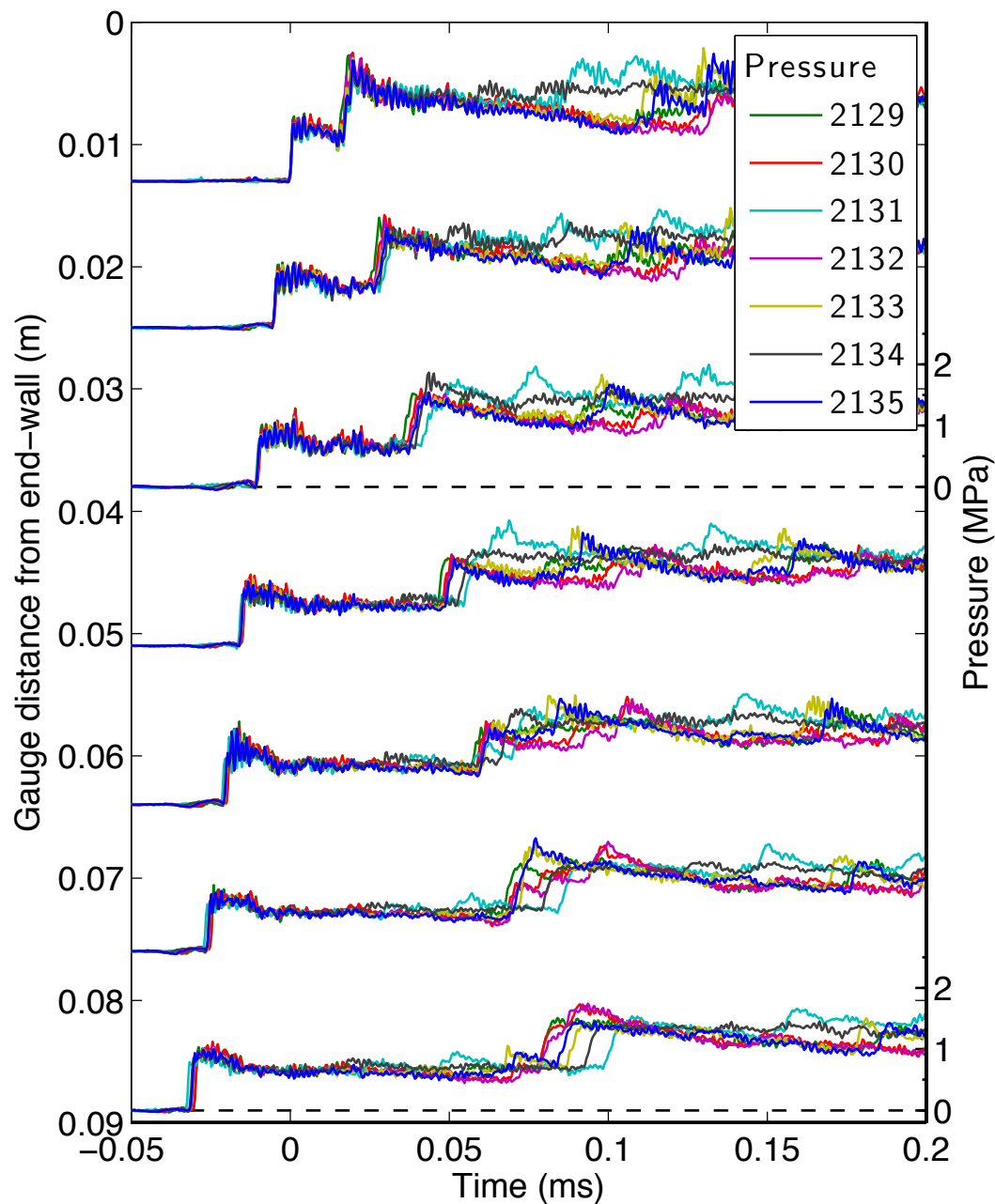


Figure E.160: Pressure traces for a detonation in stoichiometric ethylene-oxygen at fill pressure 25 kPa, part 3.

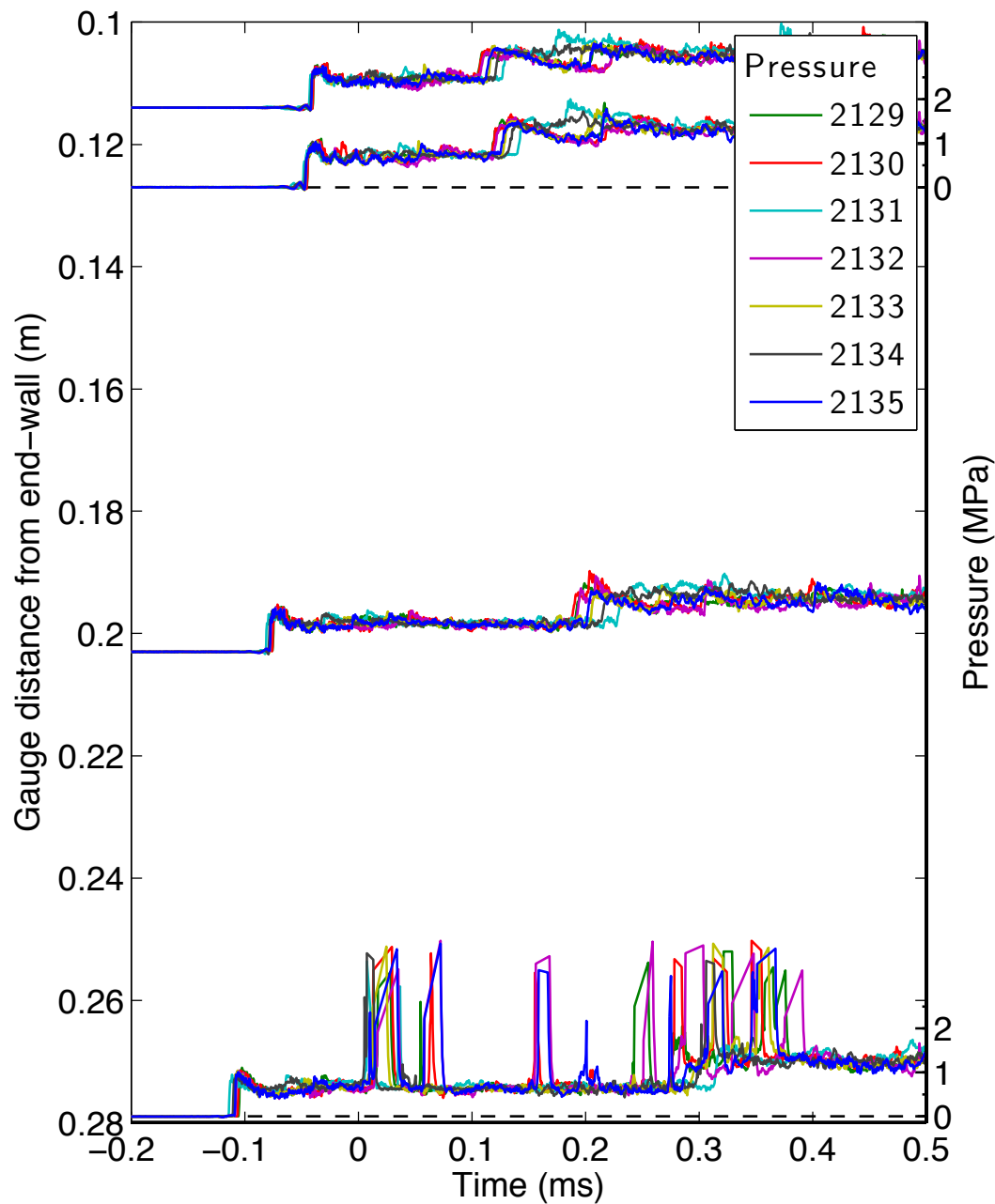


Figure E.161: Pressure traces for a detonation in stoichiometric ethylene-oxygen at fill pressure 25 kPa, part 4.

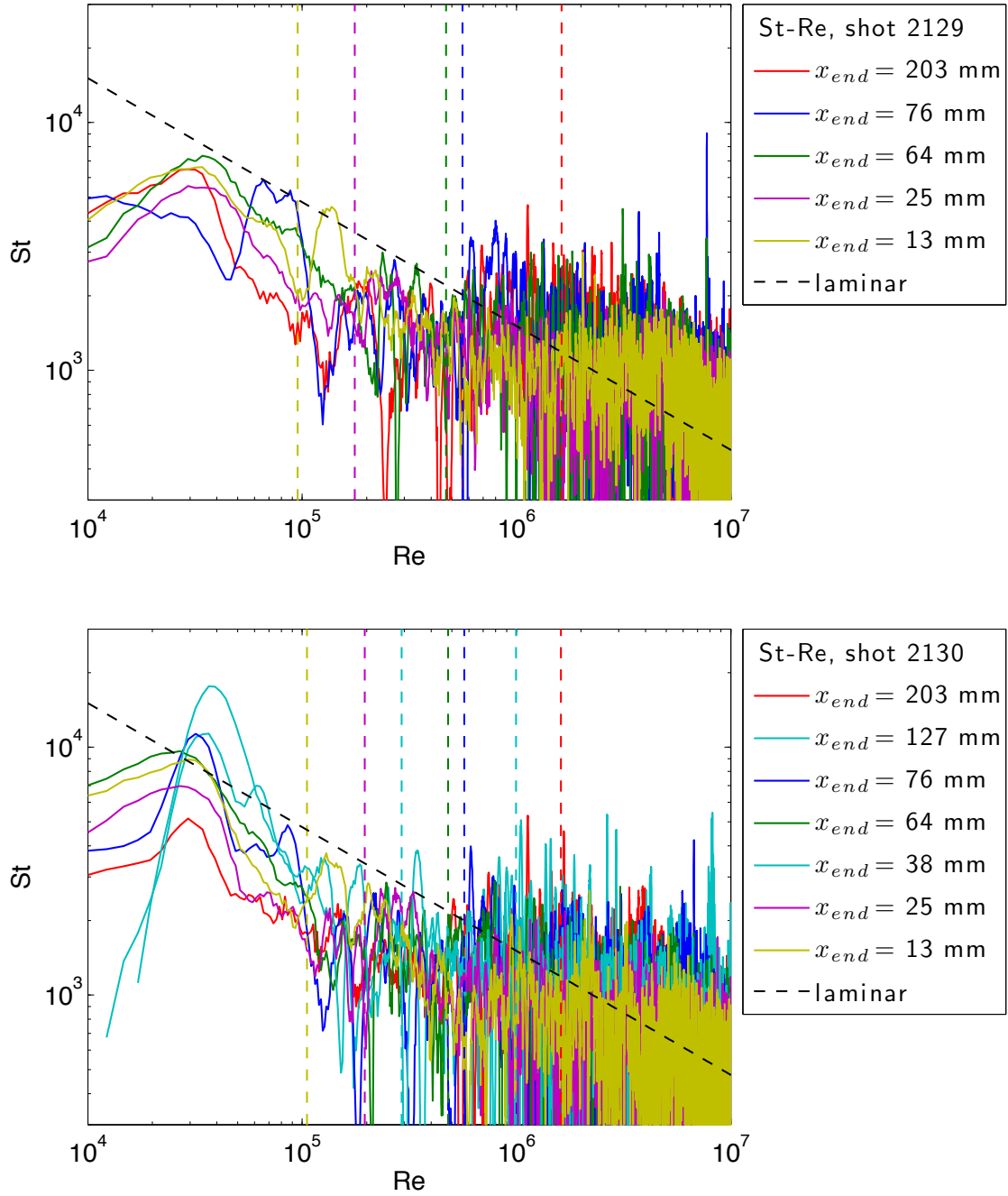


Figure E.162: Stanton-Reynolds number traces from shot 2130, a detonation in stoichiometric ethylene-oxygen at fill pressure 25 kPa. The dashed vertical lines represent the arrival of the reflected shock wave.

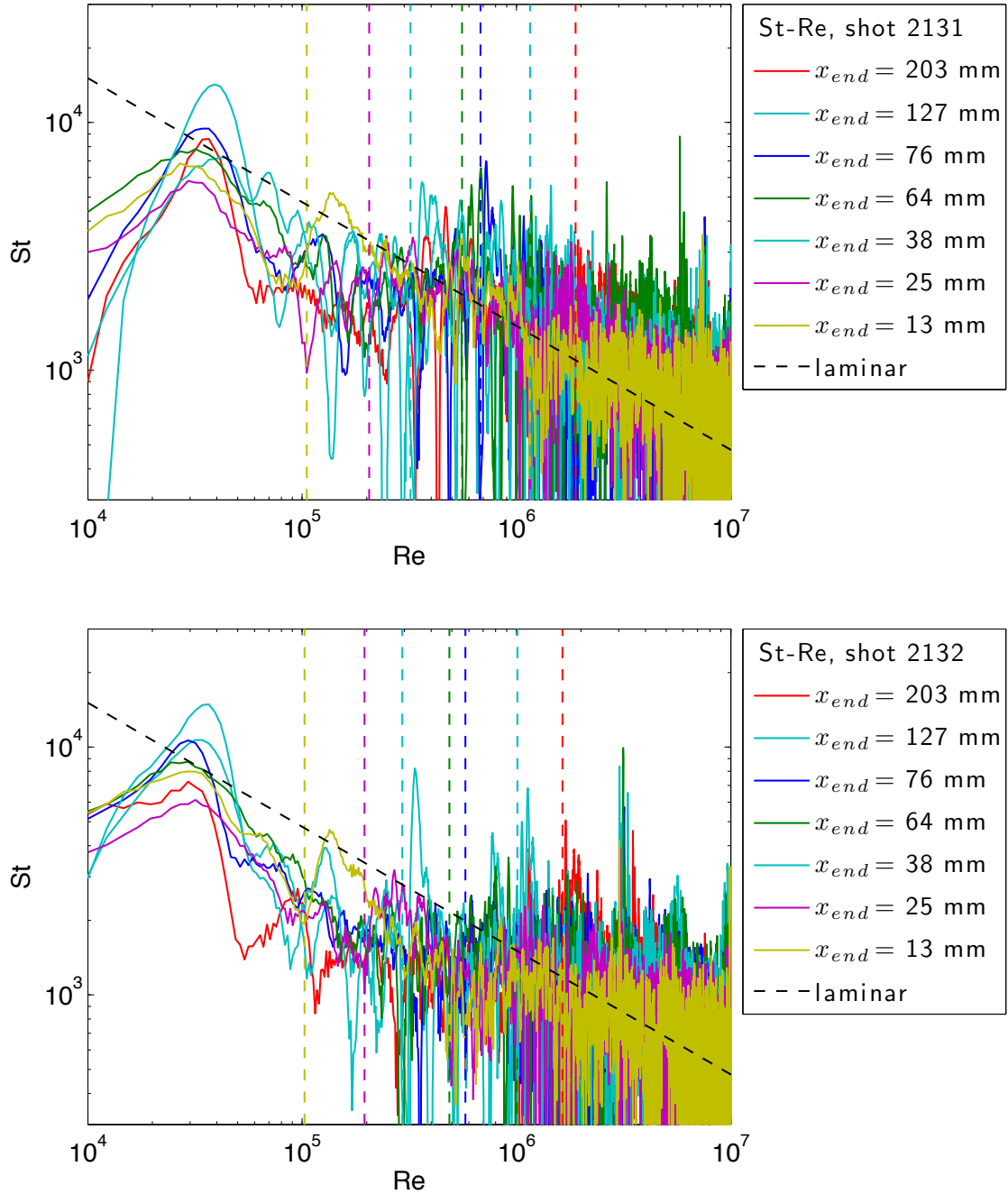


Figure E.163: Stanton-Reynolds number traces from shot 2132, a detonation in stoichiometric ethylene-oxygen at fill pressure 25 kPa. The dashed vertical lines represent the arrival of the reflected shock wave.

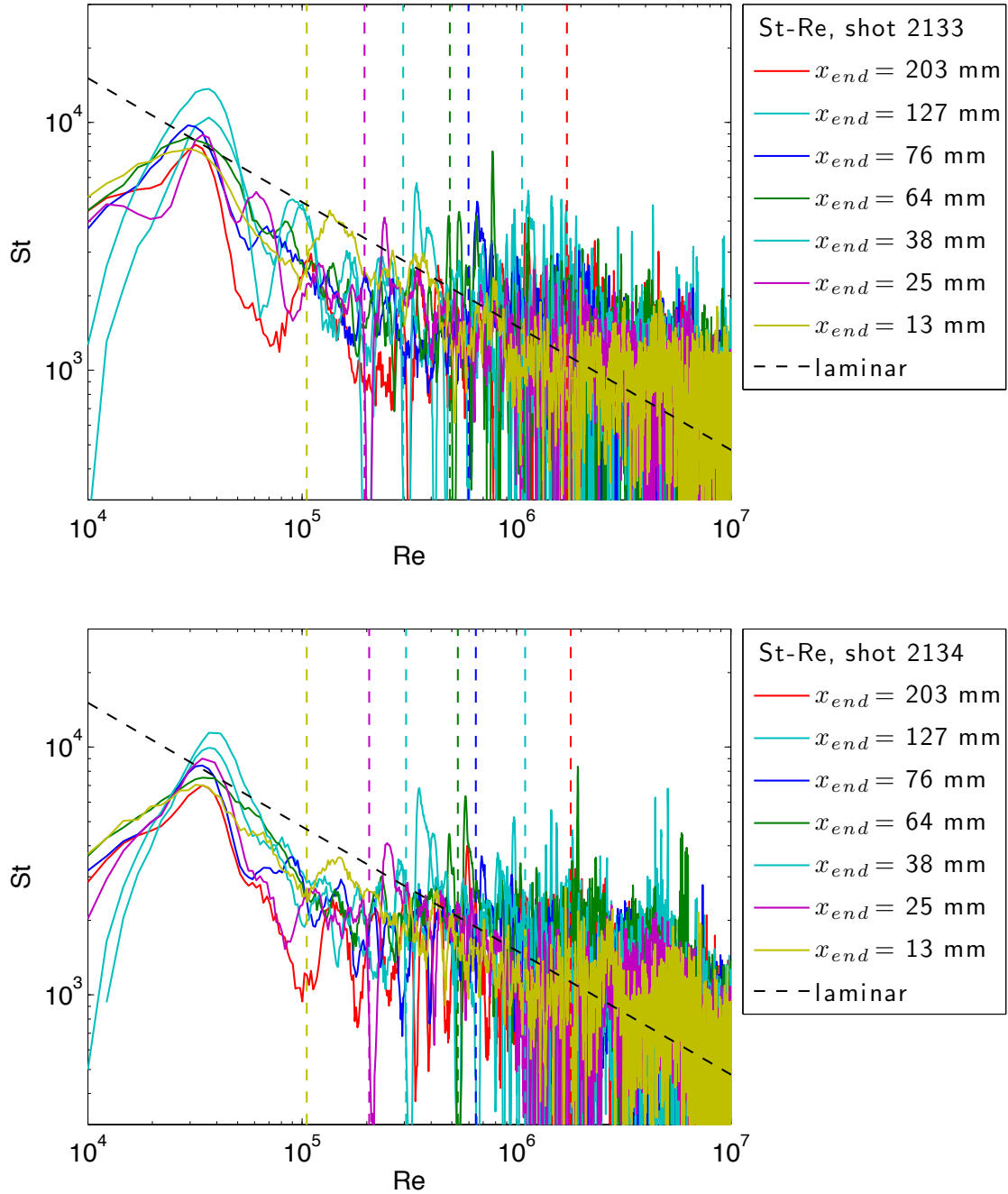


Figure E.164: Stanton-Reynolds number traces from shot 2134, a detonation in stoichiometric ethylene-oxygen at fill pressure 25 kPa. The dashed vertical lines represent the arrival of the reflected shock wave.

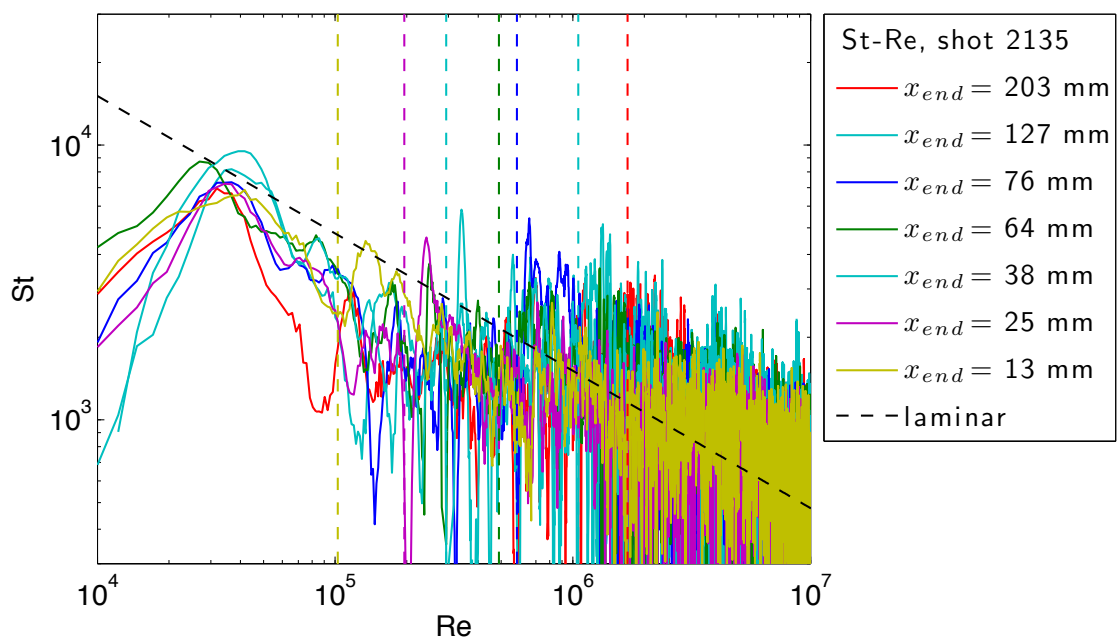


Figure E.165: Stanton-Reynolds number traces from shot 2135, a detonation in stoichiometric ethylene-oxygen at fill pressure 25 kPa. The dashed vertical lines represent the arrival of the reflected shock wave.

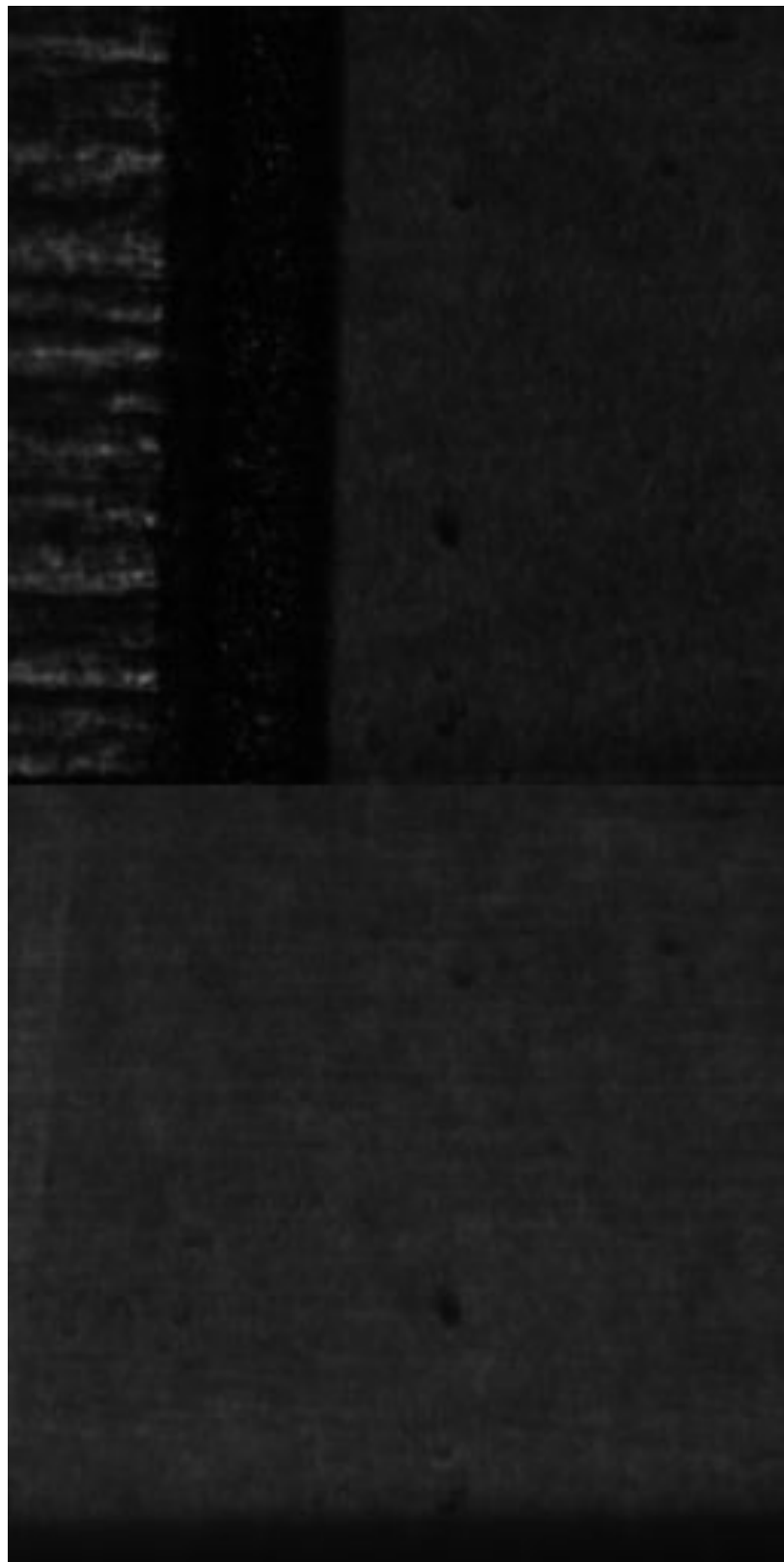


Figure E.166: Focused schlieren image of shot 2134. The field of view is approximately 14 mm wide.

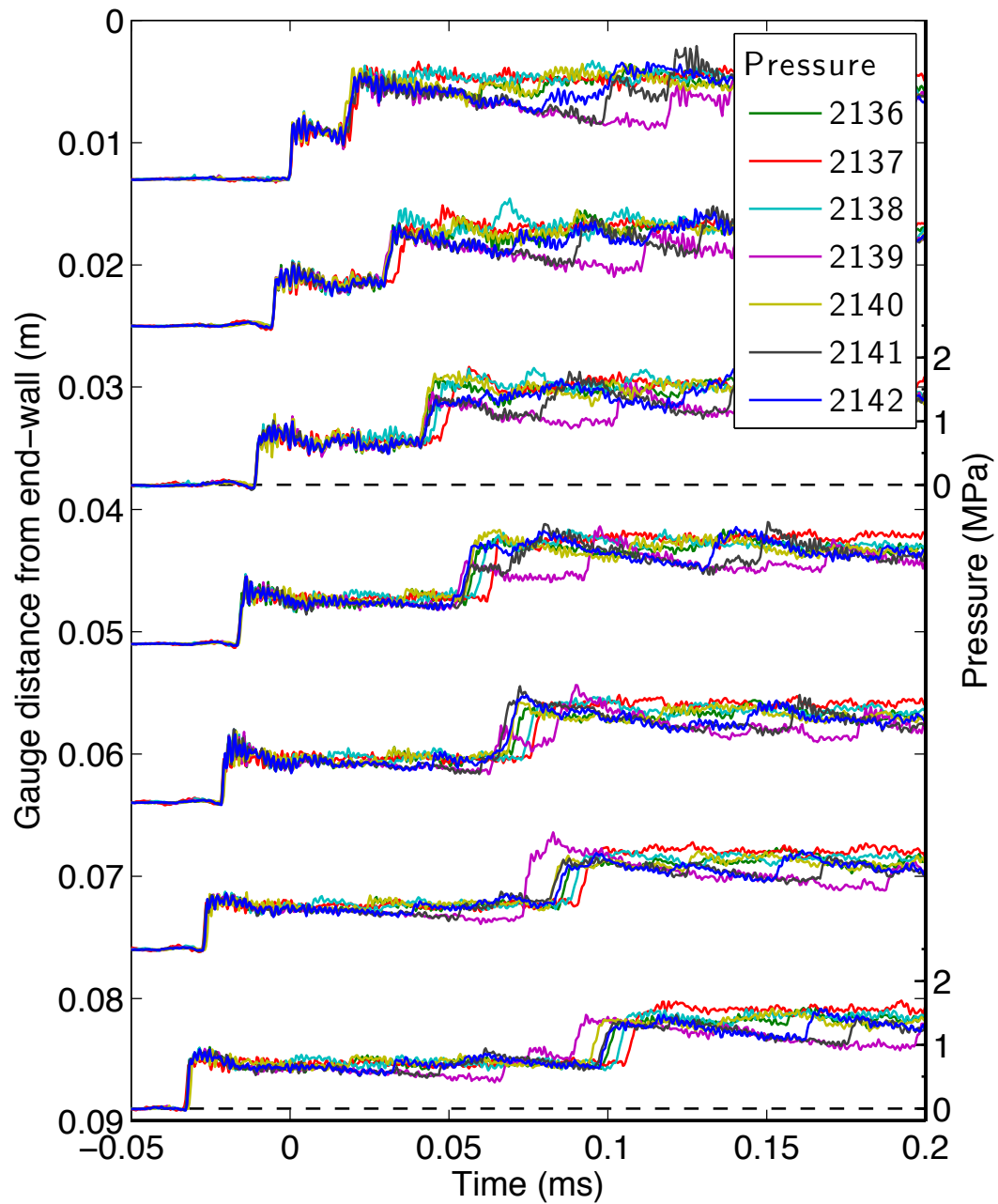


Figure E.167: Pressure traces for a detonation in stoichiometric ethylene-oxygen at fill pressure 25 kPa, part 5.

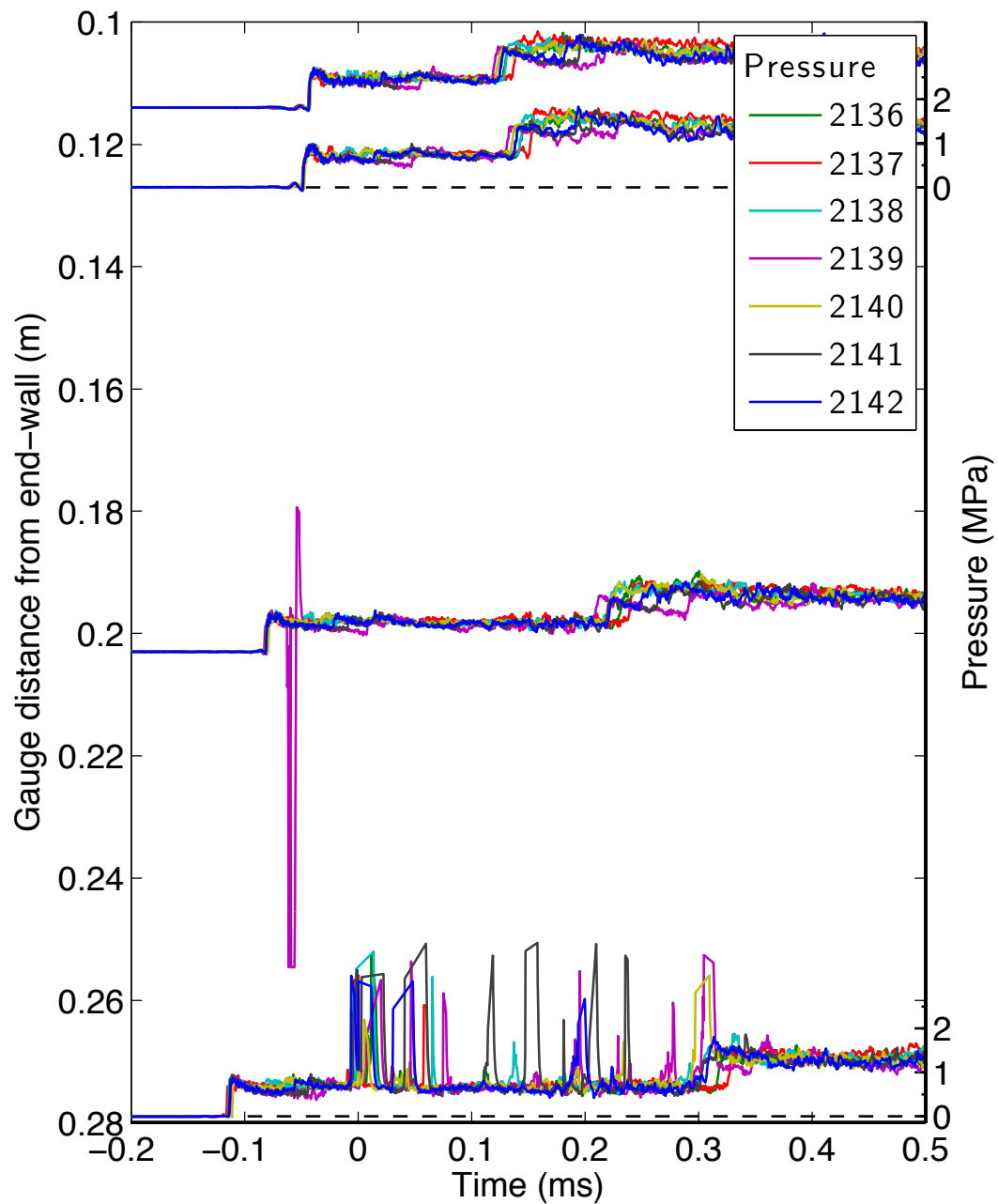


Figure E.168: Pressure traces for a detonation in stoichiometric ethylene-oxygen at fill pressure 25 kPa, part 6.

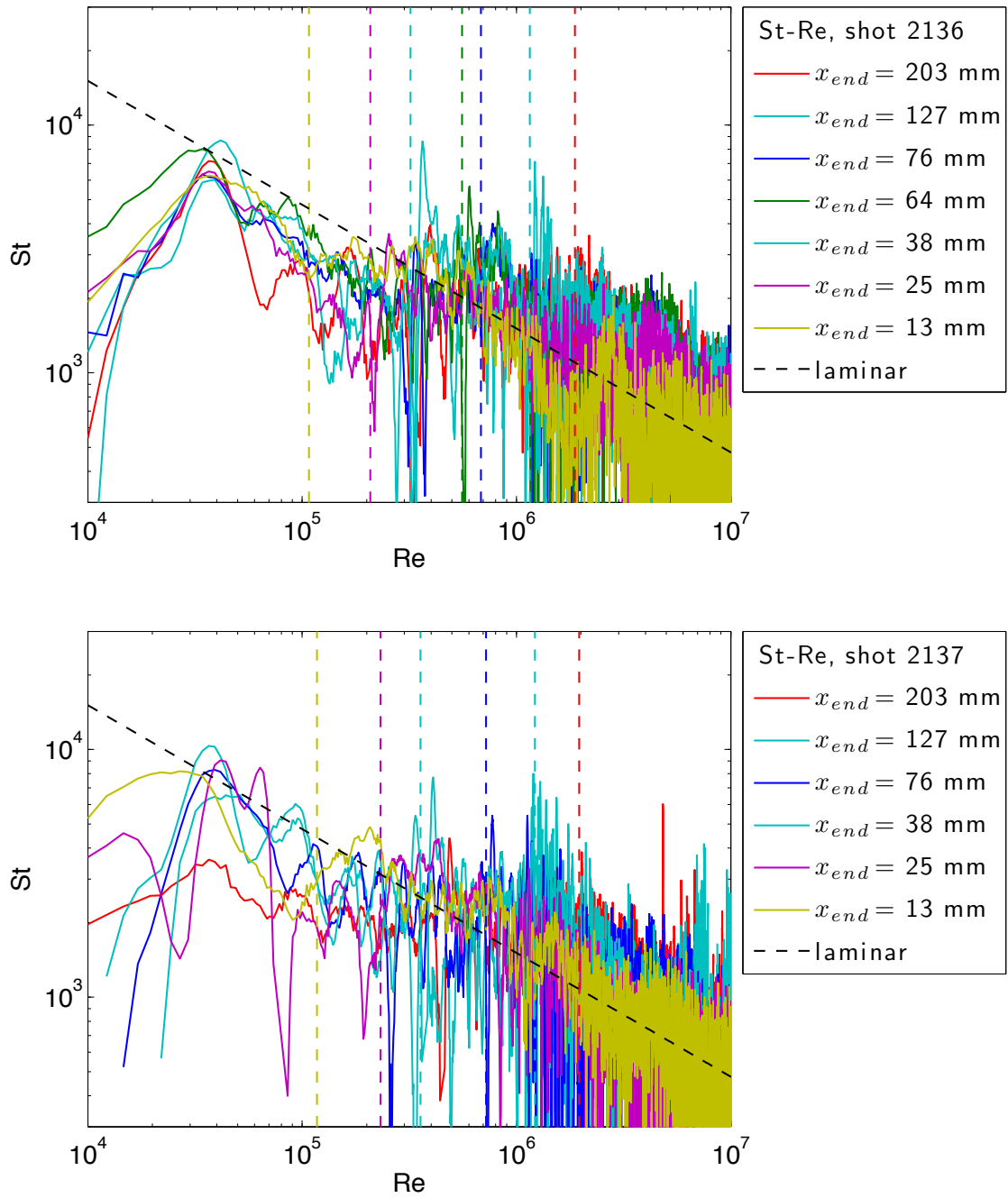


Figure E.169: Stanton-Reynolds number traces from shot 2137, a detonation in stoichiometric ethylene-oxygen at fill pressure 25 kPa. The dashed vertical lines represent the arrival of the reflected shock wave.

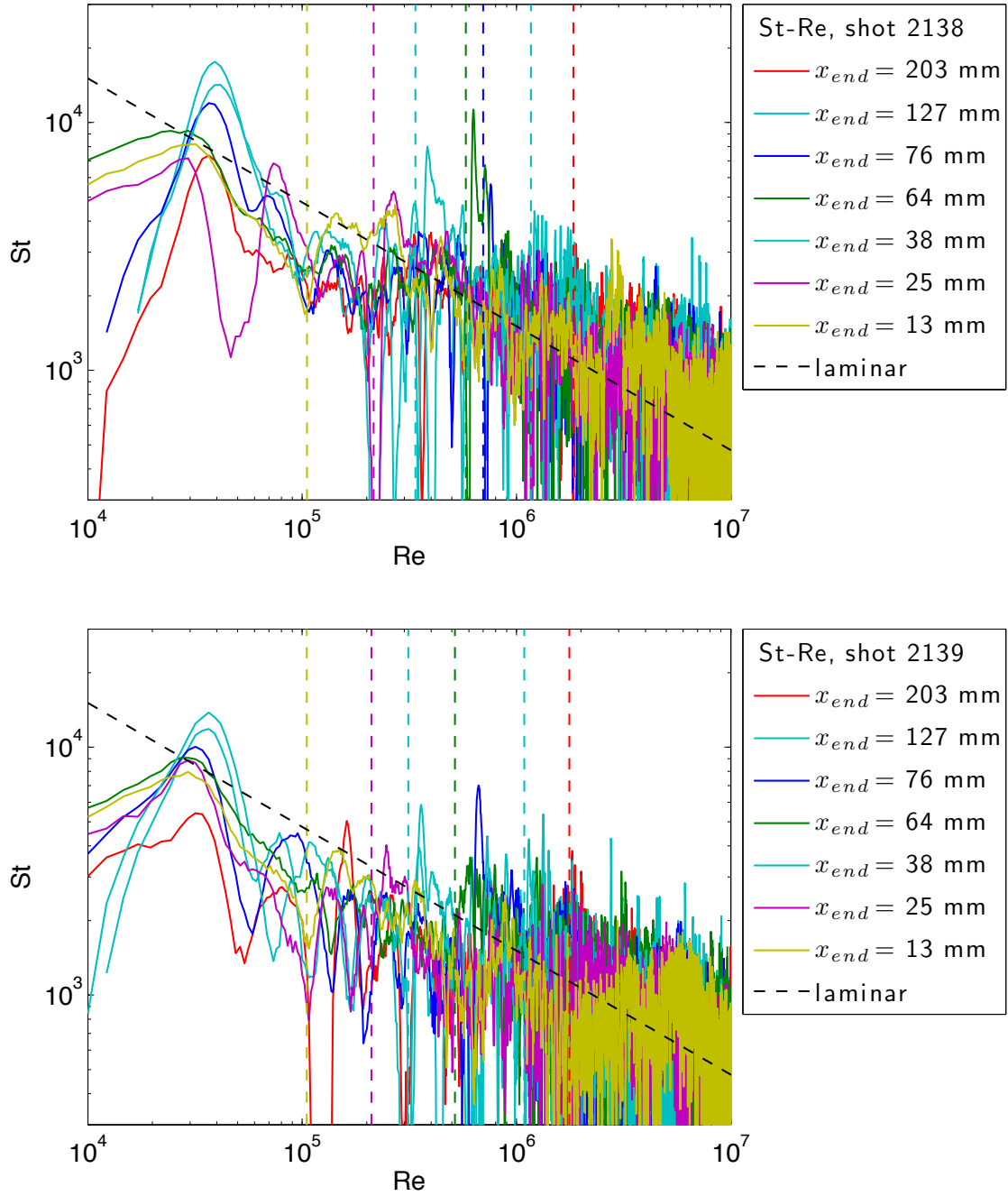


Figure E.170: Stanton-Reynolds number traces from shot 2139, a detonation in stoichiometric ethylene-oxygen at fill pressure 25 kPa. The dashed vertical lines represent the arrival of the reflected shock wave.

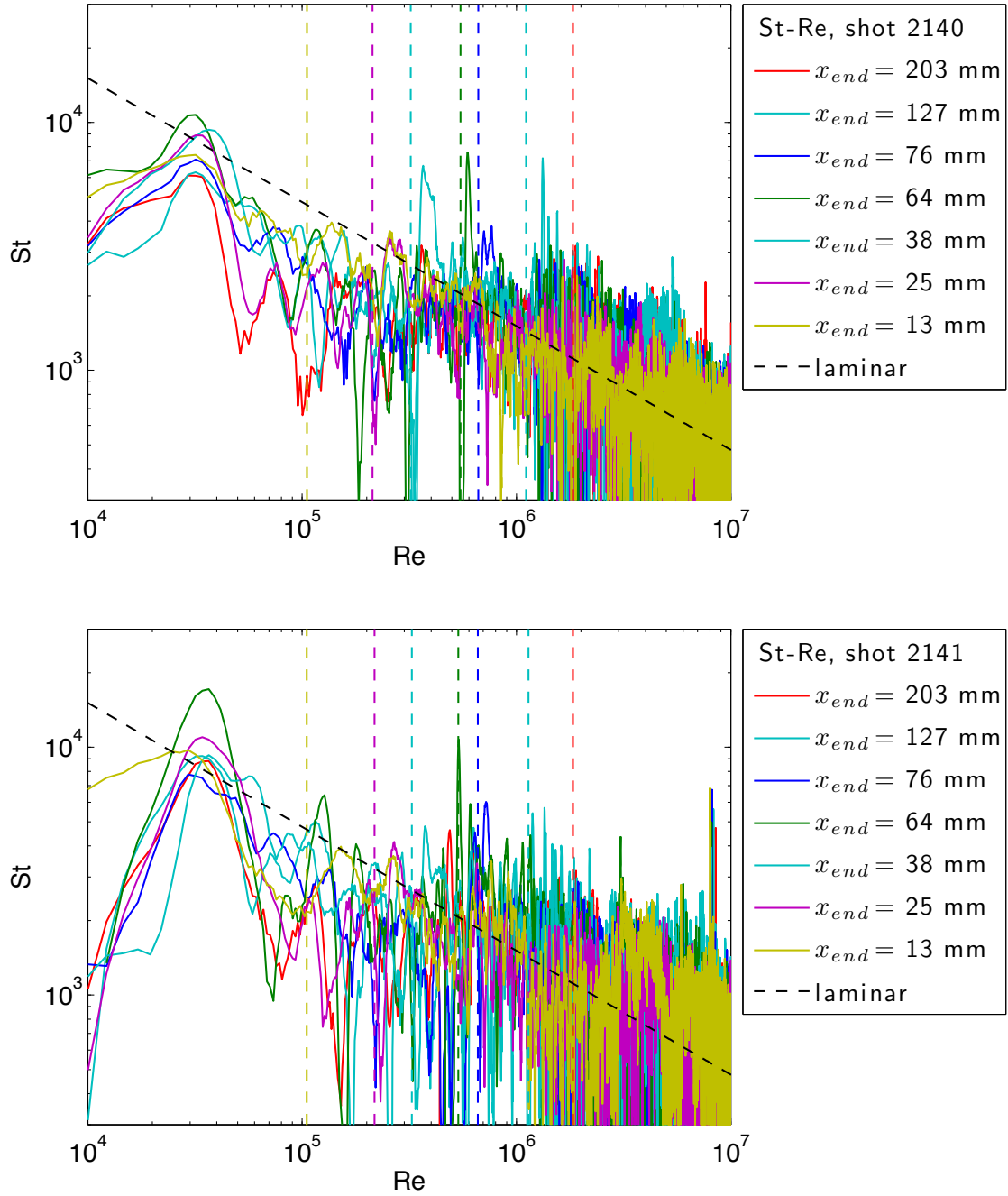


Figure E.171: Stanton-Reynolds number traces from shot 2141, a detonation in stoichiometric ethylene-oxygen at fill pressure 25 kPa. The dashed vertical lines represent the arrival of the reflected shock wave.

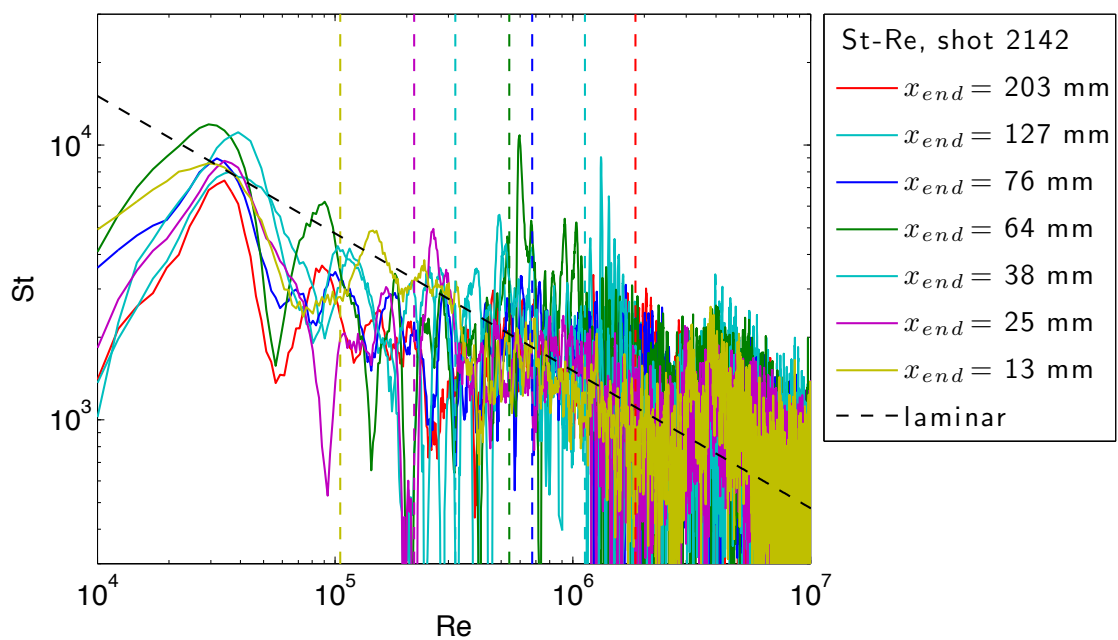


Figure E.172: Stanton-Reynolds number traces from shot 2142, a detonation in stoichiometric ethylene-oxygen at fill pressure 25 kPa. The dashed vertical lines represent the arrival of the reflected shock wave.

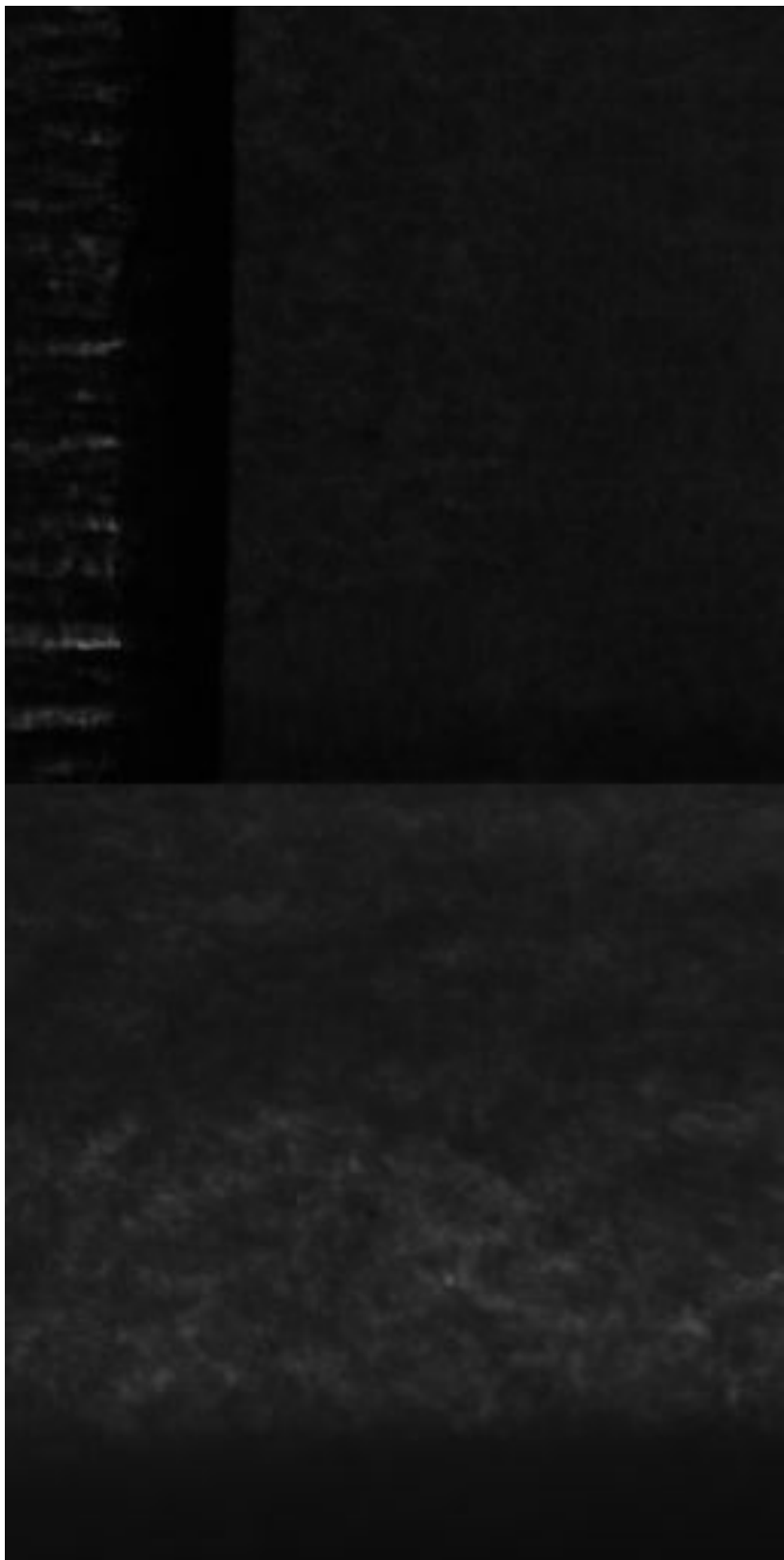


Figure E.173: Focused schlieren image of shot 2140. The field of view is approximately 14 mm wide.

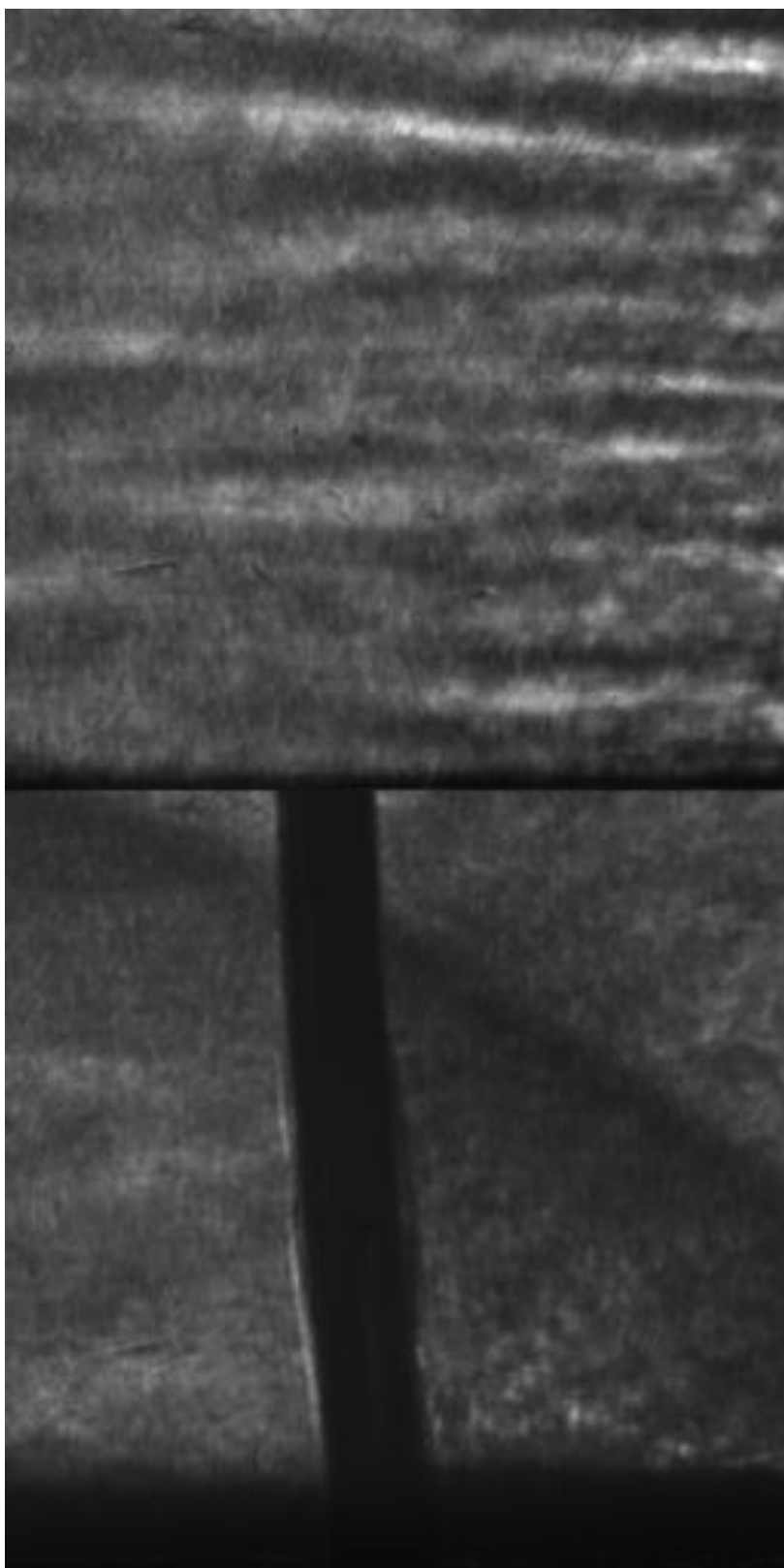


Figure E.174: Focused schlieren image of shot 2141. The field of view is approximately 14 mm wide.

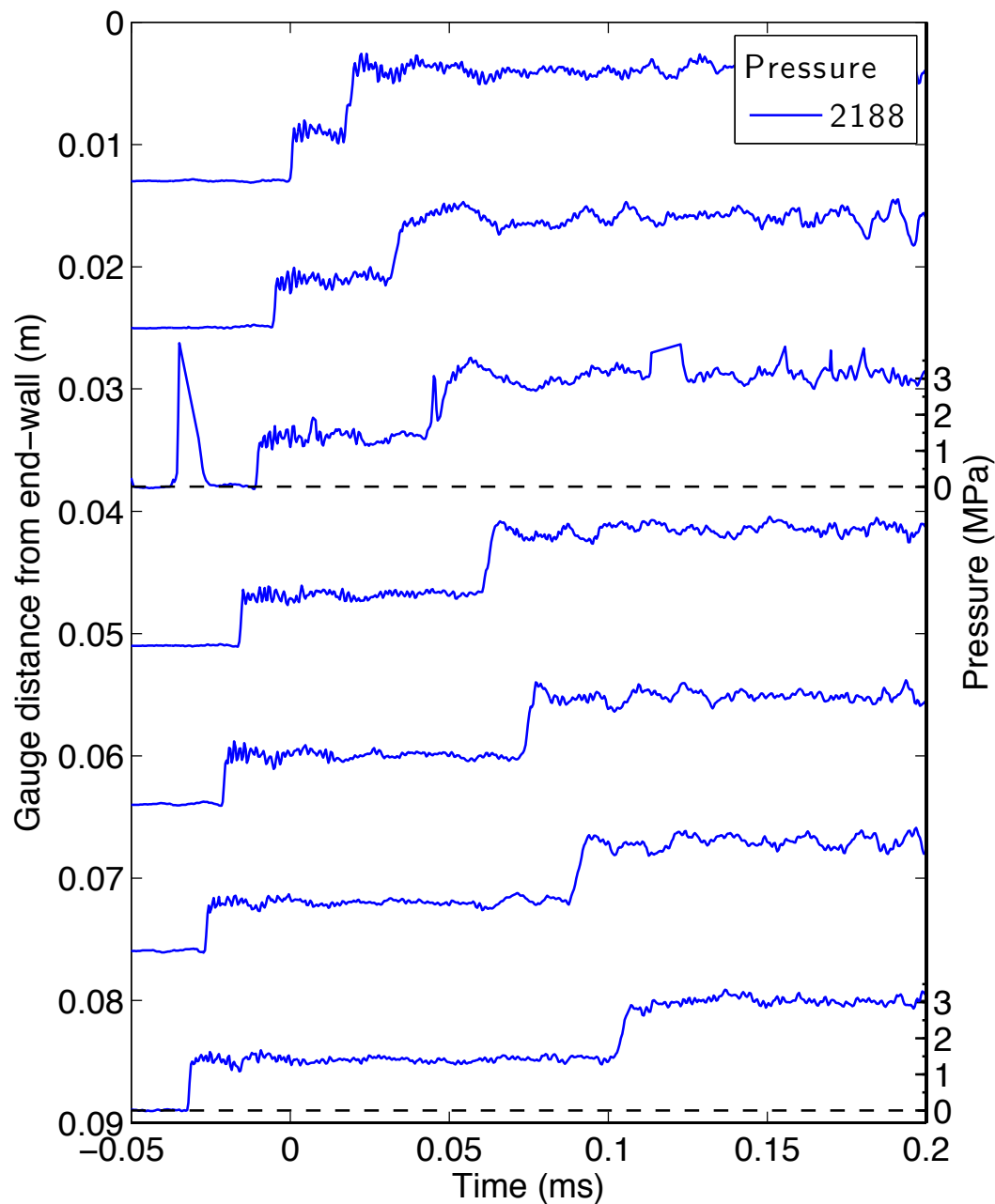


Figure E.175: Pressure traces for a detonation in stoichiometric ethylene-oxygen at fill pressure 50 kPa, part 1.

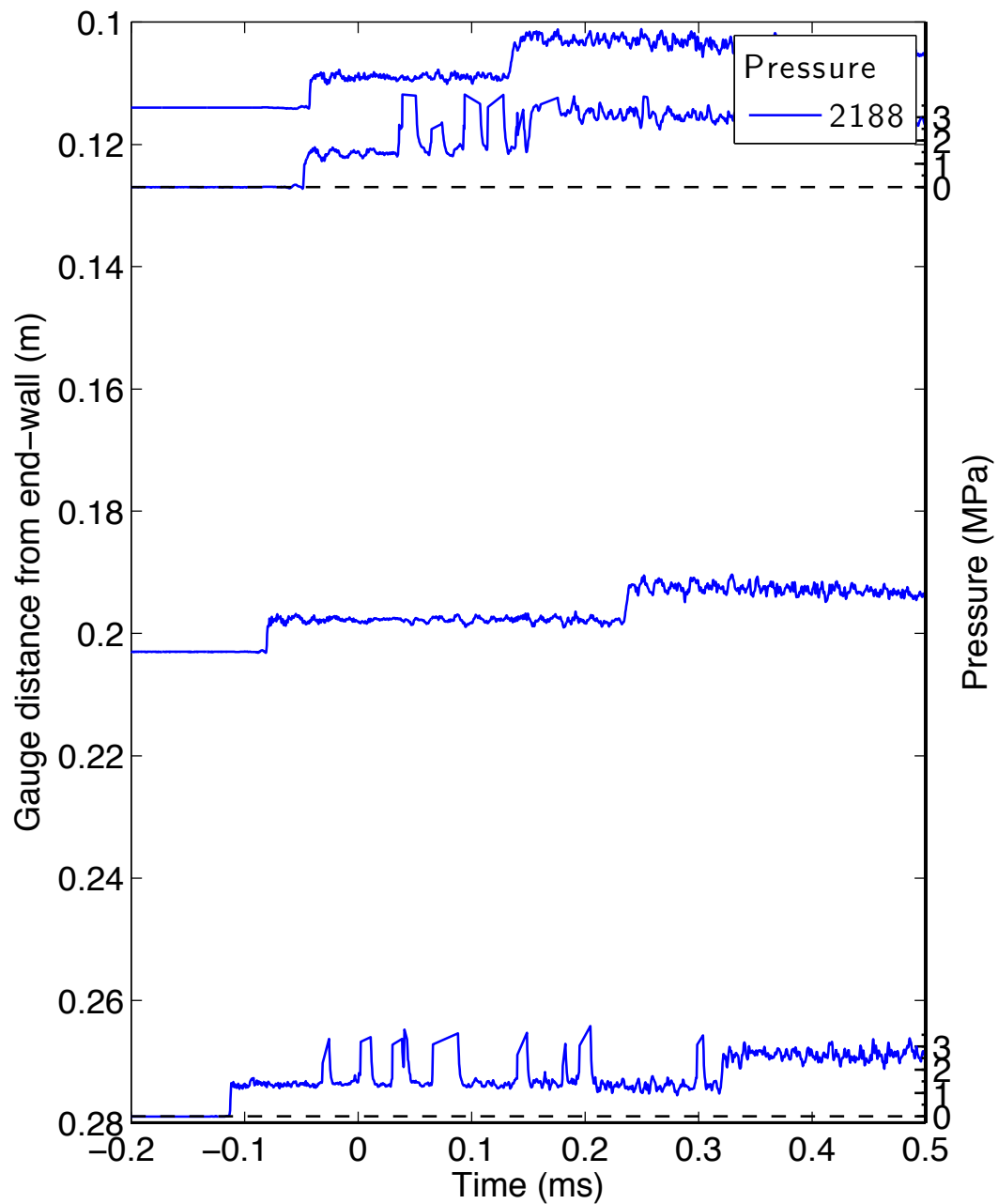


Figure E.176: Pressure traces for a detonation in stoichiometric ethylene-oxygen at fill pressure 50 kPa, part 2.

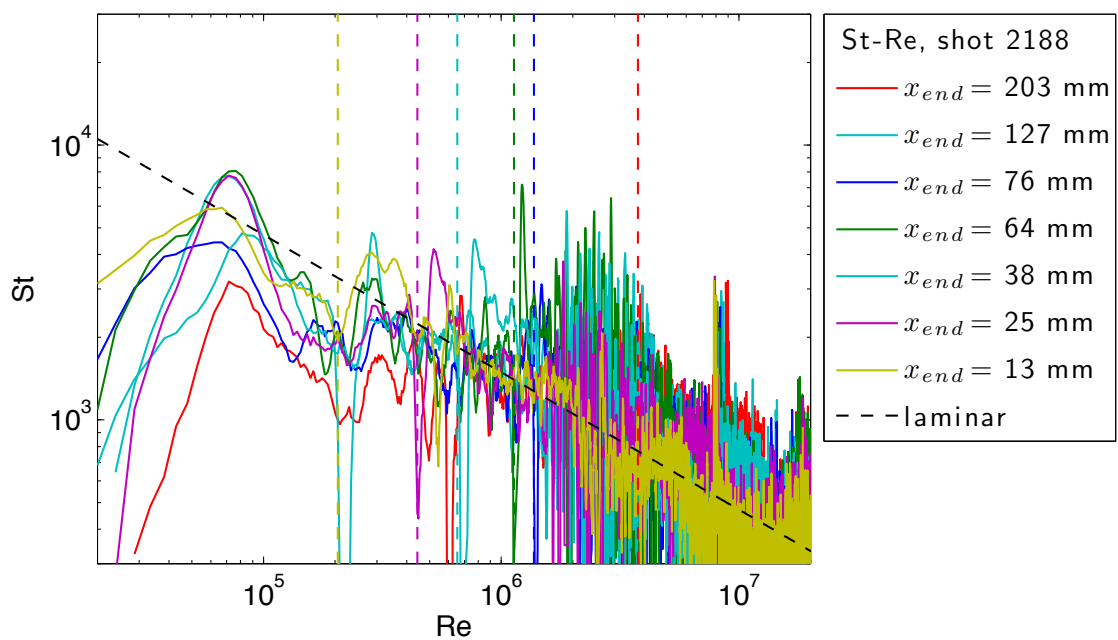


Figure E.177: Stanton-Reynolds number traces from shot 2188, a detonation in stoichiometric ethylene-oxygen at fill pressure 50 kPa. The dashed vertical lines represent the arrival of the reflected shock wave.

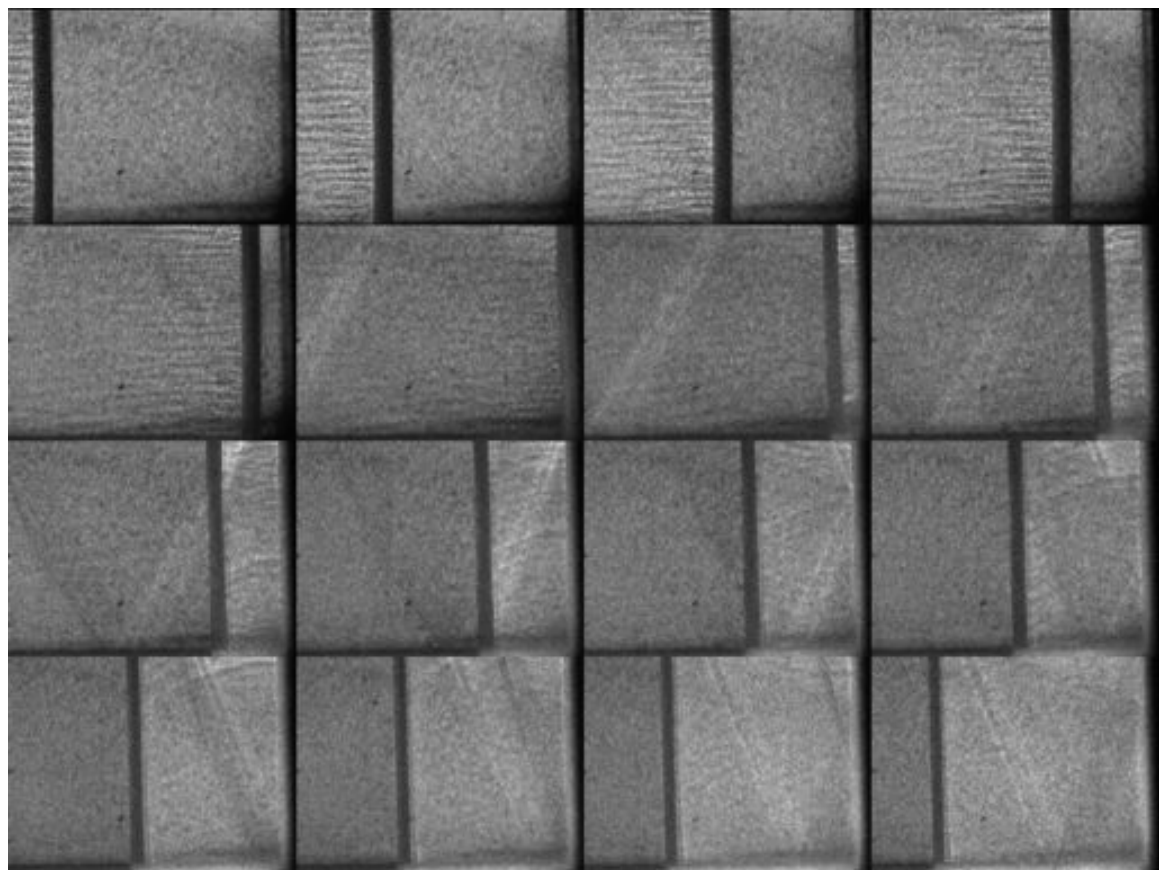


Figure E.178: Unfocused schlieren image of shot 2188. The field of view is approximately 30 mm wide.

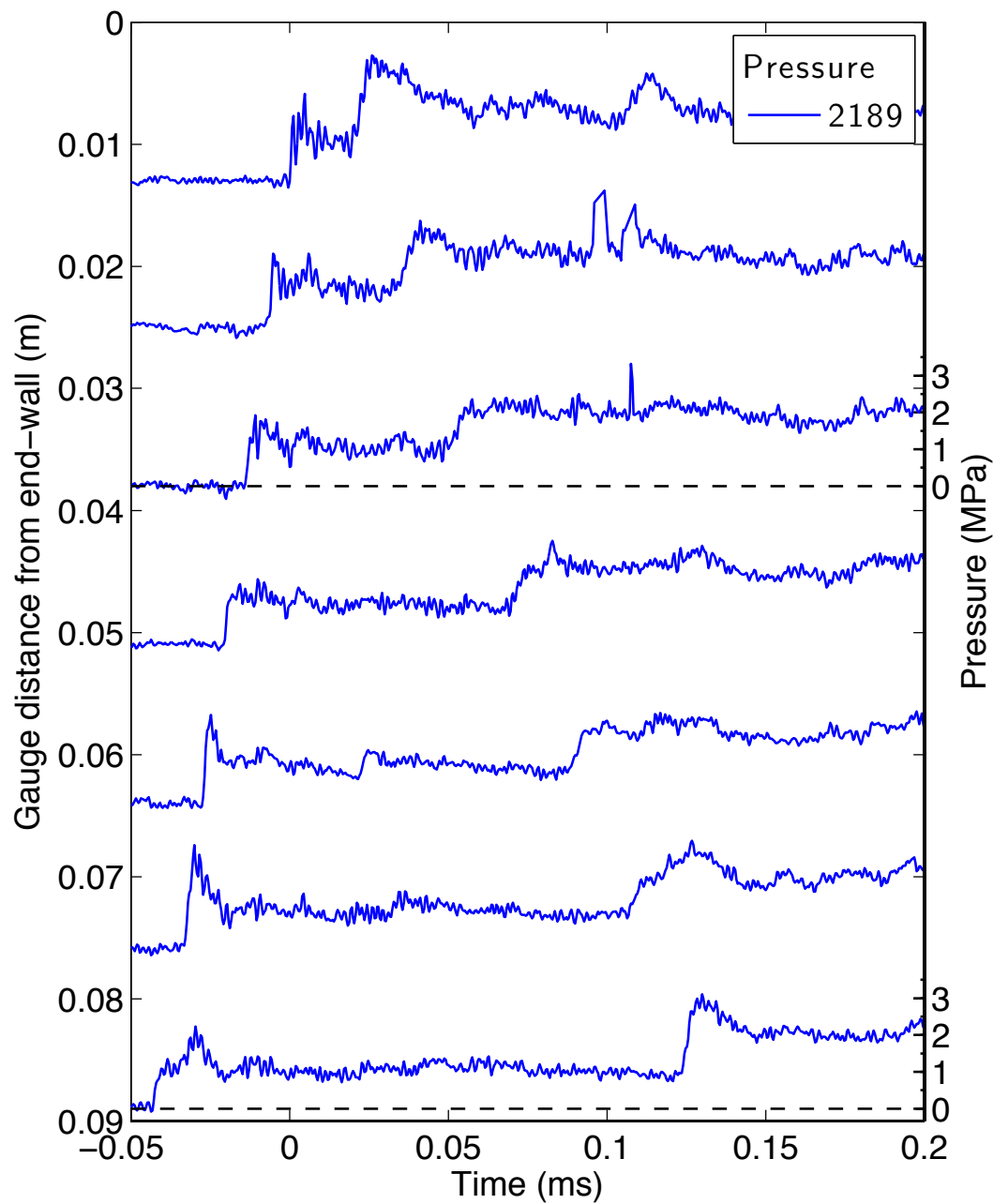


Figure E.179: Pressure traces for a detonation in stoichiometric ethylene-oxygen with 50% carbon dioxide dilution at fill pressure 50 kPa, part 1.

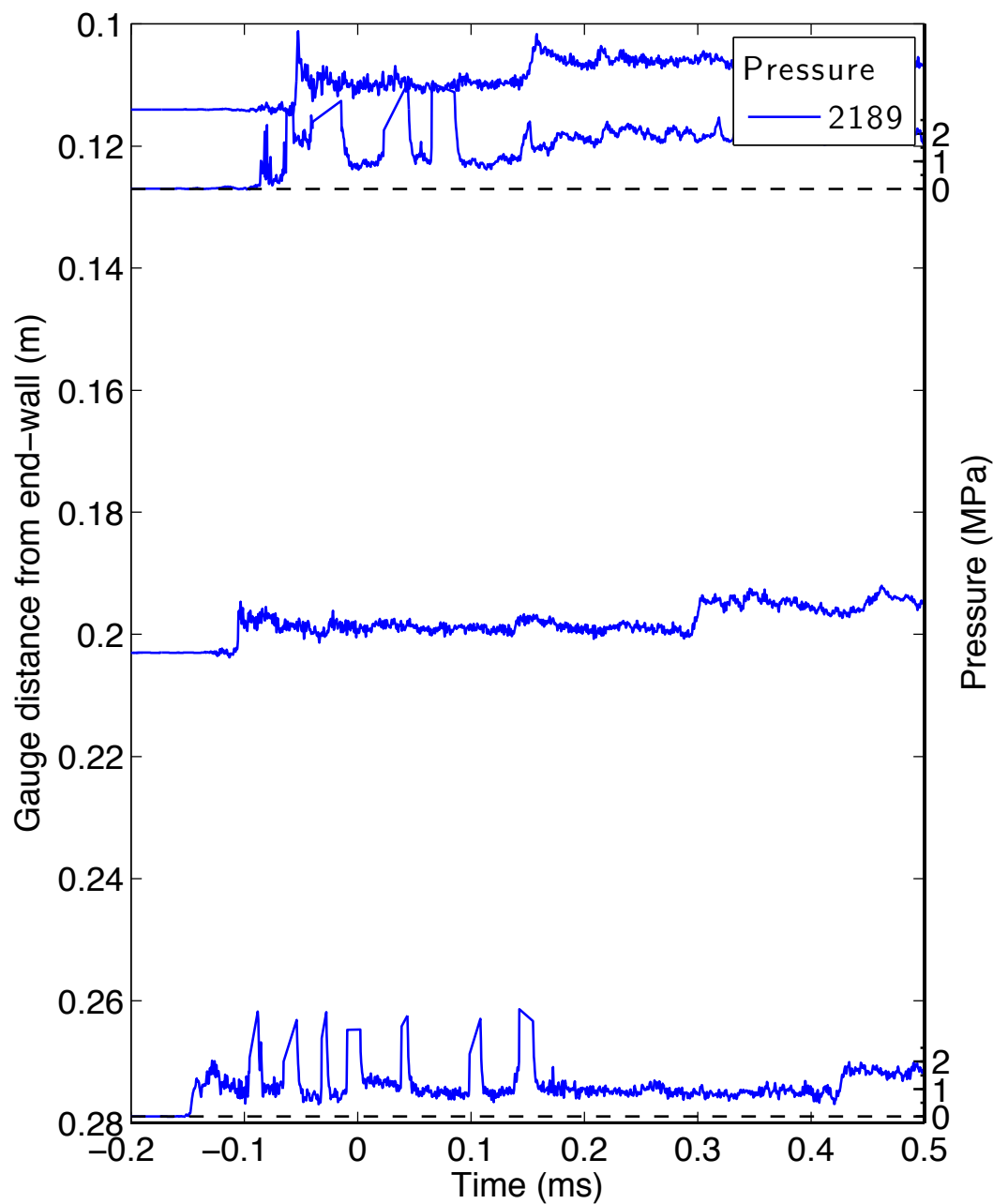


Figure E.180: Pressure traces for a detonation in stoichiometric ethylene-oxygen with 50% carbon dioxide dilution at fill pressure 50 kPa, part 2.

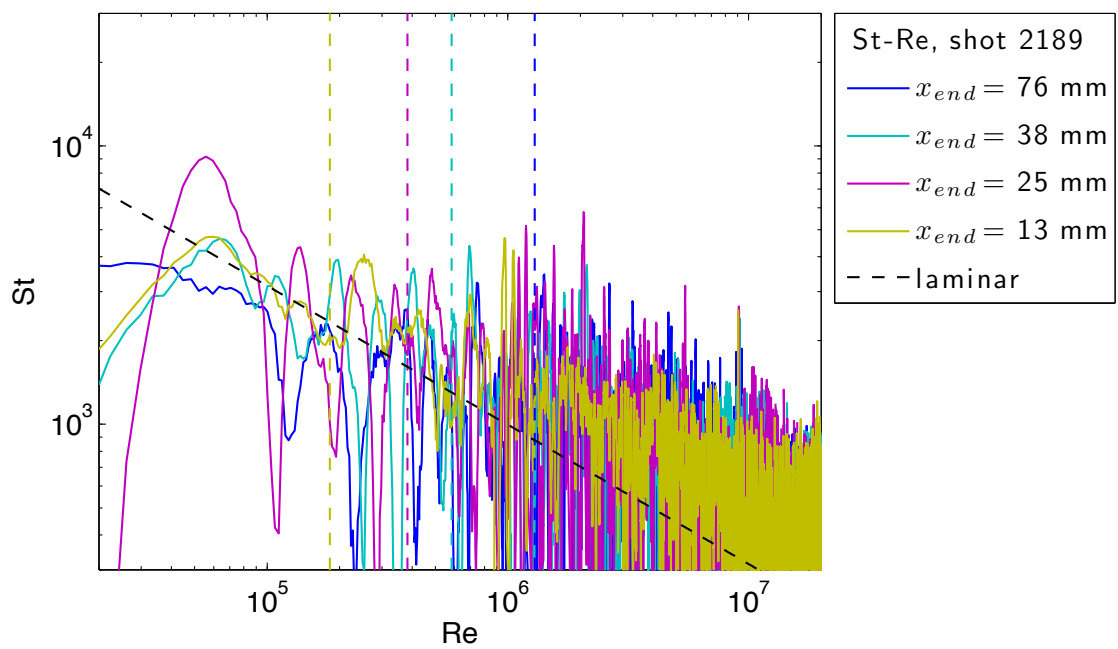


Figure E.181: Stanton-Reynolds number traces from shot 2189, a detonation in stoichiometric ethylene-oxygen with 50% carbon dioxide dilution at fill pressure 50 kPa. The dashed vertical lines represent the arrival of the reflected shock wave.

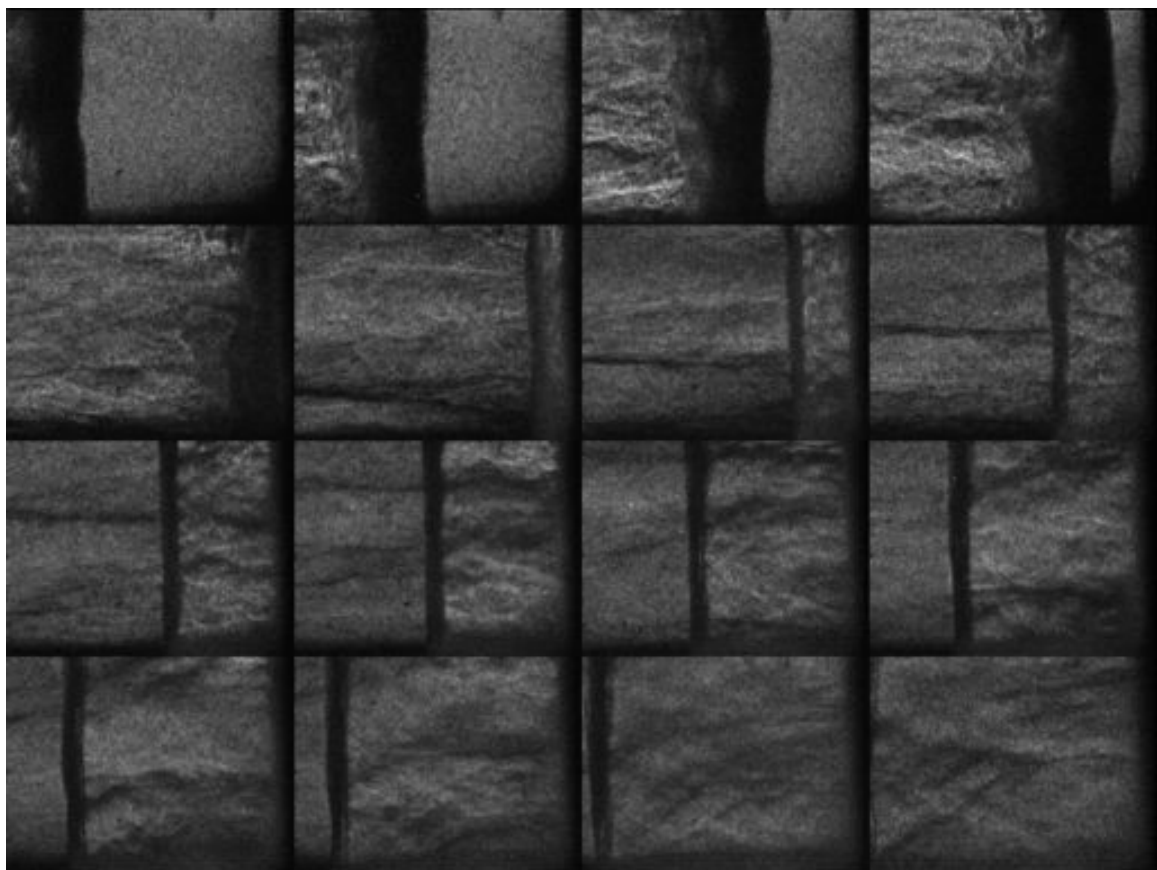


Figure E.182: Unfocused schlieren image of shot 2189. The field of view is approximately 30 mm wide.

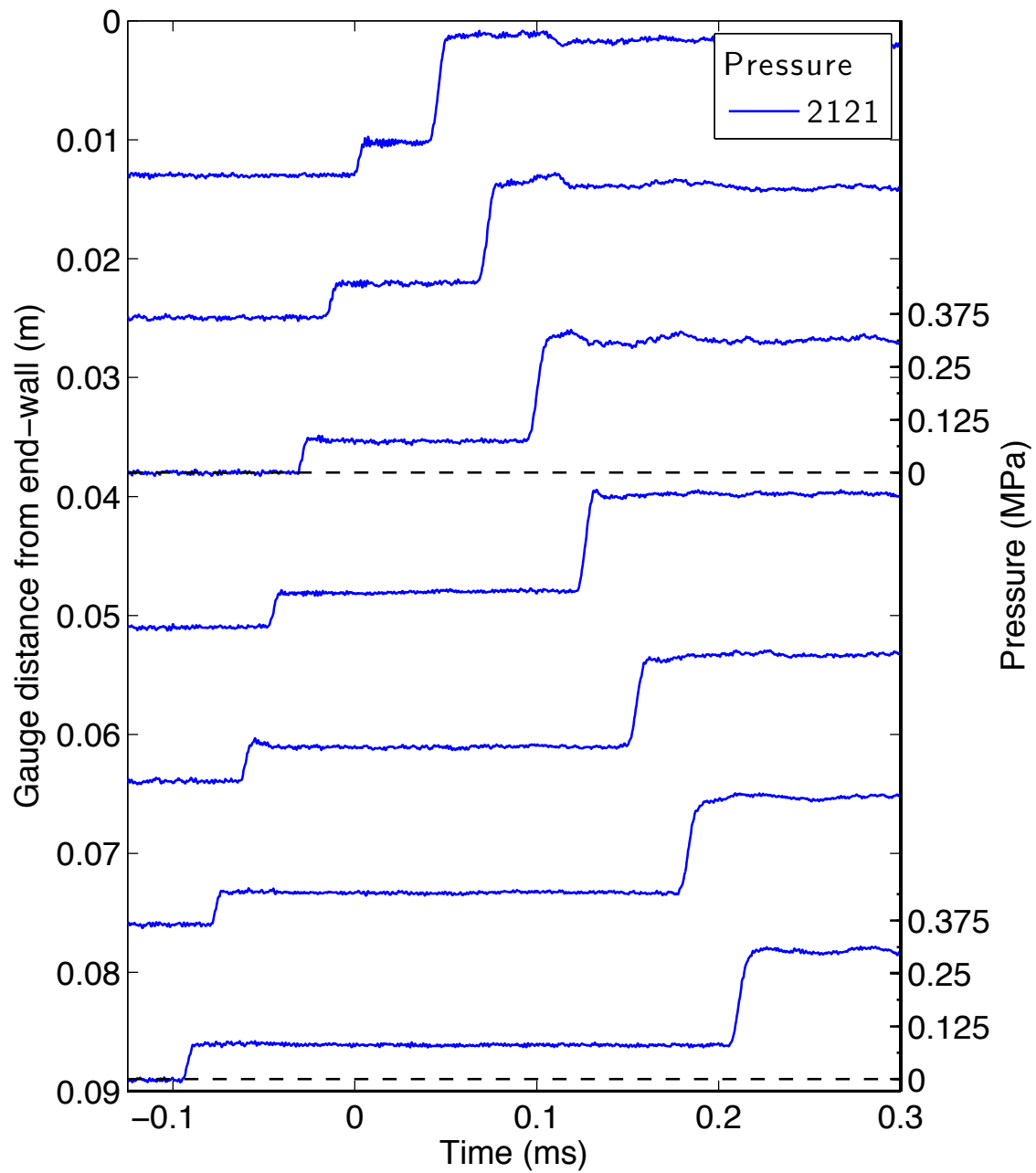


Figure E.183: Pressure traces for a shock wave in argon at fill pressure 10 kPa, part 1.

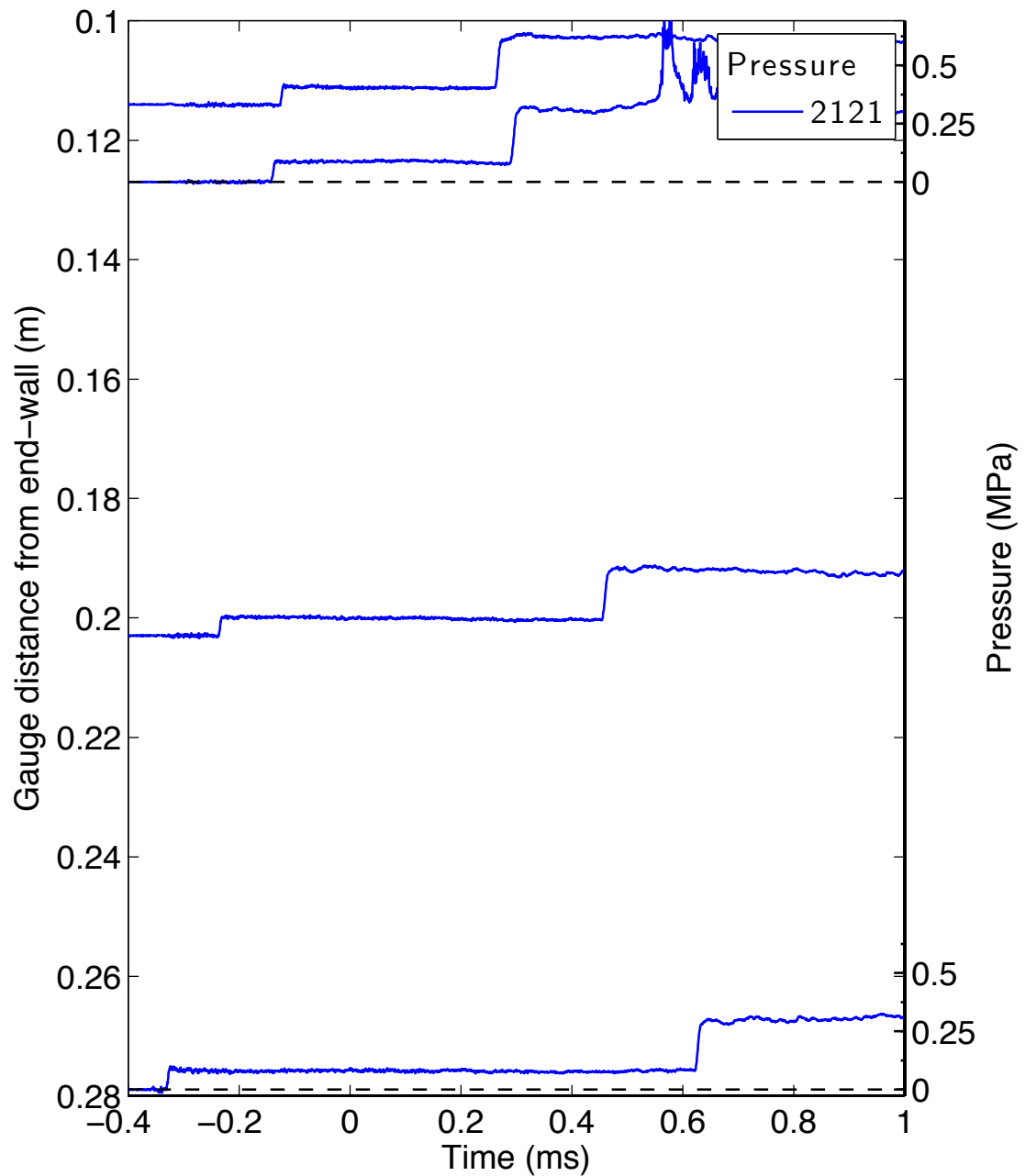


Figure E.184: Pressure traces for a shock wave in argon at fill pressure 10 kPa, part 2.

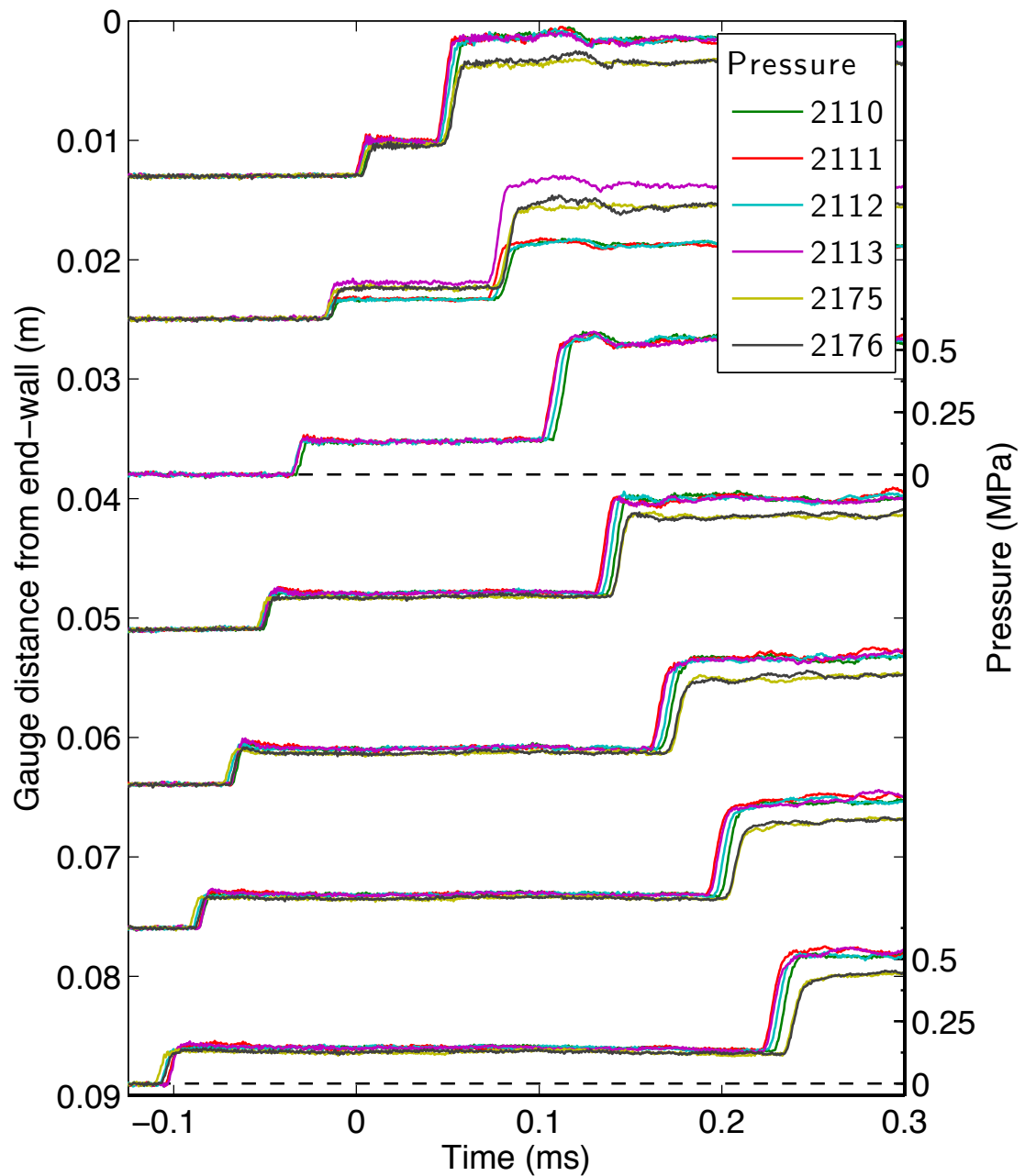


Figure E.185: Pressure traces for a shock wave in argon at fill pressure 25 kPa, part 1.

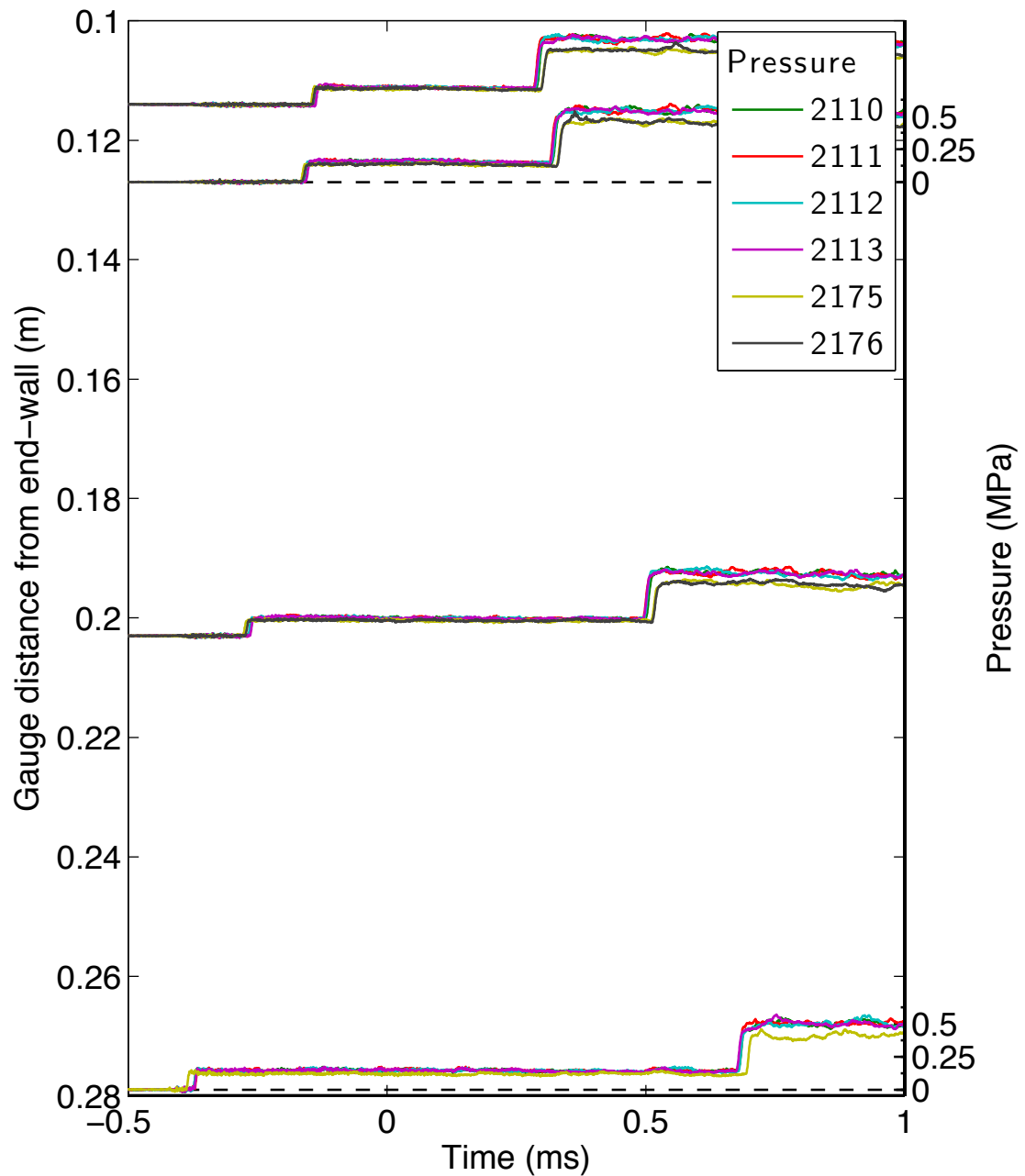


Figure E.186: Pressure traces for a shock wave in argon at fill pressure 25 kPa, part 2.

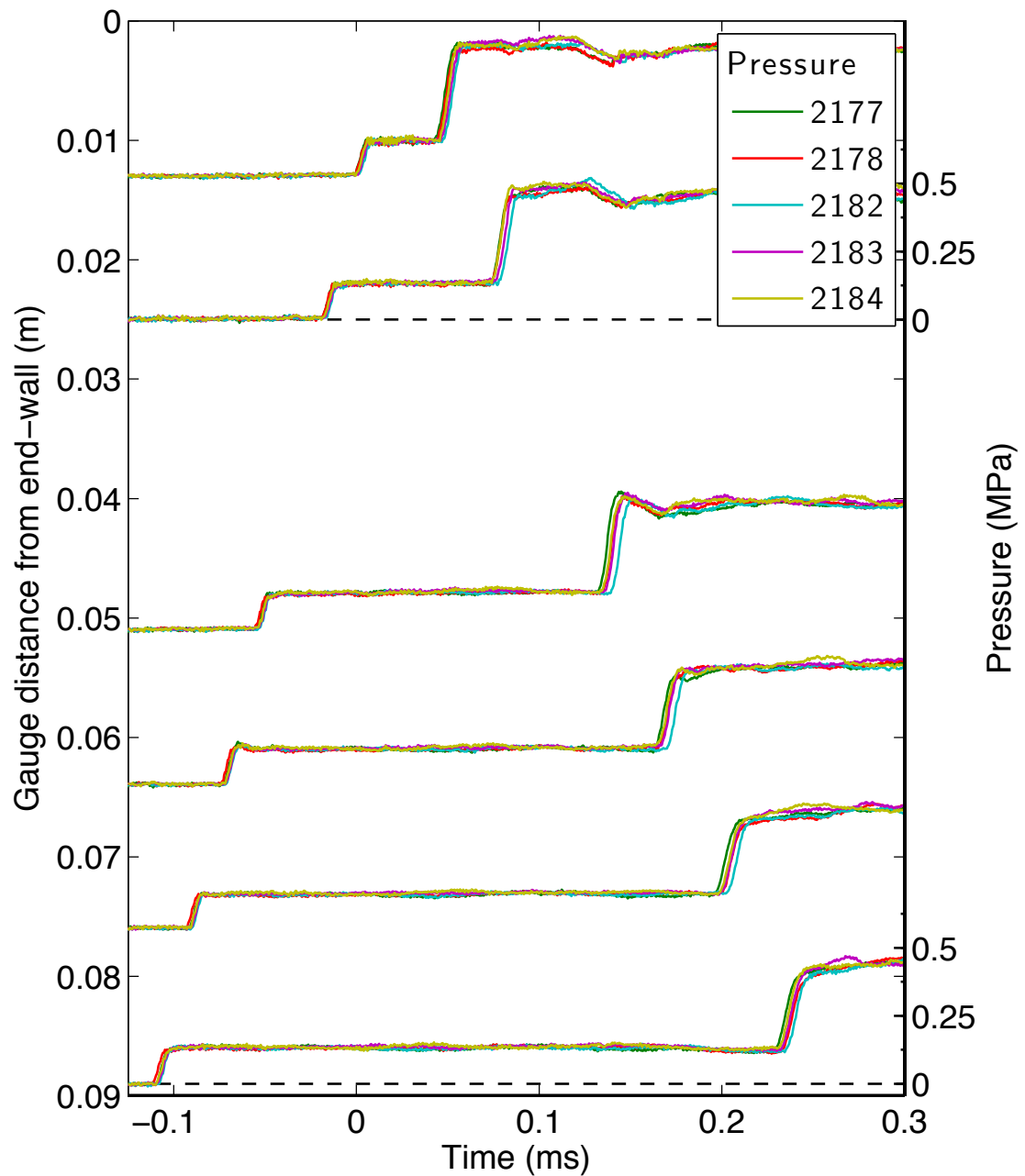


Figure E.187: Pressure traces for a shock wave in argon at fill pressure 25 kPa, part 3.

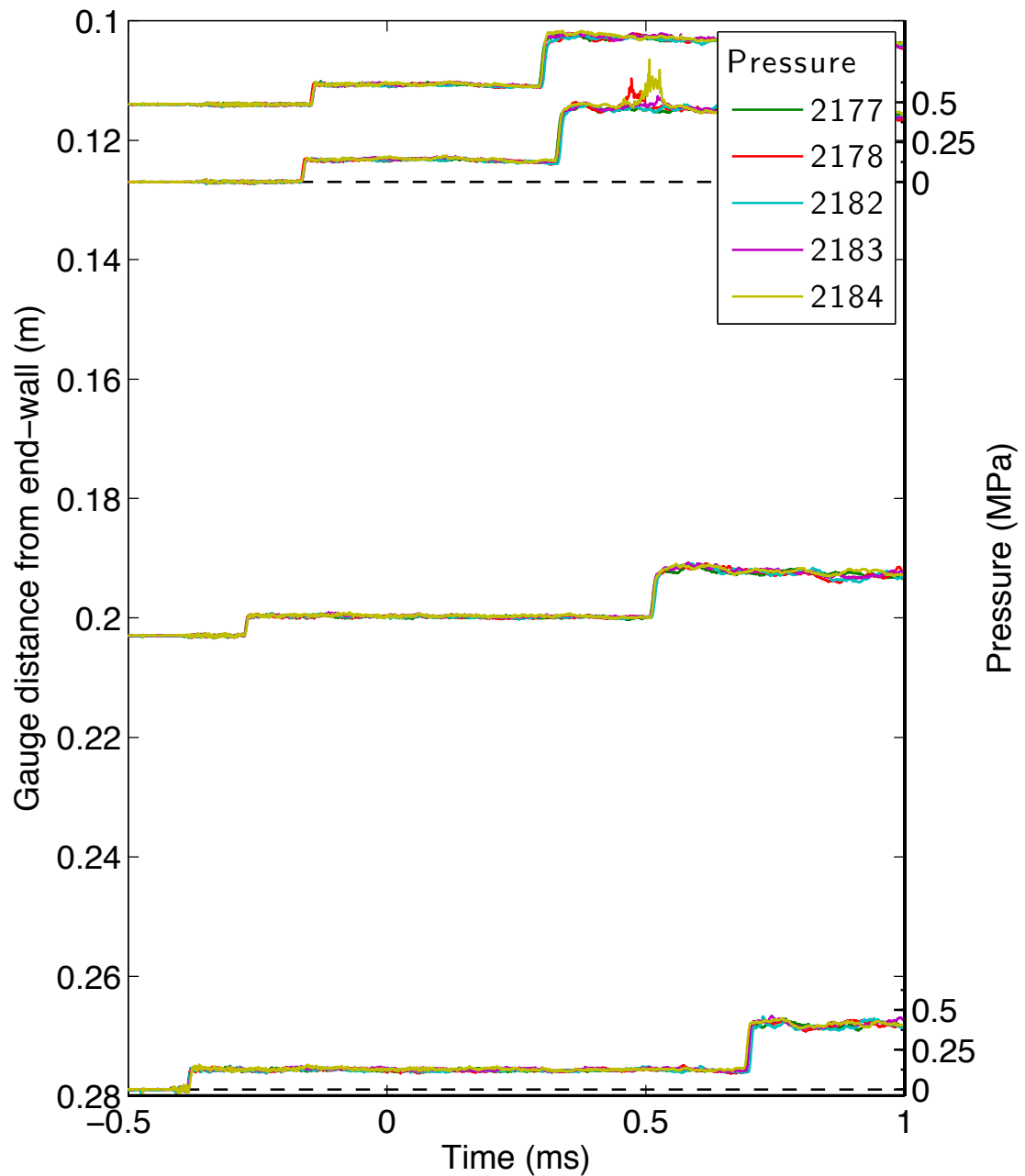


Figure E.188: Pressure traces for a shock wave in argon at fill pressure 25 kPa, part 4.

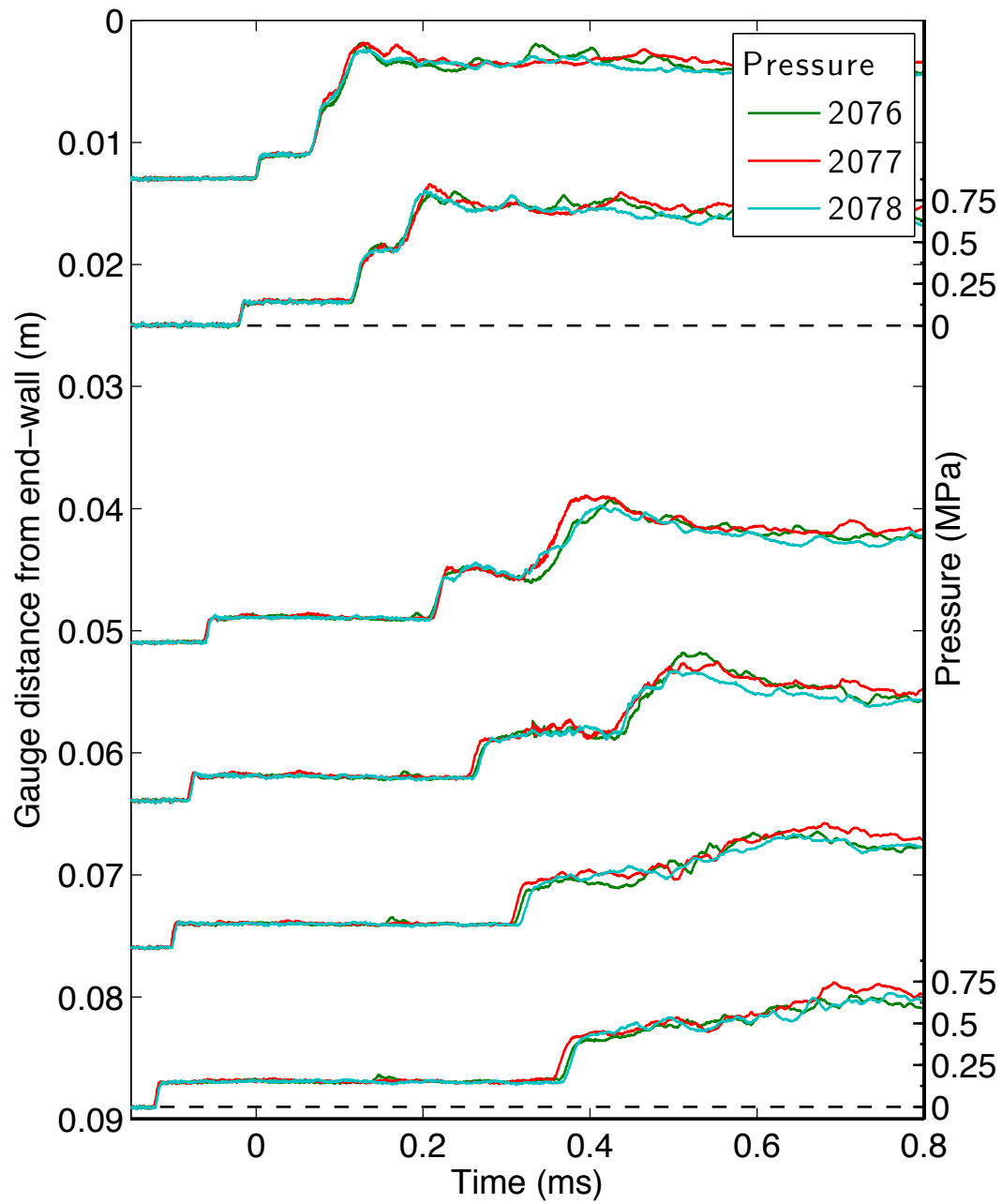


Figure E.189: Pressure traces for a shock wave in nitrous oxide at fill pressure 25 kPa, part 1.

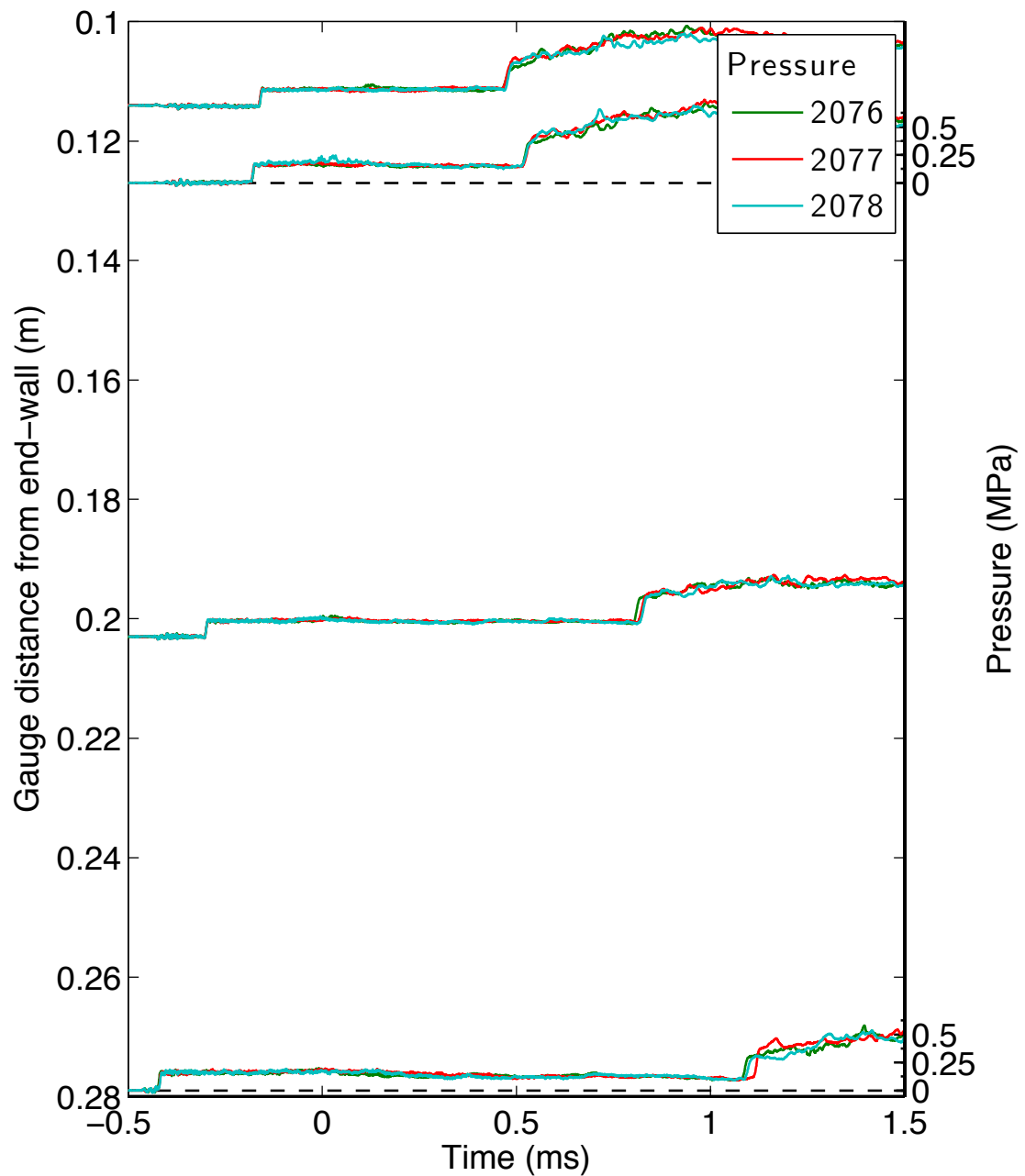


Figure E.190: Pressure traces for a shock wave in nitrous oxide at fill pressure 25 kPa, part 2.

## Appendix F

# Derivation of Laminar Boundary Layer Equations

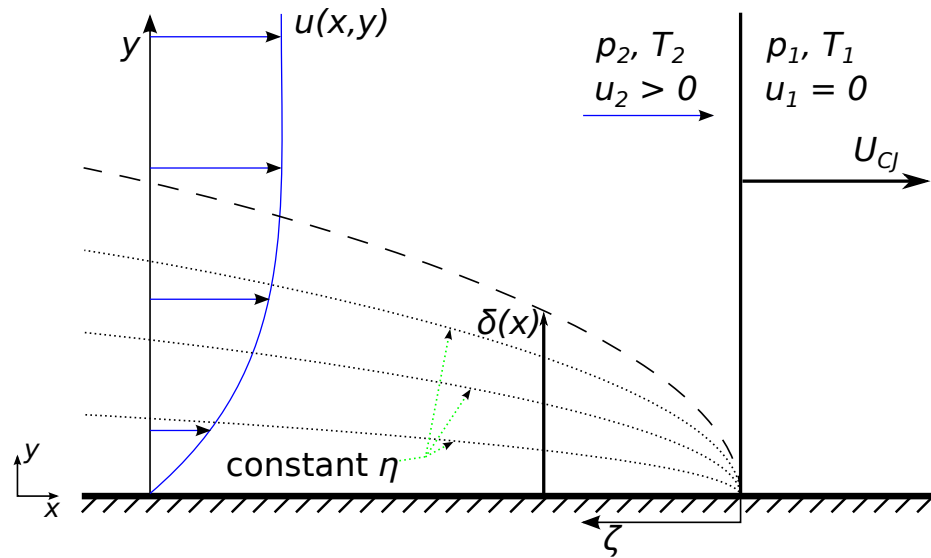


Figure F.1: Frame of reference used for boundary layer calculations.

### F.1 Boundary Layer Governing Equations

The governing equations for a two-dimensional compressible laminar boundary layer in a lab-fixed frame are the conservation of mass, momentum, and energy with the boundary layer assumption that gradients with respect to the transverse direction,  $y$ ,

are much larger than gradients with respect to the axial direction,  $x$ :

$$\frac{\partial \rho}{\partial t} + \frac{\partial \rho u}{\partial x} + \frac{\partial \rho v}{\partial y} = 0 \quad (\text{F.1})$$

$$\rho \frac{\partial u}{\partial t} + \rho u \frac{\partial u}{\partial x} + \rho v \frac{\partial u}{\partial y} = -\frac{\partial p}{\partial x} + \frac{\partial}{\partial y} \left( \mu \frac{\partial u}{\partial y} \right) \quad (\text{F.2})$$

$$\rho \frac{\partial h}{\partial t} + \rho u \frac{\partial h}{\partial x} + \rho v \frac{\partial h}{\partial y} = \frac{\partial p}{\partial t} + u \frac{\partial p}{\partial x} + \frac{\partial}{\partial y} \left( \frac{\mu}{Pr} \frac{\partial h}{\partial y} \right) + \mu \left( \frac{\partial u}{\partial y} \right)^2. \quad (\text{F.3})$$

## F.2 Definition of the Coordinate System

Variables are given in a lab fixed frame where the detonation originates at  $x = 0$ ,  $t = 0$  and proceeds in the  $+\hat{x}$ -direction. The position of the detonation as a function of time is  $X_{det}(t)$  and the detonation velocity is given by  $U_{det}(t) = U_{CJ}$ . We will be applying the Levy-Lees transformation to switch to the  $(\zeta, \eta, \tau)$  coordinate system.

$\zeta$ : Axial position,  $x$ , scaled with the location of the detonation

$$\zeta(x, t) = 1 - \frac{x}{X_{det}(t)}. \quad (\text{F.4})$$

$\eta$ : Distance from the side-wall,  $y$ , scaled with compressibility ( $\star_0$  represents  $\star$  evaluated at a constant reference state) and boundary layer thickness  $\delta$

$$\eta(x, y, t) = \frac{\int_0^y \frac{\rho(x, y', t)}{\rho_0} dy'}{\delta(x, t)}. \quad (\text{F.5})$$

$\tau$ : Time,  $t$ , scaled with the speed of the detonation and length of the detonation tube

$$\tau(t) = \frac{t U_{CJ}}{L} \quad (\text{F.6})$$

where  $L$  is the axial length of the system in the  $\hat{x}$ -direction. With this list, we can apply the chain rule to note:

$$\frac{\partial}{\partial x} \Big|_{y,t} = \frac{\partial \zeta}{\partial x} \Big|_{y,t} \frac{\partial}{\partial \zeta} \Big|_{\eta,\tau} + \frac{\partial \eta}{\partial x} \Big|_{y,t} \frac{\partial}{\partial \eta} \Big|_{\zeta,\tau} + \frac{\partial \tau}{\partial x} \Big|_{y,t} \frac{\partial}{\partial \tau} \Big|_{\zeta,\eta}^0 \quad (\text{F.7})$$

$$= -\frac{1}{L\tau} \frac{\partial}{\partial \zeta} \Big|_{\eta,\tau} + \eta_x \frac{\partial}{\partial \eta} \Big|_{\zeta,\tau} \quad (\text{F.8})$$

where, for the moment, we have left  $\eta_x$  as the derivative of  $\eta$  with respect to  $x$  at constant  $y$  and  $t$ . Similarly,

$$\frac{\partial}{\partial y} \Big|_{x,t} = \frac{\partial \zeta}{\partial y} \Big|_{x,t}^0 \frac{\partial}{\partial \zeta} \Big|_{\eta,\tau} + \frac{\partial \eta}{\partial y} \Big|_{x,t} \frac{\partial}{\partial \eta} \Big|_{\zeta,\tau} + \frac{\partial \tau}{\partial y} \Big|_{x,t}^0 \frac{\partial}{\partial \tau} \Big|_{\zeta,\eta} \quad (\text{F.9})$$

$$= \frac{\rho}{\rho_0 \delta} \frac{\partial}{\partial \eta} \Big|_{\zeta,\tau} \quad (\text{F.10})$$

$$\frac{\partial}{\partial t} \Big|_{x,y} = \frac{\partial \zeta}{\partial t} \Big|_{x,y} \frac{\partial}{\partial \zeta} \Big|_{\eta,\tau} + \frac{\partial \eta}{\partial t} \Big|_{x,y} \frac{\partial}{\partial \eta} \Big|_{\zeta,\tau} + \frac{\partial \tau}{\partial t} \Big|_{x,y} \frac{\partial}{\partial \tau} \Big|_{\zeta,\eta} \quad (\text{F.11})$$

$$= \frac{x U_{CJ}}{X_{det}^2} \frac{\partial}{\partial \zeta} \Big|_{\eta,\tau} + \eta_t \frac{\partial}{\partial \eta} \Big|_{\zeta,\tau} + \frac{U_{CJ}}{L} \frac{\partial}{\partial \tau} \Big|_{\zeta,\eta} \quad (\text{F.12})$$

$$= \frac{U_{CJ}}{L\tau} (1 - \zeta) \frac{\partial}{\partial \zeta} \Big|_{\eta,\tau} + \eta_t \frac{\partial}{\partial \eta} \Big|_{\zeta,\tau} + \frac{U_{CJ}}{L} \frac{\partial}{\partial \tau} \Big|_{\zeta,\eta}. \quad (\text{F.13})$$

### F.2.1 Transformation Inversion

Note that we can inverse the above Levy-Lees variable transformation through

$$x(\zeta, \tau) = X_{det}(\tau)(1 - \zeta) \quad (\text{F.14})$$

$$\eta(x, y, t) = \frac{\int_0^y \frac{\rho}{\rho_0} dy'}{\delta} \quad (\text{F.15})$$

$$\Rightarrow \frac{d\eta}{dy} = \frac{\rho}{\rho_0 \delta} \quad (\text{F.16})$$

$$\frac{dy}{d\eta} = \frac{\rho_0 \delta}{\rho} \quad (\text{F.17})$$

$$y = \int_0^\eta \frac{\rho_0 \delta(\zeta, \tau)}{\rho} d\eta \quad (\text{F.18})$$

$$= \rho_0 \delta \int_0^\eta \frac{RT}{p} d\eta \quad (\text{F.19})$$

$$= \frac{\rho_0 \delta R}{p} \int_0^\eta T d\eta \quad (\text{F.20})$$

$$= \frac{\rho_0 \delta}{\rho_0 T_0} \int_0^\eta \frac{h}{c_p} d\eta \quad (\text{F.21})$$

$$= \frac{\delta}{T_0 c_p} \int_0^\eta h d\eta \quad (\text{F.22})$$

where we've used the ideal gas law and assumed  $h = c_p T$  with constant  $c_p$ .

$$t = \frac{\tau L}{U_{CJ}} \quad (\text{F.23})$$

### F.2.2 Stream Function Formulation

The compressible stream function  $\Psi$  may be defined such that

$$\rho u = \rho_0 \frac{\partial \Psi}{\partial y} \quad (\text{F.24})$$

$$\rho v = -\rho_0 \left( \frac{\partial \Psi}{\partial x} + \frac{\partial}{\partial t} (\eta \delta) \right) \quad (\text{F.25})$$

so that the continuity equation is satisfied automatically. Further, let us assume

$$\Psi = u_e(\zeta)\delta(\zeta, \tau)f(\zeta, \eta) \quad (\text{F.26})$$

where  $\star_e$  represents  $\star$  evaluated in the free stream

$$\Rightarrow \Psi_\zeta = u'_e\delta f + u_e\delta_\zeta f + u_e\delta f_\zeta \quad (\text{F.27})$$

$$\Psi_\eta = u_e\delta f_\eta \quad (\text{F.28})$$

$$\Psi_{\zeta\eta} = u'_e\delta f_\eta + u_e\delta_\zeta f_\eta + u_e\delta f_{\zeta\eta} \quad (\text{F.29})$$

$$\Psi_{\eta\eta} = u_e\delta f_{\eta\eta} \quad (\text{F.30})$$

$$\Psi_\tau = u_e\delta_\tau f \quad (\text{F.31})$$

$$\Psi_{\eta\tau} = u_e\delta_\tau f_\eta. \quad (\text{F.32})$$

The velocities are thus given by

$$u = \frac{\rho_0}{\rho}\Psi_y = \frac{\rho_0}{\rho}\frac{\rho}{\rho_0\delta}\Psi_\eta = \frac{u_e}{\delta}\delta f_\eta \quad (\text{F.33})$$

$$= u_e f_\eta \quad (\text{F.34})$$

$$v = -\frac{\rho_0}{\rho}\left(\Psi_x + \frac{\partial}{\partial t}(\eta\delta)\right) \quad (\text{F.35})$$

$$= -\frac{\rho_0}{\rho}\left(-\frac{1}{L\tau}\Psi_\zeta + \eta_x\Psi_\eta + \frac{U_{CJ}}{L\tau}(1-\zeta)\eta\delta_\zeta + \eta_t\delta + \frac{U_{CJ}}{L}\eta\delta_\tau\right) \quad (\text{F.36})$$

$$\begin{aligned} &= \frac{\rho_0}{\rho}\frac{u_e\delta f}{L\tau}\left[\frac{u'_e}{u_e} + \frac{\delta_\zeta}{\delta} + \frac{f_\zeta}{f} - \eta_x L\tau \frac{f_\eta}{f} - \frac{U_{CJ}}{u_e f}(1-\zeta)\eta \frac{\delta_\zeta}{\delta}\right. \\ &\quad \left.\dots - L\tau \frac{\eta_t}{u_e f} - \frac{U_{CJ}}{u_e f}\tau\eta \frac{\delta_\tau}{\delta}\right] \end{aligned} \quad (\text{F.37})$$

$$\begin{aligned} &= \frac{\rho_0}{\rho}\frac{u_e\delta f}{L\tau}\left[\frac{u'_e}{u_e} + \frac{\delta_\zeta}{\delta} + \frac{f_\zeta}{f} - \eta_x L\tau \frac{f_\eta}{f} - \frac{U_{CJ}}{u_e f}\eta \frac{\delta_\zeta}{\delta}\right. \\ &\quad \left.\dots + \frac{U_{CJ}}{u_e f}\eta\zeta \frac{\delta_\zeta}{\delta} - L\tau \frac{\eta_t}{u_e f} - \frac{U_{CJ}}{u_e f}\tau\eta \frac{\delta_\tau}{\delta}\right] \end{aligned} \quad (\text{F.38})$$

using

$$\delta = \sqrt{\frac{\nu_0 L \tau \zeta}{U_{CJ}}} \quad (\text{F.39})$$

we have

$$\begin{aligned} v &= \frac{\rho_0}{\rho} \frac{u_e \delta f}{L \tau} \left[ \frac{u'_e}{u_e} + \frac{1}{2\zeta} + \frac{f_\zeta}{f} - \eta_x L \tau \frac{f_\eta}{f} - \frac{U_{CJ}}{u_e f} \frac{\eta}{2\zeta} + \cancel{\frac{U_{CJ}}{u_e} \frac{\eta}{2f}} \right. \\ &\quad \left. \dots - L \tau \frac{\eta_t}{u_e f} - \cancel{\frac{U_{CJ}}{u_e} \frac{\eta_t}{2f}} \right] \end{aligned} \quad (\text{F.40})$$

$$= \frac{\rho_0}{\rho} \frac{u_e \delta f}{L \tau} \left[ \frac{u'_e}{u_e} + \frac{1}{2\zeta} + \frac{f_\zeta}{f} - \eta_x L \tau \frac{f_\eta}{f} - \frac{U_{CJ}}{u_e f} \frac{\eta}{2\zeta} - L \tau \frac{\eta_t}{u_e f} \right]. \quad (\text{F.41})$$

In the case of a boundary layer behind a steady shock

$$u'_e = f_\zeta = 0 \quad (\text{F.42})$$

$$\Rightarrow v = \frac{\rho_0}{\rho} \frac{u_e \delta f}{L \tau} \left[ \frac{1}{2\zeta} - \eta_x L \tau \frac{f_\eta}{f} - \frac{U_{CJ}}{u_e f} \frac{\eta}{2\zeta} - L \tau \frac{\eta_t}{u_e f} \right]. \quad (\text{F.43})$$

### F.3 Momentum Equation

We next consider each term in the momentum equation separately.

$$\rho u_t = \rho \frac{\partial}{\partial t} \left( \frac{\rho_0}{\rho} \Psi_y \right) \quad (\text{F.44})$$

$$= \rho \frac{\partial}{\partial t} \left( \frac{\rho_0}{\rho} \frac{\rho}{\rho_0 \delta} \Psi_\eta \right) \quad (\text{F.45})$$

$$= \rho \frac{\partial}{\partial t} \left( \frac{1}{\delta} u_e \delta f_\eta \right) \quad (\text{F.46})$$

$$= \rho \left[ \frac{U_{CJ}}{L \tau} (1 - \zeta) (u'_e f_\eta + u_e f_{\eta\zeta}) + u_e \eta_t f_{\eta\eta} \right] \quad (\text{F.47})$$

$$= \frac{\rho u_e^2}{L \tau} \left[ \frac{U_{CJ}}{u_e} (1 - \zeta) \left( \frac{u'_e}{u_e} f_\eta + f_{\zeta\eta} \right) + \cancel{\frac{L \tau}{u_e} \eta_t f_{\eta\eta}} \right]. \quad (\text{F.48})$$

$$\rho u u_x = \rho_0 \Psi_y \frac{\partial}{\partial x} \left( \frac{\rho_0}{\rho} \Psi_y \right) \quad (\text{F.49})$$

$$= \frac{\rho}{\delta} \Psi_\eta \frac{\partial}{\partial x} \left( \frac{1}{\delta} \Psi_\eta \right) \quad (\text{F.50})$$

$$= \rho u_e f_\eta \frac{\partial}{\partial x} (u_e f_\eta) \quad (\text{F.51})$$

$$= \rho u_e f_\eta \left[ -\frac{1}{L\tau} u'_e f_\eta - \frac{u_e}{L\tau} f_{\zeta\eta} + u_e \eta_x f_{\eta\eta} \right] \quad (\text{F.52})$$

$$= \frac{\rho u_e^2}{L\tau} \left[ -\frac{u'_e}{u_e} f_\eta^2 - f_\eta f_{\zeta\eta} + \cancel{L\tau \eta_x f_\eta f_{\eta\eta}} \right]. \quad (\text{F.53})$$

$$\rho v u_y = -\rho_0 \left( \Psi_x + \frac{\partial}{\partial t} (\eta\delta) \right) \frac{\partial}{\partial y} \left( \frac{\rho_0}{\rho} \Psi_y \right) \quad (\text{F.54})$$

$$= -\rho_0 \left( \Psi_x + \frac{\partial}{\partial t} (\eta\delta) \right) \frac{\partial}{\partial y} \left( \frac{\rho_0}{\rho} \frac{\rho}{\rho_0 \delta} \Psi_\eta \right) \quad (\text{F.55})$$

$$= -\rho_0 \left( \Psi_x + \frac{\partial}{\partial t} (\eta\delta) \right) \frac{\partial}{\partial y} \left( \frac{1}{\delta} u_e \delta f_\eta \right) \quad (\text{F.56})$$

$$= -\rho_0 \left( \Psi_x + \frac{\partial}{\partial t} (\eta\delta) \right) \frac{\rho}{\rho_0 \delta} \frac{\partial}{\partial \eta} (u_e f_\eta) \quad (\text{F.57})$$

$$= -\frac{\rho u_e}{\delta} f_{\eta\eta} \left( \Psi_x + \frac{\partial}{\partial t} (\eta\delta) \right) \quad (\text{F.58})$$

$$= -\frac{\rho u_e}{\delta} f_{\eta\eta} \left( -\frac{1}{L\tau} \Psi_\zeta + \eta_x \Psi_\eta + \frac{U_{CJ}}{L\tau} (1-\zeta) \frac{\partial}{\partial \zeta} (\eta\delta) + \dots \eta_t \frac{\partial}{\partial \eta} (\eta\delta) + \frac{U_{CJ}}{L} \frac{\partial}{\partial \tau} (\eta\delta) \right) \quad (\text{F.59})$$

$$= -\frac{\rho u_e}{\delta} f_{\eta\eta} \left( -\frac{1}{L\tau} (u'_e \delta f + u_e \delta_\zeta f + u_e \delta f_\zeta) + \eta_x u_e \delta f_\eta \dots + \frac{U_{CJ}}{L\tau} (1-\zeta) \eta \delta_\zeta + \eta_t \delta + \frac{U_{CJ}}{L} \eta \delta_\tau \right) \quad (\text{F.60})$$

$$= \frac{\rho u_e^2}{L\tau} \left( \frac{u'_e}{u_e} f f_{\eta\eta} + \frac{\delta_\zeta}{\delta} f f_{\eta\eta} + f_\zeta f_{\eta\eta} - \cancel{L\tau \eta_x f_\eta f_{\eta\eta}} - \frac{U_{CJ}}{u_e} (1-\zeta) \eta \frac{\delta_\zeta}{\delta} f_{\eta\eta} \dots - \cancel{\frac{L\tau}{u_e} \eta_t f_{\eta\eta}} - \frac{U_{CJ}}{u_e} \tau \eta \frac{\delta_\tau}{\delta} f_{\eta\eta} \right) \quad (\text{F.61})$$

The pressure term is given by

$$\frac{\partial p}{\partial x} = -\frac{1}{L\tau} p_\zeta + \eta_x \vec{p}_\eta \cdot 0 \quad (\text{F.62})$$

$$= -\frac{p_\zeta}{L\tau} \quad (\text{F.63})$$

also, since  $p_y = 0$ , we know  $p = p_e(\zeta)$  implying

$$-\frac{\partial p}{\partial x} = -\frac{p'_e}{L\tau}. \quad (\text{F.64})$$

Lastly

$$\frac{\partial}{\partial y} \left( \mu \frac{\partial u}{\partial y} \right) = \frac{\partial}{\partial y} \left( \mu \frac{\rho}{\rho_0 \delta} \frac{\partial}{\partial \eta} \left( \frac{\rho_0}{\rho} \frac{\partial \Psi}{\partial y} \right) \right) \quad (\text{F.65})$$

$$= \frac{\partial}{\partial y} \left( \mu \frac{\rho}{\rho_0 \delta} \frac{\partial}{\partial \eta} \left( \frac{\rho_0}{\rho} \frac{\rho}{\rho_0 \delta} \frac{\partial \Psi}{\partial \eta} \right) \right) \quad (\text{F.66})$$

$$= \frac{\rho}{\rho_0 \delta} \frac{\partial}{\partial \eta} \left( \mu \frac{\rho}{\rho_0 \delta} \frac{\partial}{\partial \eta} \left( \frac{1}{\delta} u_e \delta f_\eta \right) \right) \quad (\text{F.67})$$

$$= \frac{\rho u_e}{\rho_0 \delta} \frac{\partial}{\partial \eta} \left( \mu \frac{\rho}{\rho_0 \delta} f_{\eta\eta} \right) \quad (\text{F.68})$$

$$= \frac{\rho \nu_0 u_e}{\delta^2} \frac{\partial}{\partial \eta} (C f_{\eta\eta}) \quad (\text{F.69})$$

where

$$C = \frac{\rho \mu}{\rho_0 \mu_0} \quad (\text{F.70})$$

is the Chapman-Rubesin parameter.

Thus we see after cancellation

$$0 = -\frac{\partial p}{\partial x} + \frac{\partial}{\partial y} \left( \mu \frac{\partial u}{\partial y} \right) - \rho \frac{\partial u}{\partial t} - \rho u \frac{\partial u}{\partial x} - \rho v \frac{\partial u}{\partial y} \quad (\text{F.71})$$

$$\begin{aligned} &= \frac{p'_e}{L\tau} + \frac{\rho\nu_0 u_e}{\delta^2} (C f_{\eta\eta})_\eta - \frac{\rho u_e^2}{L\tau} \left[ \frac{U_{CJ}}{u_e} (1 - \zeta) \left( \frac{u'_e}{u_e} f_\eta + f_{\zeta\eta} \right) \right] \\ &\dots - \frac{\rho u_e^2}{L\tau} \left[ -\frac{u'_e}{u_e} f_\eta^2 - f_\eta f_{\zeta\eta} \right] - \frac{\rho u_e^2}{L\tau} \left[ \frac{u'_e}{u_e} f f_{\eta\eta} + \frac{\delta_\zeta}{\delta} f f_{\eta\eta} \right] \\ &\dots + f_\zeta f_{\eta\eta} - \frac{U_{CJ}}{u_e} (1 - \zeta) \eta \frac{\delta_\zeta}{\delta} f_{\eta\eta} - \frac{U_{CJ}}{u_e} \tau \eta \frac{\delta_\tau}{\delta} f_{\eta\eta} \end{aligned} \quad (\text{F.72})$$

$$\begin{aligned} &= \frac{\nu_0 L \tau}{\delta^2 u_e} (C f_{\eta\eta})_\eta + \frac{p'_e}{\rho u_e^2} - \left( \frac{\delta_\zeta}{\delta} f - \frac{U_{CJ}}{u_e} (1 - \zeta) \eta \frac{\delta_\zeta}{\delta} - \frac{U_{CJ}}{u_e} \tau \eta \frac{\delta_\tau}{\delta} \right) f_{\eta\eta} \\ &\dots - \left( \frac{u'_e}{u_e} f + f_\zeta \right) f_{\eta\eta} - \frac{U_{CJ}}{u_e} \left( (1 - \zeta) \left( \frac{u'_e}{u_e} f_\eta + f_{\zeta\eta} \right) \right) + \frac{u'_e}{u_e} f_\eta^2 + f_\eta f_{\zeta\eta} \end{aligned} \quad (\text{F.73})$$

$$\begin{aligned} &= \frac{\nu_0 L \tau}{\delta^2 u_e} (C f_{\eta\eta})_\eta + \frac{p'_e}{\rho u_e^2} + \left( \frac{U_{CJ}}{u_e} (1 - \zeta) \eta \frac{\delta_\zeta}{\delta} + \frac{U_{CJ}}{u_e} \tau \eta \frac{\delta_\tau}{\delta} - \frac{\delta_\zeta}{\delta} f \right) f_{\eta\eta} \\ &\dots - \left( \frac{u'_e}{u_e} f + f_\zeta \right) f_{\eta\eta} - \frac{U_{CJ}}{u_e} \left[ \left( 1 - \zeta - \frac{u_e}{U_{CJ}} f_\eta \right) \left( \frac{u'_e}{u_e} + \frac{f_{\zeta\eta}}{f_\eta} \right) f_\eta \right]. \end{aligned} \quad (\text{F.74})$$

Or after rearranging and multiplying by  $\zeta u_e / U_{CJ}$

$$\begin{aligned} &\frac{1}{\delta^2} \frac{\nu_0 L \tau \zeta}{U_{CJ}} (C f_{\eta\eta})_\eta + \left( (1 - \zeta) \eta \frac{\delta_\zeta}{\delta} + \tau \eta \frac{\delta_\tau}{\delta} - \frac{u_e}{U_{CJ}} \frac{\delta_\zeta}{\delta} f \right) \zeta f_{\eta\eta} \\ &= \zeta \left\{ \left( \frac{u'_e}{U_{CJ}} f + \frac{u_e}{U_{CJ}} f_\zeta \right) f_{\eta\eta} - \frac{p'_e}{\rho u_e U_{CJ}} \right. \\ &\dots + \left. \left( 1 - \zeta - \frac{u_e}{U_{CJ}} f_\eta \right) \left( \frac{u'_e}{u_e} + \frac{f_{\zeta\eta}}{f_\eta} \right) f_\eta \right\}. \end{aligned} \quad (\text{F.75})$$

From equation (F.75), we can see that if  $p_e(\zeta) = p_e \Rightarrow p'_e = 0$ ,  $u_e(\zeta) = u_e \Rightarrow u'_e = 0$ , and  $f = f(\eta)$  implying  $f_\zeta = f_\tau = 0$  as would be the case for a boundary layer behind a shock with uniform post-shock conditions, then the entire right-hand of

equation (F.75) side equals zero. Using

$$\delta = \sqrt{\frac{\nu_0 L \tau \zeta}{U_{CJ}}} \quad (\text{F.76})$$

$$\Rightarrow \frac{\delta_\zeta}{\delta} = \frac{1}{2\zeta} \quad (\text{F.77})$$

$$\frac{\delta_\tau}{\delta} = \frac{1}{2\tau} \quad (\text{F.78})$$

gives

$$(C f_{\eta\eta})_\eta + \left( \frac{\eta}{2\zeta} - \frac{\eta}{2} + \frac{\eta}{2} - \frac{u_e}{U_{CJ}} \frac{f}{2\zeta} \right) \zeta f_{\eta\eta} = \zeta \left\{ \left( \frac{u'_e}{U_{CJ}} f + \frac{u_e}{U_{CJ}} f_\zeta \right) f_{\eta\eta} - \frac{p'_e}{\rho u_e U_{CJ}} \right. \\ \dots + \left. \left( 1 - \zeta - \frac{u_e}{U_{CJ}} f_\eta \right) \left( \frac{u'_e}{u_e} + \frac{f_{\zeta\eta}}{f_\eta} \right) f_\eta \right\} \quad (\text{F.79})$$

$$(C f_{\eta\eta})_\eta + \frac{1}{2} \left( \eta - \frac{u_e}{U_{CJ}} f \right) f_{\eta\eta} = \zeta \left\{ \left( \frac{u'_e}{U_{CJ}} f + \frac{u_e}{U_{CJ}} f_\zeta \right) f_{\eta\eta} \right. \\ \dots + \left. \left( 1 - \zeta - \frac{u_e}{U_{CJ}} f_\eta \right) \left( \frac{u'_e}{u_e} + \frac{f_{\zeta\eta}}{f_\eta} \right) f_\eta - \frac{p'_e}{\rho u_e U_{CJ}} \right\}. \quad (\text{F.80})$$

If the right-hand side is zero and  $C = 1$  we return the results given in [Schlichting \(1979\)](#):

$$f_{\eta\eta\eta} + \frac{1}{2} \left( \eta - \frac{u_e}{U_{CJ}} f \right) f_{\eta\eta} = 0. \quad (\text{F.81})$$

We also return the results of [Liu et al. \(1983\)](#) if  $\sigma = 0$ ,  $\alpha = 1$ . To show this is true, we need to return to equation (F.75) and instead use

$$\delta_{Liu} = \delta \sqrt{\frac{1}{2} \left( \frac{p_0}{U_{CJ}^2 b \rho_0 F_0} \right)^\omega} \quad (\text{F.82})$$

where

$$b = \frac{\gamma(\gamma_0 - 1)}{\gamma_0(\gamma - 1)} \frac{c_{p,0}}{c_p} \quad (\text{F.83})$$

using the terminology of Liu et al. (1983):

$$\mu = \mu_0 \left( \frac{T}{T_0} \right)^\omega \quad (\text{F.84})$$

$$F = \frac{p_e}{\rho_0 U_{CJ}^2} \quad (\text{F.85})$$

$$R = \frac{\rho_e}{\rho_0} \quad (\text{F.86})$$

$$\phi = \frac{u_e}{U_{CJ}} \quad (\text{F.87})$$

$$\beta = \frac{\rho\mu}{\rho_e\mu_e} = C \frac{\rho_0\mu_0}{\rho_e\mu_e} \quad (\text{F.88})$$

we get

$$\begin{aligned} & \frac{p_0^\omega}{U_{CJ}^{2\omega} b^\omega \rho_0^\omega F_0^\omega} \frac{\rho_e \mu_e}{\rho_0 \mu_0} (\beta f_{\eta\eta})_\eta + (\eta - \phi f) f_{\eta\eta} \\ &= 2\zeta \left\{ (\phi' f + \phi f_\zeta) f_{\eta\eta} + (1 - \zeta - \phi f_\eta) \left( \frac{\phi'}{\phi} + \frac{f_{\zeta\eta}}{f_\eta} \right) f_\eta - \frac{F_\zeta g}{R\phi} \right\} \end{aligned} \quad (\text{F.89})$$

this is precisely what Liu et al. observes except the first term is organized differently.  
To show these are equivalent observe:

$$\frac{\rho_e \mu_e}{\rho_0 \mu_0} \left( \frac{p_0}{U_{CJ}^2 b \rho_0 F_0} \right)^\omega = \frac{\rho_e}{\rho_0} \left( \frac{T_e}{T_0} \right)^\omega \left( \frac{\gamma_0(\gamma-1)}{\gamma(\gamma_0-1)} \frac{c_p}{c_{p,0}} \right)^\omega \left( \frac{p_0}{p_e} \right)^\omega \left( \frac{p_e}{\rho_0 U_{CJ}^2 F_0} \right)^\omega \quad (\text{F.90})$$

$$= R \left( \frac{T_e}{T_0} \right)^\omega \left( \frac{\gamma_0(\gamma-1)}{\gamma(\gamma_0-1)} \frac{c_p T_e}{c_{p,0} T_0} \right)^\omega \left( \frac{T_0}{T_e} \right)^\omega \left( \frac{p_0}{p_e} \right)^\omega \left( \frac{F}{F_0} \right)^\omega \quad (\text{F.91})$$

$$= R \left( \frac{\gamma_0(\gamma-1)}{\gamma(\gamma_0-1)} \frac{h_e}{h_0} \right)^\omega \left( \frac{p_0}{p_e} \right)^\omega \left( \frac{F}{F_0} \right)^\omega \quad (\text{F.92})$$

$$= R \left( \frac{p_e \rho_0}{\rho_e p_0} \right)^\omega \left( \frac{p_0}{p_e} \right)^\omega \left( \frac{F}{F_0} \right)^\omega \quad (\text{F.93})$$

$$= R^{1-\omega} \left( \frac{F}{F_0} \right)^\omega \quad \checkmark \quad (\text{F.94})$$

where we've used

$$h = \frac{\gamma}{\gamma - 1} \frac{p}{\rho}. \quad (\text{F.95})$$

Note that we've shown

$$\frac{\nu_0 L \tau \zeta}{\delta_{Liu}^2 U_{CJ}} C^* = \frac{1}{2} R^{1-\omega} \left( \frac{F}{F_0} \right)^\omega \quad (\text{F.96})$$

where  $C^*$  is either  $C$  or a derivative of  $C$ .

So our final equation is

$$(C f_{\eta\eta})_\eta + \frac{1}{2} \left( \eta - \frac{u_e}{U_{CJ}} f \right) f_{\eta\eta} = \zeta \left\{ \left( \frac{u'_e}{U_{CJ}} f + \frac{u_e}{U_{CJ}} f_\zeta \right) f_{\eta\eta} \right. \\ \left. \dots + \left( 1 - \zeta - \frac{u_e}{U_{CJ}} f_\eta \right) \left( \frac{u'_e}{u_e} + \frac{f_{\zeta\eta}}{f_\eta} \right) f_\eta - \frac{p'_e}{\rho u_e U_{CJ}} \right\} \quad (\text{F.97})$$

with initial conditions

$$f(\zeta, 0) = f_\eta(\zeta, 0) = 0 \quad (\text{F.98})$$

$$f_\eta(\zeta, \infty) = 1 \quad (\text{F.99})$$

$$u(\zeta, \eta) = u_e(\zeta) f_\eta(\zeta, \eta) \quad (\text{F.100})$$

and

$$\zeta(x, t) = 1 - \frac{x}{U_{CJ} t} \quad (\text{F.101})$$

$$\eta(x, y, t) = \frac{\int_0^y \frac{\rho(x, y', t)}{\rho_0} dy'}{\sqrt{\nu_0 \left( t - \frac{x}{U_{CJ}} \right)}}. \quad (\text{F.102})$$

### F.3.1 Ideal Free-Stream Conditions

Assuming the conditions behind the detonation are constant at the Chapman-Jouguet values, we have  $p_e = p_2$ ,  $u_e = u_2$ , and  $h_e = h_2$ . This leads to  $f$  only being a function

of  $\eta$ . Further, assuming  $C = 1$ , equation (F.80) becomes

$$f''' + \frac{1}{2} \left( \eta - \frac{f}{\Lambda} \right) f'' = 0 \quad (\text{F.103})$$

where

$$\Lambda \equiv \frac{U_{CJ}}{u_2}. \quad (\text{F.104})$$

The boundary conditions are

$$f(0) = 0 \quad (\text{F.105})$$

$$f(\infty) = 1 \quad (\text{F.106})$$

and  $u$  can be found from

$$u(\eta) = u_2 f'. \quad (\text{F.107})$$

The boundary layer thickness,  $\delta$ , at a given distance behind the shock  $x'$  can be calculated from:

$$\delta(x) = \sqrt{\frac{\nu_2 L \tau \zeta}{U_{CJ}}} \quad (\text{F.108})$$

$$= \sqrt{\frac{\nu_2 L}{U_{CJ}} \left( 1 - \frac{x}{X_s} \right) \frac{t U_{CJ}}{L}} \quad (\text{F.109})$$

$$= \sqrt{\nu_2 \left( t - \frac{x}{U_{CJ}} \right)} \quad (\text{F.110})$$

using

$$t = \frac{X_s}{U_{CJ}} \quad (\text{F.111})$$

gives

$$\delta(x) = \sqrt{\nu_2 \frac{X_s - x}{U_{CJ}}} \quad (\text{F.112})$$

and evaluating at  $x = X_s - x'$  yields

$$\delta(X_s - x') = \sqrt{\frac{\nu_2 x'}{U_{CJ}}}. \quad (\text{F.113})$$

## F.4 Energy Equation

We define  $g$  to be the non-dimensionalized enthalpy

$$g(\zeta, \eta, \tau) = \frac{h(\zeta, \eta)}{h_e(\zeta)} \quad (\text{F.114})$$

and thus we have

$$h_\zeta = (h_e g)_\zeta = h'_e g + h_e g_\zeta \quad (\text{F.115})$$

$$h_\eta = h_e g_\eta \quad (\text{F.116})$$

$$h_\tau = 0. \quad (\text{F.117})$$

We can substitute this into the conservation of energy relationship to produce

$$\rho h_t = \frac{\rho U_{CJ}}{L\tau} (1 - \zeta) h_\zeta + \rho \eta_t h_\eta + \frac{\rho U_{CJ}}{L} h_\tau \quad (\text{F.118})$$

$$= \frac{\rho U_{CJ}}{L\tau} (1 - \zeta) (h'_e g + h_e g_\zeta) + \rho \eta_t h_e g_\eta \quad (\text{F.119})$$

$$= \frac{\rho u_e}{L\tau} h_e \left[ \frac{U_{CJ}}{u_e} (1 - \zeta) \left( \frac{h'_e}{h_e} g + g_\zeta \right) + \cancel{\frac{L\tau}{u_e} \eta_t g_\eta} \right]. \quad (\text{F.120})$$

$$\rho u h_x = \rho_0 \Psi_y h_x \quad (\text{F.121})$$

$$= \rho_0 \frac{\rho}{\rho_0 \delta} \Psi_\eta \left( -\frac{1}{L\tau} h_\zeta + \eta_x h_\eta \right) \quad (\text{F.122})$$

$$= \rho u_e f_\eta \left( -\frac{1}{L\tau} (h'_e g + h_e g_\zeta) + \eta_x h_e g_\eta \right) \quad (\text{F.123})$$

$$= \frac{\rho u_e}{L\tau} h_e \left[ -\frac{h'_e}{h_e} g f_\eta - g_\zeta f_\eta + \cancel{L\tau \eta_x g_\eta f_\eta} \right]. \quad (\text{F.124})$$

$$\rho v h_y = -\rho_0 (\Psi_x + (\eta \delta)_t) h_y \quad (\text{F.125})$$

$$\begin{aligned} &= -\rho_0 \left( -\frac{1}{L\tau} \Psi_\zeta + \eta_x \Psi_\eta + \frac{U_{CJ}}{L\tau} (1 - \zeta) (\eta \delta)_\zeta + \eta_t (\eta \delta)_\eta \right. \\ &\quad \left. \dots + \frac{U_{CJ}}{L} (\eta \delta)_\tau \right) \frac{\rho}{\rho_0 \delta} h_\eta \end{aligned} \quad (\text{F.126})$$

$$\begin{aligned} &= -\frac{\rho}{\delta} h_e g_\eta \left( -\frac{1}{L\tau} u'_e \delta f - \frac{1}{L\tau} u_e \delta_\zeta f - \frac{1}{L\tau} u_e \delta f_\zeta + \eta_x u_e \delta f_\eta \right. \\ &\quad \left. \dots + \frac{U_{CJ}}{L\tau} (1 - \zeta) \eta \delta_\zeta + \eta_t \delta + \frac{U_{CJ}}{L} \eta \delta_\tau \right) \quad (\text{F.127}) \end{aligned}$$

$$\begin{aligned} &= \frac{\rho u_e}{L\tau} h_e \left[ \frac{u'_e}{u_e} f g_\eta + \frac{\delta_\zeta}{\delta} f g_\eta + f_\zeta g_\eta - \cancel{L\tau \eta_x f_\eta g_\eta} - \frac{U_{CJ}}{u_e} (1 - \zeta) \eta \frac{\delta_\zeta}{\delta} g_\eta \right. \\ &\quad \left. \dots - \cancel{\frac{L\tau}{u_e} \eta_t g_\eta} - \frac{U_{CJ}}{u_e} \tau \eta \frac{\delta_\tau}{\delta} g_\eta \right]. \quad (\text{F.128}) \end{aligned}$$

$$p_t = \frac{U_{CJ}}{L\tau} (1 - \zeta) p_\zeta + \eta_t \cancel{p_\eta^0} + \frac{U_{CJ}}{L} \cancel{p_\tau^0} \quad (\text{F.129})$$

$$= \frac{U_{CJ}}{L\tau} (1 - \zeta) p'_e \quad (\text{F.130})$$

$$= \frac{\rho u_e}{L\tau} (1 - \zeta) \frac{U_{CJ}}{u_e} \frac{p'_e}{\rho} \quad (\text{F.131})$$

$$u p_x = \frac{\rho_0}{\rho} \Psi_y \left( -\frac{1}{L\tau} p_\zeta + \eta_x \cancel{p_\eta^0} \right) \quad (\text{F.132})$$

$$= \frac{\rho_0}{\rho} \frac{\rho}{\rho_0 \delta} \Psi_\eta \left( -\frac{1}{L\tau} p'_e \right) \quad (\text{F.133})$$

$$= -\frac{1}{L\tau \delta} u_e \delta f_\eta p'_e \quad (\text{F.134})$$

$$= -\frac{\rho u_e}{L\tau} f_\eta \frac{p'_e}{\rho}. \quad (\text{F.135})$$

$$\left(\frac{\mu}{Pr}h_y\right)_y = \frac{\rho}{\rho_0\delta} \left(\frac{\mu\rho}{Pr\rho_0\delta}h_\eta\right)_\eta \quad (\text{F.136})$$

$$= \frac{\rho\mu_0}{\delta\rho_0} \left(\frac{\mu\rho}{\mu_0\rho_0} \frac{1}{Pr\delta} h_e g_\eta\right)_\eta \quad (\text{F.137})$$

$$= \frac{\rho\nu_0}{\delta^2} h_e \left(\frac{C}{Pr} g_\eta\right)_\eta. \quad (\text{F.138})$$

$$(\mu u_y)^2 = \mu \left[ \left( \frac{\rho_0}{\rho} \Psi_y \right)_y \right]^2 \quad (\text{F.139})$$

$$= \mu \left[ \frac{\rho}{\rho_0\delta} \left( \frac{\rho_0}{\rho} \frac{\rho}{\rho_0\delta} \Psi_\eta \right)_\eta \right]^2 \quad (\text{F.140})$$

$$= \mu \left[ \frac{\rho}{\rho_0\delta} \left( \frac{1}{\delta} u_e \delta f_\eta \right)_\eta \right]^2 \quad (\text{F.141})$$

$$= \frac{\mu\rho^2 u_e^2}{\rho_0^2\delta^2} f_{\eta\eta}^2 \quad (\text{F.142})$$

$$= \frac{\rho\mu_0 u_e^2}{\rho_0\delta^2} C f_{\eta\eta}^2 \quad (\text{F.143})$$

$$= \frac{\rho\nu_0 u_e^2}{\delta^2} C f_{\eta\eta}^2. \quad (\text{F.144})$$

After cancellation, we have

$$\rho h_t + \rho u h_x + \rho v h_y = p_t + u p_x + \left(\frac{\mu}{Pr}h_y\right)_y + \mu (u_y)^2 \quad (\text{F.145})$$

$$\begin{aligned}
& \frac{\rho u_e}{L\tau} h_e \left[ \frac{U_{CJ}}{u_e} (1 - \zeta) \left( \frac{h'_e}{h_e} g + g_\zeta \right) - \frac{h'_e}{h_e} g f_\eta - g_\zeta f_\eta - \frac{U_{CJ}}{u_e} (1 - \zeta) \eta \frac{\delta_\zeta}{\delta} g_\eta \right. \\
& \quad \left. \dots + \frac{u'_e}{u_e} f g_\eta + f_\zeta g_\eta + \frac{\delta_\zeta}{\delta} f g_\eta - \frac{U_{CJ}}{u_e} \tau \eta \frac{\delta_\tau}{\delta} g_\eta \right] = \frac{\rho u_e}{L\tau} (1 - \zeta) \frac{U_{CJ}}{u_e} \frac{p'_e}{\rho} \\
& \quad \dots - \frac{\rho u_e}{L\tau} f_\eta \frac{p'_e}{\rho} + \frac{\rho \nu_0}{\delta^2} h_e \left( \frac{C}{Pr} g_\eta \right)_\eta + \frac{\rho \nu_0 u_e^2}{\delta^2} C f_{\eta\eta}^2
\end{aligned} \tag{F.146}$$

$$\begin{aligned}
& \frac{U_{CJ}}{u_e} (1 - \zeta) \left( \frac{h'_e}{h_e} g + g_\zeta \right) - \frac{h'_e}{h_e} g f_\eta - g_\zeta f_\eta - \frac{U_{CJ}}{u_e} (1 - \zeta) \eta \frac{\delta_\zeta}{\delta} g_\eta + \frac{u'_e}{u_e} f g_\eta \\
& \quad \dots + f_\zeta g_\eta + \frac{\delta_\zeta}{\delta} f g_\eta - \frac{U_{CJ}}{u_e} \tau \eta \frac{\delta_\tau}{\delta} g_\eta = (1 - \zeta) \frac{U_{CJ}}{u_e} \frac{p'_e}{h_e \rho} - f_\eta \frac{p'_e}{h_e \rho} \\
& \quad \dots + \frac{L\tau \nu_0}{u_e \delta^2} \left( \frac{C}{Pr} g_\eta \right)_\eta + \frac{\nu_0 u_e L\tau}{h_e \delta^2} C f_{\eta\eta}^2
\end{aligned} \tag{F.147}$$

$$\begin{aligned}
& \frac{L\tau \nu_0}{u_e \delta^2} \left( \frac{C}{Pr} g_\eta \right)_\eta + \frac{\nu_0 u_e L\tau}{h_e \delta^2} C f_{\eta\eta}^2 + \frac{U_{CJ}}{u_e} (1 - \zeta) \eta \frac{\delta_\zeta}{\delta} g_\eta - \frac{\delta_\zeta}{\delta} f g_\eta + \frac{U_{CJ}}{u_e} \tau \eta \frac{\delta_\tau}{\delta} g_\eta \\
& = \frac{u'_e}{u_e} f g_\eta + f_\zeta g_\eta + \frac{U_{CJ}}{u_e} (1 - \zeta) \left( \frac{h'_e}{h_e} g + g_\zeta \right) - \frac{h'_e}{h_e} g f_\eta - g_\zeta f_\eta \\
& \quad \dots - (1 - \zeta) \frac{U_{CJ}}{u_e} \frac{p'_e}{h_e \rho} + f_\eta \frac{p'_e}{h_e \rho}
\end{aligned} \tag{F.148}$$

$$\begin{aligned}
& \frac{1}{\delta^2} \frac{\nu_0 L\tau \zeta}{U_{CJ}} \left( \frac{C}{Pr} g_\eta \right)_\eta + \frac{u_e^2}{\delta^2} \frac{\nu_0 L\tau \zeta}{h_e U_{CJ}} C f_{\eta\eta}^2 + (1 - \zeta) \zeta \eta \frac{\delta_\zeta}{\delta} g_\eta - \frac{u_e}{U_{CJ}} \zeta \frac{\delta_\zeta}{\delta} f g_\eta + \zeta \tau \eta \frac{\delta_\tau}{\delta} g_\eta \\
& = \zeta \left\{ \left( \frac{u'_e}{U_{CJ}} f + \frac{u_e}{U_{CJ}} f_\zeta \right) g_\eta + \left( 1 - \zeta - \frac{u_e}{U_{CJ}} f_\eta \right) \left( \frac{h'_e}{h_e} + \frac{g_\zeta}{g} - \frac{p'_e}{\rho h_e g} \right) g \right\}.
\end{aligned} \tag{F.149}$$

Note that the right-hand side is zero in the case of steady flow behind the shock. At this point, let us use

$$\delta = \sqrt{\frac{\nu_0 L\tau \zeta}{U_{CJ}}} \tag{F.150}$$

to yield

$$\begin{aligned} \left( \frac{C}{Pr} g_\eta \right)_\eta + \frac{u_e^2}{h_e} C f_{\eta\eta}^2 + (1 - \zeta) \frac{\eta}{2} g_\eta - \frac{1}{2} \frac{u_e}{U_{CJ}} f g_\eta + \frac{\zeta \eta}{2} g_\eta \\ = \zeta \left\{ \left( \frac{u'_e}{U_{CJ}} f + \frac{u_e}{U_{CJ}} f_\zeta \right) g_\eta + \left( 1 - \zeta - \frac{u_e}{U_{CJ}} f_\eta \right) \left( \frac{h'_e}{h_e} + \frac{g_\zeta}{g} - \frac{p'_e}{\rho h_e g} \right) g \right\} \end{aligned} \quad (\text{F.151})$$

$$\begin{aligned} \left( \frac{C}{Pr} g_\eta \right)_\eta + \frac{u_e^2}{h_e} C f_{\eta\eta}^2 + \left[ (1 - \zeta) \frac{\eta}{2} - \frac{1}{2} \frac{u_e}{U_{CJ}} f + \frac{\zeta \eta}{2} \right] g_\eta \\ = \zeta \left\{ \left( \frac{u'_e}{U_{CJ}} f + \frac{u_e}{U_{CJ}} f_\zeta \right) g_\eta + \left( 1 - \zeta - \frac{u_e}{U_{CJ}} f_\eta \right) \left( \frac{h'_e}{h_e} + \frac{g_\zeta}{g} - \frac{p'_e}{\rho h_e g} \right) g \right\} \end{aligned} \quad (\text{F.152})$$

$$\begin{aligned} \left( \frac{C}{Pr} g_\eta \right)_\eta + \frac{u_e^2}{h_e} C f_{\eta\eta}^2 + \frac{1}{2} \left[ \eta - \frac{u_e}{U_{CJ}} f \right] g_\eta \\ = \zeta \left\{ \left( \frac{u'_e}{U_{CJ}} f + \frac{u_e}{U_{CJ}} f_\zeta \right) g_\eta + \left( 1 - \zeta - \frac{u_e}{U_{CJ}} f_\eta \right) \left( \frac{h'_e}{h_e} + \frac{g_\zeta}{g} - \frac{p'_e}{\rho h_e g} \right) g \right\}. \end{aligned} \quad (\text{F.153})$$

If we now assume that  $C = 1$ , the Prandtl number is constant, flow properties behind the shock are constant (implying  $u'_e = f_\zeta = h'_e = g_\zeta = p'_e = 0$ ), and  $h = c_p T$ , we return the solution presented in [Schlichting \(1979\)](#):

$$\frac{1}{Pr} g_{\eta\eta} + \frac{u_e^2}{c_p T_e} f_{\eta\eta}^2 + \frac{1}{2} \left[ \eta - \frac{u_e}{U_{CJ}} f \right] g_\eta = 0. \quad (\text{F.154})$$

The solution of [Liu et al. \(1983\)](#) is returned if we take the same assumptions and choice of  $\delta$  as described above. This is proven by noting

$$\frac{\gamma - 1}{\gamma} \frac{R \phi^2}{F} = \frac{\gamma - 1}{\gamma} \frac{\rho_e}{\rho_0} \frac{\rho_0 U_{CJ}^2}{p_e} \frac{u_e^2}{U_{CJ}^2} \quad (\text{F.155})$$

$$= \frac{\gamma - 1}{\gamma} \frac{\rho_e}{p_e} u_e^2 \quad (\text{F.156})$$

$$= \frac{u_e^2}{h_e}. \quad (\text{F.157})$$

### F.4.1 Idealized Conditions

Assuming the conditions behind the detonation are constant at the Chapman-Jouguet values, we have  $p_e = p_2$ ,  $u_e = u_2$ , and  $h_e = h_2$ . This leads to  $g$  only being a function of  $\eta$ . Further assuming  $C = 1$  and the  $Pr$  number is constant equation (F.153) becomes

$$g'' + PrEc f'^2 + \frac{Pr}{2} \left[ \eta - \frac{f}{\Lambda} \right] g' = 0 \quad (\text{F.158})$$

where

$$\Lambda \equiv \frac{U_{CJ}}{u_2} \quad (\text{F.159})$$

$$Ec \equiv \frac{u_2^2}{h_2} \quad (\text{F.160})$$

the boundary conditions are

$$g(0) = \frac{h_w}{h_2} \quad (\text{F.161})$$

$$g(\infty) = 1 \quad (\text{F.162})$$

and  $h$  can be found from

$$h(\eta) = h_2 g. \quad (\text{F.163})$$